Immunomodulatory effect of minocycline on macrophage phenotype and function

K.E. Adams

Ph.D

2022

University of East London

Immunomodulatory effect of minocycline on macrophage phenotype and function

Kate Elizabeth Adams

A thesis submitted in partial fulfilment of the requirements of the University of East London for the degree of Doctor of Philosophy.

January 2022

London, UK

“You must do the things you think you cannot do.”

– Eleanor Roosevelt

Abstract

Minocycline is a second-generation semi-synthetic tetracycline antibiotic that displays additional immunomodulatory and anti-inflammatory properties. The benefit of these properties has proved to be clinically relevant, however, exact immunoregulatory mechanisms behind minocycline's non-antibiotic effects remain unveiled. In the context of inflammatory bowel disease, data has previously shown that minocycline improves mucosal recovery in colitic mice, an effect related to a potentiation of the innate immune response and enhanced inflammatory resolution. Minocycline initially enhanced monocyte recruitment to the intestine, whilst simultaneously increasing the presence of Ly6C- MHCII+ macrophages. *In vitro*, minocycline was shown to both increase and decrease proinflammatory cytokine release which was crucially seen to be time-dependant. Whether these effects derived from a direct action of minocycline on macrophages or other mechanisms is unclear. Macrophages are essential in the regulation of inflammation and resolution and can switch between M1/pro-inflammatory and M2/anti-inflammatory phenotypes, with disturbances in M1/M2 homeostasis contributing to the development and maintenance of chronic inflammation. An improved understanding of minocycline's immunoregulatory activity is key for future translational studies into human disease, thus the aim of this research was to evaluate the direct effects of minocycline on monocyte-macrophage differentiation, polarisation, and activation.

Three *in vitro* models were employed: THP-1, U-937 and human PBMCs. When differentiated in the presence of minocycline (10-50μM) with PMA (80nM) for 48hr, minocycline interrupted cellular adhesion and significantly decreased the expression of CD14 and CD86, while increasing the percentage of $CD163^{+}$ cells - an M2-associated marker. When administered to M0 macrophages polarised for 24hr to M1 (20ng/mL IFN-γ+10ng/mL LPS), or M2 (20ng/mL IL-4), minocycline significantly reduced the production of pro-inflammatory cytokines IL-1β, IL-6 and TNF-α, while in the M2 exclusively, reduced the expression of CD206 and IL-10, but increased IFN-γ and IL-12p70 production. The transcription factors *stat2, 3* and *6* were also reduced by minocycline following M1 polarization.

Conversely, when assessing the role of minocycline upon LPS-activated macrophages (100ng/mL for 24hr), minocycline-treated M1 PBMC-derived macrophages displayed maintained decreased production of IL-1β but increased TNF-α, IL-6 and IFN-y, with activated M2 macrophages also increasing and decreasing IL-12p70 and IL-10 respectively.

This data has highlighted some key regulatory effects of minocycline regarding macrophage biology and have added to the collective knowledge on minocycline's' immunomodulatory effects that can help provide more detailed context to the anti-inflammatory effects seen *in vivo*. Consequently, this advancement in knowledge will ultimately aid the development of novel therapeutic strategies for those individuals that are burdened with diseases dominated by a dysregulated immune response as seen in IBD.

Declaration

I declare that this thesis has been composed solely by myself and that it has not been submitted, in whole or in part, in any previous application for a degree. Except where stated otherwise by reference or acknowledgment, the work presented is entirely my own.

Name: Kate Elizabeth Adams

Signed: 

Date: 14 January 2022

Table of Contents

List of Tables, Figures & Illustrations

Abbreviations

BMDM | Bone Marrow-Derived Macrophage

CD | Cluster of Differentiation

DAMP | Damage/Danger Associated Molecular Pattern

IBD | Inflammatory Bowel Disease

IFN | Interferon

IL | Interleukin

IRF | Interferon Regulatory Factor

JAK | Janus Kinase

LPS | Lipopolysaccharide

MAPK | Mitogen-Activated Protein Kinase

M-CSF | Macrophage-Colony Stimulating Factor

MHC | Major Histocompatibility Complex

MMP | Matrix Metalloprotease

NF-κB | Nuclear Factor kappa B

PAMP | Pathogen Associated Molecular Pattern

PBMC | Periphery Blood Mononuclear Cell

PMA | Phorbol 12-Myristate 13-Acetate

PPAR | Peroxisome Proliferator-Activated Receptors

PRR | Pattern Recognition Receptor

SOCS | Suppressor of Cytokine Signalling

STAT | Signal Transducer and Activator of Transcription

Th | T Helper

TLR | Toll-Like Receptor

TNF | Tumour Necrosis Factor

Acknowledgements

Throughout this project so many individuals have been profoundly influential, and for every single one of them I am extremely grateful. Firstly, I would like to thank my director of studies Dr Natividad Garrido Mesa for her vision of the project and continued support and guidance throughout. I would also like to thank my supervisor's; Dr Lesley Smyth for providing both personal and professional support over the past few years, and Dr Jose Saldana for his technical and experimental input, and to each for their valuable feedback during the drafting of this manuscript.

Of course, none of this work would have been possible without funding, and for that I would like to extend a huge thank you to the University of East London for funding this project via their Excellence Studentship award. I would also like to thank the Graduate School for their provision of £1000 grant money awarded as part of the UEL Funded Internship Scheme, and to Queen Mary University London for allowing me to work within their laboratories throughout this short internship period. In addition, my research collaborator established through said scheme, Dr Jose Garrido Mesa, was instrumental in shaping this project through his extremely kind and unwavering guidance during the generation and experimentation with the PBMCs. Without his help a huge portion of this project would not have been possible, and there are not enough words to express my sincerest gratitude.

To all the technical team at the University of East London, and colleagues both past and present, thank you all so much for your professional and personal support since day one. Your kind words of advice and willingness to simply listen through the ups and downs naturally associated with pursuing a PhD have kept me smiling and sane. This journey would not have been the same without each and every one of you.

And finally, to my family and friends, in short, getting to where I am today may simply not have been possible without your continued love, support and encouragement – thank you always.

1. Introduction

1.1. Minocycline: History & applications

Tetracyclines are a family of chemical compounds derived from the tetracyclic naphthacene carboxamide ring first discovered in 1947 by Benjamin M. Duggar from a mix of natural antibiotic compounds produced by the genus *Streptomyces*, mainly composed by soil-dwelling bacteria (Duggar, 1948). The first tetracycline isolated and characterized was chlortetracycline, followed by tetracycline and other derivates. Tetracyclines can be divided into three groups based on their pharmacokinetic and antibacterial properties:

- Group 1: older derivatives with reduced bioavailability and lipophilicity than those in group 2. Examples include tetracycline, oxytetracycline, chlortetracycline, demeclocycline, lymecycline, methacycline and rolitetracycline.
- Group 2: derivatives which are almost completely absorbed and are 3–5 times more lipophilic than those in group 1 which may improve their tissue distribution. Analogues include doxycycline and minocycline.
- Group 3: new developmental compounds such as tigecycline and aminomethylcyclines. These antibiotics have been designed to target bacteria with acquired resistance to tetracyclines (Agwuh and MacGowan, 2006).

Tetracycline molecules comprise a linear fused tetracyclic skeleton made of 4 tetracyclic naphthacene carboxamide rings designated A, B, C, and D to which a variety of functional groups are attached (Figure 1.1) (Ian Chopra and Roberts, 2001; Agwuh and MacGowan, 2006). Features important for antibacterial activity among the tetracyclines require maintenance of the linear fused tetracycle, naturally occurring configurations at the A-B ring junction, and 4 dimethylamino group positions (I. Chopra and Roberts, 2001). Addition or removal of the dimethylamino group from C4 gives rise to several chemically modified tetracyclines (Golub, Suomalainen and Sorsa, 1992; Nelson, 1998a). Antibiotic and non-antibiotic characteristics of tetracyclines may be reduced by modifying the lower peripheral zone; on the other hand, modification in the upper peripheral zone enhances the attack on biological targets, particularly at positions C7 through C9 of the D ring. Chemical modifications in the upper and lower regions

of the parent structure, with the aim of improving their antimicrobial spectrum or pharmacokinetic properties, produce variably active and inactive compounds of first and second generation (Nelson, 1998a). Of those, minocycline and doxycycline are two of the most commonly used in the clinic (Smith and Leyden, 2005).

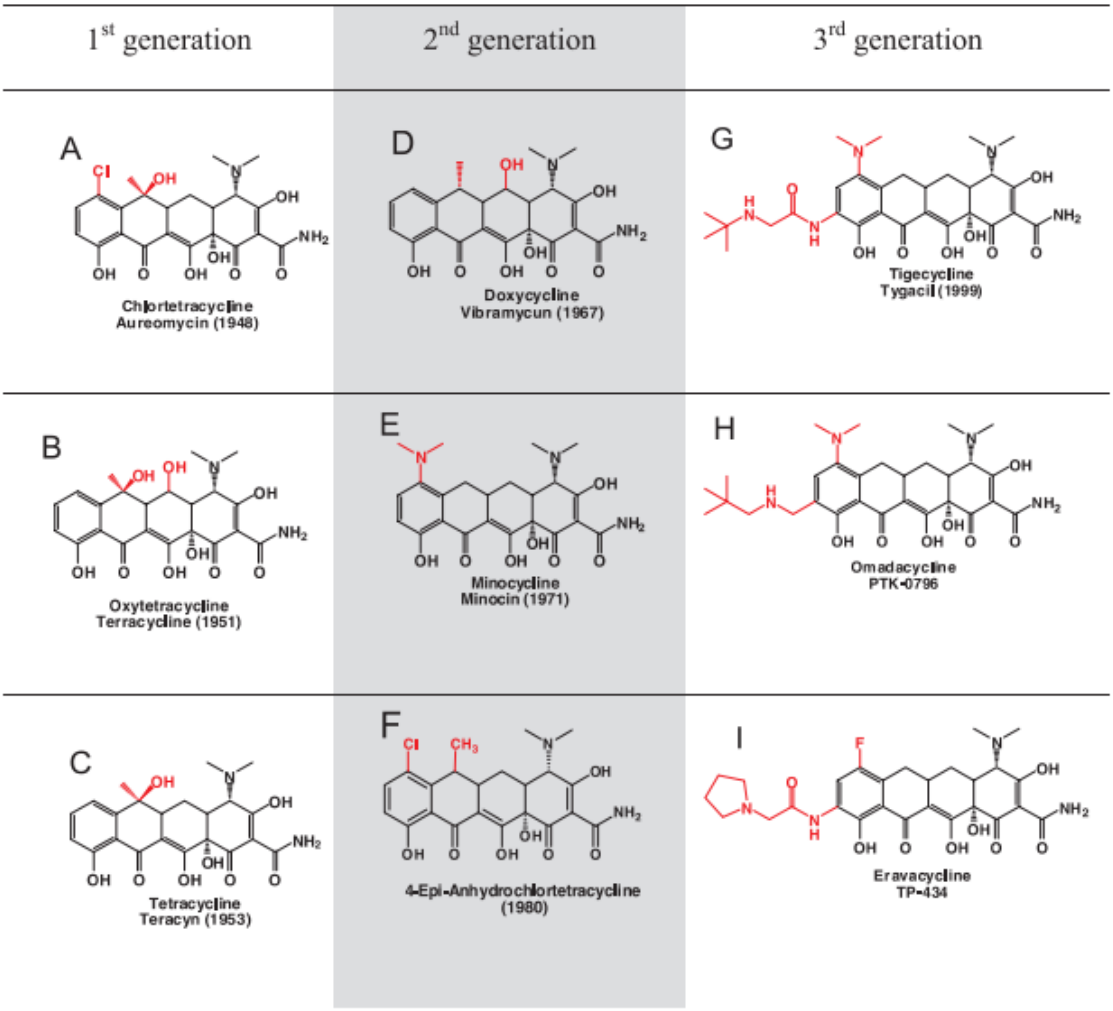

Figure 1.1: Tetracycline derivatives and their associated chemical structures. Diagram includes first, second and third generation products, with the numbers within brackets representing the year each derivative was discovered (Chiwunze et al., 2016).

Tetracyclines238 are broad-spectrum bacteriostatic antibiotics that inhibit bacterial protein synthesis through preventing the association of aminoacyl-tRNA with the bacterial ribosome, and are active against a wide range of aerobic and anaerobic bacteria, as well as other microorganisms (Schnappinger and Hillen, 1996). However, the emergence, and increase prevalence of bacterial resistance have limited their current use to infections caused by *Rickettisae, Chlamydiae, Mycoplasma pneumoniae*, and *Plasmodium* spp., as well as to the treatment of acne, respiratory tract infections and other chronic conditions caused by atypical

microorganisms which display resistance to other antibiotics (Klein and Cunha, 1995a; Sapadin and Fleischmajer, 2006a; Nelson and Levy, 2011; Falagas *et al.*, 2015; Cho *et al.*, 2018; Heaney, Mahoney and Gallagher, 2019). Their activity, in combination to being well tolerated by patients and easily produced by fermentation, made them, and continues to make them, effective and economically valuable drugs (I. Chopra and Roberts, 2001; Zakeri and Wright, 2008).

Despite their success in the context of infection, extensive research, with particular focus on minocycline, has unveiled immunomodulatory, anti-apoptotic, and anti-proliferative properties for this family of antibiotics, as well as their ability to inhibit proteolysis, angiogenesis and tumour metastasis (Golub *et al.*, 1991; Nelson, 1998b; Sapadin and Fleischmajer, 2006b; Webster and Del Rosso, 2007; Griffin *et al.*, 2010; Griffin, Ceballos and Villarreal, 2011; Garrido-Mesa, Zarzuelo and Gálvez, 2013a, p. ; Di Cerbo *et al.*, 2019). This has therefore rendered tetracyclines as a keen topic of interest for researchers globally to ascertain their use as immunomodulatory agents, which, in combination with their current application as antibiotics, may lend themselves as a novel treatment for pathologies dominated by immune dysregulation with or without microbial input.

1.2. Minocycline & its non-antibiotic properties

Minocycline is a second-generation, semi-synthetic antibiotic analogue of tetracycline with efficacy against both gram-positive and gram-negative bacterial strains through the inhibition of protein synthesis via attachment to the bacterial 30S ribosomal subunit (Asadi *et al.*, 2020). Minocycline contains a dimethylamino group at position 7 without methyl and hydroxy groups at position 5; enabling improved lipophilicity than other tetracyclines, with optimal tissue penetration (Macdonald *et al.*, 1973; Asadi *et al.*, 2020). Minocycline has an improved pharmacokinetic profile than first-generation tetracyclines when used orally. It is rapidly and almost completely absorbed (95-100%) within the stomach and GI tract (Saivin and Houin, 1988), with a longer biological half-life (11-12 hr) (Tariq, Rizvi and Anwar, 2018). Moreover, minocycline has a good safety record when used chronically, with dosages of up to 200 $mg \cdot day^{-1}$ reported to be generally safe and well-tolerated in humans (Garrido-Mesa, Zarzuelo and Gálvez, 2013a). Regarding side effects, the most common include nausea, vertigo, and mild

dizziness, and occur mainly early after its administration, subsiding following therapy discontinuation. Although generally well tolerated, for treatments spanning over 6 months it is recommended to monitor for hepatotoxicity, pigmentation and systemic lupus erythematosus, with treatment advised to be discontinued if these develop in the minority of cases (Williams, Laughlin and Lee, 1974; Klein and Cunha, 1995a; Garrido-Mesa, Zarzuelo and Gálvez, 2013a).

Minocycline has been shown to exert multiple biological modifications such as anti-apoptotic, and anti-oxidant effects, mitochondrial adaptation, inhibition of matrix metalloproteinases, alongside various anti-inflammatory effects (Sapadin and Fleischmajer, 2006c; Garrido-Mesa, Zarzuelo and Gálvez, 2013b; Haghi-Aminjan, 2017). In particular for minocycline, the therapeutic aspects beyond its function as an antibiotic have been well acknowledged within the literature, with both pre-clinical and clinical studies elucidating its anti-inflammatory and immunomodulatory properties (Sapadin and Fleischmajer, 2006c; Garrido-Mesa, Camuesco, *et al.*, 2011a; Garrido-Mesa, Zarzuelo and Gálvez, 2013b). Minocycline has been verified to exert this immunomodulatory function via alteration of immune cell activation and the subsequent release of chemical compounds such as cytokines, chemokines, nitric oxide, and matrix metalloproteases, which successively augment both inflammatory cascades and downstream immune responses in a plethora of different pathologies (Stirling *et al.*, 2005). The current literature has amounting research encompassing the beneficial effects of minocycline treatment of; acne, stroke, rheumatoid arthritis, cancers, and various neurological pathologies including Alzheimer's and multiple sclerosis, as is discussed in more detail below (Burke *et al.*, 2014; Haghi-Aminjan, 2017; Harwani, 2018a; Zhou *et al.*, 2018).

1.2.1. Anti-inflammatory actions of minocycline

Inflammation is relevant in a plethora of disease states, and several studies have already began exploring the inhibitory and stimulatory effect of minocycline with focus on the toll-like receptor (TLR)4- nuclear factor kappa B (NF-κB) inflammatory pathway. Ataie-Kachoie *et al* (2013) conducted a thorough investigation into the influence of minocycline upon constituents of the NF-κB signalling cascade, showing suppression of NF-κB in OVCAR-3 and SKOV-3 ovarian carcinoma cells. This was attributed to attenuation of upstream inhibitor

protein IκBα activation, phosphorylation, and degradation, in addition to suppression of p65 phosphorylation and nuclear translocation – a crucial mechanism for inflammatory gene transcription. This process was also described to be resultant of inhibition of transforming growth factor-β-activated kinase 1 (TAK-1) activation and dissociation from TAK1-binding protein 1 (TAB1), which are key constituents of the NF-κB signalling cascade (Ataie-Kachoie, P. *et al.*, 2013). More recently, Weiler and Dittmar (2019) also confirmed that minocycline abrogated IκBα and p65 phosphorylation leading to suppression of NF-κB and showed how treatment with minocycline inhibited the tumour necrosis factor receptor 1 (TNFR1)- tumour necrosis factor receptor-associated factor 2 (TRAF2) axis downstream of the TNFR1 in MDA-MB0435-pFDR1 cancer cells and M13SV1-Cre breast epithelial cells. They were also able to show that minocycline acted as a potent inhibitor of tumour necrosis factor alpha (TNF-α) via targeting of the NF-κB pathway, while differentially affecting all mitogen-activated protein kinases (MAPKs) (extracellular signal-regulated kinase - ERK1/2, p38 and c-Jun N-terminal protein kinase - JNK) (Weiler and Dittmar, 2019). A 2015 study conducted by Zhao and colleagues also demonstrated treatment with minocycline significantly upregulated the expression of cAMP response element-binding protein (CREB) and phosphorylated CREB (pCREB) – a transcription factor that regulates diverse cellular responses, including proliferation, survival, and differentiation, within a model of cerebral ischemia in Wistar rats (Zhao *et al.*, 2015).

In the context of neuroinflammation, it has also been observed that minocycline attenuates bacterial lipopolysaccharide (LPS)-stimulated degradation of IκBα (Nikodemova, Duncan and Watters, 2006), providing justification towards the reported interference of tetracyclines with NF-κB transcriptional activity and attenuation of the p38 MAPK cascade, which leads to the inhibition of microglia activation, inflammatory signalling, apoptosis and neurodegeneration (Yrjänheikki *et al.*, 1998; Tikka and Koistinaho, 2001; Wu *et al.*, 2002; Cui *et al.*, 2008; Defaux *et al.*, 2011; Bahrami, Morris and Pourgholami, 2012; Garrido-Mesa, Zarzuelo and Gálvez, 2013c; Santa-Cecília *et al.*, 2016). Linked to the activation of the phosphoinositide 3-kinase (PI3K)/protein kinase B (AKT) and NF-κB signalling pathways, retinoic acid receptor gamma (RARγ) also plays a role in the growth and differentiation of tumour cells, and it has been suggested to mediate the inhibitory effects of minocycline on human prostate cancer cells,

through triggering RAR signalling (Clarke *et al.*, 2004; Purton *et al.*, 2006; Yan *et al.*, 2010; Chen *et al.*, 2014; Regen *et al.*, 2014; Kadigamuwa *et al.*, 2019).

Both *in vitro* and *in vivo* studies have correlated the role of minocycline on poly-ADP ribose polymerase 1 (PARP-1) inhibition and cardio-protection (Tao *et al.*, 2010; Shahzad *et al.*, 2011). PARPs are a family of enzymes that share the ability to catalyse the transfer of ADP-ribose to target proteins (poly ADP-ribosylation), with PARP-1 best known for its involvement in DNA repair, cell proliferation and cell death (Morales *et al.*, 2014). While PARP-1 has been reported to act as a DNA damage sensor and subsequently participate in DNA repair processes crucial for protection against cell death, hyper-activated PARP-1 is noted to be destructive (Jubin *et al.*, 2017). In 2010 Tao *et al* concluded that PARP-1 enzymatic activity was directly inhibited by minocycline and protected cardiac myocytes in a model of simulated ischemia/reperfusion injury, while in 2011 Shahzad and colleagues were able to demonstrate a role of minocycline in reducing plaque size and stenosis in *de novo* atherogenesis in ApoE -/- (atherosclerosis-prone apolipoprotein E-deficient) mice receiving a high fat diet in part due to inhibition of PARP-1.

Others, however, have ascribed minocycline's role in cardio protection to interference with p38 MAPK (Sinha-Hikim *et al.*, 2011), or a reduction in high mobility group box 1 (HMGB1) resulting in a remarkable decrease in infarct size and increased cell viability (Hu *et al.*, 2010). Similar tissue protective effects of minocycline have also been observed in other organs under hypoxic conditions such as in kidneys and liver following cardio-pulmonary bypass surgery (Dhein *et al.*, 2015).

It has also been suggested that tetracyclines can interact and stabilize double stranded ribonucleic acid (dsRNA) which is involved in viral replication, and activates host defence mechanisms such as TLR3 activation of NF-κB and interferon production (Wei and Bechhofer, 2002; Ding and Voinnet, 2007; Dutta and Basu, 2011). Minocycline has also shown anti-apoptotic, anti-inflammatory, and antiviral activities in the context of human immune deficiency virus (HIV) infection which may also be mediated via interactions with dsRNAs leading to suppression of viral replication and activation of the immune response (Copeland and Brooks, 2010; Szeto *et al.*, 2010).

1.2.2. MMP inhibition

The application of tetracyclines in the field of cancer has been in continuous rise since the discovery of their potential to inhibit matrix metalloprotease (MMP) activity, in addition to reports of their antitumoral properties (Song *et al.*, 2014; Ali *et al.*, 2018; Defrancesco and Arcaini, 2018; Dong *et al.*, 2019; Antoszczak *et al.*, 2020). Extracellular matrix (ECM) degradation by MMPs is a critical step in cancer metastasis, therefore, the ability of tetracyclines to suppress MMPs activity was quickly identified of therapeutic potential in cancer treatment (Masumori *et al.*, 1994; Lokeshwar, 1999; Hidalgo and Eckhardt, 2001; Duffy, McGowan and Gallagher, 2008; Jabłońska-Trypuć, Matejczyk and Rosochacki, 2016). Tetracyclines are noted to accumulate in bone, so considering their osteotropism, tetracyclines have been found to be effective in reducing MMPs release in bone tumours and bone metastasis (Saikali and Singh, 2003; Niu *et al.*, 2008). Minocycline has also been found to inhibit metastasis and invasion to other tissues, such as pulmonary metastasis of renal adenocarcinoma (Masumori *et al.*, 1994).

The benefit of MMP inhibition with minocycline has also been researched in the context of atherosclerosis and ischemic disease. There are reports linking minocycline use with substantial reduction of plaque MMP activity and histologically verified plaque stabilization via molecular imaging, in addition to reduced occurrence of heart infarction, and subsequent myocardial damage (Ohshima *et al.*, 2010). Furthermore, blood reperfusion during cardiac ischemic events is known to cause intense oxidative stress which results in myocyte apoptosis and tissue injury and remodelling associated with MMP production. Thus, through its inhibitory action on MMP9, studies have shown the cardioprotective benefit of minocycline in ischemia-reperfusion injury models (Romero-Perez *et al.*, 2008).

The important role of nitric oxide (NO) and MMP in arthritis rendered tetracycline and its derivatives viable options in the treatment of Rheumatoid Arthritis (RA) given their inhibition of inducible NO (iNO) production by chondrocytes, synovial-derived MMP, and synoviocyte invasion (Greenwald *et al.*, 1987, 1992; Greenwald, 1994; Seftor *et al.*, 1998; Sadowski and Steinmeyer, 2001). In addition to preclinical evidence, long-term oral minocycline in conjugation to their standard therapy has been studied in RA patients, reporting a statistical

improvement in laboratory parameters (Kloppenburg et al., 1994). Furthermore, a second study with active RA refractory to disease-modifying antirheumatic drugs (DMARDS) also showed statistically significant improvement with minocycline treatment, confirming its potential as an anti-arthritic agent (Tilley, 1995).

A central hallmark of neurodegenerative disorders is the accumulation of protein aggregates, such the intraneuronal (tau or α-synuclein), and extracellular amyloid beta (Aβ) peptide misfolded proteins found in Parkinson's disease (PD) and Alzheimer's disease (AD), respectively (Maiti *et al.*, 2014). These can result in mitochondrial dysfunction, enhanced reactive oxygen species (ROS) production, and neurodegeneration (Brahmachari *et al.*, 2016; Bortolanza *et al.*, 2018). It has been recently described that minocycline can directly inhibit this protein amyloid aggregation (Socias *et al.*, 2018), and accumulating evidence has associated MMPs with the pathogenesis of PD, given their involvement in dopaminergic neuronal death and neuroinflammation (Reglodi *et al.*, 2017). Consequently, it has been remarked that minocycline can prevent dopaminergic neurodegeneration via MMP inhibition in rodent models of PD as well as in Drosophila models (Casarejos *et al.*, 2006; Radad, Moldzio and Rausch, 2010; Cankaya *et al.*, 2019).

In the context of multiple sclerosis (MS), MMPs promote inflammatory cascades in the central nervous system (CNS) and instigate axonal loss (Newman *et al.*, 2001). Here, a phase 3 trial studied the efficacy of minocycline in the risk of conversion (disease progression) from clinically isolated syndrome to established MS. The trial showed a modest effect on inflammatory disease activity by reducing the number of new lesions, cumulative combined number of unique lesions, and lesion volume at six months. Moreover, risk of conversion at six months was also significantly lower in patients treated with minocycline, but which was no longer significant after 24 months of treatment (Metz *et al.*, 2017).

Minocycline likewise abrogates oxygen-glucose deprivation-induced cell cytotoxicity, down-regulates the production and activity of MMP2 and MMP9 *in vitro*, and inhibits enzymatic activity of MMPs in the context of cerebral ischemia, consequently preserving blood-brain barrier integrity *in vivo* (Machado *et al.*, 2006; Fagan, Cronic and Hess, 2011). A completed clinical trial further supports

the use of minocycline in the treatment of ischemic stroke and demonstrated that minocycline, in conjunction with tissue plasminogen activator (tPA), greatly decreased MMP9 plasma levels, extending the treatment window from 3h to 6h, and helping to ameliorate brain haemorrhage following ischemic stroke (Murata *et al.*, 2008; Switzer *et al.*, 2011; Blacker *et al.*, 2013; Fan, Lo and Wang, 2013).

1.2.3. Cell cycle, proliferation, and apoptosis

Minocycline is able to regulate tumour proliferation both *in vitro* and *in vivo* by targeting cell cycle arrest and apoptosis (Warren, Wong-Brown and Bowden, 2019). Cell growth and proliferation are regulated by growth factor receptor signalling via the ERK pathway (Samatar and Poulikakos, 2014). Different mechanisms have been linked to this effect, highlighting the inhibition of signalling molecules and pathways linked to cancer proliferation, such as ERK and PARP-1, and increasing the susceptibility of cancerous cells to mitochondrial dysfunction, autophagy and apoptosis (Antoszczak *et al.*, 2020). Specifically, minocycline, in combination with doxycycline, was shown to have dual effects on cell proliferation (Gomes and Fernandes, 2007). Minocycline has been shown to enhance mitomycin C-induced cytotoxicity in human non-small cell lung cancer cells through down-regulating ERK1/2-mediated DNA repair protein RAD51 homolog 1 (RAD51) expression (Ko *et al.*, 2015). Moreover, considering the regulatory effects of PARP-1 on cell cycle, its inhibition could be therapeutically viable in the treatment of cancer (Alano *et al.*, 2006; Carbone *et al.*, 2008), with this effect already reported in ovarian cancer cells treated with minocycline. In addition, minocycline suppressed DNA synthesis, and down-regulated cyclins A, B, and E, resulting in cell cycle arrest in the G0 cycle, ultimately preventing cell growth and development (Pourgholami *et al.*, 2012). It has also been reported that minocycline reduces vascular smooth muscle cell proliferation by promoting an arrest in the G1 phase of the cell cycle, whilst also inhibiting smooth muscle cell (SMC) migration (Pinney *et al.*, 2003; Yao *et al.*, 2007; Shahzad *et al.*, 2011; Higashi *et al.*, 2019, 2019).

Additionally, minocycline treatment can interfere with AMP-activated protein kinase (AMPK) and PI3K-AKT-mammalian target of rapamycin (mTOR) pathways, leading to autophagy, cell dysfunction and cell death in gastric cancer cells, multiple myeloma, and glioma (Zhu, Davis and Kung, 2009; Tang *et al.*, 2014; Lu *et al.*, 2017; Wang *et al.*, 2017; Ma *et al.*, 2018; Hu and Guo, 2019).

Minocycline's ability to suppress cell growth is mediated by autophagic cell death, and endoplasmic reticulum stress-induced apoptosis as shown in glioblastoma (GBM) cells (Liu *et al.*, 2013), with additional reports also concluding an ability of minocycline to inhibit tumour growth in C6 glioma cell xenograft tumour models (Liu *et al.*, 2011). As such, minocycline has become a candidate for adjuvant therapy against malignant GBM since it reduces GBM growth both *in vitro* and in experimental mouse models (Markovic *et al.*, 2011). Minocycline was also able to activate cell autophagy through the beclin-1 signalling pathway and thus increases the antitumor activity of cisplatin in Hep-2 cells (Du *et al.*, 2011). These reports highlight further mechanisms by which minocycline has effectiveness against tumor adaptation and progression (Kondo *et al.*, 2005; Kondo and Kondo, 2006; Mulcahy Levy, Towers and Thorburn, 2017).

In leukemia cells, minocycline exerts cytotoxic effects and causes initiation of apoptosis through DNA damage, lysosomal degradation, and B-cell lymphoma-extra-large **(**Bcl-xL) deamidation (Song *et al.*, 2014; Fares *et al.*, 2015). In research using acute lymphoblastic leukemia Jurkat cells, minocycline induced apoptosis through the H2O2-mediated signalling pathway, and due to the harmless effects noted of minocycline to healthy human peripheral blood lymphocyte cells, it has been suggested that minocycline may have additional unexplored effects against leukemia (Ruiz-Moreno, Velez-Pardo and Jimenez-Del-Rio, 2018). Minocycline has also shown to be beneficial for treating vascular complications of diabetic syndrome, such as diabetic nephropathy, reducing apoptosis, renal arterial collagen and tubulointerstitial fibrosis, as well as diabetic retinopathy (Krady *et al.*, 2005; Bhatt and Addepalli, 2011; Xia *et al.*, 2011).

Due to minocycline's ability to cross the blood-brain barrier, its anti-apoptotic effect is well described in the context of neurodegenerative medicine (Chen *et al.*, 2000; Zhu *et al.*, 2002; Wang *et al.*, 2003; Pi *et al.*, 2004; Scarabelli *et al.*, 2004; Teng *et al.*, 2004, 2004; Heo *et al.*, 2006; Cui *et al.*, 2008; Antonenko *et al.*, 2010; Dumont *et al.*, 2010). The numerous mechanisms involved in the cyto-protection of minocycline are reviewed in depth by Garrido-Mesa et al. in 2013 (Garrido-Mesa, Zarzuelo and Gálvez, 2013), and include inhibition of both caspase-dependent and caspase-independent cell death.

1.2.4. Angiogenesis

The growth and metastasis of cancer are dependent on angiogenesis and lymphangiogenesis stimulated by chemical signals from tumour cells (Quintero-Fabián *et al.*, 2019). Minocycline has been shown to selectively inhibit endothelial cell growth, which constitutes a potential mechanism for its anti-angiogenic activity (Guerin *et al.*, 1992). Minocycline has the capability to inhibit angiogenesis *in vitro*, and suppress endothelial cell neovasculogenic activity by reducing Vascular endothelial growth factor (VEGF) secretion from cancer cells (Neuvonen, 1976; Gilbertson-Beadling *et al.*, 1995; Li *et al.*, 2014). Moreover, minocycline exhibits anti-angiogenic properties through suppression of hypoxia-inducible factor 1 alpha (HIF-1α) expression, which correlated with the modulation of p53 and the Akt/mTOR/p70S6K/4E-BP1 pathway in ovarian cancer, both *in vitro* and *in vivo* (Jung *et al.*, 2014; Ataie-Kachoie *et al.*, 2015).

1.2.5. Mediator release

Oral minocycline has been proven to be effective in suppressing malignant ascites in ovarian cancer cells through targeting cytokines and growth factors necessary for the development and formation of tumours (Pourgholami *et al.*, 2013). Minocycline suppressed interleukin (IL)-6, and inhibited the invasion, migration, and adhesion capacity of ovarian cancer cells, both *in vitro* and *in vivo* (Ataie-Kachoie, Morris and Pourgholami, 2013). In relation to asthma, a study in 2002 found that minocycline and doxycycline inhibited immunoglobulin E (IgE) production mediated by PBMCs from asthmatic patients *in vitro* (Smith-Norowitz *et al.*, 2002), with later studies also indicating an ability of minocycline and doxycycline to reduce peak IgE levels *in vivo* and inhibit memory IgE responses *in vitro*, mediated by targeting T cell pathways via MAPK p38 (Joks *et al.*, 2010; Joks and Durkin, 2011). Similarly, in Japanese encephalitis virus (JEV)-infected mice, minocycline treatment led to reduced levels of IL-12 and monocyte chemoattractant protein 1 (MCP-)1, and subsequent brain immune activation (Dutta *et al.*, 2010).

1.2.6. Microbiota modulation

One of the most common uses of minocycline is the treatment of acne vulgaris, where inflammation profoundly contributes to the pathophysiology of the disease, and where the combination of antibacterial and anti-inflammatory properties of minocycline is advantageous (Webster, McGinley and Leyden, 1981; Kurokawa

et al., 2009; Kircik, 2010; Maffeis and Veraldi, 2010; Ochsendorf, 2010). In particular, due to its great lipophilicity, minocycline is highly active in the pilosebaceous complex, inhibiting both the growth of *Propionibacterium acnes* and bacterial lipases, while targeting the associated inflammation (Webster, McGinley and Leyden, 1981; Maffeis and Veraldi, 2010). This added benefit also applies to other chronic inflammatory skin diseases, such as rosacea, which involves an abnormal host response including pathological collagenolysis, with phase 3 clinical studies in moderate to severe papulopustular rosacea highlighting the anti-inflammatory action of topically applied minocycline, resulting in a significant reduction of inflammatory lesions (Gold *et al.*, 2020). Both the safety and efficacy of other tetracyclines in both dermatological diseases have also been demonstrated in several clinical trials (Lane and Williamson, 1969; Golub *et al.*, 1991, 1998; Skidmore *et al.*, 2003; Monk, Shalita and Siegel, 2011; Del Rosso, 2016).

Through modulation of the microbiota and intestinal homeostasis as is discussed in more detail later, minocycline has also been shown to exert beneficial effect on pathological conditions that impact other organs, such as the cardiovascular system, with its anti-hypertensive effects associated with rebalanced gut microbiota composition (T. Yang *et al.*, 2015). An ongoing Phase 2 clinical trial investigating the effect of minocycline treatment on drug-resistant hypertensive patients aims to support this potential application (University of Florida, 2020).

1.2.7. Immune cell modulation

1.2.7.1. Monocytes & macrophages

Crucially for this project, many studies have disseminated the ability of tetracyclines to inhibit LPS-induced activation of macrophages, reducing inducible nitric oxide synthase (iNOS) activity and intracellular protein content, the production of cyclooxygenase 2 (COX-2) and MMPs, and the release of proinflammatory mediators such as interferon gamma (IFN-γ), TNF-α, IL-6 and IL-12 (D'Agostino *et al.*, 1998; Patel *et al.*, 1999). However, an enhancement of pro-inflammatory cytokine secretion including IL-1β, TNF-α and IL-6 by monocytes and macrophages is also consistently reported (Ingham, Turnbull and Kearney, 1991; Kloppenburg *et al.*, 1996; Garrido-Mesa, Rodríguez-Nogales, *et al.*, 2018a). A proteomic analysis of J774 macrophages demonstrated some significant changes in the proteome following minocycline treatment, influencing

heat shock proteins 60 and 71 reversing the downregulation and upregulation by LPS respectively, and protecting vimentin (intermediate filament protein) cleavage by LPS. The study in its entirety suggested that minocycline does not completely inhibit LPS activation, but also modulates macrophage function in the absence of LPS stimulation (Dunston *et al.*, 2011). Clear divergent results have also been obtained between peritoneal and alveolar macrophages, whereby in a model of pancreatitis-induced systemic inflammation minocycline reduced IL-1β, mannose receptor, and IL-10 expression, in addition to NF-kB activation on peritoneal macrophages, but conversely increased their expression on alveolar macrophages, promoting lung inflammation (Bonjoch *et al.*, 2015). This suggests the effect of minocycline in different macrophage subsets seems to be context dependent. Furthermore, minocycline treatment of whole-blood cultures or isolated peripheral blood mononuclear cells (PBMCs) stimulated with LPS, revealed a dose-dependent increase in TNF-α and IL-6 production, whilst dose-dependently inhibiting TNF-α and IFN-γ production induced by phytohemagglutinin (PHA) stimulation (Kloppenburg *et al.*, 1996). Due to the different leukocytes within PBMCs, this might represent disparate effects on various populations under different stimulus.

To understand the role of minocycline on macrophage activation in the context of peripheral nerve adhesion, a recent study conducted in 2021 explored the effect of lone LPS stimulation or dual treatment with minocycline on the murine macrophage cell line RAW264.7. Results showed that LPS induced abundant iNOS expression, but minocycline administration blocked this LPS-induced iNOS expression while promoting the expression of arginase-1 in a dose-dependent manner. LPS administration also increased TAK1 phosphorylation, while the addition of minocycline inhibited this process. Furthermore, the effect of minocycline on the phosphorylation of p38, JNK, ERK1/2 and p65 (well-known downstream molecules of TAK1 in the MAPK and NF-κB pathways) was also assessed. Here the authors report minocycline reversed the effect of LPS, significantly suppressing the enhanced p-p38, p-JNK, p-ERK1/2 and p-c-Jun levels. They also showed that LPS enhanced p65 phosphorylation and nuclear translocation, but minocycline treatment suppressed NF-κB signal transduction via p65 phosphorylation and nuclear translocation inhibition (Li *et al.*, 2021). Liu and Yang (2012) have also reported that 2% minocycline hydrochloride

nanoliposomes, 2% minocycline hydrochloride solution, and periocline all showed inhibition of macrophage proliferation, with all three preparations demonstrating dose- and time-dependent inhibition of proliferation of ANA-1 murine macrophages (Liu and Yang, 2012).

In the context of macrophage polarization further studies also showed that induction of an M2 microglia/macrophage phenotype by minocycline was effective in promoting blood-brain barrier remodelling and axonal regeneration, thus improving neurological functions in the context of ischemic stroke (Tao *et al.*, 2013; Y. Yang *et al.*, 2015). Additional evidence similarly indicates that macrophage phenotype switching from M1 to M2 will become a promising therapeutic strategy to protect the integrity of the blood-brain barrier after stroke, as evident in the ongoing clinical trial evaluating the safety and feasibility of autologous M2 macrophage transplantation in treatment of chronic stroke patients (NCT01845350). Despite the above observations, few studies have focused on the effect of minocycline on the TLR4-NF-κB pathway in macrophages. One paper, by Tai *et al* (2013), examined the effect of minocycline on cytokine and chemokine production in THP-1 monocytes when challenged with LPS. These authors observed that minocycline supressed TNF-α, IL-6, IFN-γ, C-X-C motif chemokine ligand 10 (CXCL10 - also known as interferon gamma-induced protein 10 (IP-10)), and MCP-1 production in a dose-dependent manner by inhibiting IκBα and IκB. They also concluded that in THP-1 monocytes minocycline did not affect the phosphorylation of ERK1/2, JNK, p38 or TAK1 (Tai *et al.*, 2013).

1.2.7.2. Dendritic cells

In reference to other leukocytes, minocycline conditioned dendritic cells (DCs) have also been shown to be resistant to subsequent maturation stimuli, with impaired major histocompatibility complex (MHC) class II, restricted exogenous antigen presentation, and decreased cytokine secretion. Minocycline treated DCs showed decreased ability to prime allogeneic-specific T cells, while increasing the expansion of cluster of differentiation (CD)$4^+$$CD25^+$Forkhead box P3 $(FoxP3)^+$ T regulatory cells, a potential that was confirmed *in vivo*, and thus preventing clinical signs of experimental autoimmune encephalitis (Svajger, Obermajer and Jeras, 2010; Kim *et al.*, 2016). In a subsequent *in vivo* study, the potential of minocycline in the generation of tolerogenic DCs was also observed,

as researchers found a synergic combination of minocycline and dexamethasone generated the highest numbers of tolerogenic DCs, which had the highest capacity to induce FoxP3$^+$ T cells, while exerting the highest programmed death ligand 1 (PD-L1)/CD86 ratio, one of the hallmarks regarding tolerogenic DC potency (Lee *et al.*, 2017; Thomson and Ezzelarab, 2018).

1.2.7.3. T Cells

The suppressive effects of tetracyclines on T-cell proliferation, activation and function have been long described (Thong and Ferrante, 1980; Kloppenburg, Verweij, A. M. Miltenburg, *et al.*, 1995; Kloppenburg *et al.*, 1996; Popovic *et al.*, 2002; Giuliani, Hader and Yong, 2005a). The influence of tetracyclines on T cell activation has been associated with an inhibitory effect on cytokine production, such as a decrease in IL–2, IFN-γ and TNF-α secretion, which could in turn reduce T cell proliferation and activation (Kloppenburg, Verweij, A. M. Miltenburg, *et al.*, 1995; Kloppenburg *et al.*, 1996). However, although no effect was observed for minocycline on T cell proliferation and IFN-γ production in rodents, more recent studies have suggested that minocycline acts to reduce T cell turnover after activation, with decreased levels of proliferating (Ki67$^+$) and activated human leukocyte antigen DR isotype (HLA-DR$^+$) cells, and increased levels of circulating naïve (CD45RA$^+$) cells in the context of autoimmune encephalitis (Popovic *et al.*, 2002; Szeto *et al.*, 2010). Reduced expression of surface markers CD25, CD40L, and HLA-DR, as well as IL-2 production, also seen in these studies, may be responsible for mediating this effect (Giuliani, Hader and Yong, 2005a; Szeto *et al.*, 2010, 2011a). An additional proposed mechanism responsible for T cell modulation is suppression of transcription activation of nuclear factor of activated T cells 1 (NFAT1), whereby minocycline has been shown to reduce its nuclear translocation following activation (Szeto *et al.*, 2011a). Minocycline has shown the ability to decrease HIV viral expression in resting CD4$^+$ T cells by reducing IL-1, IL-6 and TNF-α cytokine secretion, the expression of chemokine receptor 5 (CCR5), as well as Ki67 expression and cellular proliferation, which may be related to inhibition of NFAT1 (Szeto *et al.*, 2010, 2011a). Another report also indicated that minocycline attenuates T helper cell (Th)1 activation and the expression of IFN-stimulated genes indoleamine 2,3-dioxygenase 1 (IDO1) and tumour necrosis factor-related apoptosis-inducing ligand (TRAIL) in plasmacytoid dendritic cells and PBMCs exposed to both HIV

and influenza virus both *in vivo* and *in vitro* (Drewes *et al.*, 2014).

The role of minocycline in HIV-induced chronic immune activation has also been evaluated *in vivo* in NOD scid gamma (NSG) mice transplanted with human hematopoietic cells, which revealed a reduction in viral load and improved T-cell count with reduced expression of activation markers CD38, HLA-DR, CD69 and CCR5, and exhaustion markers programmed cell death 1 (PD-1) and cytotoxic T-lymphocyte-associated protein 4 (CTLA-4) (Singh *et al.*, 2014). Monocytes are also important HIV targets, and *in vivo* reports indicate that treatment with minocycline reduced monocyte activation, expansion and accumulation in lymph nodes upon viral infection, which correlated with neuronal protection in HIV and simian immune deficiency virus (SIV) infected mice (Campbell *et al.*, 2011).

1.2.7.4. Microglia

Modulation of microglial activation and neuroinflammation are additional non-antibiotic properties of minocycline, with reports describing how minocycline selectively inhibits M1 polarization of microglia, as shown by reduced ionized calcium-binding adapter molecule (Iba)-1 expression (Kobayashi *et al.*, 2013; H.-Y. Liu *et al.*, 2018). This leads to amelioration of transcription, nuclear translocation, and consequent activation of downstream pro-inflammatory mediators including caspase-1, glial fibrillary acidic protein (GFAP), TNF-α, iNOS, COX2 and arachidonate 5-lipoxygenase (5-LOX, ALOX5 or 5-LO) which in turn decreased IL-1β, NO, and prostaglandin E2 (PGE_2) production (Yrjänheikki *et al.*, 1999; Song *et al.*, 2004, 2006a, 2006b; Chu *et al.*, 2007; Cai, Yan and Chen, 2010). In the context of ischemia, the literature also reports that minocycline impairs T cell-microglia interaction through targeting the CD40-CD40L pathway and diminishing the ability of T cells to interact with microglia, thus resulting in decreased TNF-α and increased IL-10 production in T cell–microglia co-cultures (Giuliani, Hader and Yong, 2005a). Moreover, minocycline has shown to be beneficial in other conditions which result in ocular inflammation through modulation of microglia, such as in a light-induced retinal degeneration model, glaucoma, and a model of branch retinal vein occlusion ischemia (Zhang *et al.*, 2004; Levkovitch-Verbin *et al.*, 2006; Bosco *et al.*, 2008; Sun *et al.*, 2013; Yuan *et al.*, 2019).

Amounting data also demonstrates that minocycline is able to suppress microglial production of IL-1β, IL-6, TNF-α, nicotinamide adenine dinucleotide phosphate **(**NADPH) oxidase, and iNOS, as well as inhibit T cell egress into the brain, all of which attenuate neuropathological progression (Wu *et al.*, 2002; Zhu *et al.*, 2002; Seabrook *et al.*, 2006; Henry *et al.*, 2008). Furthermore, minocycline protection in experimental models of Alzheimer's Disease (AD) has been linked to a reduction in COX-2 and PGE_2 production, and inhibition of gliosis induced by Aβ peptide treatment in nerve growth factor (NGF)-differentiated PC-12 cells (rat pheochromocytoma cells which exhibit features of mature dopaminergic neurons) in Tg2576 mice (over express a mutant form of Aβ) (Sahoo *et al.*, 2018). Through inhibition of microglial activation and simultaneous effect on Aβ deposition, minocycline achieved a neuroprotective effect that resulted in improved cognitive impairment (Seabrook *et al.*, 2006; Sriram, Miller and O'Callaghan, 2006; Choi *et al.*, 2007).

In the context of widely recognised clinical co-morbidities chronic pain and depression, in a 2014 study Burke and colleagues investigated the association between depressive-like behaviour and mechanical allodynia. They were able to show that chronic minocycline intake reduced the expression of CD11b, a marker of microglial activation, and the M1 cytokine IL-1β in sham-SNL (L5-L6 spinal nerve ligation) rats – a model of peripheral nerve injury and neuropathic pain which also reduced neuropathic pain behaviour. On the other hand, they also demonstrated an increase in the expression of the M1 cytokines IL-1β and IL-6, the M2 microglial marker mannose receptor C-type 2 (MRC2), and the anti-inflammatory cytokine IL-10 in olfactory bulbectomized (OB)-SNL rats – a model of depression, following chronic minocycline intake (Burke *et al.*, 2014).

1.2.7.5. Neutrophils

Tetracyclines as early as the 1970s were shown to inhibit leukocyte chemotaxis using Sykes-Moore chambers and the double-filter technique. Esterly *et al* in 1978 demonstrated this suppression of chemotaxis by tetracycline in addition to a reduction in random migration (Esterly, Furey and Flanagan, 1978). Later, in 1984, Esterly and colleagues again demonstrated significant suppression of chemotaxis and random migration of autologous polymorphonuclear leukocytes from both healthy donors and those with acne receiving oral tetracycline treatment (Esterly *et al.*, 1984). More recent to those initial reports, Wasserman

and Schlichter (2007) studied the effect of minocycline in the context of intracerebral haemorrhage (ICH) whereby using dual-antibody labelling showed that neutrophils were the predominant source of TNF-α, and that intraperitoneal injection of minocycline ameliorated ICH damage. Minocycline reduced micro-vessel loss, extravasation of plasma proteins and oedema, decreased TNF-α and MMP12 expression, and reduced the number of neutrophils in the brain (Wasserman and Schlichter, 2007). In subsequent years, Walz and Cayabyab (2017) then used the modified pial vessel disruption rat model to elucidate the cellular and molecular mechanisms of cavitation in lacunar infarction. Both in the lung and cerebral cortex the migration of neutrophils across the endothelial barrier into the parenchyma plays a vital role and involves the release of MMP9. In these models, minocycline reduced MMP9 release by neutrophils and prevented cavitation (Walz and Cayabyab, 2017).

1.3. Innate immunity & the macrophage

1.3.1. Intestinal immune environment in IBD

Inflammatory bowel disease (IBD) is an umbrella term for chronic inflammatory conditions of the gut encompassing two main entities: Crohn's disease and ulcerative colitis. Both Crohn's disease and ulcerative colitis are characterized by alternating phases of clinical relapse and remission, accompanied by symptoms such as moderate to severe abdominal pain, weight loss and prolonged diarrhea (Lennard-Jones, 1989; Rogler, 2015). IBD is widely considered a multifactorial disease with its exact etiology remaining somewhat elusive, however dysregulation of normal immune responses from both the innate and adaptive systems within the intestinal mucosa are recognized as vital components in the initiation and progression of IBD pathogenesis (Park *et al.*, 2017).

Throughout the body, and especially in the gastrointestinal tract, inflammation is a tightly coordinated process characterized by sequential stages starting from acute inflammation followed terminally by inflammatory resolution which results in tissue repair and the restoration of tissue integrity and anatomical function. During this acute phase of inflammation, the terminal differentiation of monocytes to mature macrophages is disrupted and differentiation preferences a pro-inflammatory phenotype which act to promote downstream type 1 T helper (Th1) and Th17 immune responses (Elliott *et al.*, 2009; Gordon and Plüddemann, 2018; Na *et al.*, 2019a). Upon tissue damage to the epithelial lining of the gut wall, the

innate immune system detects DAMPs and PAMPs and begins to attract circulating neutrophils, which in turn infiltrate the area and recruit inflammatory monocytes from the bloodstream (Mantovani, Bonecchi and Locati, 2006).

In the context of the intestinal mucosa, the innate immune system is aptly designed to coordinate efforts between the epithelial barrier and circulating or tissue-resident specialized leukocytes, such as macrophages, DCs and innate lymphoid cells (ILCs), to mediate the homeostasis between pathogenic stimulus and intestinal immune responses. Innate immune cells accomplish this function through the secretion of chemical compounds such as cytokines and inflammatory mediators, the process of phagocytosis, different tissue remodeling properties, and the recruitment and activation of the adaptive immune system, all in the mission to eliminate the pathogenic source and reinstate homeostasis (Nowarski *et al.*, 2013).

A peaceful coexistence between host defenses and commensal bacteria is vital for healthy function within the human intestinal tract. Intestinal macrophages in the lamina propria dynamically engage with the microbiota to assure tolerance, and prevent infection by exogenous pathogens, which will stimulate the inflammatory cascades amidst the constantly fluctuating landscape (Smythies *et al.*, 2005). Coordinated efforts between the epithelial barrier and circulating or tissue-resident specialized leukocytes mediate the homeostasis between pathogenic stimulus and intestinal immune responses. These subsets of cells act in symbiosis to assess the intestinal microenvironment and mount appropriate inflammatory responses, as well as provide crucial cross-talk between the innate and adaptive systems (Geremia *et al.*, 2014). Specialization to recognize the molecular patterns of microorganisms via pattern recognition receptors (PRR), which include TLRs, and nucleotide-binding oligomerization domains (NOD), allow this efficient function to occur (Borzutzky *et al.*, 2010). Intimate cross-talk between the host and microbiome through commensal recognition via TLRs and antimicrobial peptide secretion is essential for the maintenance of symbiosis (Zigmond and Jung, 2013).

Multifaceted characteristics of the innate immunity within the gut such as impermeable epithelium, bactericidal secretion (anti-microbial peptides - AMPs) and the phagocytic function of macrophages, efficiently protect the lamina propria from microbe invasion without adaptive immune response activation (Rogler,

2015). However, in genetically susceptible individuals, defects in these protective mechanisms allow for microbes to gain entry past the epithelial barrier into the lamina propria, instigating a classic inflammatory response. The exact genetics of IBD are complex and thought to be polygenic (Wallace *et al.*, 2014), with genome-wide association studies suggesting dysregulated innate and adaptive immune systems contribute to the development and progression of IBD pathogenesis. Many susceptibility variants have been reported in genes associated with autophagy (*ATG16L1*), the IL-23/Th17 pathway (*IL-12B*), TGF-β pathway (*SMAD3*), and T-cell activation (*TAGAP*), among others (Duerr *et al.*, 2006; Hampe *et al.*, 2007; Franke *et al.*, 2010).

IBD patients experience an exacerbated immune response against microbial antigens and defects in the regulation and resolution of the inflammation, promoting perpetuation of the inflammatory cycle (Kmieć, Cyman and Ślebioda, 2017). In susceptible individuals, defects in the protective mechanisms allow for microbes to gain entry past the epithelial barrier into the lamina propria, instigating a classic inflammatory response. Modifications in autophagy (the process of self-removal of damaged cells) and antigen processing, in addition to the regulation of cellular signaling often results in a decline in pathogen clearance ultimately sponsoring the onset of an unchecked inflammatory cascade (de Mattos *et al.*, 2015).

The gastrointestinal (GI) tract is home to the largest quantity of macrophages in the body, providing crucial support in pathogen clearance, in addition to the regulation of other inflammatory responses, consequently influencing local homeostasis. This very nature means macrophages can also contribute to the development and maintenance of chronic inflammation following intestinal barrier dysfunction (C. Li *et al.*, 2018). Previous reports by Smith *et al* (2009) and Campos *et al* (2011) have surmised the role of defective macrophage function in relation to the establishment of IBD through evidence linking innate immunity gene polymorphisms, decreased pro-inflammatory cytokine production in Crohn's disease patient macrophages, and risk of developing Crohn's disease.

1.3.2. Macrophage origin & development

Originally described in 1905 by Nobel Prize winner Elie Metchnikoff, macrophages were depicted through the identification of phagocytes and his phagocytosis theory (Hao et al., 2012). In the proceeding decades, the origin and

function of macrophages has become well established. Tissue macrophages are traditionally viewed as part of the mononuclear phagocyte system (MPS), with this concept first described in 1972 by van Furth *et al*, who proposed all tissue macrophages are the terminally differentiated progeny of blood monocytes, which constitutively enter tissues under steady state conditions, and are replaced by rapidly dividing precursors from the bone marrow (BM) (van Furth *et al.*, 1972). A common macrophage and DC progenitor gives rise to both committed DC precursors and monocytes, with the development of the latter dependant on the transcription factor PU.1 and growth factors macrophage colony stimulating factor (M-CSF), granulocyte macrophage colony stimulating factor (GM-CSF), and IL-3 (Auffray *et al.*, 2007; Hettinger *et al.*, 2013; Calum C Bain and Mowat, 2014).

Their evolution begins with the differentiation of common myeloid progenitor cells in the BM. Following stimulus with M-CSF, the progenitors sequentially become macrophage colony-forming units (M-CFUs), monoblasts and pro-monocytes, which then move into the peripheral blood and differentiate into monocytes (Figure 1.2). Hematopoietic stem cells (HSCs) give continuous rise to the myeloid progenitors and consequent ephemeral lymphocyte antigen 6 complex $(Ly6C)^+$ monocytes in the blood which are then recruited into a plethora of tissues to replenish tissue-specific macrophage populations such as colonic and alveolar, in response to inflammatory stimuli. $Ly6C^+$ monocytes and their macrophage descendants are highly plastic and influence the promotion and resolution of inflammation (Gordon and Taylor, 2005; Zigmond and Jung, 2013). It is important to note however, that not all macrophages differentiate from monocytes, as it has been reported that radiation resistant Langerhans and microglial cells are seemingly maintained via local proliferation, with the most recent literature specifying initial development within the yolk sac of the developing embryo (Lawrence and Natoli, 2011). The literature also describes how major tissue-resident macrophage populations such as those mentioned above are maintained via longevity and limited self-renewal independent of further monocyte contribution, contrasting to those residing in the gut and other tissues (Zigmond and Jung, 2013).

In the context of the gastrointestinal tract, following entry into the mucosa, $Ly6C^{hi}$ monocytes undergo a process of local differentiation resulting in the generation

of mature macrophages, via a series of short-lived chemokine (C-X3-C motif) receptor 1 (CX3CR1)^{int} intermediaries, which both acquire MHCII, and lose Ly6C expression. Within days the cells then acquire the F4/80^{hi}CD64^{+}MHCII^{+}CD11c^{+}CX3CR1^{hi} phenotype typical of resident intestinal macrophages. This phenotypic differentiation of monocytes is also accompanied by acquisition of typical functions of resident intestinal macrophages, such as increased IL-10 production, enhanced phagocytic activity, acquisition of scavenger receptors and development of hypo-responsiveness to TLR ligation (Bain *et al.*, 2013). The latter, Ly6C^{low} patrolling monocytes, can be independently regarded as the terminally differentiated resident phagocyte population from the blood stream (Ginhoux and Jung, 2014), and develop from Ly6C^{hi} classical monocytes through nuclear receptor subfamily 4 group A member 1 (NR4A1)-dependent (Hanna *et al.*, 2011; Carlin *et al.*, 2013); krüppel-like factor 2 (KLF2)-dependent (Thomas *et al.*, 2016), and CCAAT/enhancer binding protein β (C/EBPb)-dependent pathways, with this continuum between Ly6C^{hi} and Ly6C^{low} monocytes recently mapped via single-cell RNA-sequencing (Mildner *et al.*, 2017). These processes appear to be unique to the intestine, with reports establishing that lung-associated Ly6C^{hi} monocytes do not undergo the same phenotypic changes (Jakubzick *et al.*, 2013).

Steady-state intestinal macrophages customarily produce low levels of TNF upon TLR ligation, however macrophages recruited during dextran sodium sulphate (DSS)-induced colitis maintain their TNF production capacity (Bain *et al.*, 2013). This may be attributable to the plasticity of macrophages, and their adaptation to an inflammatory environment. As such, it has been considered that monocytes recruited during colitis may consist of a particular subset of monocytes that has an increased capacity to produce TNF (Bonnardel and Guilliams, 2018). During intestinal inflammation, as associated with Crohn's disease and ulcerative colitis, CD14^{hi} monocyte-derived cells have also been shown to accumulate within the intestinal lamina propria (Kamada *et al.*, 2008; Thiesen *et al.*, 2014), which conversely to the Ly6C^{hi} precursors, display enhanced production of inflammatory mediators TNF-α, IL-1β and IL-6 (Rugtveit *et al.*, 1997). This population of CD14^{hi} monocyte/macrophages has also been shown to produce chemokines that attract other effector leukocytes, such as eosinophils, through production of C-C motif chemokine ligand (CCL)11 (Lampinen *et al.*, 2013). Where tissue resident macrophages traditionally express low levels of CD14, this

smaller population of CD14^{hi} macrophages is also present in the healthy mucosa, and express MHCII, CD163, CD209, and CD11c, eluding to an origin of recent CD14^{hi} monocyte emigrants (Bain *et al.*, 2013).

In a non-pathogenic state, human macrophages display an anergic signature through failure to produce pro-inflammatory cytokines, but retaining their phagocytic and bactericidal activity, all of which are compatible with their reported scavenger function (Smythies *et al.*, 2005). However, in patients with Crohn's disease, CD14^{+} macrophages display both macrophage (CD14, CD33, CD68) and DC (CD205, CD209) markers, whilst also producing increased levels of IL-6, IL-23 and TNF, and contribute to IFN-γ production by neighbouring mononuclear cells (Kamada *et al.*, 2008; de Souza and Fiocchi, 2016).

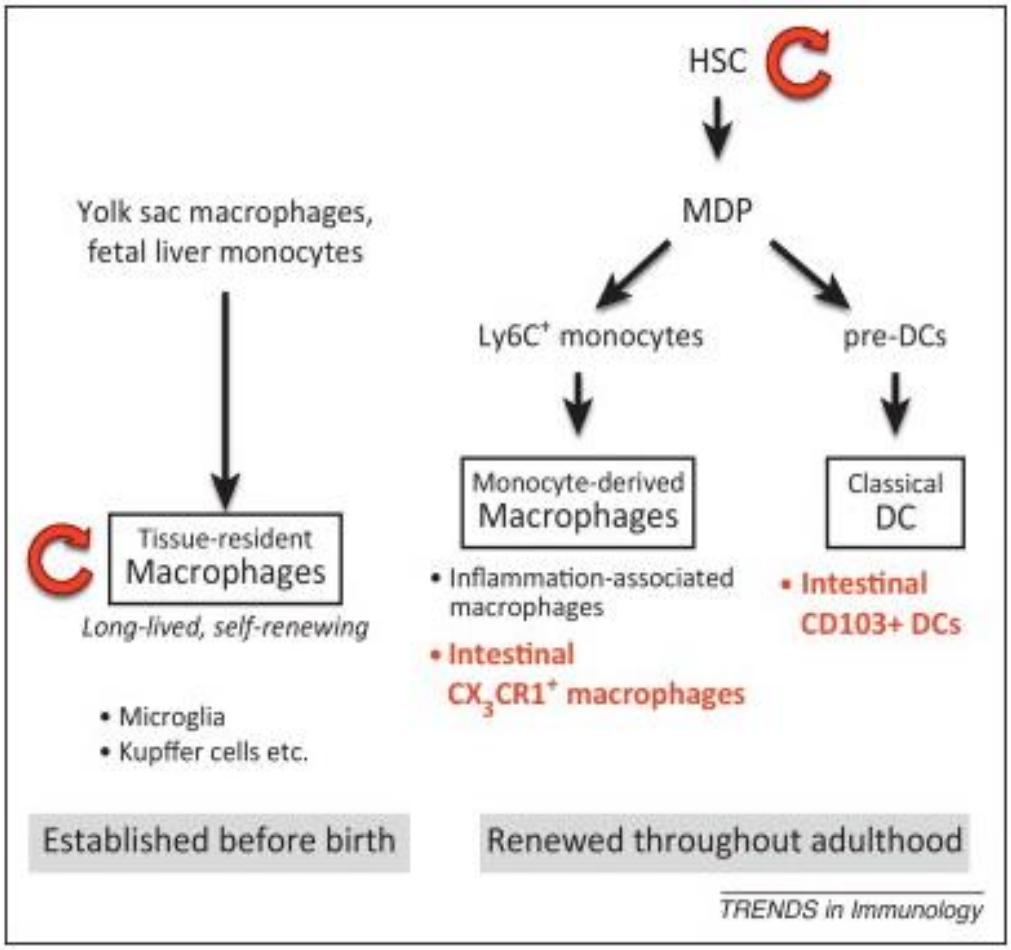

Figure 1.2: The origin of tissue resident macrophages. Macrophages established before birth are referred to as 'primitive macrophages' or 'fetal liver cells' and include microglia and Kupffer cells. These populations are maintained via longevity and limited self-renewal. Those resident within the gut express the C-X-C motif chemokine receptor and derive from Ly6C^{+} circulating blood monocytes. These populations are continuously renewed throughout adulthood from hematopoietic stem cells (HSCs) and macrophage/dendritic cell precursors (MDPs) (Zigmond and Jung, 2013).

1.3.3. LPS-induced macrophage activation

Leukocyte infiltration into sites of infection is a fundamental host defence against infection, whereby infiltrating leukocytes inactivate and clear the pathogens, rendering inflammation a primarily beneficial host response to noxious stimuli (Fearon and Locksley, 1996). However, inflammation, if excessive and prolonged can cause extensive tissue damage, contributing to the pathogenesis of many disease states (Bellingan, 2000). Therefore, as highlighted earlier, the inflammatory response must be under strict control via endogenous mechanisms (Matsukawa *et al.*, 2005). The responsiveness of cells to external stimuli such as infectious pathogens rely on the transcriptional regulation of gene expression programmes, with a network of signalling pathways working to bridge the gap between stimulation and transcription. Initiation of these pathways results in the activation of transcription factors and their subsequent translocation into the nucleus and initiation of gene transcriptional programmes (Dorrington and Fraser, 2019).

Sensing of microbial antigens by innate immune cells, such as macrophages and DCs, is mediated by PRRs that recognize pathogen associated molecular patterns (PAMPs). The more well understood family of PRRs include trans-membrane TLRs as well as intracytoplasmic NOD-like receptors (NLRs) (Geremia *et al.*, 2014; Satoh and Akira, 2016). PRR signalling cascades result in NF-κB activation, with gene transcription and production of pro-inflammatory mediators ensuring an effective innate response against pathogens (Sica and Mantovani, 2012; Chen *et al.*, 2020). The NF-κB signalling cascade regulates thousands of independent response genes encoding for cytokines, chemokines, and antimicrobial peptides, as well as additional downstream transcription factors. This pathway is vital for many crucial immunological programs including initiating inflammatory responses to pathogens by innate immune cells and the development and activation of cells responsible for adaptive immune responses (Dorrington and Fraser, 2019). PRR triggering also promotes antigen presenting cell maturation, observed by up-regulation of co-stimulatory molecules that are required for efficient antigen presentation and T cell activation, playing a crucial role in the crosstalk between innate and adaptive immune responses (Geremia *et al.*, 2014). Upon bacterial infection, macrophages utilize their PRRs to identify PAMPs and endogenous danger signals - danger-associated molecular patterns

(DAMPs). This pathogen recognition by PRRs, such as TLR4, activates macrophages to produce pro-inflammatory cytokines such as TNF-α, IL-1β, IL-6, IL-12, and NO that kill invading pathogens (Atri, Guerfali and Laouini, 2018).

TLR engagement, particularly TLR4, is stimulated by LPS- a component of Gram-negative bacteria, in addition to other microbial ligands (Figure 1.3). TLR4 ligation by LPS, is preceded by binding of LPS to the CD14 protein anchored in cholesterol (Płóciennikowska *et al.*, 2015). The innate immune system is poorly activated by LPS alone and thus requires LPS binding protein ready for transfer on CD14. In turn, LPS is chaperoned by CD14 to the LPS receptor complex comprised of TLR4 and myeloid differentiation factor 2 (MD2), which dimerizes and triggers the myeloid differentiation factor 88 (MyD88)- and adaptor toll–IL-1 receptor domain-containing adaptor inducing IFN-β (TRIF)-dependent production of pro-inflammatory cytokines and type I interferons (Bode, Ehlting and Häussinger, 2012; Płóciennikowska *et al.*, 2015). TLR4 signalling includes both MyD88-dependent and MyD88-independent pathways. In the former, TLR4 recruits toll/interleukin-1 receptor (TIR) domain-containing adaptor-inducing IFN-β, and TIR domain-containing adaptor molecule 2. Conversely, activation of the MyD88-indpendent pathway leads to the activation and translocation of IFN regulatory factor 3 (IRF3) in the nucleus, and the secretion of type I IFN (Chen *et al.*, 2017). In the MyD88-dependent pathway, TLR4 recruits MyD88, MyD88 adaptor-like, IL-1 receptor-associated kinase, and TNF receptor-associated factor 6, which induces the activation and translocation of NF-κB to the nucleus (Molteni, Gemma and Rossetti, 2016). NF-κB regulates the expression of a large number of inflammatory genes including TNF-α, IL-1β, COX2, and IL-6, but can also trigger a genetic program essential for resolution of inflammation and M2 polarization of tumour associated macrophages (TAMs) (Sica and Mantovani, 2012; Wang, Liang and Zen, 2014a; Chen *et al.*, 2020).

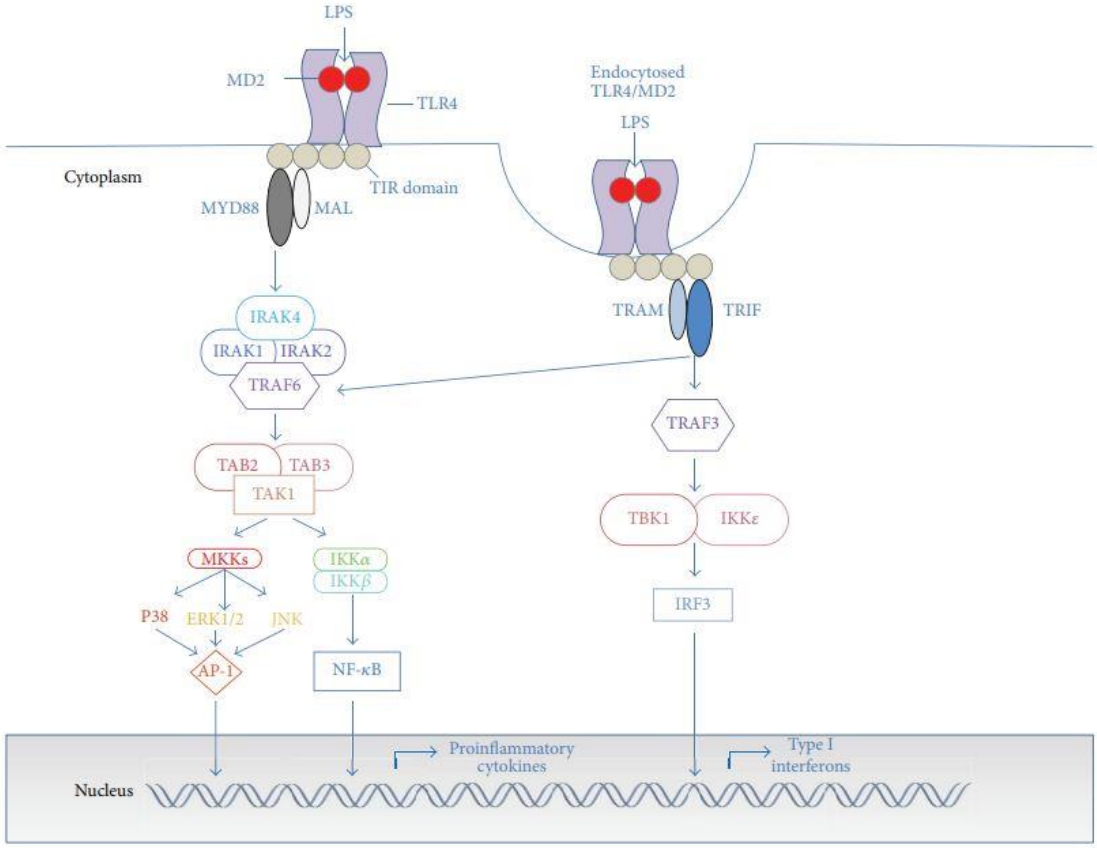

Figure 1.3: TLR4 intracellular signalling pathways. TLR signalling is triggered by ligand-induced dimerization of the receptors. TIR domains of TLR4 recruit adaptor proteins MyD88 and MAL (MyD88-dependent pathway) or TRIF and TRAM (MyD88- independent pathway). The MyD88-dependent pathway involves downstream recruitment and activation of IRAKs and TRAF6, which subsequently activate TAK1. This leads to MAP kinase kinase (MKK)-mediated activation of MAPKs and activation of the IKK complex. This complex induces activation of NF-κB and AP-1 and their translocation into the nucleus. As a result, proinflammatory cytokines are produced. The MyD88-independent pathway involves TRIF and TRAM adaptor proteins and the activation and nuclear translocation IRF3. Subsequently type I interferons are produced (Molteni, Gemma and Rossetti, 2016).

Other receptors for endotoxins like LPS include receptor for advanced glycation end products (RAGE), triggering receptor expressed by myeloid cells 2 (TREM2), and the macrophage scavenger receptors and the β_2 integrins (CD11a/CD18, CD11b/CD18 and CD11c/CD18) (Hampton *et al.*, 1991; Fenton and Golenbock, 1998; Daws *et al.*, 2003; Yamamoto *et al.*, 2011). These PRRs function to clear LPS and bacteria from blood and tissues, but if unregulated may also promote neuroinflammation and LPS toxicity.

In the context of neurodegeneration, CD11b/CD18 or compliment receptor 3 (CR3) mediate microglial ROS production, neurotoxicity and phagocytosis of neurons (Hong *et al.*, 2016; Hou *et al.*, 2017; Brown, 2019). The mechanisms of LPS-induced neurodegeneration are also mediated by the induced peripheral cytokines TNF-α and IL-1β, which induce inflammation within the brain (Skelly *et al.*, 2013). This sustained brain inflammation in response to blood endotoxin requires membrane-bound TLR4 on microglia, endothelium, perivascular macrophages, meninges or circumventricular organs, which implies longer-term effect of blood endotoxin on the brain is not mediated by blood cytokines, but by direct activation of receptors by endotoxin on the above cells to produce cytokines within the brain (Chakravarty and Herkenham, 2005; Kinsner *et al.*, 2006).

This LPS stimulation of MAPK pathways and consequent increase in NF-κB activity has also been implicated in models of sepsis. In 2017, Hung *et al* showed suppression of LPS-induced production of pro-inflammatory cytokines and mediators via downregulation of MAPK pathways and NF-κB activity using *in vitro* murine macrophage models RAW 264.7 cells and murine peritoneal macrophages (Hung *et al.*, 2017). Furthermore, in 2019, Wang and colleagues also demonstrated reduced inflammatory cytokines in the sera and bronchoalveolar lavage fluid (BALF) using a cecal ligation and puncture (CLP)-induced septic mouse model attributed to attenuation of TLR4-NF-κB/p65 activation both in the septic lung tissue and LPS-stimulated lung type II epithelial cell line A549 (Y.-M. Wang *et al.*, 2019).

In regard to IBD, there are many reported links between LPS signalling and disease instigation and progression (Candelli *et al.*, 2021). TLR4, although expressed primarily on macrophages, is also expressed at an endothelial level, where it can activate apoptosis and trigger the expression of other inflammatory cytokines (Bannerman and Goldblum, 2003). In IBD patients TLR4 expression is reported to be elevated, thus LPS activity is significantly amplified in this context (Vaure and Liu, 2014). Crosstalk between LPS and the microbiota is also contributory in the context of IBD, with links between IBD and the development of endotoxemia (Matsuoka and Kanai, 2015). This LPS-induced, chronic, low-grade systemic inflammation results in immune system dysregulation – a key mechanism in the disease pathogenesis. Furthermore, inflammatory activation of intestinal macrophages via LPS causes the cytokine production signatures shift

from anti-inflammatory (IL-10) to pro-inflammatory (IL-1, IL-6, IL-8, and TNF-α), which promotes polarization to an inflammatory M1 phenotype and propagates downstream inflammatory cascades (Wang, Chen and Wang, 2020).

On the other hand, studies have found impaired proinflammatory cytokine secretion and low levels of intracellular TNF in peripheral blood monocytes derived macrophages in Crohn's disease patients in response to *E. coli* and subsequent TLR ligation, which would indicate an impaired acute inflammatory response by macrophages in Crohn's disease that would ultimately lead to defective bacterial clearance (Smith *et al.*, 2009a; de Souza and Fiocchi, 2016). It has also been observed that LPS can cross the gut barrier and enter the bloodstream in conditions of altered permeability, such as IBD, resulting in perpetuation of both immune cell activation and continued alteration of gut permeability, resulting in a vicious circle of self-promoted inflammation (Kiecolt-Glaser *et al.*, 2018; Jaworska *et al.*, 2019). Some reports also suggest LPS may be important in stimulating autophagy in macrophages, which appears to play an important role in preventing IBD by reducing levels of ROS (Larabi, Barnich and Nguyen, 2019; Wang, Chen and Wang, 2020), while LPS is also described to promote the expression of faecal calprotectin as a direct consequence of intestinal inflammation (Førland *et al.*, 2011; D'Amico *et al.*, 2021).

1.3.4. Macrophage polarization

Macrophages are keystones in the immune population due to their phagocytic capacity and ability to adapt and adopt different phenotypes dependent on requirements dictated by their surrounding microenvironment. Recent articles have begun to establish mechanisms by which macrophages are functionally influenced by the gut (Grainger *et al.*, 2017). In the past two decades work towards elucidating the paradigm of macrophage polarization has become ever clearer, with the general consensus being that once tissue resident, macrophage populations become either M1 or M2 phenotypes, but which are also widely accepted to be transient and plastic populations (Camille and Dealtry, 2018). M1 or pro-inflammatory 'classically-activated' macrophages, act to eliminate noxious sources via cytokine and iNOS production, while M2 or anti-inflammatory 'alternatively-activated' cells promote inflammatory resolution (Hotamisligil, 2006; C. Li *et al.*, 2018). Polarization of tissue resident macrophages is determined by local external cues dictating phenotype commitment. M1 are induced by bacterial

antigens as well as IFN-γ and TNF-α, rendering the cells microbicidal and tumoricidal (Figure 1.4). M1 cells release NO and inflammatory cytokines that also promote the differentiation of Th1 and Th17 cells. On the other hand, M2 cells are generated via IL-10, IL-13, IL-4 and IL-1RA, and function to metabolize arginine and polyamines, whilst releasing anti-inflammatory cytokines, such as IL-10, ultimately contributing and driving resolution, tissue remodeling, and building of immune tolerance (Hao *et al.*, 2012; Yang *et al.*, 2013).

Much of the literature depicts this concept of dual purpose; advancing both inflammation and regeneration, however in many pathophysiological states, macrophages do not neatly ascribe to the M1/M2 paradigm. A balance between M1 and M2 phenotypic activity demonstrates a shift over time with M1 behaving as first responders, recruiting effective defense against invasion and angiogenesis, whereas M2 are essential for wound repair and tissue regeneration. The importance of M1/M2 homeostasis is further verified through evidence of delayed wound healing and fibrotic development when M1 or M2 subpopulations become unrestrained respectively. Thus, the M1/M2 nomenclature is a useful tool in describing macrophage population plasticity during inflammatory states, through correlation of observable changes in biomarkers in relation to inflammatory progression and healing (Smith *et al.*, 2017). Moreover, this classification might simply translate as different, but interchangeable functional cellular states depending on the microenvironment, an intriguing notion relevant to IBD pathogenesis (Martinez and Gordon, 2014; de Souza and Fiocchi, 2016). This “functional adaptivity” also enables macrophages to contribute to all phases of repair by promoting inflammation, removing harmful triggers, depositing extracellular matrix, stimulating cell proliferation, and releasing anti-inflammatory cues. However, when activated out of sequence, macrophages have the potential to interrupt all phases of repair, with persistent activation resulting in maladaptive chronic inflammation, and dysfunctional wound healing (Werdin *et al.*, 2009; Nathan and Ding, 2010; Gensel and Zhang, 2015).

Due to their transient nature, there are no clearly defined reliable surface markers for each macrophage population, however, some markers have been used in combinations to assign activation states. The most reliable biomarkers for these cells relate to their functional state of activation, characterized by their cytokines

production profiles. After priming with IFN-γ and LPS, or other TLR ligands, M1 macrophages are noted to overexpress pro-inflammatory cytokines such as IL-12, IL-6, IL-23, IL1-β, TNF and NO. Conversely, M2 macrophages have been identified by the overproduction of IL-10 and decreased production of said pro-inflammatory cytokines (Mosser and Edwards, 2008; Mosser and Gonçalves, 2015; Moreira Lopes, Mosser and Gonçalves, 2020).

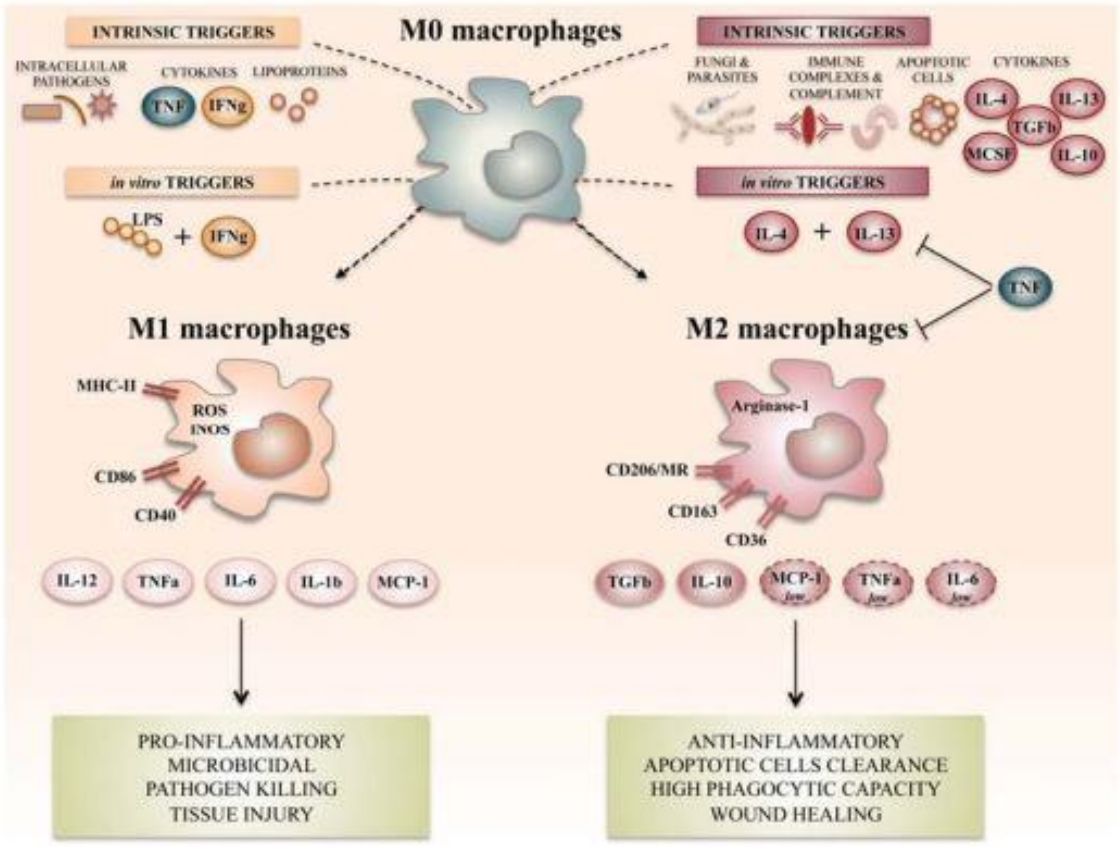

Figure 1.4: Key markers and functions of each macrophage polarization state. Different stimuli and signalling pathways induce M1 or M2 polarization, with pro-inflammatory and anti-inflammatory potentiation associated to the common M1/M2 nomenclature. Stimulation with intracellular pathogens, lipoproteins, or pro-inflammatory cytokines results in polarization of M0 macrophages to an M1 phenotype whereby they upregulate the expression of CD86, CD40, MHC-II, ROS and INOS. M1 macrophages produce high levels of pro-inflammatory mediators such as IL-12, TNF-α, IL-6, IL-1β and MCP-1 in the aim to destroy exogenous pathogens. Conversely, stimulation by fungi, parasites, immune complexes, and anti-inflammatory cytokines results in M2 polarization and upregulation of CD163, CD206, CD36 and arginase 1. M2 produce high levels of anti-inflammatory cytokines such as TGF-β and IL-10 in the goal to clear cellular debris and promote wound healing (Atri, Guerfali and Laouini, 2018).

The usual course of inflammation is traditionally described to begin with an acute phase followed by resolution, proliferation and finally tissue remodelling (Figure 1.5). However, if unresolved and left to enter a state of persistent 'chronic' inflammation, the contribution of host inflammatory mechanisms, not exogenous pathogens, becomes chiefly responsible for resultant host pathophysiology (Nathan and Ding, 2010). Conceptually, these macrophage phenotypes seem appropriate when describing the evolving states of damage and repair. As depicted below, M1 macrophages attract neutrophils and boost the inflammatory response to facilitate removal of damaged tissues, both via the release of pro-inflammatory mediators, and their enhanced phagocytic ability. Conversely, M2 cells, specifically one of the M2 subsets - M2a, then initiate the proliferative phase of repair through release of anti-inflammatory cytokines, increase cell proliferation and migration via release of arginase and Ym1, while also promoting tissue formation through secretion of growth factors (Novak and Koh, 2013; Sindrilaru and Scharffetter-Kochanek, 2013). Furthermore, while macrophages during the remodelling phase have an identifiable M2c phenotype (another M2 subset), their roles are still not entirely well understood, with the current narrative predicting that macrophages likely play a greater role via inhibiting, rather than promoting, different aspects of the remodelling phase (Daley *et al.*, 2010; Mirza and Koh, 2011; Novak and Koh, 2013; Gensel and Zhang, 2015).

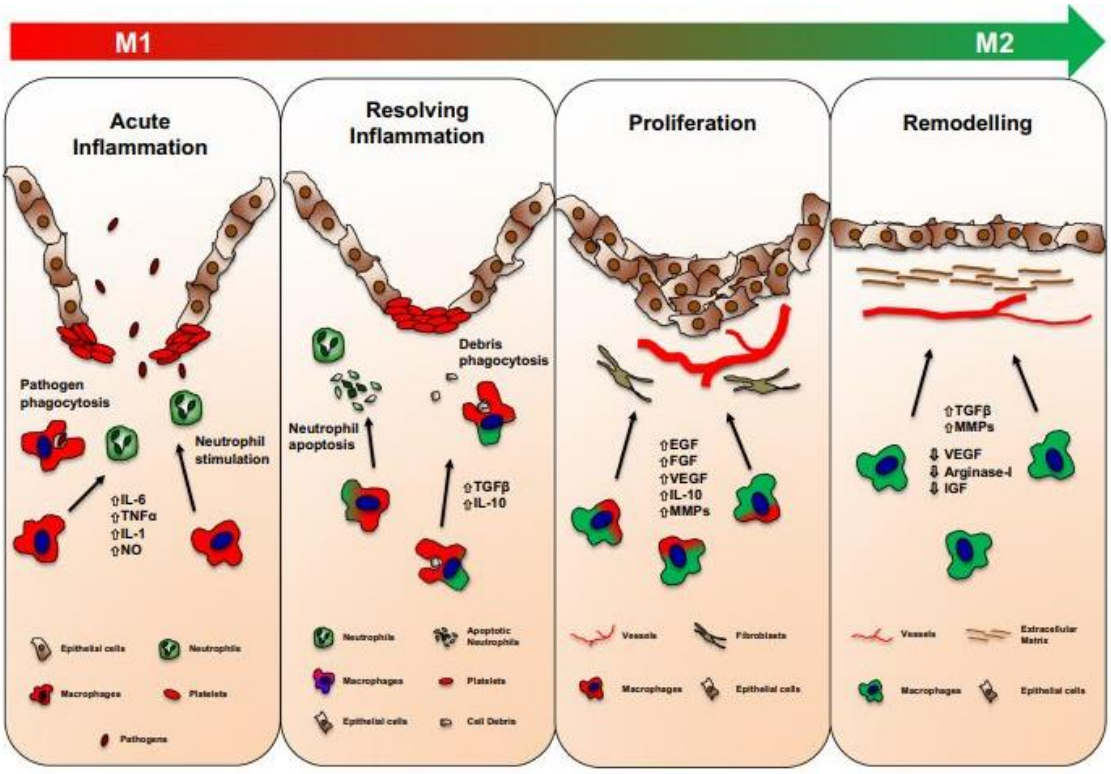

Figure 1.5: The role of macrophages and their subsets in inflammation and tissue repair. During the four key phases of tissue repair, macrophages dynamically switch their phenotype from M1 to M2. Within the acute phase, M1 macrophages produce pro-inflammatory mediators IL-6, TNF-α, IL-1, and NO, which stimulates additional innate immune cells such as neutrophils. During the second phase of resolving inflammation, macrophages initiate an M1 to M2 phenotype switch in which they acquire an anti-inflammatory phenotype and downregulate the production of inflammatory mediators, while increasing production of anti-inflammatory cytokines TGF-β and IL-10. They also initiate phagocytosis of apoptotic neutrophils and removal of damaged cells. In the third proliferation phase, M2 macrophages produce a variety of growth factors, such as EGF, FGF, and VEGF which induce the proliferation of various cell types involved in the healing process. In the final remodelling phase, macrophages contribute to the maturation of the regenerated tissue though reorganizing the extracellular matrix and vasculature architecture (Sica *et al.*, 2015).

1.3.4.1 M1 polarization

Classically activated, M1 macrophages constitute the first line of defence against intracellular pathogens and promote the Th1 polarization of $CD4^+$ T cells (Atri, Guerfali and Laouini, 2018). Microbial stimuli such as LPS, either alone or in concert with polarizing cytokines IFN-γ, TNF-α and GM-CSF, induce classically activated M1 macrophage polarization, with M1 macrophage activity and polarization dominated by TLR and IFN signalling (Sica *et al.*, 2015; Atri, Guerfali and Laouini, 2018). Engagement of additional receptors such as phagocytic Fc receptors, is also required to support robust and prolonged production of ROS (Steevels and Meyaard, 2011). M1 macrophages exhibit increased phagocytic activity and are characterized by their high antigen presentation capacity, expression of the markers CD64 and CD80 (Tarique *et al.*, 2015) and production of the pro-inflammatory cytokines IL-1β, IL-6, IL-12, IL-18, IL-23, TNF-α, and type I IFN; and several chemokines such as CXCL1, CXCL3, CXCL5, CXCL8, CXCL9, CXCL10, CXCL11, CXCL13, CXCL16; CCL2, CCL3, CCL4, CCL5, CCL8, CCL15, CCL11, CCL19, and CCL20; all of which induce downstream Th1 response activation and facilitate type I inflammation (Beyer *et al.*, 2012; Italiani *et al.*, 2014; Vogel *et al.*, 2014).

M1 macrophages are generally considered responsible for resistance against intracellular pathogens, with association to acute infection with *Listeria monocytogenes* (Shaughnessy and Swanson, 2007), *Salmonella typhi, Salmonella typhimurium* (Jouanguy *et al.*, 1999), *Mycobacterium tuberculosis* (Chacón-Salinas *et al.*, 2005), *Mycobacterium ulcerans* (Kiszewski

et al., 2006) and *Mycobacterium avium* (Murphy *et al.*, 2006). Moreover, uncontrolled M1 inflammation associated with acute infections with *E. coli* or *Streptococcus* sp. is reported to cause gastroenteritis, urinary tract infections, neonatal meningitis and sepsis (LeFebvre *et al.*, 1991).

1.3.4.2. M2 polarization

Where M1 macrophages promote inflammation and the destruction of noxious sources, M2 polarized macrophages are responsible for recovering homeostasis, promote tissue healing (Moreira Lopes, Mosser and Gonçalves, 2020), and are particularly correlated with parasitic, helminthic, and fungal infection (Atri, Guerfali and Laouini, 2018). The cytokines IL-4 and IL-13, in addition to IL-10 and TGF-β, induce the polarization of alternatively activated M2 macrophages, which express a typical IL-12^{low}IL-1^{low}IL-10^{hi} cytokine production signature (Durafourt *et al.*, 2012; Xu *et al.*, 2013; Tarique *et al.*, 2015). These cells also possess poor antigen-presentation function but act to supress the Th1 response whilst producing IL-13, CCL1, CCL2, CCL13, CCL14, CCL17, CCL18, CCL22, CCL23, CCL24, CCL26, and IL-1R production (Gordon, 2003; Martinez *et al.*, 2006; Steevels and Meyaard, 2011; Tarique *et al.*, 2015), IL-8, MCP-1, IP-10, macrophages inflammatory protein (MIP)-1β, and CCL5 (Regulated on Activation, Normal T Cell Expressed and Secreted - RANTES) in the aim to recruit neutrophils, monocytes, and T lymphocytes in an anti-inflammatory response (Verreck *et al.*, 2006). Alongside their cytokine production attributes, M2-like macrophages can also be identified based on their pattern of surface marker expression, with CD64, CD163 and CD206 commonly noted in the literature (Barros *et al.*, 2013; Tarique *et al.*, 2015).

Due to their diversity, alternatively activated M2 macrophages can be further classified into distinct subsets based upon different encountered stimuli: M2a, M2b and M2c (Vogel *et al.*, 2014; Iqbal and Kumar, 2015; Funes *et al.*, 2018). These groups are derived from different stimuli: IL-4 and/or IL-13 (M2a); immunocomplex and Toll-receptor agonist (M2b), and IL-10, TGF-β or glucocorticoid hormones (M2c) (Mantovani *et al.*, 2004; Ferrante *et al.*, 2013). More recently, further phenotypes of M2 macrophages have been described and include haemorrhage-associated macrophages (Mhem) (Boyle *et al.*, 2009), macrophages generated via oxidized phospholipids (Mox) (Kadl *et al.*, 2010), and M4 macrophages induced by chemokine ligand 4 (Gleissner *et al.*,

2010). Finally, tumour-associated macrophages (TAMs or M2d) stimulated by IL-6 and M-CSF have also been categorized as a novel M2 macrophage subset, which can directly inhibit proinflammatory M1 macrophages. These cells are characterized by IL-10^{hi}IL-12^{low}TGF-β^{low} cytokine production and decreased CXCL10, CXCL16, and CCL5 chemokine secretion (Duluc *et al.*, 2007). Thus TAMs, as their name would imply, constitute the major inflammatory component of the tumoral tissue, contributing to angiogenesis and tumour metastasis (Wu *et al.*, 2012; Sica *et al.*, 2015; Sunakawa *et al.*, 2015).

All identified subsets have the ability to secrete high levels of IL-10 and low levels of proinflammatory cytokines such as IL-12, but equally possess variations in functional biomarker expression unique to each subset (Vogel *et al.*, 2014; Iqbal and Kumar, 2015). M2a macrophages express high levels of CD86 and CD200R and low CD14 and TLR4, whilst inducing IL-10, CCL13, CCL17, and CCL22 production. M2b are characterized by higher CD80 and CD14 expression; IL-10, CCL1 and proinflammatory cytokine production, and lower HLA-DR expression and IL-12 secretion. Meanwhile, M2c have decreased CD86 and HLA-DR expression, high CD163, and are involved in preventing tissue inflammation (Pannellini *et al.*, 2004; Duluc *et al.*, 2007; Iqbal and Kumar, 2015). Within the proliferative phase, M2 macrophages possess different phenotypic profiles than those in the inflammatory phase (Daley *et al.*, 2010). IL-10 is abundant during the proliferative stage of repair that facilitates tissue remodelling and is a potent inhibitor of pro-inflammatory cytokines, chemokines and inflammasome components (Novak and Koh, 2013; Thompson *et al.*, 2013; Zigmond *et al.*, 2014), with the secretion of IL-10 a hallmark of M2b macrophages rendering them essential in the central and latter proliferative phase centred around tissue remodelling (Edwards *et al.*, 2006; Mosser and Edwards, 2008; Lech and Anders, 2013; Gensel and Zhang, 2015).

1.3.4.3. M1/M2-associated pathologies

This macrophage adaptability between acquisition of M1 and M2 phenotypes underpins their role in a plethora of diseases such as cancer, aging, obesity, and obesity-associated diabetes mellitus, arthritis, and neurodegenerative pathologies.

- **IBD**

In the context of IBD, an increased M1/M2 ratio has been reported, alongside a reduction in IL-23, TNF-α and IL-10 secretion. Correspondingly, transference of M2 macrophages has been shown to reduce colitis and increase IL-10 production in the gut, given their potential to influence other cell responses, such as increase invariant regulatory T cell and Th17 generation (Zhu *et al.*, 2014; Haribhai *et al.*, 2016). Reports have also correlated IL-10R-deficiency in IBD patients with defective macrophage function and patients possessing polymorphisms in the IL-10 promoter show a reduction in IL-10 serum levels – a trait associated with IBD (Mantovani and Marchesi, 2014; Ip *et al.*, 2017). Similarly, *in vivo* models using IL-10 or IL-10R deficient mice report spontaneous development of colitis (Kühn *et al.*, 1993; Zigmond *et al.*, 2014; Keubler *et al.*, 2015). M2 macrophages have thus been shown to contribute to the resolution of colitis via angiogenesis promotion, debris scavenging, and tissue repair (Hunter *et al.*, 2010; Weisser *et al.*, 2011; Leung *et al.*, 2013), and have therefore been frequently suggested as a possible collaborator in IBD immunotherapy for the re-establishment of mucosal tolerance and repair of injured mucosa (Haribhai *et al.*, 2016).

Moreover, isolated macrophages from the lamina propria of IBD patients are reported to have a more M1-like phenotype and produce large amounts of pro-inflammatory cytokines such as IL-12, IL-23, TNF and iNOS, and possess a strong response to bacterial stimuli (Reinecker *et al.*, 1993). During colitis, $Ly6C^{hi}$ monocytes invade the colon and differentiate into pro-inflammatory M1 macrophages. These findings testify to the capacity of $Ly6C^{hi}$ monocytes to differentiate into inflammatory cells within the gut (Rivollier *et al.*, 2012; Moreira Lopes, Mosser and Gonçalves, 2020). M1 macrophages have thus been directly implicated in IBD with an *in vitro* study by Lissner *et al* (2015) showing how M1 macrophages may contribute to the disruption of the intestinal epithelial barrier via enhanced production of TNF, which impairs the structure and function of tight junctions (Lissner *et al.*, 2015). Furthermore, in cases of IBD, $CD68^{+}$ macrophages are also reported to infiltrate the mucosa and submucosa, in addition to the muscular layer and submuscular adipose tissue in Crohn's disease (Kredel *et al.*, 2013; Kühl *et al.*, 2015). These tissue-infiltrating macrophages show expression of TLRs, notably TLR2, TLR4 and TLR5. The existence of research correlating aberrant M1 macrophage presence within a

variety of pathologies including IBD renders them a continued therapeutically viable target.

In IBD there are also marked changes to the macrophage compartment resulting from increased immigration of classical $CD14^{hi}$ monocytes, leading to the accumulation of proinflammatory $CD11c^{hi}$ monocytes/macrophages in the inflamed colon (Kamada *et al.*, 2008; Bain *et al.*, 2013; Ogino *et al.*, 2013; Bernardo *et al.*, 2018). Targeting monocyte recruitment has been widely considered in IBD, with research reporting that CCR2 is the essential chemokine receptor that mediates the entry of monocytes into the circulation and subsequent recruitment into the site of the inflamed gut, and consequently genetic ablation and antibody-mediated blockade of CCR2 is protective against mouse experimental colitis (Serbina and Pamer, 2006; Platt *et al.*, 2010; Waddell *et al.*, 2011; Neurath, 2019).

- **Cancer**

Macrophages have been noted as a major component of the leukocyte infiltrate present in varying amounts within all tumours (Noy and Pollard, 2014). As introduced previously, TAMs play a dominant role as orchestrators of cancer-related inflammation, with the narrative now correlating TAMs to malignant metastatic tumours and the promotion of tumour growth and metastasis (Evans and Alexander, 1970; Mantovani and Allavena, 2015; Mantovani *et al.*, 2017). For instance, high TAM content (characterized by increased CD64 expression) has been associated with unfavourable outcomes in patients with follicular lymphoma despite treatment with multiagent chemotherapy (Farinha *et al.*, 2005; Alvaro *et al.*, 2006).

Given that macrophages are an essential component of remodelling of the extracellular matrix, reports have linked the accumulation of M2 cells in early pancreatic adenocarcinoma in situ (PanIN) to the promotion and progression of fibrosis (Liou *et al.*, 2017). Further evidence also implicates these cells in a spectrum of tumour evolution, from initiation to metastasis. In liver inflammation and carcinogenesis, single tumour-initiating cells were found to recruit polarized M2 macrophages which aided evasion from immune clearance (Guo *et al.*, 2017). Furthermore, genetic instability is an understood hallmark of cancer, and recent evidence refers to myeloid cells as contributors to genetic instability via the production of ROS which subsequently interact with cancer stem cells (Canli *et*

al., 2017; Locati, Curtale and Mantovani, 2020). This data suggests that macrophages are involved in the early stages of carcinogenesis. Thus, the literature depicts a role by which macrophages promote invasion and metastasis and contribute to the various stages of progression, from initiation to formation of distant metastases (Doak, Schwertfeger and Wood, 2018).

More recent evidence has further surmised the role of macrophage polarization in cancer progression and metastasis. A report by Lu *et al* published in 2020 in the context of lung cancer indicates a role for Oct4 expressed by lung cancer cells in the promotion of M2 macrophage polarization via upregulation of M-CSF secretion, which resulted in growth and metastasis (Lu *et al.*, 2020). M2 polarization was also implicated in gastric cancer whereby Zhang and Li (2020) noted lactic acid was able to skew macrophages toward an M2 phenotype using THP-1 and human monocytes treated with gastric cancer cell-derived conditioned media or lactic acid (Zhang and Li, 2020). Furthermore, aberrant overexpression of tumour-derived exosomal miR-934 in colorectal cancer has been shown to promote colorectal cancer liver metastasis via regulating the crosstalk between cancer cells and TAMs, promoting M2-like TAM immunosuppressant behaviour (Zhao *et al.*, 2020).

- **Aging**

Aging has been shown by some studies to compromise macrophage recruitment, antigen presentation, phagocytosis, ROS production and cytokine production with a consensus that macrophage recruitment upon challenge is impaired in old human and murine subjects (Lloberas and Celada, 2002; Aprahamian *et al.*, 2008; Gomez *et al.*, 2008). Immune complexes, elevated cytokines, hormones, free fatty acids, oxidized low-density lipoproteins and immunoglobulins are all reported to accumulate with aging and can subsequently activate macrophages (Sambrano and Steinberg, 1995; Franceschi *et al.*, 2017). This may then promote the onset of tissue-specific low grade inflammation diminishing their ability to mount and promote an effective response during aging (Jackaman *et al.*, 2017). *In vitro* studies suggest a reduced response by macrophages to pro-inflammatory stimuli, with peritoneal and splenic macrophages from elderly mice proving to be less responsive to pro-inflammatory stimuli using administration of LPS and IFN-γ compared to those from young mice controls (Yoon *et al.*, 2004; Mahbub, Deburghgraeve and Kovacs, 2012).

Furthermore, *in vitro* production of NO, ROS, IL-6 and TNF-α by macrophages following their exposure to LPS and/or IFN-γ was shown to decrease with aging (Renshaw *et al.*, 2002; Boehmer *et al.*, 2004; Mahbub, Deburghgraeve and Kovacs, 2012). A report in 2006 by Chelvarajan *et al*, also showed genes encoding pro-inflammatory mediators such as IL-1β, IL-6, IL-12, CCL24, CCR3 and CCR5 were downregulated in splenic macrophages from healthy elderly mice compared to their younger counterparts (Chelvarajan *et al.*, 2006). On the other hand, pro-inflammatory M1-like macrophages have also been linked to aging through their high expression of the NAD-consuming enzyme CD38 and enhanced CD38-dependent NADase activity, which thereby reduces tissue NAD levels and in fact provides protection against cellular senescence (Covarrubias *et al.*, 2020). More work is therefore required in this setting to delineate macrophage contribution.

- **Arthritis**

Synovial macrophages have similar phenotype to other tissue resident macrophages, including expression of CD11b, CD14, CD16, and CD68 (Manferdini *et al.*, 2016). In RA the synovial membrane becomes hypertrophic and exhibits hallmarks of a chronic inflammatory disease, including infiltration of macrophages, neutrophils, T cells, mast cells and B cells (Alivernini *et al.*, 2016; Siouti and Andreakos, 2019). This inflammation results in pannus formation and the destruction of cartilage and bone (Firestein and McInnes, 2017). M1 macrophages have been implicated in the inflammatory chronicity of RA due to their production of potent pro-inflammatory cytokines TNF, IL-1, IL-6, IL-10, IL-12, IL-18 and TGF-β, and their stimulation of T cell response via antigen presentation (Cope *et al.*, 1992; Szekanecz *et al.*, 1995; Feldmann, Brennan and Maini, 1996; Gracie *et al.*, 1999).

Macrophage production of TNF specifically drives RA pathogenesis, with early findings using novel transgenic mouse models which contained a modified human TNF gene showing these mice developed chronic inflammatory polyarthritis, while *in vivo* administration of antibodies against human TNF effectively reversed the disease progression (Keffer *et al.*, 1991). Furthermore, using a collagen-induced model of arthritis, neutralization of TNF using antibodies significantly decreased joint swelling, histological severity and clinical disease outcome when administered both before and after establishment

of RA (Williams, Feldmann and Maini, 1992). In 1999 using a model of human/murine SCID arthritis, blocking of TNF also reduced RA related signs of inflammation (Schädlich *et al.*, 1999).

M1 macrophages also affect osteoarthritis (OA) cartilage by inhibiting genes associated with matrix production and upregulation of matrix degenerating genes, with M1-associated cytokines IL-6, IL-1β, TNF-α and oncostatin M (OSM) inducing destructive processes in chondrocytes including down regulation of collagen type II and aggrecan synthesis (Fahy *et al.*, 2014; Fernandes *et al.*, 2020). In 2017, O'Brien *et al* found that there were more macrophages in the early stages of synovial OA than when compared to late stages, and also demonstrated how synovial macrophages were decreased in pre-OA joints in comparison to normal (O'Brien *et al.*, 2017). Synovial M1 macrophages have also been reported to upregulate MMP1, MMP3, MMP13, MMP9, aggrecanases (ADAMTS), and COX-2, all of which contribute to articular degeneration (Fahy *et al.*, 2014; Manferdini *et al.*, 2016; Haltmayer *et al.*, 2019).

In recent years the use of low-intensity pulsed ultrasound (LIPUS) has been widely used as a diagnostic and therapeutic tool for arthritis (Maylia and Nokes, 1999), and in a 2019 report using a mouse model of destabilization of medial meniscus (DMM) arthritis, Zhang *et al* found that LIPUS significantly alleviated the OA symptoms via decreasing the proportion of M1 macrophages and simultaneously increasing M2 presence in the joint synovium (Zhang *et al.*, 2019). In a 2020 study, bone marrow mesenchymal stem cell-derived exosomes were shown to delay the progression of osteoarthritis via alleviating cartilage damage, reducing osteophyte formation and synovial macrophage infiltration, inhibiting M1 macrophage production and promoting M2 macrophage generation (Zhang *et al.*, 2020).

- **Neuropathology**

Inflammatory responses in the brain, demonstrated by changes in the functional properties of microglia - the brain-resident macrophages, are a common feature of human neurodegenerative diseases, and different macrophage/microglia phenotypes have been defined via changes in expression of cytokines, receptors and other markers as a response to different classes of stimuli (Walker and Lue, 2015). Widespread expression of CD40 - a marker for M1 macrophage/microglia activation, has been reported within the brains of patients with AD (Togo *et al.*,

2000). Microglia from white matter illustrated positive reactivity to the markers HLA-DR, CD16, CD32 and CD64 *ex vivo*, but not to CD14, CD80, CD163, CD200 receptor (CD200R) or CD206 (Melief *et al.*, 2012), while microglia derived from the white matter of MS patients showed a similar profile, but with significantly increased expression of CD14, suggesting a higher proportion of M1-like cells (Melief *et al.*, 2013).

In regards to gliomas, previous studies have shown as many as 30-50% of cells are non-neoplastic macrophages/microglia, with many glioblastomas containing a considerably greater proportion at around 70% (Morantz *et al.*, 1979; Rossi *et al.*, 1987; Roggendorf, Strupp and Paulus, 1996). Furthermore, $CD163^+$ and $CD204^+$ TAMs have been linked to poor disease prognosis versus $CD68^+$ TAMs, with other studies suggesting a correlation between M1-specific markers or associated pathways and glioma growth (Komohara *et al.*, 2008, 2012; Hambardzumyan, Gutmann and Kettenmann, 2016). Specifically, IL-1β was shown to promote glioma growth, and was mainly localized within the macrophage populations (Sasaki *et al.*, 1998). In 2020 Guo *et al* evaluated the polarization status of circulation-derived macrophages in patients with glioma, reporting fewer M1, and more M2 macrophages in the peripheral blood of glioma patients when compared with the healthy controls, with the number of M2a and M2b macrophages increased specifically (Guo *et al.*, 2020). This may suggest that in the context of macrophages in gliomas, the M1/M2 classification system is potentially oversimplified with the existence of numerous activation states and overlapping function forming a continuum rather than two distinct states (Sasaki, 2017). Despite these reports, the phenotype of TAMs *in vivo* has proven more complex, with the TAM gene expression profile partially overlapping with the M1 and M2 phenotypes (Szulzewsky *et al.*, 2015).

- **Obesity-associated pathology**

Obesity and hypertension, characterized by chronic, low-grade inflammation and adverse cardiac remodelling, often coexist and are major risk factors for heart failure. Given that macrophages play a key role in cardiac remodelling, a dysregulation of macrophage phenotype polarization can result in excessive inflammation and cardiac injury (Mouton *et al.*, 2020). Clinical studies and experimental models of hypertension have shown abnormalities in NO synthesis and bioavailability of macrophages (Svendsen, 1977; Llorens, Jordán and Nava,

2002; Herrera and Garvin, 2005; Schiffrin, 2014). The mechanism underpinning this development of hypertension revolves around the decreased bioavailability of NO or interference in its regulation of natriuresis. M1 macrophage production of ROS acts to scavenge NO, thereby implicating it in reduced NO bioavailability and development of hypertension. More interesting still is the role of ROS in skewing the balance of polarization towards an M1 phenotype whilst also recruiting M2 macrophages (Hermann, Flammer and Lüscher, 2006; Zhang *et al.*, 2013; Ramseyer *et al.*, 2016; Harwani, 2018b).

Metabolic shifting between glycolysis and mitochondrial oxidative phosphorylation (OXPHOS) has also been implicated in macrophage polarization, as M1 polarized macrophages primarily rely on glycolysis, while M2 macrophages rely on the tricarboxylic acid (TCA) cycle and OXPHOS. This implies factors that affect macrophage metabolism may disrupt M1/M2 homeostasis and exacerbate inflammation (Mouton *et al.*, 2020). Obesity-induced hypertension is associated with systemic and cardiac inflammation mediated in part by macrophages, which assume a pro-inflammatory M1 phenotype, especially during heart failure (Berthiaume *et al.*, 2012; Chen and Frangogiannis, 2018; Harwani, 2018b). Furthermore, clinical reports have correlated a greater number of circulating pro-inflammatory macrophages and macrophage-derived cytokines with worse clinical outcome in heart failure patients (Dick and Epelman, 2016; Andreadou *et al.*, 2019).This interaction supports the premise that curbing inflammation via controlling macrophage polarization may be a promising therapeutic option for obesity-related heart failure.

M1 macrophages are also found to be activated by lipids, lipoproteins, and cytokines within the microenvironment of white adipose tissue of obese individuals, and are shown to exacerbate inflammation in adipose tissue, trigger insulin resistance, and promote the development of obesity-associated metabolic syndromes (Osborn and Olefsky, 2012; Boutens and Stienstra, 2016). This again renders the regulation of macrophage polarization a potential therapeutic target for the prevention of obesity- or diabetes-associated pathology (Ren *et al.*, 2019). Here, exaggerated or prolonged M1 responses are involved with reports noting <10% of resident macrophages resemble M1 macrophages in white adipose tissue from lean mice, but 50% of all cells in the white adipose tissue of

obese mice possess an M1 phenotype (Weisberg *et al.*, 2003; Olefsky and Glass, 2010). The M1 macrophages subsequently produce inflammatory cytokines such as TNF-α, IL-1β, and IL-6 which counteract the insulin-sensitizing action of adiponectin and leptin, resulting in insulin resistance and development of metabolic syndrome (Kraakman *et al.*, 2014; Castoldi *et al.*, 2016). Thus, mice deficient in TNF-α, CCL2, or CCR2 are shown to have fewer M1 macrophages and higher insulin sensitivity when fed a high-fat diet compared with wild-type control mice (Hotamisligil, 2006; Bolus *et al.*, 2015).

At the molecular level, insulin resistance is promoted by a transition in macrophage polarization from an alternative M2 activation state, maintained by signal transducer and activator of transcription (STAT) 6 and peroxisome proliferator-activated receptors (PPARs), to an M1 activation state driven by NF-κB and AP-1 (Olefsky and Glass, 2010). Adipose tissue macrophages (ATMs) show highly heterogeneous characteristics, and mimic the classically activated M1, and alternatively activated M2 (Mantovani *et al.*, 2004). In lean animals, more than 90% of ATMs are M2 in phenotype, however in obese individuals both the numbers of M1 and M2 ATMs are markedly increased, although recruitment of M1 ATMs appears greater, resulting in an increase in the M1/M2 ratio and an M1/M2 phenotypic switch to M1. Treatment with pioglitazone - an insulin-sensitizing PPARγ agonist, or telmisartan - a PPARγ partial agonist, is shown to decrease number of both types of ATMs, but also the M1/M2 ratio, suggesting both the absolute numbers of M1 and M2 ATMs and the M1/M2 ratio are associated with the insulin sensitivity (Fujisaka *et al.*, 2009, 2011, 2013).

Resistin - an adipokine initially discovered to be secreted by mouse adipose tissue, is mainly elaborated by macrophages in humans (Savage *et al.*, 2001; Patel *et al.*, 2003). Resistin expression is induced by LPS in human macrophages, with experimental endotoxemia causing a dramatic rise in circulating resistin levels. Furthermore, patients with type 2 diabetes had increased serum resistin levels which were positively correlated with levels of soluble TNF-α receptor (Lehrke *et al.*, 2004). These reports suggest an alternative mode of operation by macrophages in their contribution to insulin resistance, obesity, and other inflammatory states via induction of resistin (Olefsky and Glass, 2010).

1.3.4.4. Transcriptional regulation of polarization

A network of signalling molecules, transcription factors, epigenetic mechanisms, and post-transcriptional regulators underlies the different forms of macrophage activation and polarization (Figure 1.6) (Sica and Mantovani, 2012). Key transcription factors directly associated with macrophage polarization include the Janus Kinase (JAK)/STAT family, PPARs, CREB-CCAAT/enhancer binding protein (C/EBP), NF-κB and IFN regulatory factors (IRFs) (Lawrence and Natoli, 2011; Xue et al., 2014; Funes et al., 2018). Canonical IRF/STAT signalling pathways are activated by IFNs and TLR ligation and skew macrophage polarization toward the M1 phenotype via STAT1 and STAT2, or can be activated by IL-4 and IL-13, skewing polarization toward the M2 phenotype via STAT6 (Sica and Bronte, 2007; Sica and Mantovani, 2012).

The JAK/-STAT pathway is a key promoter of M1 macrophage polarization. Stimulation of the IFN-γ receptor triggers JAK-mediated tyrosine phosphorylation and subsequent dimerization of STAT1, which subsequently binds to the promoters of genes encoding NOS2, MHC class II transactivator (CIITA) and IL-12, among others which subsequently induces the transcription of M1-associated genes (Darnell, Kerr and Stark, 1994; Martinez, Helming and Gordon, 2009). Thus, it has been reported that STAT1 deficiency in mice abolishes macrophage responsiveness to IFN-γ and IFN-α stimulation (Meraz *et al.*, 1996), with STAT1-deficient mice also possessing severe defects in immunity to intracellular bacterial and viral pathogens, which is dependent on this IFN response (Lawrence and Natoli, 2011). More recently in 2017, Liang *et al* reported that downregulation of suppressor of cytokine signalling 1 (SOCS1) could promote M1 macrophage polarization via the JAK1/STAT1 pathway, while 2 years later in 2019, Oh *et al* also found that asaronic acid could attenuate macrophage activation toward an M1 phenotype through inhibition of JAK/STAT1 signalling (Liang *et al.*, 2017; Oh *et al.*, 2019).

LPS is another well-known inducer of M1 polarization and functions through induction of IFNβ, promoting the formation of STAT1-STAT2 heterodimers that mediate the induction of M1-associated genes by forming the IFN-stimulated gene factor 3 (ISGF3) complex (Wienerroither et al., 2015; C. Li et al., 2018). The activity of NF-κB is also required for LPS-mediated M1 polarization, with the NF-κB and AP-1 pathways overlapping in M1 macrophages, suggesting cooperative

transcription factor activity (Tugal Derin, Liao Xudong, and Jain Mukesh K., 2013). However, in the LPS response specifically, induction of M1-associated genes depends on the autocrine production of IFNβ, which requires TRIF-dependent signalling from TLR4 to IRF3, and cooperation of the IFNα/β receptor (Toshchakov et al., 2002). IFNβ induces the STAT1–STAT2 heterodimer, which recruits IRF9 to form the ISGF3 complex. This complex binds to distinct cis elements found in M1 signature genes, such as *nos2, ciita* and *il12β*, highlighting a crucial role of STAT1 activity in M1 macrophage polarization (Lawrence and Natoli, 2011). However, NF-κB activation may also activate genetic programmes essential for inflammation resolution and M2 polarization of TAMs, with both *in vitro* and *in vivo* studies highlighting induction of p50 NF-κB homodimers as an essential step for M2 polarization (Lawrence and Gilroy, 2007; Hagemann et al., 2008; Porta et al., 2009).

There are nine IRFs that have been identified in mammals that bind to ISRF sequences overlapping that of ISGF3, but have specificity in the regulation of gene expression, as substantiated via research using specific phenotypes of mice with different IRF gene knockouts (Savitsky *et al.*, 2009). IRF3, 4 and 5 are involved in macrophage polarization, with IRF5 recruited to promote the expression of M1-related genes while simultaneously inhibiting M2 gene-related expression. This upregulation of IRF5 is essential for the induction of typical pro-inflammatory cytokines such as IL-12, IL-23 and TNF (Krausgruber *et al.*, 2011; Tugal Derin, Liao Xudong, and Jain Mukesh K., 2013). IRF4 was also shown to specifically regulate M2 macrophage polarization in response to parasites or chitin - a fungal cell wall component, via the histone demethylase JMJD3 (De Santa *et al.*, 2007; Satoh *et al.*, 2010). JMJD3 is strongly induced by pro-inflammatory stimuli, however the absence of JMJD3 has been noted to completely block the induction of M2 macrophages in mice challenged with helminths or chitin, indicating a greater role of JMJD3 in M2 than in M1 macrophages. Moreover, murine macrophage knockout models of additional IRFs - IRF1 and IRF2, were shown to abolish pro-inflammatory responses in response to LPS or IFN-γ stimulation, while both have been suggested to promote M1 polarization and inhibit M2-associated markers in human peripheral blood macrophages (Salkowski *et al.*, 1999; Krausgruber *et al.*, 2011). IRF6 has also been recently implicated in the negative regulation of M2 polarization of

murine bone-marrow-derived macrophages (BMDM) through inhibition of PPARγ (Li *et al.*, 2017).

The JNK signalling pathway - belonging to the superfamily of MAPKs, has three distinct isoforms; JNK1, JNK2, and JNK3, and is also reported to be required for M1 polarization, M1-related inflammation, fibrosis, insulin resistance, macrophage infiltration and expression of M1-associated genes (M. S. Han *et al.*, 2013; Zhou *et al.*, 2014; Mao *et al.*, 2015; Yang *et al.*, 2018). As such, previous studies have linked downregulation of phosphorylated JNK to polarization towards the M2 subset both in rat white adipose tissue macrophages and in the murine macrophage cell line RAW264.7 (Oliveira *et al.*, 2013; Wan and Sun, 2019).

In conjunction with the IRF/STAT/SOCS pathways, a further panel of transcription factors is involved in macrophage polarization orchestration encompassing the nuclear receptors PPARγ and PPARδ, which control distinct subsets of genes associated with M2 macrophage activation and oxidative metabolism (Odegaard *et al.*, 2007; Kang *et al.*, 2008; Sica and Mantovani, 2012). Genes associated with M2 polarization such as *arg1*, *cd206* and *ym1* are regulated by STAT6 activation following stimulation with IL-4/IL-13 (Martinez, Helming and Gordon, 2009). STAT6 regulates and synergizes with both PPARγ and Krüppel-like factor 4 (KLF4) to induce M2 genes whilst inhibiting M1 genes encoding for *tnfa*, *cox2*, *ccl5*, *inos* via sequestration of coactivators required for upstream NF-κB activation (Szanto *et al.*, 2010; Liao *et al.*, 2011; C. Li *et al.*, 2018).

In the IL-4 and IL-13 pathway, receptor binding of IL-4 I and II receptors activates JAK1 and JAK3, leading to STAT6 activation and translocation, which in turn initiates transcription of genes typical of M2 polarization such as mannose receptor (*mrc1*), resistin-like α (*retnla* or *fizz1*) and chitinase 3–like 3 (*chi3l3* or *ym1*) (Pauleau *et al.*, 2004; Junttila *et al.*, 2008; Gordon and Martinez, 2010; Wan and Sun, 2019). On the other hand, IL-10 is responsible for the activation of STAT3-mediated expression of genes encoding *il-10*, *tgfb1* and *mrc1*, which are also closely associated with an M2 phenotype (Lang *et al.*, 2002; Gordon, 2003). Studies using mice with a myeloid cell-specific knockout of IL-4 receptor-α (IL4ra) have been found to lack M2 macrophage development in models of helminth infection during Th2 cell-mediated inflammation (Herbert *et al.*, 2004).

This M2 phenotype is promoted in part by PPARγ and KLF4 (Bouhlel *et al.*, 2007a; Chawla, 2010; Liao *et al.*, 2011), whereby myeloid-specific deficiency of either factor has been shown to result in suppressed M2 macrophage polarization (Babaev *et al.*, 2005; Sharma *et al.*, 2012). Murine myeloid cells deficient of PPARγ have been shown to reduce M2-like activation and subsequently induce susceptibility to obesity, insulin resistance, and glucose intolerance (Odegaard *et al.*, 2007). Furthermore, interactions between PPARγ and STAT6, in which STAT6 acts as a cofactor, facilitating the induction of PPARγ-regulated genes, have been shown in cultured mouse primary macrophages (Szanto *et al.*, 2010). In addition, studies using KLF4 knockout mice demonstrated the role of KLF4 in the regulation of M2 macrophage polarization, providing protection to mice from obesity-induced insulin resistance (Liao *et al.*, 2011). Collectively, these findings suggest that STAT6, PPARγ and KLF-4 coordinate the M2 polarization of macrophages (Wang, Liang and Zen, 2014b).

Several members of the C/EBP family also play important roles in macrophage activation with C/EBPβ reported to regulate many M2-related genes and understood to be required for wound healing (Gordon and Martinez, 2010). C/EBPβ mediates TLR-induced expression of the M2-associated genes *arg1* and *mrc1* via the transcription factor CREB (C. Li *et al.*, 2018). In this regard, deletion of CREB binding sites has been shown to impair muscle tissue repair and inhibit expression of M2 related genes macrophage scavenger receptor 1 (*mrs1*), *il10*, IL-13 receptor subunit receptor α1 (*il13ra1*), and *arg1* within macrophages, whilst having no effect on the transcription of inflammatory, M1-associated genes (Ruffell *et al.*, 2009).

In summary, it is well established from the literature that polarization to an M1 or M2 phenotype is highly influenced by their respective transcriptional programming, and defects in these signalling cascades is directly correlated to the development of malignancies and pathogenesis.

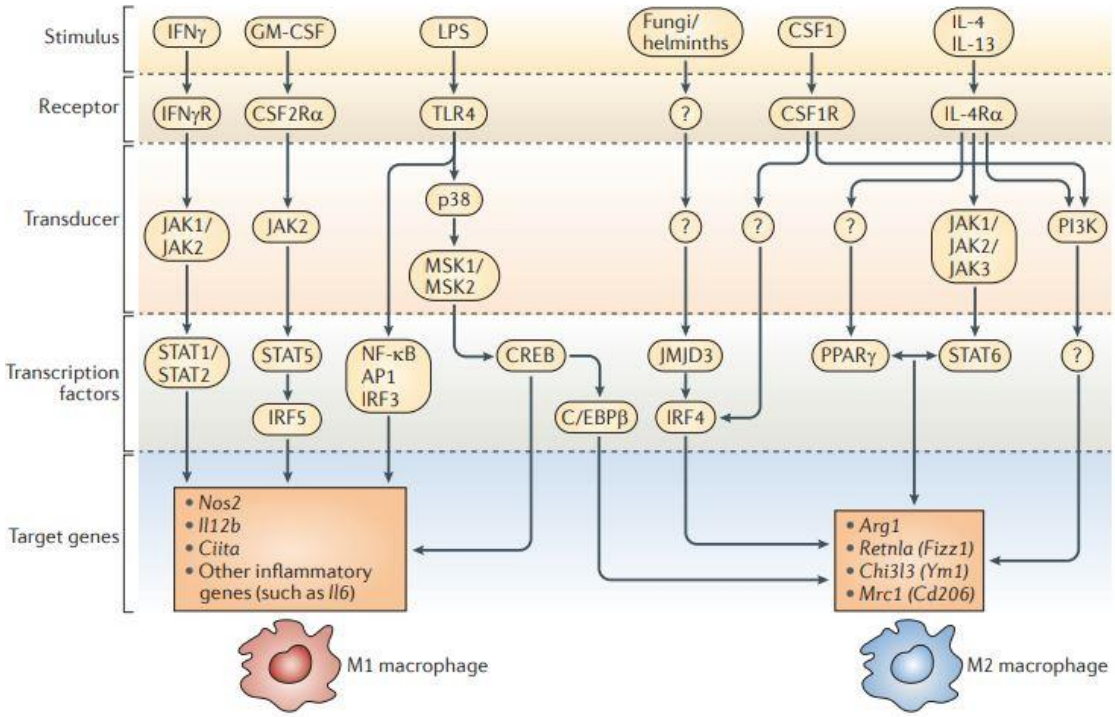

Figure 1.6: Signal transduction pathways directing M1 and M2 macrophage polarization. An initial stimulus results in the activation of sequence-specific transcription factors that mediate downstream changes. For M1 polarization 3 main stimuli have been identified: IFNγ, GM-CSF and LPS and when encountered, each bind to their respective receptors and signal via STATs, IRFs, NF-κB and AP1 resulting in M1 gene transcription. M2 polarization is dominated by IL-4/IL-13 signalling via the IL-4Rα and PPARγ/STAT6 to induce M2 associated genes. Abbreviations: Arginase 1 (Arg1); CCAAT/enhancer-binding protein-β (C/EBPβ); chitinase 3-like 3 (Chi3l3); MHC class II transactivator (Ciita); cAMP-responsive element-binding protein (CREB); colony-stimulating factor (CSF); interferon-γ (IFNγ); interleukin (IL); interferon-regulatory factor (IRF); Janus kinase (JAK); lipopolysaccharide (LPS); macrophage mannose receptor 1 (Mrc1); mitogen- and stress-activated kinase (MSK); nuclear factor-κB (NF-κB); nitric oxide synthase 2 (Nos2); phosphoinositide 3-kinase (PI3K); peroxisome proliferator-activated receptor-γ (PPARγ); resistin-like-α (Retnla); signal transducer and activator of transcription (STAT); Toll-like receptor 4 (TLR4) (Lawrence and Natoli, 2011).

1.3.5. Resolution of inflammation

Resolution and repair following an acute inflammatory response is a process mediated by tissue-resident and recruited macrophages (Watanabe *et al.*, 2019). There are three well defined mechanisms of resolution depicted in the literature which are common across different tissues and diseases and include; the cessation of neutrophil influx, neutrophil apoptosis and removal, and macrophage phenotype switch from M1 to M2 (Fullerton and Gilroy, 2016; Schett and Neurath, 2018). Remodelling and repair occur dynamically during ontogenesis and inflammation, and these processes are orchestrated by macrophages (Caprara,

Allavena and Erreni, 2020). Macrophages undergo dynamic changes during different phases of wound healing. M1-polarized macrophages mediate tissue damage and initiate inflammatory responses, while during the early stages of the repair infiltrating macrophages have an M2 phenotype. Their depletion thus inhibits the formation of a highly vascularized tissue and cellular granulation, and the development of scar tissues (van Furth and Cohn, 1968; Calum C Bain and Mowat, 2014).

Expression of Tim-4 – a phosphatidylserine (PtdSer) recognition receptor, can be used to distinguish between tissue-resident and inflammatory macrophages, with macrophages lacking Tim-4 reported to have reduced apoptotic cell engulfment properties (Albacker *et al.*, 2010). In a model of peritonitis, Schif-Zuck and colleagues show how monocyte-derived M1 macrophages undergo reprogramming, leading first to the acquisition of an M2-like phenotype characterized by high efferocytosis, and then to the concomitant expression of pro-inflammatory cytokines and IL-10 (Schif-Zuck *et al.*, 2011). They report that when the engulfing activity is at maximum, the exhausted phagocytes are further reprogrammed, leading to the generation of deactivated pro-resolving macrophages which express TGF-β and IL-10, downregulate MHC class II, and exert immunosuppressive functions.

A key event driving the resolution of inflammation is represented by the non-phlogistic monocyte–macrophage recruitment at the site of inflammation (Figure 1.7). Following the initial inflammatory influx of immune cells, macrophages scavenge apoptotic neutrophils and tissue debris via efferocytosis, thus progressively reducing pro-inflammatory stimuli – a process which is also mediated by a switch in arachidonic acid metabolism (Onali, Favale and Fantini, 2019). This macrophage clearance of neutrophils is induced by the expression of termed “find me” and “eat me” signals, such as CXCL1, sphingosine 1-phosphate, and lysophosphatidylcoline on the neutrophils themselves (Lauber *et al.*, 2003; Gude *et al.*, 2008; Truman *et al.*, 2008). Clearance of apoptotic neutrophils is essential to prevent secondary necrosis and exacerbated inflammation, whereby necrosis typically involves the loss of cell membrane integrity, in addition to uncontrolled release of intracellular organelles and enzymes into the extracellular space (Fox *et al.*, 2010). Mechanistically, neutrophil death is important to the resolution process (Wang, 2018). Neutrophil death via apoptosis prevents the

release of their toxic contents and is the first step to turning off inflammation (Ho *et al.*, 2020). Efferocytosis of apoptotic neutrophils initiates a feed-forward pro-resolution program characterized by the release of anti-inflammatory cytokines TGF-β and IL-10 from macrophages, which counteract activated proinflammatory pathways (Serhan and Savill, 2005; Watanabe *et al.*, 2019).

During the early phases of inflammation, mediators involved in the recruitment of neutrophils such as cyclooxygenase-derived PGE_2 and PGD_2 induce the expression of 15-lipoxigenase (15-LOX) in macrophages, switching to lipoxin production which marks the passage to the resolution phase (Godson *et al.*, 2000). Lipoxins act to limit the further recruitment of neutrophils to the site of inflammation, while also stimulating macrophage efferocytosis (Levy *et al.*, 2001). This process is also controlled by a variety of other agents, including, specialized pro-resolving lipid mediators (SPMs) or annexin A1 (ANXA1) (Fullerton and Gilroy, 2016; Sugimoto *et al.*, 2016). It has been demonstrated that SPMs such as maresin (MaR) 1 and 2 play pivotal roles in neutrophil recruitment inhibition with reports linking them to a decrease in neutrophil infiltration in a model of mouse zymosan-induced peritonitis (Deng *et al.*, 2014). Furthermore, ANXA1, another major protein component of the resolution cascade, and its role on neutrophil infiltration blockade has also been extensively studied in acute models of inflammation, such as DSS-induced colitis, which reveal a prominent role on neutrophil infiltration, via inhibition of neutrophil-endothelium adhesion and impairment of extravasation to sites of inflammation (Babbin *et al.*, 2008; Pederzoli-Ribeil *et al.*, 2010; Drechsler *et al.*, 2015; Hughes *et al.*, 2017). In addition, ANXA1 interacts with G-protein–coupled receptor formyl peptide receptor 2 (FPR2) to attenuate chemokine-triggered activation of integrins, thereby reducing further inflammatory cell recruitment, with ANXA1/FPR2 interaction also promoting macrophage efferocytosis (Perretti and Flower, 2004; Scannell *et al.*, 2007; Drechsler *et al.*, 2015). Cytokines and growth factors also contribute to active resolution of inflammation. IL-10 and IL-22 are among the key cytokines that limit inflammation, with genetic variants in the IL-10 receptor reported to cause early-onset Crohn's disease (Glocker *et al.*, 2009).

Mucosal healing is a widely recognized treatment goal in the management of complex IBD patients. However, remission is achieved in only a proportion of patients, many of whom lose response over time and require surgical

management (Hine and Loke, 2019). Neutrophils constitute 60% to 70% of circulating leukocytes in human blood, and in the context of IBD are recruited in abundance to the intestinal mucosa, releasing an arsenal of proteases and oxidants to execute host defence duties during the onset of inflammation (Bressenot *et al.*, 2013; Park *et al.*, 2016). Although key effectors in acute inflammation, neutrophils have been increasingly recognized to contribute to chronic inflammation via deposition of granule proteins such as α-defensins and CXCL12 that recruit monocytes to inflammatory sites (Soehnlein *et al.*, 2008, 2017). Unsurprisingly, the IBD mucosa is thus associated with prolonged neutrophil survival, with additional reports also highlighting defective neutrophil migration at the site of inflammation whereby patients affected by Crohn's disease were found to have reduced accumulation of neutrophils in the colonic mucosa at sites where the mucosal barrier was mechanically broken (Marks *et al.*, 2006). A 2011 study in which the mucosal barrier function was mechanically broken revealed a diminished infiltration of neutrophils in Crohn's disease patients, suggesting that missing sensor signals, in combination to diminished migration of neutrophils, might have an impact on the recruitment of phagocytic cells and therefore contribute to the perpetuation of inflammation in Crohn's disease (Geremia *et al.*, 2011). Conversely, in Crohn's disease, a defect in acute inflammation has also been suggested, whereby it is proposed that neutrophils in this setting fail to migrate to the inflammatory site, resulting in impaired bacterial clearance, which subsequently sustains a chronic inflammatory response (Marks *et al.*, 2006; Fournier and Parkos, 2012).

A number of additional macrophage-derived pro-resolving mediators such as eicosanoids (prostaglandins and leukotrienes), small molecules, proteins, and peptides have also been identified in relation to IBD (Caprara, Allavena and Erreni, 2020). For instance, PGD_2 and its receptor DP have been detected in long-term remission ulcerative colitis patients, with studies using DP ablation in myeloid cells reporting a decrease in the proportion of pro-resolving macrophages and worsening of the disease in both DSS-induced and 2,4,6-trinitrobenzenesulfonic acid (TNBS)-induced colitis (Vong *et al.*, 2010; Kong *et al.*, 2016). This indicates a role of PGD_2 in the resolution of mucosal inflammation. Furthermore, PGE_2 has also been associated with intestinal resolution of inflammation, with a 2011 report by Chinen *et al* demonstrating enhancement of macrophage anti-inflammatory activity by the PGE_2-EP4-cAMP axis (Chinen *et*

al., 2011). Genome-wide association studies have also identified a single-nucleotide polymorphism in the PGE_2 receptor gene in patients with Crohn's disease (Libioulle *et al.*, 2007).

Engulfment of apoptotic cells via phagocytosis signals the end of the inflammatory process to phagocytosing macrophages and alters macrophage mediator production from a pro-inflammatory M1, to an anti-inflammatory M2 phenotype (Barnig *et al.*, 2019). This further enhances phagocytosis of apoptotic cells and promotes the return to tissue homeostasis, thus suggesting that macrophage phenotype switching between M1 and M2 is essential for proper resolution of inflammation (Wynn, Chawla and Pollard, 2013; Dalli and Serhan, 2017; Smith *et al.*, 2017).

Current evidence also suggests a causal link between defects in the resolution of intestinal inflammation and altered monocyte–macrophage differentiation which results in impaired bacterial clearance and excessive IL-23 and TNF cytokine secretion in patients with IBD (Kamada *et al.*, 2008; Smith *et al.*, 2009b; Schwerd *et al.*, 2017; Bernardo *et al.*, 2018). Increased numbers of M2 macrophages, with tolerogenic and inflammation-resolving properties, are found in healthy mucosa, but by contrast, in the mucosa of IBD patients, M1 macrophages with pro-inflammatory properties are predominant (Zhu *et al.*, 2014; Lissner *et al.*, 2015). Differentiation of infiltrating monocytes to intestinal macrophages is impaired by factors such as MCP-1 during acute mucosal inflammation associated with IBD, which might contribute to impaired resolution of inflammation (Spoettl *et al.*, 2006). Moreover, resolvin and other mediators can also direct macrophage differentiation towards an M2 phenotype, further supporting a potential therapeutic role of this mucosal innate immune cell population (Titos *et al.*, 2011; Croasdell *et al.*, 2015). In patients who demonstrate a clinical response to infliximab - a chimeric monoclonal antibody against TNF-α, a distinct subset of macrophages expressing CD206 is induced and expanded compared to patients who failed to respond (Vos *et al.*, 2012). Furthermore, tofacitinib, a small molecule JAK inhibitor developed for the treatment of IBD, has been shown to affect macrophage polarization and function, increase transcription of M2 macrophage markers and increase levels of IL-10 secretion while inhibiting IFN-**γ** signalling (Zhang *et al.*, 2017; De Vries *et al.*, 2019).

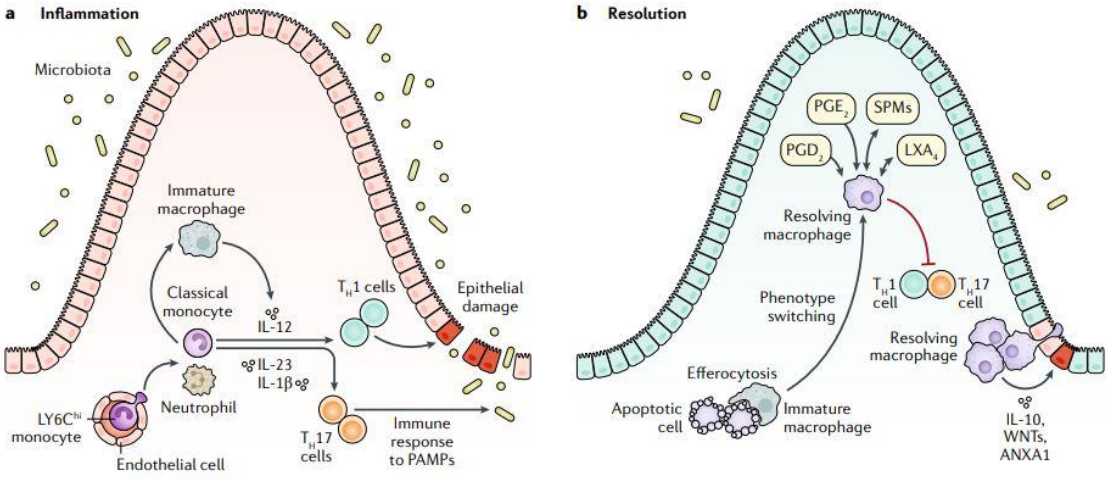

Figure 1.7: Macrophages in intestinal inflammation and resolution. [A] During intestinal inflammation neutrophils and inflammatory monocytes are recruited to mount an appropriate immune response. The differentiation of Ly6C^{hi} monocytes to mature intestinal macrophages is disrupted leading to an accumulation of Ly6C^{hi} monocytes and Ly6C^{int}MHC II^{+}CX3C1^{int} immature macrophages. When activated by PAMPs these cells produce inflammatory cytokines that promote Th1 and Th17 responses which potentiate epithelial damage. [B] In the resolution phase, efferocytosis of apoptotic neutrophils and epithelial cells induces phenotype switching of macrophages from M1 to M2. Several pro-resolving mediators, such as PGD_2, PGE_2 and lipoxin A4 (LXA4) and SPMs direct macrophage differentiation towards this M2 phenotype. Consequently the Th1 and Th17 responses are suppressed, and the epithelial barrier is re-established (Na *et al.*, 2019a).

The uptake of apoptotic cells and induction of TGF-β, IL-10, and retinoic acid also promote the development of Tregs (Liu and Cao, 2015). In models of acute inflammation such as acute peritonitis, in which decreased Tregs and defective efferocytosis drive disease progression, the accumulation of Tregs at the site of inflammation was required to enhance efferocytosis in an IL-13-dependent manner. This production of IL-13 subsequently induced IL-10 expression in macrophages, enhancing neutrophil efferocytosis and macrophage reprogramming (Proto *et al.*, 2018). Tregs derived from progenitor CD4^{+} naive T cells and promote tissue repair and regeneration via suppressing the activation and function of inflammatory macrophages through further release of anti-inflammatory cytokines IL-10 and TGF-β (van Herk and Te Velde, 2016; Lu, Barbi and Pan, 2017; J. Li *et al.*, 2018). The mechanism by which colonic macrophages signal expansion of Tregs has been described by Mortha and colleagues (Mortha *et al.*, 2014). Sensing of the microflora by TLRs on the surface of macrophages results in activation of MyD88 and secretion of IL-1β. IL-1β subsequently activates MyD88 on GM-CSF-producing RORγt^{+} type 3 innate lymphoid cells

(ILC3) resulting in GM-CSF signalling to macrophages and dendritic cells to produce IL-10 and retinoic acid. These mediators ultimately promote the conversion of helper T cells to Tregs and their subsequent expansion (Isidro and Appleyard, 2016). However under steady state conditions, intestinal macrophages cannot activate naïve $CD4^+$ T cells *in vitro* and do not migrate to the mesenteric lymph nodes (mLN), with naïve $CD4^+$ T cells appearing essentially absent from the normal mucosa (MacDonald and Pender, 1998; Schulz *et al.*, 2009). Thus, it is unlikely that macrophages can be involved in the initial priming of Tregs. Instead IL-10 production by gut resident macrophages may facilitate the secondary expansion and maintenance of $FoxP3^+$ Treg that have migrated there after initial priming in the mLN (Murai *et al.*, 2009; Hadis *et al.*, 2011; Calum C. Bain and Mowat, 2014).

Reports have linked acute Treg cell deficiency to exacerbated inflammatory immune response toward commensal intestinal bacteria which resulted in chronic inflammation as characteristic in IBD (Bollrath and Powrie, 2013; Schiering *et al.*, 2014). Retinoic acid produced by IL-4-activated macrophages acts synergistically with TGF-β to promote Treg differentiation. Hence, intestinal macrophages represent a key link between the combination of immune regulatory responses as well as type-2 responses in the process of resolving tissue inflammation and promoting mucosal healing (Broadhurst *et al.*, 2012; Hine and Loke, 2019). Elevated levels of IL-10 and diminished IL-17A and RORγt levels can also influence the differentiation of pro-inflammatory Th17 into anti-inflammatory Tr1 cells and therefore have an impact on the resolution of inflammation cascade (Gagliani *et al.*, 2015; Schett and Neurath, 2018).

1.4. Project rationale & aim

The use of tetracyclines as immunomodulatory antibiotics has attracted particular interest in pathologies with both a dysregulated immune response and a confirmed or suspected microbial component. Their approved use for periodontitis and acne are clear examples of the potential of this synergistic combination. Furthermore, other classes of antibiotics such as macrolides have had their immunomodulatory properties elucidated in the recent decades and have been proven beneficial in non-infectious diseases particularly in the lungs such as asthma, chronic obstructive pulmonary disease (COPD) and cystic fibrosis (Labro and Abdelghaffar, 2001; Zimmermann *et al.*, 2018; Reijnders *et*

al., 2020). Given the role of the microbiota in intestinal inflammation, tetracyclines have been studied extensively in experimental models of colitis. This synergy between antibiotic function and immunomodulation has proven effective in this setting, with preclinical studies reporting that minocycline treatment ameliorates experimental colitis by modulating both the microbiota and the intestinal immune response (Garrido-Mesa, Camuesco, et al., 2011; Garrido-Mesa, Utrilla, et al., 2011).

This anti-inflammatory effect of minocycline has been confirmed in different models of intestinal inflammation, as well as in comparison with other members of the tetracycline family, such as tetracycline, doxycycline and tigecycline, which highlighted the superiority of 2nd and 3rd generation tetracycline analogues regarding their non-antibiotic pharmacological potential (Garrido-Mesa, Camuesco, *et al.*, 2011b; Garrido-Mesa, Utrilla, *et al.*, 2011a; Garrido-Mesa, Algieri, Rodriguez-Nogales, Maria Pilar Utrilla, *et al.*, 2015; Garrido-Mesa, Algieri, *et al.*, 2018). Minocycline specifically has shown beneficial effects in this regard, initially ascribed to the reduction of iNOS and MMP expression, as well as PARP-1 inhibition in murine models of acute and chronic colitis induced by treatment with DSS or TNBS (Huang *et al.*, 2009).

Minocycline's beneficial effects have been further elucidated using the same murine models of chemically induced colitis in which minocycline treatment was proven to significantly reduce the disease activity index and histological damage to the colonic tissue when compared to the untreated colitic mice. This effect was accompanied by a significant reduction in expression of pro-inflammatory cytokines such as TNF-α and IL-1β, and a reduction in colonic MPO activity (a marker for neutrophil infiltration) and iNOS expression. In addition, a reversal of the decline in mucus thickening which occurs during colitis was observed, via upregulation of MUC-2 (mucin-2) and TFF-3 (trefoil factor-3) expression (Garrido-Mesa, Camuesco, *et al.*, 2011a). In the same year, Garrido-Mesa and colleagues then assessed the effect of minocycline in combination with the probiotic *Escherichia coli* Nissle 1917 again using the DSS-induced colitis model. Here they reported a reduction in histological score and improved colon length, in addition to a reduction of *tnf-α, il-1β, il-2, mip-2, mcp-1, icam-1, inos* and *mmp9* mRNA expression, but an increase in *muc-3* and *zo-1* (Garrido-Mesa, Utrilla, *et al.*, 2011a). Importantly, minocycline performed on par, or better in respect to the

markers evaluated when administered alone or in combination with *Escherichia coli* Nissle 1917. Later in 2015, a study conducted by Garrido-Mesa *et al* corroborated this data, again showing an anti-inflammatory action of minocycline when compared to doxycycline (Garrido-Mesa, Rodríguez-Nogales, *et al.*, 2018b). These findings encourage the application of current, or novel chemically modified tetracyclines (CMTs) to manage the inflammatory relapses that characterise IBD pathology, in combination with maintenance therapies devoid of adverse effect, a strategy that has proven effective in chronic models of colitis (Garrido-Mesa, Utrilla, *et al.*, 2011a; Garrido-Mesa, Algieri, Rodriguez-Nogales, Maria Pilar Utrilla, *et al.*, 2015).

The most recent work published in 2018 focused then on understanding how minocycline may specifically influence the immune cell populations both circulating in the blood as well as those present in the lamina propria in the colon during intestinal inflammation. Using the mouse model of DSS-induced colitis, the effects of minocycline were observed at 2- and 4-days post treatment. Here, there appeared to be a time-dependant influence of minocycline whereby at 2 days post treatment minocycline increased the colon mRNA expression of *il-2, il-10, ccl2* and *ccl11*, in addition to increasing the cytokine concentration of IL-1β, IL-6, IL-4, IL-22 and GM-CSF in colonic explants. Conversely, at 4 days post treatment, contradictory data was obtained, whereby minocycline elicited a decrease in IL-1β and IL-6 cytokine production, while not effecting IL-4 (Garrido-Mesa, Rodríguez-Nogales, *et al.*, 2018b). Furthermore, this study also attributed minocycline's intestinal anti-inflammatory effect to a possible potentiation of the innate immune response in the intestine, leading to an earlier resolution of the inflammatory process. This was due to them reporting a higher number of pro-inflammatory Ly6C^{+}MHC II+ macrophages located in the gut at initial stages of the inflammatory process, which then differentiated into a pro-resolving Ly6C^{-} MHCII^{+} phenotype. This was also accompanied by an earlier and enhanced resolution of the inflammatory process and expression of the resolving enzyme ALOX15 in the intestine of minocycline treated mice, which also showed increased IL-22 production, a cytokine that it's key in epithelial regeneration (Garrido-Mesa, Rodríguez-Nogales, *et al.*, 2018b). Of note, the latter ascribed the immediate effect observed with minocycline to the potentiation of innate immune protection driven by macrophages, rather than an immunosuppressive effect,

which results in the potentiation of mucosal healing (Garrido-Mesa, Rodríguez-Nogales, *et al.*, 2018a).

When studied *in vitro*, minocycline elicited similar modification of biomarkers, with separate experiments conducted by Garrido Mesa *et* al assessing the effect of minocycline using RAW264.7 (murine macrophages). Using this model, the researchers reported a reduction in the production of pro-inflammatory cytokines such as IL-8 and the production of nitrite, two contributors to inflammation when challenged with LPS (Garrido-Mesa, Utrilla, *et al.*, 2011b). Then, when applied to *in vitro* murine BMDMs, minocycline resulted in conflicting data, whereby an increase in proinflammatory cytokines IL-1β, TNF-α, and IL-6 was observed following LPS challenge (Garrido-Mesa, Rodríguez-Nogales, *et al.*, 2018b).

However, despite these reports and extensive research into minocycline within the perspective of colitis, there remains no definitive data on the specific mechanism of action minocycline has upon macrophage development, function, and phenotype especially in the context of IBD. The data summarized above indicate that minocycline causes an increased presence of pro-inflammatory macrophages within the gut at initial stages of the inflammatory process, which then change into pro-resolving M2 macrophages later. On the other hand, *in vitro* studies using BMDM and the RAW264.7 cell line indicate conflicting data whereby minocycline caused both a decrease and increase in pro-inflammatory markers in each cell model respectively following 24hr LPS stimulation. So, while minocycline's actions within the immune system are generally deemed anti-inflammatory, as depicted throughout this chapter, there is controversy when assessed *in vitro* and at different durations post treatment regarding the effect of minocycline in macrophages specifically.

Therefore, the aim of this project is to:

'Characterize the direct effects of minocycline on macrophage biology, with primary focus on macrophage differentiation, phenotype and function, and to subsequently investigate the mechanisms mediating these effects.'

To achieve this aim, the project was sub-divided into 4 key objectives represented by the 4 results chapters (3-6).

1. Study the effects of minocycline on monocyte-macrophage differentiation (Chapter 3)
2. Study the effects of minocycline on macrophage activation with LPS (Chapter 4)
3. Study the effects of minocycline on macrophage polarization to M1 and M2 subsets (Chapter 5)
4. Study the effects of minocycline on LPS activation of M1 and M2 pre-polarized subsets (Chapter 6)

It is expected that the data obtained within this project will add to the collective knowledge regarding minocycline's' immunomodulatory effects and provide more detail as to the mechanism by which minocycline elicits its anti-inflammatory effects previously seen when administered *in vivo* and *in vitro*. Furthermore, data disseminated within this thesis is expected to highlight the direct influence of minocycline on macrophage biology specifically, understanding how it may alter macrophage phenotype acquisition and response to inflammatory stimulus.

This novel insight will support future exploration and innovation of further modified minocycline derivatives through identification of biological pathways responsible for any changes observed in macrophage biology, consequently allowing for new targeting moieties. Novel derivatives such as chemically modified tetracyclines (CMTs) could, in future, not only be tailored to suit distinct immunomodulatory mechanisms, but designed to also lack antibiotic function thus removing the ever-growing issue of antibiotic resistance. The data housed within this project could also support drug repurposing of minocycline, in addition to other immunomodulatory tetracyclines for conditions with both a microbial and inflammatory basis. Exploration and identification of new applications for drugs such as minocycline that are already certified safe and in general circulation with society will ultimately allow for rapid drug development and the proposition of new therapeutic alternatives, especially in developing countries where the cost of drug development is a barrier.

Consequently, this advancement in knowledge and understanding of how minocycline directly influences macrophage function will ultimately aid those individuals that are burdened with diseases that are dominated by a dysregulated immune response such as IBD, RA and neuropathologies like MS, and thus provide relief to present and future patients.

2. Materials & methodology

All product and source details can be found in Appendix A1 unless otherwise mentioned. Drugs were obtained in powder form and prepared following manufacturer instructions. Minocycline and dexamethasone were prepared by reconstitution in dimethyl sulfoxide (DMSO) to a concentration of 50mM ready for subsequent serial dilution using RPMI 1640 prior to use in assays. Final DMSO dilutions ranged from 0.1%-0.02% when minocycline and dexamethasone were added at 10μM-50μM respectively. Dexamethasone was included as a positive control given its established use as an immunosuppressant at a final concentration of 50μM as to provide direct comparison to the top concentration of minocycline used. For THP-1 and U-937 experiments, an independent vehicle control of DMSO was included at a final dilution of 1:1000 (0.1%) which was equal to the final concentration within the top concentrations of minocycline used at 50μM (Chapter 3 and 4), and then later at 25μM (DMSO at 0.05% final dilution) (Chapter 5 and 6). During all experimentation with peripheral blood mononuclear cells (PBMCs), DMSO was incorporated at the same final concentration of 1:1000 in all conditions to equalise the DMSO concentration across all samples. This was done due to limited cellular material available and thus inability to include an independent DMSO vehicle control. In the PBMC experiments both minocycline at 50μM, and dexamethasone were not tested, again due to limited cellular material and prior identification of cellular toxicity of minocycline at this concentration.

When selecting the drug concentrations used in this study is important to note that the concentration of a compound cells are exposed to *in vivo* depends on factors such as the pharmacokinetic and pharmacodynamic properties of the compound, whereas under *in vitro* conditions, drug concentration is considered constant (Checkley et al., 2015). Therefore, direct comparisons can be difficult to make meaning selection of concentrations to use for *in vitro* assays are often determined empirically. The recommended dose of minocycline in adults is 100-200 milligrams (mg) which may be divided into multiple doses in a 24-hour period, with no more than 400mg per day to be prescribed. In children the dose is calculated based on body weight with an initial dose usually 4mg per kilogram (kg) of body weight followed by 2 mg/kg every 12 hours but with the maximal dose equating to no more than an adult (Minocycline Advanced Patient

Information, 2022; Minocycline Dosage (Dynacin, Minocin), 2022). In contrast dexamethasone is advised to be dosed between 0.5-9mg per day if being used as an immunosuppressant or anti-inflammatory agent (Dexamethasone Dosage Guide + Max Dose, Adjustments, 2021). Conversely, in experimental models of colitis minocycline is often reported to be administered between 20 and 50 mg/kg, likely due to the differences in metabolism and pharmacokinetics in small rodent models (Huang et al., 2009; Garrido-Mesa, Camuesco, et al., 2011; Garrido-Mesa, Utrilla, et al., 2011; Garrido-Mesa et al., 2018). Loosely converted to molarity minocycline would therefore be approximately 200-400μM/mL, while dexamethasone is much lower around 0.1-20μM/mL. When consulted, the literature displayed many reports of minocycline being used at a wide range of concentrations between 0.2-40μM (0.1μg/mL-0.4mg/mL) in *in vitro* assays (Smith-Norowitz et al., 2002; Kalish and Koujak, 2004; Tai et al., 2013; Garrido-Mesa et al., 2015; Sun et al., 2020), while dexamethasone is generally lower between 0.01-10μM when used for immortalized cell lines (Sporstøl et al., 2007; Kim et al., 2017), but comparatively higher when used on primary cells such as PBMCs between 1nM-1mM (De et al., 2002; Falchi et al., 2015; de Almeida et al., 2019). With all evidence considered it was decided to use minocycline at 3 ascending concentrations, 10μM, 25μM and 50μM which both allowed for comparisons with previous *in vitro* data and remained below usual therapeutic dosing. For dexamethasone 50uM was selected to guarantee an effect in both immortalised cell lines and primary cells even though this exceeded usual dose recommendations. From these concentrations it would be possible to understand any effect of minocycline administered at a sub-optimal dose in the context of a well-known immunosuppressant administered to excess which may allow for more robust conclusions to be drawn.

Lipopolysaccharides from *Escherichia coli* O55:B5 (LPS) was obtained in powder form and reconstituted in RPMI 1640 at 1mg/mL ready for later dilution using RPMI 1640 to working concentrations of 100ng/mL or 10ng/mL as indicated. LPS is a component of the cell wall of the gram-negative bacteria, E. coli which induces an immune response and promotes the secretion of pro-inflammatory cytokines (Maldonado, Sá-Correia and Valvano, 2016; Liu et al., 2018). LPS O55:B5 has been derived from a serotype of E. coli O55:B5, which is part of a subdivision based on its O-antigen component often regarded as the virulence factor (Orskov and Orskov, 1992). This serotype was selected in part due to its

reported absence from a healthy biome, but also given the work conducted within this thesis aimed to study innate immune responses *in vitro* and as such LPS-serotype was not important considering serotype is defined by surface antigen and therefore would be more relevant for *in vivo* experimentation or if using co-culture systems (Fratamico et al., 2016). Phorbol 12-myristate 13-acetate (PMA) was obtained in powder form and reconstituted to 1mg/mL in DMSO and aliquoted for later use. All reconstituted aliquots were stored at -20°c and protected from light.

2.1. *In vitro* cell culture and macrophage differentiation

2.1.1. THP-1 & U-937 cell lines

THP-1 (human monocytes derived from acute monocytic leukaemia) and U-937 (human monocytes derived from histiocytic lymphoma) cell lines were obtained from frozen aliquots provided by colleagues both at the University of East London (UK) and University of Roehampton (UK). Cells had been tested for mycoplasma contamination prior to acquisition and long-term storage in liquid nitrogen. Unless otherwise stated all cells were cultured in RPMI 1640 cell culture media formulated with L-glutamine and no HEPES, and externally supplemented with 10% heat deactivated foetal bovine serum (FBS) – hereto referred to as complete media. Parallel cultures were also maintained in the same media externally supplemented with additional 1% penicillin and streptomycin in case of contamination to main cultures. If required to be used, these cells were removed from antibiotic-supplemented media and further cultured in antibiotic-free complete media for at least 1 passage cycle prior to use. This was employed to ensure minocycline was the only antibiotic agent present in the experimental cultures as to not interfere with any biological function of minocycline. Cell lines were maintained in accordance with American Type Culture Collection (ATCC) guidance, and stored in 5% CO_2 humidity at 37°c. For experimentation, cells were utilised between passages 5 and 25, at which time cultures were discarded and a new aliquot was thawed. To validate the cultures, cells were first checked for homogeneity and consistency regarding forward and side scatter profiles before being characterized via multicolour flow cytometry by assessing the surface marker expression of CD14 and CD11b. This was conducted following thawing of new aliquots, and within every flow cytometry experiment to allow consistent monitoring of cultures.

For differentiation to macrophages, on day 1 cells were plated at a density of $8x10^5$cells/mL in 24 well plates in 500µL complete media (antibiotic-free) – a final total of $4x10^5$ cells/well. PMA at 80nM was added to each well, and plates were left to incubate at 37°c and 5% CO_2 humidity for 48hr. All experimental parameters inclusive of seeding density, well size, PMA concentration and incubation times were pre-optimized based on review of the literature (data shown in chapter 3.1.1). On day 3, supernatant containing PMA and un-differentiated non-adherent cells were carefully aspirated and discarded, and wells were replenished with 500µL fresh complete media. Plates were returned to the incubator for a further 72hr to allow for macrophage maturation, and on day 6 differentiated macrophages were ready for collection or further experimentation. Cell morphology, plate adhesion, clustering and elongation was first assessed via captured images using the EVOS™ XL transmitted light digital inverted microscope (AMG – Advanced Microscopy Group, USA). Cell purity and assessment of successful differentiation was then characterised via multicolour flow cytometry by evaluating the surface marker expression of CD14 and CD86. As before, this characterisation was checked within all flow cytometry analysis to ensure homogeneity and reproducibility.

2.1.2. Peripheral blood mononuclear cells

PBMCs were obtained from 4 consenting donors at Queen Mary University London (UK) as a kind gift from Dr Jose Garrido Mesa and colleagues. To comply with all Human Tissue Act (HTA) regulations and ethics, cells were not personally handled or used until PBMCs were terminally differentiated into macrophages and no longer within the confines of ethical or HTA licensing. To summarize how the macrophages were generated the following protocol was used. Venous blood was collected with 10% v/v sodium citrate to avoid clotting and spun at 240xg for 20min. Most of the platelet-rich plasma was then discarded and replaced with an equal volume of RMPI 1640 media. The blood was carefully layered into tubes containing Histopaque 1119 and Histopaque 1077 and spun at 400xg for 30min. PBMCs were collected and transferred to a separate tube and washed with sterile phosphate buffered saline (PBS). Red blood cells were lysed by adding ice cold ultrapure water and gently pipetting for 30sec, before the addition of 3.6% NaCl to recover the osmotic balance. Samples were spun at 350xg for 10min. Isolated PBMCs were finally plated at $2x10^5$ cells per 10cm plate in 10mL RPMI 1640

containing 20% FBS and human M-CSF (hM-CSF) at 50ng/mL, with 20% FBS utilized for increased nutrient support throughout the differentiation process. Cells were kept in the incubator at 37°c and 5% CO_2 humidity for 6 days to differentiate. On day 3 or 4, 5mL of media was removed and discarded from each plate with care taken not to disturb the cells attached at the bottom, and each plate was refreshed with 5mL of RPMI 1640 + 20% FBS + hM-CSF (50ng/mL). Plates were returned to the incubator until day 6. On day 6, all culture media was gentle aspirated and kept to one side while the differentiated macrophages were collected via the addition of Accutase® for 10min. Cells were then washed twice using sterile PBS, before being re-plated in the same aspirated media at $2.5x10^4$ cells/well in 96 well plates and returned to the incubator for 24hr ready to begin experimentation on day 7. On day 6, an aliquot of cells was taken for differentiation characterisation via multicolour flow cytometry. Here, cells were assessed for upregulation of surface markers CD14, CD16, CD11b and CD86, in addition to visual assessment of cellular morphology.

Experiments were conducted in 96 well plates for flow cytometric analysis and cytokine determination to keep well volume low and subsequently maintain high cytokine concentration for downstream detection. To provide enough or sufficient cellular material for genetic analysis, cells were plated at $4.5x10^5$ cells/well in 6 well plates but followed the same experimental protocols in preparation for downstream lysis and RNA isolation.

2.2. Experimental design

2.2.1. Effect of minocycline on THP-1 & U-937 PMA-induced macrophage differentiation

When studying the effect of minocycline on PMA-induced differentiation (Figure 2.1), monocyte cultures were pre-treated with minocycline at 10μM, 25μM or 50μM, dexamethasone at 50μM, or DMSO at a final concentration of 1:1000 for 2hr prior to the addition of 80nM PMA. PMA concentration was determined by optimisation experiments which were conducted and outlined in chapter 3 section 3.1.1. Cells were incubated for a further 48hr, at which time supernatant was removed and discarded alongside the un-differentiated non-adherent cells before wells were replenished with fresh complete media for the final 72hr incubation. An untreated PMA-only control was included, in addition to undifferentiated monocytes to provide intra-experimental proof of differentiation. For analysis on

day 6, first, images were captured from a representative well for each condition using the system outlined in section 2.1.1. to allow for morphological comparison. Next, supernatant was aspirated and stored at -70°c for future cytokine determination using enzyme-linked immunosorbent assays (ELISA). Next, 500µL of ice-cold PBS was added to each well and the adherent macrophages were detached via gentle scraping with a sterile 1mL syringe plunger. Cells were collected and stored for downstream viability and surface marker analysis using multicolour flow cytometry, or genetic analysis using RT-qPCR. An aliquot of cells from each well were also retained to calculate absolute cell counts using a light microscope, haemocytometer, and trypan blue.

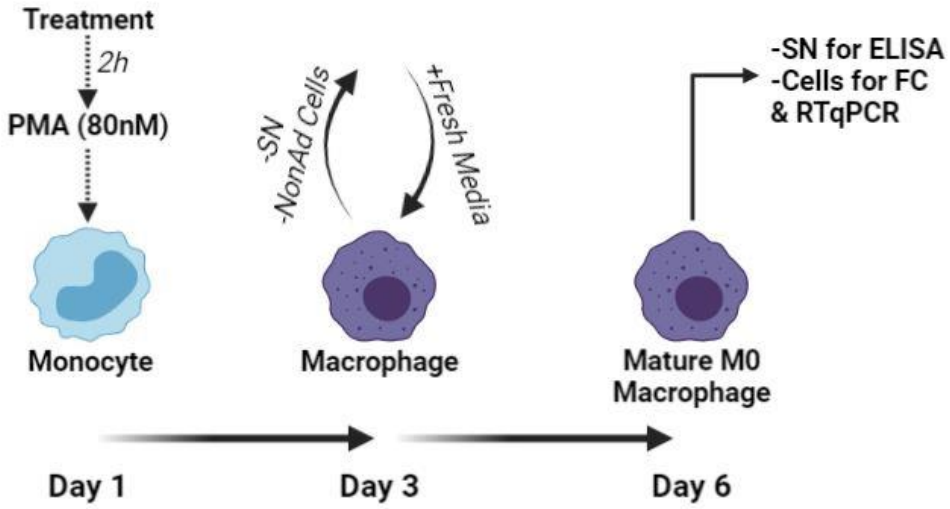

Figure 2.1: Schematic representation of the standard protocol followed to study the effect of minocycline on PMA-induced differentiation of THP-1 and U-937 monocytes. The designation of 'treatment' refers to minocycline (MINO) at 10µM, 25µM or 50µM, dexamethasone (DEX) at 50µM, or DMSO at a final concentration of 1:1000. PMA = phorbol 12-myristate 13-acetate; SN = supernatant; NonAd cells = non-adherent cells; ELISA = enzyme-linked immunosorbent assay; FC = Flow cytometry; RTqPCR = reverse transcriptase quantitative polymerase chain reaction.

2.2.2. Effect of minocycline on LPS-induced macrophage activation

2.2.2.1. THP-1 & U-937

To generate 'activated' macrophages, first, monocytes were differentiated into 'resting' M0 macrophages following the protocol outlined in section 2.1.1. Once fully transformed at the completion of the differentiation protocol on day 6, LPS at 100ng/mL was added to each well and plates were returned to the incubator

for a further 24hr. This concentration of LPS was frequently used in the literature (Bode, Ehlting and Häussinger, 2012; Ti *et al.*, 2015; Liu *et al.*, 2020). After 24hr (day 7), supernatants were aspirated and stored at -70°c for future cytokine determination by ELISA, and cells were collected following the same procedure outlined in section 2.2.1. ready for flow cytometric or RT-qPCR analysis.

To study the effect of minocycline on LPS-induced activation of M0 macrophage populations, mature M0 macrophages were pre-treated with minocycline at 10μM, 25μM or 50μM, dexamethasone at 50μM, or DMSO at a final concentration of 1:1000 for 2hr prior to the addition of LPS at 100ng/mL. Three independent control wells were included; one containing LPS only to assess the effect of each pre-treatment, one untreated M0 macrophage to characterize activated populations, and an un-differentiated monocyte sample taken from culture for continued determination of successful monocyte-macrophage differentiation. Cultures were returned to the incubator for a further 24hr, whereby on day 7, supernatants were collected and stored at -70°c for future cytokine determination, and cells were processed as outlined in section 2.1.1 above. This protocol is depicted below in Figure 2.2.

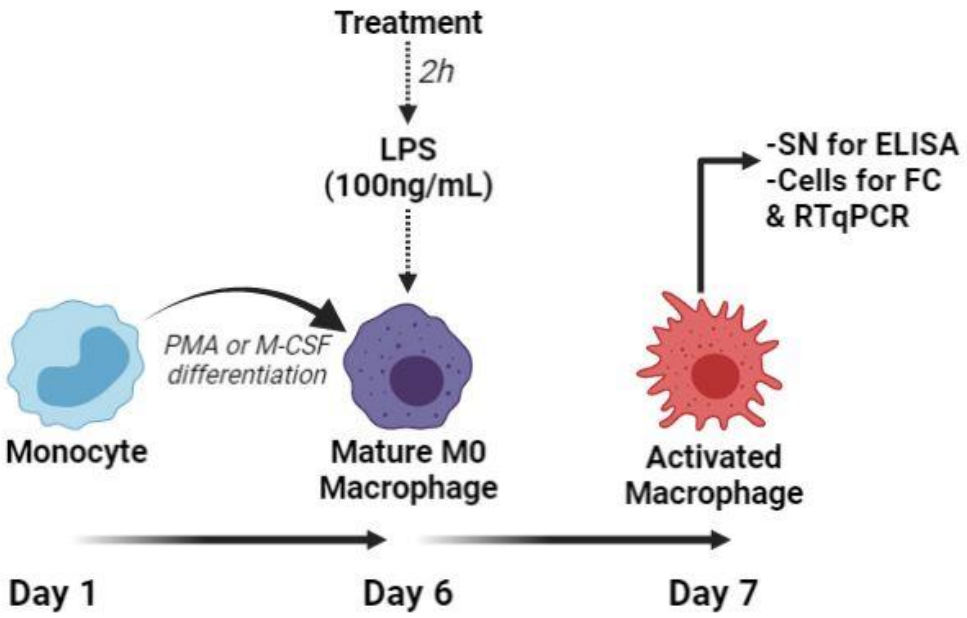

Figure 2.2: Schematic representation of the standard protocol followed to study the effect of minocycline on LPS-induced activation of M0 macrophages. The designation of 'treatment' refers to minocycline (MINO) at 10μM, 25μM or 50μM, dexamethasone (DEX) at 50μM, or DMSO at a final concentration of 1:1000. PMA = phorbol 12-myristate 13-acetate; M-CSF = macrophage colony stimulating factor; LPS = lipopolysaccharides from *Escherichia coli* O55:B5; SN =

supernatant; ELISA = enzyme-linked immunosorbent assay; FC = Flow cytometry; RTqPCR = reverse transcriptase quantitative polymerase chain reaction.

2.2.2.2. PBMC-derived macrophages

To assess LPS-activation of PBMC-derived macrophages, PBMC's were first differentiated to mature 'resting' M0 macrophages following the 7-day protocol outlined in section 2.1.2. M0 macrophages were pre-treated for 2h with minocycline at 10μM or 25μM, before the administration of LPS at 100ng/mL for a further 24hr. In this instance all wells contained DMSO at a final dilution of 1:1000 to normalise the vehicle exposure across all treatments. An untreated M0, and LPS-only control was also included. On day 8, supernatant was removed and stored at -70°c for future cytokine determination, and cells were detached via incubation with Accutase® for 10 minutes at room temperature, before being washed twice with sterile PBS and collected for surface marker analysis via flow cytometry and gene analysis using RT-qPCR.

2.2.3. Effect of minocycline on cytokine-induced macrophage polarization

To polarize 'resting' M0 macrophages to distinct M1 and M2 populations, macrophages were first generated following protocols previously outlined in sections 2.1.1. and 2.1.2. for THP-1 and PBMCs respectively. Once differentiated, M0 macrophages were treated with IFN-γ (20ng/mL) + LPS (10ng/mL) for M1 macrophage polarization, or IL-4 (20ng/mL) for M2 macrophage polarization. Agents and concentrations were determined from literary review (Genin *et al.*, 2015; Bertani, Mozetic, Fioramonti, Luliani, *et al.*, 2017). Plates were incubated at 37°c at 5% humidity for 24hr, at which point supernatant was aspirated and stored for cytokine determination, and cells were collected following the relevant collection procedures highlighted in sections 2.1.1. and 2.1.2. ready for flow cytometric and RT-qPCR analysis.

Then, to study the effect of minocycline on macrophage polarization (Figure 2.3.), cultures were pre-treated with minocycline at 10μM or 25μM, for 2hr before the addition of the polarizing agents. Macrophage cultures were returned to the incubator for 24hr, at which time supernatant and cells were again collected and processed for ELISA, flow cytometry and RT-qPCR as described before. For all experiments an unpolarized M0 control was included, in addition to an untreated M1 or M2 polarized control. For the PBMC experiments DMSO was again

included in all conditions at a final concentration of 1:1000. For THP-1 an individual DMSO control was included.

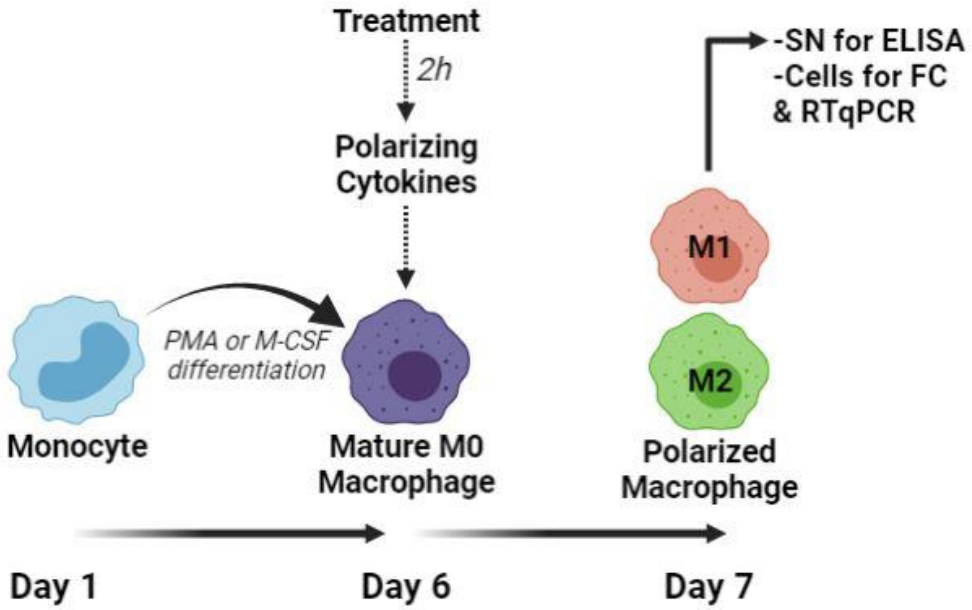

Figure 2.3: Schematic representation of the standard protocol followed to study the effect of minocycline on M1/M2 macrophage polarisation. The designation of 'treatment' refers to minocycline at 10μM or 25μM, or DMSO at a final concentration of 1:1000 (THP-1 only. The designation 'polarising cytokines' refers to interferon gamma (IFN-γ) (20ng/mL) + lipopolysaccharides from *Escherichia coli* O55:B5 (LPS) (10ng/mL) for M1 polarisation, or interleukin 4 (IL-4) (20ng/mL) for M2 polarisation. PMA = phorbol 12-myristate 13-acetate; M-CSF = macrophage colony stimulating factor; SN = supernatant; ELISA = enzyme-linked immunosorbent assay; FC = Flow cytometry; RTqPCR = reverse transcriptase quantitative polymerase chain reaction.SN = supernatant; ELISA = enzyme-linked immunosorbent assay; FC = Flow cytometry; RTqPCR = reverse transcriptase quantitative polymerase chain reaction.

2.2.4. Effect of minocycline on LPS-induced M1/M2 macrophage activation

To assess the effect of LPS-activation of M1 and M2 polarized macrophages and the subsequent influence of minocycline upon this, THP-1 and PBMC-derived macrophages were first generated as described before (sections 2.1.1. and 2.1.2. respectively), and M0 cultures were then polarised to M1 or M2 subsets following a 24h incubation with IFN-γ (20ng/mL) + LPS (10ng/mL) for M1, or IL-4 (20ng/mL) for M2 as outlined in section 2.2.3. After 24hr, supernatant was gently removed and discarded, and cultures were replenished with 500μL fresh complete media. LPS at 100ng/mL was then added to each well, and plates were again returned to the incubator for a further 24hr, at which point supernatant and cells were

collected for ELISA, flow cytometry and RT-qPCR following the previously outlined procedures.

To assess the effect of minocycline upon this process (Figure 2.4.), the polarized macrophages were pre-treated with minocycline at 10μM or 25μM for 2hr prior to the addition of LPS at 100ng/mL. Cultures were returned to the incubator for a further 24hr after which they were processed as previously described. Here, an LPS only control was included, in addition to a non-activated sample for each phenotype. For THP-1 a separate vehicle control was included, and for PBMC DMSO was administered to all conditions at a final concentration of 1:1000.

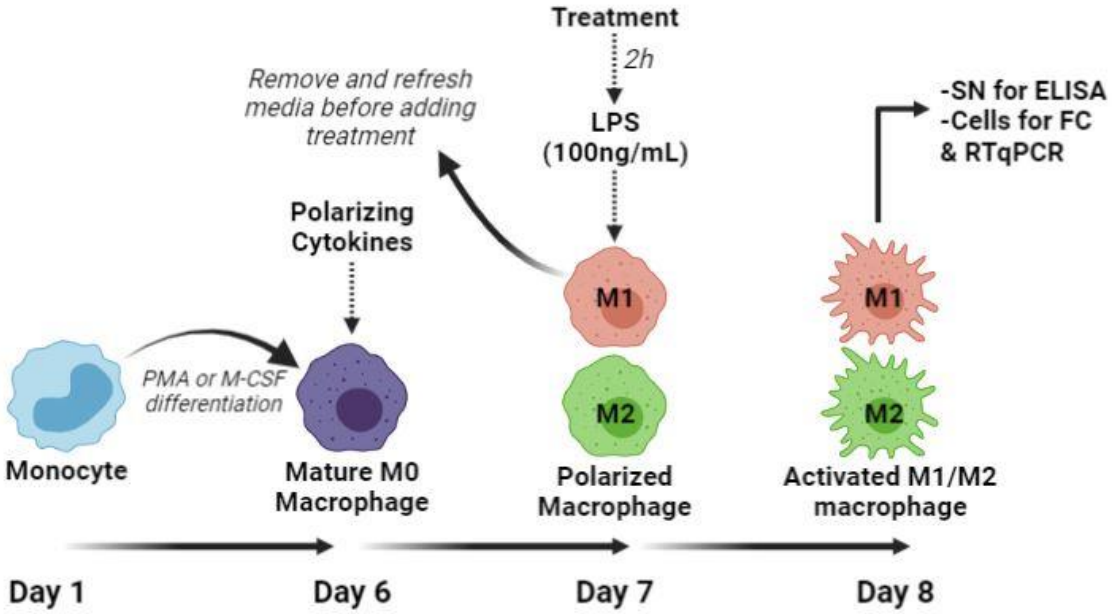

Figure 2.4: Schematic representation of the standard protocol followed to study the effect of minocycline on LPS-induced activation of M1/M2 macrophage subsets. The designation of 'treatment' refers to MINO (10μM and 25μM) and DMSO (1:1000). The designation 'polarising cytokines' refers to interferon gamma (IFN-γ) (20ng/mL) + lipopolysaccharides from *Escherichia coli* O55:B5 (LPS) (10ng/mL) for M1 polarisation, or interleukin 4 (IL-4) (20ng/mL) for M2 polarisation. PMA = phorbol 12-myristate 13-acetate; M-CSF = macrophage colony stimulating factor; SN = supernatant; ELISA = enzyme-linked immunosorbent assay; FC = Flow cytometry; RTqPCR = reverse transcriptase quantitative polymerase chain reaction.SN = supernatant; ELISA = enzyme-linked immunosorbent assay; FC = Flow cytometry; RTqPCR = reverse transcriptase quantitative polymerase chain reaction.

2.3. Multicolour flow cytometry

2.3.1. Cell collection & staining

At the completion of each experimental protocol, cells were collected as previously outlined, stained, and analysed by multicolour flow cytometry. For cell staining, cells were first pelleted via centrifugation at 400xg for 5min, resuspended in 100µL 1X PBS containing Zombie Aqua™ Fixable Viability stain (1:200) and kept in the dark for 15min at 4°c. Cells were then pelleted again following the same centrifugation step, washed with 200µL 1X PBS, re-pelleted, and resuspended in 100µL staining buffer containing (1X PBS + 2% FBS) and Human TruStain FcX™ (1:100). This was left to incubate in the dark for 10min at 4°c. Samples were again pelleted and washed with staining buffer, before incubation with a surface staining antibody cocktail as detailed in Table 2.1. below. Cell pellets were resuspended in 100µL staining buffer, and antibodies were added directly into each well at a final dilution of 1:100. Samples were left to incubate in the dark for 30min at 4°c, at which time cells were pelleted and washed 3 times using cell staining buffer before a final resuspension in 300µL staining buffer. Individual FMO (fluorescence minus 1) controls were included for each fluorochrome used, following the same staining procedure.

	Laser	**Violet (405nm)**			**Blue (488nm)**		**Yellow/Green (561nm)**	
	Fluorochrome	*BV650*	*BV711*	*BV785*	*FITC*	*PerCP-cy™5.5*	*PE*	*PE-Cy™7*
THP-1 U-937	**Antibody**	Anti-CD80	Anti-CD163	Anti-CD206	Anti-CD14	-	Anti-CD86	Anti-CD11b
	Isotype	Mouse IgG1, κ	Mouse IgG1, κ	Mouse IgG1, κ	Mouse IgG1, κ	-	Mouse IgG1, κ	Mouse IgG1, κ
	Clone	2D10	GHI/61	15-2	63D3	-	BU63	CBRM1/5
	Stock Concentration	100pg/mL	200µg/mL	100µg/mL	400µg/mL	-	50µg/mL	400µg/mL
PBMCs	**Antibody**	Anti-CD80	Anti-CD163	Anti-CD11b	Anti-CD14	Anti-CD206	Anti-CD86	-
	Isotype	Mouse IgG1, κ	Mouse IgG1, κ	Mouse IgG1, κ	Mouse IgG1, κ	Mouse IgG1, κ	Mouse IgG1, κ	-
	Clone	2D10	GHI/61	ICRF44	63D3	15-2	BU63	-
	Stock Concentration	100pg/mL	200µg/mL	100µg/mL	400µg/mL	400µg/mL	50µg/mL	-

Table 2.1: Flow cytometry antibody panels.

2.3.2. Flow cytometry analysis gating strategy

Samples were acquired using a BD FACSCelesta™ flow cytometer (Beckton, Dickinson & Company, USA) with a 3-laser configuration, and data was analysed using the FlowJo™ LLC software (Beckton, Dickinson & Company, USA). The gating strategy followed is illustrated below in Figure 2.5. First, all acquired cells were selected based on FSC and SSC properties relating to cellular size and granularity before the exclusion of duplets. Next, live cells were selected based on negative fluorescence of the viability marker used. From here, all subsequent surface marker analysis was performed on this live, single-cell population. Data was expressed as a percentage (%) of the parent population, or as the density of expression presented as mean fluorescence intensity (MFI).

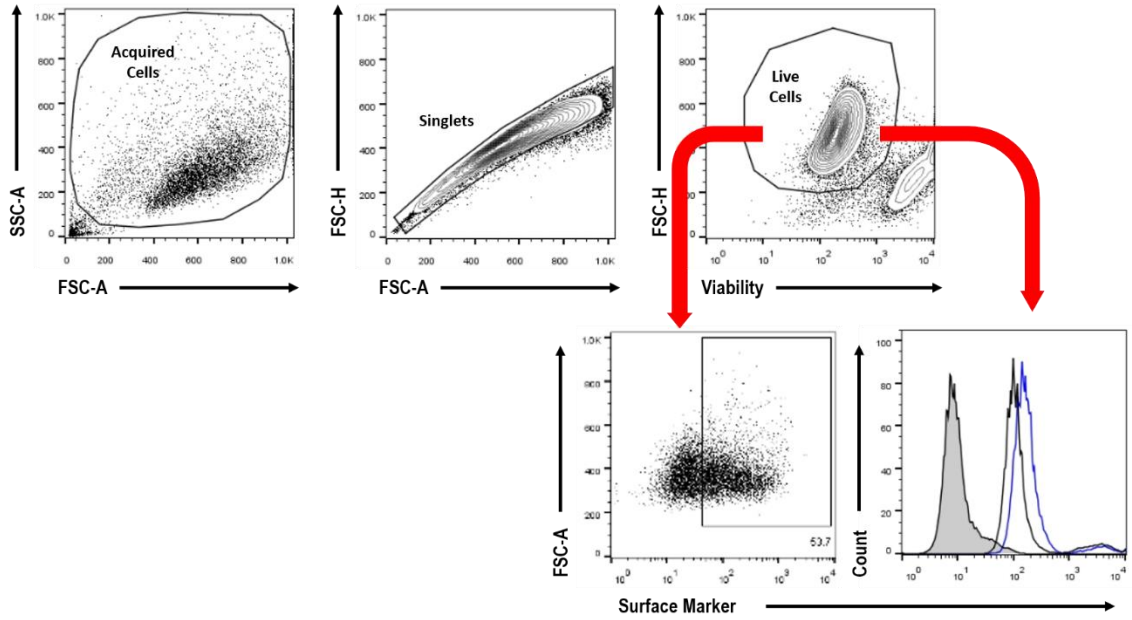

Figure 2.5: Representative gating strategy used for all flow cytometry data analysis. Cells are sequentially isolated by size and granularity, excluded for duplets, , and those negative for the viability dye – live cells (left to right). All subsequent analysis was performed on this defined live, singlet cell population.

2.4. Cytokine production determination

2.4.1. Multiplex assay

To obtain a preliminary cytokine production profile a 13-plex LEGENDplex™ (Biolegend®, UK) assay was performed which included the analytes indicated below in Table 2.2. The assay uses beads that can be differentiated by size and fluorescence intensities, with each bead set conjugated with a specific antibody. These then serve as the capture beads for a particular analyte. Since the beads are differentiated by size (forward versus side scatter) and PE fluorescence intensity via flow cytometry, analyte-specific populations can then be segregated and fluorescent signal quantified. The concentration of each analyte is then determined using a standard curve generated within the same assay.

Cytokine	M1 Macrophage	M2 Macrophage
IL-10		✓
IL-6	✓	✓
IL-4		✓
IL-1RA		✓
IL-23	✓	
IL-1β	✓	
IL-12p40	✓	
IL-12p70	✓	
IP-10 (CXCL10)	✓	
TNF-α	✓	
IFN-y	✓	
TARC (CCL17)		✓
Arginase		✓

Table 2.2: Target cytokines included in the 13-plex human macrophage/microglia LEGENDplex™ panel.

The assay was performed following the manufacturer protocol without alteration. Briefly, collected, and stored supernatants were thawed on ice, spun at 400xg for 5min to pellet cellular material. Once prepared 25µL of each experimental supernatant or the supplied standards were added to each of the wells within a 96-well, V bottom plate, in parallel to the supplied assay buffer and conjugated beads. Each bead set served as the capture antibody for each of the 13 analytes. This was left to incubate for 2hr in the dark at room temperature with continuous shaking at 800rpm on an orbital shaker (all subsequent shaking was performed at this speed). After 2hr the plate was spun at 300xg for 5min, the supernatant was discarded, and bead pellet washed with 200µL/well of supplied wash buffer. Bead pellets were then resuspended in 25µL/well of supplied detection

antibodies, and left to incubate at room temperature, in the dark for 1hr with continuous shaking. After 1hr, 25µL/well of Streptavidin-phycoerythrin (SA-PE) was added and returned to the shaker for 30min in the dark at room temperature. The plate was then spun to pellet the beads, washed with 200µL/well of supplied wash buffer before a final centrifugation and resuspension in 150µL/well wash buffer. Samples were analysed using the BD LSRFortessa™ flow cytometer (Beckton, Dickinson & Company, USA). The concentration of each analyte was determined using the LEGENDplex™ Data Analysis Software (Version 8) provided. Figure 2.6. below outlines the gating strategy followed to analyse the multiplex data. First, each of the 2 bead sets were gated, before each individual target bead population was identified using the APC versus PE scatter plots automatically by the software.

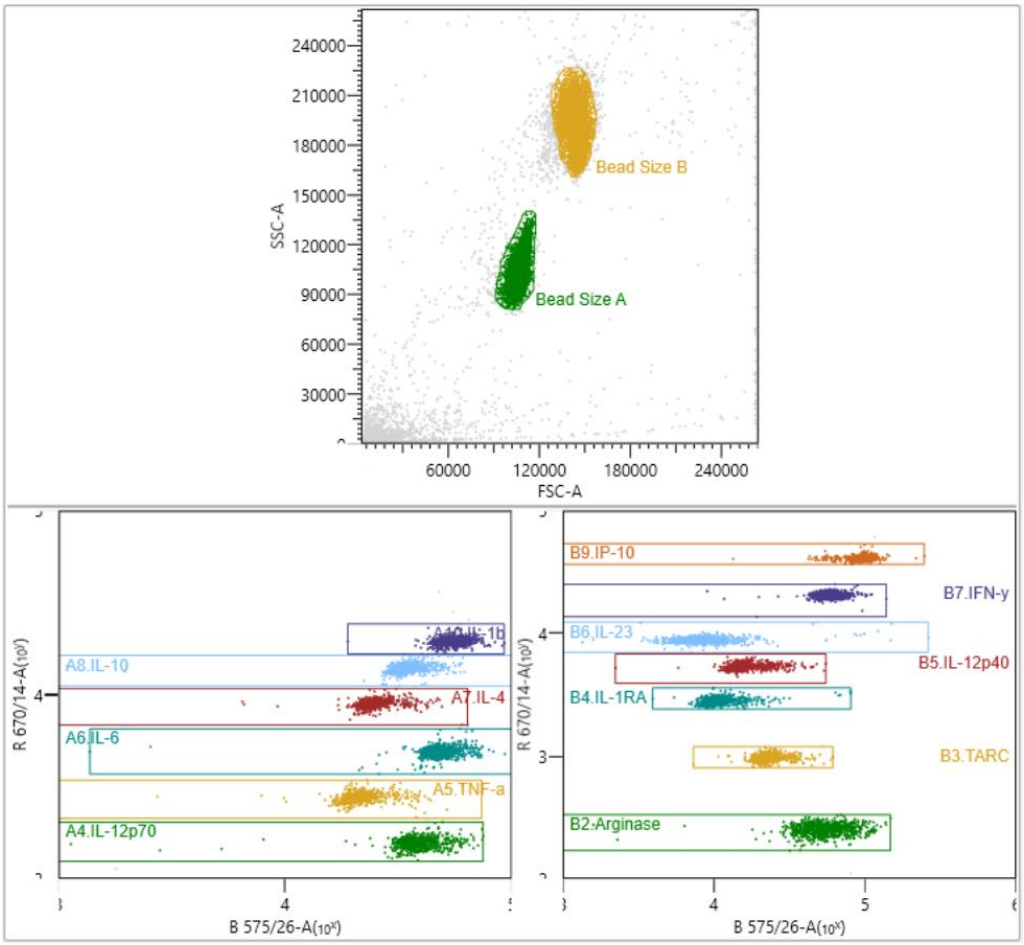

Figure 2.6: LEGENDplex™ gating strategy using the LEGENDplex™ Data Analysis Software (Version 8). Forward and side scatter parameters are used to first identify A and B bead populations. All 13 sub-populations are then gated based on their PE versus APC fluorescence to define each analyte within the A and B bead clusters. From here subsequent standard curves can be generated by the software using plated standards, of which unknown sample cytokine concentrations can be determined.

The internal standard curves were then applied and used to determine cytokine concentration within the 'unknown' experimental samples. As this assay served as a preliminary screen for cytokine selection for downstream validation, only 2 PBMC donor samples were included in the assay, in addition to 2 different THP-1 experiments. This was due to only having 1 96-well plate worth of reagents within the kit. The cytokines deemed necessary for corroboration based on the preliminary data from the multiplex assay were validated using an ELISA in which all biological replicates were measured.

2.4.2. Sandwich enzyme-linked immunosorbent assay (ELISA)

Collected and stored supernatant samples were thawed on ice and spun at 400xg for 5min. The concentration of the cytokines IL-10, IL-4, IL-12(p70), IL-12/IL-23(p40) and IFN-γ was then measured using the human ELISA MAX™ Deluxe Sets from Biolegend® (UK), while TNF-α, IL-1β and IL-6 concentrations were determined using the human uncoated ELISA kits from Thermo Fisher Scientific (UK). Cytokine concentration was assessed following manufacturer instructions. Briefly, Nunc Immuno Maxisorp 96-well plates were coated with capture antibody (1X) diluted in coating buffer and left to incubate overnight at 4°c. On day 2, plates were washed 4 times with wash buffer (1X PBS + 0.05% Tween®-20), before standards and experimental supernatant was added and left to incubate with shaking for 2hr at room temperature. Standards were diluted according to manufacturer instructions. Assay diluent was included as the negative control. Experimental supernatant was diluted to fall within the detection range of each assay used as indicated in Tables 2.3 and 2.4 below and was estimated based on the preliminary raw data obtained from the multiplex assay.

ELISA	Concentration Range (pg/mL)	THP-1 Supernatant Dilution		
		M0 + LPS	M1 + LPS	M1 Pol
IL-10	3.9-250	ND	ND	ND
IL-4	3.9-250	ND	ND	ND
IFN-γ	7.8-500	ND	1:20	1:20
TNF-α	4-500	ND	ND	ND
IL-6	2-200	1:10	1:20	1:20
IL-1β	2-150	ND	1:2	1:2
IL-12p40	62.5-4000	ND	ND	ND
IL-12p70	15.6-1000	ND	ND	ND

Table 2.3: THP-1 supernatant dilutions for enzyme-linked immunosorbent assay cytokine determination. ND = no dilution; M0 + LPS = supernatant samples from: M0 macrophage + LPS (100ng/mL); M1 + LPS = M1 polarized macrophage + LPS (100ng/mL); M1 Pol = M1 macrophage polarization.

ELISA	Concentration Range (pg/mL)	PBMC Supernatant Dilution				
		M0 + LPS	M1 + LPS	M2 + LPS	M1 Pol	M2 Pol
IL-10	3.9-250	1:20	ND	1:40	1:20	ND
IL-4	3.9-250	ND	ND	1:5	ND	1:300
IFN-γ	7.8-500	ND	ND	ND	1:10	ND
TNF-α	4-500	1:50	1:10	1:50	1:50	ND
IL-6	2-200	1:200	1:100	1:200	1:200	ND
IL-1β	2-150	ND	ND	1:5	1:5	ND
IL-12p40	62.5-4000	ND	ND	ND	ND	ND
IL-12p70	15.6-1000	ND	ND	ND	1:5	ND

Table 2.4: PBMC supernatant dilutions for enzyme-linked immunosorbent assay cytokine determination. ND = no dilution; M0 + LPS = supernatant samples from: M0 macrophage + LPS (100ng/mL); M1 + LPS = M1 polarized macrophage + LPS (100ng/mL); M2 + LPS = M2 polarized macrophage + LPs (100ng/mL); M1 Pol = M1 macrophage polarization; M2 Pol = M2 macrophage polarization.

Plates were washed 4 times with wash buffer and incubated with 1X detection antibody for a further 1hr at room temperature. Plates were washed 4 times before a final incubation with 1X Avidin-HRP for 30min at room temperature with shaking. Wells were washed 5 times before incubation with 3,3′,5,5′-Tetramethylbenzidine TMB substrate (1:1 solution of substrate A and B) for 15-30min in the dark. The reaction was then stopped with the addition of stop

solution (for Biolegend® assays) or 2N H_2SO_4 (for Invitrogen assays) and the absorbance was read at 450nm and 570nm using the Synergy HTX multi-mode reader (Agilent, BioTek, UK) running the Gen5 software. Experimental samples were run in duplicate, and unknown concentrations were determined through comparison with the generated standard curve within each assay. The absorbance of the unknown samples was then used to calculate the cytokine concentration based on the known absorbance and concentration values of the standards.

2.5. Evaluation of gene expression

2.5.1. RNA extraction

For the analysis of gene expression, cells were collected using the same procedures previously detailed in sections 2.1.1. and 2.1.2. for THP-1 and PBMCs respectively and stored in Monarch DNA/RNA Protection Reagent at -70°c until needed. Samples were then thawed on ice and total RNA was isolated using the Monarch Total RNA Miniprep Kit according to manufacturer's instructions. Briefly, cells were lysed via addition of an equal volume of RNA lysis buffer (500µL) and the sample was transferred to a gDNA removal column fitted with a collection tube. Samples were spun at 13000rpm for 30sec (all consequent centrifugation steps were performed at the same settings) and the flow through collected. An equal volume of ≥95% ethanol was then mixed with the flow through before being transferred to an RNA purification column. Samples were spun for another 30sec. For on-column DNase 1 treatment, columns were first washed with 500µL RNA wash buffer before being spun and treated with diluted DNase 1 in DNase 1 reaction buffer. Samples were left at room temperature for 15min. Columns were washed with 500µL RNA priming buffer, spun, and washed twice with RNA wash buffer. For the final wash samples were spun for 2min. To elute the isolated RNA, 50µL of nuclease-free water was added directly onto the column matrix and spun one last time into a RNase-free microcentrifuge tube. RNA concentration was quantified using the Thermo Scientific NanoDrop™ 1000 Spectrophotometer (Thermo Fisher Scientific, USA) and stored at -70°c prior to downstream application. RNA concentrations from THP-1 samples ranged from 200-1200ng/µL, and samples were deemed 'pure' with 260/280 and 260/230 absorbance ratios above 1.8, with most samples ≥2. RNA was extracted from

PBMC donors 3 and 4, and concentrations ranged from 5-60ng/μL, with purity over 1.8 for both ratios.

2.5.2. RT-qPCR

To evaluate mRNA expression, ≤1μg of RNA was reverse transcribed into cDNA using the LunaScript® RT SuperMix Kit according to manufacturer's instructions, assuming a 1:1 conversion of RNA - cDNA. Samples were generated using the Bio-Rad T100™ Thermal Cycler (UK). Real-time quantitative polymerase chain reaction (RT-qPCR) amplification and detection was then performed using the AriaMX Real-time PCR System (Agilent, USA) and their specified optical-grade tube strips. Each reaction was composed of 1ng cDNA, 4μL Luna® Universal qPCR Master Mix, 10μM specific forward and reverse KicqStart® SYBR® Green Primer, and nuclease-free water for a final reaction volume of 20μL. The exact primer sequences and thermocycling protocol are detailed below in Tables 2.5. and 2.6. respectively.

Gene	Annealing T (°c)	Sequence (5'-3')	
Beta-actin	60	Fw	GACGACATGGAGAAAATCTG
		Rv	ACCCAATCCAGATGTCTATG
TLR4	60	Fw	GATTTATCCAGGTGTGAAATCC
		Rv	TATTAAGGTAGAGAGGTGGC
SOCS3	60	Fw	CCTATTACATCTACTCCGGG
		Rv	ACTTTCTCATAGGAGTCCAG
STAT1	60	Fw	ACCCAATCCAGATGTCTATG
		Rv	GAGCCTGATTAAATCTCTGG
STAT2	60	Fw	ATATAAGATCCAGGCCAAAGG
		Rv	CAGTAGCTCGATTAGGGTAG
STAT3	60	Fw	GGTACATCATGGGCTTTATC
		Rv	TTTGCTGCTTTCACTGAATC
STAT6	60	Fw	CACAGCTTGATAGAAACTCC
		Rv	GTTTCCAAATCTGGATCCTC
IRF5	60	Fw	CTCAGCCCTACAAGATCTAC
		Rv	CTGCACCAAAAGAGTAATCC
PPARγ	60	Fw	AAAGAAGCCAACACTAAACC
		Rv	TGGTCATTTCGTTAAAGGC

Table 2.5: KicqStart® SYBR® Green Primer sequences used in real-time PCR.

Cycle Step	Temperature (°c)	Time (sec)	Cycles
Initial Denaturation	95	60	1
Denaturation	95	15	40
Extension	60	30	

Table 2.6: Thermocycling protocol used for real-time PCR analysis.

Data was analysed using the Agilent AriaMX software. Samples were run in triplicate, with a no-RT (RNA samples reverse transcribed with buffer not containing active reverse transcriptase enzyme) and no-template control (samples containing no cDNA) also included in each experiment to assess for potential contaminations. To normalise mRNA expression, the expression of the housekeeping gene *beta-actin* (*ACTB*) was measured within all samples. In addition, pre-calculated primer efficiencies using known concentrations of cDNA for each gene were incorporated into the analysis, with RNA relative quantification calculated using the Pfaffl method detailed below, where '*E*' refers to the primer efficiency, GOI to the Gene of interest and HKG to the housekeeping gene. Data was subsequently reported as gene expression ratio.

$$Gene\ expression\ ratio = \frac{(E_{GOI})^{\Delta Ct\ GOI}}{(E_{HKG})^{\Delta Ct\ HKG}}$$

2.6. Phospho-protein intracellular staining & assessment

To evaluate the activation of STAT3, phosphorylation of the tyrosine705 residue was determined by intracellular staining and flow cytometric analysis. Prior to the addition of minocycline, protocol optimization occurred to determine both optimal incubation times and LPS concentration. THP-1 cells were prepared as described in section 2.1.1., however in this instance cultures were activated with LPS at 100ng/mL or 1µg/mL for 8 different incubation durations: 30sec, 1min, 10min, 15min, 30min, 2hr, 6hr and 24hr, with or without sodium vanadate (a competitive inhibitor for protein phosphotyrosyl phosphatases) at 0.1%. At the completion of each time point the reaction was stopped by removing and discarding the supernatant and immediately fixing the cells using 300µL pre-warmed Fixation Buffer (BioLegend®). Cells were suspended by gentle pipetting and incubated for 15min at 37°c. Cells were spun at 350xg for 5min. The supernatant was then discarded, and pellets washed twice with Cell Staining Buffer (BioLegend®). With gentle vortexing, cells were then permeabilised by adding pre-chilled True-Phos™ Perm Buffer (BioLegend®) and left to incubate at -20°c overnight. Cells were spun at 500xg for 5min and resuspended in cell staining buffer.

An antibody cocktail containing human anti-STAT3 Phospho (Tyr705) (FITC) and anti-STAT3 (PE) was added to the samples and left to incubate in the dark for 30min at room temperature. Cells were finally washed twice and resuspended in cell staining buffer ready for flow cytometry analysis. Mouse IgG1, κ isotype controls conjugated with PE and FITC were included in separate tubes, in addition to an unstained sample. Samples were acquired using the BD FACSCelesta™ flow cytometer (Beckton, Dickinson & Company, USA) and analysed using the FlowJo™ LLC software (Beckton, Dickinson & Company, USA).

For analysis, a similar gating strategy was utilised as the one depicted in section 2.3.2, Figure 2.5, whereby cells were first selected based upon FSC and SSC profile, and isolated for singlets, with all subsequent analysis performed on this single cell homogenous population. No viability dye was included in these experiments. As these experiments were for preliminary selection of appropriate LPS incubation periods prior to the addition of minocycline and confirmation of assay success, samples were run in duplicate, with each experiment performed only once. This was to allow assessment of various independent variables such as time, LPS concentration and inclusion of sodium vanadate.

2.7. Data analysis

For THP-1 experimentation, all conditions were run in triplicate, and each experiment was conducted 3 times. For PBMC experiments each condition was run in duplicate using 4 independent donors. Data was analysed and represented as mean +/- SD within each individual experiment, or if biological replicates were pooled, data was presented as mean ± SEM. This is indicated within the corresponding figure legends. Differences between means were tested for significance using one-way or two-way analysis of variance (ANOVA) with the appropriate *post hoc* least significance test – Dunnett's or Bonferroni. For cell line experiments with only one variable, a one-way ANOVA was performed with *post hoc* Dunnett's versus the control. For PBMC experiments in which multiple donors are plotted together a two-way ANOVA was utilised with *post hoc* Bonferroni. All statistical analyses were performed using the Prism GraphPad software (USA), with a level of significance (alpha) of 0.05.

For presented data, all replicated experiments were pooled and shown in the main body of the thesis. Data corresponding to supplemental data can be found in the appendix and is indicated in each relevant chapter and figure legend. Figures throughout the main body of the thesis are showing a representative flow cytometry plot for each condition (corresponding to the median value within each triplicate), and histogram overlays again selected from one representative experiment displaying the matched plot frequency data.

3. Results: Effect of minocycline on monocyte-macrophage differentiation

As outlined earlier in chapter 1 section 1.3, previous reports have highlighted the increased proportion of macrophages within the colon of colitis-induced murine models when treated with minocycline (Garrido-Mesa, Rodríguez-Nogales, *et al.*, 2018b). This begins to suggest a potential role of minocycline within the differentiation process of monocytes to macrophages given that circulating monocytes are the key cell population for replenishing intestinal macrophage populations (Smythies *et al.*, 2006; Bain *et al.*, 2013). Therefore, this chapter aims to assess the effect of minocycline when added during this differentiation process using a reproducible and reliable protocol for THP-1 and U-937 monocyte-macrophage differentiation with PMA.

3.1. Characterizing PMA-induced monocyte-macrophage differentiation

3.1.1. Protocol optimization

To study the effects of minocycline on monocyte-macrophage differentiation, it was essential to establish a reproducible and reliable protocol for *in vitro* differentiation of human monocytic cell lines THP-1 and U-937 into macrophages. This protocol was also used to generate the macrophages for all subsequent experimentation with minocycline. When added to monocytic cells *in vitro* PMA drives the differentiation of monocytes to macrophages, at which point the cells change morphology - becoming granular and elongated, and transform from suspension to adherent thus affixing to the surface of the flask or culture plate (Chanput, Mes and Wichers, 2014; Starr *et al.*, 2018). The cells also alter their surface marker expression profiles, through upregulation of surface markers such as CD14 and CD11b, as well as a litany of other surface proteins such as CD80, CD86, CD13, CD11c, CD35 and TIM-3 (Zamani *et al.*, 2013; Forrester *et al.*, 2018; Schmid *et al.*, 2018). It is worth noting that assessment of CD11b expression throughout all proceeding THP-1 and U937 analysis was performed using the clone CBRM1/5. The CBRM1/5 antibody recognises the activated form of CD11b rather than total protein, which is also referred to as Mac-1, CR3 and C3biR within the literature (Zhou *et al.*, 2013). CBRM1/5 binds to an activation-specific epitope of human Mac-1 on the surface of monocytes following

stimulation with phorbol esters such as PMA but does not recognise its inactivated counterpart. Given the role of the CD11b integrin in numerous cell-cell interactions such as leukocyte activation, adhesion and migration (Ho and Springer, 1982; Solovjov, Pluskota and Plow, 2005), using the antibody CBRM1/5 allowed the assessment of minocycline on these processes.

Monocyte-macrophage differentiation using PMA is a well-documented technique (Chanput, Mes and Wichers, 2014; Gatto *et al.*, 2017), but the literature, although plentiful on this topic, is also widely varying with no universally established baseline protocol. To establish a reliable and reproducible protocol for the generation of PMA-differentiated macrophages, experiments were initially conducted which explored variables such as cell density (1-6x10^5cells/well), and PMA concentration (8-200nM). Successful generation of mature macrophages was determined first via adherent cell counts with microscopic images also captured to demonstrate morphological change and cellular adherence, then by assessing cell viability, and CD14 and CD11b surface marker expression (Camilli *et al.*, 2016; Lund *et al.*, 2016; Gatto *et al.*, 2017). This optimization work was carried out in both cell lines – THP-1 and U-937, with THP-1 data shown here in Figures 3.1 – 3.5 and the U-937 data located in Appendix A2.

The first set of experiments explored 4 different PMA titrations (8nM – 200nM) in combination with 4 different cell seeding densities (1x10^5 – 6x10^5 cells/well) in a final volume of 500µL/well using 24 well plates. 24 well plates were selected to keep subsequent cytokine concentrations high to allow for accurate detection and measurement by ELISA. This reasoning also dictated the total well volume of 500µL. This initial experiment was assessed by adherent cell counts taken after 48hr PMA treatment and 72hr resting. Figure 3.1. below shows no significant change in the total number of adherent cells when plated at 1x10^5 cells/well amongst any of the PMA titrations tested (Figure 3.1A). There were also comparatively less cells collected at the cessation of the protocol with this cell density versus the other seeding densities. Although cellular morphology changed in accordance with the literary reports, with cells elongating (Figure 3.1E), no significant change in adherence values was reported. When assessing cells seeded at 2x10^5 cells/well, PMA at 80nM resulted in the greatest number of adherent cells collected, with a significant increase in total adherent cells compared to the untreated control, increasing by an average of 400,000 cells

(p<0.0001) (Figure 3.1B). Although the other titrations also resulted in significant increases in the number of adherent cells, increasing the total by an average of 74,700, 245,000, and 220,000 cells for 8nM, 162nM and 200nM respectively, PMA at 80nM resulted in significantly greater total adherent cell numbers versus these titrations (p<0.0001). When compared with the cellular morphology characteristics (Figure 3.1F) this increase in cell total can be seen across all concentrations tested, although the elongation is comparable between variables.

Superiority of 80nM PMA was also reported in the seeding density at $4x10^5$ cells/well (Figure 3.1C and G), whereby 80nM was the only titration to exert any significant increase in total adherent cells. Here, 80nM resulted in an average of 570,000 more adherent cells versus the untreated control (p=0.0064). Meanwhile, cell morphology continued to show successful differentiation through elongation and increased confluency. The final seeding density at $6x10^5$ cells/well saw 163nM PMA as the only concentration to elicit a change in total number of adherent cells, with an increase of 390,000 cells versus the untreated control (p=0.0041) (Figure 3.1D). 163nM also increased the total number of adherent cells significantly more than 80nM, up from 415,000 to 685,000 (p=0.0474). Despite 162nM seeming to result in better clustering of the cells (Figure 3.1H) versus the other conditions, at this seeding density many more cells were becoming adherent in the untreated well, and in general total number of cells recovered were similar to those at $4x10^5$ cells/well (Figure 3.1C and D).

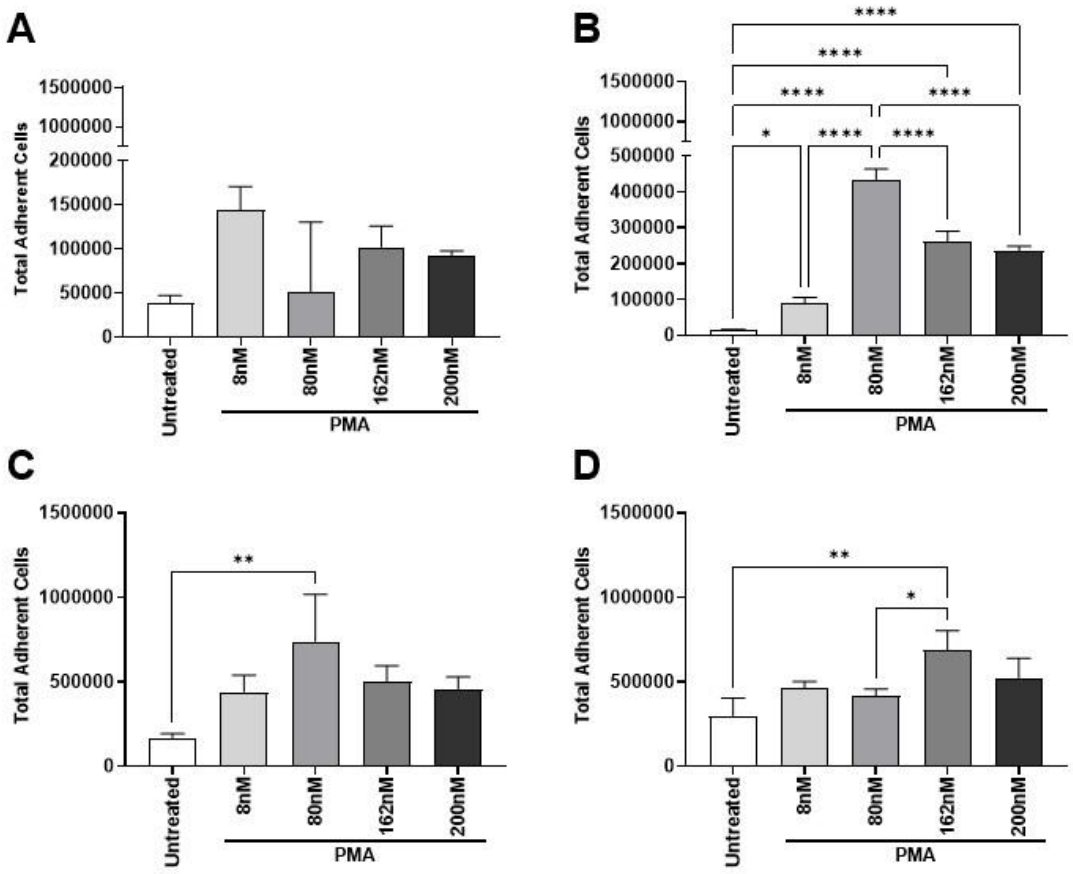
A
B
C
D
Total Adherent Cells
1500000
1000000
500000
200000
150000
100000
50000
400000
300000
0
Untreated
8nM
80nM
162nM
200nM
PMA
*
**
****

E

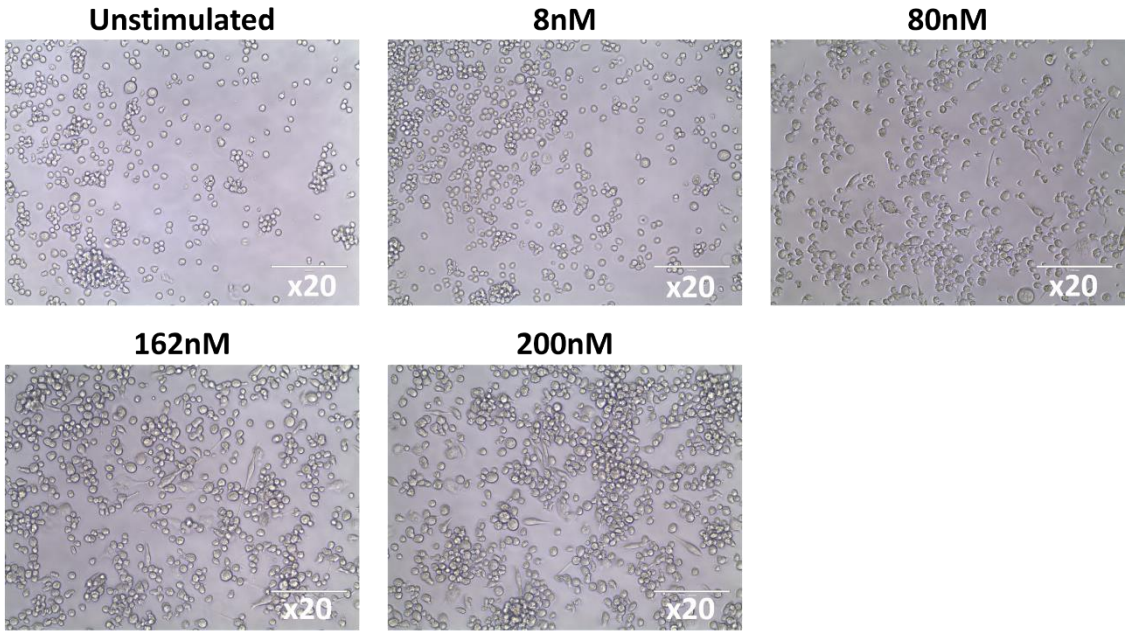
Unstimulated
8nM
80nM
x20
x20
x20
162nM
200nM
x20
x20

F

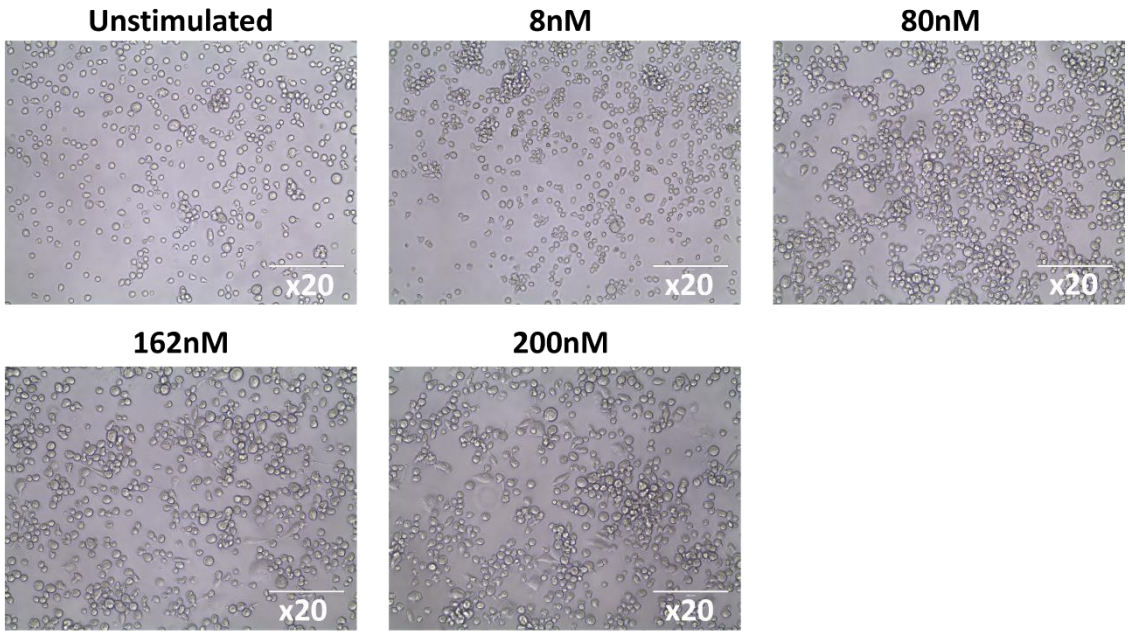
Unstimulated
8nM
80nM
x20
x20
x20
162nM
200nM
x20
x20

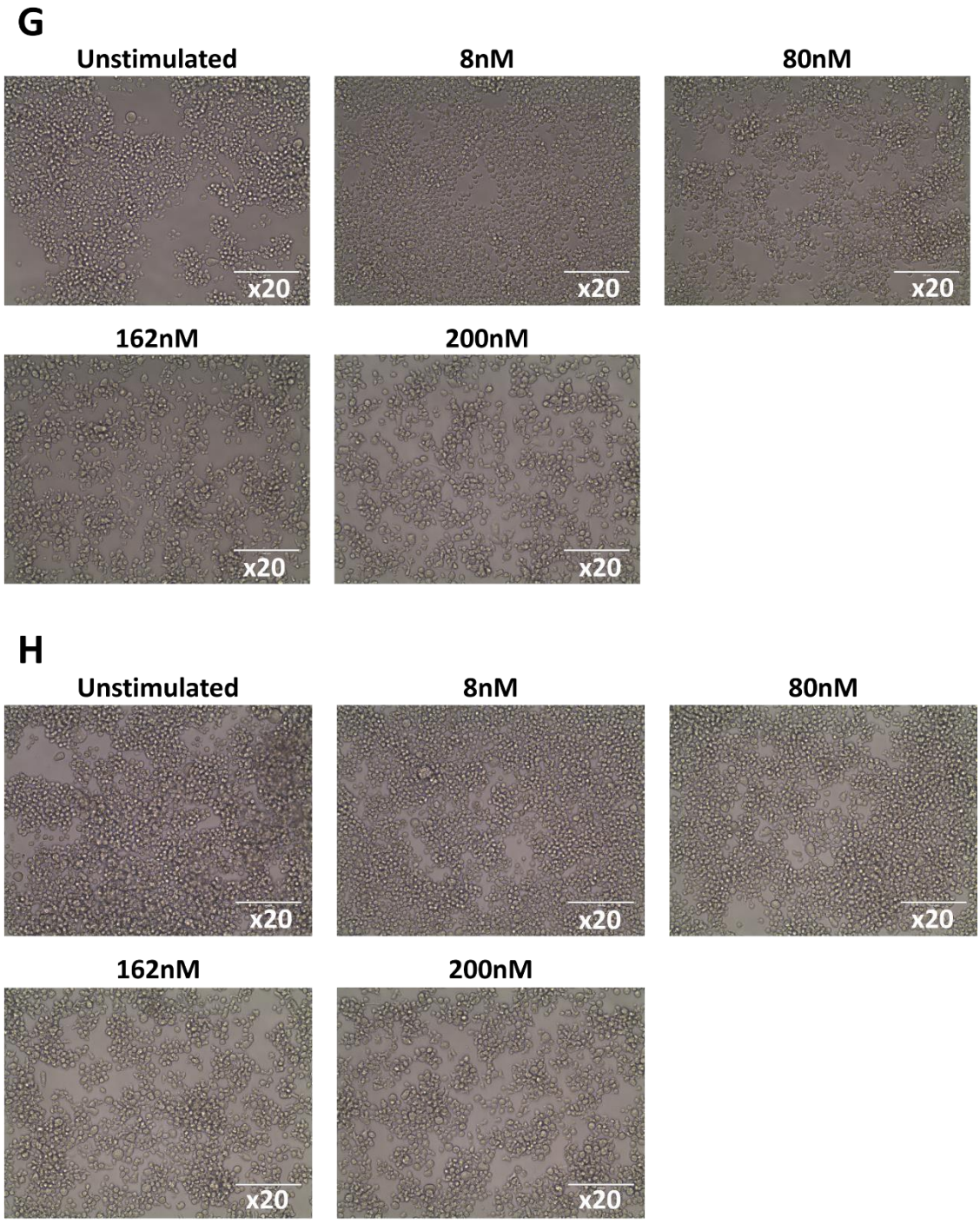

Figure 3.1: Optimization 1 - Assessment of total adherent cell counts with different cell seeding densities and PMA titrations. Data obtained after 48hr PMA treatment at either 8nM, 80nM, 162nM or 200nM, followed by 72hr resting in replenished media. Bar graphs showing the total number of adherent cells recovered from wells seeded at; [A] $1x10^5$ cells/well. [B] $2x10^5$ cells/well. [C] $4x10^5$ cells/well. [D] $6x10^5$ cells/well. Cell counts obtained via counting with trypan blue and haematocytometer. Microscopic images taken at x20 magnification for cells seeded at; [E] $1x10^5$ cells/well. [F] $2x10^5$ cells/well. [G] $4x10^5$ cells/well. [H] $6x10^5$ cells/well. Data represents 1 experiment comprising triplicate values. Data presented as Mean ± SD. Images present 1 representative well from each condition. One-way ANOVA with post hoc Bonferroni. *p<0.05; **p<0.01; ****p<0.0001.

The second set of experiments continued to assess seeding densities at $2x10^5$ – $6x10^5$ cells/well, while incorporating an intermediate PMA concentration of 120nM, alongside 80nM, 162nM and 200nM. For these experiments the lowest seeding density of $1x10^5$ cells was discontinued due to very low numbers of adherent cells obtained previously, and 8nM was also removed from the panel due to limited effect of this concentration in the previous experiments. 120nM was included to assess whether an intermediate concentration between 80nM and 162nM had better influence on cell adherence given these 2 concentrations had both previously been demonstrated to produce superior differentiation.

Figure 3.2A below shows no significant effect of any of the PMA titrations when administered to cells seeded at $2x10^5$ cells/well. Although the previous experiment reported a significant increase by 80nM, here only a slight increase is observed. Regarding morphological changes, all PMA titrations transformed the cells from spherical to elongated versus the untreated control (Figure 3.2D). Figure 3.2B shows the results for the seeding density of $4x10^5$ cells/well and highlights a significant increase in adherent cells elicited by all PMA titrations. Here, all concentrations resulted in significantly higher average numbers of adherent cells versus the untreated control; 80nM (p=0.0011), 120nM (p=0.0063), 162nM (p=0.0009), and 200nM (p=0.0232). This similar influence was also observed in morphology, with all titrations resulting in cellular elongation and clustering (Figure 3.2E).

The final seeding density of $6x10^5$ cells/well saw 80nM perform the best, with a significant increase in the average number of adherent cells up by $1.1x10^6$ (p=0.0014) versus the untreated control (Figure 3.2C). PMA at 120nM and 162nM also resulted in significant increases in total adherent cells, up from 124,000 to 870,000 (p=0.0251) and 806,000 (p=0.0431) respectively versus the untreated group. Once again, all PMA titrations seemed to perform equally regarding changing cellular morphology (Figure 3.2F). Despite total number of adherent cells recovered, the density of $6x10^5$ cells generated more pronounced differentiation characteristics with cells appearing clustered and highly confluent which could potentially have detrimental effect on cellular viability. This potential decline in culture viability may then affect downstream protocols in which cells would remain in culture for a further 48hr and influence acquired live cells, and both surface marker expression and cytokine production analysis. Therefore,

given that the $4x10^5$ seeding density resulted in the next highest total of adherent cells recovered, this was selected for continued experimentation. 80nM was also selected for continued assessment given its superior influence on cellular adherence.

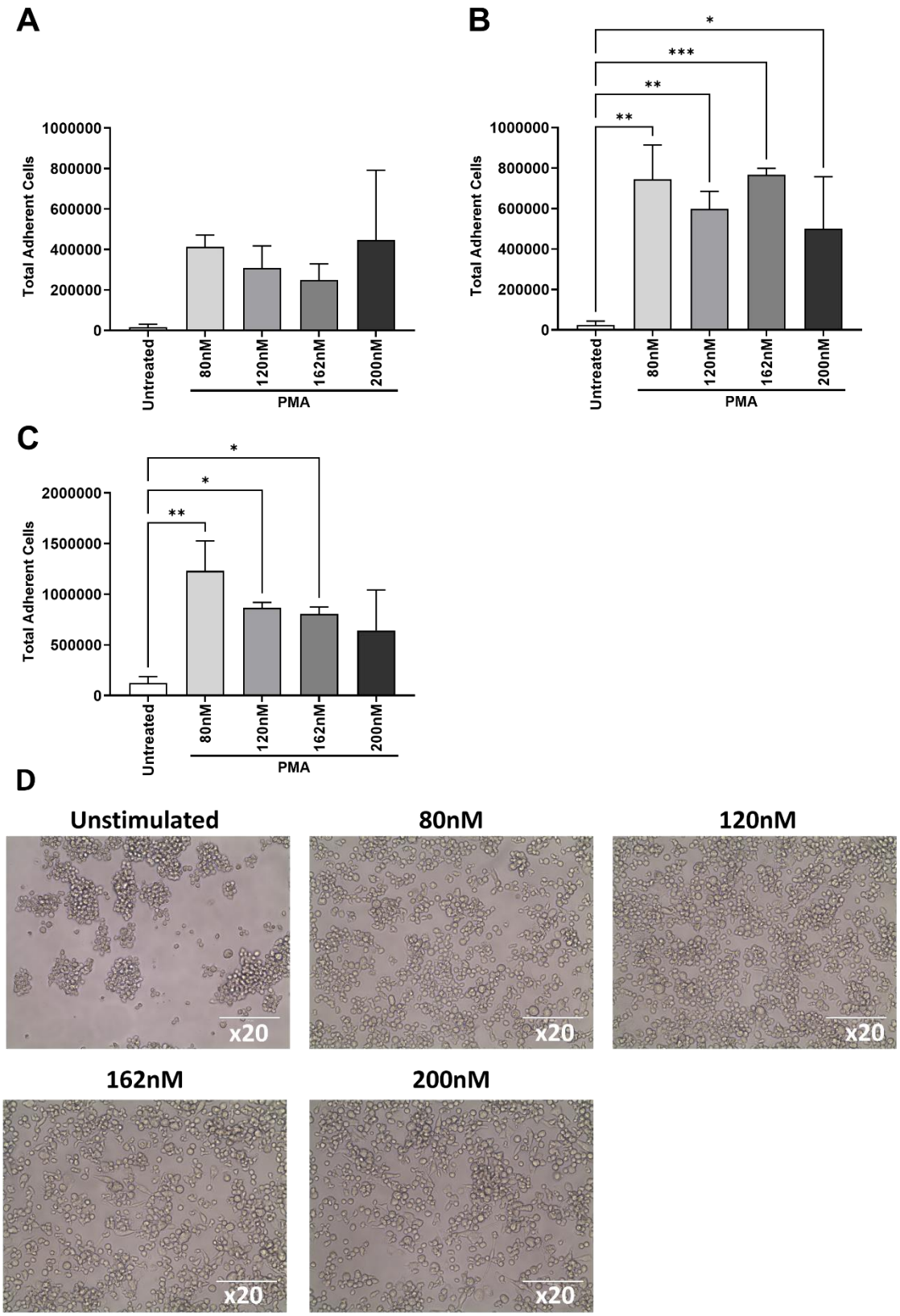

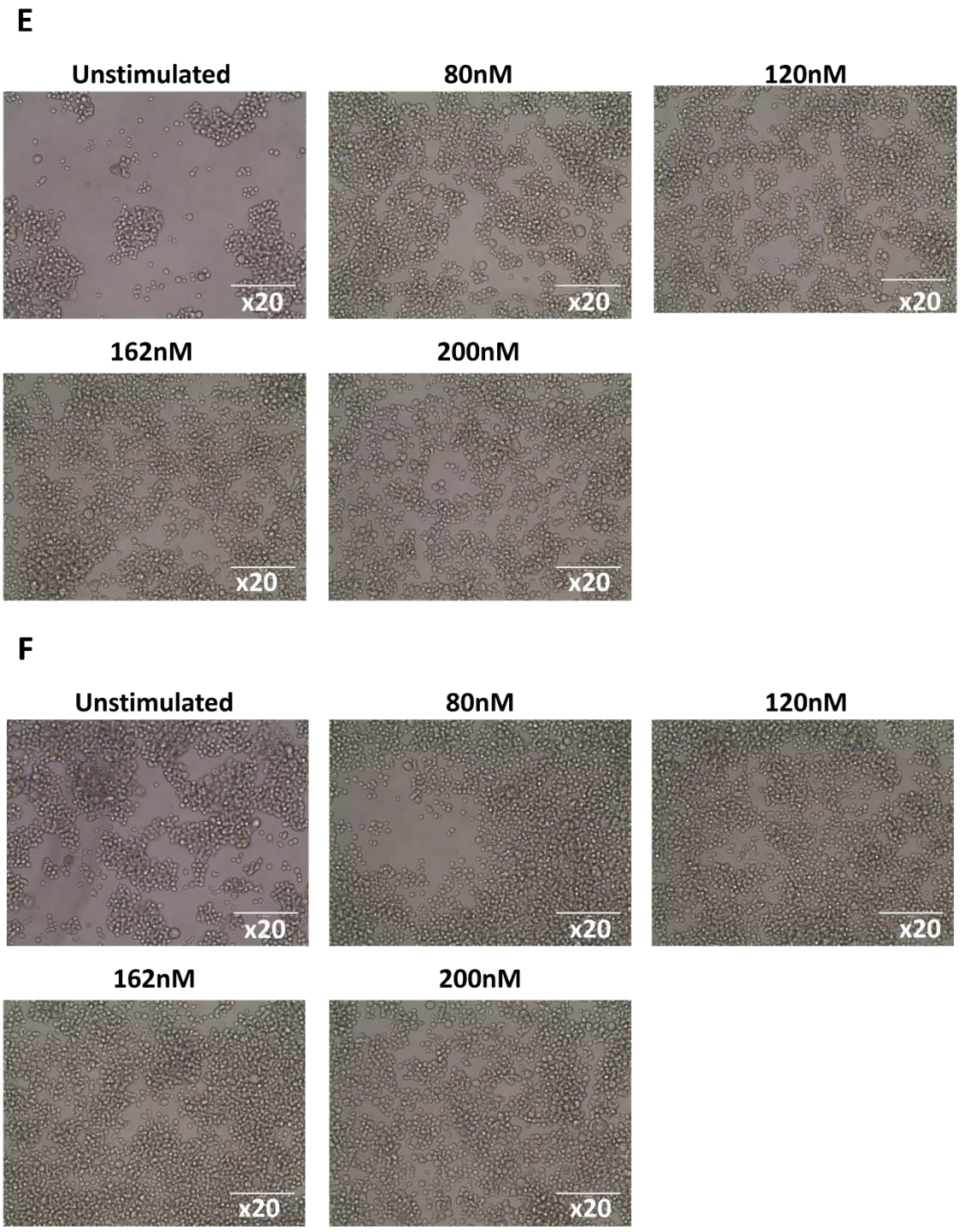

Figure 3.2: Optimization 2 - Assessment of total adherent cell counts with different cell seeding densities and PMA titrations. Data obtained after 48hr PMA treatment at either 80nM, 120nM, 162nM or 200nM, followed by 72hr resting in replenished media. Bar graphs showing the total number of adherent cells recovered from wells seeded at; [A] $2x10^5$ cells/well. [B] $4x10^5$ cells/well. [C] $6x10^5$ cells/well. Cell counts obtained via counting with trypan blue and haematocytometer. Microscopic images taken at x20 magnification for cells seeded at; [D] $2x10^5$ cells/well. [E] $4x10^5$ cells/well. [F] $6x10^5$ cells/well. Data represents 1 experiment comprising triplicate values. Data presented as Mean ± SD. Images present 1 representative well from each condition. One-way ANOVA with post hoc Bonferroni. *p<0.05; **p<0.01; ***p<0.001.

The final set of experiments next explored a lower titration of PMA at 40nM to assess whether a similar outcome could be produced with a lower concentration versus 80nM as PMA is known to be toxic to cells at high concentrations, and may induce an activated phenotype (S. Han *et al.*, 2013; Lund *et al.*, 2016). Here cells were plated at the previously selected density of $4x10^5$ cells/well in 24 well plates and treated with 40nM and 80nM before being assessed via adherent cell counts, as well as viability and surface marker expression of CD14 and CD11b using flow cytometry. Figure 3.3. below shows once again 80nM as the more potent concentration in increasing cellular adherence, significantly increasing the total number of adherent cells by 330'000 (p=0.0018) and 176'000 (p=0.0383) versus the untreated control and 40nM respectively (Figure 3.3A). A visible difference in these adherent cell numbers can also be seen in the microscopic images whereby 80nM resulted in greater confluency (Figure 3.3B).

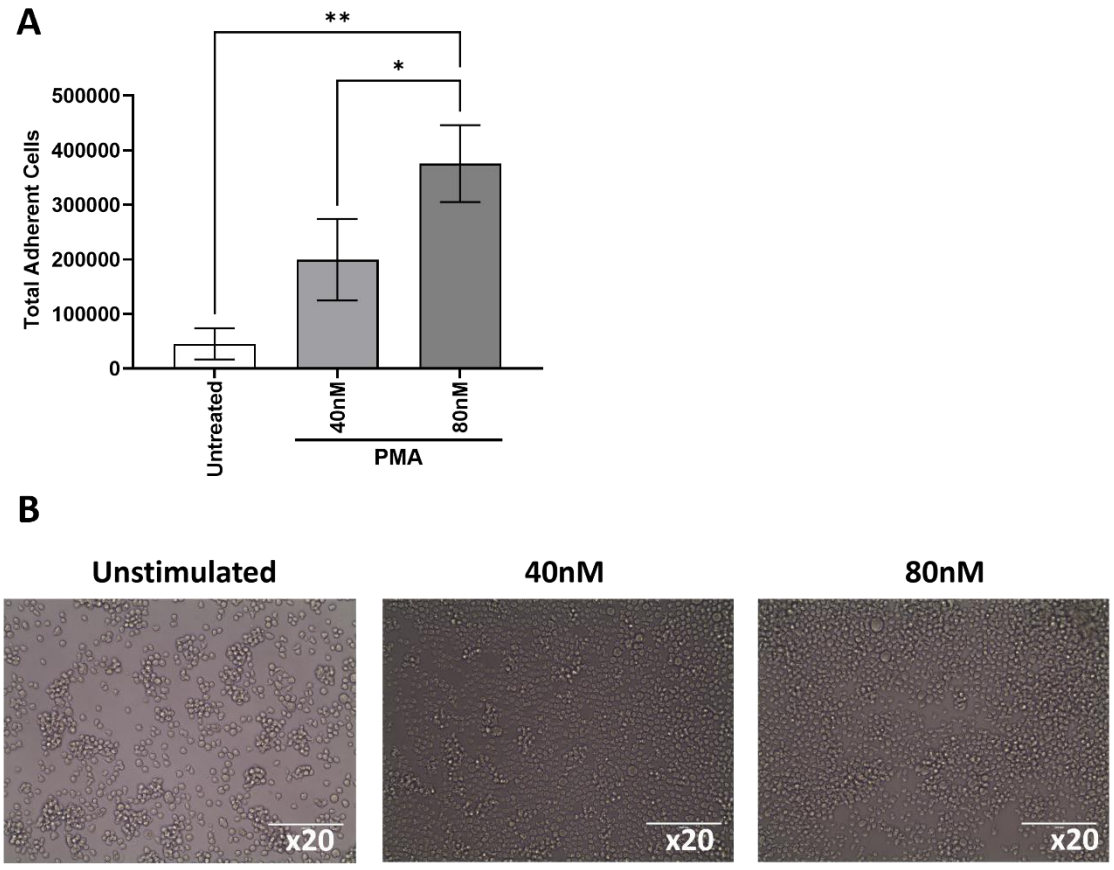

Figure 3.3: Optimization 3 - Assessment of total adherent cell counts when seeded at 4x105 cells/well and treated with 40nm or 80nM PMA. Data obtained after 48hr PMA treatment at either 40nM or 80nM, followed by 72hr resting in replenished media. [A] Bar graph showing the total number of adherent cells recovered. Cell counts obtained via counting with trypan blue and haematocytometer. [B] Microscopic images taken at x20 magnification for PMA at 40nM or 80nM.

Data represents 1 experiment comprising triplicate values. Data presented as Mean ± SD. Images present 1 representative well from each condition. One-way ANOVA with post hoc Bonferroni. *p<0.05; **p<0.01.

Once counted, the cells were stained using the Zombie Aqua viability dye (BioLegend®). In Figure 3.4., there is no alteration in viability seen with either concentration of PMA, with both 40nM and 80nM remaining directly comparable to the untreated control.

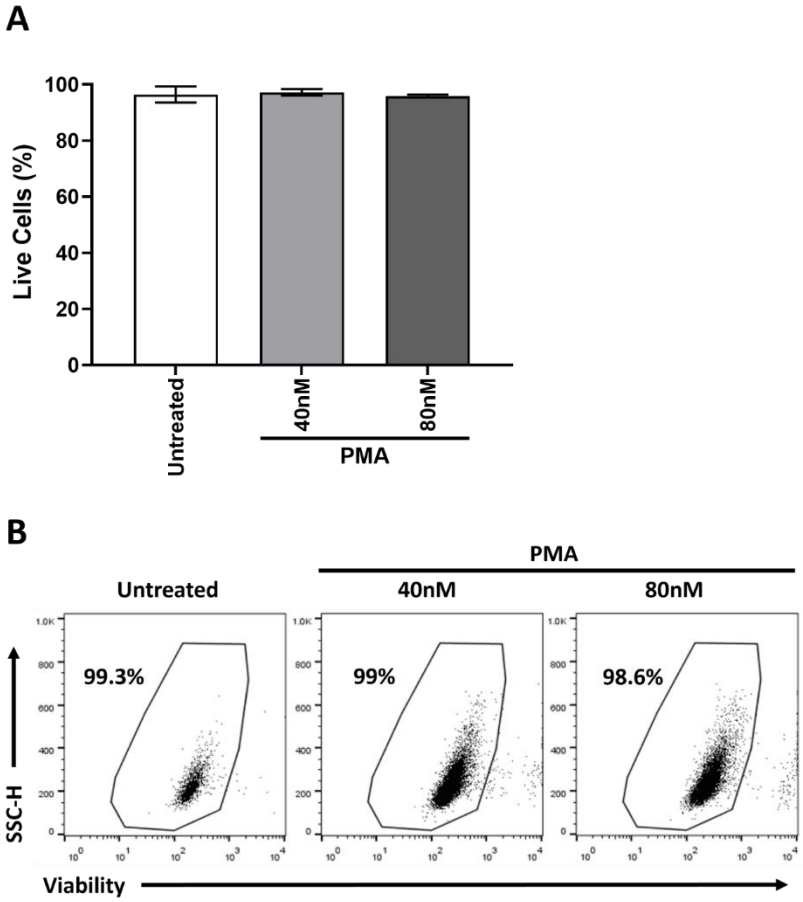

Figure 3.4: Optimization 3 - Assessment of cell viability following treatment with 40nM or 80nM PMA. Data obtained after 48hr PMA treatment at either 40nM or 80nM followed by 72hr resting in replenished media. [A] Bar graph showing the percentage of live cells (%) (Zombie Aqua^{neg}). [B] Representative dot plots showing the percentage of live cells (%) (Zombie Aqua^{neg}). Data represenats 1 experiment comprising of triplicate values and is presented as mean ± SD. One-way ANOVA with post hoc Bonferroni applied.

Finally, cells were assessed for surface marker expression of CD14 and CD11b. Figure 3.5A, C and E show with 80nM resulting in a 36% increase in the percentage of $CD14^+$ cells versus the untreated control (p<0.0001), and 27% increase versus 40nM (p<0.0001). Moreover, this change in expression was also noted for the density of CD14 expression, in which 80nM significantly increased the CD14 MFI by 2.7-fold versus the untreated control (p=0.0054) and 1.2-fold versus 40nM (p=0.0231) (Figure 3.5B and D). A similar trend was also seen when assessing CD11b expression, whereby 80nM increased the percentage of $CD11b^+$ cells from 13% to 29% versus the untreated control (p=0.0006), and from 22% to 29% versus the 40nM group (p=0.0404). This was not, however, seen in the density of CD11b expression where no significant change was noted for either concentration versus the untreated group (Figure 3.5B and F). Overall, this data confirmed 80nM as the optimal concentration to induce monocyte-macrophage differentiation using THP-1 cells, resulting in increased cell adherence, upregulation of CD14 and activated CD11b, while having no detrimental effect on cell viability.

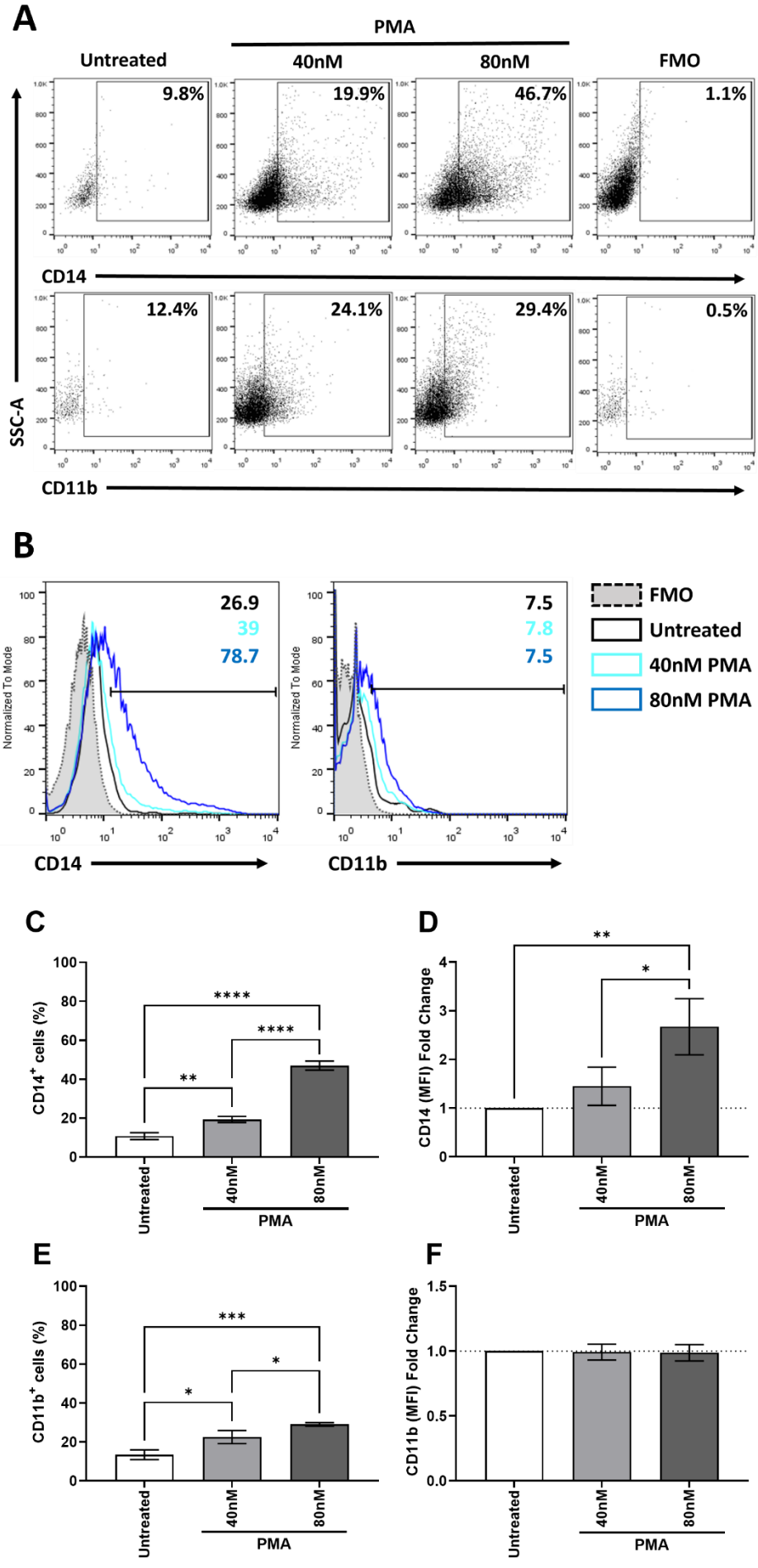
A
PMA
Untreated
40nM
80nM
FMO
9.8%
19.9%
46.7%
1.1%
CD14
12.4%
24.1%
29.4%
0.5%
SSC-A
CD11b
B
26.9
39
78.7
7.5
7.8
7.5
Normalized To Mode
FMO
Untreated
40nM PMA
80nM PMA
CD14
CD11b
C
CD14+ cells (%)
****
****
**
Untreated
40nM
80nM
PMA
D
CD14 (MFI) Fold Change
**
*
E
CD11b+ cells (%)
***
*
*
F
CD11b (MFI) Fold Change

Figure 3.5: Optimization 3: CD14/CD11b expression profile of cells treated with 40nM or 80nM PMA. Data obtained from adherent cells after 48hr PMA treatment at either 40nM or 80nM, and 72hr resting. [A**]** Representative dot plots showing the percentage of $CD14^+$ (top) and $CD11b^+$ (bottom) cells. [B] Representative histograms showing mean fluorescent intensity (MFI) for CD14 (left) and CD11b (right). Numbers indicate MFI of live gated population. [C—F] Bar graphs showing the percentage of $CD14^+$ [C] and $CD11b^+$ [E] cells, and MFI values for CD14 [D] and CD11b [F] displayed as fold change versus the untreated control. Plots and histograms illustrate one representative experiment. Bar graphs represent 1 experiment comprising of triplicate values. Data presented as mean ± SD. One-way ANOVA with post hoc Bonferroni applied. *p<0.05; **p<0.01; ***p<0.001; ****p<0.0001.

The final verified monocyte-macrophage differentiation protocol was selected based upon the optimization results and used cells seeded at $4x10^5$cells/well in 24 well plates, with the addition of 80nM PMA for 48hr. Then, non-adherent cells were removed, the media replenished, and cells rested for a further 72hr. This protocol was followed for all subsequent experimentation with both the THP-1 and U-937 cell lines.

3.1.2. Macrophage characterization: Surface marker evaluation

To further characterise the PMA-induced differentiation model, 4 additional surface proteins were evaluated: CD80, CD86, CD206 and CD163, in addition to CD14 and activated CD11b epitope. The expression of pan macrophage markers CD14 and CD11b (Mahnke *et al.*, 1997; Schlereth *et al.*, 2016), pro-inflammatory M1-associated markers CD80 and CD86 (Tarique *et al.*, 2015), and pro-resolving M2-associated markers CD206 and CD163 (Rőszer, 2015) were selected based upon literary reports. As discussed in chapter 2, section 2.2.1., marker expression was determined at cessation of the protocol at 72hr via multicolour flow cytometry.

When compared to the unstimulated THP-1 monocytes, PMA significantly increased the expression of the LPS receptor CD14, as shown by an increase in both the percentage of $CD14^+$ cells (4.1-fold), and the density of CD14 expression (MFI) (4.5-fold) versus the monocyte control (Figure 3.6). Despite the literature reporting an increase in CD11b following monocyte-macrophage differentiation (Schwende *et al.*, 1996; Starr *et al.*, 2018), in this study PMA treatment resulted in a reduction of CD11b expression, both in percentage of $CD11b^+$ cells (0.8-fold)

and CD11b mean fluorescence intensity (MFI) (0.5-fold) versus the monocyte control (Figure 3.6A, B, E and F).

The pro-inflammatory M1-associated markers CD80 and CD86 were also consistently upregulated within the PMA-derived macrophage cultures (M0) although failed to reach statistical significance in some instances (Figure 3.7). Here, PMA resulted in a 3.2-fold increase in the percentage of $CD80^+$ cells, and a 2.7-fold increase in $CD86^+$ cells. The density of expression (MFI) of these markers were also increased with a fold change of 1.5 for CD80, and 4 for CD86.

Conversely, data regarding expression of M2 markers was inconsistent across the replicates (Figure 3.8). When assessing the percentage of $CD163^+$ and $CD206^+$ cells, there was a range of between 0.9-1.7-fold change witnessed for CD163 expression, and 0.2-1 for CD206 (Figure 3.8A, C and E). However, this pattern was not so pronounced in the density of expression (Figure 3.8B, D and F). Therefore, it was concluded that the level of expression of these markers was largely unchanged by PMA, possibly explaining the low reproducibility of the data amongst replicates.

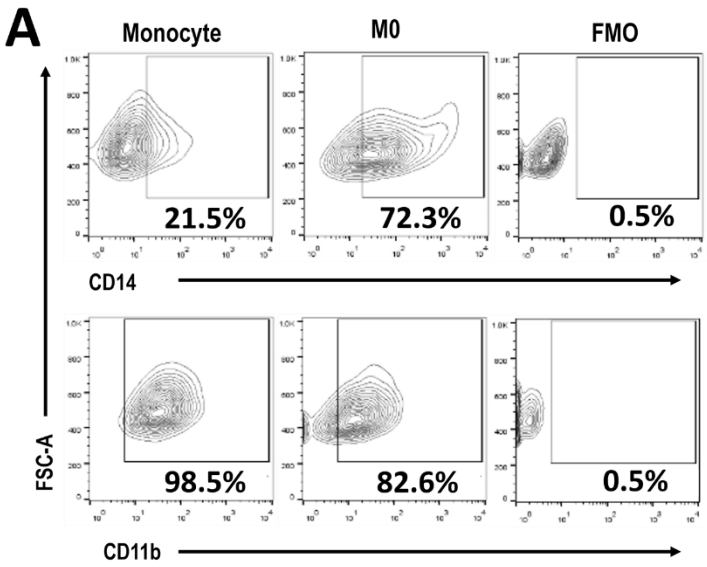
A
Monocyte
M0
FMO
21.5%
72.3%
0.5%
CD14
98.5%
82.6%
0.5%
FSC-A
CD11b

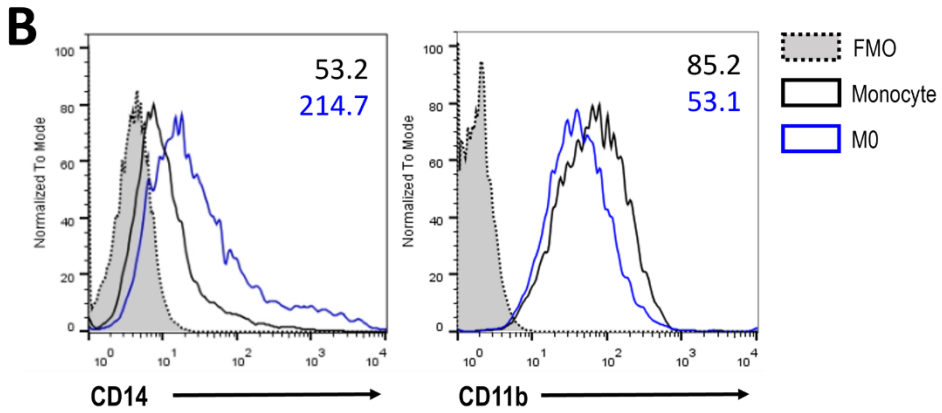
B
53.2
214.7
85.2
53.1
Normalized To Mode
CD14
CD11b
FMO
Monocyte
M0

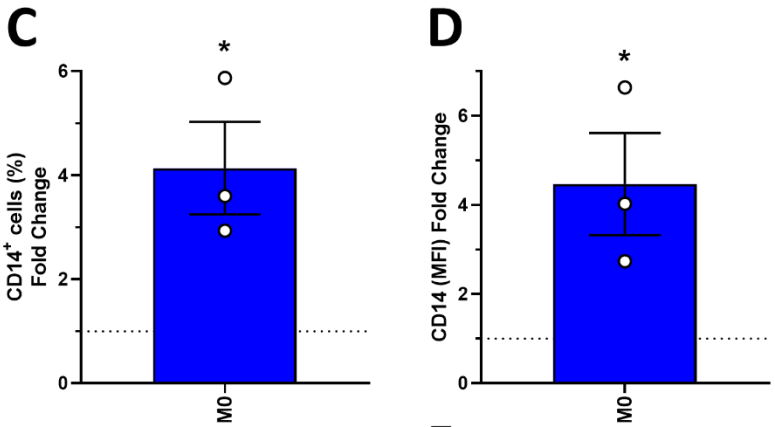
C
CD14+ cells (%) Fold Change
M0

D
CD14 (MFI) Fold Change
M0

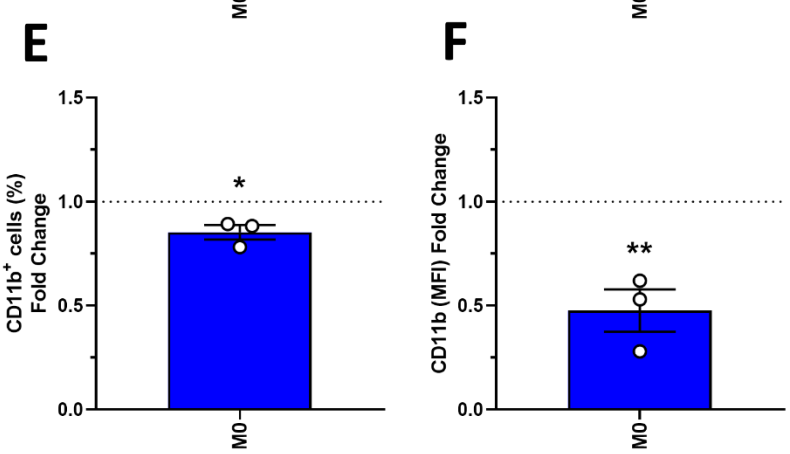
E
CD11b+ cells (%) Fold Change
M0

F
CD11b (MFI) Fold Change
M0

Figure 3.6: CD14 and CD11b expression profile of PMA- differentiated THP-1 macrophages. Data obtained from adherent cells after 48hr of 80nM PMA treatment and 72hr resting. [A] Representative contour plots showing the percentage of $CD14^+$ (top) and $CD11b^+$ (bottom) cells. [B] Representative histograms showing mean fluorescent intensity (MFI) for CD14 (left) and CD11b (right). Numbers indicate MFI of live gated population. [C—F] Bar graphs showing the percentage of $CD14^+$ [C] and $CD11b^+$ [E] cells, and MFI values for CD14 [D] and CD11b [F] both displayed as fold change versus the THP-1 monocyte control. Data compares THP-1 monocytes from culture and PMA-differentiated M0 macrophages. Plots and histograms illustrate one representative experiment. Data for U-937 can be found in Appendix A3.1. Graphs represent 3 independent experiments each comprised of triplicate values. Data presented as mean ± SEM. One-way ANOVA with post hoc Dunnett's applied versus the unstimulated THP-1 monocyte indicated at 1. *$p<0.05$; **$p<0.01$;.

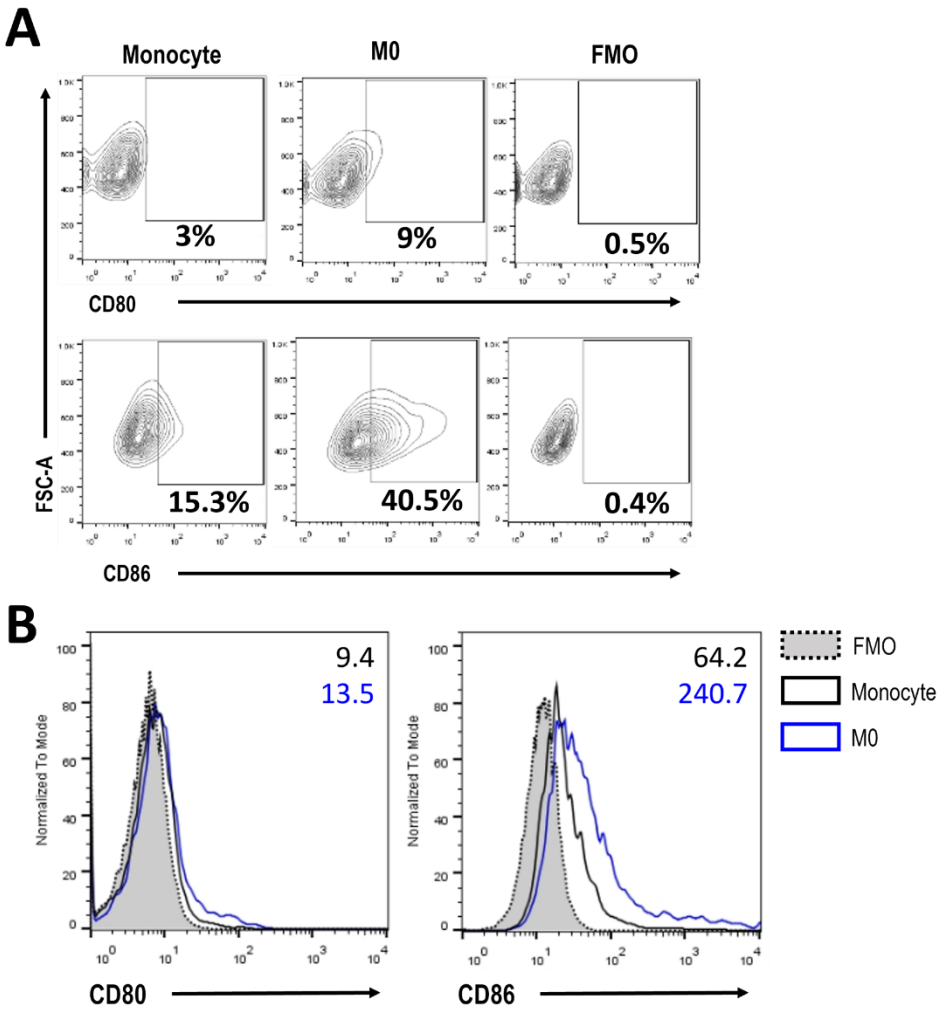
A
Monocyte
M0
FMO
3%
9%
0.5%
CD80
FSC-A
15.3%
40.5%
0.4%
CD86
B
9.4
13.5
64.2
240.7
Normalized To Mode
CD80
CD86
FMO
Monocyte
M0
C
CD80+ cells (%) Fold Change
M0
D
CD80 (MFI) Fold Change
M0
E
CD86+ cells (%) Fold Change
M0
F
CD86 (MFI) Fold Change
*
M0

Figure 3.7: CD80 and CD86 expression profile of PMA- differentiated THP-1 macrophages. Data obtained from adherent cells after 48hr of 80nM PMA treatment and 72hr resting. [A] Representative contour plots showing the percentage of $CD80^+$ (top) and $CD86^+$ (bottom) cells. [B] Representative histograms showing mean fluorescent intensity (MFI) for CD80 (left) and CD86 (right). Numbers indicate MFI of live gated population. [C—F] Bar graphs showing the percentage of $CD80^+$ [C] and $CD86^+$ [E] cells, and MFI values for CD80 [D] and CD86 [F] both displayed as fold change versus the THP-1 monocyte control. Data compares THP-1 monocytes from culture and PMA-differentiated M0 macrophages. Plots and histograms illustrate one representative experiment. Data for U-937 can be found in Appendix A3.2. Graphs represent 3 independent experiments each comprised of triplicate values. Data presented as mean ± SEM. One-way ANOVA with post hoc Dunnett's applied versus the unstimulated THP-1 monocyte indicated at 1. *$p<0.05$.

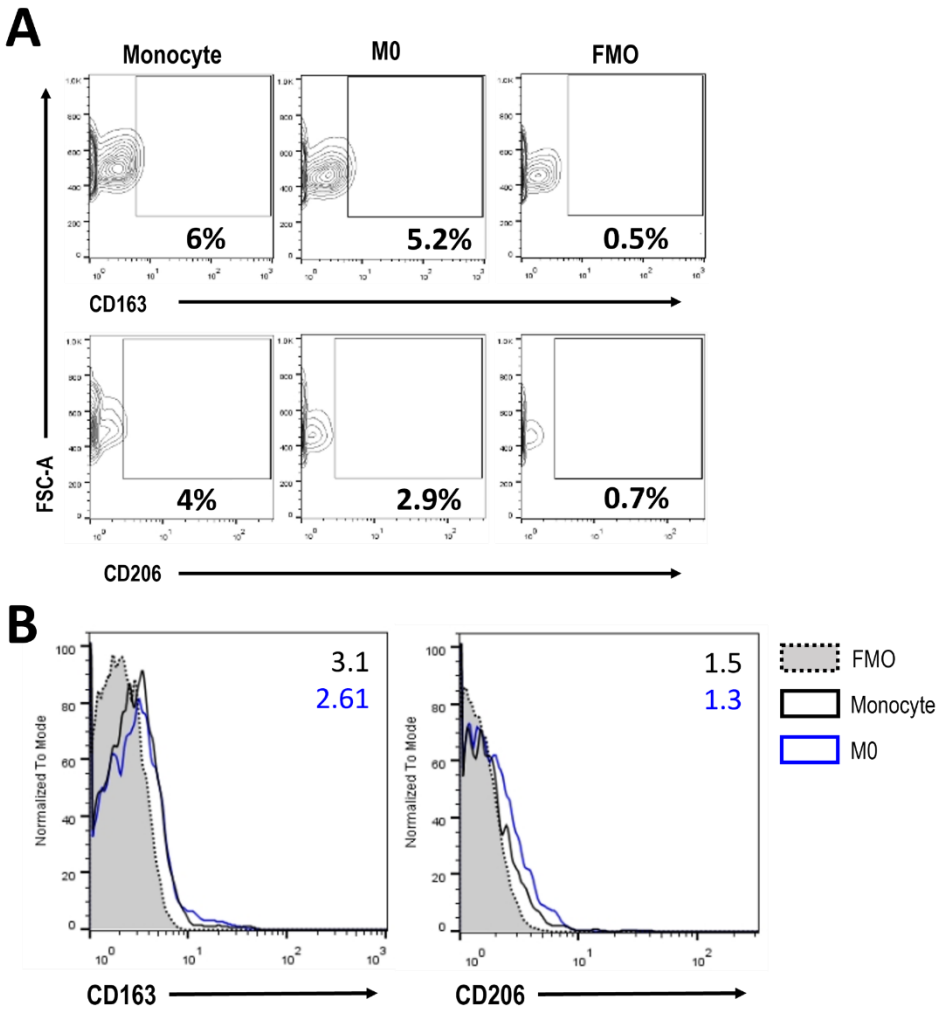
A
Monocyte
M0
FMO
6%
5.2%
0.5%
CD163
FSC-A
4%
2.9%
0.7%
CD206
B
3.1
2.61
1.5
1.3
Normalized To Mode
FMO
Monocyte
M0
CD163
CD206
C
D
CD163+ cells (%) Fold Change
CD163 (MFI) Fold Change
M0
E
F
CD206+ cells (%) Fold Change
CD206 (MFI) Fold Change

Figure 3.8: CD163 and CD206 expression profile of PMA- differentiated THP-1 macrophages. Data obtained from adherent cells after 48hr of 80nM PMA treatment and 72hr resting. [A] Representative contour plots showing the percentage of $CD163^+$ (top) and $CD206^+$ (bottom) cells. [B] Representative histograms showing mean fluorescent intensity (MFI) for CD163 (left) and CD206 (right). Numbers indicate MFI of live gated population. [C—F] Bar graphs showing the percentage of $CD163^+$ [C] and $CD206^+$ [E] cells, and MFI values for CD163 [D] and CD206 [F] both displayed as fold change versus the THP-1 monocyte control. Data compares THP-1 monocytes from culture and PMA-differentiated M0 macrophages. Plots and histograms illustrate one representative experiment. Data for U-937 can be found in Appendix A3.3. Graphs represent 3 independent experiments each comprised of triplicate values. Data presented as mean ± SEM. One-way ANOVA with post hoc Dunnett's applied versus the unstimulated THP-1 monocyte indicated at 1.

3.2. Characterising the effect of minocycline on monocyte-macrophage differentiation

3.2.1. Cellular Viability

It was first crucial to ascertain whether the different concentrations of minocycline tested were having a detrimental effect on culture viability. This was important as a decline in cellular viability may directly influence the total number of adherent cells, the surface marker expression profile, in addition to rendering minocycline at the chosen concentrations unsuitable as a therapeutic. To do this, cells were pre-treated with either minocycline (10μM, 25μM or 50μM), alongside the controls, prior to the addition of PMA (80nM), and both adherent and non-adherent cells were collected after the 48hr and 72hr incubation periods. These 3 titrations of minocycline were selected based upon previous reports whereby concentrations were calculated from effective *in vivo* dosing regimens (Garrido-Mesa, Camuesco, *et al.*, 2011a) and to allow identification of any concentration dependant changes. Dexamethasone (50μM) was included as a positive control within the experiment given its known immunosuppressant action (Giles *et al.*, 2018), alongside dimethyl sulfoxide (DMSO – 1:1000) as the vehicle control. Both adherent and non-adherent cell populations were stained using a viability dye (Zombie Aqua – BioLegend®) and analysed via flow cytometry. The Zombie Aqua reagent is an amine-reactive fluorescent dye that is non-permeant to live cells but permeant to cells with compromised membranes. This enables the discrimination between viable 'live' versus dead cells within the sample.

In this set of experiments, a significant decline in the percentage of live cells was noted with 50μM minocycline reducing the viability by 0.8-fold in the adherent population (p=0.0133) which was not witnessed in the non-adherent counterpart (Figure 3.9A-B). Conversely, no reduction in viability was noted with the lower concentrations of minocycline at 10μM and 25μM, or with the vehicle or dexamethasone controls when compared to the untreated PMA-induced macrophage group. In summary, although minocycline was shown to have toxicity to the cultures at 50μM, there was no considerable change in viability at 48hr with the lower doses of minocycline, in either the adherent or non-adherent populations when compared to the untreated PMA-induced macrophage group.

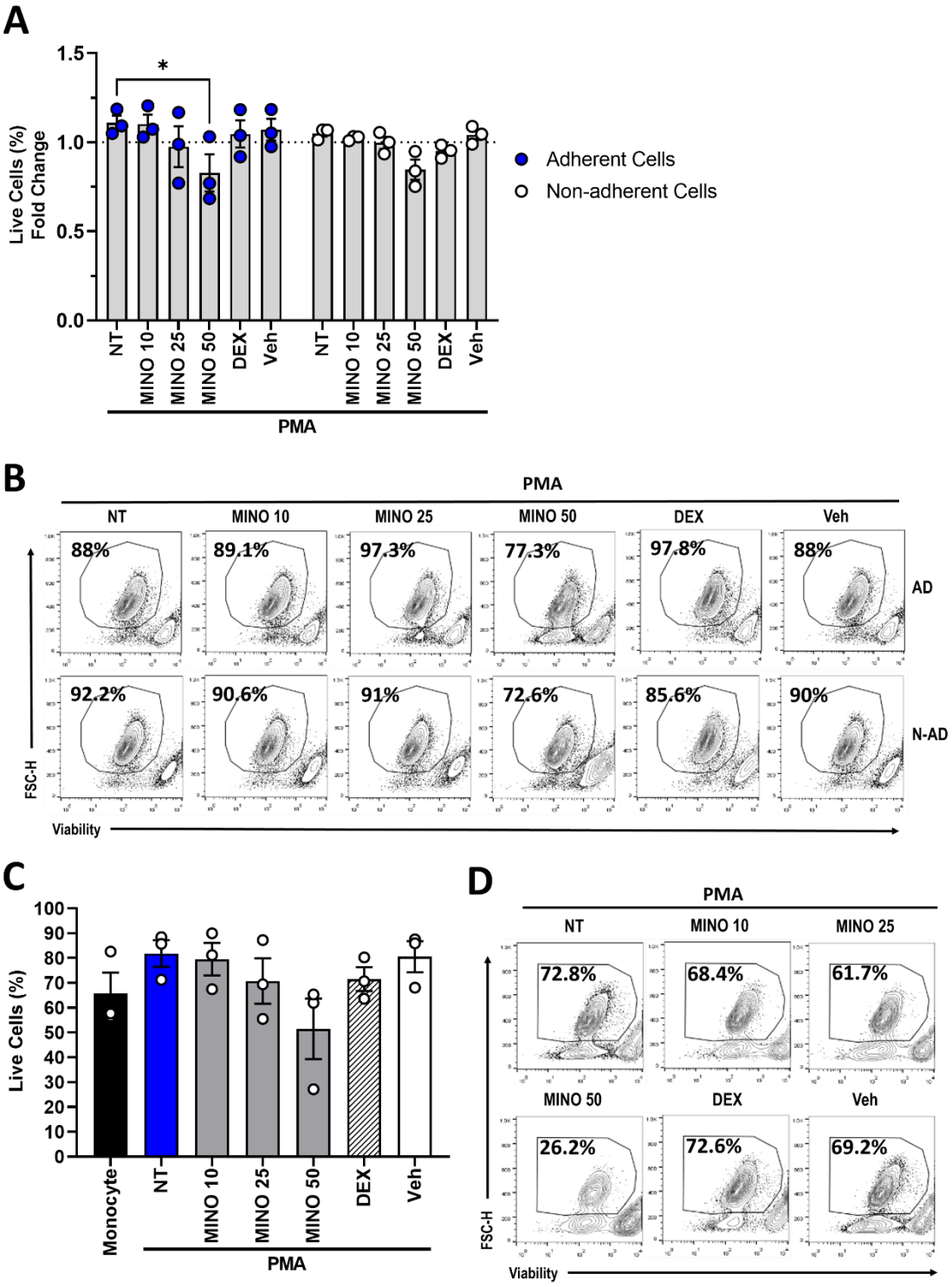

Figure 3.9: Effect of minocycline on cell viability during PMA-induced THP-1 differentiation. [A] Bar graph showing the percentage of live cells (%) (Zombie Aqua^{neg}) following 48hr of 80nM PMA treatment for both the adherent and non-adherent populations. [B] Representative contour plots showing the percentage of live cells (%) (Zombie Aqua^{neg}) at 48hr for adherent (AD) and non-adherent (N-AD) populations. [C] Bar graph showing the percentage of live cells (%) (Zombie Aqua^{neg}) after 48hr 80nM PMA treatment and 72hr resting.

[D] Representative contour plots showing the percentage of live adherent cells (%) (Zombie Aqua^{neg}) after 48hr 80nM PMA treatment and 72hr resting. NT = untreated PMA-induced macrophage, MINO 10 = Minocycline 10μM, MINO 25 = Minocycline 25μM, MINO 50 = Minocycline 50μM, DEX = Dexamethasone 50μM, Veh = DMSO vehicle control 1:1000. Data represents 3 independant experiments each comprised of triplicate values and is presented as mean ± SEM. Data for U-937 can be found in Appendix A4. One-way ANOVA with post hoc Dunnett's applied versus the NT group. *p<0.05.

When cells were collected at 72hr, a reduction in cell viability of adherent cells was seen in groups treated with minocycline at 25μM and 50μM (Figure 3.9C & D) with an 11.1% and 30.3% decrease in the percentage of live cells respectively versus the untreated PMA-induced macrophage (NT) control group. These observations, although below the range of statistical significance suggest that minocycline may exhibit a low level of toxicity at higher concentrations in relation to a decrease in cellular viability. The data obtained from the 48hr time point also indicated a reduction of adherent cells numbers, thus the reduced number of adherent cells seen at 72hr may be attributable both to a direct effect of minocycline on cell adherence via direct alteration in differentiation or as a consequence of cell death.

3.2.2. Cellular morphology & adherence

Following the initial investigation which explored if minocycline would have any effect upon the cellular viability, the next study explored adherence properties indicative of successful monocyte-macrophage differentiation. Previous *in vivo* reports have indicated an influx of macrophages within the colon of colitic mice following treatment with minocycline (Garrido-Mesa, Rodríguez-Nogales, *et al.*, 2018b), therefore, it was of interest to establish whether this phenomenon was attributable to a direct effect of minocycline on the process of monocyte-macrophage differentiation. To do that, cells were again pre-treated with minocycline (10μM, 25μM or 50μM), two hours prior to the addition of PMA (80nM) to allow a small time-window in which minocycline or the control treatments could exert any action in the absence of PMA. A monocyte control group containing THP-1 monocytes was also included to compare the characteristics of PMA-differentiated cells. After 48hr, supernatant containing non-adherent thus undifferentiated cells were removed, and adherent cultures were replenished with fresh media and left to mature for a further 72hr.

After 72hr, adherent cells were imaged, collected, and counted before surface marker expression and cell viability was assessed via flow cytometry. Figure 3.10B below illustrates the morphological change of the cells with the addition of PMA whereby the cells become clustered and elongated in nature. However, with the pre-treatment of minocycline, cultures seem to lack these features and instead resemble cells in the monocyte control group. This may suggest an interference of minocycline within the differentiation process, inhibiting the monocytes from fully acquiring macrophage-like properties (Figure 3.10B).

When differentiated, monocytes transform from suspension to adherent cells, therefore cell counts of adherent cells provided an initial data set relating a potential influence of minocycline on the macrophage differentiation process using THP-1cells shown below in Figure 3.10. The results gained from these counts revealed firstly a 10-fold increase in the number of adherent cells within the PMA-treated group when compared with the undifferentiated monocyte control. This was then reduced by 7.7-fold, 9-fold and 8.6-fold following treatment with minocycline (MINO) at 10μM, 25μM and 50μM respectively (p>0.05). A decline in adherence was also noted within the dexamethasone (DEX) treated group but to a lesser degree with a 0.7-fold reduction versus the PMA only condition. There were no significant changes in cellular adherence elicited by the DMSO vehicle (Veh) control (Figure 3.10A). This experiment was replicated using the U-937 cell line following the same protocol, yielding like-for-like results (Appendix A5). Here minocycline at all concentrations tested reduced the total number of adherent cells when compared with the PMA-differentiated group. These cell counts provide further support that a reduction in adherent cells is a real effect of minocycline and not simply a result of drug toxicity. It must also be noted that, although without PMA treatment, monocytes may still partially differentiate and adhere due to the hydrophilic plate surface which may help explain the existence of a small number of adherent cells in the monocyte control group. This adherence did not however alter phenotype as will be shown later in section 3.2.3.

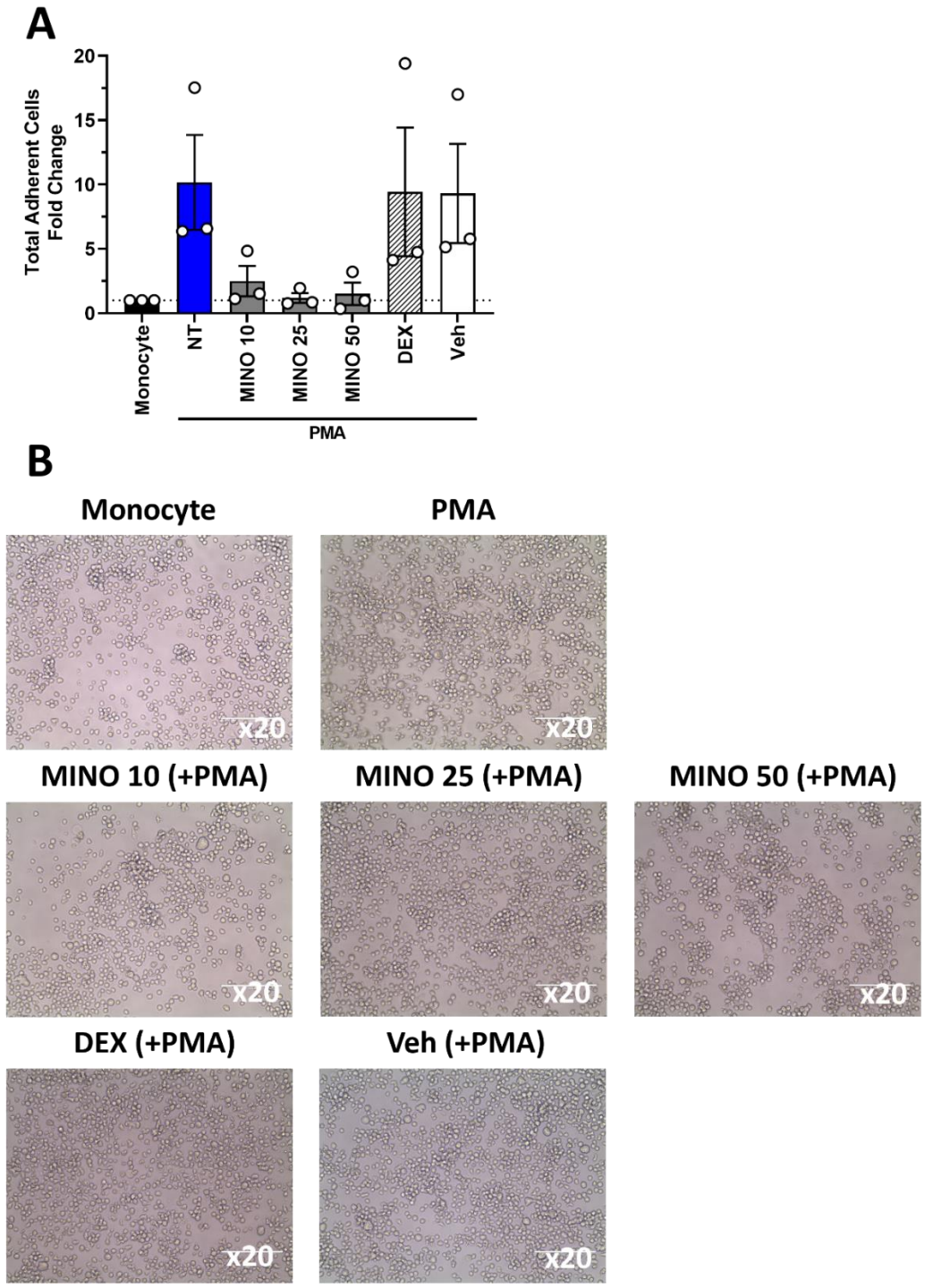

Figure 3.10: Effect of minocycline on cellular adherence and morphology during PMA-induced THP1 monocyte differentiation. [A] Bar graph showing the total number of adherent cells after 48h of 80nM PMA treatment and 72hr resting. Data showed as fold change versus the untreated THP-1 monocyte control indicated at 1. [B] Representative microscopic images at x20 magnification. NT = no treatment, MINO 10 = Minocycline 10μM, MINO 25 = Minocycline 25μM, MINO 50 = Minocycline 50μM, DEX = Dexamethasone 50μM, Veh = DMSO vehicle control 1:1000. Data represents 3 independent experiments each comprised of triplicate values and is presented as mean ± SEM. Data for U-937 can be found in Appendix A5. One-way ANOVA with post hoc Dunnett's applied versus the NT group.

3.2.3. Surface marker expression

With a reproducible surface marker profile generated for the baseline M0 macrophages outlined in section 3.1.2., the effect of minocycline treatment on the expression of CD14, CD11b, CD80, CD86, CD163 and CD206 was assessed as before, to assess if minocycline has any effect on the differentiation process. Although 50μM was previously noted to have adverse effect on culture viability it was included in this set of analysis as a maximum concentration to aid identification of any dose responses. Nevertheless, results from this value were, and should be considered with caution.

Firstly, the expression of CD14 was reduced in samples pre-treated with minocycline (MINO), with 10μM, 25μM and 50μM reducing the percentage of $CD14^+$ cells by 39%, 39.2% and 38.9% respectively when compared with the PMA-differentiated group ($p>0.05$) (Figure 3.11A-D). This was further reflected in the density of expression (MFI) with all concentrations of minocycline reducing the MFI for CD14 by a fold change of 2.6-3 times ($p<0.05$) (Figure 3.11A-D). Notably, no clear changes were observed in dexamethasone treated samples when compared with the PMA-differentiated group (NT).

Regarding CD11b expression in its active form, minocycline exerted no significant effect on the percentage of $CD11b^+$ cells or on the density of CD11b expression (Figure 3.11A-F). However, whereas dexamethasone (DEX) had little effect on CD14 expression, Figure 3.11B & F highlights a significant influence of dexamethasone on CD11b expression, causing a 1.2-fold increase in CD11b MFI ($p=0.0017$).

Regarding the M1-associated markers CD80 and CD86, minocycline treatment did not have any statistically significant impact on the percentage of $CD80^+$ cells, whereas minocycline at the lowest concentration of 10μM resulted in a visual decrease in the density of CD80 expression, reducing the MFI by 0.4-fold versus the PMA-differentiated group (NT) (Figure 3.12A-D). Minocycline did however influence CD86 expression, where it reversed the initial up-regulation caused by PMA differentiation, visually lowering the percentage of $CD86^+$ cells between 10.2%-13.6% ($p>0.05$), and MFI between 2.6 and 2.8-fold ($p<0.01$) (Figure 3.12A, B-F). In relation to dexamethasone, which increased the percentage of $CD80^+$ cells ($p=0.0099$) and MFI ($p=0.0814$) (Figure 3.12A-C & D), minocycline

was able to reduce CD80 expression to a greater degree than dexamethasone. Furthermore, minocycline appeared to be able to reduce the percentage of $CD86^+$ cells to a greater degree than dexamethasone, while remaining comparable in its effect on the density of CD86 expression (Figure 3.12A, B, E and F).

When assessing the effect of minocycline on the M2-associated markers CD163 and CD206 a consistent effect was witnessed with 50μM minocycline treatment which caused a subtle increase in expression across both markers (Figure 3.13). Here 50μM minocycline resulted in a 4.5% increase in the percentage of $CD163^+$ cells, and a 2.4% increase in $CD206^+$ cells when compared to the PMA-differentiated group (NT) (Figure 3.13A, C-D). Similarly, the density of CD163 and CD206 expression was increased by 50μM minocycline by 0.3 and 0.2-fold versus the PMA-differentiated group respectively (Figure 3.13B, E and F). Although the effect of dexamethasone was of greater magnitude in this regard, eliciting a 56.3% increase, and 26.9-fold increase in the percentage of $CD163^+$ cells and density of expression respectively, and an 16% increase and 1.6-fold increase in CD206 percentage and density.

Finally, amongst all variables tested no changes were observed with the DMSO vehicle control (Veh). The fact that DMSO had no effect on surface marker expression provided confidence when analysing the direct effect of minocycline on these proteins.

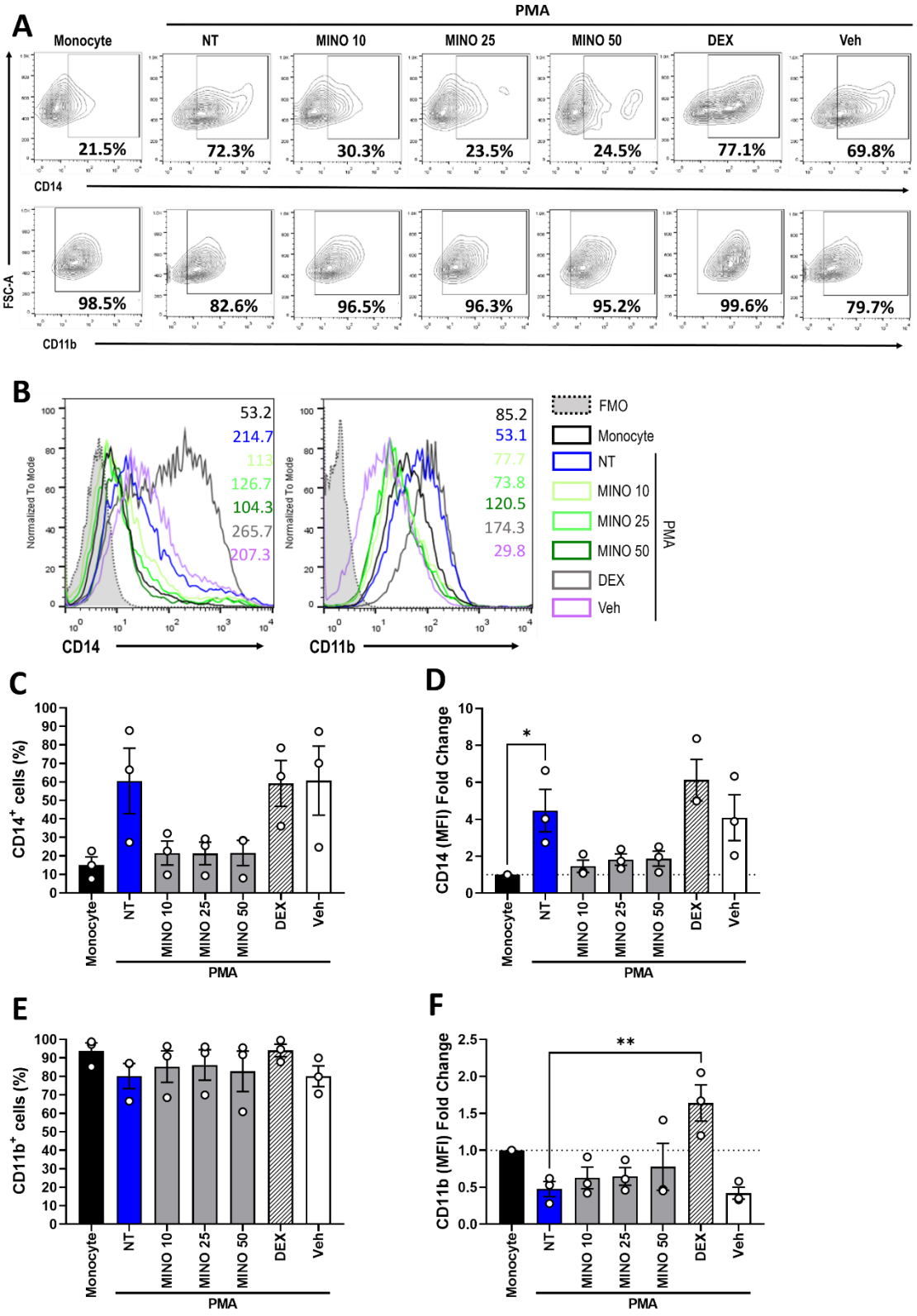
A
PMA
Monocyte
NT
MINO 10
MINO 25
MINO 50
DEX
Veh
21.5%
72.3%
30.3%
23.5%
24.5%
77.1%
69.8%
CD14
FSC-A
98.5%
82.6%
96.5%
96.3%
95.2%
99.6%
79.7%
CD11b
B
Normalized To Mode
53.2
214.7
113
126.7
104.3
265.7
207.3
85.2
53.1
77.7
73.8
120.5
174.3
29.8
CD14
CD11b
FMO
Monocyte
NT
MINO 10
MINO 25
MINO 50
DEX
Veh
PMA
C
CD14+ cells (%)
D
CD14 (MFI) Fold Change
E
CD11b+ cells (%)
F
CD11b (MFI) Fold Change

Figure 3.11 Effect of minocycline on CD14 and CD11b expression of PMA-differentiated THP-1 macrophages. Data obtained from adherent cells after 48hr of 80nM PMA treatment and 72hr resting. [A] Representative contour plots showing the percentage of $CD14^+$ (top) and $CD11b^+$ (bottom) cells. [B] Representative histograms showing mean fluorescent intensity (MFI) of CD14 (left) and CD11b (right). Numbers indicate MFI of live gated population. [C-F] Bar graphs showing the percentage of $CD14^+$ [C] and $CD11b^+$ [E] cells, and MFI values for CD14 [D] and CD11b [F] displayed as fold change versus the THP-1 monocyte indicated at 1. NT = untreated PMA-differentiated M0 macrophage, MINO 10 = Minocycline 10μM, MINO 25 = Minocycline 25μM, MINO 50 = Minocycline 50μM, DEX = Dexamethasone 50μM, Veh = DMSO vehicle control 1:1000. Plots and histograms illustrate one representative experiment. Graphs represent 3 independent experiments each comprised of triplicate values. Data for U-937 can be found in Appendix A6. Data presented as mean ± SEM. One-way ANOVA with post hoc Dunnett's applied versus the unstimulated THP-1 monocyte. *p<0.05; **p<0.01.

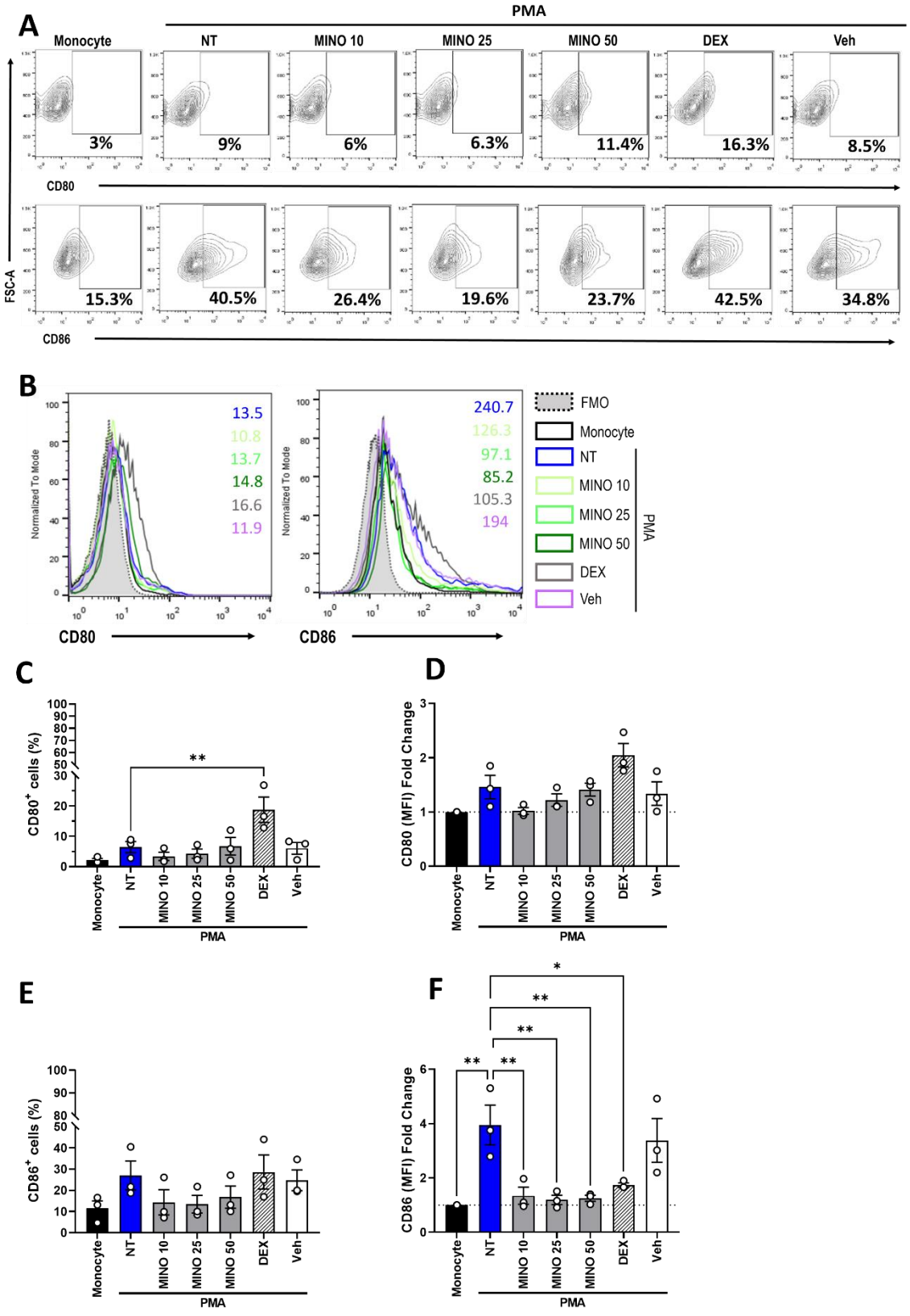
A
PMA
Monocyte
NT
MINO 10
MINO 25
MINO 50
DEX
Veh
3%
9%
6%
6.3%
11.4%
16.3%
8.5%
CD80
FSC-A
15.3%
40.5%
26.4%
19.6%
23.7%
42.5%
34.8%
CD86
B
Normalized To Mode
13.5
10.8
13.7
14.8
16.6
11.9
240.7
126.3
97.1
85.2
105.3
194
CD80
CD86
FMO
Monocyte
NT
MINO 10
MINO 25
MINO 50
DEX
Veh
PMA
C
CD80+ cells (%)
**
D
CD80 (MFI) Fold Change
E
CD86+ cells (%)
F
CD86 (MFI) Fold Change
*
**

Figure 3.12: Effect of minocycline on CD80 and CD86 expression of PMA-differentiated THP-1 macrophages. Data obtained from adherent cells after 48hr of 80nM PMA treatment and 72hr resting. [A] Representative contour plots showing the percentage of $CD80^+$ (top) and $CD86^+$ (bottom) cells. [B] Representative histograms showing mean fluorescent intensity (MFI) of CD80 (left) and CD86 (right). Numbers indicate MFI of live gated population. [C-F] Bar graphs showing the percentage of $CD80^+$ [C] and $CD86^+$ [E] cells, and MFI values for CD80 [D] and CD86 [F] displayed as fold change versus the THP-1 monocyte indicated at 1. NT = untreated PMA-differentiated macrophage, MINO 10 = Minocycline 10μM, MINO 25 = Minocycline 25μM, MINO 50 = Minocycline 50μM, DEX = Dexamethasone 50μM, Veh = DMSO vehicle control 1:1000. Plots and histograms illustrate one representative experiment. Graphs represent 3 independent experiments each comprised of triplicate values. Data for U-937 can be found in Appendix A6. Data presented as mean ± SEM. One-way ANOVA with post hoc Dunnett's applied versus the unstimulated THP-1 monocyte. *p<0.05; **p<0.01.

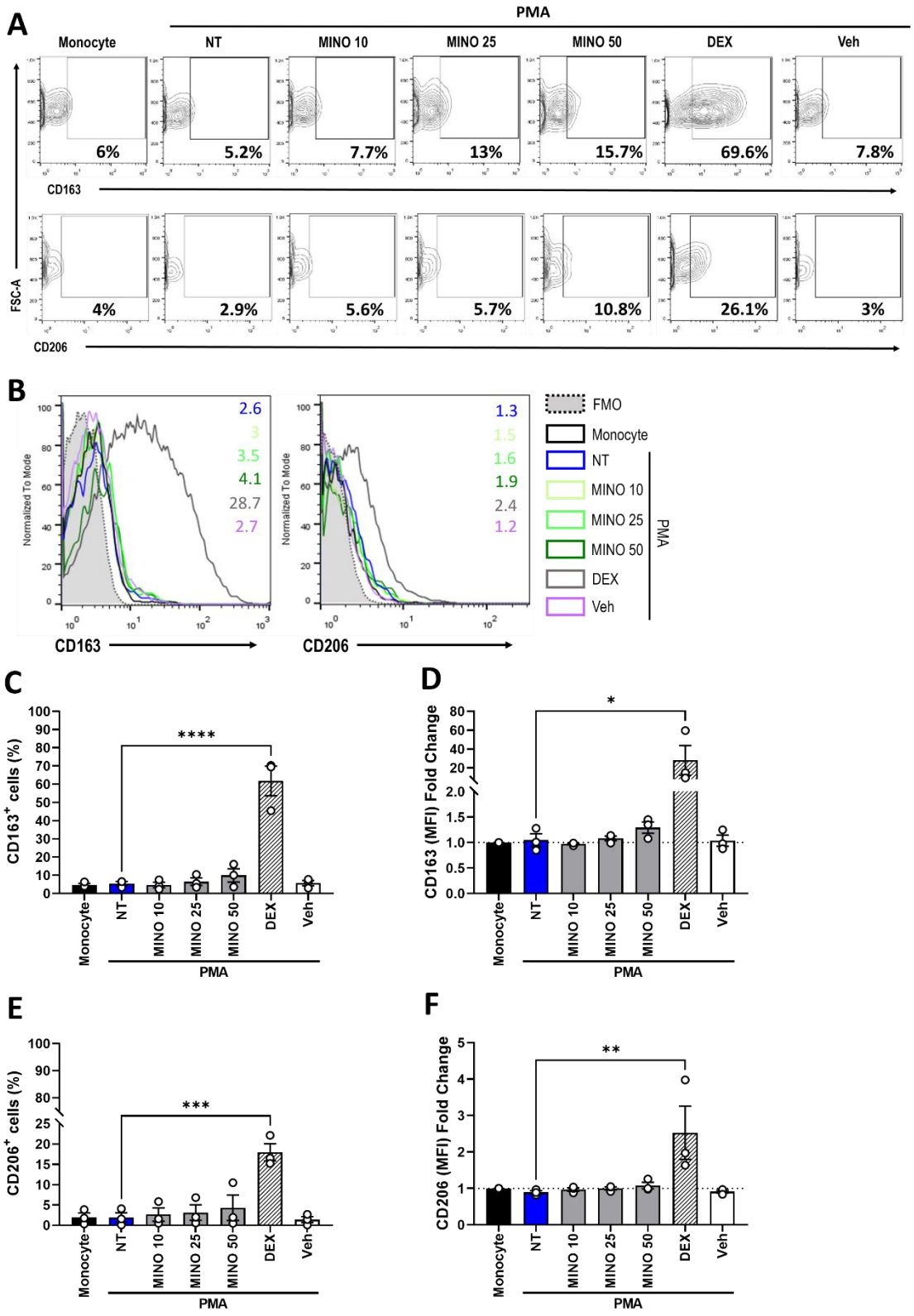
A
PMA
Monocyte
NT
MINO 10
MINO 25
MINO 50
DEX
Veh
6%
5.2%
7.7%
13%
15.7%
69.6%
7.8%
CD163
FSC-A
4%
2.9%
5.6%
5.7%
10.8%
26.1%
3%
CD206
B
Normalized To Mode
2.6
3
3.5
4.1
28.7
2.7
1.3
1.5
1.6
1.9
2.4
1.2
CD163
CD206
FMO
Monocyte
NT
MINO 10
MINO 25
MINO 50
DEX
Veh
PMA
C
CD163+ cells (%)
****
D
CD163 (MFI) Fold Change
*
E
CD206+ cells (%)
***
F
CD206 (MFI) Fold Change
**

Figure 3.13: Effect of minocycline on CD163 and CD206 expression of PMA-differentiated THP-1 macrophages. Data obtained from adherent cells after 48hr of 80nM PMA treatment and 72hr resting. [A] Representative contour plots showing the percentage of $CD163^+$ (top) and $CD206^+$ (bottom) cells. [B] Representative histograms showing mean fluorescent intensity (MFI) of CD163 (left) and CD206 (right). Numbers indicate MFI of live gated population. [C-F] Bar graphs showing the percentage of $CD163^+$ [C] and $CD206^+$ [E] cells, and MFI values for CD163 [D] and CD206 [F] displayed as fold change versus the THP-1 monocyte indicated at 1. NT = untreated PMA-differentiated macrophage, MINO 10 = Minocycline 10μM, MINO 25 = Minocycline 25μM, MINO 50 = Minocycline 50μM, DEX = Dexamethasone 50μM, Veh = DMSO vehicle control 1:1000. Plots and histograms illustrate one representative experiment. Graphs represent 3 independent experiments each comprised of triplicate values. Data for U-937 can be found in Appendix A6. Data presented as mean ± SEM. One-way ANOVA with post hoc Dunnett's applied versus the unstimulated THP-1 monocyte. *p<0.05; **p<0.01; ***p<0.001; ****p<0.0001.

3.3. Discussion

The data shown in this chapter highlights a few key things; first, minocycline seems to inhibit the differentiation of monocytes to macrophages when administered during PMA-driven differentiation. This was evident by the reduction in total number of adherent cells recovered in cells treated with minocycline versus the untreated PMA-only control. Second, minocycline was shown to have influence on the terminal phenotype of the differentiated macrophages, reducing CD14 and CD86 expression, while subtly upregulating the expression of M2-associated markers CD163 and CD206.

Macrophages play a central role in this process as they clear and phagocytose bacteria, bacterial wall components and apoptotic cells (Fullerton and Gilroy, 2016; Na *et al.*, 2019a). The literature provides multiple avenues of evidence that support the premise of monocyte recruitment being the key mechanism of replenishment for intestinal macrophage populations (Smythies *et al.*, 2006; Bain *et al.*, 2013). This hypothesis is supported by the fact that mature macrophages in the adult mucosa have poor proliferative capacity, further suggesting an unlikely role of *in situ* self-renewal in macrophage replenishment (Calum C. Bain and Mowat, 2014). Although it is not completely understood why the mucosa would require continuous recruitment and differentiation of monocytes, a feasible explanation could be the repeated exposure of this region to commensal microbiota and thus the requirement to monitor this interaction closely which is especially poignant in IBD (Jones *et al.*, 2018). This is supported by data highlighting a greater proportion of macrophages in the gut of IBD patients as well

as colitic mouse models (Garrido-Mesa, Rodríguez-Nogales, *et al.*, 2018b; Liu *et al.*, 2019; Mitsialis *et al.*, 2020).

Monocytes are heterogeneous populations with most murine blood monocytes expressing high levels of surface protein Ly6C ($Ly6C^{hi}$) (Auffray *et al.*, 2007), and although historically deemed inflammatory, in recent years their designation has shifted and are now often categorised as 'classical' monocytes due to their fulfilment of roles previously attributed to generic monocytes (Geissmann, Jung and Littman, 2003). The second subset of murine monocytes are termed 'resident' as they are located in both resting and inflamed tissue, and are defined by low Ly6C ($Ly6C^{low}$) expression, as well as increased expression of chemokine receptor CX3CR1 and LFA-1 integrin (Sunderkotter *et al.*, 2004). In humans, equivalent populations of these monocytes exist with $CD14^{hi}$ $CD16^{-}$ resembling the inflammatory monocytes in mice, and $CD14^{low}CD16^{+}$ similar in phenotype to the resident populations (Ingersoll *et al.*, 2010). The primary function of $Ly6C^{low}$ monocytes has recently been elucidated to behave more like phagocytes in the bloodstream, patrolling and maintaining the vascular integrity, and as a result are sometimes referred to as 'patrolling' monocytes (Auffray *et al.*, 2007). Their human equivalent $CD14^{low}CD16^{+}$ monocytes share many parallel gene expression pattens, so although yet to be fully confirmed, it is likely these subsets of cells behave in a similar fashion, acting to patrol the bloodstream and phagocytose pathogens (Ingersoll *et al.*, 2010).

During development, embryonic-derived macrophages are the key population in the colon; however, throughout adulthood monocyte-derived macrophages (MDMs) gradually replace these macrophages and become the predominant population, with studies agreeing that, both during homeostasis and inflammation, colonic macrophages originate from circulating monocytes (Rivollier *et al.*, 2012; Zigmond *et al.*, 2012; Bain *et al.*, 2013, 2014). Monocytes are initially recruited to the colon in a CCR2-dependent manner, in addition to increased secretion of CCL2, CCL7 and CCL8 from intestinal epithelial cells in response to gram-positive bacterial sensing and are proinflammatory in nature. After entering the colon, the monocytes begin differentiation into macrophages, manifesting in the acquisition of MHC II expression in addition to upregulation of CD11b, CD14, CD16 and CD64 (Spöttl *et al.*, 2001; Boyette *et al.*, 2017; Jones *et al.*, 2018).

In IBD, monocytes recruited to sites of inflammation differentiate into macrophages that maintain their pro-inflammatory M1 phenotype, expressing high levels of CD80 and CD86, instead of transitioning to the characteristic anti-inflammatory M2 phenotype which express greater levels of CD163 and CD206 (Tarique *et al.*, 2015; Mily *et al.*, 2020; Veloso *et al.*, 2020). Although these mechanisms remain poorly understood, speculation suggests a role of the proinflammatory milieu (Isidro and Appleyard, 2016). The work published by Garrido-Mesa *et al* in 2018 reported a role of minocycline with possible potentiation of the innate immune response in the intestine, which lead to an earlier resolution of the inflammatory process. This was deduced by data highlighting a higher number of pro-inflammatory Ly6C^{+}MHC II+ macrophages located in the gut of colitic mice at initial stages of the inflammatory process, which then differentiated into a pro-resolving Ly6C^{-}MHCII^{+} phenotype (Garrido-Mesa, Rodríguez-Nogales, *et al.*, 2018b). The data shown here in this chapter partially coincided with these observations in which minocycline was shown to influence the latter phenotype of M0 macrophage populations from that which displays an initial inflammatory signature to that which is more anti-inflammatory.

On the other hand, contradictory evidence was also reported whereby minocycline does not in fact directly promote monocyte-macrophage differentiation, but instead inhibits this process as seen by the reduction in adherent cells following minocycline treatment. This was also accompanied by an earlier and enhanced resolution of the inflammatory process and expression of the resolving enzyme ALOX15 in the intestine of minocycline treated mice, which also showed increased IL-22 production, a cytokine that it's key in epithelial regeneration (Garrido-Mesa, Rodríguez-Nogales, *et al.*, 2018b). The second finding of this chapter indicates that minocycline has influence on the terminal phenotype of the differentiated macrophages. Given that CD14 plays a crucial role in antigen recognition and immune cell activation, LPS binding, synthesis and release of proinflammatory mediators, alongside its role in phagocytic clearance and cellular apoptosis (Zamani *et al.*, 2013), a consistent reduction in the expression of CD14 as a result of minocycline may highlight an inhibitory role of minocycline in suppressing proinflammatory stimuli in response to bacterial antigen. Thus, a significant reduction in CD14 could suggest a role of minocycline in decreasing macrophage sensitivity to pathogenic stimulus, potentially

suggesting a key role of minocycline in dampening the ability of macrophages to respond to invading bacteria. This may, in part, help explain why mice treated with minocycline showed earlier inflammatory resolution compared to untreated controls, and why an initial influx in inflammatory macrophages had no detrimental effect on downstream resolution.

Moreover, Zigmond and colleagues in 2012 demonstrated that daily administration of a depleting CCR2 antibody commencing 2 days after colitis induction with DSS in mice reduced monocyte-derived cell infiltration in the colon, weight loss, and colonic damage (Zigmond *et al.*, 2012). Here treatment with minocycline resulted in a decrease in monocyte-macrophage differentiation independent of CCR2 signalling. Given that these data are in different *in vivo* and *in vitro* systems, it remains possible that minocycline may alleviate inflammation through inhibition of monocyte differentiation, whilst not influencing monocyte infiltration and thus differentiation to other cell types such as dendritic cells.

Similarly, CD86 was significantly downregulated upon minocycline treatment. CD80/86 are the main co-stimulatory molecules expressed on the surface of macrophages and other antigen-presenting cells. Although macrophages function to internalize antigens ready for presentation to T-cells via the MHC-II molecules, CD86 and CD80 are required for complete T-cell activation. CD86 and CD80 interact with the T-cell co-receptor CD28 which results in the induction of various signalling pathways within the T cell including those controlled by NF-κB, MAPK, PI3K and AKT (Jimenez-Uribe *et al.*, 2019; Parker, 2019). A downregulation of this marker could again suggest a role of minocycline treatment with desensitization of macrophages to later stimulus as well as their ability to recruit additional immune cell populations, and ability to further stimulate T-cell activation or the induction of tolerance. Although minocycline has previously been reported to directly alter T cell activation and function through downregulation of the CD40 ligand (CD40L), inhibition of TNF-α production, suppression of activation via the T cell receptor (TCR)/CD3 complex, and impairment of nuclear factor of activated T cells (NFAT)-mediated transcriptional activation (Kloppenburg, Verweij, A. M. M. Miltenburg, *et al.*, 1995; Giuliani, Hader and Yong, 2005b; Szeto *et al.*, 2011b), no data currently exists linking an alteration in macrophage phenotype due to minocycline treatment and downstream T cell activation via CD80/CD80 binding. The data here showing a reduction in CD80

and CD86 suggests that minocycline could potentially alter T cell function via macrophage interaction, however further studies would be required to confirm this.

Although the effect of minocycline on the expression of the CD163 and CD206 was not statistically significant, there still appears to be a concentration dependant change in the percentage of $CD206^+$ and $CD163^+$ cells. Despite being statistically non-significant the presence of slight increases in expression may still yield promising avenues of investigation considering these scavenger receptors bind a litany of ligands and promote the removal of non-self targets via processes such as endocytosis and phagocytosis, and promote bacteria-induced pro-inflammatory cytokine production (Fabriek *et al.*, 2009; PrabhuDas *et al.*, 2017; Nielson *et al.*, 2020). Furthermore, this data may indicate a role of minocycline in the induction of an M2 pro-resolving phenotype.

It was also interesting to compare the effect of minocycline with the known immunosuppressant dexamethasone. Although dexamethasone was able to upregulate the pro-resolving proteins CD163 and CD206 significantly more than minocycline, here minocycline had greater inhibitory action on the expression of CD14 and CD86, while also altering the expression of CD163 and CD206 in a similar manner to dexamethasone. With the literature providing a mechanism of action of dexamethasone on macrophage apoptosis, suppression of antitumoral activity and inhibiting naïve T cell proliferation and differentiation (Giles *et al.*, 2018; Ai *et al.*, 2020), the ability of minocycline to provide greater or comparable influence on macrophage surface marker expression without inducing cell apoptosis may render minocycline a viable therapeutic candidate in limiting inflammation and possible T cell activation through modification of macrophage phenotype as opposed to inducing cell death. Furthermore, given its designation as an immunosuppressant, dexamethasone may result in systemic immune suppression, an unwanted side effect. This may therefore render minocycline a potential competitive candidate within the setting of monocyte-macrophage differentiation.

Taken into consideration alongside the current literature, the data described in this chapter seems contradictory to previously reported monocyte infiltration into the colon lamina propria *in vivo* to a direct effect of minocycline upon monocyte-macrophage differentiation (Garrido-Mesa, Rodríguez-Nogales, *et al.*, 2018b).

Data in this chapter in fact suggest that minocycline negatively influences monocyte-macrophage differentiation, thus, while earlier reported monocyte infiltration may remain true, it may not be correlated necessarily to an abundance of macrophages. Additionally, through modification of macrophage phenotype, the data in this chapter suggest minocycline may also cause desensitisation of macrophages to ongoing endogenous stimulus such as invading pathogen while increasing their function as phagocytes.

4. Results: Effect of minocycline on the response of M0 macrophages to LPS activation

Chapter 3 explored and discussed the potential effects of minocycline on PMA-induced monocyte-macrophage differentiation *in vitro* using the THP-1 and U-937 cell lines. This data highlighted a potential role of minocycline in inhibiting full differentiation of 'patrolling' monocytes, while simultaneously altering the terminal phenotype of the macrophages to that which may render them desensitized to inflammatory stimulus. The second objective of the project was to assess whether minocycline may also modify macrophage phenotype and function when resting 'M0' macrophages were challenged with the inflammatory stimulus lipopolysaccharides from *Escherichia coli* O55:B5 (LPS) as would happen in the inflamed colon of IBD sufferers due to bacteria influx because of epithelial barrier dysfunction.

To test this hypothesis, both THP-1 and U-937 were first fully differentiated using the previously described protocol using PMA (Figure 2.1). At 72hr, and the termination of differentiation, the now mature 'M0' macrophages were pre-treated with minocycline at 10μM, 25μM and 50μM, 50μM dexamethasone, or the DMSO vehicle control at a final dilution of 1:1000 for 2hr before the addition of 100ng/mL LPS. After 24hr supernatant was carefully removed and stored for cytokine determination, and adherent cells were harvested for downstream surface marker evaluation. The full protocol can be found in chapter 2 Figure 2.2. These investigations were also replicated in U-937 whose data is within the appendix, indicated within the relevant figure legends.

4.1. THP-1

4.1.1. Characterising LPS activation of M0 THP-1 macrophages

It was imperative to first assess the influence of LPS on the resting 'M0' macrophages prior to introducing minocycline, dexamethasone and DMSO to provide a reliable and replicable model for comparison. Figures 4.1, 4.2 and 4.3 below illustrate the effect of LPS activation on the pattern of expression of CD14, CD11b, CD80, CD86, CD163 and CD206 on the differentiated THP-1 macrophages. This antibody panel was kept consistent from the previous

objective with the purpose of monitoring key proteins across the M1/M2 subsets, and functional macrophage markers under a different biological stimulus. It must be noted however that the antibody clones used for cell line versus PBMC analysis are different. Clone CBRM1/5 which binds to the active conformation of CD11b was used for THP-1 and U937 analysis, consistent with the pervious chapter, however clone ICRF44 which recognises total protein was used for all PBMC experiments meaning these data sets should be viewed and scrutinised independently. Here, it is important to note that although the experiment was performed 3 independent times, this LPS characterisation was only applied to replicates; 2 and 3, as the first experiment did not include a PMA only control and thus the data could not be normalised in this instance.

Data obtained from this characterisation highlights first, a down-regulation of the LPS chaperone molecule CD14 (Figure 4.1A-D), reflected in the density of CD14 expression (MFI) when compared to the un-activated M0 macrophage control. Similarly, the percentage of activated $CD11b^+$ cells did not change significantly following LPS stimulation, while a decrease in MFI versus the un-activated M0 control can be seen but failed to reach significance (Figure 4.1A, B, E and F). Regarding the pro-inflammatory markers CD80 and CD86, LPS appeared to have opposing influence. Firstly, activation with LPS resulted in a 1.4-fold increase in the percentage of $CD80^+$ cells when compared to the un-activated control (Figure 4.2A and C), while no discernible change was noted in the density of expression (Figure 4.2B and D). On the other hand, the percentage of $CD86^+$ was largely unchanged following LPS simulation (Figure 4.2 A and E), whereas the density of CD86 significantly declined across all replicates versus the control group (p=0.0141) (Figure 4.2 B and F). Finally, both M2-associated proteins CD163 and CD206 significantly decreased following 24hr incubation with LPS with the exception of CD206 density of expression (Figure 4.3), although it must be observed that the baseline expression of both proteins even prior to activation was distinctly low, especially for CD206 expression.

Although the literature clearly identifies CD14 as a key molecule in chaperoning LPS on the cell membrane (Bode, Ehlting and Häussinger, 2012; Płóciennikowska *et al.*, 2015), a downregulation of CD14 upon LPS activation reported here was not necessarily unpredicted and could be attributed to proteolysis of the membrane bound CD14 on the cell surface. This ‘shedding’,

which may also occur intracellularly, manifests following LPS exposure and phagocytosis of bacteria (Delgado *et al.*, 1999; Ciesielska, Matyjek and Kwiatkowska, 2021).

As for CD80 and CD86, it has previously been validated that macrophages express low levels of CD80 and CD86 at basal level, with both molecules being induced by LPS or IFN-γ (Lim *et al.*, 2005), with other reports also indicating the ability of LPS to activate APCs via TLR-4 which increases CD80/CD86 expression in monocytes (Rivellese *et al.*, 2014; Taddio *et al.*, 2021). While the CD80 and CD86 monomers work in tandem with MHC and CD28 to induce activation of $CD4^+$ T cells, CD80 has been reported to have more potent binding affinity to both CD28 and the T-cell negative regulator cytotoxic T-lymphocyte antigen 4 (CTLA-4), with slower disassociation and faster binding kinetics than CD86. This could go some way to explaining why CD80 is seen to be consistently increased in this THP-1 macrophage model while CD86 is reduced, with the hypothesis that LPS in this model is promoting a phenotype that preferences a more potent CD80 effector molecule. Although these reports provide rationale, there remains little evidence on the regulation of CD80 and CD86 in response to LPS specifically in macrophages, meaning this data should be used as a baseline to provide direct comparison with minocycline treated cultures in the interim, until further signalling studies have been conducted.

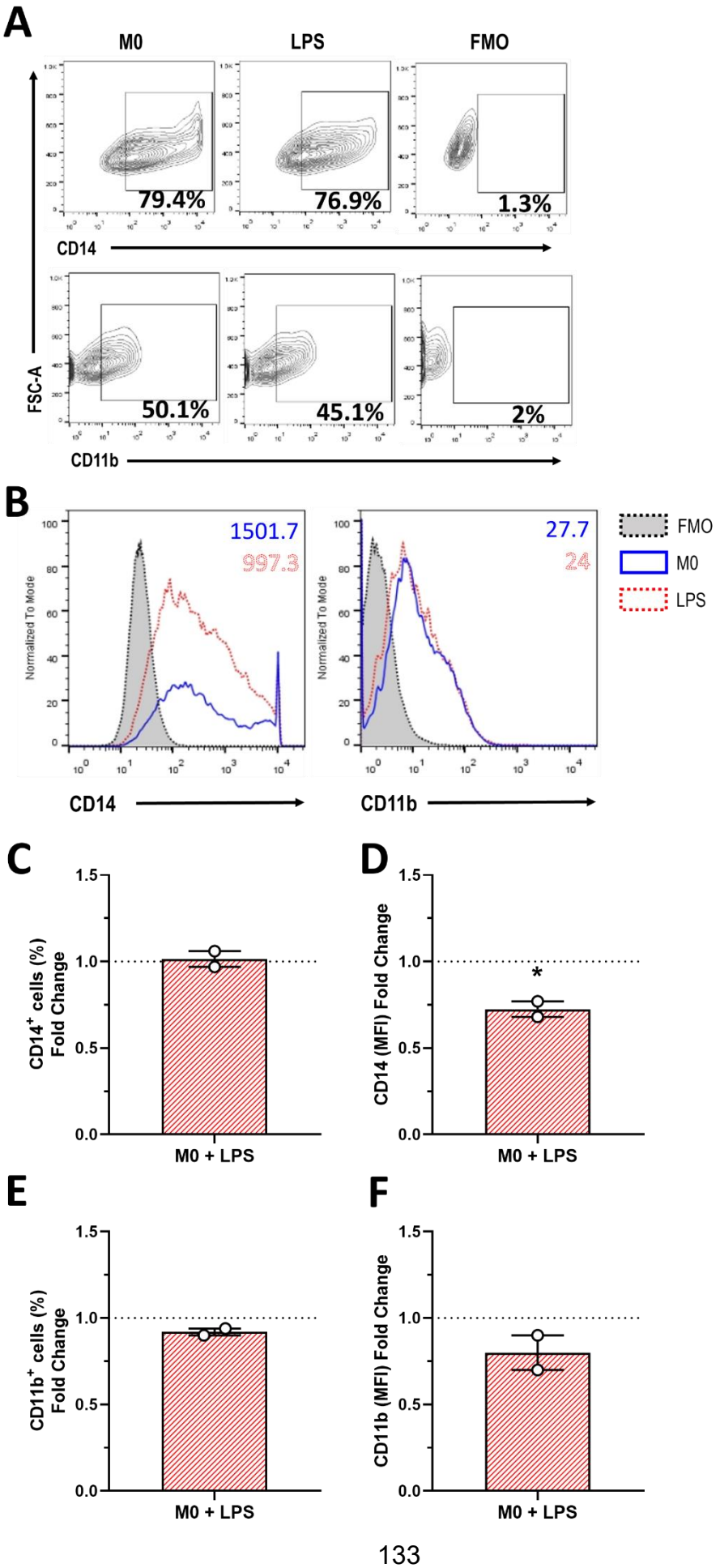
A
M0
LPS
FMO
79.4%
76.9%
1.3%
CD14
FSC-A
50.1%
45.1%
2%
CD11b
B
1501.7
997.3
27.7
24
Normalized To Mode
FMO
M0
LPS
CD14
CD11b
C
CD14+ cells (%) Fold Change
M0 + LPS
D
CD14 (MFI) Fold Change
*
M0 + LPS
E
CD11b+ cells (%) Fold Change
M0 + LPS
F
CD11b (MFI) Fold Change
M0 + LPS

Figure 4.1: CD14 and CD11b expression profile of LPS-activated M0 THP-1 macrophages. Data obtained after 24hr incubation of differentiated M0 macrophages with LPS (100ng/mL). [A] Representative contour plots showing the percentage of $CD14^+$ (top) and $CD11b^+$ (bottom) cells. [B] Representative histograms showing mean fluorescent intensity (MFI) for CD14 (left) and CD11b (right). Numbers indicate MFI of live gated population. [C-F] Bar graphs showing the percentage of $CD14^+$ [C] and $CD11b^+$ [E] cells, and MFI values for CD14 [D] and CD11b [F]. Data normalised and displayed as fold change versus the un-activated M0 macrophage indicated at 1. Graphs represents 2 independent experiments each comprised of triplicate values. Data for U-937 found in appendix A7. Data presented as mean ± SEM. Unpaired *t* test performed versus the un-activated M0 macrophage. *$p<0.05$.

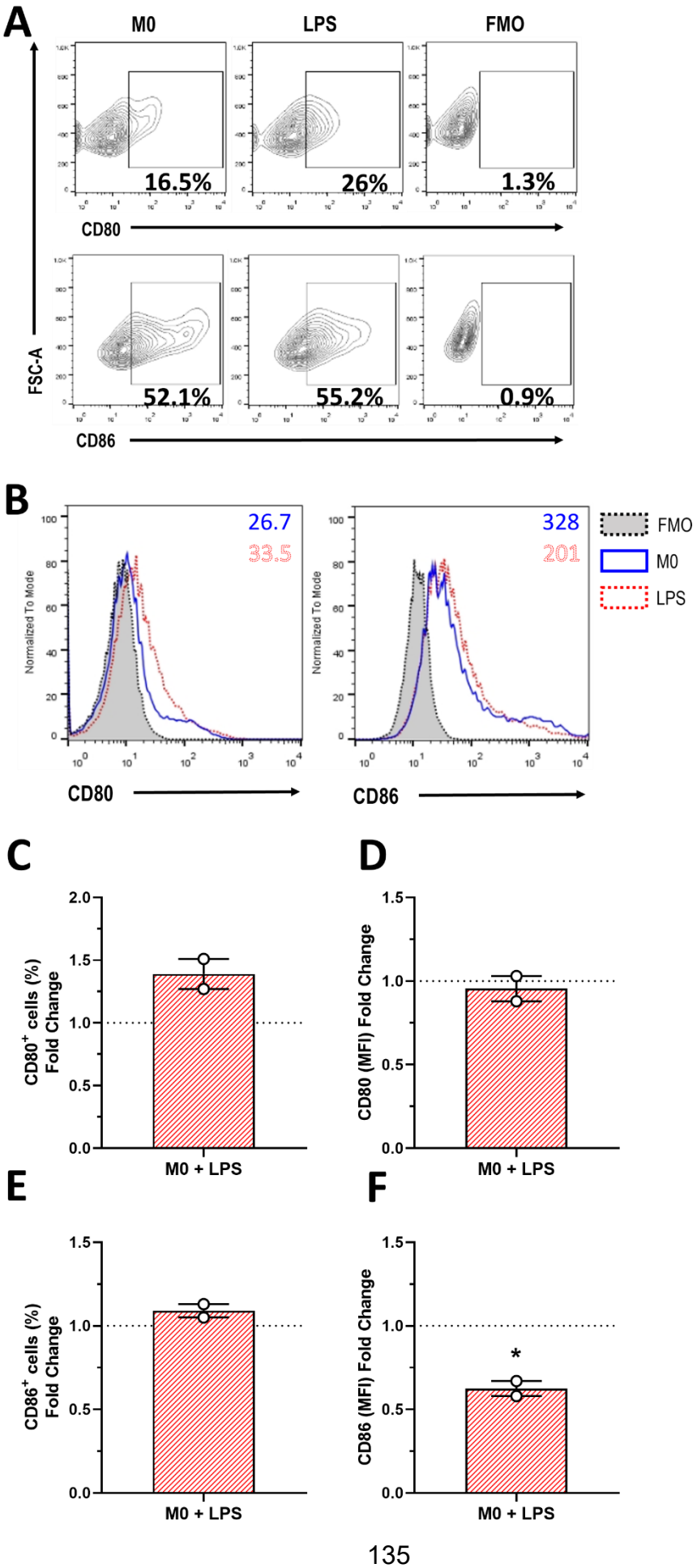
A
M0
LPS
FMO
16.5%
26%
1.3%
CD80
FSC-A
52.1%
55.2%
0.9%
CD86
B
26.7
33.5
328
201
FMO
M0
LPS
Normalized To Mode
CD80
CD86
C
D
CD80+ cells (%) Fold Change
CD80 (MFI) Fold Change
M0 + LPS
E
F
CD86+ cells (%) Fold Change
CD86 (MFI) Fold Change
*

Figure 4.2: CD80 and CD86 expression profile of LPS-activated M0 THP-1 macrophages. Data obtained after 24hr incubation of differentiated M0 macrophages with LPS (100ng/mL). [A] Representative contour plots showing the percentage of $CD80^+$ (top) and $CD86^+$ (bottom) cells. [B] Representative histograms showing mean fluorescent intensity (MFI) for CD80 (left) and CD86 (right). Numbers indicate MFI of live gated population. [C-F] Bar graphs showing the percentage of $CD80^+$ [C] and $CD86^+$ [E] cells, and MFI values for CD80 [D] and CD86 [F]. Data normalised and displayed as fold change versus the un-activated M0 macrophage indicated at 1. Graphs represent 2 independent experiments each comprised of triplicate values. Data for U-937 found in appendix A7. Data presented as mean ± SEM. Unpaired *t* test performed versus the un-activated M0 macrophage. *$p<0.05$.

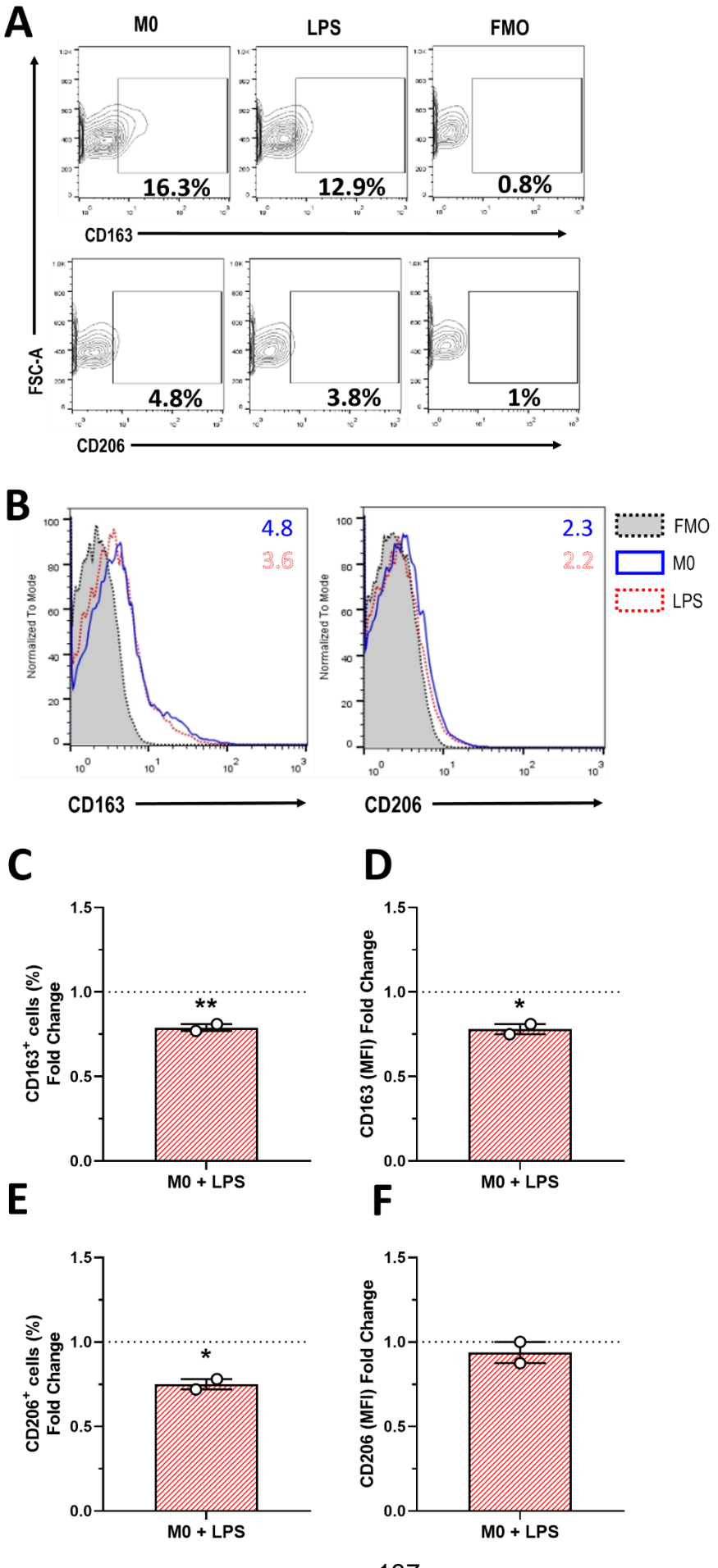
A
M0
LPS
FMO
16.3%
12.9%
0.8%
CD163
4.8%
3.8%
1%
FSC-A
CD206
B
4.8
3.6
2.3
2.2
Normalized To Mode
FMO
M0
LPS
CD163
CD206
C
D
CD163+ cells (%) Fold Change
CD163 (MFI) Fold Change
**
*
M0 + LPS
E
F
CD206+ cells (%) Fold Change
CD206 (MFI) Fold Change
*
M0 + LPS

Figure 4.3: CD163 and CD206 expression profile of LPS-activated M0 THP-1 macrophages. Data obtained after 24hr incubation of differentiated M0 macrophages with LPS (100ng/mL). [A] Representative contour plots showing the percentage of $CD163^+$ (top) and $CD206^+$ (bottom) cells. [B] Representative histograms showing mean fluorescent intensity (MFI) for CD163 (left) and CD206 (right). Numbers indicate MFI of live gated population. [C-F] Nested bar graphs showing the percentage of $CD163^+$ [C] and $CD206^+$ [E] cells, and MFI values for CD163 [D] and CD206 [F]. Data normalised and displayed as fold change versus the un-activated M0 macrophage indicated at 1. Graphs represent 2 independent experiments each comprised of triplicate values. Data for U-937 found in appendix A7. Data presented as mean ± SEM. Unpaired *t* test performed versus the un-activated M0 macrophage. *p<0.05; **p<0.01.

4.1.2. Effect of minocycline on LPS-activation of M0 THP-1 macrophages

Having established the effect of LPS activation on M0 macrophages, the next step was to assess the effect of minocycline on this process when introduced 2hr prior to, and throughout stimulation with LPS. Data displayed below in Figure 4.4A and C shows a reduction in the percentage of $CD14^+$ cells, with a 14.2% reduction exerted by 25μM (p=0.0591) and 36.7% by 50μM (p<0.0001) minocycline, which also displayed a correlation between the concentration of minocycline and the degree of reduction when compared to the LPS-activated control. This outcome was further reflected in the density of CD14 expression (Figure 4.4B and D) with both 25μM (p=0.9679) and 50μM (p<0.2186) minocycline causing a significant decrease in MFI by a fold change of 0.9 and 0.6 respectively versus the LPS control. When compared to the positive control dexamethasone, in this instance minocycline demonstrated superior effect.

When assessing the effect of minocycline on CD11b expression in its active state, an 11.5% reduction in the percentage of $CD11b^+$ cells was exerted by 25μM minocycline (p=0.9194) versus the LPS only group (Figure 4.4A and E). Here, however, minocycline at 50μM resulted in a significant increase in the density of CD11b expressed (p=0.0421), while 10μM and 25μM displayed no change. This influence of 50μM minocycline should be interpreted with caution however, given the evidence presented in the previous chapter regarding the toxicity of minocycline at this concentration (Figure 4.4B and F).

When analysing the data obtained from the M1-associated surface markers CD80 and CD86 opposing consequences of minocycline were observed. First, the expression of CD80 was unanimously modified by treatment with

minocycline, with all concentrations resulting in significant upregulation of both the percentage of $CD80^+$ cells, as well as the density of CD80 expression (Figure 4.5A-D). Minocycline at 25μM was the most potent modifier in the instance of the percentage of $CD80^+$ cells, causing a significant increase in $CD80^+$ cells by 74.7% (p<0.0001). However, minocycline at 50μM more potently increased the density of CD80 expression with a 9.2-fold increase in MFI (p<0.0001) versus the LPS treatment group. The inverse however was seen when analysing CD86, which appears to consolidate the negative effect of LPS versus the un-activated macrophage control as noted previously. Here a correlation between minocycline concentration and the degree of reduction in the percentage of $CD86^+$ cells (Figure 4.5A and E) was noted. Minocycline at 25μM and 50μM reduced the percentage of $CD86^+$ cells by 7% (p=0.9285) and 18.5% (p=0.2826) respectively versus the LPS only control. Data obtained for the density of CD86 expression also indicated a reduction elicited by 50μM minocycline, in which the MFI was decreased by 0.86-fold (p=0.9487) (Figure 4.5B and F). With CD80, minocycline exceeded the response seen by dexamethasone, providing far better marker modification, however in the case of CD86 it acted to counter dexamethasone's effect, which itself seems to behave in a way that restores the negative effect of LPS to that of a non-activated baseline.

Arguably the most prominent data from these experiments was the effect of minocycline on the M2-associated markers CD163 and CD206. In this regard, minocycline at all concentrations caused significant upregulation of the percentage of both proteins, with 25μM again providing the most prominent change in expression (Figure 4.6). Minocycline at 25μM resulted in the conversion of almost 100% of cells to express both markers, with an increase of 85.8% in $CD163^+$ cells, and 91.9% of $CD206^+$ cells, up from 12% and 5% respectively in the LPS only group (Figure 4.6A, C and E). This modification was also reflected in the density of expression but failed to reach significance, with minocycline at 25μM causing a 11.1-fold increase in CD163, and a 10-fold increase in CD206 (Figure 4.6B, D and F). Here however, minocycline at 50μM was more potent resulting in a 24.4-fold and 20.6-fold increase in CD163 and CD206 density of expression respectively (Figure 4.6B, D and F). When compared to the dexamethasone treated group, minocycline was shown to have a greater ability to increase the expression of both markers.

Regarding the DMSO vehicle control, there were few notable changes in expression of any of the markers included in the analysis. The data presented in this section reflect that obtained from the THP-1 cell line, however results achieved using U-937 was unanimous in minocycline's influence on expression profiles, especially the M2-related markers. This data can be found in appendix A10.

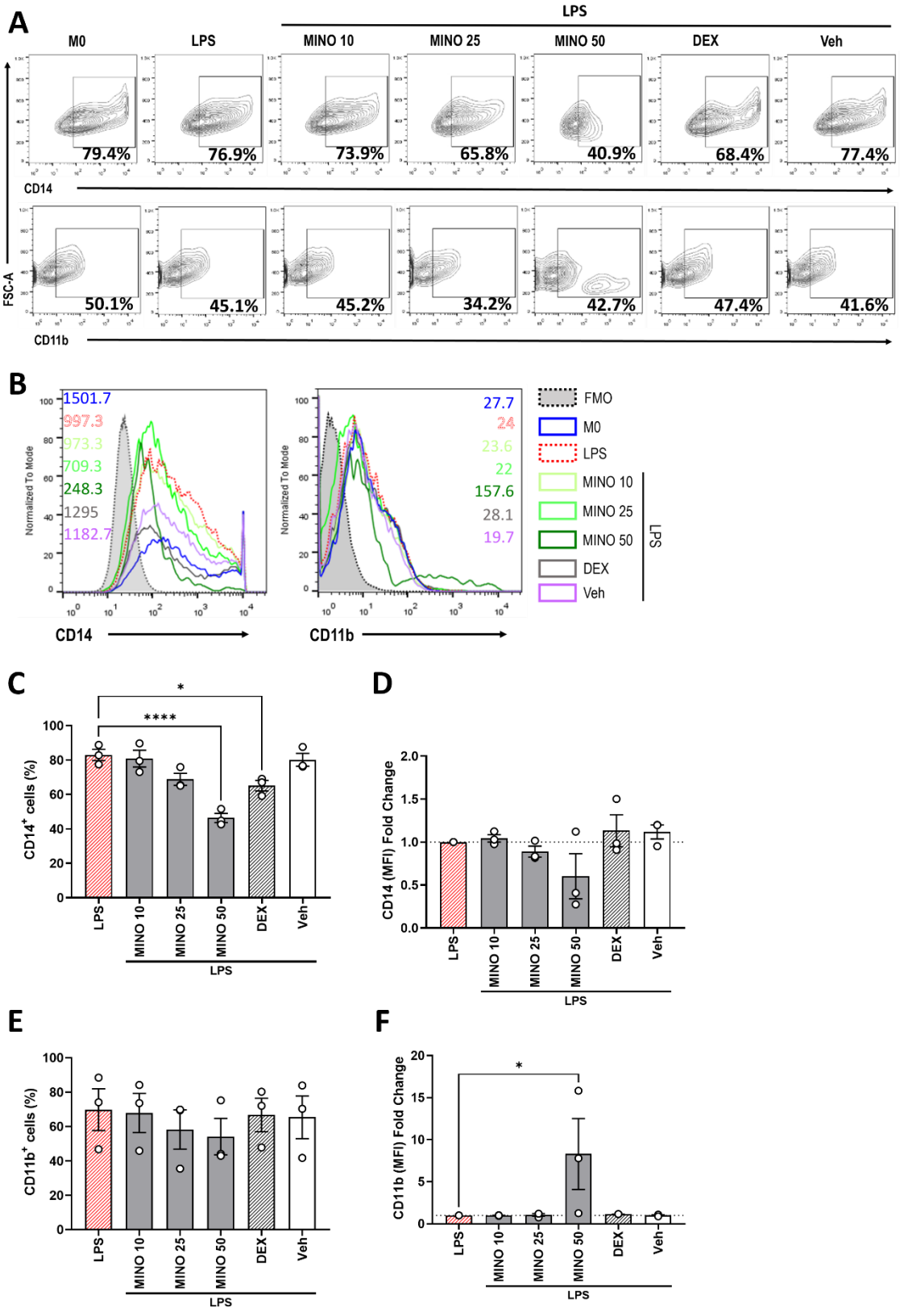
A
LPS
M0
LPS
MINO 10
MINO 25
MINO 50
DEX
Veh
79.4%
76.9%
73.9%
65.8%
40.9%
68.4%
77.4%
CD14
FSC-A
50.1%
45.1%
45.2%
34.2%
42.7%
47.4%
41.6%
CD11b
B
1501.7
997.3
373.3
709.3
248.3
1295
1182.7
27.7
24
23.6
22
157.6
28.1
19.7
Normalized To Mode
CD14
CD11b
FMO
M0
LPS
MINO 10
MINO 25
MINO 50
DEX
Veh
LPS
C
CD14+ cells (%)
*
****
LPS
MINO 10
MINO 25
MINO 50
DEX
Veh
LPS
D
CD14 (MFI) Fold Change
LPS
MINO 10
MINO 25
MINO 50
DEX
Veh
LPS
E
CD11b+ cells (%)
LPS
MINO 10
MINO 25
MINO 50
DEX
Veh
LPS
F
CD11b (MFI) Fold Change
*
LPS
MINO 10
MINO 25
MINO 50
DEX
Veh
LPS

Figure 4.4: Effect of minocycline on CD14 and CD11b expression following LPS activation of M0 THP-1 macrophages. Data obtained after 24hr incubation of differentiated M0 macrophages with LPS (100ng/mL). MINO 10 = Minocycline 10μM, MINO 25 = Minocycline 25μM, MINO 50 = Minocycline 50μM, DEX = Dexamethasone 50μM, Veh = DMSO vehicle control 1:1000. [A] Representative contour plots showing the percentage of $CD14^+$ (top) and $CD11b^+$ (bottom) cells. [B] Representative histograms showing mean fluorescent intensity (MFI) for CD14 (left) and CD11b (right). Numbers indicate MFI of live gated population. [C-F] Bar graphs showing the percentage of $CD14^+$ [C] and $CD11b^+$ [E] cells, and MFI values for CD14 [D] and CD11b [F]. MFI values have been normalised and displayed as fold change versus the un-activated M0 macrophage control indicated at 1. Graphs representative of 3 independent experiments each comprised of triplicate values. Data for U-937 can be found in appendix A10. Data presented as mean ± SEM. One-way ANOVA with post hoc Dunnett's applied versus the LPS-activated M0 macrophage. *p<0.05; ****p<0.0001.

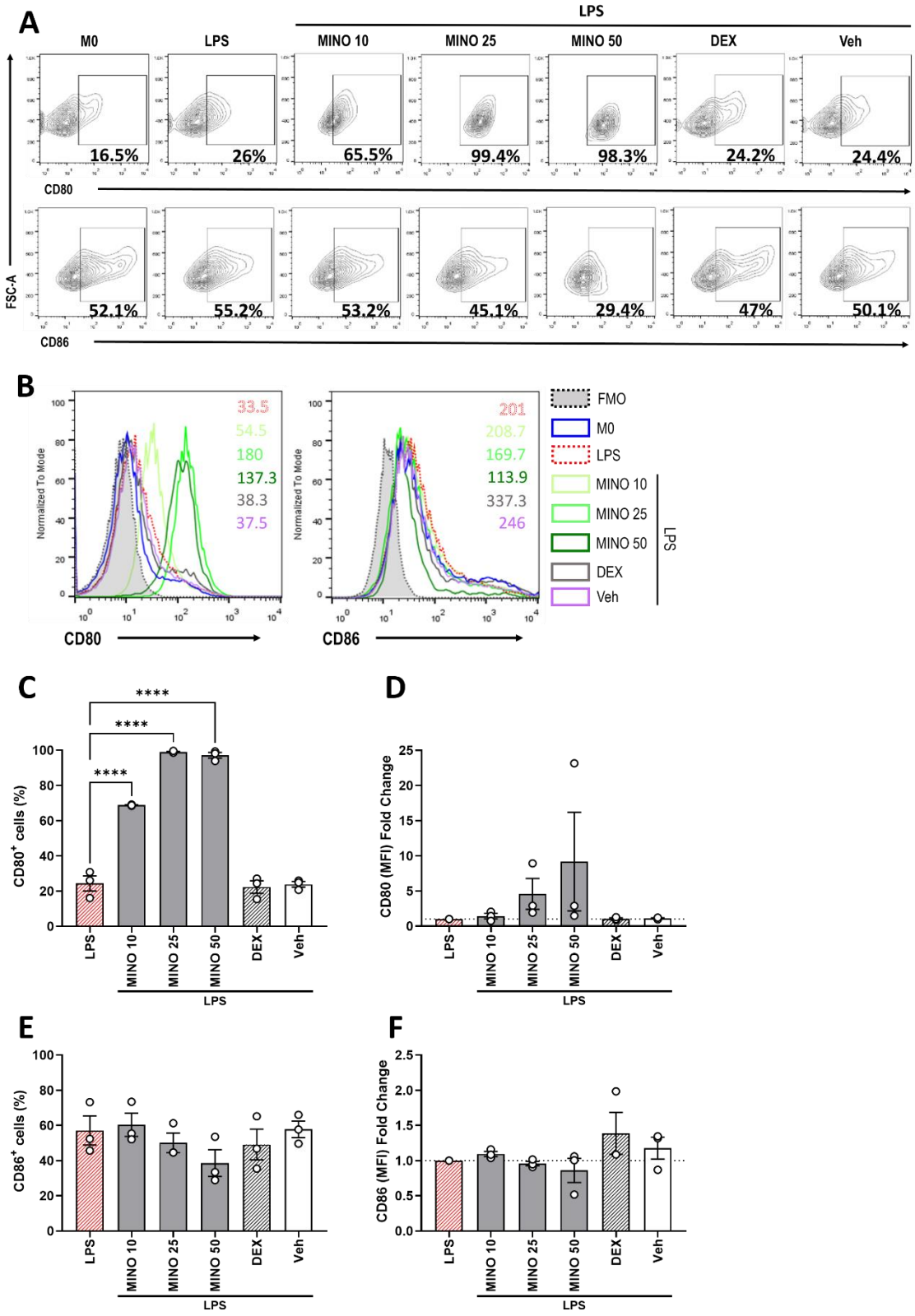
A
LPS
M0
LPS
MINO 10
MINO 25
MINO 50
DEX
Veh
16.5%
26%
65.5%
99.4%
98.3%
24.2%
24.4%
CD80
FSC-A
52.1%
55.2%
53.2%
45.1%
29.4%
47%
50.1%
CD86
B
Normalized To Mode
33.5
54.5
180
137.3
38.3
37.5
201
208.7
169.7
113.9
337.3
246
CD80
CD86
FMO
M0
LPS
MINO 10
MINO 25
MINO 50
DEX
Veh
LPS
C
CD80+ cells (%)
****
****
****
LPS
MINO 10
MINO 25
MINO 50
DEX
Veh
LPS
D
CD80 (MFI) Fold Change
LPS
MINO 10
MINO 25
MINO 50
DEX
Veh
LPS
E
CD86+ cells (%)
LPS
MINO 10
MINO 25
MINO 50
DEX
Veh
LPS
F
CD86 (MFI) Fold Change
LPS
MINO 10
MINO 25
MINO 50
DEX
Veh
LPS

Figure 4.5: Effect of minocycline on CD80 and CD86 expression following LPS activation of M0 THP-1 macrophages. Data obtained after 24hr incubation of differentiated M0 macrophages with LPS (100ng/mL). MINO 10 = Minocycline 10μM, MINO 25 = Minocycline 25μM, MINO 50 = Minocycline 50μM, DEX = Dexamethasone 50μM, Veh = DMSO vehicle control 1:1000. [A] Representative contour plots showing the percentage of $CD80^+$ (top) and $CD86^+$ (bottom) cells. [B] Representative histograms showing mean fluorescent intensity (MFI) for CD80 (left) and CD86 (right). Numbers indicate MFI of live gated population. [C-F] Bar graphs showing the percentage of $CD80^+$ [C] and $CD86^+$ [E] cells, and MFI values for CD80 [D] and CD86 [F]. MFI values have been normalised and displayed as fold change versus the un-activated M0 macrophage control indicated at 1. Graphs representative of 3 independent experiments each comprised of triplicate values. Data for U-937 can be found in appendix A10. Data presented as mean ± SEM. One-way ANOVA with post hoc Dunnett's applied versus the LPS-activated M0 macrophage. ****p<0.0001.

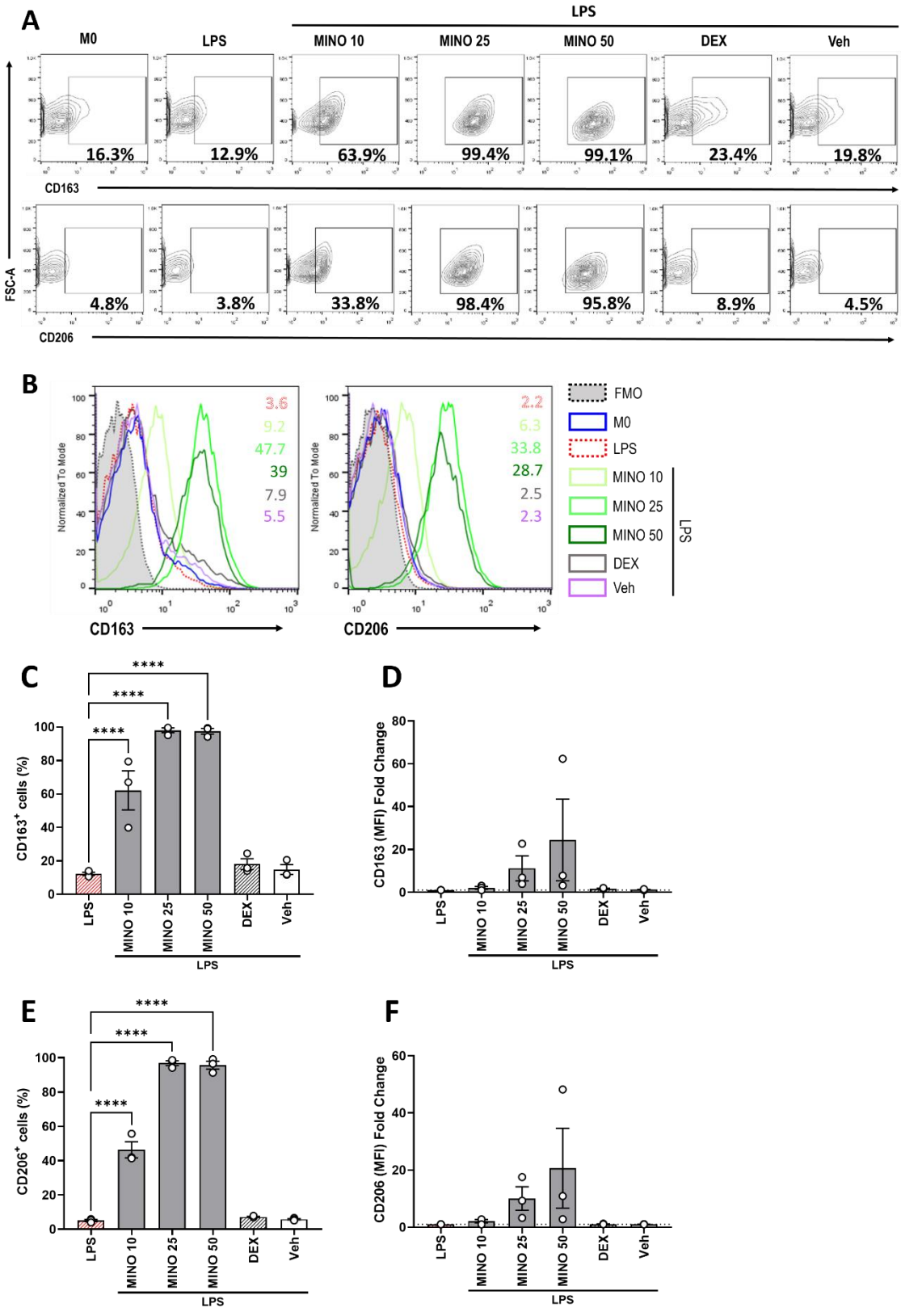
A
LPS
M0
LPS
MINO 10
MINO 25
MINO 50
DEX
Veh
16.3%
12.9%
63.9%
99.4%
99.1%
23.4%
19.8%
CD163
FSC-A
4.8%
3.8%
33.8%
98.4%
95.8%
8.9%
4.5%
CD206
B
Normalized To Mode
3.6
9.2
47.7
39
7.9
5.5
2.2
6.3
33.8
28.7
2.5
2.3
CD163
CD206
FMO
M0
LPS
MINO 10
MINO 25
MINO 50
DEX
Veh
LPS
C
CD163+ cells (%)
****
****
****
LPS
MINO 10
MINO 25
MINO 50
DEX
Veh
LPS
D
CD163 (MFI) Fold Change
LPS
MINO 10
MINO 25
MINO 50
DEX
Veh
LPS
E
CD206+ cells (%)
****
****
****
LPS
MINO 10
MINO 25
MINO 50
DEX
Veh
LPS
F
CD206 (MFI) Fold Change
LPS
MINO 10
MINO 25
MINO 50
DEX
Veh
LPS

Figure 4.6: Effect of minocycline on CD163 and CD206 expression following LPS activation of M0 THP-1 macrophages. Data obtained after 24hr incubation of differentiated M0 macrophages with LPS (100ng/mL). MINO 10 = Minocycline 10μM, MINO 25 = Minocycline 25μM, MINO 50 = Minocycline 50μM, DEX = Dexamethasone 50μM, Veh = DMSO vehicle control 1:1000. [A] Representative contour plots showing the percentage of $CD163^+$ (top) and $CD206^+$ (bottom) cells. [B] Representative histograms showing mean fluorescent intensity (MFI) for CD163 (left) and CD206 (right). Numbers indicate MFI of live gated population. [C-F] Bar graphs showing the percentage of $CD163^+$ [C] and $CD206^+$ [E] cells, and MFI values for CD163 [D] and CD206 [F]. MFI values have been normalised and displayed as fold change versus the un-activated M0 macrophage control indicated at 1. Graphs representative of 3 independent experiments each comprised of triplicate values. Data for U-937 can be found in appendix A10. Data presented as mean ± SEM. One-way ANOVA with post hoc Dunnett's applied versus the LPS-activated M0 macrophage. ****$p<0.0001$.

4.2. PBMC

4.2.1. Characterising LPS activation of M0 PBMC macrophages

To evaluate whether the findings obtained from the two independent cell lines were translatable, primary macrophages in the form of M-CSF-expanded PBMCs were used. A collaboration with Dr Jose Garrido Mesa at Queen Mary University London (UK) was established, who kindly provided the PBMC-derived, M-CSF-expanded primary macrophages from four individual donors. To maintain consistency between *in vitro* methodologies, once generated, these resting 'M0' macrophages were handled following the same experimental protocol as the THP-1 and U-937 cell lines, with sequential pre-treatment with minocycline for 2hr prior to 24hr stimulation with LPS as noted in chapter 2, section 2.2.2. Protocol modification came in respect to treatment groups included in the analysis, as due to limited cell numbers, it was not possible to include either the dexamethasone or minocycline (50μM) conditions. The vehicle control was also adjusted to account for this restriction in cellular material and in this instance was included in all conditions at the same final concentration (1:1000) to ensure any changes witnessed were due to a direct effect of the different treatments. As this was the first study conducted using the PBMC-derived macrophages, it was important to first establish if minocycline at 10μM and 25μM had any adverse effect on culture viability. Results shown in Figure 4.7 below indicate no negative effect of either LPS or minocycline on the viability of the donor cells, with no identifiable change in the percentage of live cells.

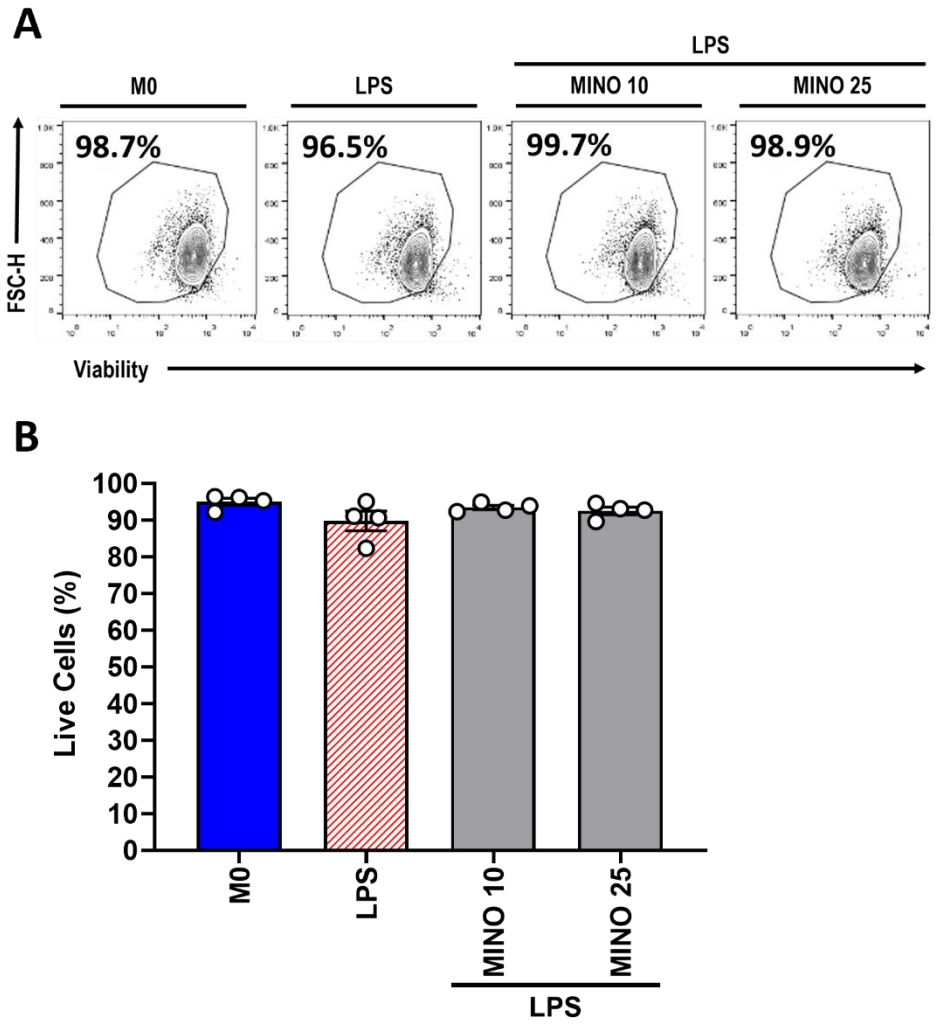

Figure 4.7: Effect of LPS and minocycline on PBMC-derived macrophage culture viability. Data obtained after 24hr incubation of M-CSF-expanded M0 macrophages with LPS (100ng/mL). MINO 10 = Minocycline 10μM, MINO 25 = Minocycline 25μM. [A] Representative contour plots showing the percentage of live cells (Zombie Aqua^{neg}). [B] Bar graph showing the percentage of live cells. Plots illustrate one representative donor. Graphs represent pooled data obtained from 4 individual donors each comprised of duplicate values. Data presented as mean ± SEM. One-way ANOVA with post hoc Dunnett's applied versus the LPS-activated M0 macrophage.

Given the evidence that there was no adverse effect on viability within the experimental model, the effect of LPS upon each of the 6 surface markers used previously was next characterised. Figure 4.8 outlines the effect of 24hr LPS activation on CD14 and CD11b expression. Here LPS had no clear influence on the percentage of CD14^{+} cells when compared to the un-activated M0 baseline control (Figure 4.8A and C). However, stimulation with LPS resulted in a significant reduction in the density of expression reflected in all 4 donors (Figure 4.8B and D). Similarly, the expression of total CD11b was consistently downregulated, reflected in both the percentage of CD11b^{+} cells and density of

expression (Figure 4.8A, B, E and F). These changes were similar with the data obtained from the characterisation of LPS on THP-1-derived macrophages. In addition to the previous evidence provided regarding cause for reduced expression of CD14, other reports also suggest high-dose LPS may results in a decline in CD14 expression due to stimulation of IFN-γ production (Landmann *et al.*, 1991). Similarly, the data below which indicates a decrease in CD11b expression may be further explained by the integral role of CD11b in cellular adhesion and migration during inflammation, which has previously been corroborated to decline at 24hr post LPS stimulation, although this clone (ICRF44) does not distinguish activated protein which would be indicative of an influence upon CD11b function (Lukácsi *et al.*, 2020).

When evaluating the M1-associated markers CD80 and CD86, LPS upregulated both proteins, which was reflected both in the percentage of positively expressing cells and the density of marker expression, and across all donors studied (Figure 4.9A-F). This data was coherent with the literary reports for this model (Rivellese *et al.*, 2014), and could indicate that cells of primary origin like the PBMCs, versus their immortalised counterpart like THP-1, behave more homogenously which may be associated, at least in part, with the genetic modification that accompanies cell lines with pathogenic origin like the leukemic cell lines THP-1 and U-937.

Finally, data gathered for CD163 and CD206 showed significant reduction in both markers, reflected in the percentage of positive cells and the density of expression, with slight variation in magnitude between donor cells (Figure 4.10A-F). Reassuringly, these data were entirely consistent with the THP-1 profile and provided further corroboration between both the different *in vitro* models, as well as proof of concept for the protocol designed and used for LPS-activation of macrophages.

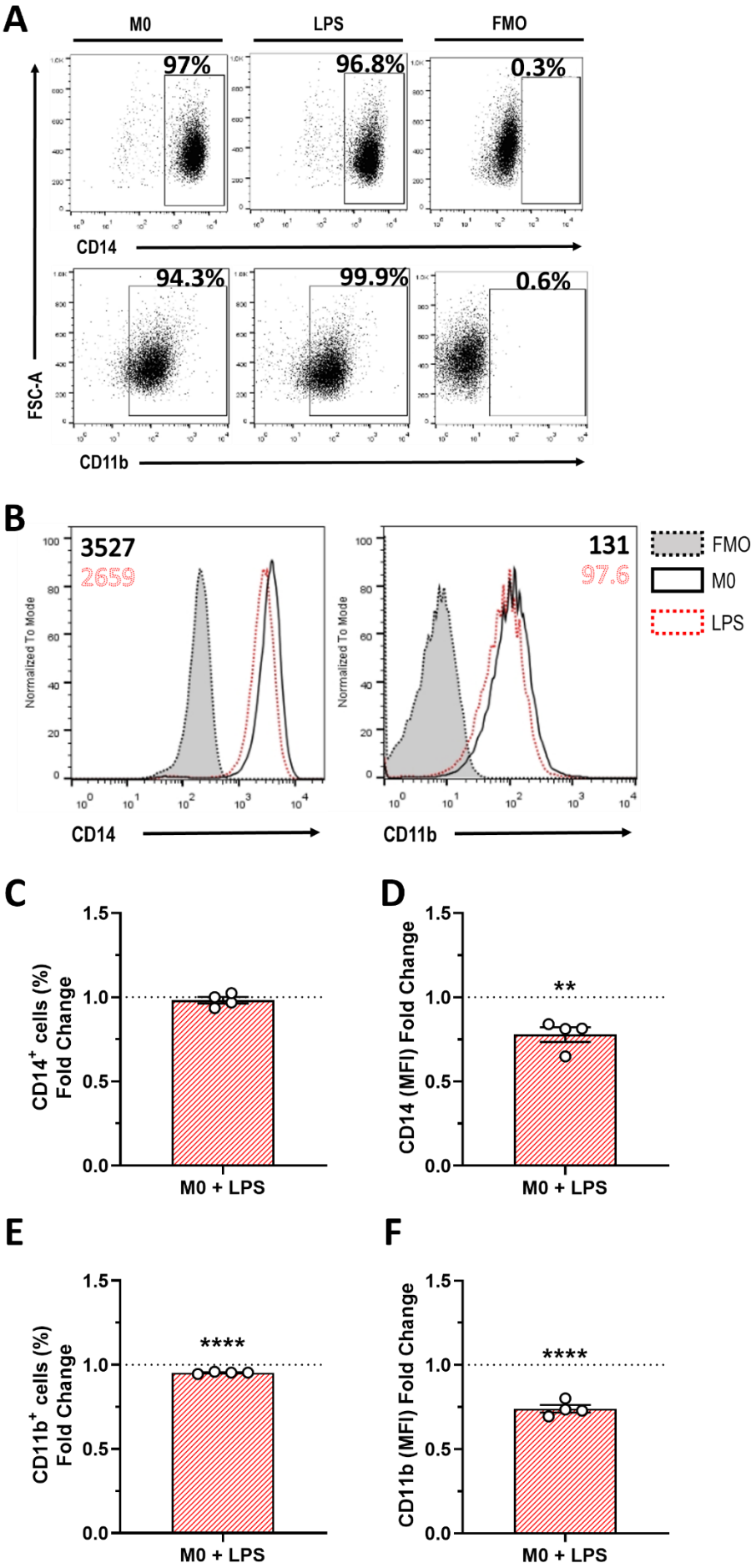
A
M0
LPS
FMO
97%
96.8%
0.3%
CD14
94.3%
99.9%
0.6%
FSC-A
CD11b
B
3527
2659
131
97.6
FMO
M0
LPS
Normalized To Mode
CD14
CD11b
C
CD14+ cells (%) Fold Change
M0 + LPS
D
CD14 (MFI) Fold Change
**
M0 + LPS
E
CD11b+ cells (%) Fold Change
****
M0 + LPS
F
CD11b (MFI) Fold Change
****
M0 + LPS

Figure 4.8: CD14 and CD11b expression profile of LPS-activated PBMC-derived M0 macrophages. Data obtained after 24hr incubation of M-CSF-expanded M0 macrophages with LPS (100ng/mL). [A] Representative dot plots showing the percentage of $CD14^+$ (top) and $CD11b^+$ (bottom) cells. [B] Representative histograms showing mean fluorescent intensity (MFI) for CD14 (left) and CD11b (right). Numbers indicate MFI of live gated population. [C-F] Bar graphs showing the percentage of $CD14^+$ [C] and $CD11b^+$ [E] cells, and MFI values for CD14 [D] and CD11b [F]. Data normalised and displayed as fold change versus the un-activated M0 macrophage indicated at 1. Plots and histograms illustrate one representative donor. Graphs represent data from 4 individual donors each comprised of duplicate values. Data presented as mean ± SEM. Unpaired *t* test applied versus the un-activated M0 macrophage. **p<0.01; ****p<0.0001.

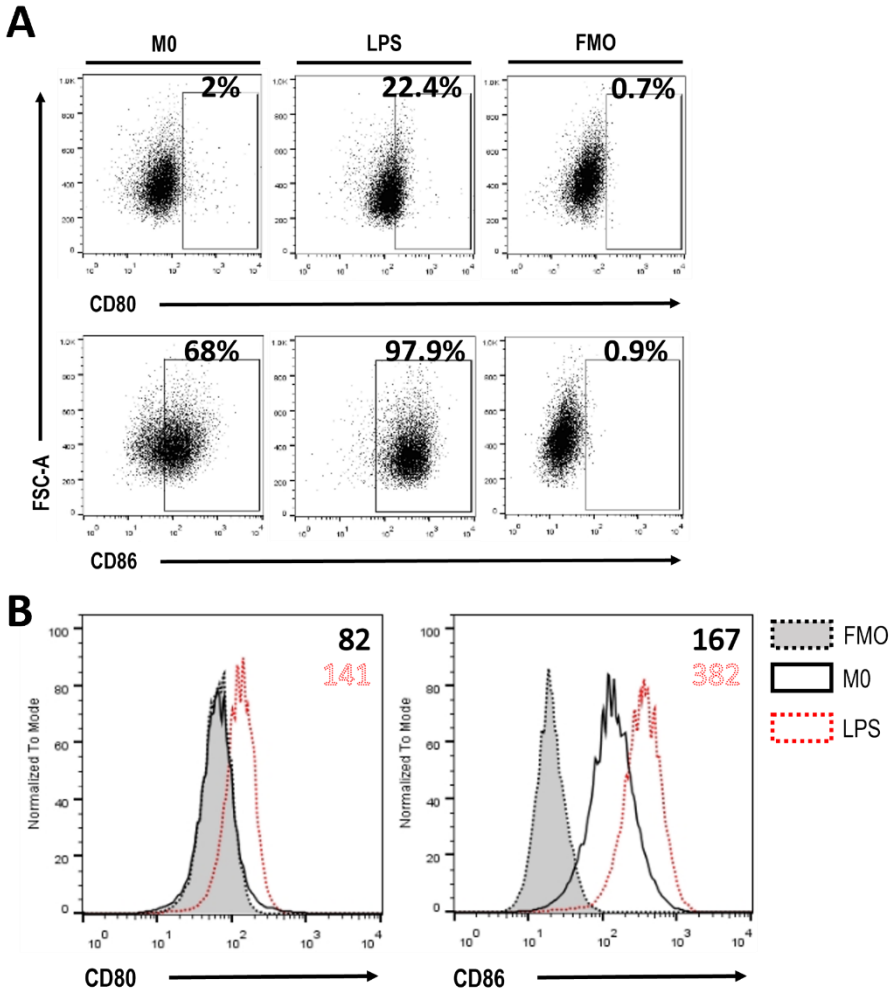
A
M0
LPS
FMO
2%
22.4%
0.7%
CD80
68%
97.9%
0.9%
FSC-A
CD86
B
82
141
167
382
FMO
M0
LPS
Normalized To Mode
CD80
CD86

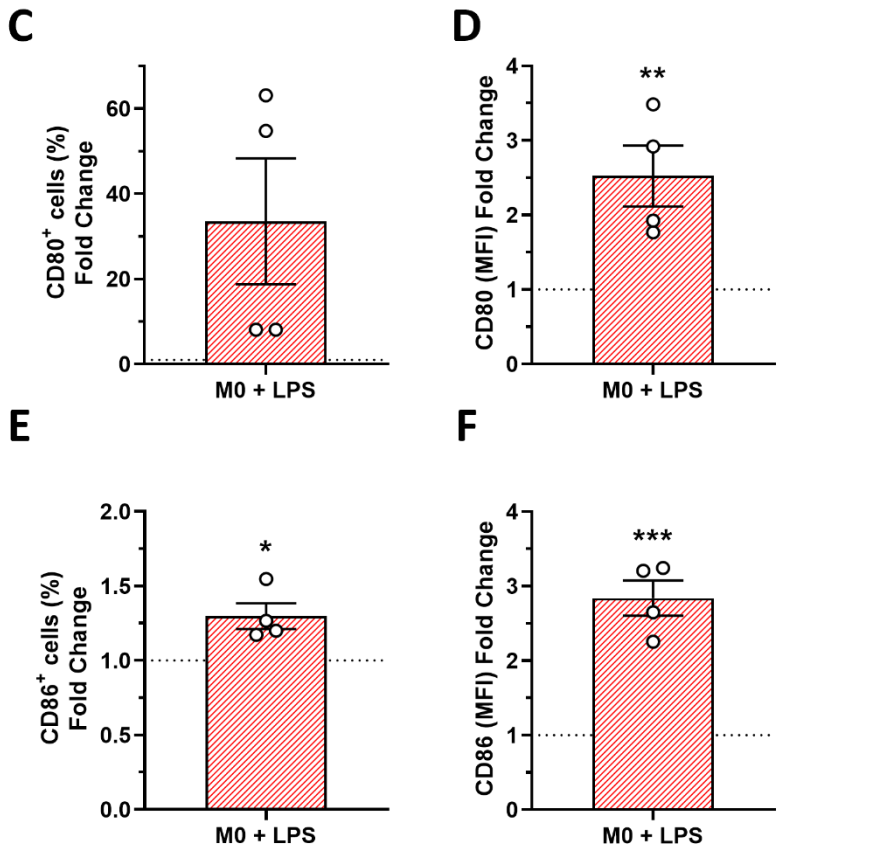
C
CD80+ cells (%) Fold Change
M0 + LPS
D
CD80 (MFI) Fold Change
**
M0 + LPS
E
CD86+ cells (%) Fold Change
*
M0 + LPS
F
CD86 (MFI) Fold Change
***
M0 + LPS

Figure 4.9: CD80 and CD86 expression profile of LPS-activated PBMC-derived M0 macrophages. Data obtained after 24hr incubation of M-CSF-expanded M0 macrophages with LPS (100ng/mL). [A] Representative dot plots showing the percentage of $CD80^+$ (top) and $CD86^+$ (bottom) cells. [B] Representative histograms showing mean fluorescent intensity (MFI) for CD80 (left) and CD86 (right). Numbers indicate MFI of live gated population. [C-F] Bar graphs showing the percentage of $CD80^+$ [C] and $CD86^+$ [E] cells, and MFI values for CD80 [D] and CD86 [F]. Data normalised and displayed as fold change versus the un-activated M0 macrophage indicated at 1. Plots and histograms illustrate one representative donor. Graphs represent data from 4 individual donors each comprised of duplicate values. Data presented as mean ± SEM. Unpaired *t* test applied versus the un-activated M0 macrophage. *p<0.05; **p<0.01; ***p<0.001.

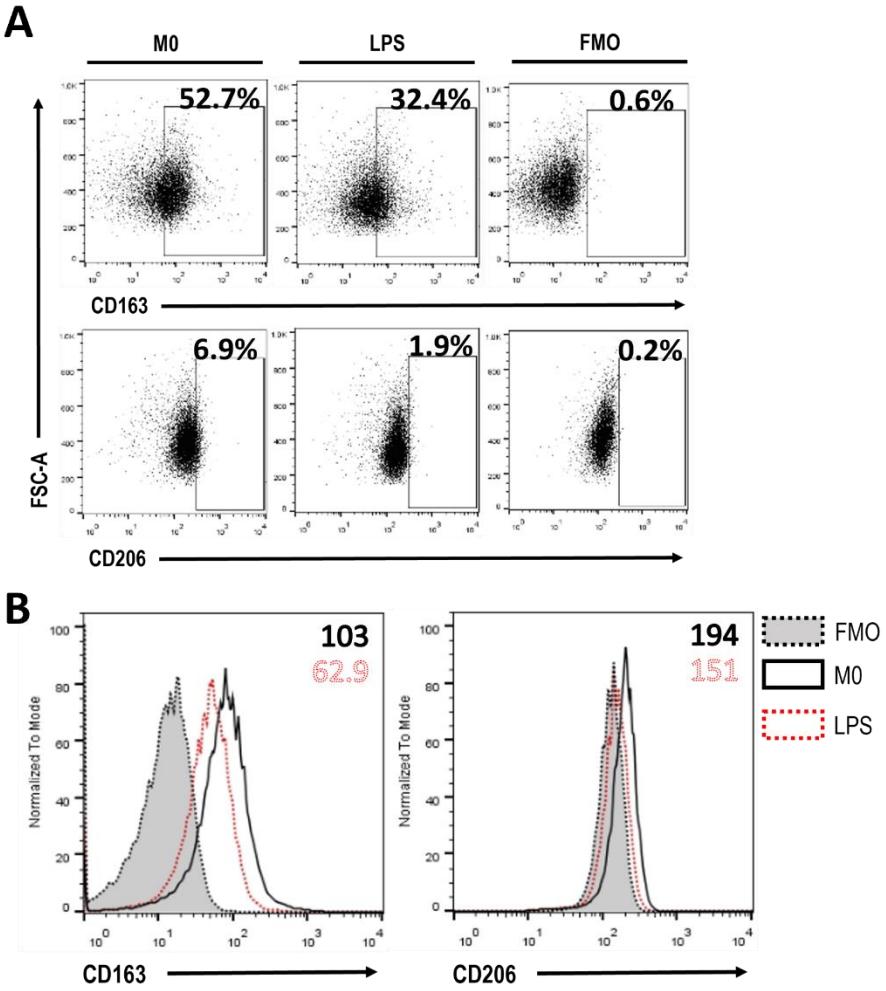
A
M0
LPS
FMO
52.7%
32.4%
0.6%
CD163
6.9%
1.9%
0.2%
FSC-A
CD206
B
103
62.9
194
151
Normalized To Mode
FMO
M0
LPS
CD163
CD206
C
D
CD163+ cells (%) Fold Change
CD163 (MFI) Fold Change
**
***
M0 + LPS
E
F
CD206+ cells (%) Fold Change
CD206 (MFI) Fold Change
***
***
M0 + LPS

Figure 4.10: CD163 and CD206 expression profile of LPS-activated PBMC-derived M0 macrophages. Data obtained after 24hr incubation of M-CSF-expanded M0 macrophages with LPS (100ng/mL). [A] Representative dot plots showing the percentage of $CD163^+$ (top) and $CD206^+$ (bottom) cells. [B] Representative histograms showing mean fluorescent intensity (MFI) for CD163 (left) and CD206 (right). Numbers indicate MFI of live gated population. [C-F] Bar graphs showing the percentage of $CD163^+$ [C] and $CD206^+$ [E] cells, and MFI values for CD163 [D] and CD206 [F]. Data normalised and displayed as fold change versus the un-activated M0 macrophage indicated at 1. Plots and histograms illustrate one representative donor. Graphs represent data from 4 individual donors each comprised of duplicate values. Data presented as mean ± SEM. Unpaired *t* test applied versus the un-activated M0 macrophage. **p<0.01; ***p<0.001.

4.2.2. Effect of minocycline during LPS-activation of PBMC-derived M0 macrophages

To next assess the effect of minocycline on the LPS-induced activation of PBMC-derived M0 macrophages, minocycline at 10μM and 25μM was administered to the M0 macrophages for 2hr prior to the addition of LPS (100ng/mL). Following 24hr incubation surface marker expression was evaluated. Firstly, minocycline elicited no discernible change in either the percentage of $CD14^+$ cells or the density of CD14 expression (Figure 4.11A-D), nor the expression of CD11b (Figure 4.11A and E).

On the other hand, a subtle increase in CD80 expression resulted from treatment with minocycline, causing a 2% and 9% increase in the percentage of $CD80^+$ cells by 10μM and 25μM respectively (Figure 4.12A and C). This upregulation by minocycline was further mirrored in the density of CD80 expression with a 0.1-fold increase by 10μM minocycline (p=0.9969), and a 0.3-fold increase by 25μM minocycline (p=9111) (Figure 4.12B and D). Values obtained for CD86 showed no distinguishable change in the percentage of $CD86^+$ cells by minocycline (Figure 4.12A and E), nor in the density of CD86 (Figure 4.12B and F).

Finally, the M2-associated markers CD163 and CD206 also revealed negligible change in expression incited by minocycline treatment with no definable difference in CD163 (Figure 4.13A, B, C and D), or CD206 (Figure 4.13A, B, C, E and F). From these experiments, subtle changes in CD80 expression driven by minocycline was congruent with the THP-1 findings. In addition, despite the data for the M2-associated markers CD163 and CD206 remaining below statistical

significance, trends in expression did not refute those found previously, with no conflicting data to counter the narrative implied by the THP-1 results.

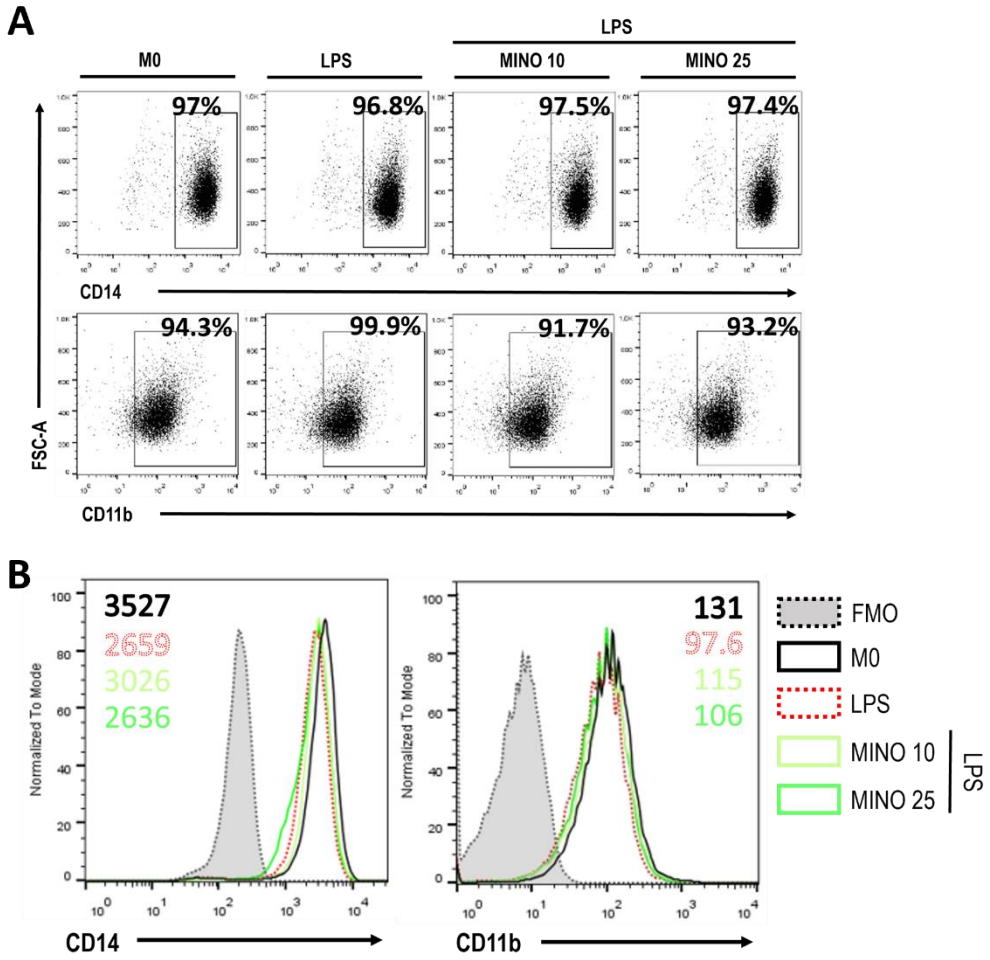
A
M0
LPS
LPS
MINO 10
MINO 25
97%
96.8%
97.5%
97.4%
CD14
94.3%
99.9%
91.7%
93.2%
FSC-A
CD11b
B
3527
2659
3026
2636
131
97.6
115
106
Normalized To Mode
FMO
M0
LPS
MINO 10
MINO 25
LPS
CD14
CD11b
C
CD14+ cells (%)
M0
LPS
MINO 10
MINO 25
LPS
D
CD14 (MFI) Fold Change
**
E
CD11b+ cells (%)
**
F
CD11b (MFI) Fold Change
****

Figure 4.11: Effect of minocycline on CD14 and CD11b expression following LPS activation of PBMC-derived M0 macrophages. Data obtained after 2hr pre-treatment with minocycline and 24hr incubation of M-CSF-expanded M0 macrophages with LPS (100ng/mL). MINO 10 = Minocycline 10μM, MINO 25 = Minocycline 25μM. [A] Representative dot plots showing the percentage of $CD14^+$ (top) and $CD11b^+$ (bottom) cells. [B] Representative histograms showing mean fluorescent intensity (MFI) for CD14 (left) and CD11b (right). Numbers indicate MFI of live gated population. [C-F] Bar graphs showing the percentage of $CD14^+$ [C] and $CD11b^+$ [E] cells, and MFI values for CD14 [D] and CD11b [F]. MFI values normalised and displayed as fold change versus the un-activated M0 macrophage control indicated at 1. Plots and histograms illustrate one representative donor. Graphs represent data from 4 individual donors each comprised of duplicate values. Data presented as mean ± SEM. One-way ANOVA with post hoc Dunnett's applied versus the LPS-activated M0 macrophage. $^{**}p<0.01$; $^{***}p<0.0001$.

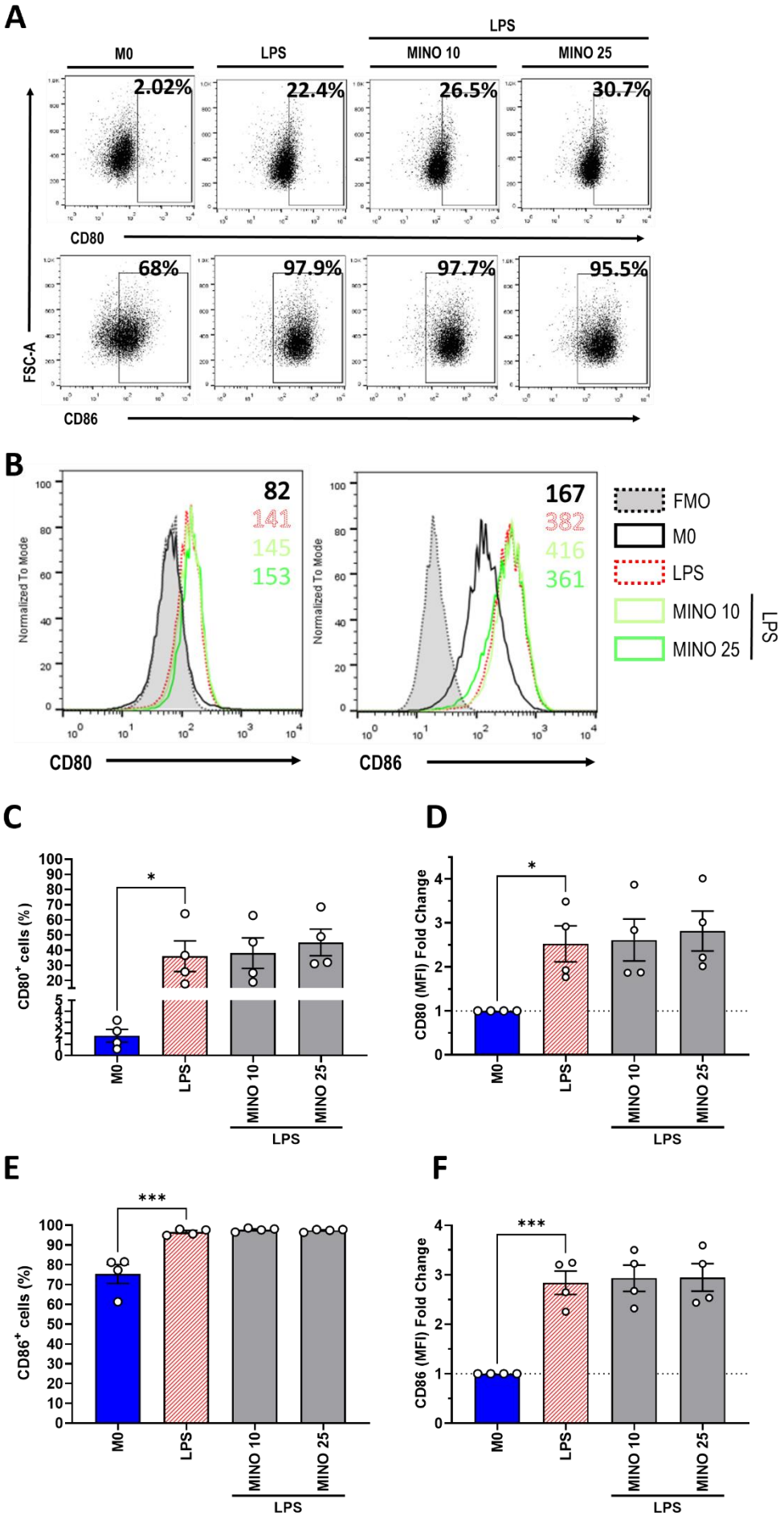
A
LPS
M0
LPS
MINO 10
MINO 25
2.02%
22.4%
26.5%
30.7%
CD80
68%
97.9%
97.7%
95.5%
FSC-A
CD86
B
82
141
145
153
167
382
416
361
Normalized To Mode
FMO
M0
LPS
MINO 10
MINO 25
LPS
CD80
CD86
C
CD80+ cells (%)
D
CD80 (MFI) Fold Change
E
CD86+ cells (%)
F
CD86 (MFI) Fold Change
M0
LPS
MINO 10
MINO 25
LPS

Figure 4.12: Effect of minocycline on CD80 and CD86 expression following LPS activation of PBMC-derived M0 macrophages. Data obtained after 2hr pre-treatment with minocycline and 24hr incubation of M-CSF-expanded M0 macrophages with LPS (100ng/mL). MINO 10 = Minocycline 10μM, MINO 25 = Minocycline 25μM. [A] Representative dot plots showing the percentage of $CD80^+$ (top) and $CD86^+$ (bottom) cells. [B] Representative histograms showing mean fluorescent intensity (MFI) for CD80 (left) and CD86 (right). Numbers indicate MFI of live gated population. [C-F] Bar graphs showing the percentage of $CD80^+$ [C] and $CD86^+$ [E] cells, and MFI values for CD80 [D] and CD86 [F]. MFI values normalised and displayed as fold change versus the un-activated M0 macrophage control indicated at 1. Plots and histograms illustrate one representative donor. Graphs represent data from 4 individual donors each comprised of duplicate values. Data presented as mean ± SEM. One-way ANOVA with post hoc Dunnett's applied versus the LPS-activated M0 macrophage. *p<0.05; ***p<0.001.

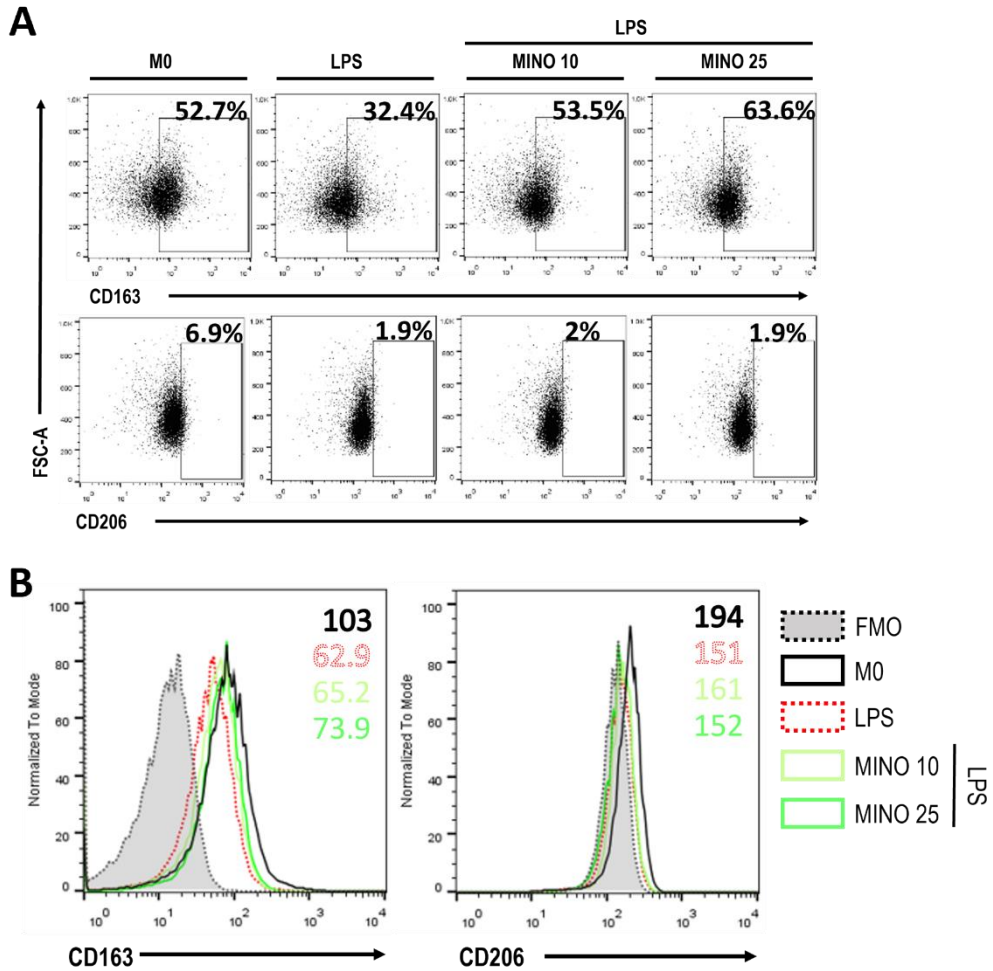
A
LPS
M0
LPS
MINO 10
MINO 25
52.7%
32.4%
53.5%
63.6%
CD163
6.9%
1.9%
2%
1.9%
FSC-A
CD206
B
103
62.9
65.2
73.9
194
151
161
152
Normalized To Mode
FMO
M0
LPS
MINO 10
MINO 25
LPS
CD163
CD206

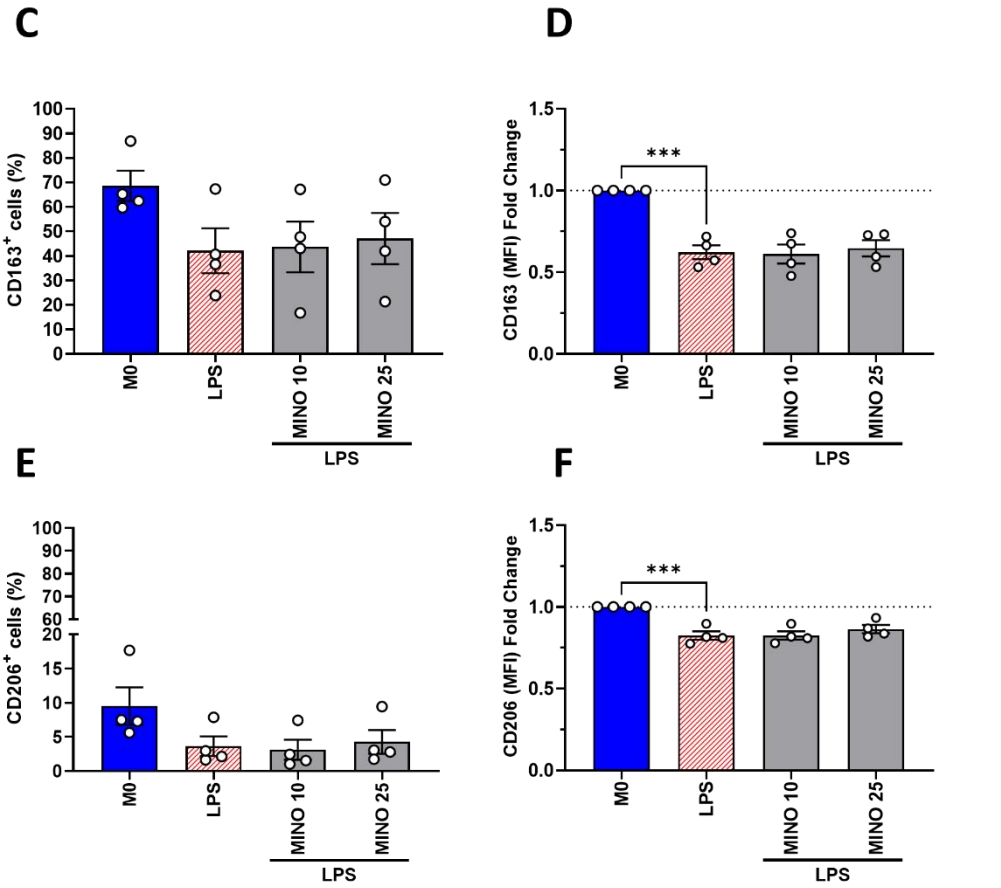
C
D
CD163+ cells (%)
CD163 (MFI) Fold Change
***
M0
LPS
MINO 10
MINO 25
LPS
E
F
CD206+ cells (%)
CD206 (MFI) Fold Change
***
M0
LPS
MINO 10
MINO 25
LPS

Figure 4.13: Effect of minocycline on CD163 and CD206 expression following LPS activation of PBMC-derived M0 macrophages. Data obtained after 2hr pre-treatment with minocycline and 24hr incubation of M-CSF-expanded M0 macrophages with LPS (100ng/mL). MINO 10 = Minocycline 10μM, MINO 25 = Minocycline 25μM. [A] Representative dot plots showing the percentage of $CD163^+$ (top) and $CD206^+$ (bottom) cells. [B] Representative histograms showing mean fluorescent intensity (MFI) for CD163 (left) and CD206 (right). Numbers indicate MFI of live gated population. [C-F] Bar graphs showing the percentage of $CD163^+$ [C] and $CD206^+$ [E] cells, and MFI values for CD163 [D] and CD206 [F]. MFI values normalised and displayed as fold change versus the un-activated M0 macrophage control indicated at 1. Plots and histograms illustrate one representative donor. Graphs represent data from 4 individual donors each comprised of duplicate values. Data presented as mean ± SEM. One-way ANOVA with post hoc Dunnett's applied versus the LPS-activated M0 macrophage. ***p<0.001.

4.3. Cytokine production profile of LPS-Activated M0 macrophages

Having explored the effect of minocycline on surface marker expression following LPS activation of resting M0 macrophages, the cytokine production profiles of the LPS-activated cells were next assessed to evaluate macrophage function in the presence of minocycline. Monocytes and macrophages produce a wide variety of cytokines dependant on both endogenous and exogenous stimulus, with some promoting downstream inflammation (TNF-α, IL-6, IL-1β, IL-12), while others propagate pro-resolving cellular mechanisms (Rossol *et al.*, 2011). The NF-κB signalling cascade following interaction of LPS with its receptor complex CD14/TLR4, and consequent activation of both MyD88 and TRIF pathways has been fully deciphered and reported in the literature (O'Neill, Golenbock and Bowie, 2013; Ciesielska, Matyjek and Kwiatkowska, 2021). Thousands of independent response genes encoding cytokines, chemokines and antimicrobial peptides, in addition to downstream transcription factors are modulated by these signalling events and are vital for many crucial immunological programs including initiating inflammatory responses to pathogens by other innate immune cells, and the development and activation of cells responsible for adaptive immune responses (Dorrington and Fraser, 2019). Thus, it is imperative to evaluate any changes in the expression of these biochemical mediators to understand minocycline's potential regulatory ability.

For this cytokine determination, M0 macrophages were first generated using the THP-1 and PBMCs, before pre-treatment with minocycline for 2hr prior to activation with LPS (100ng/mL) for an additional 24hr. After 24hr the culture supernatant was collected and stored before the cytokine concentration was determined by ELISA. It was chosen to discontinue use of the U-937 cell line at this stage due to limited resources and time restraints and given the existence of almost duplicate data achieved between both cell lines up to this point.

The initial phase of this research utilized a 13-plex human macrophage/microglia LEGENDplex™ multiplex assay kit from Biolegend® (UK). This technique allowed for the simultaneous determination of 13 different analytes; TNF-α, IFN-γ, IL-1β, IL-10, IL-4, IL-6, IL-23, IL-1RA, IP-10, IL-12p40, IL-12p70, TARC (CCL17), and Arginase within the cell culture supernatant, and was made possible with the kind support of the UEL Graduate School through a PGR Internship Scheme award, in collaboration with Dr Jose Garrido Mesa at Queen Mary University London (UK). For this analysis a representative selection of samples from both the LPS-activated THP-1 and PBMC protocols were used. One sample from donor 3 and donor 4 was included, alongside one full experiment from the investigations using THP-1 which incorporated triplicate values. This decision was based upon limited assay capacity, and the desire to gain as much preliminary insight into possible cytokine production modification due to minocycline which could later be corroborated using standard ELISA kits. This preliminary data obtained can be found in appendix A17.

As this procedure only incorporated limited sample numbers and thus yielded limited data sets where statistical analysis was not always possible, these findings required clarification using ELISAs. Therefore, based on the preliminary data from the LEGENDplex™ assay the following cytokines were selected to be corroborated; IL-4 and IL-10 as M2 macrophage indicators, and IFN-γ, IL-1β, IL-6, TNF-α, IL-12p40, and IL-12p70 as M1-associated cytokines. As outlined, the cytokine concentration was determined from the experimental supernatant acquired at the cessation of the protocol at 24hr post-LPS stimulation, and like the previous investigations, it was crucial to first evaluate the effect of the LPS-activation upon the M0 macrophage cultures prior to intervention with minocycline.

When first considering the characterisation data from the THP-1 supernatant an adverse effect of the DMSO vehicle control was immediately evident. Figure 4.14 outlines both the impact of LPS, in addition to the vehicle control on the production of classically inflammatory mediators and highlights an increase in the production of IL-1β, IL-6 and TNF-α (Figure 4.14A2-A4). This effect was then seen to be further exacerbated by DMSO by a significant margin. Conversely the data for IFN-γ displays limited effect by either LPS or LPS+DMSO (Figure 4.14 A1). For the 2 subunits of IL-12 there was indeterminate influence of LPS or the vehicle whereby no significant change was observed (Figure 4.14 A5 and A6). In relation to the M2 anti-inflammatory mediators IL-4 and IL-10, no influence of LPS was seen for IL-4 production, but with DMSO causing an increase which remained below statistical significance (Figure 4.15 A1). Conversely, there was a significant increase in IL-10 production seen in the vehicle treated group when compared to the un-activated control (Figure 4.15 A2).

When assessing the data obtained from the PBMC supernatant, all cytokines were significantly increased following 24hr stimulation with LPS when compared to the un-activated control, with the exception being IL-4 (Figure 4.14 B2-B4, and Figure 4.15 B2). Results for IL-4 were inconclusive regarding an effect of LPS on PBMC-derived M0 macrophages, with no significant changes in production across any of the donors tested (Figure 4.15 B1). It should be noted however that raw data collected for the IL-12 subunits were near, or on the minimum detection limit of the assay which may explain variation between donors and occurrence of large standard deviation between duplicate readings. This should also be taken into consideration when assessing the effect of minocycline in the proceeding section.

M1 pro-inflammatory macrophages are typically induced by Th1 cytokines, such as IFN-γ and TNF-α, or by bacterial LPS as in this experimental model of macrophage activation. These macrophages characteristically produce and secrete high levels of pro-inflammatory cytokines such as TNF-α, IL-1β, IL-6, IL-12, and IFN-γ, and commonly low levels of IL-10 (Shapouri-Moghaddam *et al.*, 2018). This conventional characterisation is in direct agreement with the data achieved in this study, however here an unpredicted increase in IL-10 production following LPS stimulation was also seen. IL-10, a traditional M2-associated cytokine, plays a crucial role in maintaining homeostasis of potent prophylactic

immune responses while limiting immune-mediated physiological damage (Couper, Blount and Riley, 2008). Despite this classification macrophages are noted in the literature to produce IL-10 in response to TLR ligands such as LPS through involvement of MAPKs and transcription factors including CREB and NF-κB (Cao *et al.*, 2006; Vliet *et al.*, 2013). In a 2015 study, Sanin, Prendergast and Mountford detailed early and rapid release of IL-10 by macrophages via the activation of CREB, downstream of TLR2 and TLR4 through phosphorylation of p38 and ERK1/2 (Sanin, Prendergast and Mountford, 2015). This may help explain why an increase in IL-10 was consistently reported in this study.

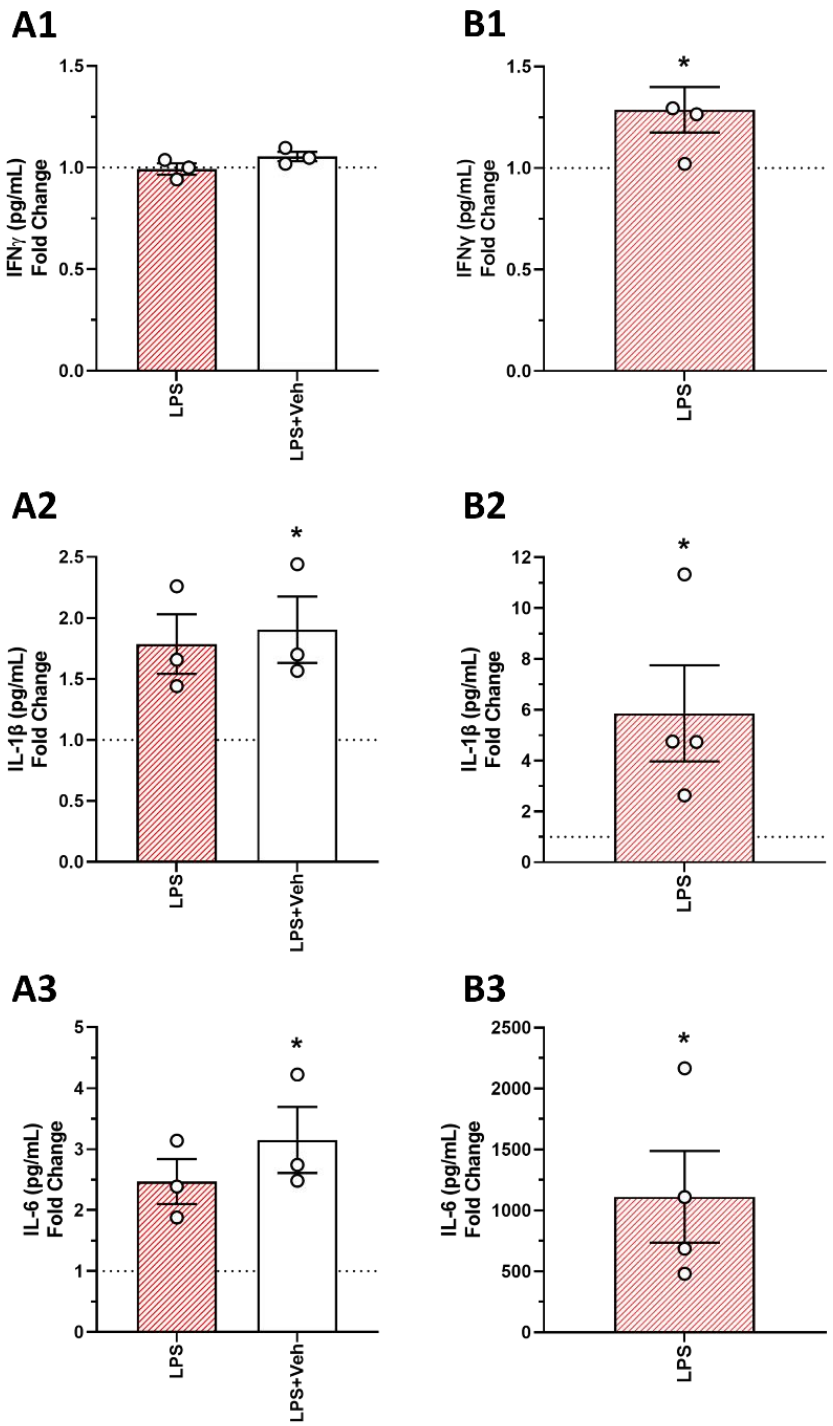
A1
IFNγ (pg/mL) Fold Change
1.5
1.0
0.5
0.0
LPS
LPS+Veh
B1
*
IFNγ (pg/mL) Fold Change
1.5
1.0
0.5
0.0
LPS
A2
IL-1β (pg/mL) Fold Change
2.5
2.0
1.5
1.0
0.5
0.0
*
LPS
LPS+Veh
B2
*
IL-1β (pg/mL) Fold Change
12
10
8
6
4
2
0
LPS
A3
IL-6 (pg/mL) Fold Change
5
4
3
2
1
0
*
LPS
LPS+Veh
B3
*
IL-6 (pg/mL) Fold Change
2500
2000
1500
1000
500
0
LPS

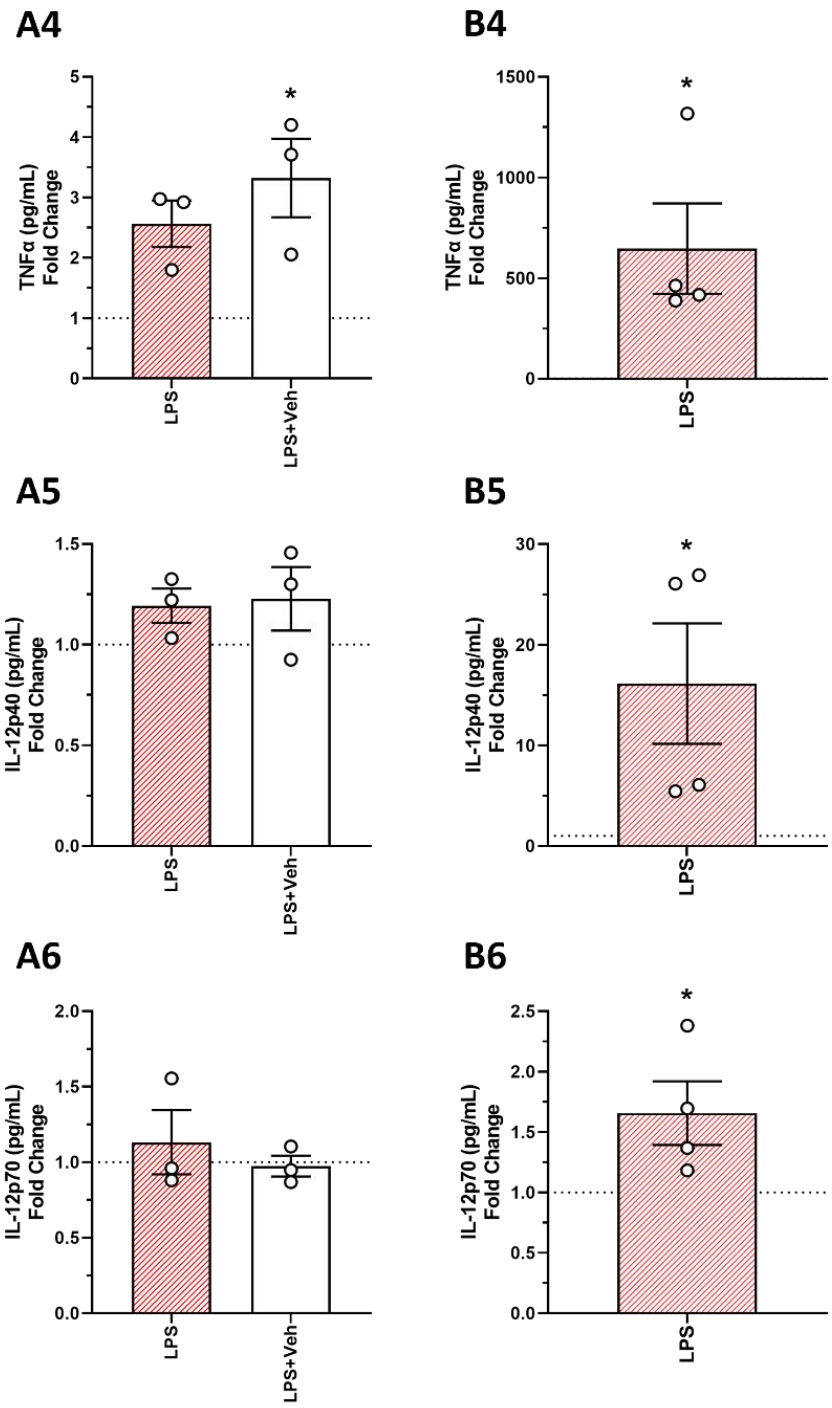

Figure 4.14: M1-associated cytokine production by LPS-activated THP-1 (Panel A) and PBMC-derived (Panel B) M0 macrophages. Data obtained from supernatant analysis after 24hr incubation of M0 macrophages with LPS (100ng/mL). Veh = DMSO vehicle control (1:1000). Bar graphs showing data for the M1-associated cytokines IFN-γ [1], IL-1β [2], IL-6 [3], TNF-α [4], IL-12p40 [5] and IL-12p70 [6]. Data presented as relative fold change versus the un-activated M0 control indicated at 1. Graphs represent data from 3 repeated experiments each comprising triplicate readings for THP-1 [Panel A], and 4 donors each comprising of duplicate values for PBMCs [Panel B]. Data presented as mean ± SEM. One-way ANOVA with post hoc Dunnett's [Panel A] or unpaired *t* test [Panel B] applied versus the un-activated M0 macrophage. *p<0.05.

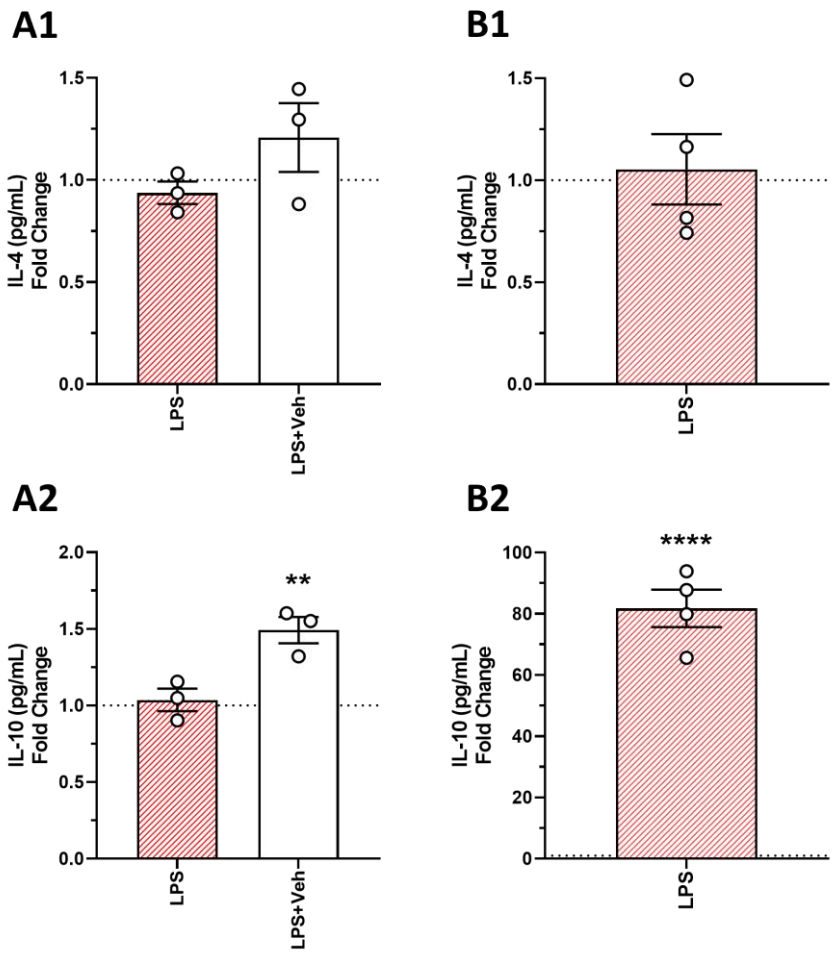

Figure 4.15: M2-associated cytokine production by LPS-activated THP-1 (Panel A) and PBMC-derived (Panel B) M0 macrophages. Data obtained from supernatant analysis after 24hr incubation of M0 macrophages with LPS (100ng/mL). Veh = DMSO vehicle control (1:1000). Bar graphs showing data for M2-associated cytokines IL-4 [1] and IL-10 [2]. Data presented as relative fold change versus the un-activated M0 control indicated at 1. Graphs represent data from 3 repeated experiments each comprising triplicate readings for THP-1 [Panel A], and 4 donors each comprising of duplicate values for PBMCs [Panel B]. Data presented as mean ± SEM. One-way ANOVA with post hoc Dunnett's [Panel A] or unpaired *t* test [Panel B] applied versus the un-activated M0 macrophage. ***p*<0.01; *****p*<0.0001.

4.4. Effect of minocycline on the cytokine production of LPS-activated M0 macrophages

Having now established baseline data and characterised the effect of LPS on the production of both pro- and anti-inflammatory related cytokines from M0 macrophages, the next stage was to introduce minocycline treatment and assess any changes induced by minocycline. Given the potent influence of the vehicle control within the THP-1 samples on this biomarker, which was witnessed across almost all variables tested, it was decided to use this as the positive 'stimulated'

control when analysing the effect of minocycline. This was thought to provide the most biologically relevant conclusions given the dominant effect of DMSO which in all circumstances acted to exacerbate any effect of LPS alone. By correlating changes induced by minocycline to this new positive LPS+Veh control it would be possible to assess whether minocycline produced compound pro-inflammatory action or acted to reverse the over-production elicited by the LPS+DMSO combination treatment.

When first assessing the data relating to M1, pro-inflammatory molecules, 25μM minocycline was seen to counter the potent effect of the LPS+Veh treatment by significantly reducing the production of IFN-γ in the THP-1 samples (Figure 4.16A1). However, where the THP-1 data is universal in minocycline's function at reducing IFN-γ production, there is contradictory results reflected by the PBMC data in which minocycline at 25μM was now shown to increase IFN-γ production (p=0.0086) (Figure 4.16B1). On the contrary, minocycline at 25μM resulted in a significant reduction in IL-1β cytokine production in the PBMC model compared to the LPS only control (p=0.0293) but remained unchanged in the THP-1 samples (Figure 4.16A2 and B2). IL-6 was also similar in its disparity between models, showing minocycline at both concentrations decrease the concentration of IL-6 in THP-1, with 10μM and 25μM reducing by 0.75- (p=0.0141) and 0.72-fold (p=0.0079) respectively, but failing to reach significance in the PBMC macrophages (Figure 4.16A3 and B3).

Data reflecting modification of TNF-α were again more distinct in the THP-1 model, with 10μM minocycline exerting superior reduction when compared to the LPS+DMSO control (p=0.0369) (Figure 4.16A4). This was not, however, echoed in the PBMC samples where there were no significant changes in TNF-α production by either concentration of minocycline versus the LPS only control group (Figure 4.16B4). Negligible change was also witnessed when visualising the data for the IL-12p40 subunit, but IL-12p70 was seen to be reduced by both concentrations of minocycline in the THP-1 model, by 0.86- (p=0.0274) and 0.84-fold (p=0.0164) by 10μM and 25μM versus the LPS+Veh control group, which was not reflected in the PBMCs (Figure 4.16A6 and B6). However, as stated earlier, the data for these parameters were on the limit of the assay range of sensitivity which may render this finding inconclusive and requiring corroboration using a more sensitive assay.

For data pertaining to the anti-inflammatory M2 cytokines a universal decrease in the production of IL-10 was witnessed following treatment with minocycline at either 10μM or 25μM which was consistent across both cellular models and all biological replicates (Figure 4.17A1 and B1). Furthermore, IL-4 was also seen to be reduced by minocycline at both concentrations within the THP-1 model although failed to reach statistical significance (Figure 4.17A2), and was not corroborated in the PBMCs(Figure 4.17B2).

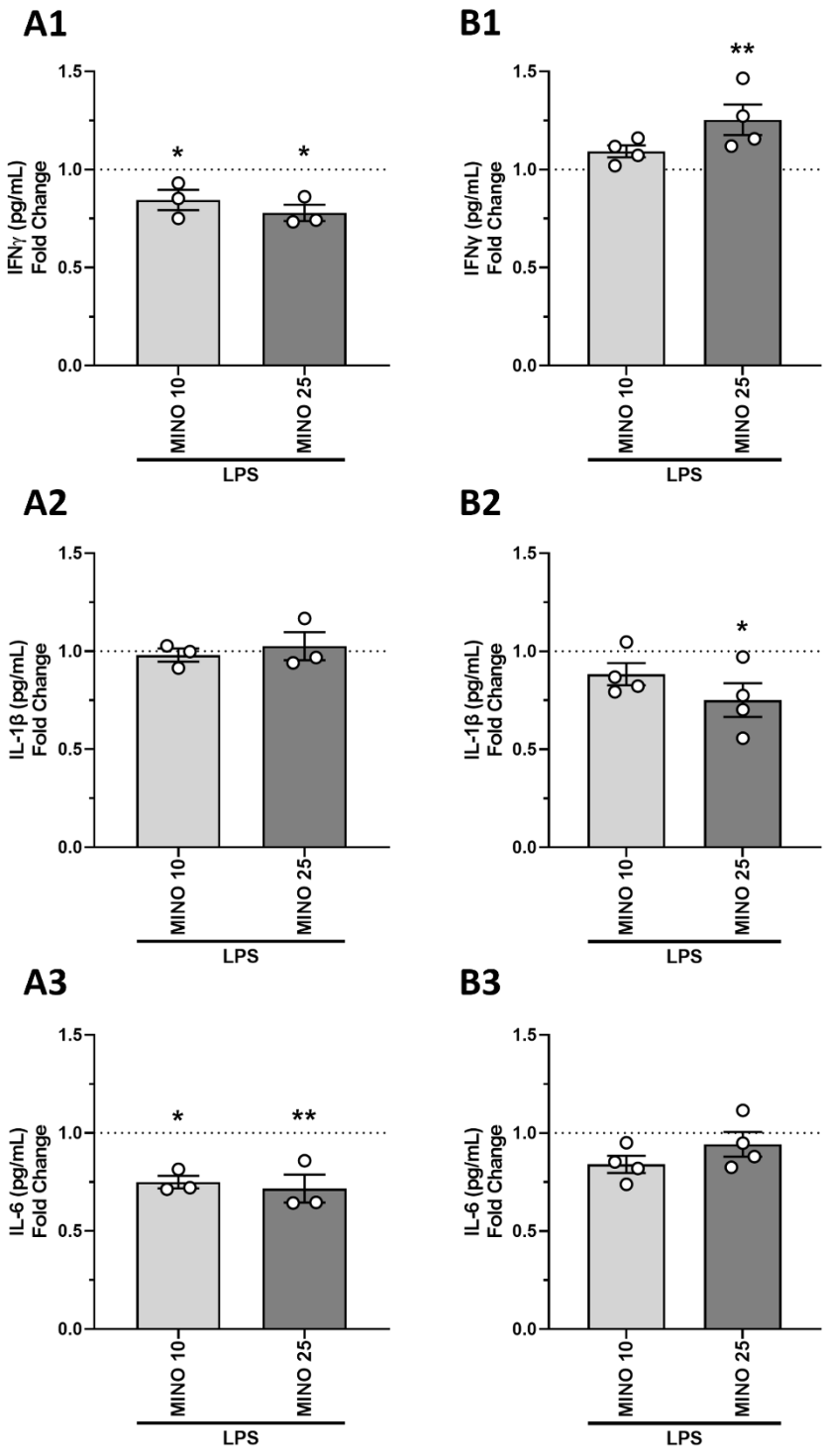

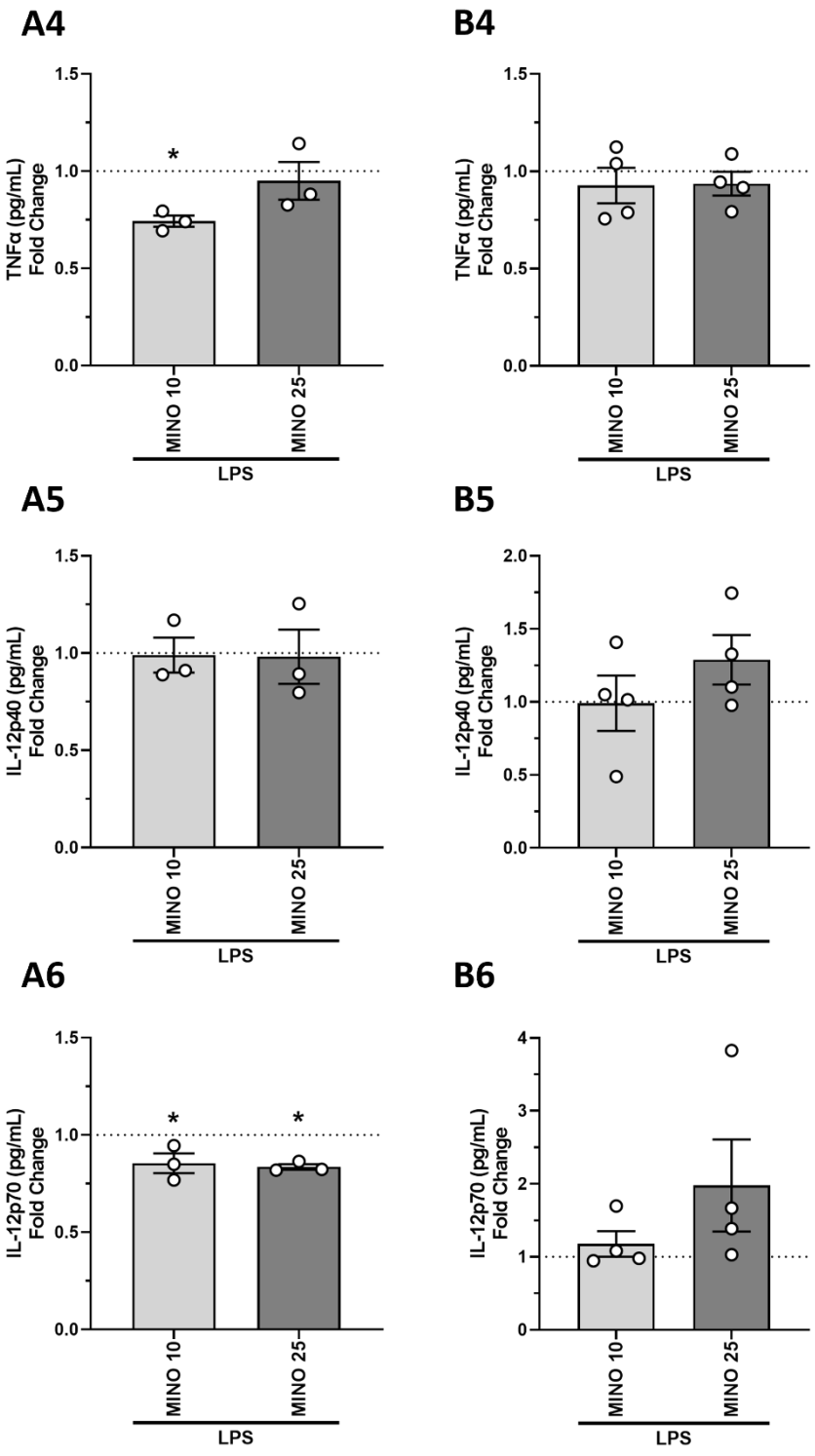

Figure 4.16: Effect of minocycline on M1-associated cytokine production by LPS-activated THP-1 (Panel A) and PBMC-derived (Panel B) M0 macrophages. Data obtained from supernatant analysis after 2hr pre-treatment with minocycline and 24hr incubation of M0 macrophages with LPS (100ng/mL). MINO 10 = minocycline 10μM, MINO 25 = minocycline 25μM, Veh = DMSO vehicle control (1:1000). Bar graphs showing data for M1-associated cytokines IFN-γ [1], IL-1β [2], IL-6 [3], TNF-α [4], IL-12p40 [5] and IL-12p70 [6]. Data presented as relative fold change versus the LPS+DMSO-activated M0 [Panel A], or LPS-activated M0 [Panel B]

macrophage control indicated at 1. Graphs represent data from 3 repeated experiments each comprising triplicate readings for THP-1 [Panel A], and 4 donors each comprising of duplicate values for PBMCs [Panel B]. Data presented as mean ± SEM. One-way ANOVA with post hoc Dunnett's applied versus the relevant control in each panel. *p<0.05; **p<0.01.

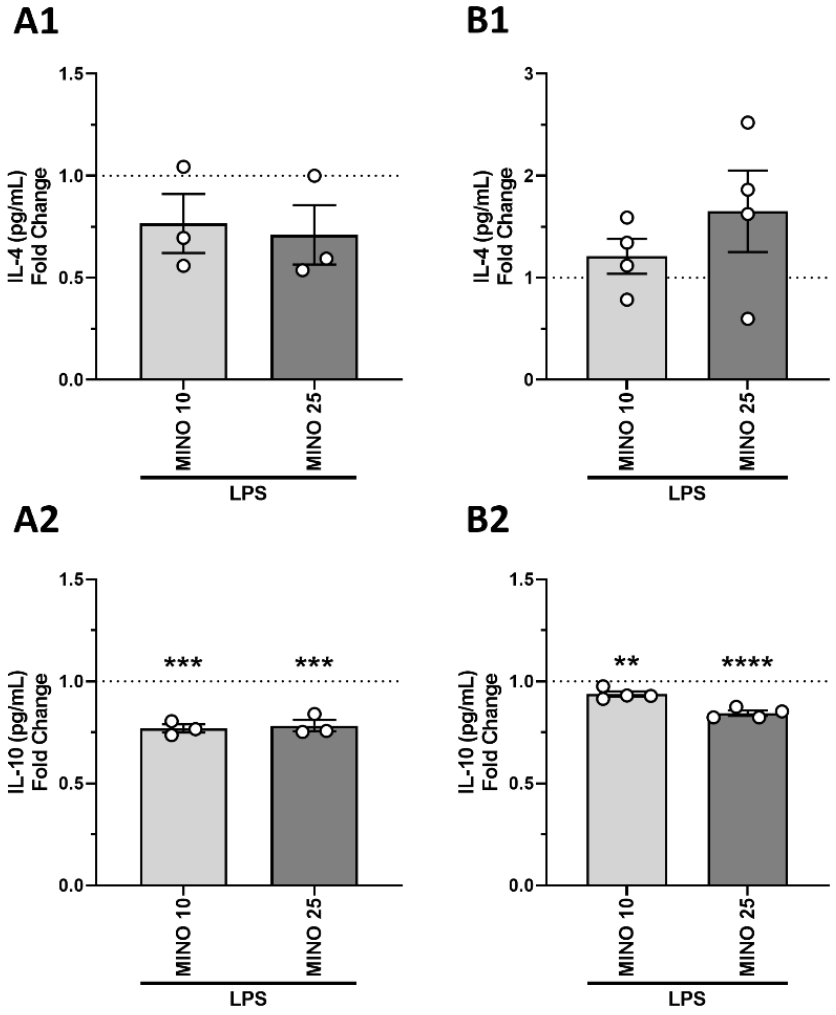

Figure 4.17: Effect of minocycline on M2-associated cytokine production by LPS-activated THP-1 (Panel A) and PBMC-derived (Panel B) M0 macrophages. Data obtained from supernatant analysis after 2hr pre-treatment with minocycline and 24hr incubation of M0 macrophages with LPS (100ng/mL). MINO 10 = minocycline 10μM, MINO 25μM = minocycline 25, Veh = DMSO vehicle control (1:1000). Bar graphs showing data for M2-associated cytokines IL-4 [1] and IL-10 [2]. Data presented as relative fold change versus the LPS+DMSO-activated M0 [Panel A], or LPS-activated M0 [Panel B] macrophage control indicated at 1. Graphs represent data from 3 repeated experiments each comprising triplicate readings for THP-1 [Panel A], and 4 donors each comprising of duplicate values for PBMCs [Panel B]. Data presented as mean ± SEM. One-way ANOVA with post hoc Dunnett's applied versus the relevant control in each panel. **p<0.01; ***p<0.001; ****p<0.0001.

4.5. Influence of minocycline on M0 macrophage gene expression following LPS-activation

The data so far described in this chapter suggest that minocycline may affect the way in which resting M0 macrophages respond to LPS stimulation, as suggested by downregulation of CD14 - a protein that works in tandem with TLR4 for recognition of LPS and initiating intracellular signalling (Arroyo-Espliguero *et al.*, 2004), in addition to, decreases in CD86 expression, and upregulation of CD80 which are commonly considered to be pro-inflammatory molecules (Subauste, Malefyt and Fuh, 1998; Nolan *et al.*, 2009) Furthermore, section 4.6 highlights potent roles of minocycline on the production of classical pro-inflammatory cytokines such as TNF-α, IL-1β and IL-6, in addition to the M2-associated cytokine IL-10, all of which are regulated by key transcriptional programmes. Based on these findings it was imperative to explore how the transcriptional machinery may be being affected by minocycline to help explain the previously obtained data. Furthermore, as discussed in more detail later in the chapter, previous reports have already outlined minocycline's influence on the NF-κB signalling pathway, causing alterations in NF-κB itself, alongside accessory molecules within microglia and monocyte models (Cai *et al.*, 2011; Ataie-Kachoie, P. *et al.*, 2013; Weiler and Dittmar, 2019). With published reports showing that minocycline directly affects NF-κB signalling, it was decided to focus on parallel mechanisms given the data generated so far, in conjunction with evidence that minocycline can, and does influence intracellular signalling pathways in macrophages.

It was decided to investigate upstream regulators or NF-κB, along the TLR4/LPS axis which included the expression of genes encoding for TLR-4, STAT3 and SOCS3. The expression of these proteins have central roles not only in the LPS-signalling cascade, but also in macrophage polarization and phenotype commitment, with close association to key effector molecules such as STAT6 and STAT1, and importantly function as inhibitory molecules for pro-inflammatory drivers such as NF-κB and AP-1 (Pålsson-McDermott and O'Neill, 2004; Nakano *et al.*, 2015; H. Li *et al.*, 2018). To test this hypothesis, the same standard macrophage activation protocol was employed which utilised a 2hr pre-incubation of resting M0 macrophages with minocycline prior to activation with LPS (100ng/mL).

As the protocol now aimed to evaluate changes in gene expression through assessment of RNA, the incubation time with LPS was reduced from 24hr to 4hr given any modification due to minocycline of RNA is observable at an earlier time point than whole protein expression. This is a common place understanding within the literature in regards to mRNA analysis (Ben-Ari *et al.*, 2010). After 4hr, cells were lysed and processed for RNA as described in chapter 2, section 2.5, before being reverse transcribed to cDNA and input into qPCR reactions using gene sequence specific primers.

Once more, the first phase aimed to characterise the effect of LPS alone on the gene expression profiles of the THP-1 and PBMC samples, before minocycline treatment was introduced. Figure 4.18 below shows some interesting genetic regulation of target genes, with LPS resulting in significant increased expression of TLR-4 within the PBMC samples ($p<0.0157$) (Figure 4.18B1), and SOCS3 ($p<0.0211$) (Figure 4.18B3), with STAT3 also displaying increased expression by 2.5-fold versus the un-activated control but failing to reach significance (Figure 4.18B2). Data obtained from the THP-1 model however were somewhat less distinct, showing parallel upregulation of SOCS3 (Figure 4.18A3), but minimal change in STAT3 (Figure 4.18 A2) and a reverse influence of LPS on TLR4 expression with significant decrease in expression ($p=0.0002$) (Figure 4.18A1). Although these data are generally in agreement or non-conflicting, the significant decrease in TLR4 in the THP-1 samples was unexpected and forced careful consideration of any effect potentially seen with minocycline treatment for this gene. Furthermore, it should be recognised that the relative change in gene expression was far more pronounced in the PBMC samples, possible due to their primary origin and absence of genetic modification.

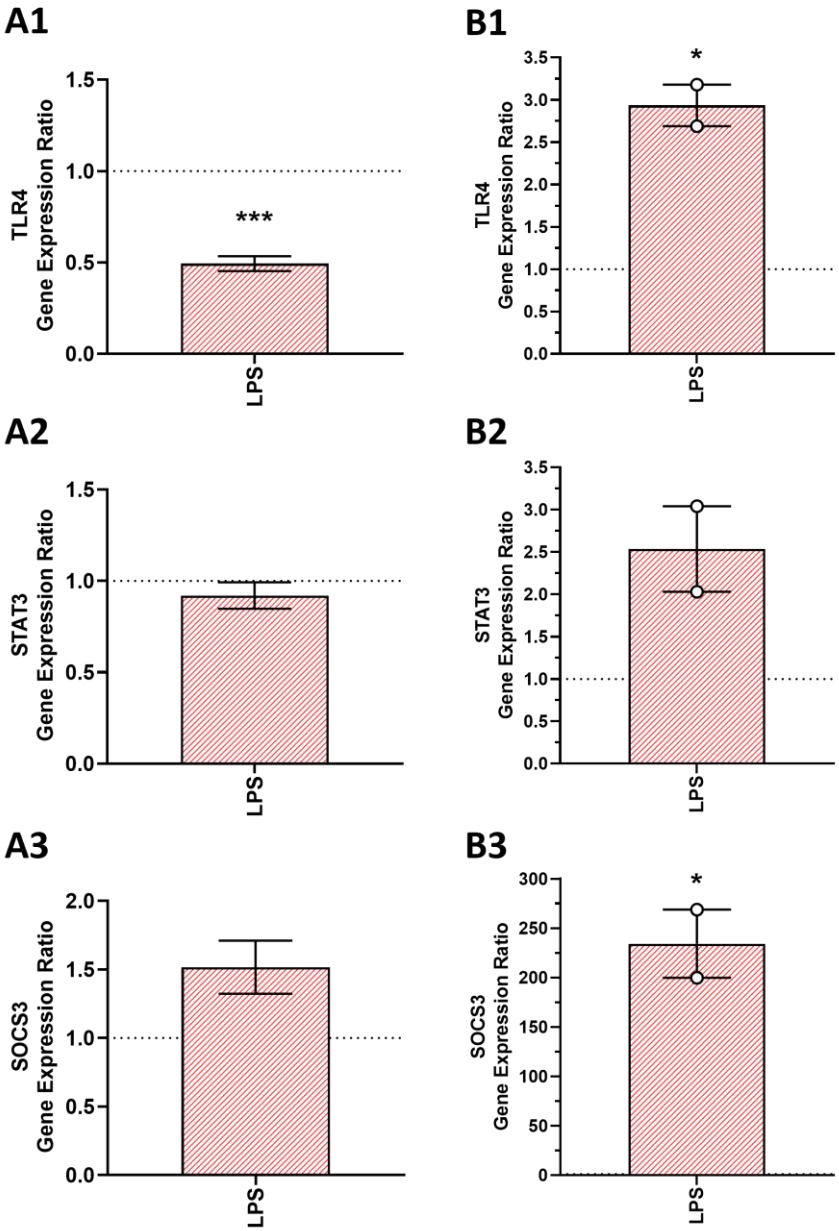

Figure 4.18: Genetic analysis of LPS-cascade related proteins in LPS-activated THP-1 (Panel A) and PBMC-derived (Panel B) M0 macrophages. Data obtained from RT-qPCR analysis of samples taken after 4hr incubation of M0 macrophages with LPS (100ng/mL). Bar graphs showing relative gene expression ratio versus the un-activated M0 control indicated at 1, as calculated using the Pfaffl equation. Graphs represent pooled data from 3 repeated experiments each comprising triplicate readings for THP-1 [Panel A], and 2 donors each comprising of duplicate values for PBMCs [Panel B]. Data presented as mean ± SEM. Un-paired *t* Test performed versus the control. *p<0.05; ***p<0.001.

With baseline data determined, effect of minocycline within this LPS stimulatory model was next evaluated. First, 25μM minocycline significantly increased the expression of TLR4 in the THP-1 model when compared to the LPS only control (p=0.0208) (Figure 4.19A1), however, this was not corroborated in the PBMCs (Figure 4.19A1). Regarding the STAT3/SOCS3 axis, data from the PBMC samples, although statistically not significant and marginal, appears to show an inverse correlation whereby minocycline simultaneously increases the expression of SOCS3 and decreases STAT3 (Figure 4.19 B2 and B3). This increase in SOCS3 was also reflected in the THP-1 model (Figure 4.19 A3) with minocycline at 25μM causing a 0.42-fold increase in gene expression ratio versus the LPS only control. STAT3 was also suggested to be increased by minocycline treatment in the THP-1 samples (Figure 4.19A2). The limited size of the study which was only able to incorporate 2 donor samples should be noted and therefore any conclusions drawn should be done so with some caution.

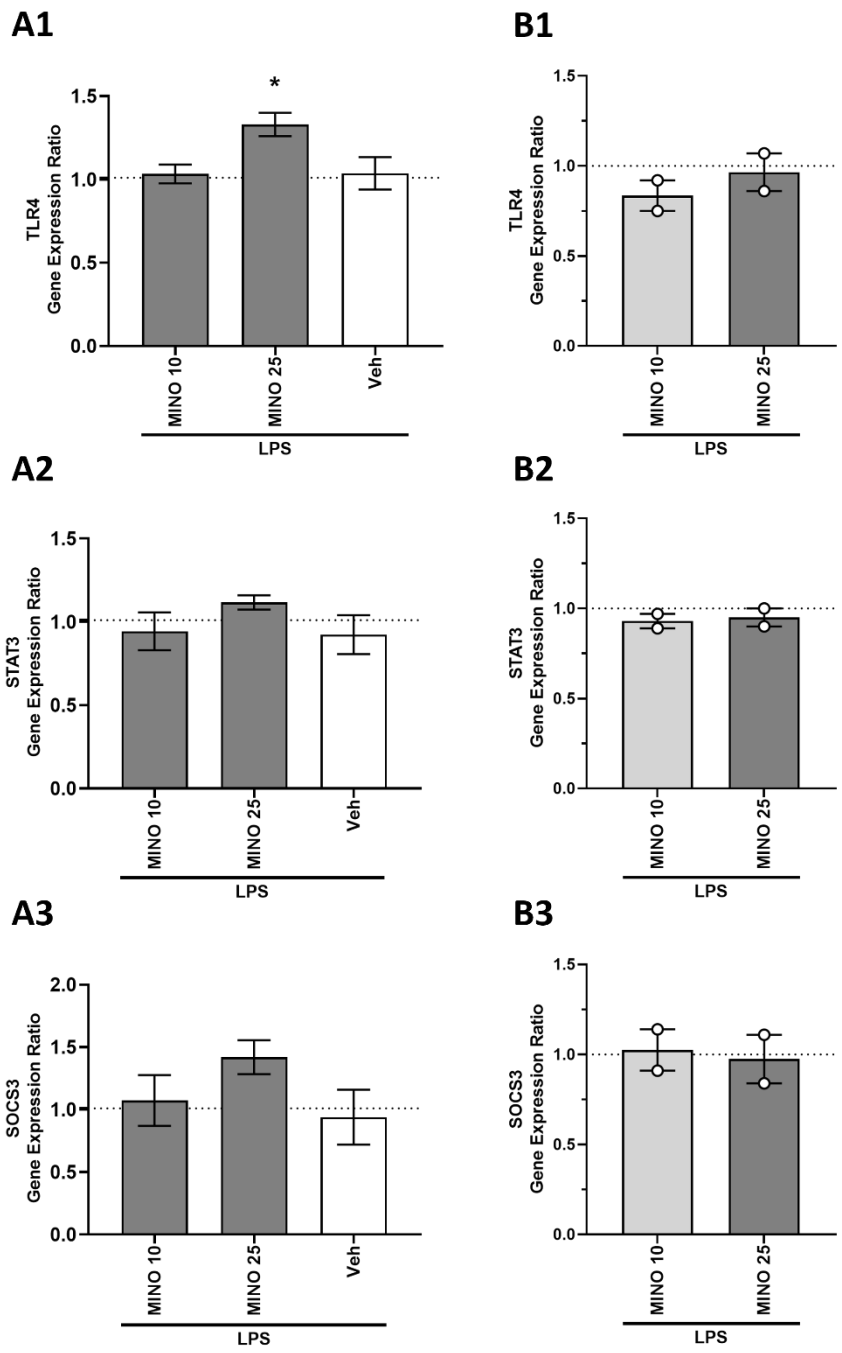

Figure 4.19: Effect of minocycline on the genetic expression of LPS-cascade related proteins in LPS-activated THP-1 (Panel A) and PBMC-derived (Panel B) M0 macrophages. Data obtained from RT-qPCR analysis of samples taken after 2hr pre-treatment with minocycline and 4hr incubation of M0 macrophages with LPS (100ng/mL). Bar graphs showing the relative gene expression ratio versus the LPS-activated M0 control indicated at 1, as calculated using the Pfaffl equation. Graphs represent pooled data from 3 repeated experiments each comprising triplicate readings for THP-1 [Panel A], and 2 donors each comprising of duplicate values for PBMCs [Panel B]. Data presented as mean ± SEM. One-way ANOVA with post hoc Dunnett's performed versus the untreated control. *p<0.05.

4.6. Intracellular flow cytometry detection of p-STAT3(Tyr705)

When LPS binds to its receptor complex, an intracellular signal transduction is produced which results in changes of both gene expression and the production of pro-inflammatory cytokines IFN-γ, IL-1β, IL-6, TNF-α and IL-12 (Meng and Lowell, 1997). These cytokines require the activation of the P38/MAPK pathway which instigates a series of cytokine-mediated autocrine and paracrine feedback loops which act to re-modify LPS-induced cytokine production (Bode, Ehlting and Häussinger, 2012). An example of this autocrine feedback-loop is the release of IFN-β, a cytokine required for LPS-induced release of IL-10 (Lobo-Silva *et al.*, 2017; Karimi *et al.*, 2020). IL-10 then acts to trigger sustained activation of STAT3 and the regulation of SOCS3 expression (Cevey *et al.*, 2019; Degboé *et al.*, 2019). However, STAT3 activation may also be induced by other cytokines such as IL-6 which is inversely insensitive to SOCS3 – an endogenous inhibitor of STAT3 (Bode, Ehlting and Häussinger, 2012; Rottenberg and Carow, 2014). STAT3 was the first member of the STAT family identified that was activated by the IL-6 cytokine family, and since has been shown to be tyrosine phosphorylated in response to this, and a variety of other stimuli (Crepaldi *et al.*, 2001; Nishiki *et al.*, 2004; Giurisato *et al.*, 2018; Balic *et al.*, 2020).

STAT3 activation is crucial for the transmission of anti-inflammatory signals in macrophages and has been demonstrated in mice whereby deletion of the STAT3 gene in macrophages lead to spontaneous development of enterocolitis rendering the animals highly susceptible towards LPS-mediated shock and septic peritonitis (Takeda *et al.*, 1999; Matsukawa *et al.*, 2003). This inflammatory response was attributed to the inability of IL-10 to mediate its anti-inflammatory effect on the macrophages in the absence of STAT3, and resulted in an enhanced production of inflammatory cytokines, including TNF-α, IL-1β, IL-6, IL-12, and IFN-γ. Furthermore, these STAT3-deficient macrophages also experienced impaired bactericidal activity which reduced their ability to eradicate bacterial infection (Takeda *et al.*, 1999; Matsukawa *et al.*, 2005; Bode, Ehlting and Häussinger, 2012).

The data from the previous section alludes to a possible influence of minocycline on the STAT3/SOCS3 axis despite the limited size of data sets generated. In addition to the associated cytokine production data from section 4.6, which reports significant decreases in pro-inflammatory mediators IFN-γ, IL-6, IL-1β, as well as the potent activator of STAT-3 - IL-10, it was deemed interesting to pursue this line of enquiry using THP-1 and investigate if minocycline had any effect on the phosphorylation of the tyrosine residue of STAT3 and thus its activation status and function. As this technique was not abundant in the literature regarding this particular cell line with many using the more traditional method of western blotting, it was first important to test both the BioLegend® optimized protocol, in combination with the cellular model and LPS activation method used here to generate a positive control baseline ready for future intervention with minocycline. After consulting the literature, two frequently applied LPS incubation periods of 30min and 2hr were selected (Guo, Jin and Chen, 2014; Hemmati, Haque and Gritsman, 2017; Chiu *et al.*, 2018; Giurisato *et al.*, 2018) to apply to the differentiated M0 macrophages maintaining use of LPS at 100ng/mL, at which point cells were immediately collected and fixed, permeabilized, and stained for p-STAT3(Tyr705) (FITC), and native STAT3 (PE). Expression of these proteins were then assessed via flow cytometry.

Data displayed in Figure 4.20 shows a clear baseline expression of native STAT-3 in both the unstimulated M0 macrophages, as well as the LPS-activated samples, with >90% increase in expression detected versus the isotype control (Figure 4.20A). This was also reflected in the density of STAT3 expression (MFI), alongside no distinct change between the 2 incubation times. When considering the effect of LPS at each time point on the expression of p-STAT3(Tyr705) however, there is almost no shift in expression detected between either treatment group versus the isotype control, or the different incubation lengths (Figure 4.21).

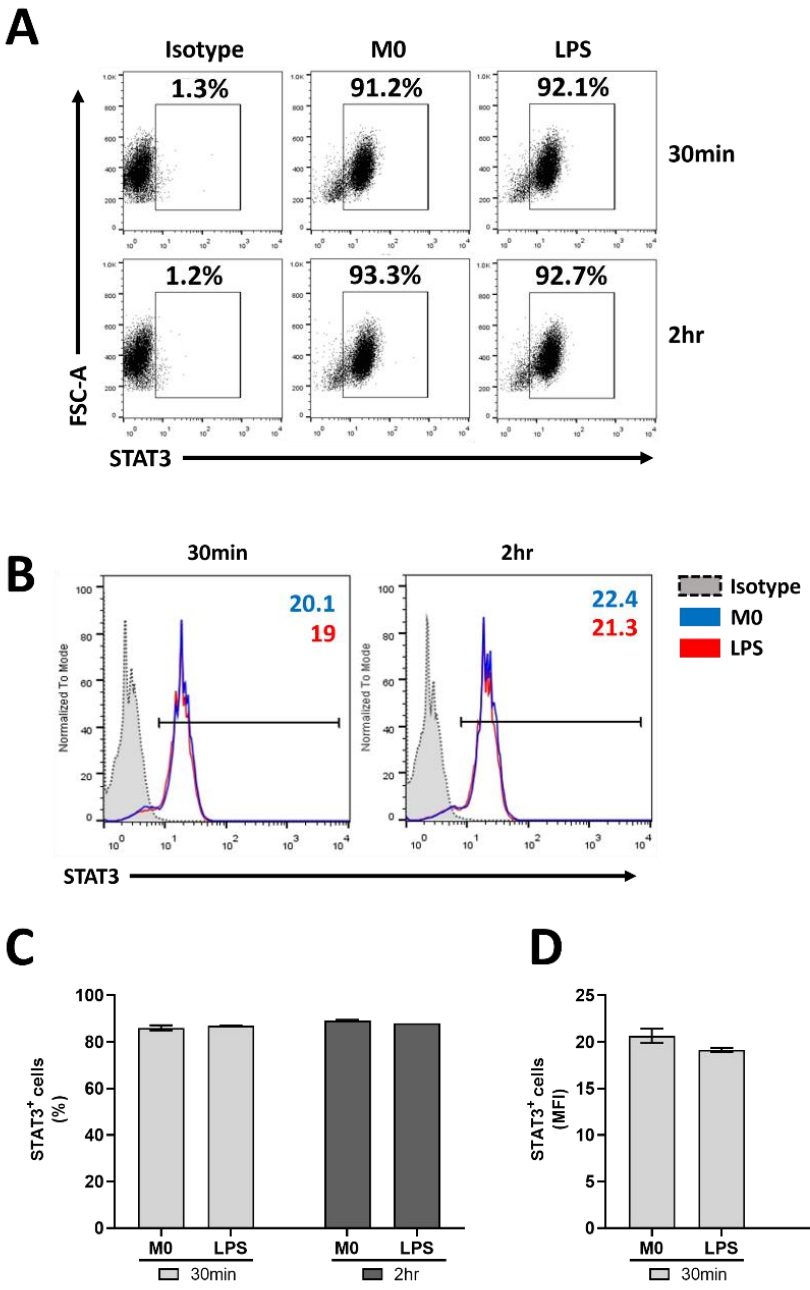

Figure 4.20: Characterising STAT3 expression at 30min and 2hr following LPS activation of THP-1 M0 macrophages. Data obtained after incubation of differentiated M0 macrophages with LPS (100ng/mL) at the indicated time points. [A] Representative dot plots showing the percentage of native STAT3⁺ cells at 30min (top) and 2hr (bottom). [B] Representative histograms showing mean fluorescent intensity (MFI) of STAT3 at 30min (left) and 2hr (right). Numbers indicate MFI of live gated population. Bar graphs showing the percentage of STAT3⁺ cells [C], and MFI values for STAT3 [D]. Plots and histograms illustrate one representative experiment. Graphical data represent 1 experiment comprising of duplicate values. Data presented as mean ± SD. Two-way ANOVA with post hoc Bonferroni.

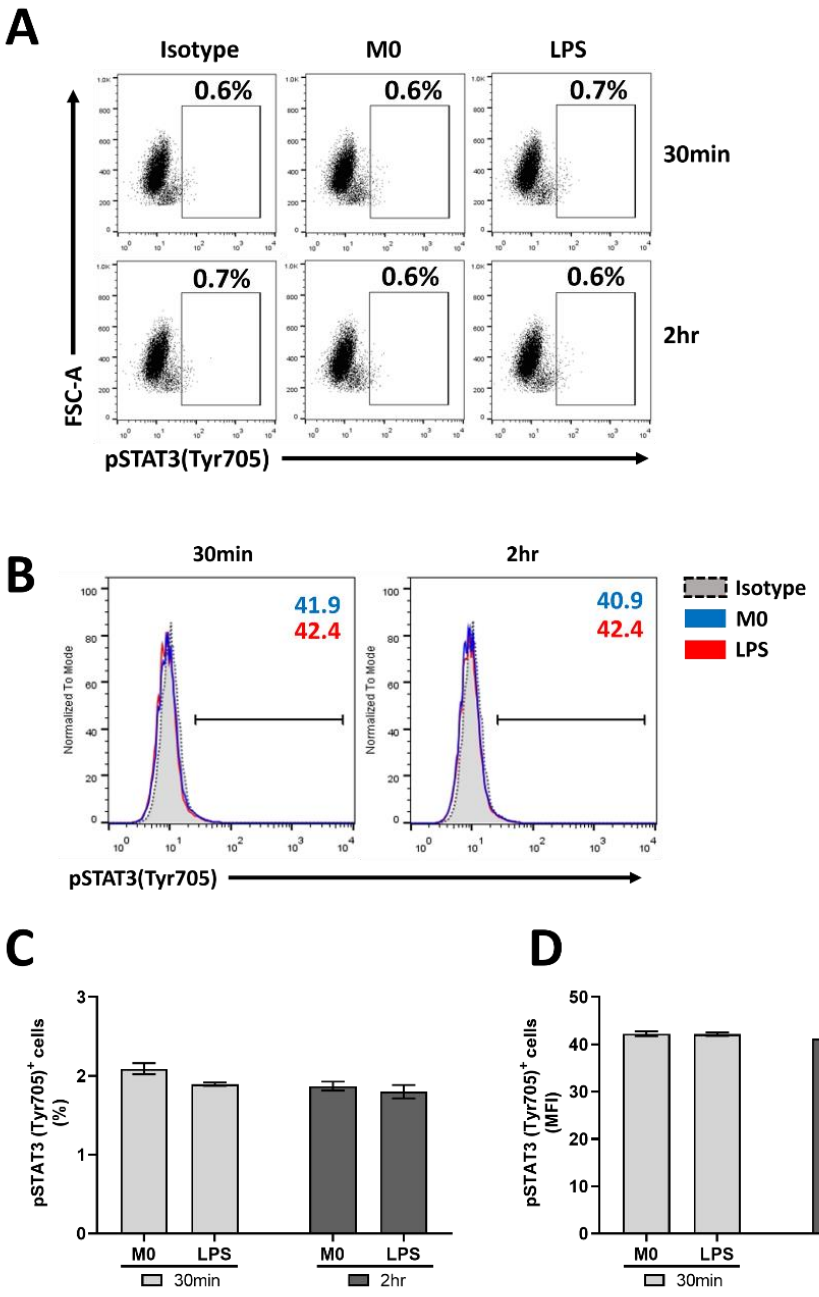

Figure 4.21: Characterising p-STAT3(Tyr705) expression at 30min and 2hr following LPS activation of THP-1 M0 macrophages. Data obtained after incubation of differentiated M0 macrophages with LPS (100ng/mL) at the indicated time points. [A] Representative dot plots showing the percentage of p-STAT3(Tyr705)$^+$ cells at 30min (top) and 2hr (bottom). [B] Representative histograms showing mean fluorescent intensity (MFI) of p-STAT3(Tyr705) at 30min (left) and 2hr (right). Numbers indicate MFI of live gated population. Bar graphs showing the percentage of p-STAT3(Tyr705)$^+$ cells [C], and MFI values for p-STAT3(Tyr705) [D]. Plots and histograms illustrate one representative experiment. Graphical data represent 1 experiment comprising of duplicate values. Data presented as mean ± SD. Two-way ANOVA with post hoc Bonferroni.

Having failed to induce a change in p-STAT3(Tyr705) expression using the time points initially selected, the range of incubation times was expanded to incorporate both earlier and later periods in the awareness that the point of peak phosphorylation may simply have been missed. A higher dose of LPS at 1µg/mL was also incorporated due to some published reports using this concentration when analysing STAT3 phosphorylation (Guo, Jin and Chen, 2014; Cronin *et al.*, 2016; X. Liu *et al.*, 2018). This second set of experiments repeated the same experimental procedures, this time fixing samples after 15min, 6hr and 24hr stimulation with LPS at either the original 100ng/mL, or the increased concentration of 1µg/mL.

Once again, a well-defined expression of native STAT3 was seen across all treatment groups versus the isotype control (Figure 4.22). The data also indicates no significant influence exerted by either the incubation time or LPS concentration reported across both the percentage of $STAT3^{+}$ cells (Figure 4.22C) or density of STAT3 expression (Figure 4.22D). The only identifiable difference was noted in samples stimulated with LPS for 24hr which showed a 6%-15% increase in the percentage of $STAT3^{+}$ cells compared to those left for 15min and 6hr respectively. Results for p-STAT3(Tyr705) indicated for a second time no clear increase in expression induced by LPS activation at either concentration or across any of the incubation periods used (Figure 4.23). Moreover, whilst LPS at either concentration appeared to have a negative impact on the percentage of p-$STAT3(tyr705)^{+}$ cells, the overall percentage expression was <2.5% rendering this change likely inconsequential.

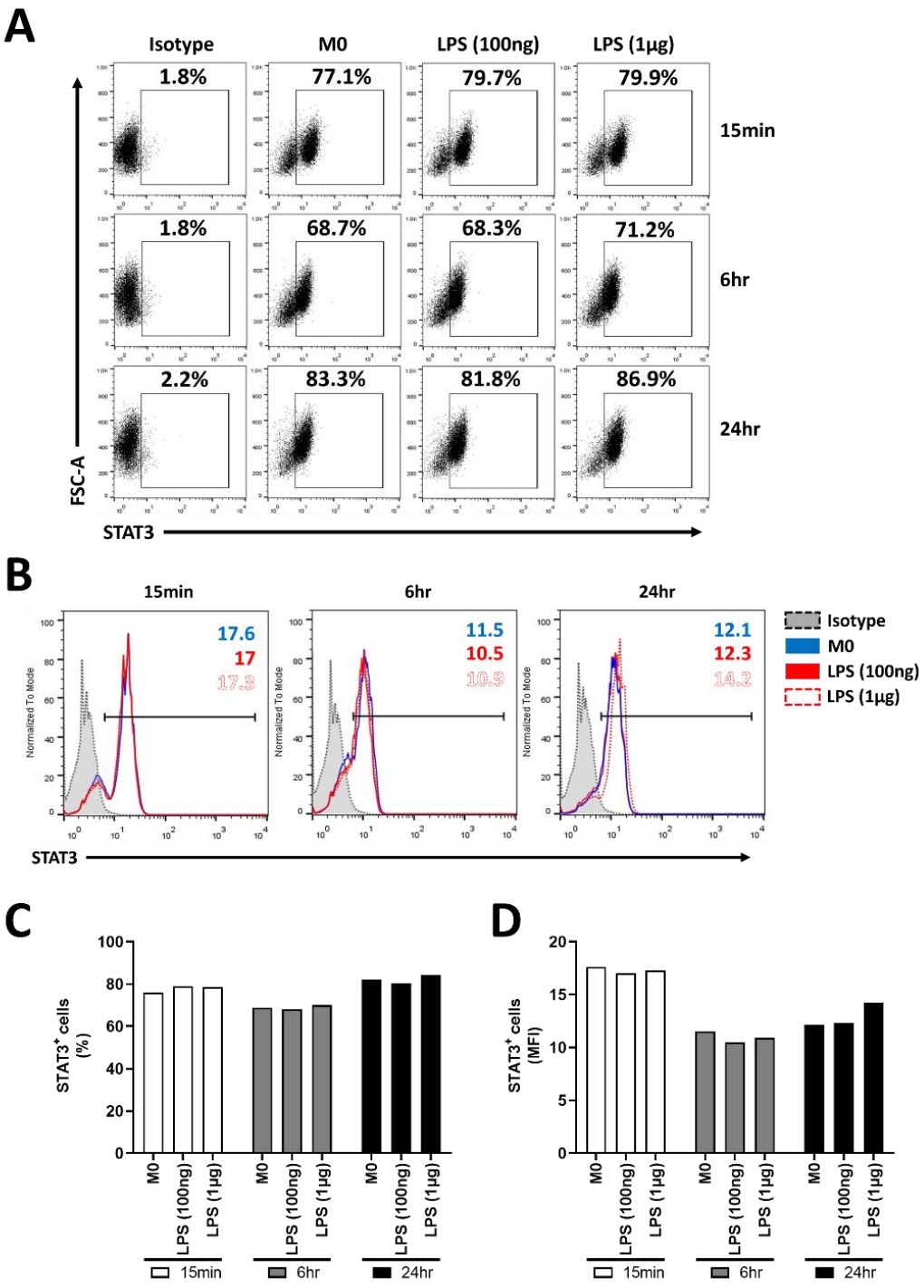

Figure 4.22: Characterising STAT3 expression at 15min, 6hr and 24hr following LPS activation of THP-1 M0 macrophages. Data obtained after incubation of differentiated M0 macrophages with LPS at 100ng/mL or 1µg/mL for the indicated time periods. [A] Dot plots showing the percentage of native STAT3⁺ cells at 15min (top), 6hr (middle) and 24hr (bottom). [B] Histograms showing mean fluorescent intensity (MFI) of STAT3 at 15min (left), 6hr (middle) and 24hr (right). Numbers indicate MFI of live gated population. Bar graphs showing the percentage of STAT3⁺ cells [C], and MFI values for STAT3 [D]. All data represent 1 experiment comprising of individual values. No statistics available.

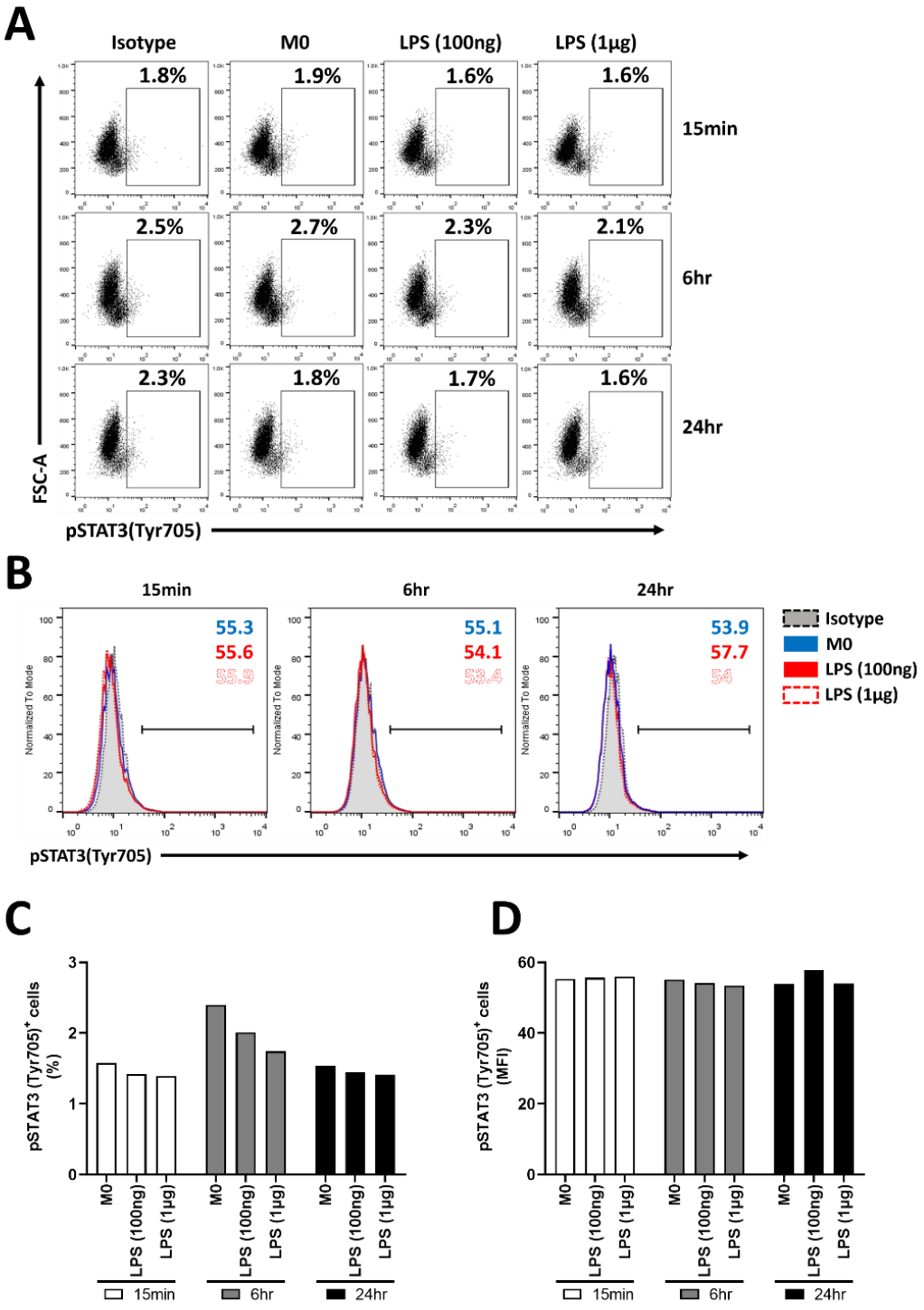

Figure 4.23: Characterising p-STAT3(Tyr705) expression at 15min, 6hr and 24hr following LPS activation of THP-1 M0 macrophages. Data obtained after incubation of differentiated M0 macrophages with LPS at 100ng/mL or 1µg/mL for the indicated time periods. [A] Dot plots showing the percentage of native p-STAT3(Tyr705)$^+$ cells at 15min (top), 6hr (middle) and 24hr (bottom). [B] Histograms showing mean fluorescent intensity (MFI) of p-STAT3(Tyr705) at 15min (left), 6hr (middle) and 24hr (right). Numbers indicate MFI of live gated population. Bar graphs showing the percentage of p-STAT3(Tyr705)$^+$ cells [C], and MFI values for p-STAT3(Tyr705) [D]. All data represent 1 experiment comprising of individual values. No statistics available.

With no identifiable detection of p-STAT3(Tyr705) following LPS-activation of THP-1 M0 macrophages despite changing variables such as incubation period and stimulation concentration, a final hypothesis considered the possibility of a de-phosphorylation event occurring within the cultures rendering it impossible to detect the phosphorylated protein within the samples. Therefore, the last experiments incorporated the phosphatase inhibitor sodium vanadate (0.1%) into all experimental reagents to rule out dephosphorylation of STAT3 as a cause for low-no detection via flow cytometry. It was also decided to continue using the highest concentration of LPS at 1µg/mL and incorporate even earlier time points of 30sec, 1min and 10min to maximise the chances of positive p-STAT3(tyr705) detection.

Data collected from this experiment again illustrated defined expression of native STAT3, independent of incubation time or the presence of the phosphatase inhibitor sodium vanadate (Figure 4.24). A potential increase in the percentage of expression was seen after 10min stimulation with LPS in the non-inhibitor group whereby the percentage of $STAT3^{+}$ cells increased by 7.6% (Figure 4.24C), however this change was negligible when assessing MFI (Figure 4.24D). Unfortunately, the changes in variables again made no discernible difference in p-STAT3(Tyr705) expression with both the percentage and density of expression remaining comparable with the isotype control (Figure 4.25).

After completing all three pilot studies it was concluded that it was not possible to confirm upregulation of p-STAT3(Tyr705) by LPS stimulation in this experimental model by ICFC when using this staining protocol. However, it was possible to remove dephosphorylation due to the presence of phosphatases through reagent supplementation with sodium vanadate as a cause for a lack of pSTAT3(Tyr704) detection. Despite utilising parallel LPS concentrations and incubation times to that reported in the literature, for reasons that remain undetermined, these experiments were unable to define a baseline protocol and as such not possible to continue with assessing the effect of minocycline intervention in this instance.

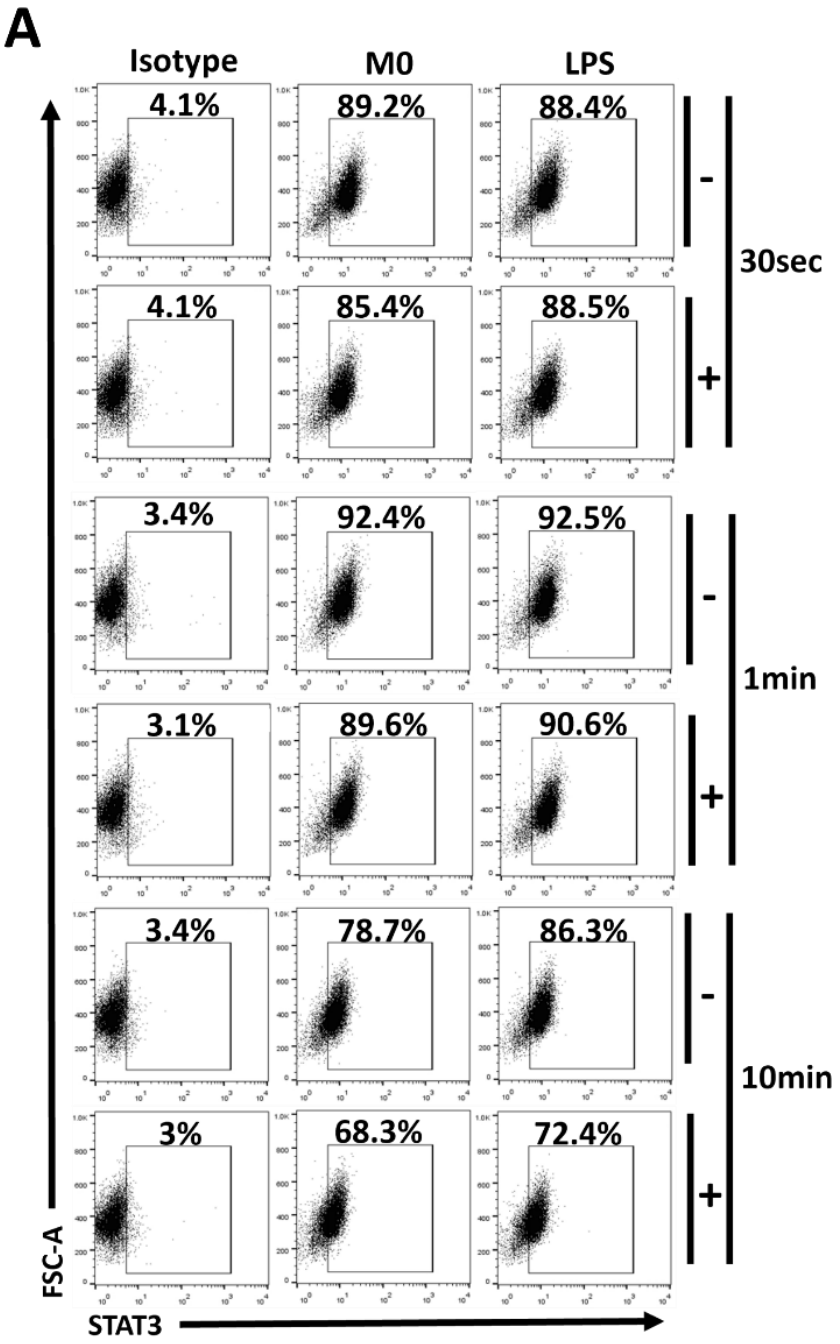
A
Isotype
M0
LPS
4.1%
89.2%
88.4%
-
30sec
4.1%
85.4%
88.5%
+
3.4%
92.4%
92.5%
-
1min
3.1%
89.6%
90.6%
+
3.4%
78.7%
86.3%
-
10min
3%
68.3%
72.4%
+
FSC-A
STAT3

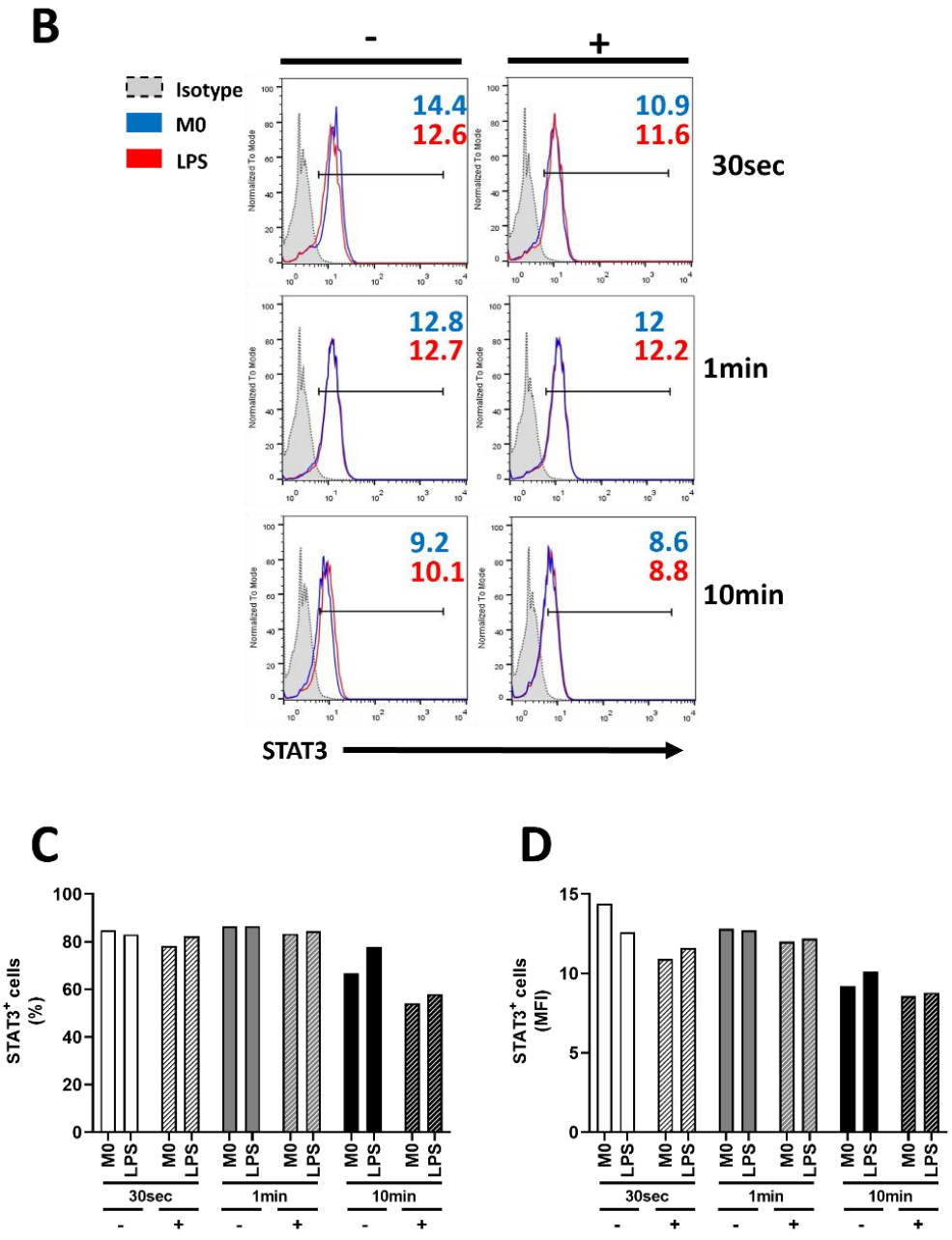

Figure 4.24: Characterising STAT3 expression at 30sec, 1min and 10min following LPS activation of THP-1 M0 macrophages. Data obtained after incubation of differentiated M0 macrophages with LPS at 1µg/mL for the indicated time periods. Culture and ICFC reagents were supplemented with (+) or without (-) sodium vanadate (0.1%). [A] Dot plots showing the percentage of native STAT3⁺ cells at 30sec (top), 1min (middle) and 10min (bottom). [B] Histograms showing mean fluorescent intensity (MFI) of STAT3 at 30sec (top), 1min (middle) and 10min (bottom). Numbers indicate MFI of live gated population. Bar graphs showing the percentage of STAT3⁺ cells [C], and MFI values for STAT3 [D]. All data represent 1 experiment comprising of individual values. No statistics available.

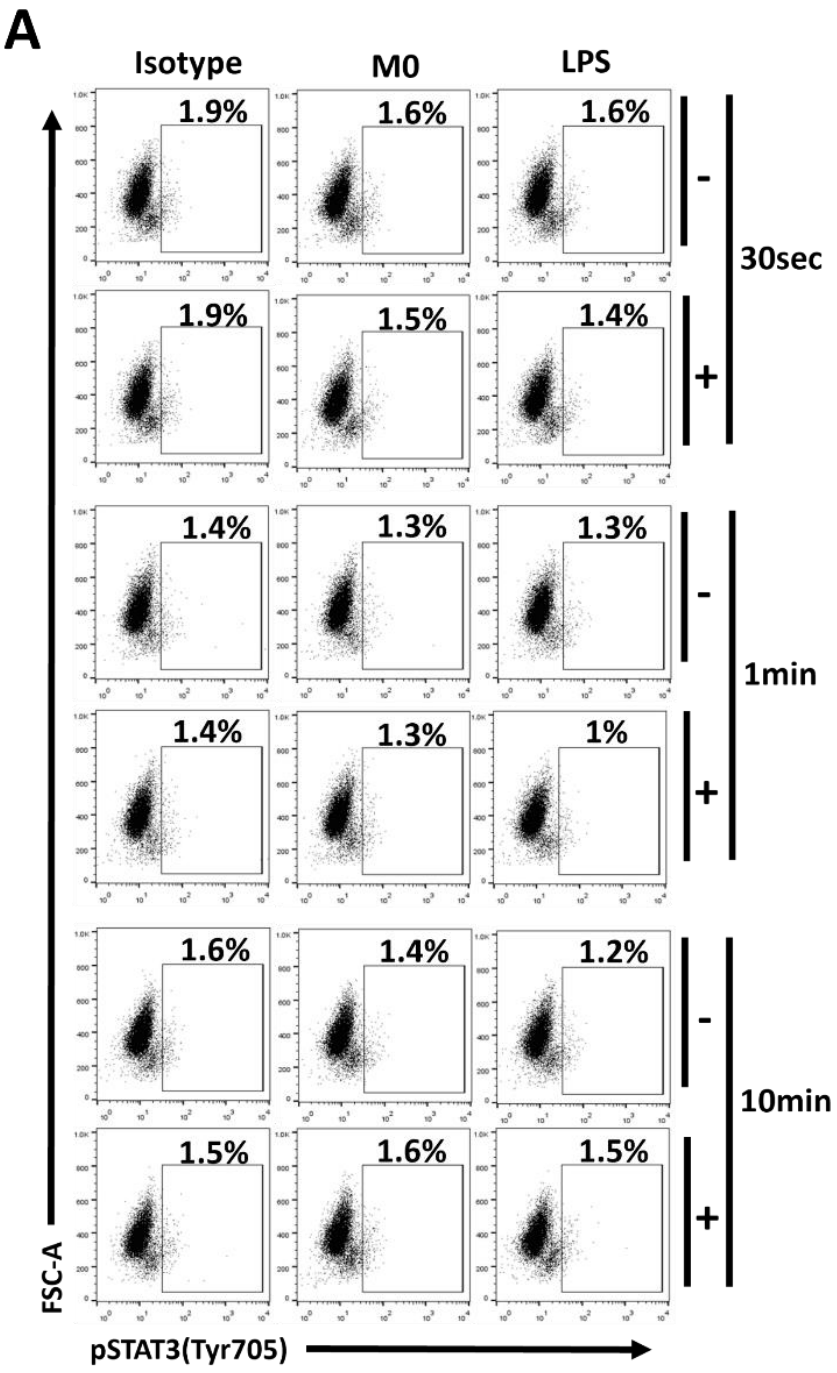
A
Isotype
M0
LPS
1.9%
1.6%
1.6%
-
30sec
1.9%
1.5%
1.4%
+
1.4%
1.3%
1.3%
-
1min
1.4%
1.3%
1%
+
1.6%
1.4%
1.2%
-
10min
1.5%
1.6%
1.5%
+
FSC-A
pSTAT3(Tyr705)

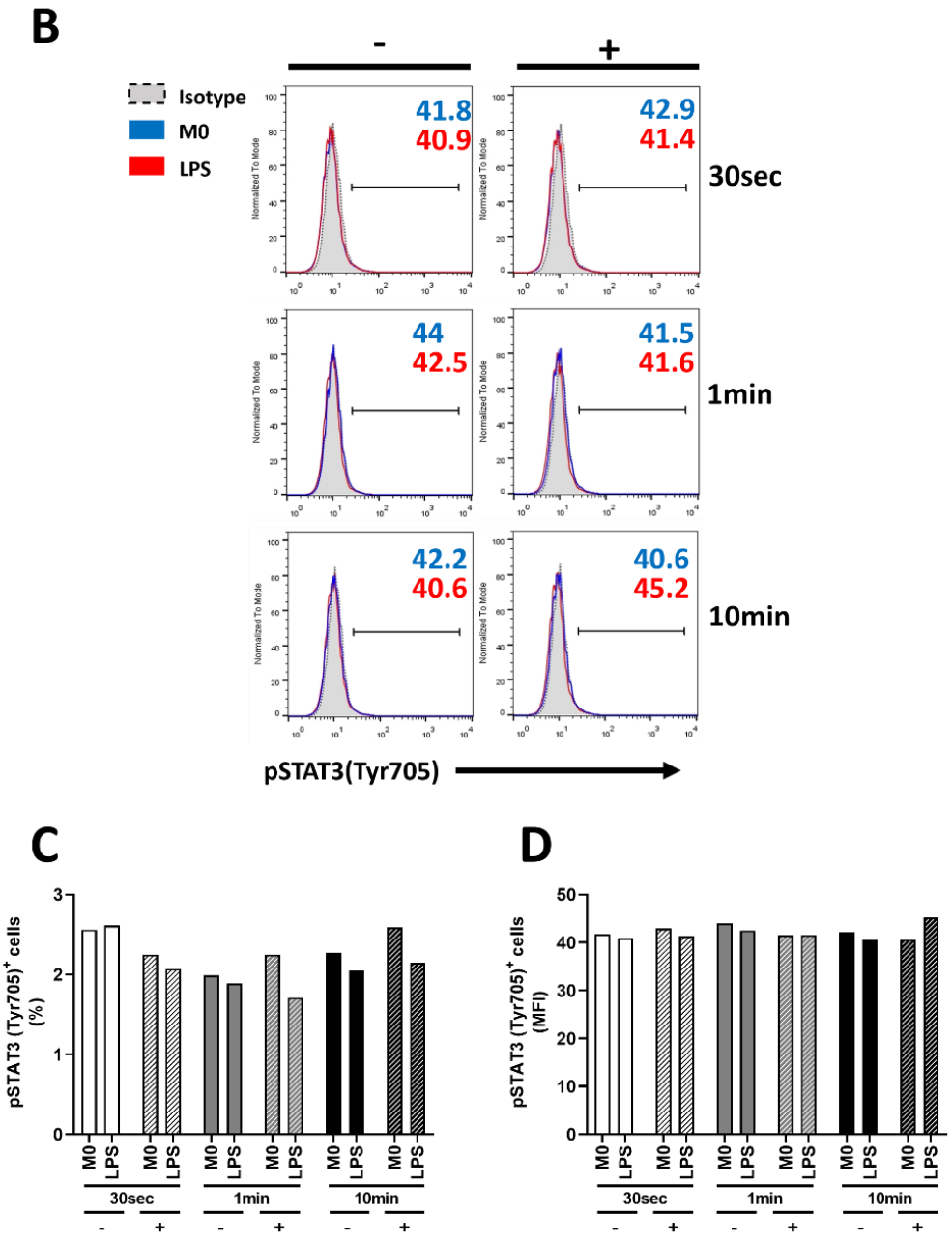

Figure 4.25: Characterising p-STAT3(Tyr705) expression at 30sec, 1min and 10min following LPS activation of THP-1 M0 macrophages. Data obtained after incubation of differentiated M0 macrophages with LPS at 1µg/mL for the indicated time periods. Culture and ICFC reagents were supplemented with (+) or without (-) sodium vanadate (0.1%). [A] Dot plots showing the percentage of native p-STAT3(Tyr705)$^+$ cells at 30sec (top), 1min (middle) and 10min (bottom). [B] Histograms showing mean fluorescent intensity (MFI) of p-STAT3(Tyr705) at 30sec (top), 1min (middle) and 10min (bottom). Numbers indicate MFI of live gated population. Bar graphs showing the percentage of p-STAT3(Tyr705)$^+$ cells [C], and MFI values for p-STAT3(Tyr705) [D]. All data represent 1 experiment comprising of individual values. No statistics available.

4.7. Chapter discussion

The usual course of inflammation begins with an acute phase followed by resolution, however if unresolved and left to enter a state of persistent 'chronic' infection, the contribution of host inflammatory mechanisms, not exogenous pathogens, becomes chiefly responsible for resultant host pathophysiology (Nathan and Ding, 2010). A large proportion of the global disease burden can be attributed at least in part to non-resolving inflammation with both acute and chronic states coexisting for extended periods, which suggests continual self-re-initiation of inflammatory cascades. A prominent example of this self-perpetuation occurs in Crohn's disease and Ulcerative Colitis in which infiltration of macrophages and other immature myeloid cells are prominent (Mantovani *et al.*, 2008; Davies and Abreu, 2015).

Cells of the innate immune system play vital roles in host defence against infection via sensing PAMPs and DAMPs. Different classes of germline-encoded PRRs which include TLRs then initiate and regulate the ensuing downstream responses (Akira, Uematsu and Takeuchi, 2006; Takeuchi and Akira, 2010). Activation of these PRRs by exogenous ligands such as LPS trigger multiple inflammasome signalling pathways which result in the production of pro-inflammatory mediators and subsequently induce adaptive immune responses (Iwasaki and Medzhitov, 2004; Cui *et al.*, 2015).

Monocyte and macrophage populations in the gut can alter markedly in both Crohn's disease and Ulcerative Colitis, seeing the accumulation of $CD14^{hi}CD11c^{hi}$ phenotypes (Grimm *et al.*, 1995; Rugtveit *et al.*, 1997; Bain *et al.*, 2013), which produce high levels of pro-inflammatory cytokines such as TNFα, IL-1β, IL-6, IL-12, and IL-23, and respond in an abnormal manner to commensal bacteria (Kamada *et al.*, 2008). In 2008, Kameda *et al* reported an increase in $CD14^{+}$ macrophages in the colon mucosa of Crohn's disease patients which produced large amounts of pro-inflammatory cytokines, IL-23 and TNF-α in response to commensal bacteria when compared with those from normal individuals and ulcerative colitis patients (Kamada *et al.*, 2008). Furthermore, although the number of M2-like macrophages has also been reported to be increased in the mucosa of both Crohn's disease and Ulcerative Colitis patients, the balance of macrophage phenotypes was shifted towards a pro-inflammatory

state, indicated by a higher ratio of $iNOS^+$ versus $CD163^+$ cells compared with normal intestinal tissue (Lissner *et al.*, 2015).

The responsiveness of cells to external stimuli such as infectious pathogens also rely on the transcriptional regulation of gene expression programmes, with a network of signalling pathways working to bridge the gap between stimulation and transcription. Initiation of these pathways results in the activation of transcription factors, their subsequent translocation into the nucleus and initiation of gene transcriptional programmes. The NF-κB signalling cascade regulates thousands of independent response genes encoding for cytokines, chemokines, antimicrobial peptides, as well as additional downstream transcription factors. This pathway is vital for many crucial immunological programs including initiating inflammatory responses to pathogens by innate immune cells, and the development and activation of cells responsible for adaptive immune responses (Dorrington and Fraser, 2019).

Several studies have already been conducted exploring the inhibitory and stimulatory effect of minocycline with focus on the TLR4-NF-κB inflammatory pathway. Ataie-Kachoie *et al* (2013) conducted a thorough investigation into the influence of minocycline upon constituents of the NF-κB signalling cascade, showing suppression of NF-κB in OVCAR-3 and SKOV-3 ovarian carcinoma cells. This was attributed to attenuation of upstream IκBα activation, phosphorylation, and degradation, in addition to suppression of p65 phosphorylation and nuclear translocation – a crucial mechanism for inflammatory gene transcription. This process was also described to be resultant of inhibition of TAK-1 activation and dissociation from TAB1 (Ataie-Kachoie, P. *et al.*, 2013). More recently Weiler and Dittmar (2019) also confirmed that minocycline abrogated IκBα and p65 phosphorylation leading to suppression of NF-κB and showed how treatment with minocycline inhibited the TNFR1-TRAF2 axis downstream of the TNF receptor 1 (TNFR1) in MDA-MB0435-pFDR1 cancer cells and M13SV1-Cre breast epithelial cells. They were also able to show that minocycline acted as a potent inhibitor of TNF-α via targeting of the NF-κB pathway, while differentially affecting all MAPK kinases (ERK1/2, p38 and JNK) acting to inhibit or stimulate their activation (Weiler and Dittmar, 2019). Lastly, a study conducted by Zhao and colleagues demonstrated treatment with minocycline significantly upregulated the expression of the transcription factors

CREB and pCREB within a model of cerebral ischemia in Wistar rats (Zhao *et al.*, 2015).

Despite the above observations, few studies have focused on the effect of minocycline on the TLR4-NF-κB pathway in macrophages. One paper, by Tai *et al* (2013), examined the effect of minocycline on cytokine and chemokine production in THP-1 monocytes when challenged with LPS. These authors observed that minocycline supressed TNF-α, IL-6, IFN-γ, IP-10, and MCP-1 production in a dose-dependent manner by inhibiting IκBα and IκB. They also concluded that in THP-1 monocytes minocycline did not affect the phosphorylation of ERK1/2, JNK, p38 or TAK1 (Tai *et al.*, 2013). The existing data summarising the inhibitory effect of minocycline on the NF-κB cascade in alternate biological models of monocytic cells suggest that minocycline may also be targeting this pathway in macrophages. Two upstream regulators of the NF-κB axis are the proteins CD14 and TLR4 which were assessed in this chapter.

As previously referenced, CD14 is an LPS receptor anchored to the cell membrane via glycosylphosphatidyl inositol found on monocyte and macrophage populations (Haziot *et al.*, 1988). In addition to the membrane form, a soluble form of CD14 is present in the blood, primarily due to shedding of this membrane form (Bazil and Strominger, 1991). LPS and LPS binding protein (LBP) form a tertiary complex with CD14 which enables the transfer of LPS to TLR4 and MD-2. The signalling pathways activated by TLR4 in response to LPS have been extensively studied and require adapter proteins in order to operate, which include myeloid differentiation factor 88 (MyD88), MyD88 adaptor-like protein (Mal, also known as TIRAP), TIR-containing adapter molecule (TRIF, also known as TICAM-1), and TRIF-related adapter molecule (TRAM, also known as TICAM-2) (Pålsson-McDermott and O'Neill, 2004).

Despite previous *in vitro* studies showing that cells lacking the membrane CD14 receptor, such as the endothelial and epithelial cells, can still respond to complexes of LPS and soluble CD14 (Pugin *et al.*, 1993) via an as yet unidentified receptor, other models using transgenic mice that overexpress CD14 are reported to be more sensitive to LPS-induced shock than CD14-expressing controls (Ferrero *et al.*, 1993; Tamura *et al.*, 1999), while animals deficient in CD14 altogether show little or no response to a dose of LPS that is 10-fold higher than a 100% lethal dose for CD14- expressing mice (Haziot *et al.*, 1996; Ebong

et al., 2001). Furthermore, hypo-responsiveness of macrophages to activation via TLRs is a cardinal feature of resident intestinal macrophages. Signalling molecules such as CD14, MyD88, TRAF-6, MD2, TRIF, and IRAK1 appear to be downregulated in mature intestinal macrophages (Smythies *et al.*, 2005), while mechanisms that inhibit TLR signalling and/or NF-κB activation appear to be over-expressed in gut-resident macrophages (Smythies *et al.*, 2010). This suggests molecules responsible for propagating TLR signalling are preferentially targeted rather than TLR expression itself (Calum C. Bain and Mowat, 2014).

The data presented in this chapter begin to suggest a protagonist action of minocycline in reducing CD14 expression while simultaneously reducing the production of pro-inflammatory mediators such as TNF-α, IL-6, IL-1β and IL-12 from LPS-activated M0 macrophages *in vitro*. This may not only modify macrophage phenotype from an established pro-inflammatory state ($CD14^{hi}CD86^{+}$) back towards a typical hypo-responsive intestinal macrophage baseline ($CD14^{low}$), but also provides support that propagation of TLR signalling in response to minocycline in this instance is not necessarily due to direct modification of TLR4 expression, but rather an influence on its soluble counterpart CD14. Considering the widely documented existence of increased macrophage CD14 expression in IBD patients and experimental models, a potent inhibitory effect exerted by minocycline as reported in this chapter on this protein may have beneficial therapeutic application in reducing innate cell LPS-sensitivity.

Moreover, $CD14^{hi}$ monocyte and macrophage populations in the mucosa of IBD patients are thought to support pathogenic T cell function through the production of IL-23 and expression of CD40, CD80 and CD86 (Rugtveit *et al.*, 1997). Activation of T cells occurs through peptides presented by interaction of major histocompatibility complex (MHC) that interact with select T cell receptors (TCRs), resulting in the initiation of various signalling cascades (Parker, 2019). Co-stimulatory molecules CD80 and CD86 are key molecules in this regard and have similar but also distinct functions. Binding to CD28 promotes T cell activation, whereas binding of CD80/CD86 to CTLA-4 results in downregulation of T cell function – a critical stage in inhibiting the immune response following infection resolution (Freeman *et al.*, 1995; Rugtveit *et al.*, 1997).

The T cell co-receptor CD28, interacts with CD80 (B7-1) and CD86 (B7-2) which are expressed on the surface of activated antigen presenting cells such as macrophages. Consequently, several signalling pathways, including those controlled by NF-κB, MAPK, PI3K and AKT are induced (Chen and Flies, 2013; Yao, Zhu and Chen, 2013). Their distinction is also apparent concerning their time of expression with CD86 expression dominating in the early stages of the immune response being upregulated rapidly in response to infection, while CD80 often occurs in the latter stages at the site of inflammation (Lanier *et al.*, 1995; NEWTON *et al.*, 2004).

The literature contains a growing body of evidence which propose these different functional consequences of CD28 engagement by CD80 and CD86. Using a murine model of acute myeloid leukemia, Matulonis *et al* illustrated superiority of CD80 in its capacity to protect the host against wild-type tumour challenge in addition to eradicating residual disease (Matulonis *et al.*, 1996). In the context of stimulation by irradiated P815 transfectants and co-stimulation of $CD8^+$ T lymphocytes, CD80 again was reported to be superior versus CD86 (Gajewski, 1996). Whilst finally in models of experimental allergic encephalomyelitis (EAE) administration of anti-CD80 mABs resulted in increased IL-4 production in mice, while inhibiting CD86/CD28 interaction *in vitro* decreased the production of IFN-γ (Kuchroo *et al.*, 1995; Racke *et al.*, 1995). This data, in combination with other reports suggests a situation whereby CD80 co-stimulation promotes the development of Th1 cells, while co-stimulation with CD86 preferences Th2 differentiation (Slavik, Hutchcroft and Bierer, 1999).

Further published evidence also points to a crucial role of this CD28-CD80/CD86 system in the regulation of inflammation in the context of both autoimmunity and aberrant innate immune responses (Nolan *et al.*, 2009). In 2007 Hoshino *et al* demonstrated the ability of CD28 on the surface of neutrophils to activate macrophages via engagement of the CD80/CD86 complex (Hoshino *et al.*, 2007). In proceeding years Nolan *et al* utilised an *in vivo* model of murine cecal ligation and puncture (CLP) and determined that CD80/CD86 signal via NF-κB to induce cytokines such as IL-6 using CD80/86$^{-/-}$ mice, and a novel CD40/80/86$^{-/-}$ murine model, while further CLP *in vivo* investigations illustrated an improvement in survival and attenuation of pro-inflammatory cytokines via deletion or blockade of CD80 and CD86 (Nolan *et al.*, 2008). These reports showing deletion of CD80

but not CD86 is directly correlated with better overall survival suggests that CD80 is the dominant receptor in regulating lethal outcomes in the early innate immune response through the direct attenuation of IL-6.

Within the *in vitro* model of LPS-activated M0 macrophages shown in this chapter, minocycline was able to exert distinct influence on CD80 and CD86 expression, causing a significant increase and decrease respectively. Given the understanding that CD80 is a more potent effector molecule for the induction of $CD4^+$ Th1 cells which function to recognize antigens presented by MHC class I or II molecules and play a vital role in the identification and eradication of intracellular pathogens such as bacteria (Romagnani, 2000), it could be hypothesised that minocycline may behave in a way that aims to potentiate downstream humoral immunity in the form of Th1 recruitment and activation. Considering attenuation of IL-6 by minocycline is also reported here in this chapter which occurs via NF-κB signalling – another molecule previously reported to be inhibited by minocycline, a dual action of minocycline begins to be proposed, one that both promotes additional downstream pro-inflammatory response but dampens the macrophages own participation in inflammation potentiation.

Moreover, the literature attributes co-stimulation of CD28 and CD86 with Th2 cell response, a $CD4^+$ subset responsible for evoking not only antibody response and eosinophil accumulation, but the inhibition of several macrophage functions rendering them regulators of phagocyte-independent responses (Zhu and Paul, 2008; Zhu, 2015). The data disseminated here highlights the ability of minocycline in downregulating CD86 expression which may correlate with both reduced downstream Th2 populations, thus limiting their negative regulatory function on the macrophages themselves, in addition to potentially limiting M2 macrophage associated pathology following phenotype switching such as fibrosis and tumour formation as a direct result of both minocycline and the release of IL-4 and IL-13 from Th2 populations (Tjiu *et al.*, 2009).

Modification of CD14, CD80 and CD86 were not the only defined outcome of minocycline intervention reported in this chapter. A clear upregulation of the M2-associated surface markers CD163 and CD206 was also shown (Nielson *et al.*, 2020). Both proteins are expressed by macrophages but can be differentially regulated, with CD163 expression modified by IL-10 stimulation, and CD206

upregulated by IL-4 and IL-13 (Mosser and Edwards, 2008; Nielson *et al.*, 2020). These scavenger receptors are highly expressed by macrophages and act to bind a variety of ligands, promoting the removal of non-self or altered-self targets. They perform these functions via endocytosis, phagocytosis, adhesion, and signalling, which results in the elimination of degraded or harmful substances (PrabhuDas *et al.*, 2017).

CD163 is a 130-kDa membrane protein, with its expression restricted to the monocytic–macrophage linage. $CD163^{+}$ macrophages may originate from extravasation of monocytes, or may represent macrophage activation switching (Porcheray *et al.*, 2005), with reports concluding regulation of CD163 a feature of macrophage differentiation to 'alternatively activated' M2-type macrophages (Barros *et al.*, 2013). Bacteria are reported to bind human CD163, with studies describing sensor-like function of CD163 in response to *Streptococcus* mutants, *Escherichia coli*, and *Staphylococcus aureus*, rather than behaving as an endocytic receptor. In these reports, expression of CD163 promoted bacteria-induced production of pro-inflammatory cytokine TNF-α and the recognition and phagocytosis of the bacteria (Kneidl *et al.*, 2012).

On the other hand, CD206 is a complex 175 kDa membrane-bound protein comprising different extracellular domains, a transmembrane segment, and a cytoplasmic tail (Taylor *et al.*, 1990). Much like CD163, CD206 is an efficient endocytic receptor and continuously recycles between the cell surface and endosomal compartments with <30% expressed in the plasma membrane at baseline (Gazi and Martinez-Pomares, 2009). It recognises a wide variety of ligands including mannose, collagen and peptide hormones, in addition to allergens and microbial products such as LPS (Zamze *et al.*, 2002; Gazi and Martinez-Pomares, 2009; Martinez-Pomares, 2012). Despite this ability to recognize and bind pathogens, the contribution of CD206 to host defence against infection is obscured. In a 2002 study, Lee *et al* showed an inability of CD206 deficient (MR -/-) wild-type mice to remove collagen peptide hormones and lysosomal hydrolases (Lee, 2002), while Taylor *et al* reported an inability to induce phagocytosis by CD206 independently using both *in vivo* and *in vitro* methodologies (Taylor, Gordon and Martinezpomares, 2005).

When related to IBD, studies into mucosal healing in IBD patients who received the anti-TNF-α therapy adalimumab illustrated both a loss of $CD14^{hi}$ macrophages, in addition to accumulation of $CD206^{+}$ macrophages which resulted in pro-restorative action. From these data they suggest a possible phenotypic 'switch' of pro-inflammatory macrophages ($CD14^{hi}$) to anti-inflammatory populations ($CD206^{+}$) in the Crohn's Disease patients (Vos *et al.*, 2012). Moreover, studies conducted in 2016 report the induction of regulatory M2 macrophages by treatment with anti-TNF antibodies – a current major therapeutic intervention for the treatment of IBD, which were accompanied by increased levels of autophagy when compared to an IFN-γ-induced M1 macrophage control (Levin *et al.*, 2016).

A meta-analysis of placebo-controlled trials conducted in 2008 evaluated the safety and efficacy of TNF antagonists for the treatment of Crohn's disease. The authors assessed fourteen luminal Crohn's disease trials encompassing 3995 patients and reported the anti-TNF therapy (infliximab and adalimumab combined) was more effective than placebo for the induction of clinical remission at 4 weeks, also showing significant effect on 1-year maintenance of steroid-free remission (Peyrin–Biroulet *et al.*, 2008). Although clearly an effective therapeutic strategy, reports also highlight the requirement of IL-10 signalling in macrophages to enable successful response following anti-TNF mAb administration. Koelink *et al* recently proved the necessity of IL-10 for the anti-TNF induction of macrophage polarization from an M1-M2 $CD163^{+}CD206^{+}$ phenotype (Koelink *et al.*, 2020). Their data supports the narrative that macrophages become fixed as an M1 phenotype and continue to secrete pro-inflammatory cytokines in the absence of IL-10 and cannot convert to their M2 counterpart.

The data illustrated in this chapter highlight minocycline's potent ability to upregulate the expression of both CD163 and CD206 despite originating from inflammatory 'patrolling' ($CD14^{+}$) monocyte precursors, and with 24hr exposure to LPS at a therapeutically high dose. This, in combination with a decrease in CD14, and reductionist action of TNF-α secretion by activated macrophages in these experiments appears to corroborate previous reports whereby this phenotype 'switching' (M1 to M2) is seen upon anti-TNF therapy.

The data reported in this chapter simultaneously shows minocycline promote not only this phenotype switch from M1 to M2, but also reduce M1-driven pro-inflammatory cytokine release. Moreover, although minocycline was also shown to reduce IL-10 production, it was not possible to ascertain any defined effect of minocycline on IL-10 signalling mediated through the STAT3/SOCS3 axis as discussed earlier in section 4.8. Importantly, these results may render minocycline another safe and effective treatment strategy for IBD given its similarity in function to current therapies such as anti-TNF-α which does not appear to rely on IL-10 signalling.

5. Results: Effect of minocycline on the response of M0 macrophages to M1 or M2 polarization

Macrophages are a key cell type in the immune response due to their ability to adapt and adopt different phenotypes dependent on requirements dictated by their surrounding microenvironment, with recent articles beginning to establish mechanisms by which macrophages are functionally influenced by the gut (Muller, Matheis and Mucida, 2020; Viola and Boeckxstaens, 2020; Wang, Chen and Wang, 2020; Yang *et al.*, 2021). In the past two decades work towards elucidating the paradigm of macrophage polarization has become ever clearer with the general consensus being that once tissue resident, macrophage populations become either M1 or M2 phenotypes, but which are also widely accepted to be transient and plastic populations (Camille and Dealtry, 2018).

M1 or pro-inflammatory 'classically-activated' macrophages act to eliminate exogenous pathogens via cytokine and inducible nitric-oxide synthase (iNOS) production, while M2 anti-inflammatory 'alternatively-activated' cells promote inflammation anergy and resolution (Hotamisligil, 2006; C. Li *et al.*, 2018). Polarization of macrophages is determined by local external cues dictating phenotype commitment. M1 are induced by bacterial antigens as well as IFN-γ, LPS and TNF-α, rendering the cells microbicidal and tumoricidal, and subsequently release nitric oxide (NO) and inflammatory cytokines that promote the differentiation of Th1 and Th17 T helper cells. On the other hand, M2 cells are generated via interleukin (IL)-10, IL-13, IL-4 and IL-1RA (receptor agonist) and function to metabolize arginine and polyamines whilst releasing anti-inflammatory cytokines, such as IL-10, ultimately contributing and driving resolution, tissue remodeling and building of immune tolerance (Hao *et al.*, 2012; Yang *et al.*, 2013).

Much of the literature depicts this concept of dual purpose; advancing both inflammation and regeneration, however in many pathophysiological conditions, macrophages do not neatly ascribe to the M1/M2 paradigm (Rőszer, 2015; Artyomov, Sergushichev and Schilling, 2016; Jinnouchi *et al.*, 2020). A balance between M1 and M2 phenotypic activity demonstrates shift over time with M1 generally behaving as first responders recruiting both effective defense against invasion through secretion of pro-inflammatory mediators in addition to

angiogenesis, whereas M2 are essential for wound repair and tissue regeneration in the latter stages of inflammation resolution (Orecchioni *et al.*, 2019; Yunna *et al.*, 2020). The importance of M1/M2 homeostasis is further verified through evidence of delayed wound healing and fibrotic development when M1 or M2 subpopulations become unrestrained respectively (Hesketh *et al.*, 2017). The literature also supports the role of M1 macrophages in inflammatory-mediated responses displayed during the early stages of the normal tissue repair process, whereby they are characterized by high expression of CD80 and CD86 (Bertani, Mozetic, Fioramonti, Iuliani, *et al.*, 2017; Raggi *et al.*, 2017; Feito *et al.*, 2019).Thus the M1/M2 nomenclature is a useful tool in describing macrophage population plasticity during inflammatory states through correlation of observable changes in biomarkers in relation to inflammatory progression and healing (Smith *et al.*, 2017). This chapter, therefore, aims to explore the potential role of minocycline on the polarization process from resting M0 macrophages to polarized M1 or M2 phenotypes through *in vitro* polarization of THP-1 and PBMC-derived macrophages.

5.1. THP-1

5.1.1. Characterising *in vitro* polarization of THP-1 macrophages

Following the completion of objectives 1 and 2 in the previous chapters, which explored the effect of minocycline on macrophage differentiation and activation with exogenous LPS respectively, the next objective aimed to assess if minocycline could influence the phenotype acquisition of macrophages if introduced during the polarization process. To begin these investigations, as before, a reliable protocol for polarization of M0 macrophages to both M1 and M2 subsets needed to be established. While the literature is relatively universal in the stimuli required to drive M1 and M2 polarization with IFN-γ and LPS or IL-4 used respectively (Genin *et al.*, 2015; Bertani, Mozetic, Fioramonti, Luliani, *et al.*, 2017), there was some disparity in stimulus concentration as well as incubation periods, meaning some optimization occurred to decipher the best combination of polarization agents for this model supported by the pre-established protocols in the literature (Tjiu *et al.*, 2009; Laskar *et al.*, 2013; Chanput, Mes and Wichers, 2014; Shiratori *et al.*, 2017). Administration of 20ng/mL IFN-γ was a consistent feature across reports therefore this was tested and kept consistent throughout

the optimization process (A11 & A12) (Chanput *et al.*, 2013; Vogel *et al.*, 2014; Shiratori *et al.*, 2017).

However, despite multiple attempts utilizing varying conditions for M2 macrophage generation encompassing lone stimulation using IL-4 (Appendix A11.1-11.4), dual stimulation with IL-4 and IL-13 (Appendix A11.5-11.7), and differing incubation periods (24 and 48 hr) (Appendix A11.8-11.11), a distinguishable M2 phenotype could not be established using the THP-1 model, therefore intervention with minocycline was continued using the M1 model only in this instance. Based on the results obtained a final polarization protocol of 20ng/mL IFN-γ + 10ng/mL LPS was established for M1 macrophage generation. It should also be noted that discontinuation with U-937 was also decided at this stage given the limited literature using this cell line for polarization studies and failure to induce distinct M1 or M2 populations (Appendix A12). In addition, use of 50μM minocycline and the positive control dexamethasone was also discontinued from the treatment panels due to the toxic effects seen with this top concentration of minocycline (chapter 3), and requirement to prioritise treatment groups due to material availability.

To assess the role of minocycline on macrophage polarization it was first imperative to characterise the effect of the polarizing stimuli upon surface marker expression. To do this, THP-1 monocytes were first differentiated to resting M0 macrophages following 48hr PMA (80nM) incubation and subsequent 72hr resting in replenished media as before. At this point (Day 5) cells were treated with IFN-γ (20ng/mL) + LPS (10ng/mL) for a further 24hr, at which time supernatant was aspirated and discarded, and cells were collected and stained for surface marker evaluation by multicolour flow cytometry. As within previous chapters, the surface marker panel stayed consistent, incorporating pan-macrophage markers CD14 and CD11b (with the CD11b antibody clone selection for THP-1 and PBMC also remaining consistent), M1-associated markers CD80 and CD86, and M2-associated markers CD163 and CD206.

Data presented below in Figures 5.1, 5.2 and 5.3 illustrate acquisition of an M1 phenotype by the resting M0 THP-1-derived macrophages with increased expression of CD14 (Figure 5.1A-D), and the co-stimulatory molecules CD80 and CD86 (Figure 5.2A-F) when compared to the un-polarized M0 baseline. This was

reflected in both the percentage of positive cells and the density of marker expression (MFI).

However, where upregulation of these markers was pronounced following 24hr polarization with IFN-γ and LPS, CD11b expression in its active form was inconclusive with no consistent modification exerted by the M1 polarizing stimuli (Figure 5.1A, B, E and F). The M2-associated marker CD163 was shown to increase following M1-polarizaing with the percentage of $CD163^+$ cells increasing by 1.5-fold when compared to the un-polarized control (Figure 5.3A and C). However, the density of CD163 expression (MFI) was largely unchanged (Figure 3.3 B and D). Data for CD206 was also inconsistent in both the percentage of $CD206^+$ cells and the density of CD206 expression (Figure 5.3A, B, E and F). Considering the raw obtained values, the fluctuation in CD163 and CD206 response may be attributed to the very low baseline expression of these markers and as such CD206 and CD163 MFI were defined as unchanged following polarization.

The interaction of LPS with the CD14-TLR4 receptor complex modulates the host innate immune response (Płóciennikowska *et al.*, 2015; Tsukamoto *et al.*, 2018; Ciesielska, Matyjek and Kwiatkowska, 2021). A lack of CD14 therefore hampers the macrophage response to LPS with reports corroborating this narrative whereby CD14-deficient macrophages did not undergo the same polarization and cytokine production as wild type ($CD14^+$) macrophages (Gangloff *et al.*, 2005; da Silva *et al.*, 2017). Therefore, the data presented here, in combination with the data within the literature depict a distinct M1 phenotype with increased expression of CD14, CD80 and CD86 when compared to unstimulated M0 macrophages, and thus successful polarization within this model (Raggi *et al.*, 2017).

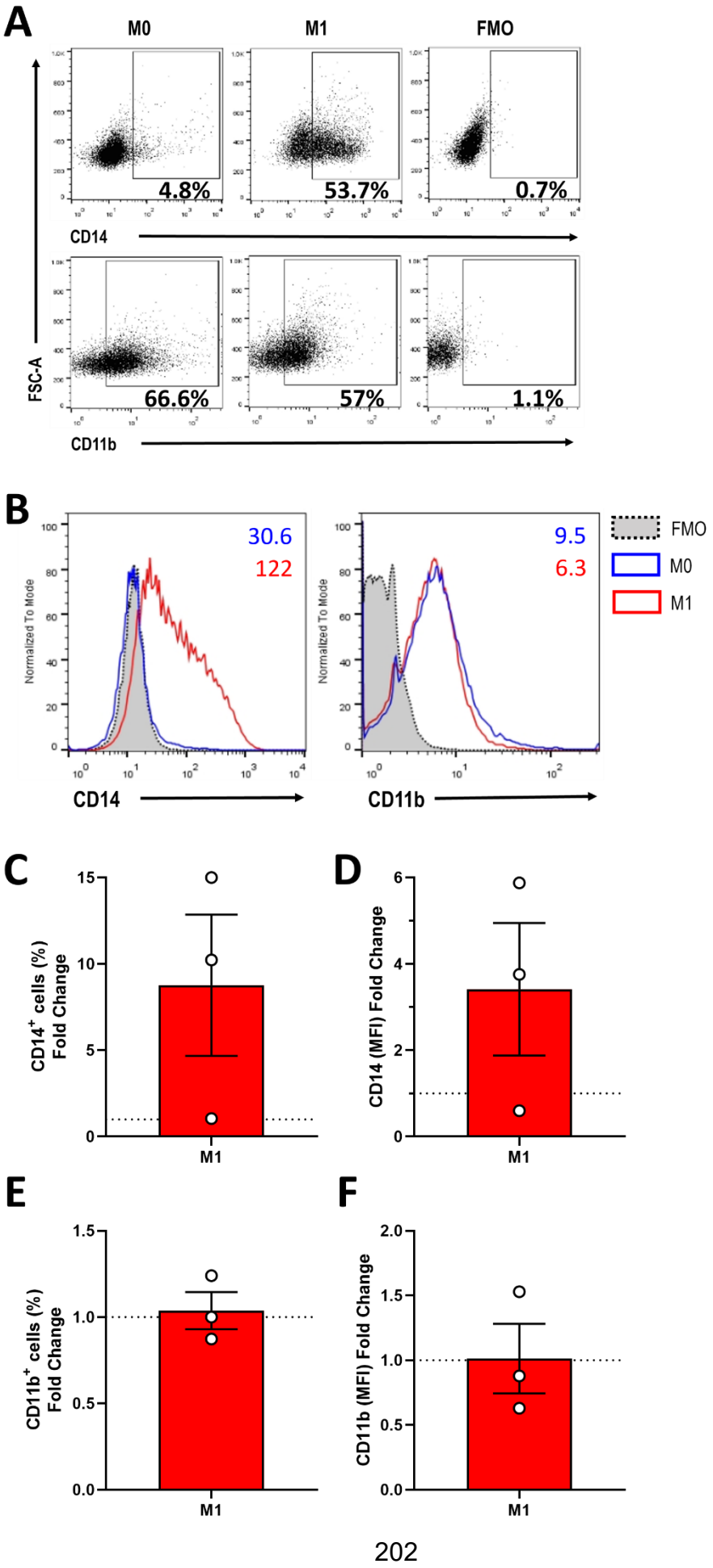
A
M0
M1
FMO
4.8%
53.7%
0.7%
CD14
FSC-A
66.6%
57%
1.1%
CD11b
B
30.6
122
9.5
6.3
FMO
M0
M1
Normalized To Mode
CD14
CD11b
C
CD14+ cells (%) Fold Change
M1
D
CD14 (MFI) Fold Change
M1
E
CD11b+ cells (%) Fold Change
M1
F
CD11b (MFI) Fold Change
M1

Figure 5.1: CD14 and CD11b expression profile of M1-polarized THP-1 macrophages. Data obtained after 24hr incubation of differentiated M0 macrophages with M1 polarizing agents IFN-γ (20ng/mL) + LPS (10ng/mL). [A] Representative dot plots showing the percentage of $CD14^+$ (top) and $CD11b^+$ (bottom) cells. [B] Representative histograms showing mean fluorescent intensity (MFI) for CD14 (left) and CD11b (right). Numbers indicate MFI of live gated population. [C-F] Bar graphs showing the percentage of $CD14^+$ [C] and $CD11b^+$ [E] cells, and MFI values for CD14 [D] and CD11b [F]. Data normalised and displayed as fold change versus the un-polarized M0 macrophage control. Data represents 3 replicated experiments each comprising of triplicate values. Data presented as mean ± SEM. Unpaired *t* test applied versus the un-polarized M0 macrophage.

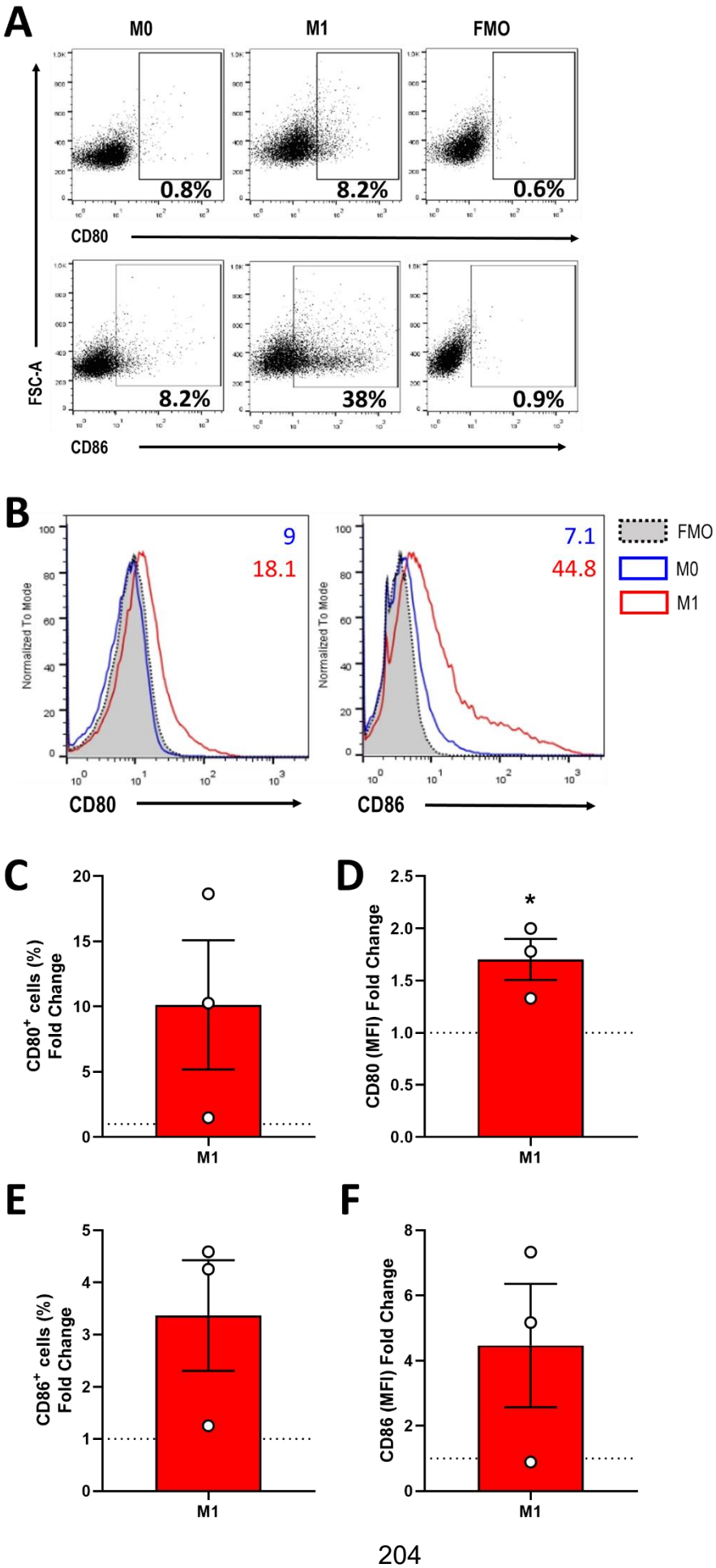
A
M0
M1
FMO
0.8%
8.2%
0.6%
CD80
8.2%
38%
0.9%
FSC-A
CD86
B
9
18.1
7.1
44.8
FMO
M0
M1
Normalized To Mode
CD80
CD86
C
CD80+ cells (%) Fold Change
M1
D
CD80 (MFI) Fold Change
*
M1
E
CD86+ cells (%) Fold Change
M1
F
CD86 (MFI) Fold Change
M1

Figure 5.2: CD80 and CD86 expression profile of M1-polarized THP-1 macrophages. Data obtained after 24hr incubation of differentiated M0 macrophages with M1 polarizing agents IFN-γ (20ng/mL) + LPS (10ng/mL). [A] Representative dot plots showing the percentage of $CD80^+$ (top) and $CD86^+$ (bottom) cells. [B] Representative histograms showing mean fluorescent intensity (MFI) for CD80 (left) and CD86 (right). Numbers indicate MFI of live gated population. [C-F] Bar graphs showing the percentage of $CD80^+$ [C] and $CD86^+$ [E] cells, and MFI values for CD80 [D] and CD86 [F]. Data normalised and displayed as fold change versus the un-polarized M0 macrophage control. Data represents 3 replicated experiments each comprising of triplicate values. Data presented as mean ± SEM. Unpaired *t* test applied versus the un-polarized M0 macrophage. *$p<0.05$.

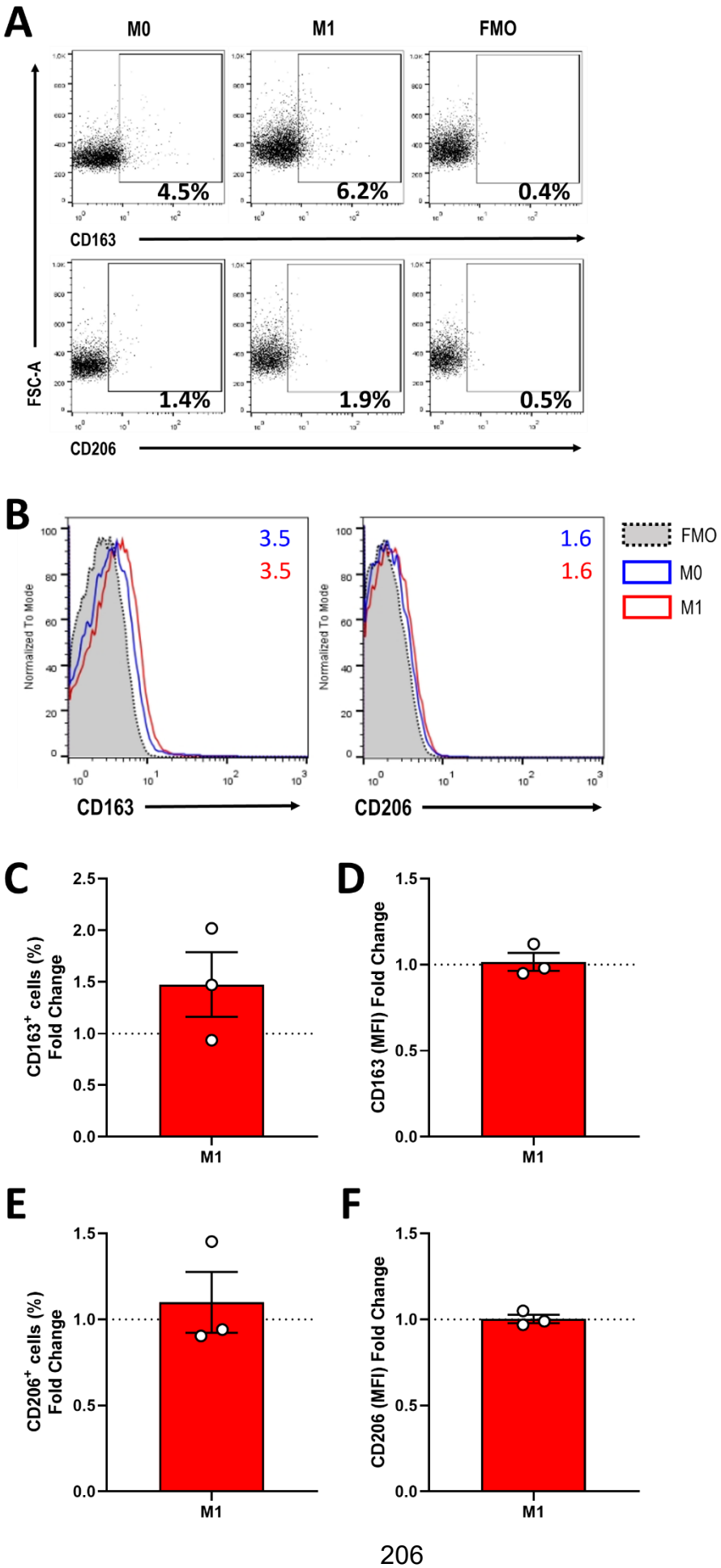
A
M0
M1
FMO
4.5%
6.2%
0.4%
CD163
1.4%
1.9%
0.5%
FSC-A
CD206
B
3.5
3.5
1.6
1.6
FMO
M0
M1
Normalized To Mode
CD163
CD206
C
CD163+ cells (%) Fold Change
M1
D
CD163 (MFI) Fold Change
M1
E
CD206+ cells (%) Fold Change
M1
F
CD206 (MFI) Fold Change
M1

Figure 5.3: CD163 and CD206 expression profile of M1-polarized THP-1 macrophages. Data obtained after 24hr incubation of differentiated M0 macrophages with M1 polarizing agents IFN-γ (20ng/mL) + LPS (10ng/mL). [A] Representative dot plots showing the percentage of $CD163^+$ (top) and $CD206^+$ (bottom) cells. [B] Representative histograms showing mean fluorescent intensity (MFI) for CD163 (left) and CD206 (right). Numbers indicate MFI of live gated population. [C-F] Bar graphs showing the percentage of $CD163^+$ [C] and $CD206^+$ [E] cells, and MFI values for CD163 [D] and CD206 [F]. Data normalised and displayed as fold change versus the un-polarized M0 macrophage. Data represents 3 replicated experiments each comprising of triplicate values. Data presented as mean ± SEM. Unpaired *t* test applied versus the un-polarized M0 macrophage.

5.1.2. Effect of minocycline during M1 polarization of THP-1 macrophages

With an M1 subset of macrophages successfully generated based on the previous surface marker phenotyping data, treatment with minocycline at the two lower concentrations of 10μM and 25μM was next introduced to assess a potential effect of minocycline upon this polarization process. Macrophages were differentiated from their monocyte precursor using PMA as described in chapter 2 section 2.1.1 and were pre-treated with minocycline for 2hr prior to the addition of the M1 polarizing agents IFN-γ (20ng/mL) + LPS (10ng/mL). Cultures were incubated for a further 24hr to allow for full polarization as per the optimized protocol, at which point supernatant was collected and stored for cytokine determination, and cells were collected and stained for flow cytometric analysis.

Data outlined in Figure 5.4 below shows a small reduction in the percentage of $CD14^+$ cells by 11.5% following treatment with minocycline at 25μM versus the no treatment (NT) group (Figure 5.4 A and C). This inhibitory effect of minocycline was also reflected in the density of CD14 expression whereby 25μM resulted in a 0.9-fold decrease in MFI versus the baseline M1 group (Figure 5.4B and D). In this regard, minocycline at the lower concentration of 10μM did not elicit any clear change in CD14 expression. Conversely, no definable influence of minocycline intervention on the expression of active CD11b was reported (Figure 5.4A, B, E and F). What should be noted however, is the adverse effect on CD11b expression exerted by the DMSO vehicle control (Veh) which caused an increase in both the percentage of $CD11b^+$ cells, as well as the density of CD11b expression (MFI).

When assessing the effect on the co-stimulatory molecules CD80 and CD86 an opposing influence of minocycline was seen. Where M1 polarization in the

absence of minocycline increased the percentage of $CD80^+$ cells from <1% to a modest 8% versus the un-polarized control (Figure 5.5A and C), administration of minocycline at 10μM and 25μM caused significant upregulation, up by 83% and 91.6% respectively (p<0.0001) versus the M1-polarized (NT) group (Figure 5.5A and C). This meant that treatment with minocycline at the highest concentration of 25μM resulted in almost 100% of cells now expressing CD80 versus only 8% without treatment. Moreover, this was duplicated in the density of expression data which show a clear correlation between minocycline concentration and CD80 expression with 10μM inducing a 5.5-fold increase in CD80 expression, and 25μM a significant 19.1-fold increase versus the M1-polarized (NT) group (p<0.0001) (Figure 5.5B and D).

Despite an inhibitory effect elicited by minocycline in the previous chapters, when added during M1 polarization minocycline on this occasion did not influence any coherent changes in CD86 expression (Figure 5.5A, B, E and F), although both the percentage and density of expression appear to be consistent with the data displayed in previous chapters despite failing to reach significance. However, once again, an influence of the vehicle upon this marker was noted whereby DMSO appeared to inhibit CD86 expression compared to the M1 control. Reports alluding to the effect of DMSO on surface marker expression in this macrophage model remain absent meaning it is only possible to speculate the cause of this modification, and instead report the conclusion that in respect to minocycline no obvious alteration in CD86 expression occurred.

Finally, when analysing the influence of minocycline on the M2-associated markers CD163 and CD206, results echoed those obtained in chapter 4 whereby intervention resulted in robust upregulation of both proteins (Figure 5.6). In parallel to the data obtained from assessing CD80, minocycline at 25μM resulted in almost 100% of cells now expressing both CD163 and CD206, with an increase of 94.5% and 96.7% respectively (p<0.0001) (Figure 5.6A, C and E). This significant upregulation was further mirrored in the density of expression with a 20-fold, and 18.3-fold increase in MFI for CD163 and CD206 respectively versus the untreated M1 control which itself had little to no change versus the un-polarized M0 group (p<0.0001) (Figure 5.6B, D and F). Although minocycline at 25μM was the more potent of the two concentrations used, 10μM continued to elicit the same responses, just at a lower magnitude. From this data minocycline

was shown to simultaneously inhibit CD14 expression, while upregulating CD80, CD163 and CD206 despite a strong pro-inflammatory baseline created by the M1-polarizing stimuli.

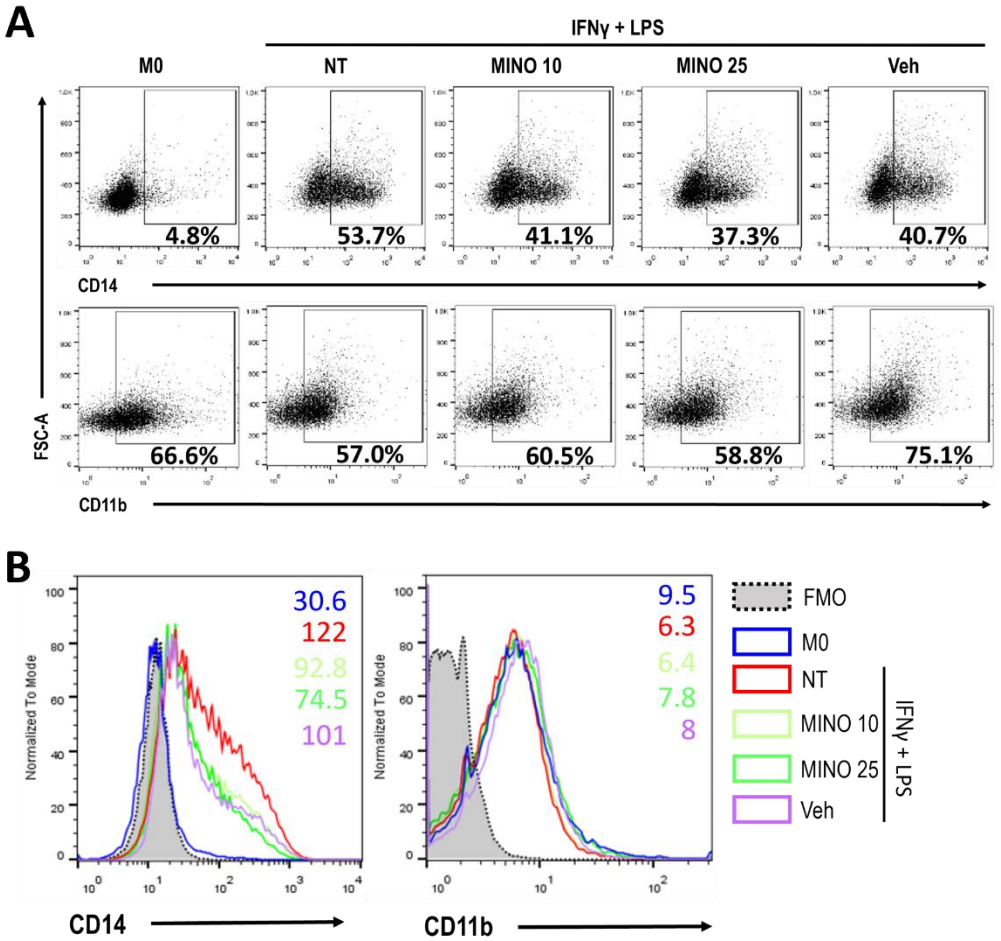
A
IFNγ + LPS
M0
NT
MINO 10
MINO 25
Veh
4.8%
53.7%
41.1%
37.3%
40.7%
CD14
FSC-A
66.6%
57.0%
60.5%
58.8%
75.1%
CD11b
B
30.6
122
92.8
74.5
101
9.5
6.3
6.4
7.8
8
Normalized To Mode
FMO
M0
NT
MINO 10
MINO 25
Veh
IFNγ + LPS
CD14
CD11b
C
CD14+ cells (%)
D
CD14 (MFI) Fold Change
E
CD11b+ cells (%)
F
CD11b (MFI) Fold Change
IFNγ + LPS

Figure 5.4: Effect of minocycline on CD14 and CD11b expression following M1 polarization of THP-1 macrophages. Data obtained after 24hr incubation of differentiated M0 macrophages with M1 polarizing agents IFN-γ (20ng/mL) and LPS (10ng/mL). [A] Representative dot plots showing the percentage of $CD14^+$ (top) and $CD11b^+$ (bottom) cells. [B] Representative histograms showing mean fluorescent intensity (MFI) of CD14 (left) and CD11b (right). Numbers indicate MFI of live gated population. [C-F] Bar graphs showing the percentage of $CD14^+$ [C] and $CD11b^+$ [E] cells, and MFI values for CD14 [D] and CD11b [F]. MFI values normalised and displayed as fold change versus the un-polarized M0 macrophage control. NT = untreated M1 macrophage, MINO 10 = Minocycline 10μM, MINO 25 = Minocycline 25μM, Veh = DMSO vehicle control (1:1000). Data represents 3 replicated experiments each comprising of triplicate values. Data presented as mean ± SEM. One-way ANOVA with post hoc Dunnett's applied versus the untreated (NT) M1 macrophage control.

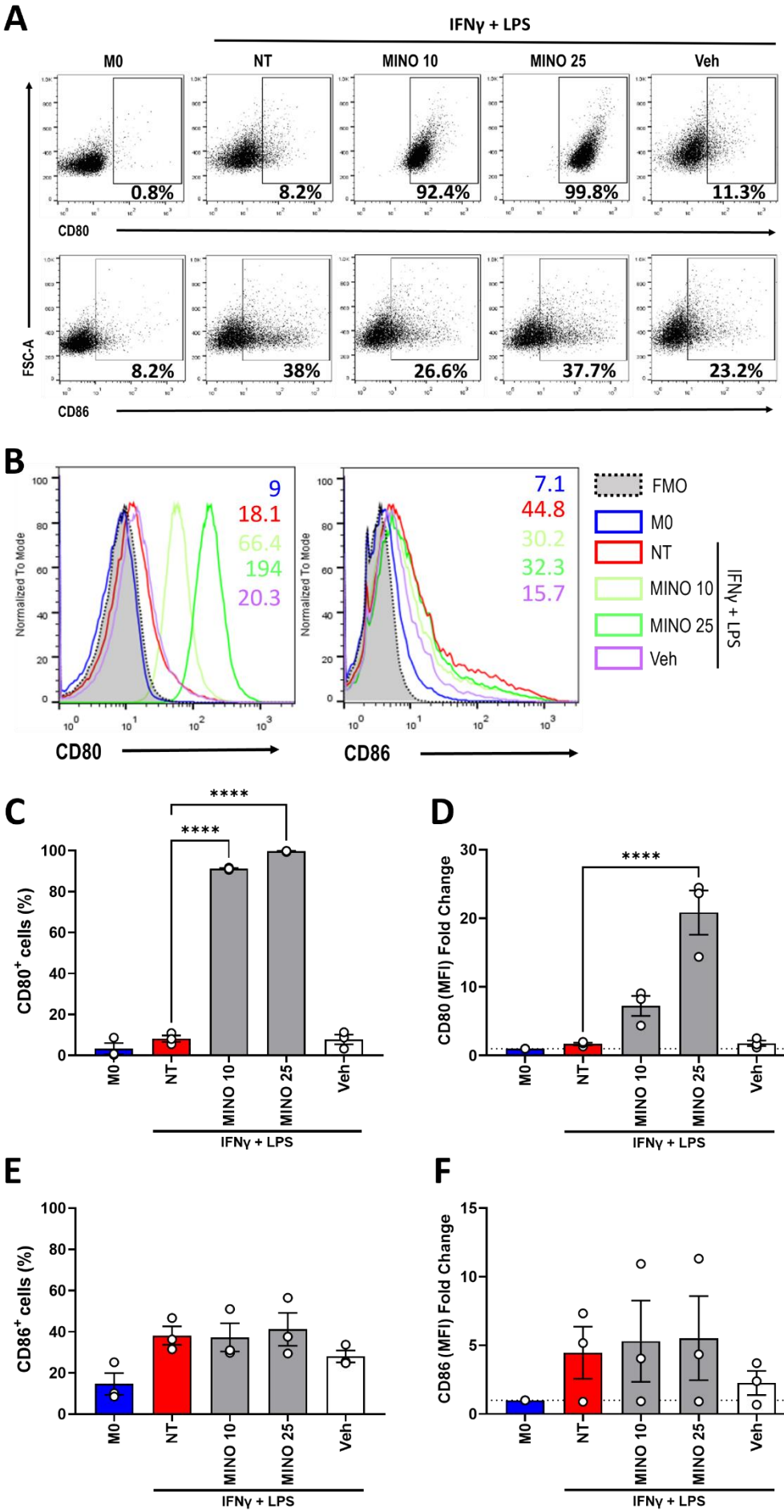
A
IFNγ + LPS
M0
NT
MINO 10
MINO 25
Veh
0.8%
8.2%
92.4%
99.8%
11.3%
CD80
FSC-A
8.2%
38%
26.6%
37.7%
23.2%
CD86
B
Normalized To Mode
9
18.1
66.4
194
20.3
7.1
44.8
30.2
32.3
15.7
FMO
M0
NT
MINO 10
MINO 25
Veh
IFNγ + LPS
CD80
CD86
C
CD80+ cells (%)
****
****
M0
NT
MINO 10
MINO 25
Veh
IFNγ + LPS
D
CD80 (MFI) Fold Change
****
IFNγ + LPS
E
CD86+ cells (%)
IFNγ + LPS
F
CD86 (MFI) Fold Change
IFNγ + LPS

Figure 5.5: Effect of minocycline on CD80 and CD86 expression following M1 polarization of THP-1 macrophages. Data obtained after 24hr incubation of differentiated M0 macrophages with M1 polarizing agents IFN-γ (20ng/mL) and LPS (10ng/mL). [A] Representative dot plots showing the percentage of $CD80^+$ (top) and $CD86^+$ (bottom) cells. [B] Representative histograms showing mean fluorescent intensity (MFI) of CD80 (left) and CD86 (right). Numbers indicate MFI of live gated population. [C-F] Bar graphs showing the percentage of $CD80^+$ [C] and $CD86^+$ [E] cells, and MFI values for CD80 [D] and CD86 [F]. MFI values normalised and displayed as fold change versus the un-polarized M0 macrophage control. NT = untreated M1 macrophage, MINO 10 = Minocycline 10μM, MINO 25 = Minocycline 25μM, Veh = DMSO vehicle control 1:1000. Data represents 3 replicated experiments each comprising of triplicate values. Data presented as mean ± SEM. One-way ANOVA with post hoc Dunnett's applied versus the untreated (NT) M1 macrophage control. ****$p<0.0001$.

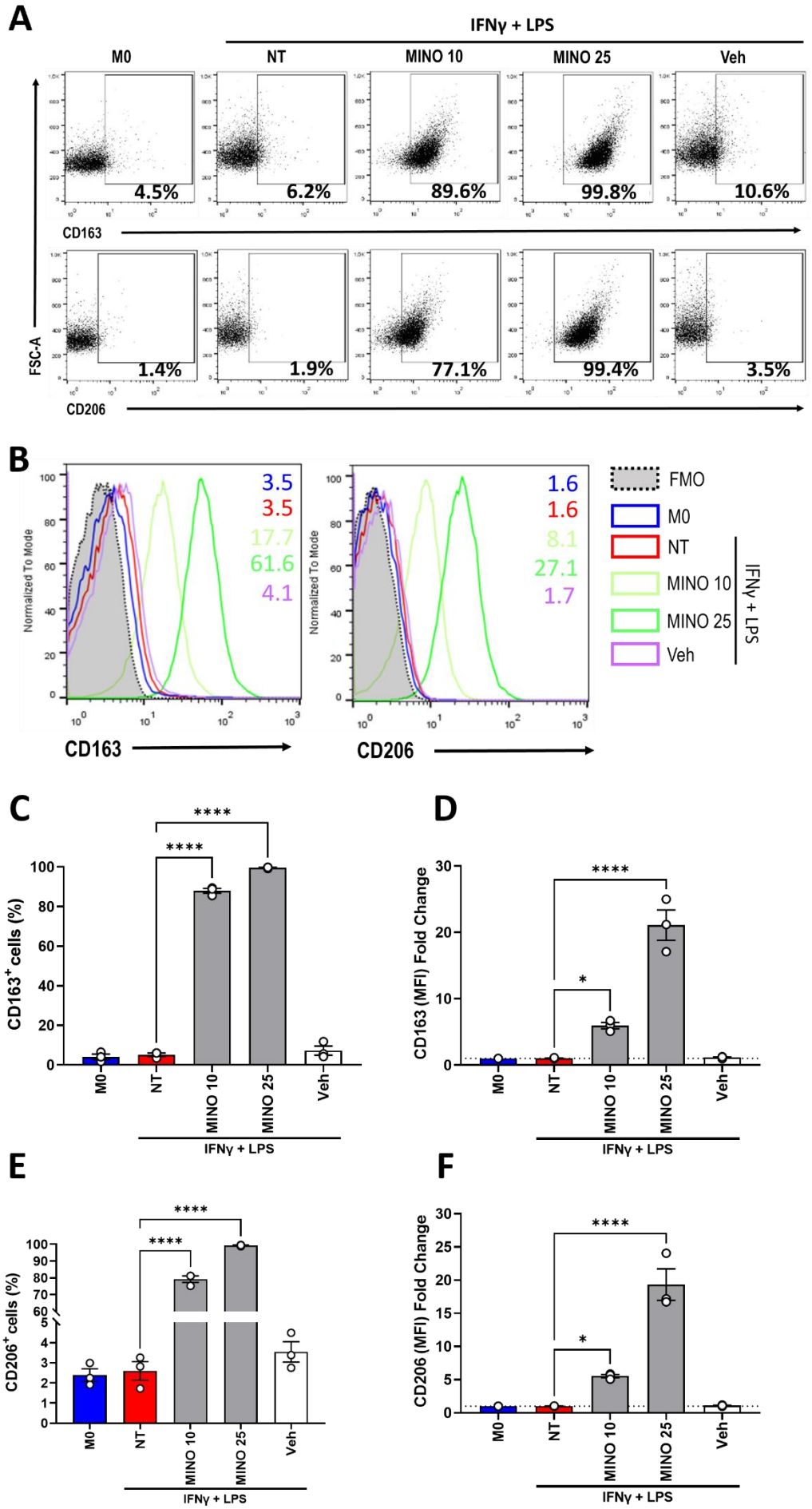
A
IFNγ + LPS
M0
NT
MINO 10
MINO 25
Veh
4.5%
6.2%
89.6%
99.8%
10.6%
CD163
FSC-A
1.4%
1.9%
77.1%
99.4%
3.5%
CD206
B
Normalized To Mode
3.5
3.5
17.7
61.6
4.1
1.6
1.6
8.1
27.1
1.7
CD163
CD206
FMO
M0
NT
MINO 10
MINO 25
Veh
IFNγ + LPS
C
CD163+ cells (%)
****
****
M0
NT
MINO 10
MINO 25
Veh
IFNγ + LPS
D
CD163 (MFI) Fold Change
****
*
M0
NT
MINO 10
MINO 25
Veh
IFNγ + LPS
E
CD206+ cells (%)
****
****
M0
NT
MINO 10
MINO 25
Veh
IFNγ + LPS
F
CD206 (MFI) Fold Change
****
*
M0
NT
MINO 10
MINO 25
Veh
IFNγ + LPS

Figure 5.6: Effect of minocycline on CD163 and CD206 expression following M1 polarization of THP-1 macrophages. Data obtained after 24hr incubation of differentiated M0 macrophages with M1 polarizing agents IFN-γ (20ng/mL) and LPS (10ng/mL). [A] Representative dot plots showing the percentage of $CD163^+$ (top) and $CD206^+$ (bottom) cells. [B] Representative histograms showing mean fluorescent intensity (MFI) of CD163 (left) and CD206 (right). Numbers indicate MFI of live gated population. [C-F] Bar graphs showing the percentage of $CD163^+$ [C] and $CD206^+$ [E] cells, and MFI values for CD163 [D] and CD206 [F]. MFI values normalised and displayed as fold change versus the un-polarized M0 macrophage control. NT = untreated M1 macrophage, MINO 10 = Minocycline 10μM, MINO 25 = Minocycline 25μM, Veh = DMSO vehicle control 1:1000. Data represents 3 replicated experiments each comprising of triplicate values. Data presented as mean ± SEM. One-way ANOVA with post hoc Dunnett's applied versus the untreated (NT) M1 macrophage control. *p<0.05; ****p<0.0001.

5.2. PBMC

5.2.1. Characterising *in vitro* polarization of PBMC-derived macrophages

Having used THP-1 as an initial *in vitro* system to assess the effect of minocycline on macrophage polarization, the findings were next validated using PBMC-derived macrophages. This also provided an opportunity to gain insight into the effect of minocycline on M2 macrophage subsets as successful M2-polarization of PBMC-derived macrophages was much more prominent in the literature with Dr Jose Garrido Mesa also possessing an established protocol (Orecchioni *et al.*, 2019; Y. Wang *et al.*, 2019). Proceeding with this experimental protocol, PBMCs were first differentiated into M0 macrophages following M-CSF expansion of isolated monocytes and were subsequently pre-treated with minocycline for 2hr prior to incubation for a further 24hr with IFN-γ (20ng/mL) + LPS (10ng/mL) for polarization to M1, or IL-4 (20ng/mL) to produce M2 macrophages. This procedure, and all subsequent sample collection was kept consistent with the THP-1 investigations, whereby supernatant was collected and stored at the termination of the protocol, and cells were collected and stained for surface marker expression analysis.

As before, it was imperative to first phenotype the polarized subsets in the absence of minocycline to ensure distinct and consistent macrophage populations were generated. Figure 5.7A-D below profile the change in CD14 expression following polarization to each of the two phenotypes. Here a subtle decrease in the percentage of $CD14^+$ cells was identified, as well as a decrease

in the density of CD14 expression in both M1 and M2 populations, with the reduction seen to a greater extent in the M1 phenotype and in the density of expression (p=0.0131). Data was similar in respect to total CD11b expression (Figure 5.7A, B, E and F) whereby all donors illustrated a decrease in the percentage of $CD11b^+$ cells and the density of CD11b expression in the M1 cultures. On the contrary, M2 polarization resulted in CD11b upregulation as shown by the MFI, while the percentage of positive cells remained largely unchanged versus the M0 baseline.

The influence of M1/M2 macrophage polarization on CD80 expression was more distinct, with all donors showing a significant increase in the percentage of positive cells, by a magnitude of 64-fold change versus the M0 baseline, which was further reflected in the increased MFI values in the M1 cultures (Figure 5.8A-D). CD80 was also seen to be partially increased following M2 polarization but to a far lesser degree than the M1 samples. This change was also seen in the values obtained for density of CD80 expression with a modest 1.7-fold increase. Results pertaining to CD86 were less pronounced but reached statistical significance with increases in the percentage of $CD86^+$ cells across both phenotypes, and a significant upregulation in CD86 MFI, with 5.6- and 3.2-fold increases for M1 and M2 respectively when compared to the un-polarized baseline (Figure 5.8A, B, E and 8F).

Finally, regarding the M2-associated markers CD163 and CD206 (Figure 5.9), data attributed to M1 polarization highlighted a decrease in both the percentage of $CD163^+$ and $CD206^+$ cells, in addition to a decrease in the density of expression of both markers (Figure 5.9A, C and E). Influence of M2 polarization on CD163 was slightly less clear with opposing discrepancies seen across the 4 donors (Figure 5.9A-D). In contrast, M2 induction resulted in a significant increase in the number of $CD206^+$ cells which was corroborated in the mean fluorescence values whereby all donors displayed upregulation of CD206 MFI (Figure 5.9B, E and F). This data indicates an M1 phenotype acquisition characterized by a decline in CD11b, CD163 and CD206 expression, in addition to potent upregulation of CD80 and CD86 when compared to the un-polarized M0 control. Conversely, M2 phenotype can be identified through an increase in CD11b and CD206 versus the un-polarized M0 control, with marginal increases also in CD80 and CD86 versus M0 but to a far lesser degree than the M1.

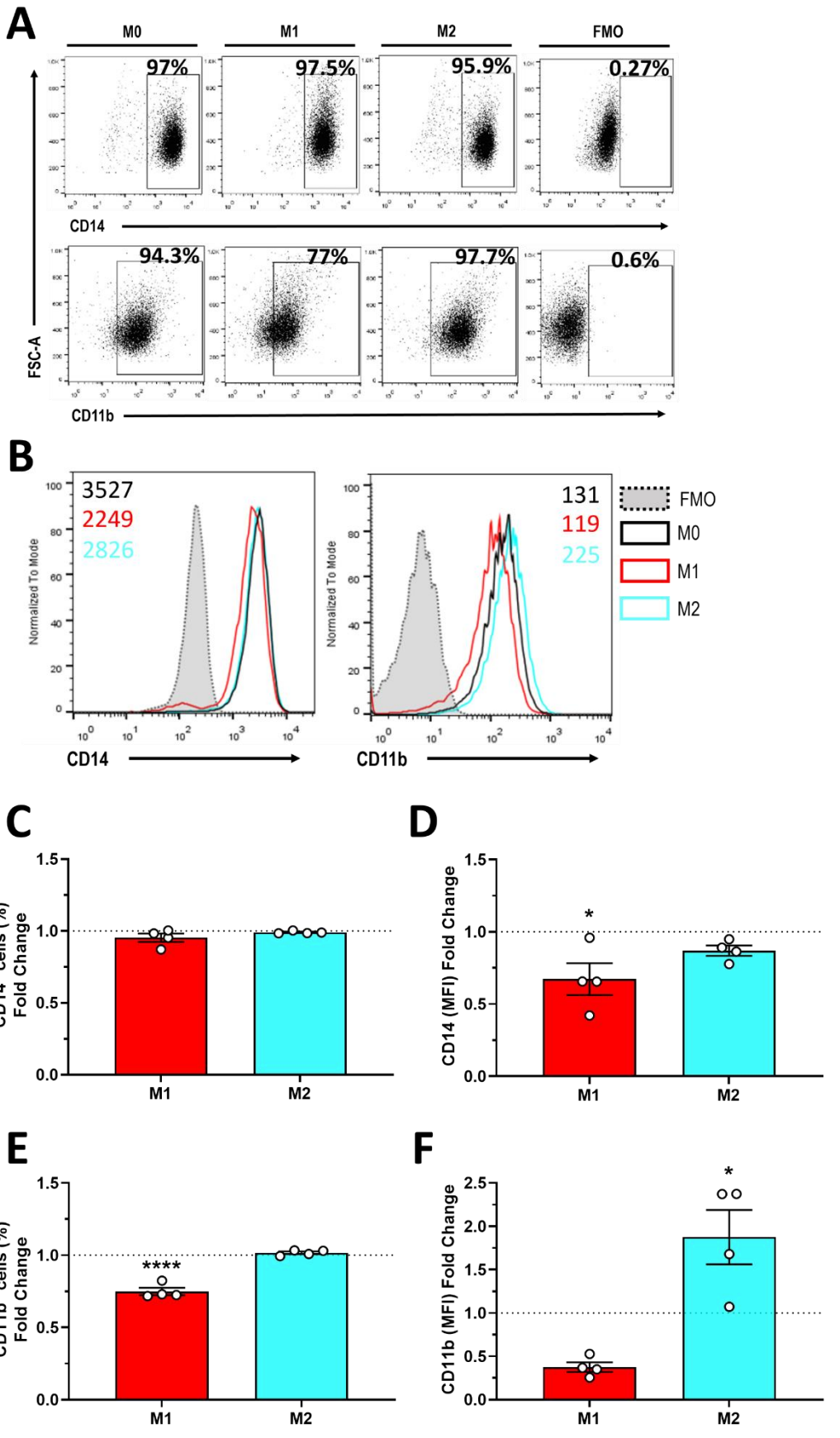
A
M0
M1
M2
FMO
97%
97.5%
95.9%
0.27%
CD14
94.3%
77%
97.7%
0.6%
FSC-A
CD11b
B
3527
2249
2826
131
119
225
FMO
M0
M1
M2
Normalized To Mode
CD14
CD11b
C
CD14+ cells (%) Fold Change
M1
M2
D
CD14 (MFI) Fold Change
*
E
CD11b+ cells (%) Fold Change
****
F
CD11b (MFI) Fold Change
*

Figure 5.7: CD14 and CD11b expression profile of M1 and M2 polarized PBMC-derived macrophages. Data obtained after 24hr incubation of M-CSF-expanded M0 macrophages with M1 (IFN-γ 20ng/mL + LPS 10mg/mL) or M2 (IL-4 20ng/mL) polarizing agents. [A] Representative dot plots showing the percentage of $CD14^+$ (top) and $CD11b^+$ (bottom) cells. [B] Representative histograms showing mean fluorescent intensity (MFI) of CD14 (left) and CD11b (right). Numbers indicate MFI of live gated population. [C-F] Bar graphs showing the percentage of $CD14^+$ [C] and $CD11b^+$ [E] cells, and MFI values for CD14 [D] and CD11b [F]. Values normalised and displayed as fold change versus the un-polarized M0 macrophage. Data represents 4 donors, each comprising of duplicate values. Data presented as mean ± SEM. One-way ANOVA with post hoc Dunnett's applied versus the un-polarized M0 macrophage. *p<0.05; ****p<0.0001.

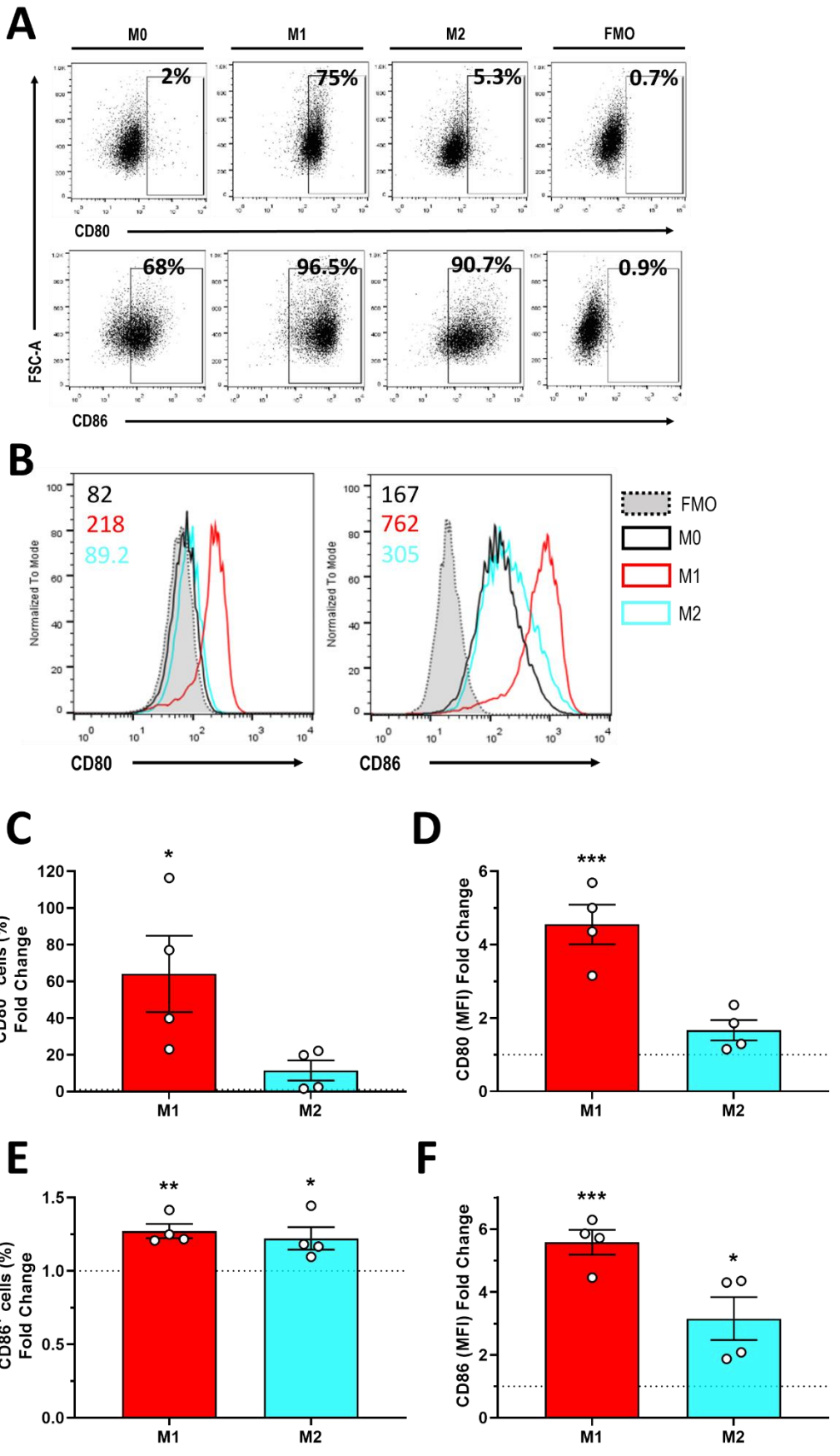
A
M0
M1
M2
FMO
2%
75%
5.3%
0.7%
CD80
68%
96.5%
90.7%
0.9%
FSC-A
CD86
B
82
218
89.2
167
762
305
Normalized To Mode
FMO
M0
M1
M2
CD80
CD86
C
CD80+ cells (%) Fold Change
M1
M2
D
CD80 (MFI) Fold Change
E
CD86+ cells (%) Fold Change
F
CD86 (MFI) Fold Change

Figure 5.8: CD80 and CD86 expression profile of M1 and M2 polarized PBMC-derived macrophages. Data obtained after 24hr incubation of M-CSF-expanded M0 macrophages with M1 (IFN-γ 20ng/mL + LPS 10mg/mL) or M2 (IL-4 20ng/mL) polarizing agents. [A] Representative dot plots showing the percentage of $CD80^+$ (top) and $CD86^+$ (bottom) cells. [B] Representative histograms showing mean fluorescent intensity (MFI) of CD80 (left) and CD86 (right). Numbers indicate MFI of live gated population. [C-F] Bar graphs showing the percentage of $CD80^+$ [C] and $CD86^+$ [E] cells, and MFI values for CD80 [D] and CD86 [F]. Values normalised and displayed as fold change versus the un-polarized M0 macrophage. Data represents 4 donors, each comprising of duplicate values. Data presented as mean ± SEM. One-way ANOVA with post hoc Dunnett's applied versus the un-polarized M0 macrophage. *p<0.05; **p<0.01; ***p<0.001.

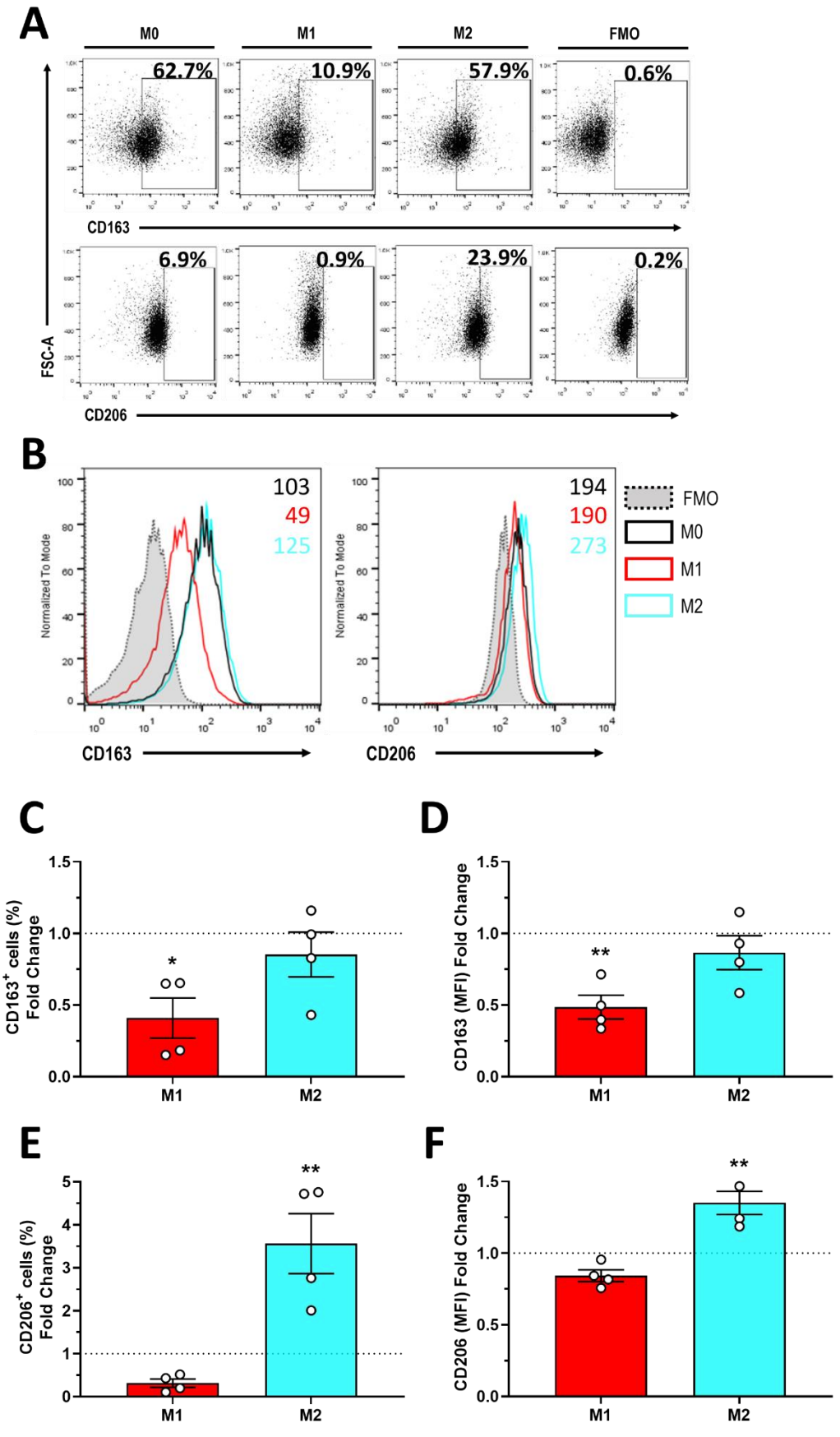
A
M0
M1
M2
FMO
62.7%
10.9%
57.9%
0.6%
CD163
6.9%
0.9%
23.9%
0.2%
FSC-A
CD206
B
103
49
125
194
190
273
FMO
M0
M1
M2
Normalized To Mode
CD163
CD206
C
CD163+ cells (%) Fold Change
M1
M2
D
CD163 (MFI) Fold Change
E
CD206+ cells (%) Fold Change
F
CD206 (MFI) Fold Change

Figure 5.9: CD163 and CD206 expression profile of M1 and M2 polarized PBMC-derived macrophages. Data obtained after 24hr incubation of M-CSF-expanded M0 macrophages with M1 (IFN-γ 20ng/mL + LPS 10mg/mL) or M2 (IL-4 20ng/mL) polarizing agents. [A] Representative dot plots showing the percentage of $CD163^+$ (top) and $CD206^+$ (bottom) cells. [B] Representative histograms showing mean fluorescent intensity (MFI) of CD163 (left) and CD206 (right). Numbers indicate MFI of live gated population. [C-F] Bar graphs showing the percentage of $CD163^+$ [C] and $CD206^+$ [E] cells, and MFI values for CD163 [D] and CD206 [F]. Values normalised and displayed as fold change versus the un-polarized M0 macrophage. Data represents 4 donors, each comprising of duplicate values. Data presented as mean ± SEM. One-way ANOVA with post hoc Dunnett's applied versus the un-polarized M0 macrophage. *p<0.05; **p<0.01.

5.2.2. Effect of minocycline during M1/M2 polarization of PBMC-derived macrophages

Overall, despite some divergence from the common literary narrative, the data presented in section 5.2.1. confirms successful polarization of PBMC-derived macrophages to both M1 and M2 subsets. Having established an un-treated baseline for both phenotypes with respect to surface marker expression profiles exploration into any potential modification by minocycline began.

When studying the effect of minocycline treatment during macrophage polarization, no significant alteration in CD14 expression was noted as reflected in both the percentage of $CD14^+$ cells in each culture, and the density of CD14 expression (Figure 5.10). These findings did not directly corroborate those seen when exploring the effect of minocycline using THP-1-derived M1 macrophages in which a distinct inhibitory effect was reported (section 5.1.2). Regarding total CD11b expression, again no discernible change was seen in protein expression following administration of minocycline at either concentration or in either polarized culture (Figure 5.11).

When analysing results gained for CD80, data once more failed to fully corroborate the previous THP-1 findings. No statistically significant changes in the percentage of $CD80^+$ cells or CD80 MFI among the M1 macrophages were seen (Figure 5.12A, B, C and D). Furthermore, although data pertaining to the M1 populations were insignificant, they showed a potential decrease in expression following minocycline intervention. This reduction was further reflected in the M2 macrophages where minocycline at 25μM seemed to subtly decrease the number of $CD80^+$ cells (Figure 5.12A and E), however data concerning CD80 MFI illustrated no clear modification. Data for CD86 was

similarly ambiguous showing no influence of minocycline on the percentage of positive cells in ether phenotype, or MFI in the M1 cultures (Figure 5.13A-E). There was, however, distinct modification of CD86 MFI within the M2 populations whereby minocycline significantly reduced this parameter by 10μM (p=0.0018) and 25μM (p=0.0001), the latter being the more potent modifier (Figure 5.13F).

Finally, it was of interest to see if the marked increase in both CD163 and CD206 seen in the THP-1 model would be replicated using the primary PBMC macrophages. In this regard only visible increases in the percentage of $CD163^+$ cells and density of CD163 expression can be seen in the M1 model. Additionally, data obtained from the M2 model also failed to indicate any clear effect of minocycline treatment on CD163 expression (Figure 5.14A, B, E and F). Minocycline failed to induce any significant change in either the percentage of $CD163^+$ or $CD206^+$ cells, or in density of expression within the M1 cultures when compared to the untreated control (Figure 5.15A-D). A key finding during this investigation, however, was the inhibitory effect of minocycline intervention on CD206 expression within the M2 model. Here, a notable decrease in the number of $CD206^+$ cells can be seen, as well as a significant reduction in the density of CD206 expression exerted by 25μM minocycline (p=0.0175) (Figure 3.15A, B, E and F).

Considering the data obtained minocycline was shown to have limited influence on CD14, CD11b, CD80 and CD163 expression when administered during either M1 or M2 polarization. Some modification was seen in relation to CD86 expression whereby minocycline decreased the density of CD86 expression within the M2 cultures only, while the most prominent change was in respect to CD206 expression. Here minocycline had distinct influence on both the percentage of $CD206^+$ cells and the density of CD206 expression when administered during M2 polarization, causing a decline in expression. Given this unforeseen finding, in addition to the results gained from the rest of the chapter so far, it was essential to next understand the influence of minocycline on the cytokine production profiles of the two subsets which may aid in the interpretation of these data in their entirety.

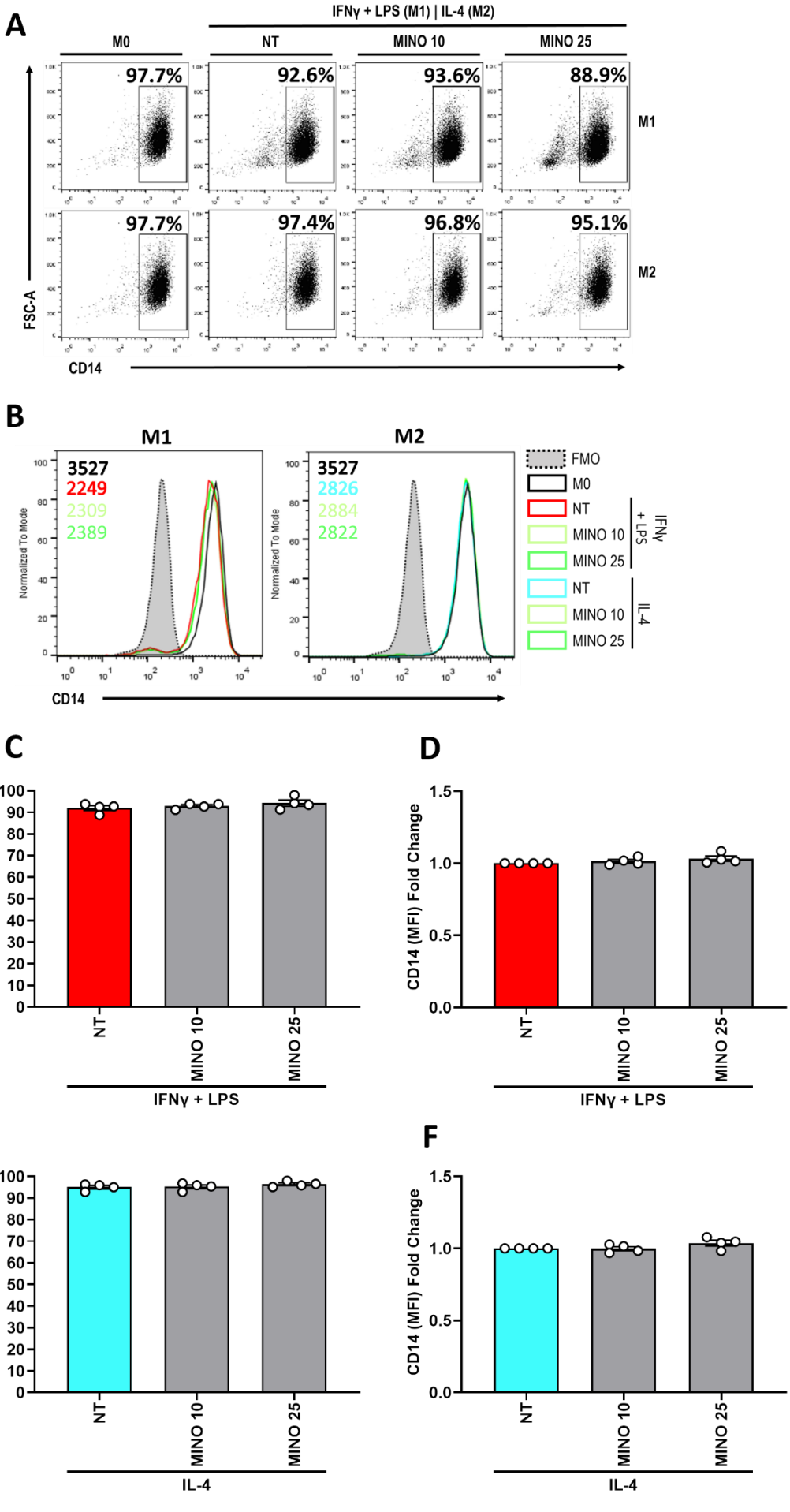
A
IFNγ + LPS (M1) | IL-4 (M2)
M0
NT
MINO 10
MINO 25
97.7%
92.6%
93.6%
88.9%
M1
97.7%
97.4%
96.8%
95.1%
M2
FSC-A
CD14
B
M1
M2
3527
2249
2309
2389
3527
2826
2884
2822
Normalized To Mode
CD14
FMO
M0
NT
MINO 10
MINO 25
IFNγ + LPS
NT
MINO 10
MINO 25
IL-4
C
CD14+ cells (%)
NT
MINO 10
MINO 25
IFNγ + LPS
D
CD14 (MFI) Fold Change
NT
MINO 10
MINO 25
IFNγ + LPS
E
CD14+ cells (%)
NT
MINO 10
MINO 25
IL-4
F
CD14 (MFI) Fold Change
NT
MINO 10
MINO 25
IL-4

Figure 5.10: Effect of minocycline on CD14 expression following M1 or M2 polarization of PBMC-derived macrophages. Data obtained after 2hr pre-treatment with minocycline and 24hr incubation of M-CSF-expanded M0 macrophages with M1 (IFN-γ 20ng/mL + LPS 10mg/mL) or M2 (IL-4 20ng/mL) polarizing agents. NT = no treatment, MINO 10 = Minocycline 10μM, MINO 25 = Minocycline 25μM. [A] Representative dot plots showing the percentage of $CD14^+$ cells in M1 (top) or M2 (bottom) macrophage cultures following the addition of polarizing agents. [B] Representative histograms showing mean fluorescent intensity (MFI) for CD14 in M1 (left) or M2 (right) macrophages. Numbers indicate MFI of live gated population. [C-F] Bar graphs showing the percentage of $CD14^+$ M1 [C] and $CD14^+$ M2 [E] polarized macrophages, and CD14 MFI values for M1 [D] and M2 [F] populations. MFI normalised and displayed as fold change versus the non-treatment (NT) group indicated at 1. Plots and histograms illustrate one representative donor. Graphical data represent data from 4 donors each comprising of duplicate values. Data presented as mean ± SEM. One-way ANOVA with post hoc Dunnett's applied versus the un-treated M1 or M2 control.

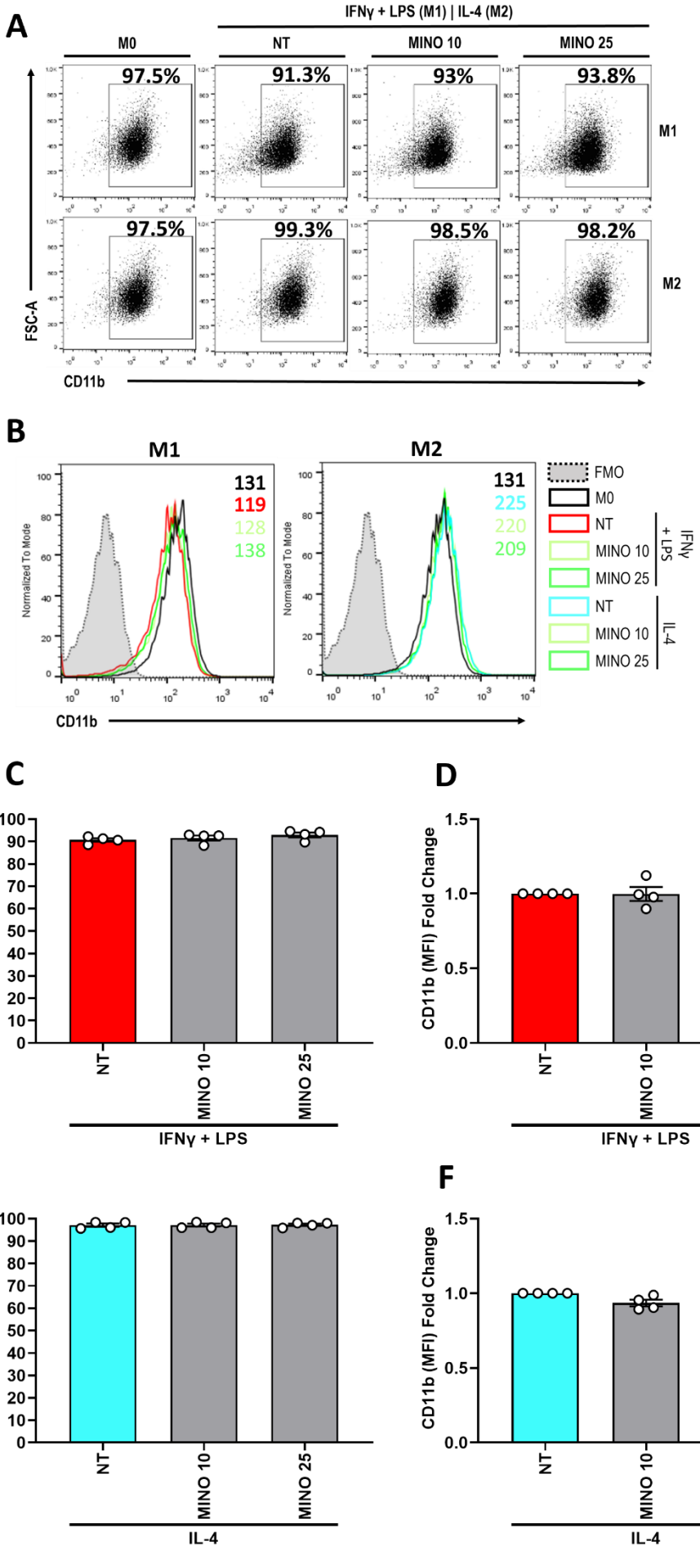
A
IFNγ + LPS (M1) | IL-4 (M2)
M0
NT
MINO 10
MINO 25
97.5%
91.3%
93%
93.8%
M1
97.5%
99.3%
98.5%
98.2%
M2
FSC-A
CD11b
B
M1
M2
131
119
128
138
131
225
220
209
Normalized To Mode
CD11b
FMO
M0
NT
MINO 10
MINO 25
IFNγ + LPS
NT
MINO 10
MINO 25
IL-4
C
CD11b+ cells (%)
NT
MINO 10
MINO 25
IFNγ + LPS
D
CD11b (MFI) Fold Change
NT
MINO 10
MINO 25
IFNγ + LPS
E
CD11b+ cells (%)
NT
MINO 10
MINO 25
IL-4
F
CD11b (MFI) Fold Change
NT
MINO 10
MINO 25
IL-4

Figure 5.11: Effect of minocycline on CD11b expression following M1 or M2 polarization of PBMC-derived macrophages. Data obtained after 2hr pre-treatment with minocycline and 24hr incubation of M-CSF-expanded M0 macrophages with M1 (IFN-γ 20ng/mL + LPS 10mg/mL) or M2 (IL-4 20ng/mL) polarizing agents. NT = no treatment, MINO 10 = Minocycline 10μM, MINO 25 = Minocycline 25μM. [A] Representative dot plots showing the percentage of $CD11b^+$ cells in M1 (top) or M2 (bottom) macrophage cultures following the addition of polarizing agents. [B] Representative histograms showing mean fluorescent intensity (MFI) for CD11b in M1 (left) or M2 (right) macrophages. Numbers indicate MFI of live gated population. [C-F] Bar graphs showing the percentage of $CD11b^+$ M1 [C] and $CD11b^+$ M2 [E] polarized macrophages, and CD11b MFI values for M1 [D] and M2 [F] populations. MFI normalised and displayed as fold change versus the non-treatment (NT) group indicated at 1. Plots and histograms illustrate one representative donor. Graphical data represent data from 4 donors each comprising of duplicate values. Data presented as mean ± SEM. One-way ANOVA with post hoc Dunnett's applied versus the un-treated M1 or M2 control.

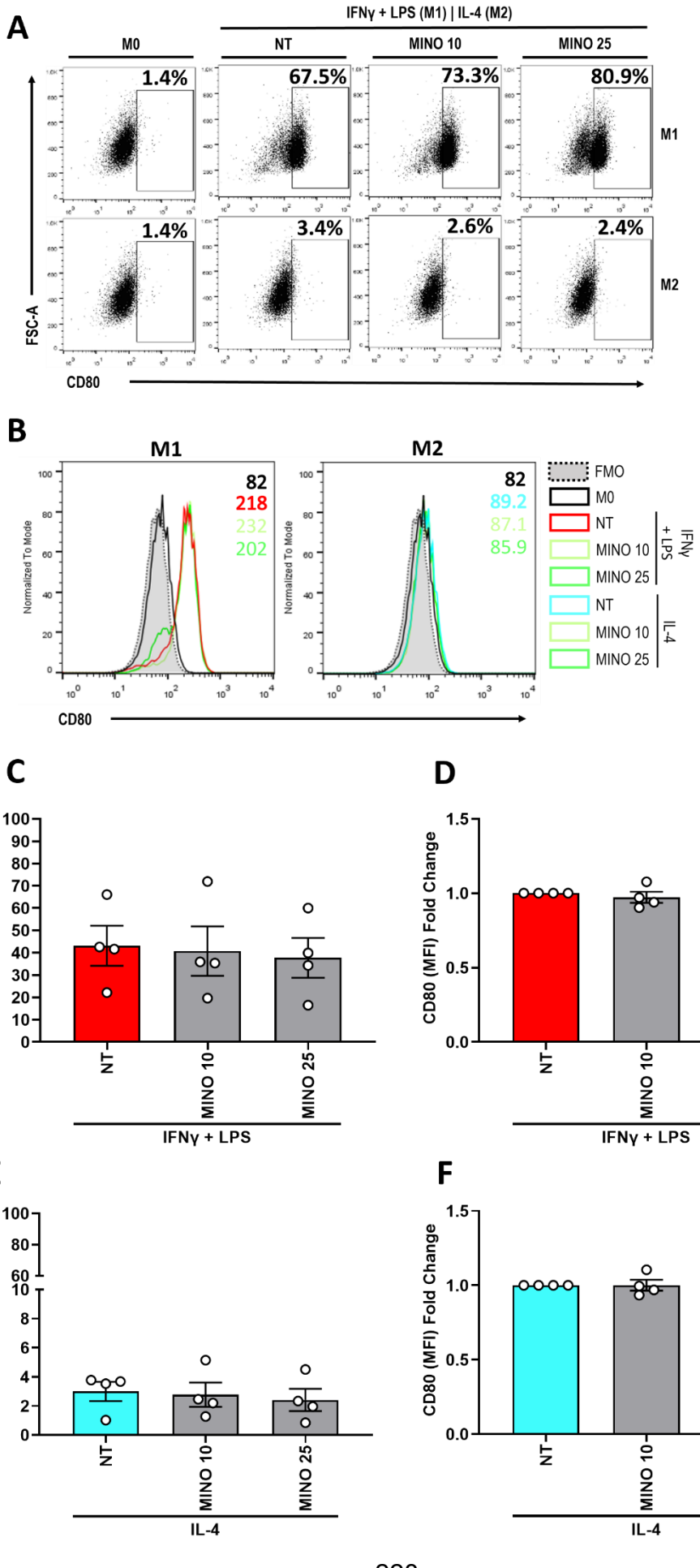
A
IFNγ + LPS (M1) | IL-4 (M2)
M0
NT
MINO 10
MINO 25
1.4%
67.5%
73.3%
80.9%
M1
1.4%
3.4%
2.6%
2.4%
M2
FSC-A
CD80
B
M1
M2
82
218
232
202
82
89.2
87.1
85.9
Normalized To Mode
FMO
M0
NT
MINO 10
MINO 25
IFNγ + LPS
NT
MINO 10
MINO 25
IL-4
CD80
C
CD80+ cells (%)
NT
MINO 10
MINO 25
IFNγ + LPS
D
CD80 (MFI) Fold Change
NT
MINO 10
MINO 25
IFNγ + LPS
E
CD80+ cells (%)
NT
MINO 10
MINO 25
IL-4
F
CD80 (MFI) Fold Change
NT
MINO 10
MINO 25
IL-4

Figure 5.12: Effect of minocycline on CD80 expression following M1 or M2 polarization of PBMC-derived macrophages. Data obtained after 2hr pre-treatment with minocycline and 24hr incubation of M-CSF-expanded M0 macrophages with M1 (IFN-γ 20ng/mL + LPS 10mg/mL) or M2 (IL-4 20ng/mL) polarizing agents. NT = no treatment, MINO 10 = Minocycline 10μM, MINO 25 = Minocycline 25μM. [A] Representative dot plots showing the percentage of $CD80^+$ cells in M1 (top) or M2 (bottom) macrophage cultures following the addition of polarizing agents. [B] Representative histograms showing mean fluorescent intensity (MFI) for CD80 in M1 (left) or M2 (right) macrophages. Numbers indicate MFI of live gated population. [C-F] Bar graphs showing the percentage of $CD80^+$ M1 [C] and $CD80^+$ M2 [E] polarized macrophages, and CD80 MFI values for M1 [D] and M2 [F] populations. MFI normalised and displayed as fold change versus the non-treatment (NT) group indicated at 1. Plots and histograms illustrate one representative donor. Graphical data represent data from 4 donors each comprising of duplicate values. Data presented as mean ± SEM. One-way ANOVA with post hoc Dunnett's applied versus the un-treated M1 or M2 control.

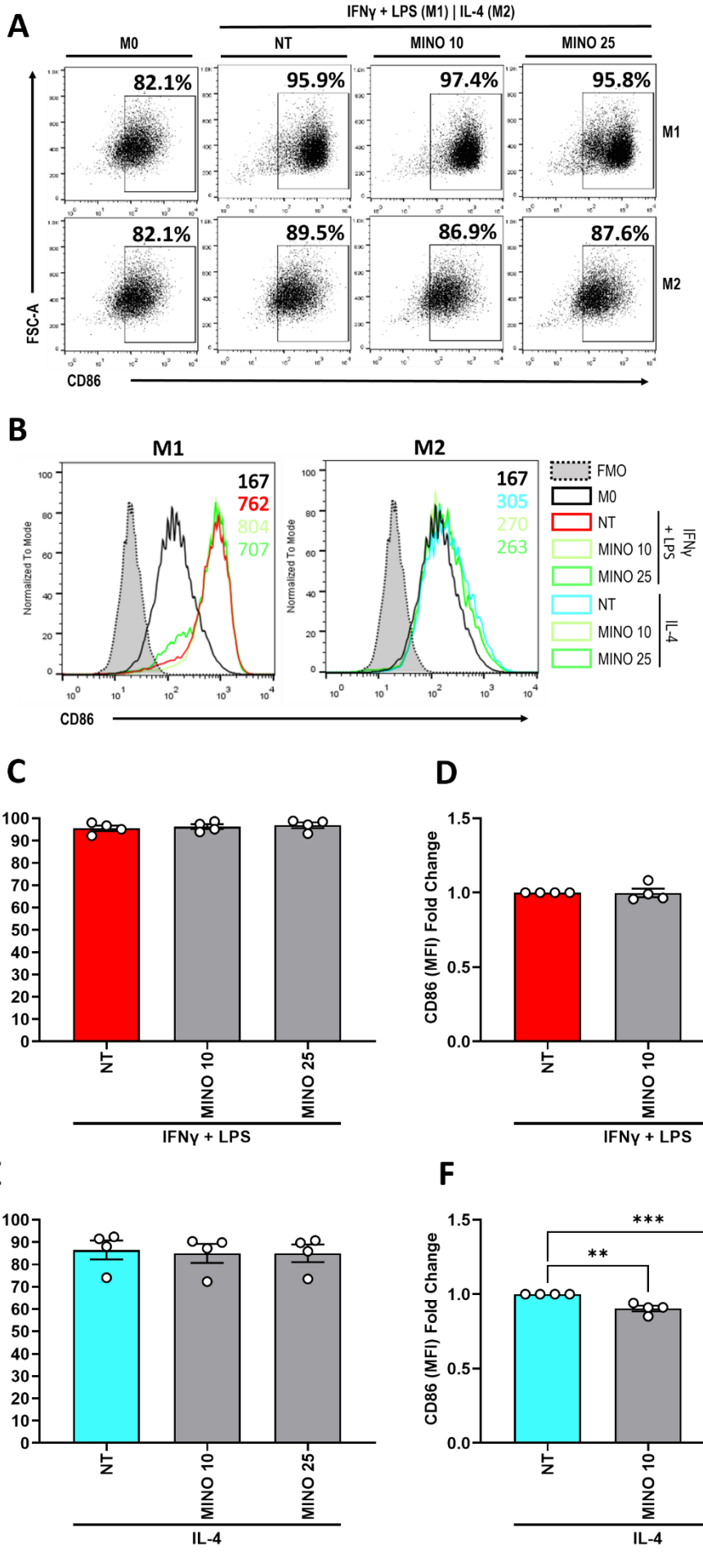
A
IFNγ + LPS (M1) | IL-4 (M2)
M0
NT
MINO 10
MINO 25
82.1%
95.9%
97.4%
95.8%
M1
82.1%
89.5%
86.9%
87.6%
M2
FSC-A
CD86
B
M1
M2
167
762
804
707
167
305
270
263
Normalized To Mode
FMO
M0
NT
MINO 10
MINO 25
IFNγ + LPS
NT
MINO 10
MINO 25
IL-4
CD86
C
CD86+ cells (%)
NT
MINO 10
MINO 25
IFNγ + LPS
D
CD86 (MFI) Fold Change
NT
MINO 10
MINO 25
IFNγ + LPS
E
CD86+ cells (%)
NT
MINO 10
MINO 25
IL-4
F
CD86 (MFI) Fold Change
***
**
NT
MINO 10
MINO 25
IL-4

Figure 5.13: Effect of minocycline on CD86 expression following M1 or M2 polarization of PBMC-derived macrophages. Data obtained after 2hr pre-treatment with minocycline and 24hr incubation of M-CSF-expanded M0 macrophages with M1 (IFN-γ 20ng/mL + LPS 10mg/mL) or M2 (IL-4 20ng/mL) polarizing agents. NT = no treatment, MINO 10 = Minocycline 10μM, MINO 25 = Minocycline 25μM. [A] Representative dot plots showing the percentage of $CD86^+$ cells in M1 (top) or M2 (bottom) macrophage cultures following the addition of polarizing agents. [B] Representative histograms showing mean fluorescent intensity (MFI) for CD86 in M1 (left) or M2 (right) macrophages. Numbers indicate MFI of live gated population. [C-F] Bar graphs showing the percentage of $CD86^+$ M1 [C] and $CD86^+$ M2 [E] polarized macrophages, and CD86 MFI values for M1 [D] and M2 [F] populations. MFI normalised and displayed as fold change versus the non-treatment (NT) group indicated at 1. Plots and histograms illustrate one representative donor. Graphical data represent data from 4 donors each comprising of duplicate values. Data presented as mean ± SEM. One-way ANOVA with post hoc Dunnett's applied versus the un-treated M1 or M2 control. $^{**}p<0.01$; $^{***}p<0.001$.

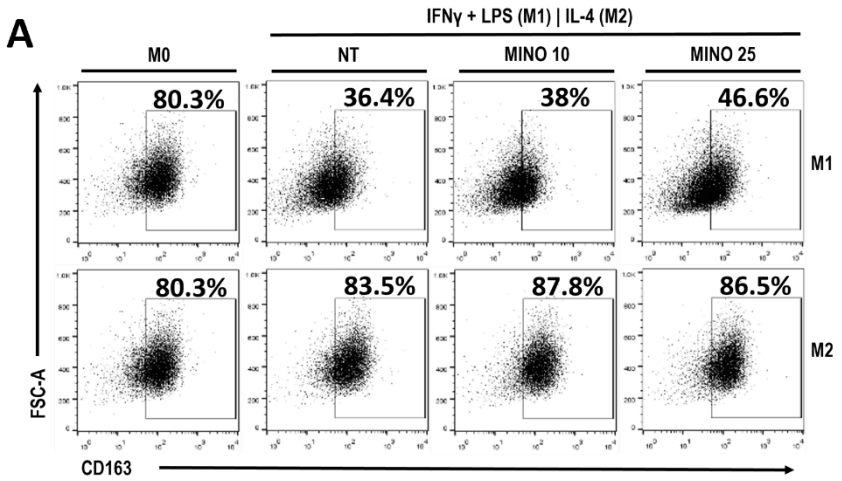
A
IFNγ + LPS (M1) | IL-4 (M2)
M0
NT
MINO 10
MINO 25
80.3%
36.4%
38%
46.6%
M1
80.3%
83.5%
87.8%
86.5%
M2
FSC-A
CD163

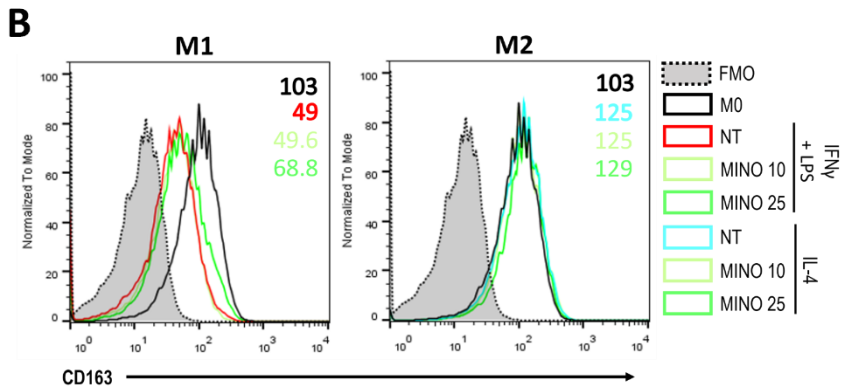
B
M1
M2
103
49
49.6
68.8
103
125
125
129
Normalized To Mode
FMO
M0
NT
MINO 10
MINO 25
IFNγ + LPS
NT
MINO 10
MINO 25
IL-4
CD163

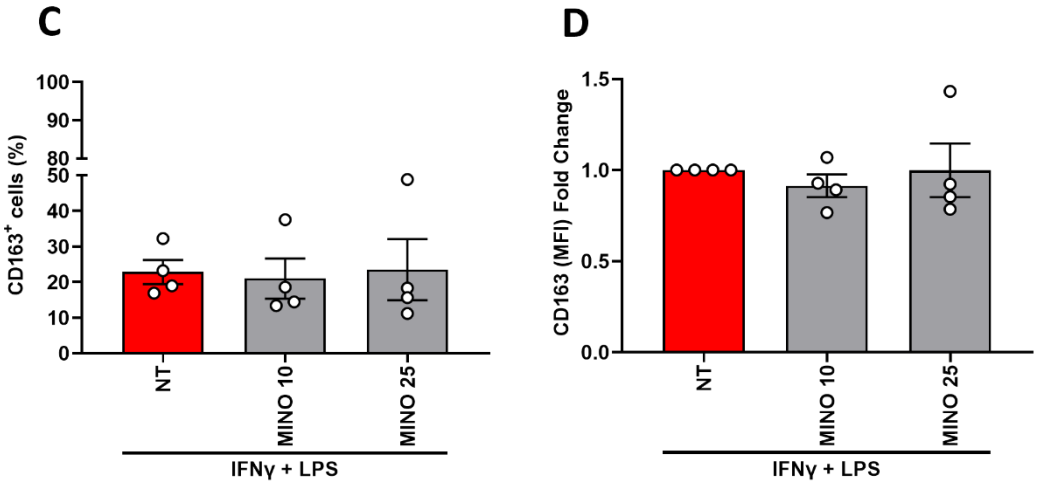
C
CD163+ cells (%)
NT
MINO 10
MINO 25
IFNγ + LPS

D
CD163 (MFI) Fold Change
NT
MINO 10
MINO 25
IFNγ + LPS

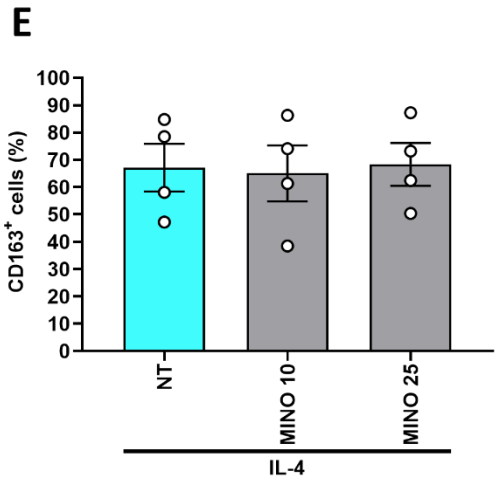
E
CD163+ cells (%)
NT
MINO 10
MINO 25
IL-4

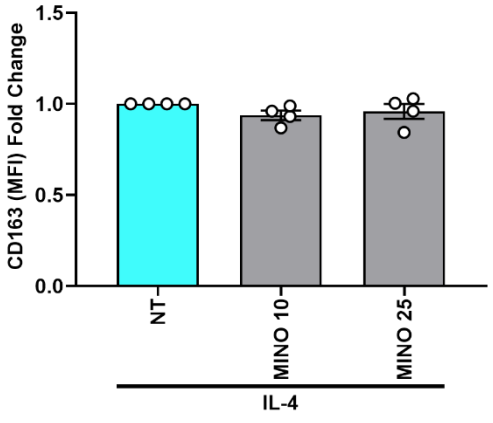
F
CD163 (MFI) Fold Change
NT
MINO 10
MINO 25
IL-4

Figure 5.14: Effect of minocycline on CD163 expression following M1 or M2 polarization of PBMC-derived macrophages. Data obtained after 2hr pre-treatment with minocycline and 24hr incubation of M-CSF-expanded M0 macrophages with M1 (IFN-γ 20ng/mL + LPS 10mg/mL) or M2 (IL-4 20ng/mL) polarizing agents. NT = no treatment, MINO 10 = Minocycline 10μM, MINO 25 = Minocycline 25μM. [A] Representative dot plots showing the percentage of $CD163^+$ cells in M1 (top) or M2 (bottom) macrophage cultures following the addition of polarizing agents. [B] Representative histograms showing mean fluorescent intensity (MFI) for CD163 in M1 (left) or M2 (right) macrophages. Numbers indicate MFI of live gated population. [C-F] Bar graphs showing the percentage of $CD163^+$ M1 [C] and $CD163^+$ M2 [E] polarized macrophages, and CD163 MFI values for M1 [D] and M2 [F] populations. MFI normalised and displayed as fold change versus the non-treatment (NT) group indicated at 1. Plots and histograms illustrate one representative donor. Graphical data represent data from 4 donors each comprising of duplicate values. Data presented as mean ± SEM. One-way ANOVA with post hoc Dunnett's applied versus the un-treated M1 or M2 control.

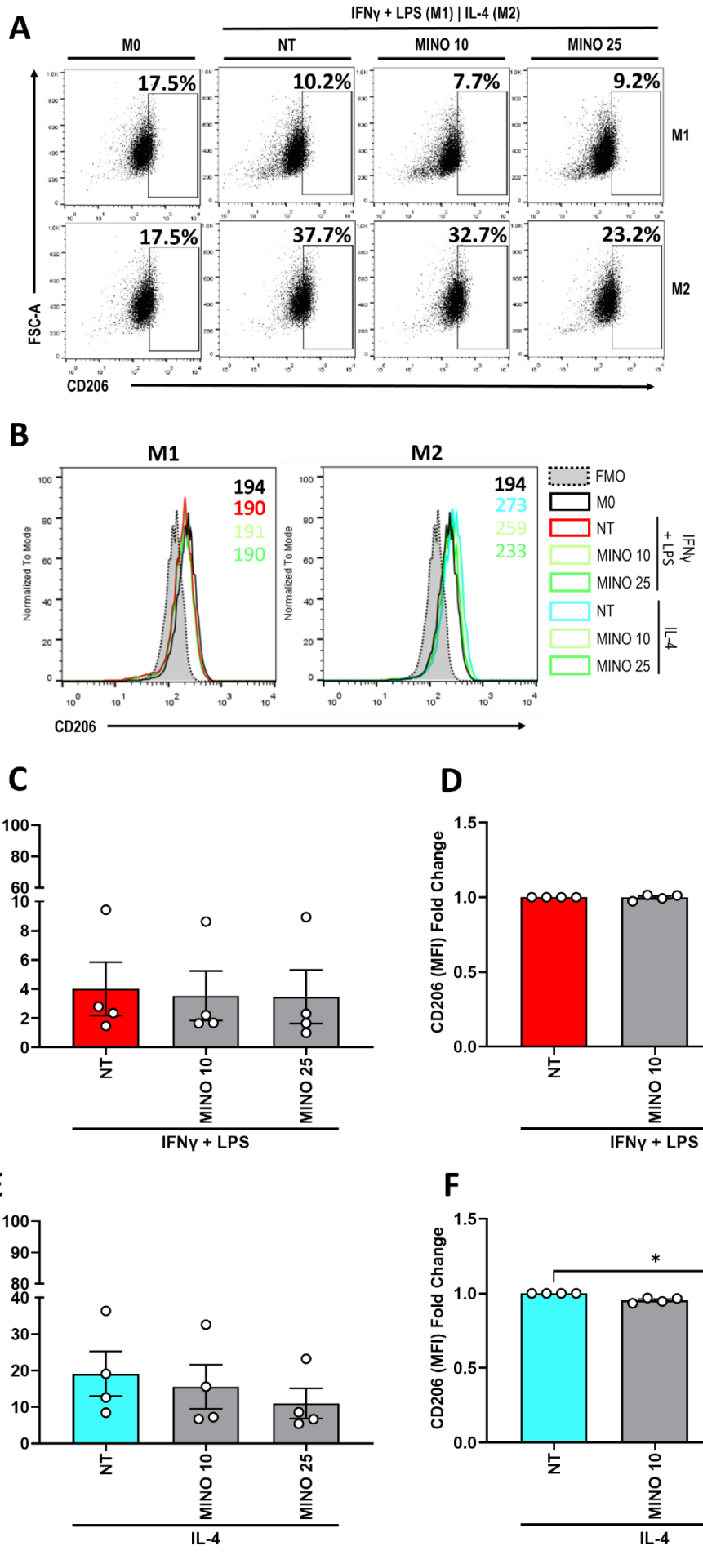
A
IFNγ + LPS (M1) | IL-4 (M2)
M0
NT
MINO 10
MINO 25
17.5%
10.2%
7.7%
9.2%
M1
17.5%
37.7%
32.7%
23.2%
M2
FSC-A
CD206
B
M1
M2
194
190
191
190
194
273
259
233
Normalized To Mode
CD206
FMO
M0
NT
MINO 10
MINO 25
IFNγ + LPS
NT
MINO 10
MINO 25
IL-4
C
CD206+ cells (%)
NT
MINO 10
MINO 25
IFNγ + LPS
D
CD206 (MFI) Fold Change
NT
MINO 10
MINO 25
IFNγ + LPS
E
CD206+ cells (%)
NT
MINO 10
MINO 25
IL-4
F
CD206 (MFI) Fold Change
*
NT
MINO 10
MINO 25
IL-4

Figure 5.15: Effect of minocycline on CD206 expression following M1 or M2 polarization of PBMC-derived macrophages. Data obtained after 2hr pre-treatment with minocycline and 24hr incubation of M-CSF-expanded M0 macrophages with M1 (IFN-γ 20ng/mL + LPS 10mg/mL) or M2 (IL-4 20ng/mL) polarizing agents. NT = no treatment, MINO 10 = Minocycline 10μM, MINO 25 = Minocycline 25μM. [A] Representative dot plots showing the percentage of $CD206^+$ cells in M1 (top) or M2 (bottom) macrophage cultures following the addition of polarizing agents. [B] Representative histograms showing mean fluorescent intensity (MFI) for CD206 in M1 (left) or M2 (right) macrophages. Numbers indicate MFI of live gated population. [C-F] Bar graphs showing the percentage of $CD206^+$ M1 [C] and $CD206^+$ M2 [E] polarized macrophages, and CD206 MFI values for M1 [D] and M2 [F] populations. MFI normalised and displayed as fold change versus the non-treatment (NT) group indicated at 1. Plots and histograms illustrate one representative donor. Graphical data represent data from 4 donors each comprising of duplicate values. Data presented as mean ± SEM. One-way ANOVA with post hoc Dunnett's applied versus the un-treated M1 or M2 control. *p<0.05.

5.1. Cytokine Production Profile of M1/M2 Polarized Macrophages

Macrophage phenotype commitment is orchestrated by the local cytokine milieu with classically activated M1 macrophages typically induced by Th1 cytokines such as IFN-γ, or as a result of bacterial LPS recognition, while alternatively activated M2 macrophages are determined by Th2 cytokines IL-4 and IL-13 (Sica and Mantovani, 2012). Each subset can further be defined by their consequent expression of distinct surface markers as explored previously, as well as the production of characteristic cytokines and chemokines. Once polarized, M1 cells are recognised to produce high levels of pro-inflammatory cytokines TNF-α, IL-1β, IL-6 and IL-12, enabling them to promote the removal of pathogens and perform anti-microbial and anti-tumoral activities. Conversely, M2 macrophages are characterised to produce IL-10, IL-4 and TGF-β with the aim to scavenge and phagocytose debris and apoptotic cells, in addition to promoting tissue repair and wound healing via their pro-angiogenic and pro-fibrotic properties (Locati, Mantovani and Sica, 2013; Murray *et al.*, 2014; Braga, Agudelo and Camara, 2015).

5.1.1. THP-1 cytokine production profile

Sections 5.1.2 and 5.2.2 within this chapter have already begun to decipher a modulatory role of minocycline in respect to the surface marker signatures of these two macrophage subsets, with THP-1 experiments illustrating potent upregulation of M2-associated markers CD163 and CD206, in addition to CD80,

while data obtained from the PBMC investigations highlighted an inhibitory role of minocycline on CD206 expression within M2 cells. Having identified possible functionally significant outcomes of minocycline based on surface marker expression, it was imperative to now assess any modification of minocycline on the cytokine production profiles of these two phenotypes. As with surface marker expression work began by characterising the polarized phenotypes in respect to their cytokine production properties. Figure 5.16 below illustrates the increased production of M1-associated pro-inflammatory cytokines IFN-γ (p=0.0008) (Figure 5.16A and B1), IL-1β (p=0.0037) (Figure 5.16A and B2) and TNF-α (p=0.0012) (Figure 5.16A and B4), with IL-6 (Figure 5.16A and B3) and IL-12p40 (Figure 5.16A and B5) appearing to increase but remaining under the threshold of significance. IL-12p70 however remained unchanged (Figure 5.16A and B6). Furthermore, when polarized to M1, THP-1 macrophages indicate no change, or a decline in M2-associated cytokine expression with both IL-4 (Figure 5.16A and C1) and IL-10 (Figure 5.16A and C2) remaining comparative with the un-polarized M0 control. These data further validated the polarization protocol used and provided additional evidence to support the successful *in vitro* polarization of THP-1-derived macrophages.

Previously data alluded to a potential influence of the vehicle control DMSO as indicated in section 5.1.2 within this cellular model. Therefore, the cytokine production profile of the M1 cells when treated with the DMSO control in the absence of minocycline was also characterised. Figure 5.17 displays the findings from this investigation, identifying amplified production of the pro-inflammatory cytokines IFN-γ, TNF-α, and IL-12p40, with IL-12p70 also increased but not statistically significant (Figure 5.17A1, A4-A6). IL-6 was also partially affected by the vehicle (Figure 5.17A3). Conversely, changes to IL-1β production were ill-defined with both positive and negative effects of the vehicle observed (Figure 5.17A2). Moreover, this augmentation of cytokine production extended to the M2-associated cytokines whereby IL-4 appeared to increase versus the un-treated M1 control (Figure 5.17C1), and L-10 was increased back to an un-polarized M0 baseline across all replicates (Figure 5.17C2). Given these results which show an influence of the vehicle control on cytokine production, it was decided to adjust the subsequent analytical approach and utilize the vehicle-treated group as the intra-experimental control when assessing the effect of minocycline.

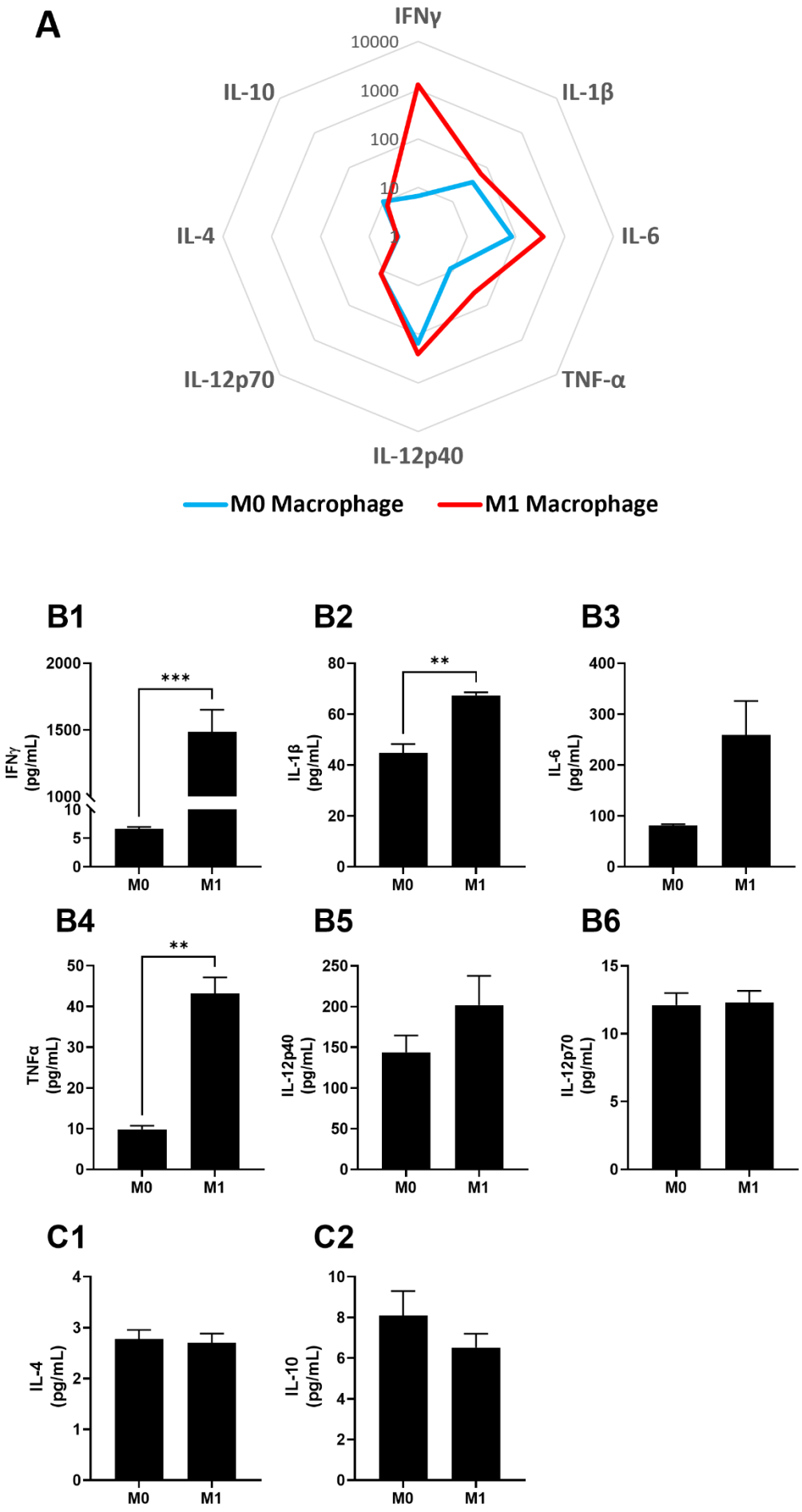
A
IFNγ
10000
1000
100
10
1
IL-1β
IL-6
TNF-α
IL-12p40
IL-12p70
IL-4
IL-10
M0 Macrophage
M1 Macrophage
B1
IFNγ (pg/mL)
2000
1500
1000
10
5
0
***
M0
M1
B2
IL-1β (pg/mL)
80
60
40
20
0
**
M0
M1
B3
IL-6 (pg/mL)
400
300
200
100
0
M0
M1
B4
TNFα (pg/mL)
50
40
30
20
10
0
**
M0
M1
B5
IL-12p40 (pg/mL)
250
200
150
100
50
0
M0
M1
B6
IL-12p70 (pg/mL)
15
10
5
0
M0
M1
C1
IL-4 (pg/mL)
4
3
2
1
0
M0
M1
C2
IL-10 (pg/mL)
10
8
6
4
2
0
M0
M1

Figure 5.16: Cytokine production from M1-polarized THP-1-derived macrophages. Data obtained from supernatant analysis after 24hr incubation of M0 macrophages with the M1 polarizing agents IFN-γ (20ng/mL) and LPS (10ng/mL). [A] Radar plot illustrating relative change in cytokine production between M0 and M1 macrophages. Bar graphs showing the production of M1-associated cytokines IFN-γ [B1], IL-1β [B2], IL-6 [B3], TNF-α [B4], IL-12p40 [B5] and IL-12p70 [B6], and M2-associated cytokines IL-4 [C1] and IL-10 [C2]. Graphs represent averaged triplicate data from 3 repeated experiments. Data presented as mean ± SEM with unpaired t test. **p<0.01; ***p<0.001.

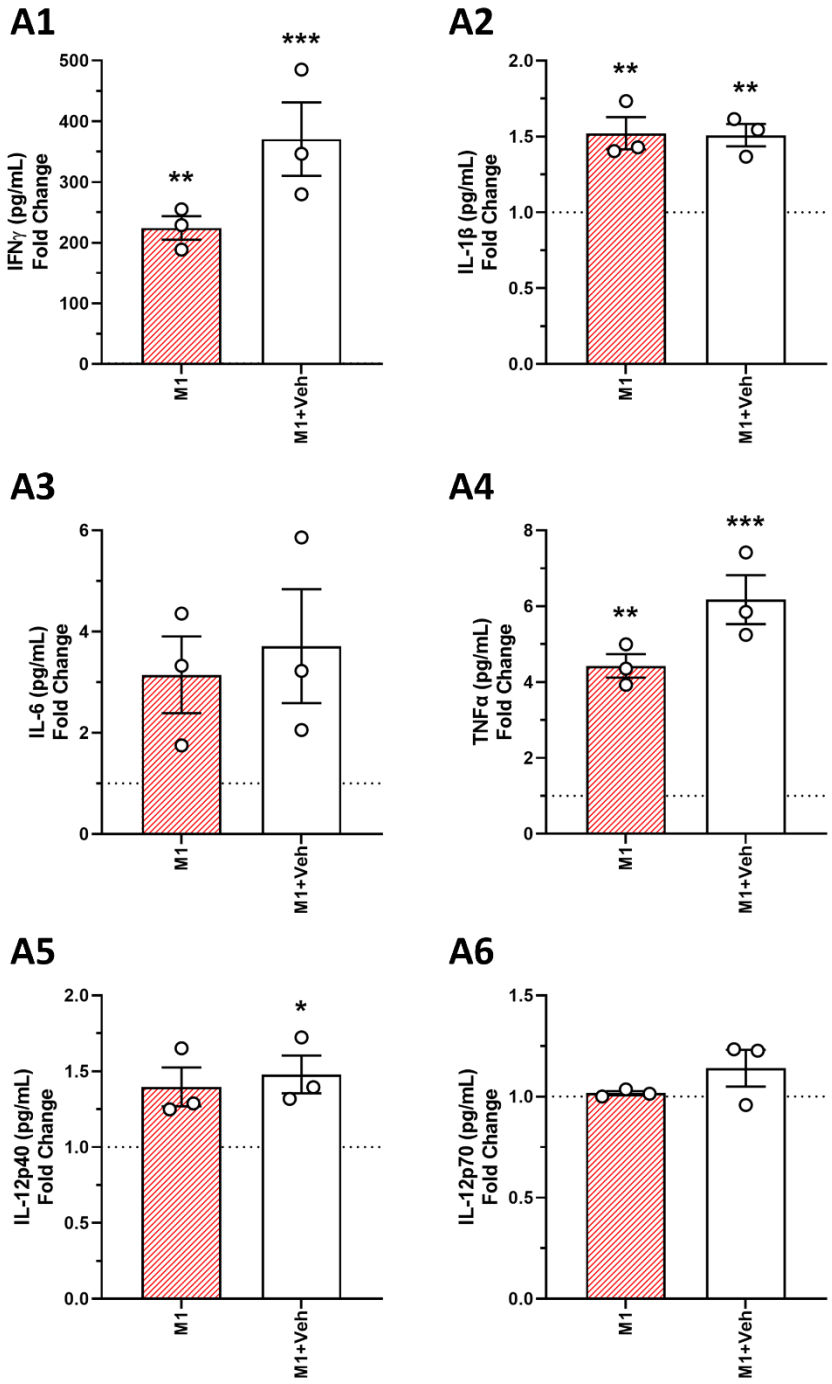

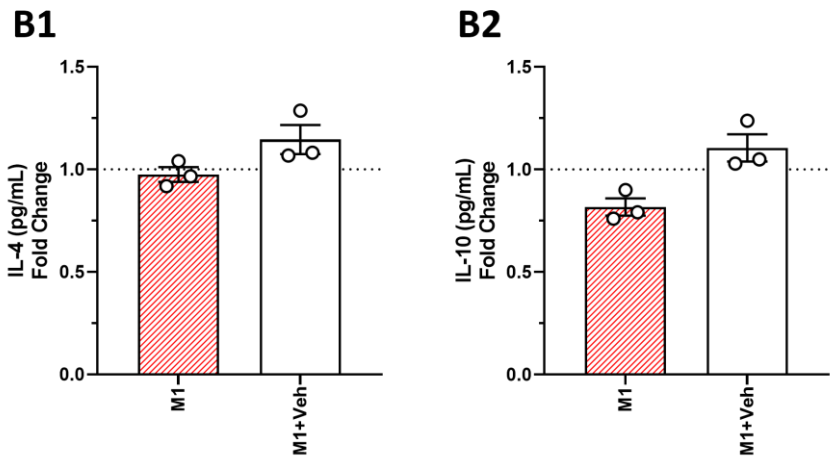

Figure 5.17: Cytokine production from vehicle treated, M1-polarized THP-1-derived macrophages. Data obtained from supernatant analysis after 24hr incubation of M0 macrophages with the M1 polarizing agents IFN-γ (20ng/mL) and LPS (10ng/mL) in the presence of the DMSO vehicle control (1:1000). Bar graphs showing the production of M1-associated cytokines IFN-γ [A1], IL-1β [A2], IL-6 [A3], TNF-α [A4], IL-12p40 [A5] and IL-12p70 [A6], and M2-associated cytokines IL-4 [B1] and IL-10 [B2]. Graphs represent data from 3 repeated experiments each comprising triplicate readings. Data presented as mean ± SEM. One-way ANOVA with post hoc Dunnett's applied versus the un-treated M1. *p<0.05; **p<0.01; ***p<0.001.

5.1.2. PBMC cytokine production profile

As with the THP-1 model, characterisation of the polarized phenotypes regarding their cytokine production values occurred. Figure 5.18 below clearly defines the effect of M1 polarization on the enhanced production of all pro-inflammatory M1-associated cytokines when compared to both the M0 and M2 cultures (Figure 5.18B1-B6). Inversely, IL-4 – a potent anti-inflammatory mediator is significantly upregulated in the M2-polarized cells (Figure 5.18C1), while IL-10 - a key immuno-modulatory M2 cytokine, was significantly increased following M1 polarization to a greater extent than that seen in the M2 which appears to be reduced versus the un-polarized M0 (Figure 5.18C2).

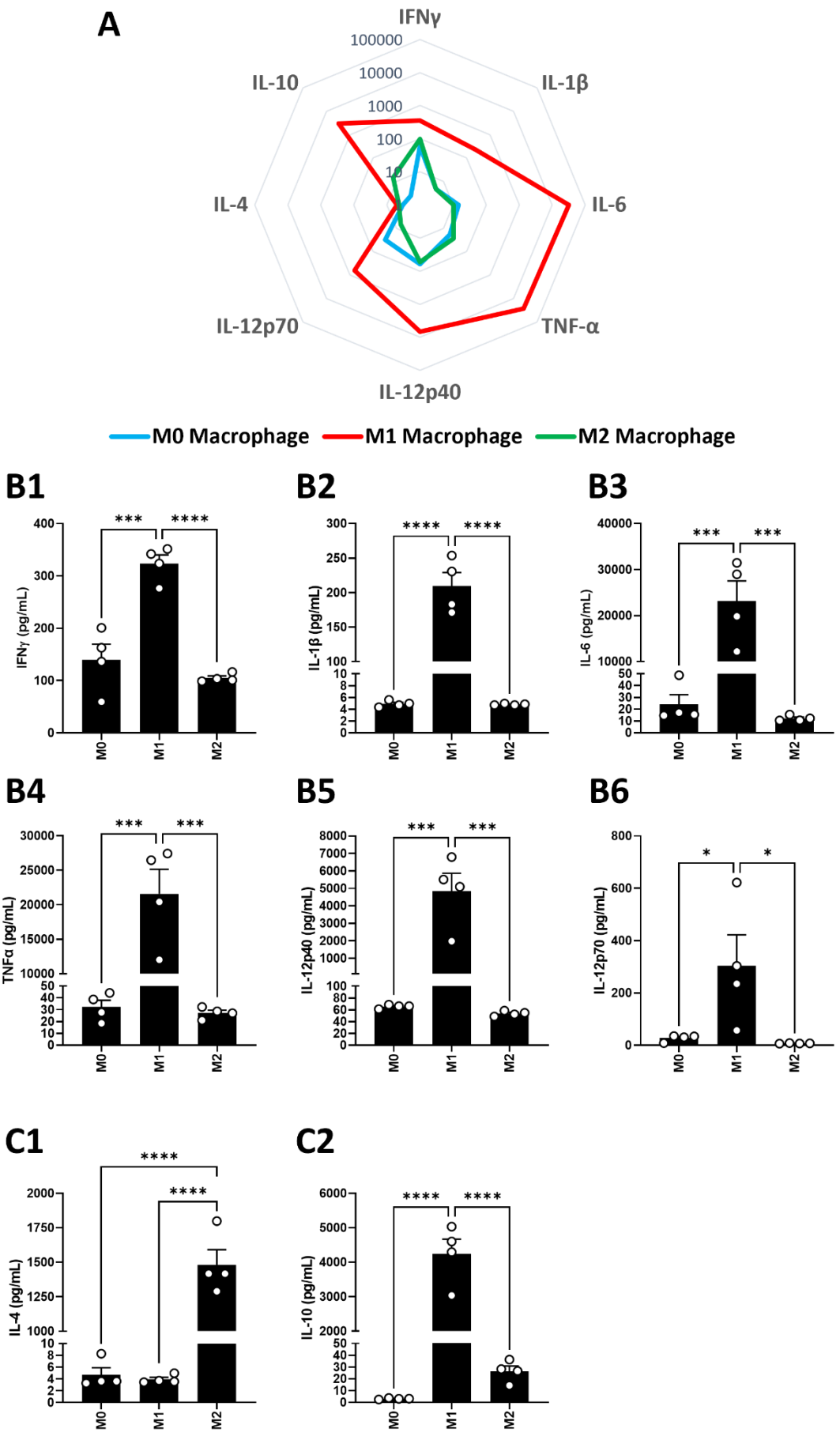
A
IFNγ
IL-1β
IL-6
TNF-α
IL-12p40
IL-12p70
IL-4
IL-10
100000
10000
1000
100
10
M0 Macrophage
M1 Macrophage
M2 Macrophage
B1
IFNγ (pg/mL)
B2
IL-1β (pg/mL)
B3
IL-6 (pg/mL)
B4
TNFα (pg/mL)
B5
IL-12p40 (pg/mL)
B6
IL-12p70 (pg/mL)
C1
IL-4 (pg/mL)
C2
IL-10 (pg/mL)
M0
M1
M2

Figure 5.18: Cytokine production from M1 and M2-polarized PBMC-derived macrophages. Data obtained from supernatant analysis after 24hr incubation of M0 macrophages with the M1 polarizing agents IFN-γ (20ng/mL) and LPS (10ng/mL), or M2 polarizing agent IL-4 (20ng/mL). [A] Radar plot illustrating relative change in cytokine production between M0, M1 and M2 macrophages. Bar graphs showing the production of M1-associated cytokines IFN-γ [B1], IL-1β [B2], IL-6 [B3], TNF-α [B4], IL-12p40 [B5] and IL-12p70 [B6], and M2-associated cytokines IL-4 [C1] and IL-10 [C2]. Graphs represent data obtained from 4 donors each comprised of duplicate readings. Data presented as mean ± SEM. Two-way ANOVA with post hoc Tukey's. *p<0.05; ***p<0.001; ****p<0.0001.

5.2. Effect of minocycline on cytokine production by polarized macrophage subsets

The results obtained for M1-associated cytokines when minocycline was administered during M1 polarization are presented in Figure 5.19, where a consistent inhibitory effect of minocycline on the production of IFN-γ (Figure 5.19A1), IL-1β (Figure 5.19A2) and IL-6 (Figure 5.19A3) can be seen using THP-1 cells when compared to the M1+DMSO (M1+Veh) group. Here, minocycline at the lower concentration of 10μM reduced IFN-γ and IL-1β to a greater extent than the highest dose of 25μM, however a positive correlation between minocycline concentration and cytokine production for IL-6 can been seen, with 25μM now being the more potent modifier. Data pertaining to the PBMC samples corroborated some of these findings, whereby IL-1β and IL-6 were reduced with a correlation between minocycline concentration and cytokine production versus the untreated control again seen (Figure 5.19B2 and B3). Regarding IFN-γ however, data from the PBMCs were less defined, with generally no change in production (Figure 5.19B1).

This correlation between concentration and inhibition of cytokine production was further displayed in the results for IL-12p70 using the THP-1 cells with a reduction in expression induced by minocycline across all biological replicates (Figure 5.19A6). This was not, however, replicated in the PBMCs (Figure 5.19B6). Furthermore, data for TNF-α and IL-12p40 were difficult to define in the THP-1 model, however is significantly reduced in the PBMCs by both minocycline concentrations (Figure 5.19A4 and B4). Both IL-12 subunits in this model however showed insignificant results, which may in part be attributed to samples ranging around the lower detection limit of the assay in this instance.

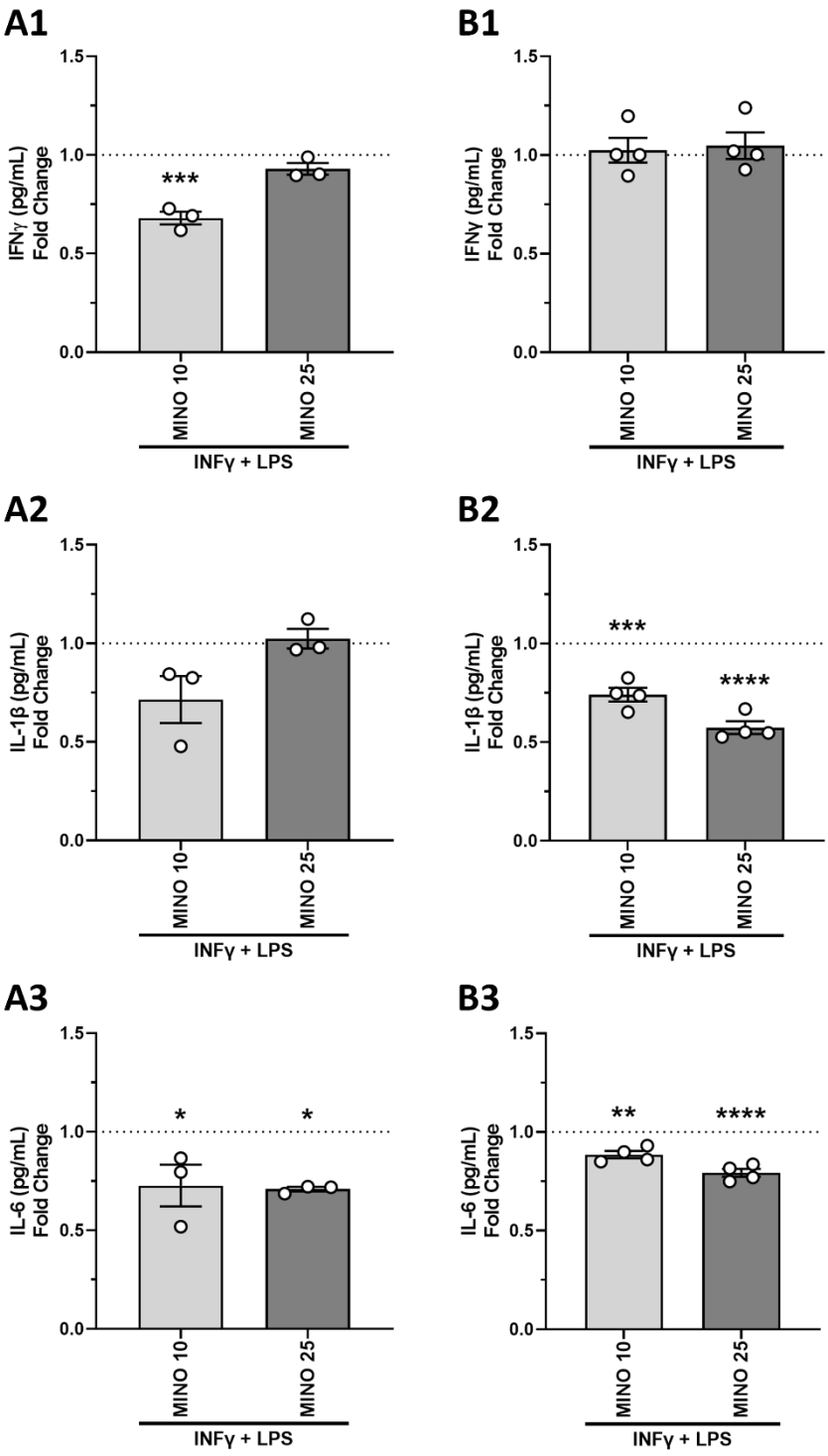
A1
B1
A2
B2
A3
B3
IFNγ (pg/mL) Fold Change
IL-1β (pg/mL) Fold Change
IL-6 (pg/mL) Fold Change
1.5
1.0
0.5
0.0
***
****
**
*
MINO 10
MINO 25
INFγ + LPS

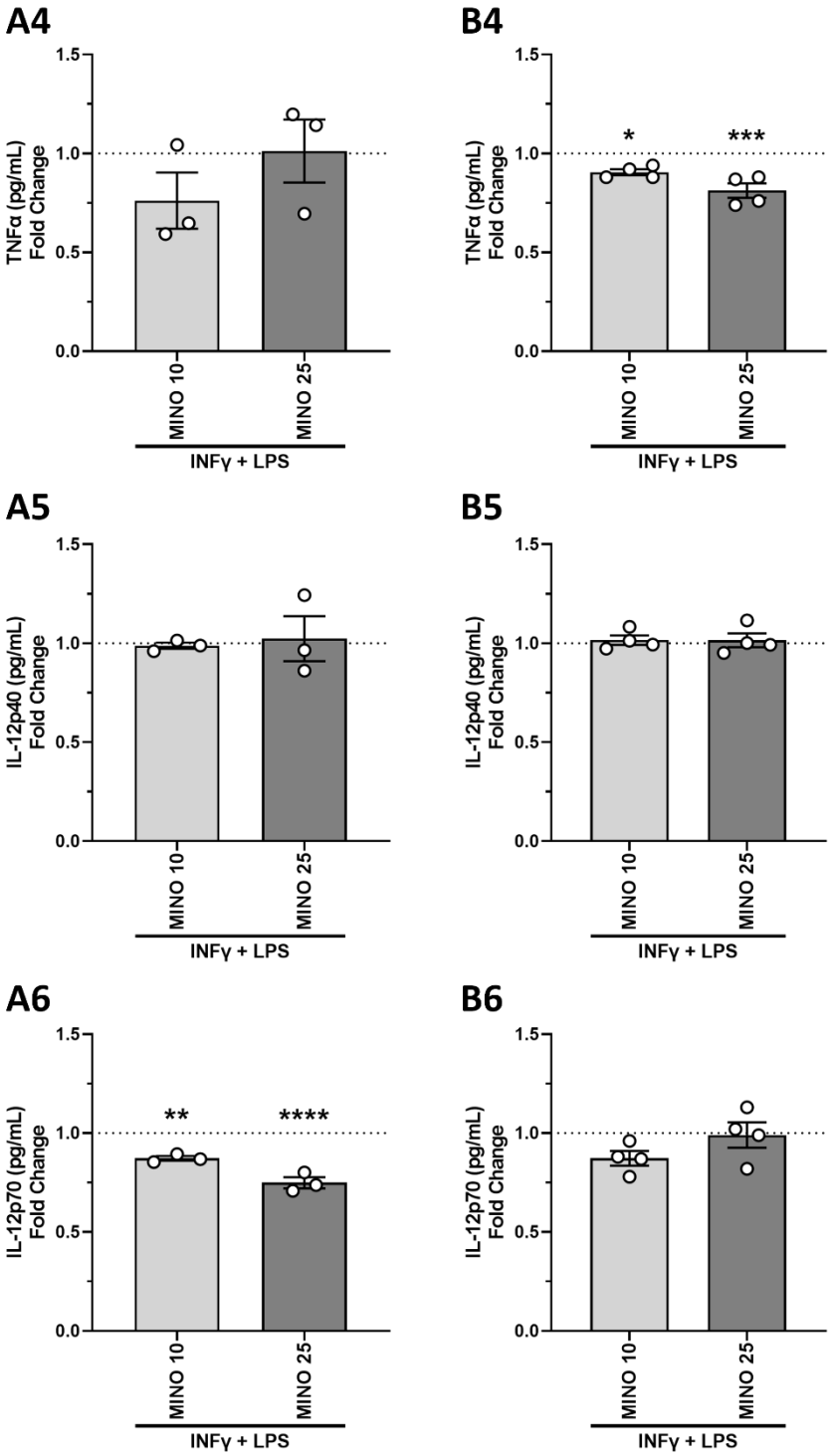

Figure 5.19: Effect of minocycline on M1 cytokine production from M1-polarized THP-1 and PBMC-derived macrophages. Data obtained from supernatant analysis after 2hr pre-incubation with minocycline and 24hr incubation of M0 macrophages with the M1 polarizing agents IFN-γ (20ng/mL) and LPS (10ng/mL). MINO 10 = minocycline 10μM, MINO 25 = minocycline 25μM, Veh = DMSO vehicle control (1:1000). Bar graphs showing data collected from THP-1 [Panel A] and PBMC [Panel B] experimental samples for M1-associated cytokines IFN-γ [1], IL-1β [2], IL-6 [3], TNF-α [4], IL-12p40 [5] and IL-12p70 [6]. Bar graphs showing the relative fold change versus the M1+Veh [Panel A] or untreated M1 [Panel B] control indicated at 1. Graphs represent data

from 3 repeated experiments each comprising triplicate readings for THP-1 [Panel A], and 4 donors each comprising of duplicate values for PBMCs [Panel B]. Data presented as mean ± SEM. One-way ANOVA with post hoc Dunnett's applied versus the relevant control. *p<0.05; **p<0.01; ***p<0.001; ****p<0.0001.

When assessing the influence of minocycline on the production of M2-associated cytokines IL-4 and IL-10 when administered during M1 macrophage polarization, minocycline at either, or both concentrations caused significant downregulation in the production of both IL-4 (Figure 5.20A1 and B1) and IL-10 (Figure 5.20A2 and B2) across all biological replicates of THP-1 and PBMC donors.

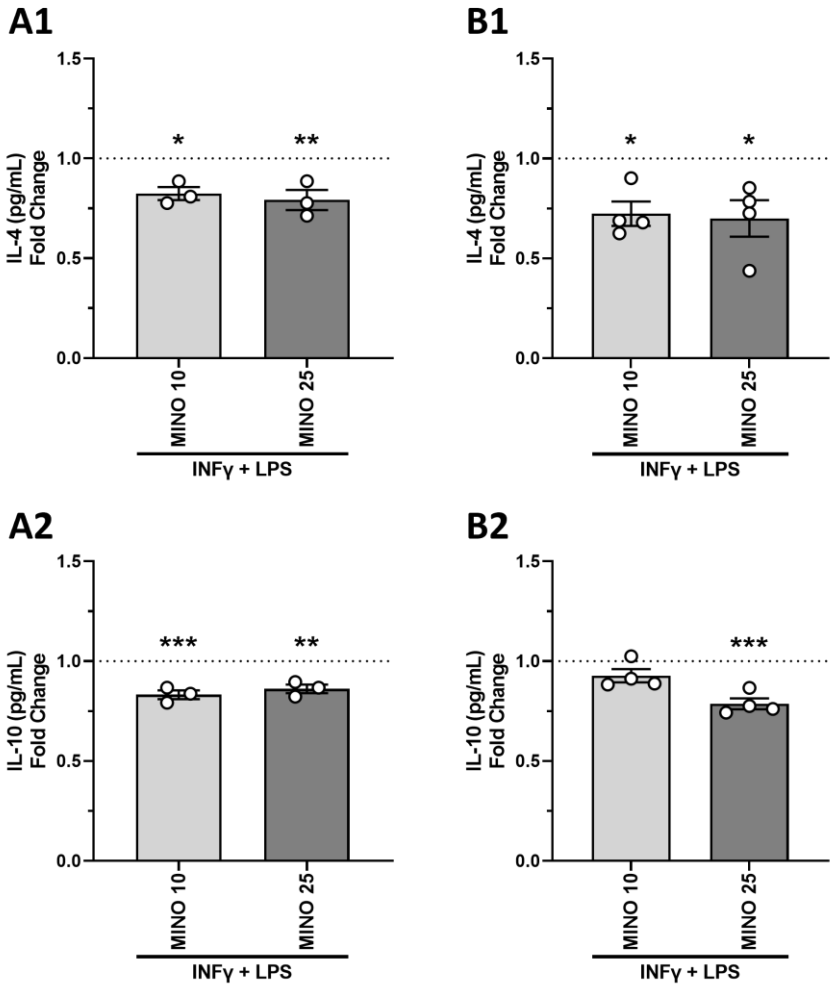

Figure 5.20: Effect of minocycline on M2 cytokine production from M1-polarized THP-1 and PBMC-derived macrophages. Data obtained from supernatant analysis after 24hr incubation of M0 macrophages with the M1 polarizing agents IFN-γ (20ng/mL) and LPS (10ng/mL). MINO 10 = minocycline 10μM, MINO 25 = minocycline 25μM, Veh = DMSO vehicle control (1:1000). Bar graphs showing data collected from THP-1 [Panel A] and PBMC [Panel B] experimental samples for M2-associated cytokines IL-4 [1] and IL-10 [2]. Bar graphs showing the relative fold change versus the M1+Veh [Panel A], or untreated M1 [Panel B] control indicated at 1. Graphs represent

data from 3 repeated experiments each comprising triplicate readings for THP-1 [Panel A], and 4 donors each comprising of duplicate values for PBMCs [Panel B]. Data presented as mean ± SEM. One-way ANOVA with post hoc Dunnett's applied versus the relevant control. *p<0.05; **p<0.01; ***p<0.001.

Having successfully polarized PBMC-derived macrophages into an M2 phenotype via incubation with IL-4, it was also possible to assess any effect of minocycline on this functionally distinct subset of cells. Figure 5.21 below presents the data from these experiments. In relation to the production of M1-associated pro-inflammatory cytokines, minocycline treatment at 25μM resulted in a significant increase of IFN-γ among all donors (p<0.0001) (Figure 5.21A1). This suggests an ability of minocycline to reverse the typical anti-inflammatory cytokine secretion of M2 macrophages to a signature more characteristic of its pro-inflammatory M1 counterpart. Inversely, a possible inhibitory effect of minocycline was reported regarding TNF-α production whereby treatment with 25μM minocycline resulted in decreased production versus the M2 only control (Figure 5.21A4). Interestingly, IL-12p70 was also significantly upregulated in this model by minocycline, with 25μM causing increased production across all donors (p<0.0001) (Figure 5.21A6). All remaining results using this model pertaining to the M1-associated cytokines were ambiguous or inconsistent (Figure 5.21A2, A3 and A5).

Data achieved from studying the effect of minocycline on M2-associated cytokines during M2 polarization showed a partial but statistically significant reduction in IL-4 (Figure 5.21B1), while on the other hand, IL-10 production was significantly inhibited by 25μM minocycline treatment (p=0.0007) displaying a decrease in IL-10 further below the M2 baseline (Figure 5.21B2). If only considering data that was either corroborated between models as in the case of the M1 investigation or was identified in most donors for the M2, a modification pattern exerted by minocycline begins to be unveiled whereby minocycline actively reduced potent pro-inflammatory mediators such as IL-1β, IL-6 and TNF-α, whilst simultaneously reducing anti-inflammatory mediators IL-4 and IL-10 independent of phenotype.

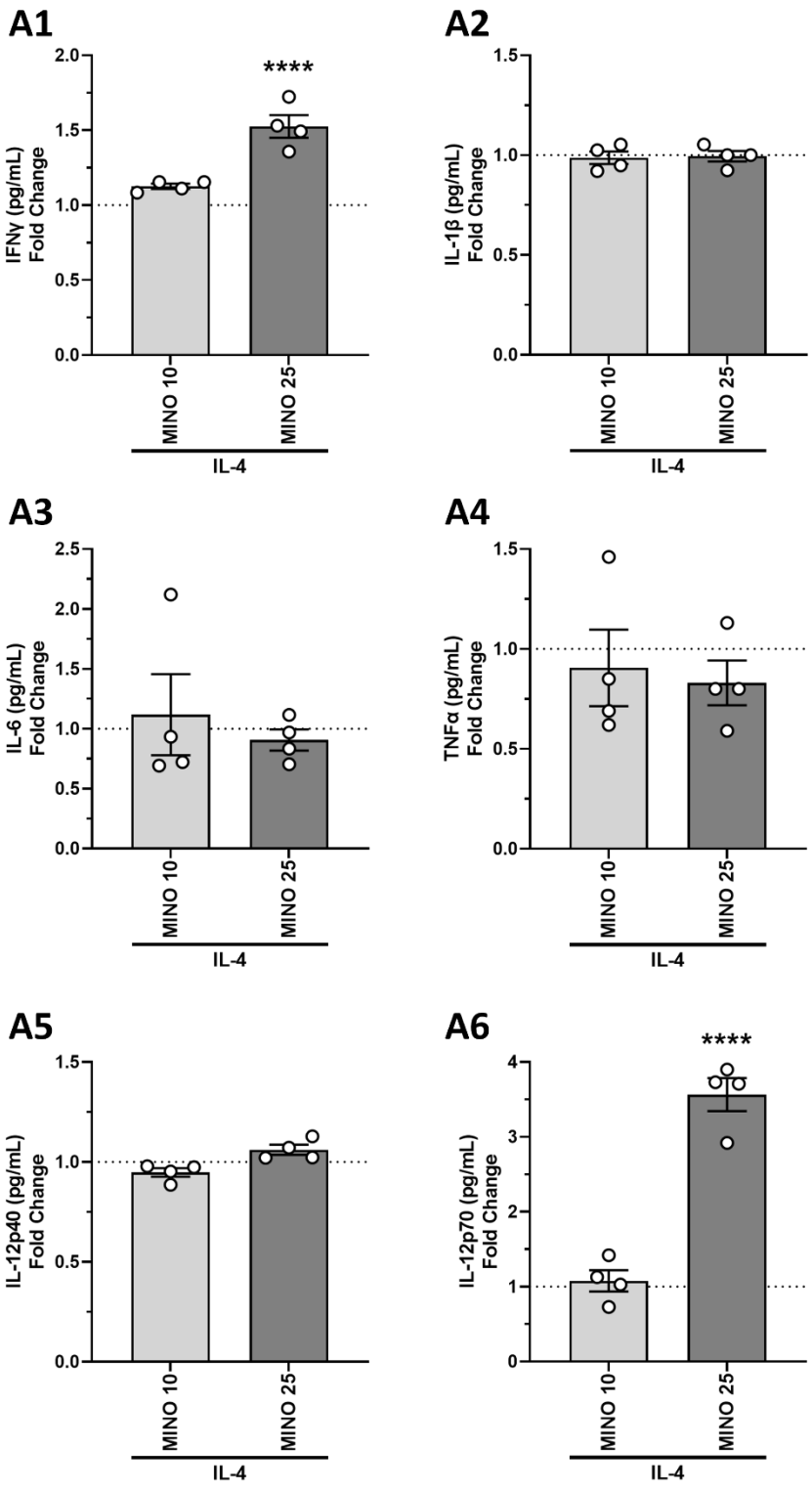
A1
IFNγ (pg/mL) Fold Change
2.0
1.5
1.0
0.5
0.0
****
MINO 10
MINO 25
IL-4
A2
IL-1β (pg/mL) Fold Change
1.5
1.0
0.5
0.0
MINO 10
MINO 25
IL-4
A3
IL-6 (pg/mL) Fold Change
2.5
2.0
1.5
1.0
0.5
0.0
MINO 10
MINO 25
IL-4
A4
TNFα (pg/mL) Fold Change
1.5
1.0
0.5
0.0
MINO 10
MINO 25
IL-4
A5
IL-12p40 (pg/mL) Fold Change
1.5
1.0
0.5
0.0
MINO 10
MINO 25
IL-4
A6
IL-12p70 (pg/mL) Fold Change
4
3
2
1
0
****
MINO 10
MINO 25
IL-4

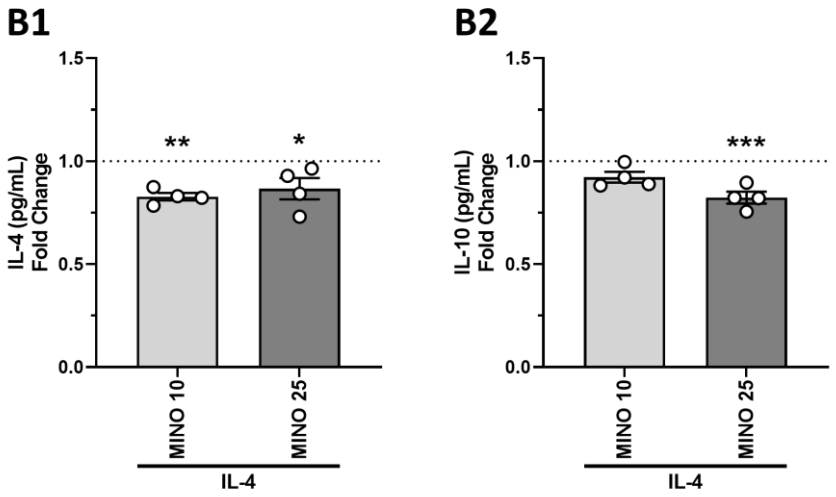

Figure 5.21: Effect of minocycline on cytokine production from M2-polarized PBMC-derived macrophages. Data obtained from supernatant analysis after 24hr incubation of M0 macrophages with the M2 polarizing agent IL-4 (20ng/mL). MINO 10 = minocycline 10μM, MINO 25 = minocycline 25μM. Bar graphs showing data collected from PBMCs of 4 individual donors for experimental samples for M1-associated cytokines IFN-γ [A1], IL-1β [A2], IL-6 [A3], TNF-α [A4], IL-12p40 [A5] and IL-12p70 [A6] and M2-associated cytokines IL-4 [B1] and IL-10 [B2]. Bar graphs showing the relative fold change versus the untreated M2 control indicated at 1. Graphs represent data from 4 donors each comprising of duplicate values. Data presented as mean ± SEM. One-way ANOVA with post hoc Dunnett's applied versus the relevant control. **p*<0.05; ***p*<0.01; ****p*<0.001; *****p*<0.0001.

5.3. Influence of minocycline on M1/M2 macrophage gene expression

The final endeavour was to understand if minocycline may be directly influencing the transcriptional regulation driving M1 and M2 polarization by assessing key transcription factors via genetic analysis. M1 and M2 macrophage sub-populations represent two opposing poles of a dynamically changing state of activation and function and the transcription factors prominent within these processes are widely described and include STATs, IRFs, KLFs, C/EPBs and NF-κB (H. Li *et al.*, 2018). These signal transducers are potent proteins in the commitment of macrophage polarization to either an M1 or M2 phenotype, respectively (Tugal Derin, Liao Xudong, and Jain Mukesh K., 2013; H. Li *et al.*, 2018; Wang *et al.*, 2018). Coupled to pivotal STAT proteins such as STAT1, STAT2 and STAT6, additional genes such as *irf5* and *pparg* also have central roles in macrophage polarization and phenotype commitment to M1 or M2, by closely associating to these key effector molecules and functioning as inhibitory

molecules or pro-inflammatory drivers (Krausgruber *et al.*, 2011; Tugal Derin, Liao Xudong, and Jain Mukesh K., 2013; Wang, Liang and Zen, 2014b; Abdalla *et al.*, 2020).

Data presented earlier in this chapter suggests a role of minocycline in M2 phenotype acquisition in THP-1 and PBMC models as represented by upregulation of surface markers CD163 and CD206, even when previously polarized to a pro-inflammatory M1 phenotype, with further modifications in CD80 and CD86 expression patterns. Consistent inhibition of M1-associated pro-inflammatory mediators IL-1β, IL-6 and TNF-α was also reported, with significant modification of the anti-inflammatory mediator IL-10 also occurring as a result of minocycline treatment. Secretion of proinflammatory mediators such as IL-6 and IFN-γ are primarily controlled by the activation and nuclear translocation of NF-κB, in tandem with other proteins such as STAT1, STAT3, IRF4 and AP-1 (Kapoor *et al.*, 2015; Parker, 2019). The cytokine production analysis described in section 5.4 highlights consistent inhibition in the production of these pro-inflammatory mediators upon minocycline treatment, all of which are characteristic downstream products of typical M1 macrophages, induced via the same transcriptional programmes. These cytokine profiles indicate an influence of minocycline upon M1 macrophage differentiation and activity, in relation to their ability to secrete proinflammatory cytokines, as opposed to M2 where the data also suggests minocycline acts to regulate macrophage polarisation and promote an M2 phenotype, but which is coupled with consistent downregulation of M2-associated IL-10 release. Given these findings, which were highly correlated with a potential disruption in macrophage phenotype acquisition and function, exploration into how the transcriptional machinery may be modified by minocycline began to help explain the somewhat conflicting narratives.

5.3.1. Genetic profile of polarized populations

The effect of minocycline on the transcription on the genes *stat1, stat2, stat3, stat6, irf5* and *pparg* were evaluated by RT-qPCR using the New England BioLabs (NEB) Sybr Green system. Both THP-1- and PBMC-derived macrophages were again generated following the same differentiation protocols as previously described, before being pre-treated with minocycline or the vehicle for 2hr prior to the addition of polarizing agents IFN-γ (20ng/mL) + LPS (10ng/mL) for M1, or IL-4 (20ng/mL) for M2 for an additional 4hr. At the termination of the

protocol cells were collected and lysed in preparation for RNA extraction, cDNA synthesis, and qPCR analysis.

To begin, the expression of the genes of interest within the untreated baseline phenotypes were defined before assessing any modification exerted by minocycline. Figure 5.22 below highlights the expression profile of the selected M1-associated genes, illustrating an increased expression of both *stat1* (Figure 5.22A1 and B1) and *stat2* (Figure 5.22A2 and B2) within the M1 polarized macrophages when compared to the unpolarized control. What was unexpected, however, was the higher gene expression signature for *irf5* found in the M2 cultures (Figure 5.22B3), whilst this gene did not change significantly in the THP-1 model, and in fact appeared to be reduced (Figure 5.22A3).

Regarding the M2-associated genes *stat6, stat3* and *pparg*, Figure 5.23 shows a lack of consistency regarding *stat6* expression, with disparity between the two donors, and no clear change seen within the THP-1 cells following M1 polarization and compared to the M0 control (Figure 5.23A1 and B1). Relatively parallel data between the cellular models was however seen with *stat3*, with a consistent increase in *stat3* following M1 polarization versus the M0 group (Figure 5.23A2 and B2). Similarly, *pparg* expression was consistent whereby downregulation occurred in the M1 cultures, coupled with a significant increase in the PBMC M2 polarized cells (Figure 3.23A3 and B3). In summary, the genetic signature of M1 polarized macrophages was defined by increased expression of *stat1* and *stat2, stat3* but reduced *pparg*, while M2 was defined through increased expression of *irf5* and *pparg* when compared to the unpolarized M0 control.

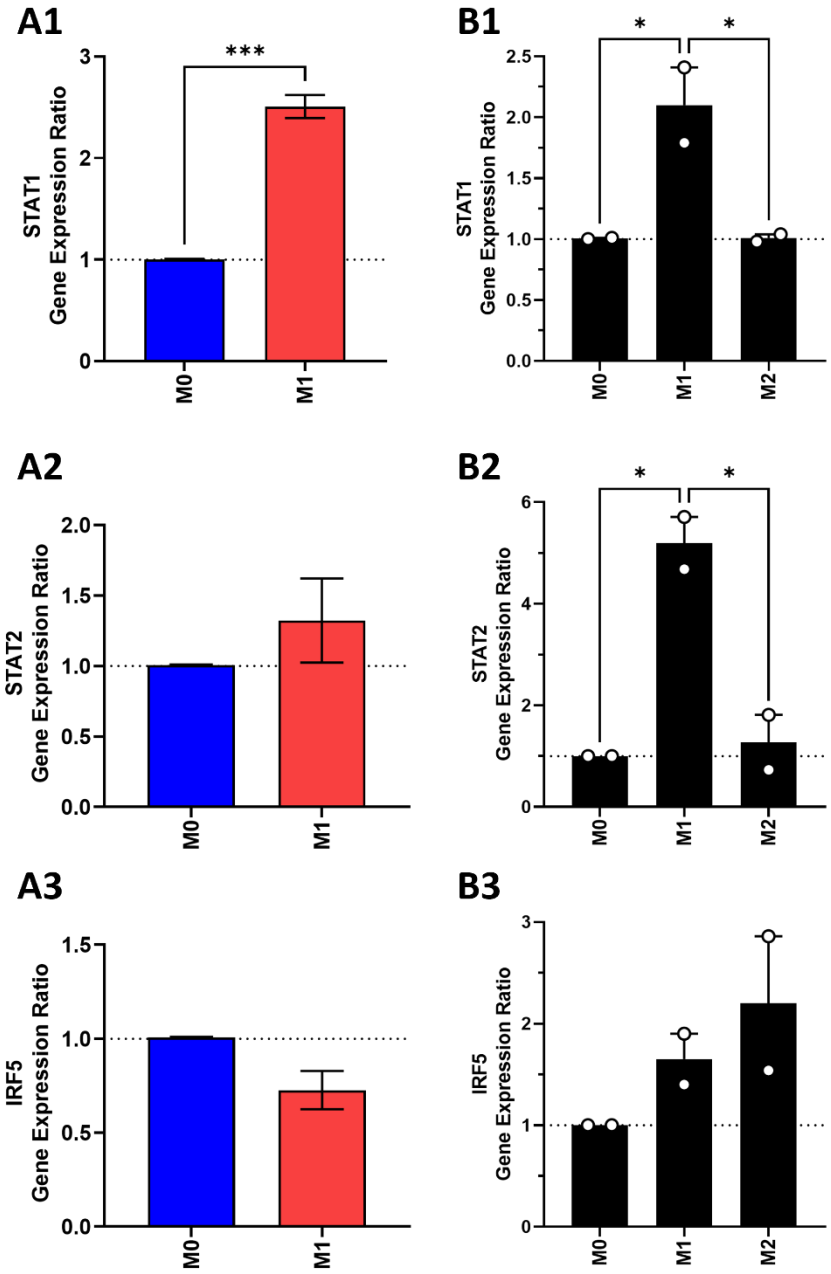

Figure 5.22: M1-associated gene expression from M1 and M2-polarized THP-1 and PBMC-derived macrophages. Data obtained from RT-qPCR analysis of whole cell lysate after 4hr incubation of M0 macrophages with M1 polarizing agents IFN-γ (20ng/mL) and LPS (10ng/mL), or M2 polarizing agent IL-4 (20ng/mL). Bar graphs showing data collected from THP-1 [Panel A] and PBMC [Panel B] experimental samples for M1-associated transcription factors STAT1 [1], STAT2 [2] and IRF5 [3]. Bar graphs showing the relative change in gene expression ratio versus the unpolarized M0 control indicated at 1. Graphs represent averaged triplicate data from 3 repeated experiments for THP-1 [Panel A], or from 2 donors each comprising of triplicate values for PBMCs [Panel B]. Data presented as mean ± SEM. Unpaired t test [Panel A] or One-way ANOVA with post hoc Bonferroni [Panel B] applied. *p<0.05; ***p<0.001.

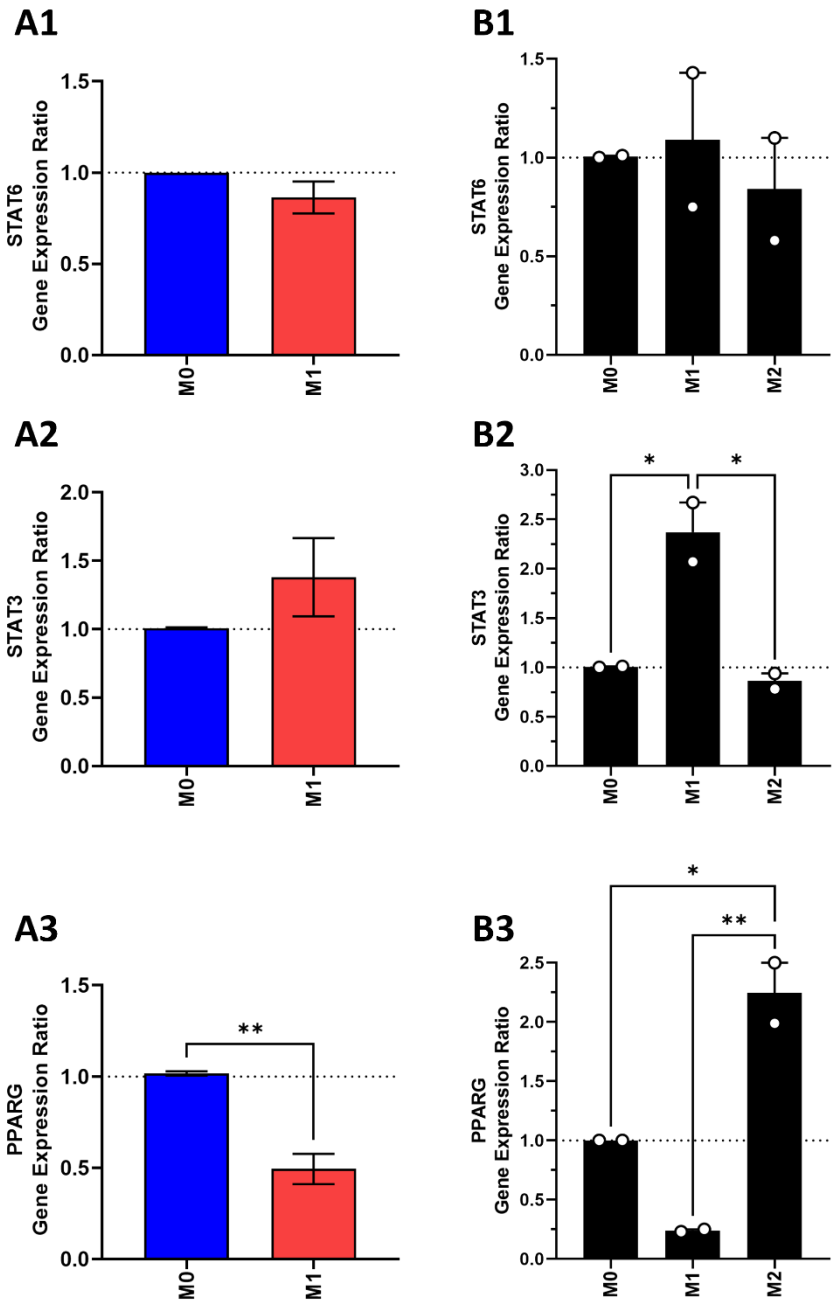

Figure 5.23: M2-associated gene expression of M1 and M2-polarized THP-1 and PBMC-derived macrophages. Data obtained from RT-qPCR analysis of whole cell lysate after 4hr incubation of M0 macrophages with M1 polarizing agents IFN-γ (20ng/mL) and LPS (10ng/mL), or M2 polarizing agent IL-4 (20ng/mL). Bar graphs showing data collected from THP-1 [Panel A] and PBMC [Panel B] experimental samples for M2-associated transcription factors STAT6 [1], STAT3 [2] and PPARG [3]. Bar graphs showing the relative change in gene expression ratio versus the unpolarized M0 control indicated at 1. Graphs represent averaged triplicate data from 3 repeated experiments for THP-1 [Panel A], or from 2 donors each comprising of triplicate values for PBMCs [Panel B]. Data presented as mean ± SEM. Unpaired *t* test [Panel A] or One-way ANOVA with post hoc Bonferroni [Panel B] applied. *p<0.05; **p<0.01.

5.3.2. Effect of minocycline on M1/M2 transcription factors

To understand whether minocycline can affect the expression of key transcription factors to contextualise the previous findings its role on M1 genes when administered during M1 polarization was first assessed. Figure 5.24 outlines these findings, showing largely inconclusive data obtained from the THP-1 model with no statistically definable changes in expression when compared to the untreated (NT) control (Figure 5.24 Panel A). Moreover, there was inconsistent data achieved with the PBMC-derived macrophages whereby both donors illustrated inverse results in relation to *stat1* and *irf5* (Figure 5.24B1 and B3). A significant decrease in *stat2* expression exerted by minocycline at each concentration was however identified in the PBMC samples which was consistent between both donors studied versus the untreated (NT) M1 control group (Figure 5.24B2).

Regarding the M2-associated genes *stat6, stat3* and *pparg*, the THP-1 model saw minocycline seeming to increase all genes to a similar magnitude versus the control but failing to reach significance (Figure 5.25 Panel A). On the other hand, minocycline acted to inhibit the expression of *stat6* and *stat3* following M1 polarization in the PBMC samples, a response elicited by either 10μM or 25μM minocycline (Figure 5.25B1 and B2). An absence of significant modulation was also reflected in the PBMC samples for expression values pertaining to *pparg* whereby minocycline appeared to exert no modification when compared to the untreated control (Figure 5.25B3).

Having established a possible role of minocycline on gene expression during M1 polarization, the PBMC-derived M2 macrophage model was next utilised to assess any influence of minocycline on this distinct subset. Here no clearly definable modification of the M1 transcription factors *stat1, stat2* or *irf5* was found, with marginal downregulation of *stat1* and *stat2* observed (Figure 5.26C). Similar data was also obtained when evaluating the M2-associated genes, whereby parallel discrepancies between donors is illustrated with wide variation between donor values rendering the results difficult to interpret (Figure 5.27C).

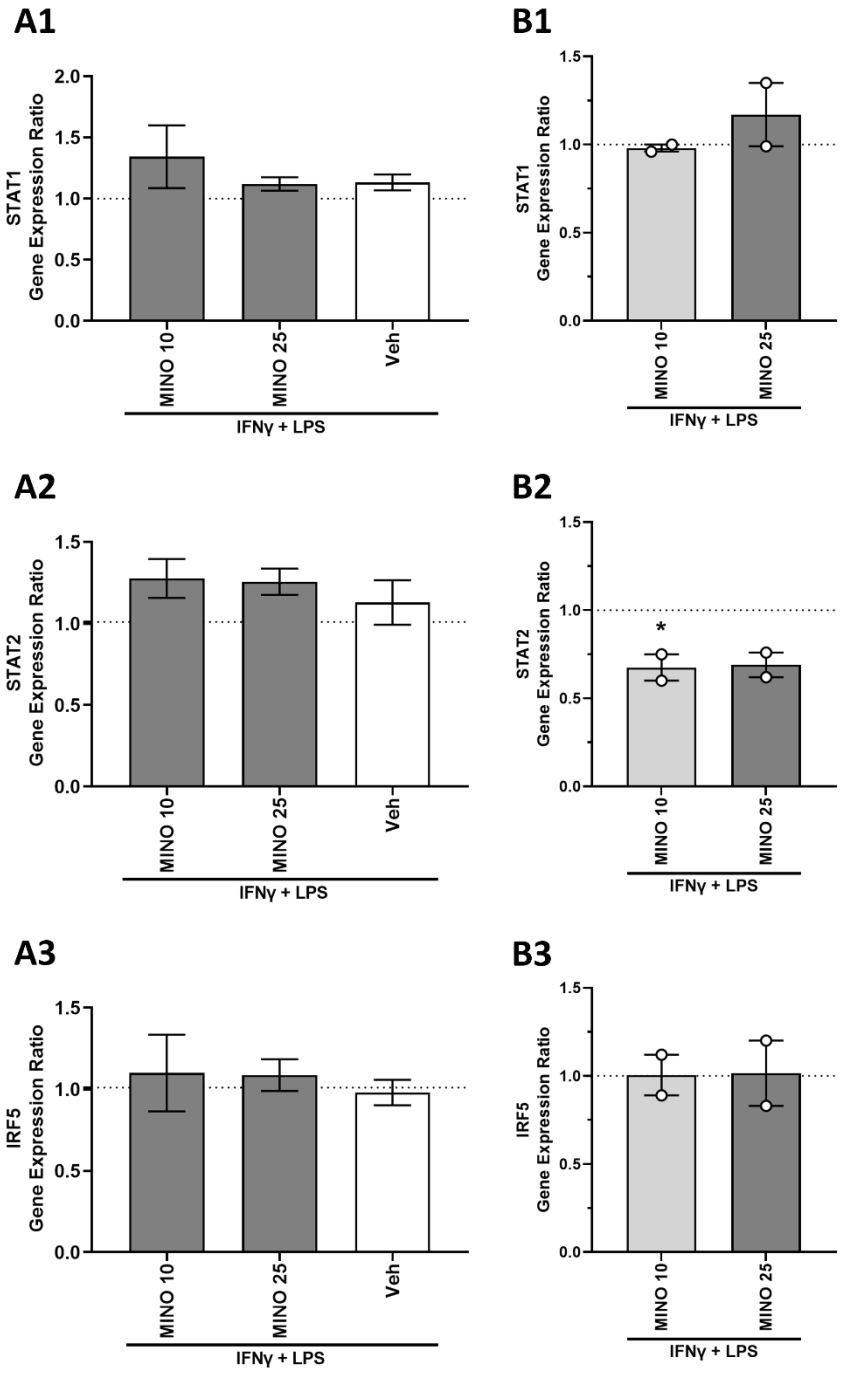

Figure 5.24: Effect of minocycline on M1-associated gene expression from M1-polarized THP-1 and PBMC-derived macrophages. Data obtained from RT-qPCR analysis of whole cell lysate following 2hr pre-treatment with MINO or Veh and additional 4hr incubation of M0 macrophages with M1 polarizing agents IFN-γ (20ng/mL) and LPS (10ng/mL). NT = no treatment, MINO 10 = minocycline 10μM, MINO 25 = minocycline 25μM, Veh = DMSO 1:1000. Bar graphs showing data collected from THP-1 [Panel A] and PBMC [Panel B] experimental samples for M1-associated transcription factors STAT1 [1], STAT2 [2] and IRF5 [3]. Bar graphs showing the relative change in gene expression ratio versus the untreated (NT) M1 control indicated at 1. Graphs represent averaged triplicate data from 3 repeated experiments for THP-1 [Panel A], or

from 2 donors each comprising of triplicate values for PBMCs [Panel B]. Data presented as mean ± SEM. One-way ANOVA with post hoc Dunnett's versus the NT control applied. *p<0.05.

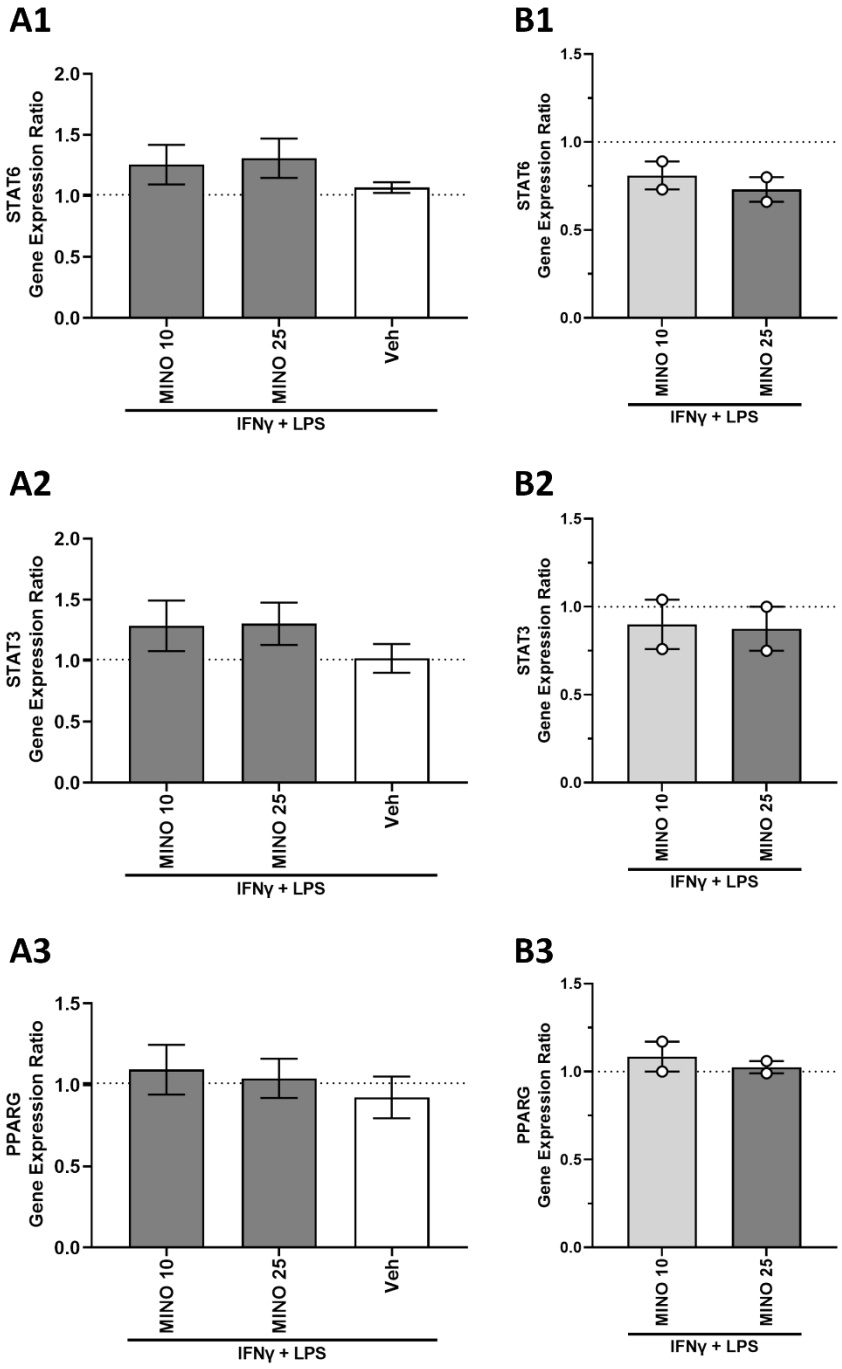

Figure 5.25: Effect of minocycline on M2-associated gene expression from M1-polarized THP-1 and PBMC-derived macrophages. Data obtained from RT-qPCR analysis of whole cell lysate following 2hr pre-treatment with MINO or Veh and additional 4hr incubation of M0 macrophages with M1 polarizing agents IFN-γ (20ng/mL) and LPS (10ng/mL). NT = no treatment, MINO 10 = minocycline 10μM, MINO 25 = minocycline 25μM, Veh = DMSO 1:1000. Bar graphs showing data collected from THP-1 [Panel A] and PBMC [Panel B] experimental samples for M2-associated transcription factors STAT6 [1], STAT3 [2] and PPARG [3]. Bar graphs showing the relative change in gene expression ratio versus the untreated (NT) M1 control indicated at 1.

Graphs represent averaged triplicate data from 3 repeated experiments for THP-1 [Panel A], or from 2 donors each comprising of triplicate values for PBMCs [Panel B]. Data presented as mean ± SEM. One-way ANOVA with post hoc Dunnett's versus the NT control applied.

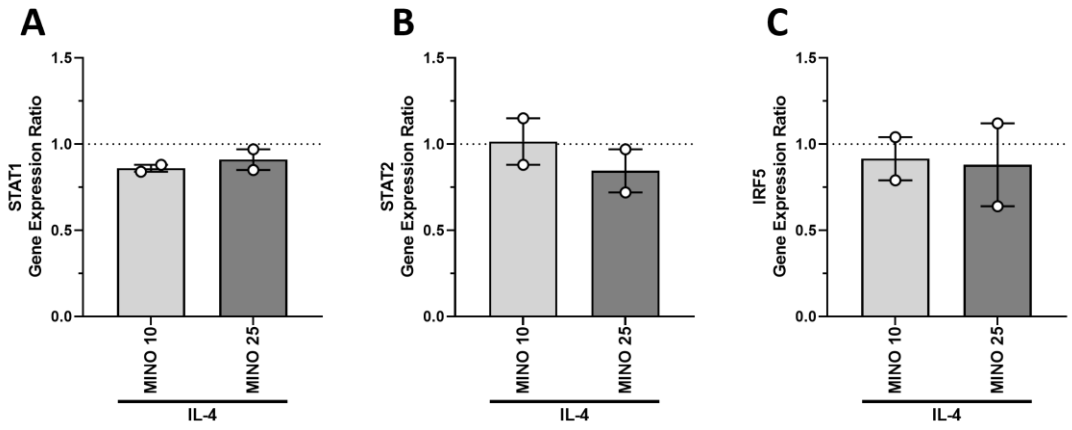

Figure 5.26: Effect of minocycline on M1-associated gene expression of M2-polarized PBMC-derived macrophages. Data obtained from RT-qPCR analysis of whole cell lysate following 2hr pre-treatment with MINO and additional 4hr incubation of M0 macrophages with M2 polarizing cytokine IL-4 (20ng/mL). NT = no treatment, MINO 10 = minocycline 10μM, MINO 25 = minocycline 25μM. Bar graphs showing data collected from PBMC samples for M1-associated transcription factors STAT1 [A], STAT2 [B] and IRF5 [C]. Bar graphs showing the relative change in gene expression ratio versus the untreated (NT) M2 control indicated at 1. Graphs represent data from 2 donors each comprising of triplicate values. Data presented as mean ± SEM. One-way ANOVA with post hoc Dunnett's versus the untreated M2 control applied.

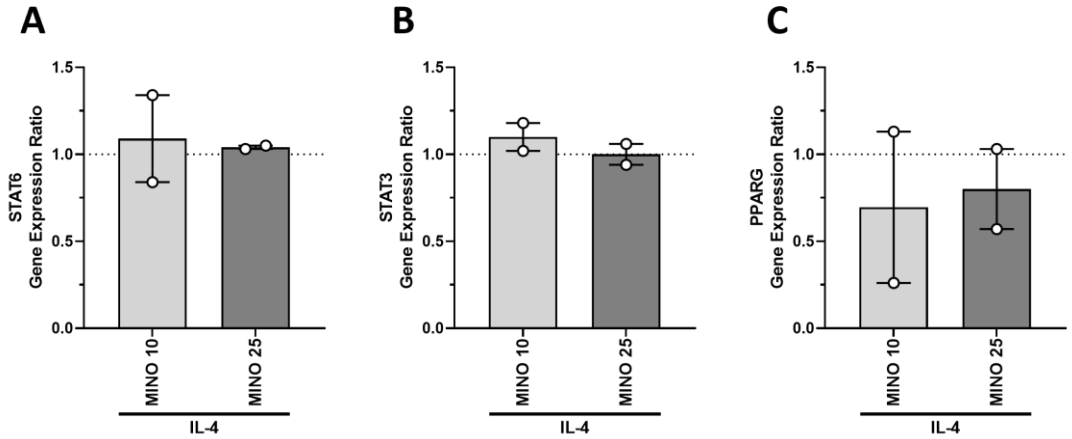

Figure 5.27: Effect of minocycline on M2-associated gene expression of M2-polarized PBMC-derived macrophages. Data obtained from RT-qPCR analysis of whole cell lysate following 2hr pre-treatment with MINO and additional 4hr incubation of M0 macrophages with M2 polarizing cytokine IL-4 (20ng/mL). NT = no treatment, MINO 10 = minocycline 10μM, MINO 25 = minocycline 25μM. Bar graphs showing data collected from PBMC samples for M2-associated transcription factors STAT6 [A], STAT3 [B] and PPARG [C]. Bar graphs showing the relative change in gene expression ratio versus the untreated (NT) M2 control indicated at 1. Graphs represent data from 2 donors each comprising of triplicate values. Data presented as mean ± SEM. One-way ANOVA with post hoc Dunnett's versus the untreated M2 control applied.

5.4. Chapter discussion

The data disseminated in this chapter indicate a few key modifications to macrophage polarization and function induced by minocycline which may prove therapeutically relevant for the treatment of IBD. Firstly, in section 5.1.2. a potent role of minocycline was displayed, both in the induction of surface markers CD80, CD163 and CD206, and simultaneous downregulation of CD14 within the THP-1 macrophage model. These data categorically imply an influence of minocycline in the phenotypic switch from pro-inflammatory M1, to anti-inflammatory M2, in addition to rendering cells hyporesponsive to further TLR activation by the TLR4 ligand LPS. However, although this data was conclusive and corroborated across biological replicates, the same effects were not witnessed when translating the investigation to primary PBMC in section 5.2.2. This disparity between cellular models was disappointing, so although robust data was achieved in the THP-1, a lack of substantiation by the second model renders the data somewhat inconclusive and would require further verification.

Data for CD80 in the PBMC model in particular did not directly corroborate those seen when exploring the effect of minocycline using THP-1-derived M1 macrophages in which a distinct inhibitory effect was reported (section 5.1.2). However, it must be noted that in the PBMC-derived cells the overall percentage of $CD80^{+}$ cells in this instance remained below 6% across all conditions and donors, which thus may render the minocycline data inconsequential. On the other hand, CD86 expression was seen to reduce within the M2 macrophage model which was in fact consistent with the THP-1 findings, and although not reaching statistical significance, alluded to the inhibitory action of minocycline on CD86 expression.

The other major discrepancy was in regard to CD206 which was reduced by treatment with minocycline in the PBMC-derived M2 macrophages. This was to some extent unpredicted given the data acquired during the THP-1 investigations whereby minocycline potently upregulated CD206 expression even when an inflammatory M1 baseline was established. Given this data which supports an inverse effect within the M2 cultures, a potential regulatory role of minocycline on phenotype commitment and plasticity began to be suggested. The data reported in this chapter may allude to role whereby minocycline acts to upregulate M2-associated markers such as CD206 on baseline or ‘activated’ cells in the intent

of dampening their pro-inflammatory contribution, whilst simultaneously reducing M2-like markers on already defined M2 populations in order to maintain phenotype homeostasis and reduce the risk of M2-associated pathophysiology.

Furthermore, another unforeseen result was highlighted in section 5.2.1. pertaining to the initial phenotyping of M1 polarized PBMC macrophages in which CD14 was seen to decline. Given the understanding that CD14 plays a vital role in LPS binding and latter TLR4 signalling, which is a prominent function of M1 macrophages, it was surprising to see a decline in expression within this population. However, as mentioned previously, CD14 has the ability to shed from the cell surface membrane and become soluble (sCD14), with papers reporting that while enhanced shedding of CD14 during sepsis models *in vivo* can be witnessed, this does not directly reduce the binding of LPS to monocytes/macrophages (Rokita and Menzel, 1997). With no papers further categorizing or suggesting cause for CD14 downregulation following M1 polarization, it was hypothesised that incubation with potent inflammatory stimulants like IFN-γ and LPS may mimic sepsis-like inflammation and thus lead to membrane bound CD14 (mCD14) shedding which is reflected in this reduced surface expression. Moreover, as this has not been directly correlated to reduced LPS binding and therefore TLR4-intiation of inflammatory cascades attributed to M1 macrophages, in combination with the other characteristic markers of successful M1 induction, M1 polarization was still deemed successful despite this reduction in CD14.

Furthermore, it was also noted during these investigations described in section 5.1.2 an influence of the DMSO vehicle control upon activated CD11b surface marker expression within the THP-1 model. Given the absence of any adverse effect of the vehicle during all previous flow cytometry analysis, a potential ‘sensitization’ of the macrophages following M1 polarization to the chemical DMSO in relation to this CD11b may have occurred. This may be due, in part, to reported increases in CD11b in its active conformation (Mac-1) when exposed to ligands which cause cellular activation such as DMSO (Hynes, 2002). However, this remains speculative due to no clearly identified literary sources to either support or refute this hypothesis at the time or writing. Therefore, what is important to note from this CD11b data is simply a lack of potentiation or inhibitory effect of minocycline when compared to either the M1 or vehicle groups.

It was also interesting to note however the decreased expression of CD11b total protein in the M1 polarized PBMC macrophages but opposing increase in M2 outlined in section 5.2.1. This was curious given that inflammation can be categorised through recruitment of leukocytes to the site of injury or infection which is facilitated by integrins such as Mac-1 – the activated confirmation of CD11b/CD18 (Ley *et al.*, 2007). This adhesion molecule experiences rapid activation that increases the affinity for its ligands and subsequently mediates rolling, firm adhesion, and transmigration of leukocytes into inflamed tissue (Dunne *et al.*, 2003; Fan and Ley, 2015). Macrophages express Mac-1 which also has functional diversity and ability to bind a large repertoire of proteins and proteoglycans such as ICAM-1 and fibrinogen (Wolf *et al.*, 2018). Thus, one would expect its expression to increase following potent inflammatory insult in the form of M1 polarizing which was not seen. However, despite its major role in host defence, CD11b is also implicated in tissue regeneration, and thrombosis development, which may provide some insight as to why this protein was increased on the surface of M2 polarized macrophages. Reports have also begun to elucidate another mechanism which could explain the upregulation of CD11b on M2 macrophages in the form of macrophage efflux following inflammation. a report by Cao *et al* in 2005 showed that inflammatory macrophages do not die locally by apoptosis; but rather migrate into the lymphatics and finally into the circulation. This macrophage efflux is enhanced considerably following cell activation and its acceleration dependent on integrin Mac-1 (Cao *et al.*, 2005). This paper suggests that Mac-1 may play an important role in the removal of local inflammatory macrophages and in their subsequent migration to the lymph nodes, which may aid in providing an explanation to CD11b upregulation in M2 macrophages but not M1.

Despite discrepancies regarding surface marker expression, far more consistent and consequential results were achieved when assessing cytokine production following minocycline treatment. It was outlined in section 5.4. consistent modification of key cytokines IL-1β, IL-6, TNF-α, IFN-γ and IL-10 following intervention of M1 or M2 polarization with minocycline which may have fundamental influence on downstream inflammatory signalling. Firstly, IL-1β is a potent pro-inflammatory cytokine that is crucial for host-defence responses to infection and injury. However, despite being essential for resistance to infections,

IL-1β may also exacerbate damage during chronic disease and acute tissue injuries (Lopez-Castejon and Brough, 2011). Inflammatory stimuli cause activation of the signalling adaptor MyD88 which is known to stimulate C/EBP, that in turn confers upregulation of IL-1β gene expression in response to the TLR4 ligand LPS (Zhang and Rom, 1993; Lu *et al.*, 2009). Activation of IL-1β triggers local immune responses by stimulating T cell proliferation and guiding of neutrophils to sites of infection via IL-1β/IL-1R complexes, and the further activation of NF-κB and MAPK pathways which upregulate additional pro-inflammatory cytokines such as IL-6 and TNF-α (Guarda and So, 2010; Sahoo *et al.*, 2011).

Although largely beneficial to the host defence during infections and metabolic processes, over production of IL-1β results in sterile inflammation, which can increase the risk of developing metabolic and autoinflammatory diseases among IBD patients. In the context of the macrophage lineage, IL-1β has been shown to promote the differentiation of monocytes to M1-like macrophages, induce type 1 immune responses, polarize αβ $CD4^+$ T cells towards T helper cell type 1 (Th1), and favour the differentiation of αβ $CD4^+$ T cells towards Th17 in combination with IL-6 and IL-23 (Acosta-Rodriguez *et al.*, 2007; Schenk *et al.*, 2014; Hutton *et al.*, 2016; Bent *et al.*, 2018). Reports also link an overproduction of IL-1β in both IBD patients and murine models illustrating a function of IL-1β in the development of mucosal inflammation (Mahida, Wu and Jewell, 1989). Furthermore, elevations in IL-1β levels have been associated with increased IBD severity (Ligumsky *et al.*, 1990), with a 2010 study by Bauer *et al* exploring the role of the NLRP3 inflammasome in intestinal inflammation, reporting that mice who lacked NLRP3, and therefore had reduced IL-1β production, were often characterised by a decrease in DSS-colitis and TNBS-colitis severity when compared to the control (Bauer *et al.*, 2010). In section 5.3. treatment with minocycline consistently and potently reduced the production of IL-1β, regardless of polarization status.

Similarly, IL-6 is a multifunctional cytokine that is secreted by both immune and non-immune cells, and functions via binding to the IL-6 receptor (IL-6R) and gp130. This subsequently activates the JAK-STAT3 signalling pathway which acts to regulate inflammatory responses (Wang *et al.*, 2020). IL-6 has been found at higher levels in various diseases, including IBD (Műzes *et al.*, 2012), while its inhibition in other autoimmune diseases such as rheumatoid arthritis has also

proven to be beneficial (Mircic and Kavanaugh, 2009). In experimental models of colitis there is growing evidence that IL-6 is a major contributory cytokine within the chronic phase of inflammation. In the year 2000, two large *in vivo* experimental colitis studies were published and indicated that IL-6 secreted by both T cells and macrophages were key protagonists to disease progression (Atreya *et al.*, 2000; Yamamoto *et al.*, 2000). Additionally, more recent findings further implicate the role of IL-6 in the maintenance of inflammation in mice lacking the common cytokine gamma chain, whereby in a model of spontaneous colitis, application of antibodies to the IL-6 receptor prevented intestinal inflammation due to the induction of apoptosis in $CD4^+$ T cells (Kai *et al.*, 2005).

In regard to immune cell function, the IL-6/IL-6Rα complex has been described to favour a transition from neutrophil to monocyte infiltration during early inflammatory events. Endothelial activation by proinflammatory molecules results in the secretion of chemo-attractants, which in turn recruit the influx of neutrophils and induction of IL-6Rα shedding (becoming sIL-6Rα) from their membranes. This IL-6/sIL-6Ra signalling subsequently controls leucocyte infiltration (Hurst *et al.*, 2001; Marin *et al.*, 2001). *In vitro* studies confirm that these sIL-6Rα mediated events regulate both chemokine and adhesion molecule expression, and consequently control the intermediary factors involved in resolving inflammation. A disruption in this IL-6 trans-signalling control of leucocyte trafficking may therefore be significant at the onset of chronic disease as in the case of IBD relapse (Jones *et al.*, 2005; Gabay, 2006). It was again shown in this chapter that minocycline potently inhibited the production of IL-6 when added during M1 or M2 polarization *in vitro*.

Likewise, TNF-α has long been considered one of the most essential factors promoting the inflammatory process with correlation to diseases such as rheumatoid arthritis and IBD. TNF-α plays a prominent role in bridging the innate and adaptive phases of immunity, in addition to modulating cell proliferation, and apoptotic processes (Popa *et al.*, 2007). Two types of TNF-α receptors, type I (TNFR1, p55 or CD120a) and type II (TNFR2, p75 or CD120b) are present on the plasma membrane of virtually all cell types except erythrocytes, and although they share structural homology, they induce separate cytoplasmic signalling cascades following receptor-ligand binding, as well as differing in binding affinity

(Ma, 2001). Upon stimulation, the intracellular domain of TNFR1 binds to the TNF receptor-associated death domain (TRADD) protein, which further activates either the apoptotic pathway, via Fas-associated death domain (FADD), or the pro-inflammatory pathway, via TNF receptor-associated factor 2 (TRAF2). This results in the activation of nuclear factor-κB (Popa *et al.*, 2007; Kalliolias and Ivashkiv, 2016).

In the context of IBD, increased levels of TNF-α have been found in the intestinal mucosa, serum, and faeces of IBD juvenile patients when compared with healthy donor controls (Pirenne *et al.*, 1992; Breese *et al.*, 1994). In murine experimental colitis models, selective inhibition of soluble TNF-α *in vivo* was sufficient to reduce inflammation, with blocking of both soluble and membrane-bound forms proving even more efficient in this action, which was accompanied by continuous and stable remission (Perrier *et al.*, 2012). Many studies have also implicated TNF-α in the degradation of the epithelial barrier and subsequent regulation of tight-junctions. In a 2013 study, Su *et al* reported that TNFR2 mediates MLCK up-regulation and colitis development upon transfer of normal $CD4^{+}CD45RB^{hi}$ cells to $Tnfr2^{-/-}Rag1^{-/-}$ recipient mice (Su *et al.*, 2013). Other studies have in parallel shown how TNF-α influences the distribution of JAMA in the tight junctions, with $Jama^{-/-}$ mouse models eliciting disrupted epithelial barrier function, rendering them highly susceptible to dextran sulphate sodium (DSS)-induced colitis (Ozaki *et al.*, 1999; Laukoetter *et al.*, 2007; Vetrano *et al.*, 2008).

Given the documented research, the use of TNF antagonists has been approved by the Food and Drug Administration of USA (FDA) for the treatment of IBD and has revolutionized its medical management. Four inhibitors are currently available; infliximab, adalimumab, certolizumab pegol, and golimumab, which function by inhibiting disease activity resulting in mucosal healing (Slevin and Egan, 2015; Gajendran *et al.*, 2018). Although proven to have good efficacy in relation to the induction of remission in moderately severe Crohn's disease patients who have previously failed treatment with standard therapies, registered systemic side effects linked with infection and inflammation in the skin and joints, development of non-Hodgkin's lymphoma, and activation of latent tuberculosis have been recorded (Cleynen and Vermeire, 2012; Targownik and Bernstein, 2013; Gubernatorova and Tumanov, 2016). The data disseminated in this chapter show clear inhibition of all three cytokines; IL-1β, IL-6 and TNF-α exerted

by minocycline treatment during macrophage polarization to M1 and M2 subsets. Given the current literature, in combination with these findings, it was hypothesised that minocycline may have modulatory influence on pathologies such as mucosal inflammation, tissue degradation, leukocyte trafficking, epithelial barrier dysfunction, and the activation of inflammatory resolution mechanisms via down regulation of these potent mediators. Furthermore, minocycline may present as a viable option in the setting of IBD management versus current anti-TNF therapies given its established safe pharmacological profile, in addition to its ability to not only inhibit TNF-α secretion from macrophages, but also concurrently downregulate other contributory pro-inflammatory mediators.

Conversely, results presented in section 5.3 whereby minocycline intervention of M2 macrophage polarization simultaneously caused increased production of typical pro-inflammatory mediators IFN-γ and IL-12, whilst inhibiting the potent anti-inflammatory cytokine IL-10. This was unexpected based upon the previous surface marker expression profiling in which a role of minocycline in promoting an M2 phenotype was identified. IFN-γ is well documented to have pleiotropic immunomodulatory properties on both the innate and adaptive immune responses, and is involved in host protection as well as post-infection immunopathology (Burke and Young, 2019; Mezouar and Mege, 2020). It is a soluble homodimer secreted by activated CD4 and CD8 T cells, γδ T cells, natural killer cells, B cells and APCs such as macrophages (Kasahara *et al.*, 1983; Gao *et al.*, 2003; Harris *et al.*, 2005; Yu *et al.*, 2006; Robinson *et al.*, 2009). IFN-γ signalling is regulated via controlled expression of two receptors; IFNGR1 and IFNGR2 whose distribution is varied across many cell types (Kak, Raza and Tiwari, 2018). During inflammation, macrophages secrete IL-12 and IL-18 which activate natural killer and T cells to produce IFN-γ. This is turn further activates the macrophages and elicits their polarization to M1 (Fultz *et al.*, 1993), resulting in auxiliary downstream pro-inflammatory mediator release such as IL-12 (Schroder *et al.*, 2004). The coordination of IL-12 and IFN-γ link pathogen recognition by innate cells to the induction of specific immunity through amplifying or stabilizing the Th1 response via a positive feedback loop (Boehm *et al.*, 1997).

In relation to IBD, IFN-γ is noted to be overproduced by macrophages in the lamina propria within colitis rodent models, which was also correlated with disproportional, dominant Th1 responses and thus is seen as a key contributor to

IBD progression (Powrie and Leach, 1995; Fiocchi, 1998; Monteleone *et al.*, 1998). This dominance of Th1 phenotype and excessive secretion of INF-γ is also implicated in Crohn's disease patients when compared with healthy controls (Hugot *et al.*, 1996). Further critical in the context of IBD, macrophage-derived IFN-γ has been associated with restraint of bacterial growth with reports demonstrating administration of IFN-γ inhibitors in IFN-γ $^{-/-}$ BALB/c and A/J mouse models result in increased Legionella pneumophila bacterial growth in infected macrophages (Salins *et al.*, 2001), while IFNGR$^{-/-}$ bone marrow-derived macrophage studies showed increased *Chlamydia pneumoniae* load (Rothfuchs *et al.*, 2001). Further articles also correlate a decreased resistance to bacterial, viral, and parasitic infections in animals lacking IFN-γ or IFNGR1 (Suzuki *et al.*, 1988; van den Broek *et al.*, 1995; Pearl *et al.*, 2001). Furthermore, upregulation of MHC I by IFN-γ has been associated with the increased potential of cytotoxic T cell recognition of peptides, and thus the host response to pathogens and cell-mediated immunity (Johnson and Pober, 1990; Chang *et al.*, 1992). Thus, although noted to potentiate inflammation within an IBD setting and encourage pro-inflammatory dominance, IFN-γ is essential for bacterial elimination – a key driver of IBD pathology. Therefore, increased production by minocycline noted within the M2 cultures may simultaneously allow for exaggerated bacterial recognition and neutralization, while also reducing confounding pro-inflammatory cytokine release minimising local and systemic damage.

On the contrary, IL-10 is a potent anti-inflammatory and immune-suppressive cytokine, produced by cells of both innate and adaptive immunity (Moore *et al.*, 2001; Mollazadeh *et al.*, 2019). It is a noncovalent alpha helical homodimer with the IL-10 receptor (IL-10R) consisting of two fractions; IL10R1 and IL10R2 which are expressed on the surface of most hematopoietic cells, including T cells, B cells, and macrophages (Oft, 2014). During infection IL-10 inhibits the activity of Th1 cells, natural killer cells, and macrophages, and although all are required for optimal pathogen clearance, dysregulation results in aberrant tissue damage. Thus, consequently, IL-10 can both impede pathogen clearance but also ameliorate immunopathology. M2-like macrophages are able to secrete high levels of IL-10 and low or negligible levels of proinflammatory cytokines such as IL-12 (Vogel *et al.*, 2014). Ablation of IL-10 signalling has been reported to promote severe and often fatal immunopathology in various infectious models

(Gazzinelli *et al.*, 1996; Hunter *et al.*, 1997; Li, Corraliza and Langhorne, 1999). IL-10 alone, and through cooperation with Th1 cytokines is also able to regulate Th2 responses to prevent the overproduction of IL-4, IL-5 and IL-13, which are attributed to the development of severe fibrosis (Schandené *et al.*, 1994; Wynn, 2004; Couper, Blount and Riley, 2008).

In the setting of IBD, IL-10 plays an important physiological role with genetic models of IL-$10^{-/-}$ mice developing the disease (Berg *et al.*, 1996; Glocker *et al.*, 2009). This may be due, in part, to its potent anti-inflammatory action as seen in models of bacterial endotoxemia. In these animal models chronic LPS administration results in vascular shock and death via production of inflammatory cytokines IL-12 and IL-23 from upstream TLR signalling. A regulatory side effect of LPS stimulation is the induction of IL-10 which behaves as a negative regulator through STAT3 of IL-12 and IL-23, which is highlighted in IL-$10^{-/-}$ models whereby the animals become extremely sensitive to the LPS-induced shock (Berg *et al.*, 1995). Moreover, other authors also report expansion of pro-inflammatory Th17 cells and suppression of Tregs in similar *in vivo* IL-$10^{-/-}$ models (Chaudhry and Rudensky, 2013).

The data displayed in section 5.4. showed an inverse relationship of IFN-γ and IL-10 when minocycline was administered during M2 polarization of PBMC-derived macrophages. Here minocycline concurrently inhibited IL-10 production while causing an increase in IFN-γ and IL-12. Given the current literature, and as the same outcome was not reported amongst the M1 populations, a homeostatic role of minocycline on M2 macrophage phenotype was considered, whereby it seems to regulate the usual biology of M2 subsets. By limiting IL-10 production but promoting IFN-y and IL-12, minocycline may have therapeutically consequential influence on maintaining host response to pathogens through preserving the pathogen recognition ability of $CD4^+$ T cells and natural killer cells, and stabilising the Th1 response, but also limiting the macrophages' own ability to produce pathologically high levels of other pro-inflammatory mediators like IL-6, IL-1β and TNF-α.

It must also be observed that an unexpected significant increase in IL-10 following polarization to M1 using the PBMCs was described. When consulted, the literature provided rationale for this finding with reports highlighting the ability of macrophages to produce IL-10 in response to TLR receptor ligands such as LPS

through involvement of MAPKs and transcription factors (Elcombe *et al.*, 2013; Vliet *et al.*, 2013; Sanin, Prendergast and Mountford, 2015). This IL-10 induction following LPS is also attributed to a negative feedback system whereby it is produced in order to inhibit IL-12 and IL-23 production, downstream expression of other pro-inflammatory mediators, in addition to continued signalling via surface PRRs (Berg *et al.*, 1995; Oft, 2014). Furthermore, given previous evidence that macrophages can produce high levels of IL-10 Baseler *et al* identified a role of autocrine IL-10 in maintaining M1 macrophage metabolic equilibrium via regulation of mTOR and NO production following LPS stimulation (Baseler *et al.*, 2016). These reports, in conjunction with the cytokine profiling, suggest polarization via IFN-γ and LPS incubation of PBMC-derived macrophages results in increased production of IL-10 which may aid in internal inflammation regulation whilst also providing cellular protection from LPS-induced shock as previously reported in IL-$10^{-/-}$ murine models (Berg *et al.*, 1995).

Finally, when assessing the expression of transcription factors key to modulating M1/M2 macrophage polarization with and without minocycline treatment some unexpected results were obtained. In section 5.5.1. an increased expression of *stat1* and *stat2* following M1 macrophage polarization was reported. This upregulation in expression is consistent with the literature which widely describes M1 polarization to be promoted by JAK–STAT signalling via interaction with IFN-γ. Here, activation of the IFN-γ receptor triggers JAK-mediated tyrosine phosphorylation and dimerization of STAT1 (Darnell, Kerr and Stark, 1994). Studies into macrophages from STAT$1^{-/-}$ mice report a dependency of STAT1 on gene expression following stimulation by type I IFNs and IFN-γ (Ohmori and Hamilton, 1997). Similar studies using STAT1-deficient mice also demonstrated consequential severe defects in immunity to intracellular bacterial and viral pathogens given their dependency on IFN/STAT1 signalling (Durbin *et al.*, 1996). In relation to STAT2, the most prominent active STAT complex is the STAT1–STAT2 heterodimer, which recruits IRF9 to form the IFN-stimulated gene factor 3 (ISGF3) complex. This complex subsequently binds to interferon-stimulated response elements (ISREs), which are found in M1 signature genes (Lawrence and Natoli, 2011).

The data shown in this chapter is consistent with the scientific consensus in this regard, with clear evidence that *stat1/stat2* expression plays a critical role in M1

macrophage polarization. What was unexpected, however, was the higher gene expression signature for *irf5* found in the M2 cultures. The literature is almost universal in its depiction of IRF5 as a major regulator of M1 polarization (Krausgruber *et al.*, 2011; Sun *et al.*, 2016; Corbin *et al.*, 2020), with experiments using IRF5 siRNA therapy correlated to phenotype switching from M1 to M2 (Sun *et al.*, 2016), and others showing that IRF5 directly activates transcription of M1 proinflammatory cytokines, such as IL-12 and IL-23, and repressing its transcription severely impairs the expression of these cytokines (Krausgruber *et al.*, 2011). At present, no reports can be found to substantiate any reasoning for an increase in *irf5* expression within the M2 population.

Moreover, significant and consistent upregulation of *pparg* within the M2 polarized PBMC macrophages shown in section 5.5.1. is corroborated by the current literature with plentiful published data supporting its role in M2 polarization (Lawrence and Natoli, 2011; Luo *et al.*, 2017). PPAR-γ is a key regulator of lipid metabolism in macrophages and boasts potent anti-inflammatory properties that modulates the immune inflammatory response (Ricote *et al.*, 1999). PPAR-γ activation alleviates inflammatory response through several mechanisms, including the interference and trans-repression of genes such as NF-κB and STAT (Ricote *et al.*, 1998; Lehrke and Lazar, 2005; Pascual *et al.*, 2005). Activation of PPAR-γ was recently found to play an important role in macrophages polarization, with STAT6 acting as a cofactor in PPAR-γ-mediated gene regulation, suggesting a crosstalk between PPAR-γ and the IL-4–STAT6 axis in the regulation of M2 phenotype acquisition (Szanto *et al.*, 2010; Villanueva and Tontonoz, 2010). The activation of PPAR-γ induces a phenotypic change of macrophages from M1 to M2 at sites of inflammation, with the absence of PPAR-γ signalling resulting in continued secretion of pro-inflammatory cytokines by macrophages (Bouhlel *et al.*, 2007b; Abdalla *et al.*, 2020). Reports have also linked a disruption of PPAR-γ to impaired M2 macrophage activation (Odegaard *et al.*, 2007).

However, the data illustrating *stat3* amplification following M1 macrophage polarization and not M2 were somewhat unexpected given a key role of STAT3 in mediating anti-inflammatory effects of IL-10 via ameliorating inflammatory responses and inhibiting pro-inflammatory cytokine production (Riley *et al.*, 1999; Takeda *et al.*, 1999). STAT3 activation in macrophages enhances macrophage

proliferation and survival, while also potentiating angiogenesis, immune tolerance, extracellular matrix remodelling, and efferocytosis (Kujawski *et al.*, 2008; Campana *et al.*, 2018). Furthermore, previous data in murine models of septic peritonitis indicated a role of STAT3 as an important regulator of macrophages in inflammation maintenance (Matsukawa *et al.*, 2003). However, STAT3 was initially discovered as a transcription factor activated by IL-6 family cytokines through gp130, and only in the presence of STAT3 was IL-10 able to down regulate inflammatory cytokine TNF-α in macrophages (Zhong, Wen and Darnell, 1994; Riley *et al.*, 1999). Furthermore, mechanistically, IL-10 induces the phosphorylation of STAT3 in macrophages thereby intercepting inflammatory responses to LPS or other PRR stimulants via downstream signalling and inhibition of pro-inflammatory mediators (Oft, 2014). In summary, these reports, taken in conjunction with the cytokine profiling of both generated macrophage phenotypes outlined in section 5.2 may suggest an autocrine activation of STAT3 within the M1 cultures as a result of high IL-6 and IL-10 production, which may provide rationale to the increased gene expression seen in this model.

Finally, given the literature, it was unexpected to see an increase in *stat6* displayed by the M1 cultures, in addition to a decrease in expression following M2 polarization. M2 macrophage polarization involves phosphorylation of the tyrosine residue, and subsequent activation of STAT6. This process then mediates the transcriptional activation of M2 macrophage-specific genes such as arginase 1 (*Arg1*), mannose receptor 1 (*Mrc1*), resistin-like α (*Retnla* / *Fizz1*) and chitinase-like protein 3 (*Chil3* / *Ym1*), in addition to the chemokine genes *Ccl17* and *Ccl24* (Goenka and Kaplan, 2011). IL-4 activates STAT6 via the IL-4 receptor (IL-4R1 and IL-4R2) to regulate M1/M2 polarization via a STAT6-dependent pathway (He *et al.*, 2020). The critical role of STAT6 in M2 polarization is further reflected in the correlation between enhanced M2 gene expression following STAT6 overexpression, and inversely abolished M2 gene expression in macrophages deficient in STAT6 (Yu *et al.*, 2019). Again, no current reports provide reasonable explanation as to why *stat6* would be declined in M2 and up in M1 macrophages, however, clear inconsistency between donors may simply imply the generation of unreliable results due to limited replicates. Future analysis of the effect of minocycline should be interpreted with this undefined baseline in mind.

When treatment with minocycline was introduced as outlined in section 5.5.2. a depression of *stat3* and *stat6* expression within M1 macrophage cultures was shown which was not replicated following M2 polarization. Binding of IL-10 to the IL-10 receptor complex results in activation of intracellular signal-transduction, via Jak1-mediated activation of STAT3 - a key mediator of the anti-inflammatory effects of IL-10 (Riley *et al.*, 1999). As mentioned in chapter 4, reports utilising STAT3 knock-out murine models have depicted STAT3 as a crucial protein for the transmission of anti-inflammatory signals in macrophages whereby deletion of the gene resulted in the spontaneous development of enterocolitis and increased susceptibility to LPS-mediated shock and septic peritonitis (Takeda *et al.*, 1999; Matsukawa *et al.*, 2003). This is attributed to the unregulated inflammatory response observed in the experimental animals, in addition to the inability of IL-10 to mediate its suppressive effects. *In vitro* macrophage models also report impaired bactericidal activity in $STAT3^{-/-}$ cells which resulted in a reduced ability to clear bacterial infections (Matsukawa *et al.*, 2003). Further gene expression studies have further supported this narrative, indicating a requirement of STAT3 by IL-10 in order to impart its activation program following LPS stimulation (Lang *et al.*, 2002). Although IL-10 signalling can also trigger the phosphorylation of STAT1 and STAT5, STAT3 is the transducer of the inhibitory signal and is an essential anti-inflammatory and deactivating factor (Moore *et al.*, 2001; Lang, 2005).

In the context of STAT6, IL-4 and IL-13 promote alternative macrophage activation by inducing the tyrosine phosphorylation and dimerization of STAT6, which in turn regulates a distinct gene expression programme that is distinct from, and in some respects antagonistic to, M1 activation (Gordon, 2003; Olefsky and Glass, 2010). Many genes associated with M2 macrophages are regulated by STAT6, including resistin-like-α (Retnla, or FIZZ1), arginase 1 (Arg1), chitinase 3-like 3 (Chi3l3 or YM1), and CD206 (macrophage mannose receptor 1 - Mrc1) (Lawrence and Natoli, 2011). STAT6 has diverse and complex functions in mediating distinct gene expression profiles in a variety of cell types involved in inflammation. While STAT6 is required for normal immune function, it has been implicated as a crucial factor in the development of pathologies such as excessive mucus production, Th2 cell accumulation, tissue remodelling, and hyper-responsiveness (Thai *et al.*, 2005; Kuperman and Schleimer, 2008; Maier, Duschl

and Horejs-Hoeck, 2012). The expression of MHC class II by macrophage in response to IL-13 are also greatly impaired in STAT6-deficient mice (Takeda *et al.*, 1996). STAT6 has also been attributed to colitis exacerbation, with a 2005 study by Elrod *et al* reporting a significant increase in disease activity index and production of IFN-γ in STAT6$^{-/-}$ mice versus wildtype upon induced DSS colitis (Elrod *et al.*, 2005). This supported the hypothesis that STAT6 is an important regulator of IBD pathogenesis, partially through modulation of IFN-γ.

As outlined previously, interferons play a key role in the host defence against viruses and infection. Both IFN receptors (Type 1 and type 2) signal through the JAK-STAT pathway, in which JAKs phosphorylate STATs, followed by translocation to the nucleus for the induction of IFN-stimulated genes (Schroder *et al.*, 2004). Type 1 IFN signalling activates STAT1 and STAT2 which create a heterodimer and associate with interferon regulatory factor-9 (IRF9) to form IFN-stimulated gene factor-3 (ISGF3), while type 2 IFN signalling activates STAT1 only, whose homodimer binds to DNA at γ-activated sequence (GAS) elements (Rauch, Müller and Decker, 2013). To better understand STAT2 signalling, *stat2*$^{-/-}$ models have been utilised and showed the animals becoming unresponsive to type 1 IFNs and subsequently sensitive to infection (Park *et al.*, 2000). Indirect studies have further suggested that the type I IFN autocrine/paracrine loop regulates lymphocyte function with reports demonstrating downregulation of lymphopoiesis and the promotion of memory T cell survival (Lin, Dong and Cooper, 1998; Marrack, Kappler and Mitchell, 1999).

The findings within this chapter, therefore, could further support the hypothesis that sees minocycline exert a regulatory role over anti-inflammatory phenotype switching in respect to decreased *stat3* and *stat6,* however this conclusion is difficult to ascertain given that the earlier data in section 5.3. may correlate increased *stat3* expression to autocrine signalling by IL-10 and IL-6, both of which were reported to be decreased by minocycline in this M1 model. Therefore, a subsequent decrease in *stat3* expression may simply be a direct influence of a reduction in stimulatory cytokine production, or directly due to minocycline inhibiting gene expression thus STAT3 protein transcription and translation. Meanwhile, a reduction in *stat2* and *stat6* driven by minocycline may indicate a regulatory function of minocycline over the macrophage phenotype acquisition and plasticity as simultaneous reduction of both the pro-inflammatory driver *stat2*

and the anti-inflammatory mediator *stat6* was seen. This could cooperatively allow the dampening of further pro-inflammatory stimulation, in addition to limiting an aberrant switch to potent anti-inflammatory programmes which may result in the development of M2 macrophage pathophysiology. Furthermore, a lack of genetic modification by minocycline within the M2 cultures in relation to either M1 or M2 associated transcription factors may indicate preferential function of minocycline on macrophages in pre-established pro-inflammatory states. This could prove therapeutically beneficial whereby minocycline doesn't seem to drastically alter the biology of anti-inflammatory macrophage populations but exerts potent modification of inflammatory subsets.

Accumulating evidence supports the idea that enforcing a pro-resolving M2 macrophage phenotype might be a novel therapeutic approach to control intestinal inflammation and restore tissue integrity (Na *et al.*, 2019b). This idea is corroborated by evidence demonstrating how most classic IBD therapies such as mesalazine and infliximab already affect macrophage function through inhibition of inflammatory signalling pathways and/or inducing polarization of alternatively activated macrophages (Bantel *et al.*, 2000; Vos *et al.*, 2012). In murine models of DSS-induced colitis whereby individuals are deficient in M2 polarized macrophages, researchers report a higher susceptibility of these animals to the colitis stimuli (Takada *et al.*, 2010). Further human studies have also identified IBD susceptibility loci being strongly correlated with promotors regulated in response to LPS, and thus macrophage activation and phenotype acquisition (Baillie *et al.*, 2017), with additional evidence suggesting a causal link between altered macrophage phenotype and defects in the resolution of intestinal inflammation (Smith *et al.*, 2009b).

Here, further support to the concept of utilizing macrophage polarization and phenotype plasticity in the regulation of inflammation has been provided. In this instance inflammation management is exerted by treatment with minocycline administered during macrophage polarization where concurrent modification of surface marker expression, cytokine production and transcription factor expression is noted, all of which seem to restrain aberrant macrophage function whilst not hindering their ability to respond to potential antigen challenge.

6. Results: Effect of minocycline on the response of M1/M2 macrophage subsets to LPS activation

Chapters 4 and 5 have outlined and discussed the effect of minocycline on how resting M0 macrophages respond to the inflammatory stimulus LPS, in addition to its influence on the acquired phenotype following *in vitro* polarization to M1 and M2 subsets. This chapter next explores the role of minocycline on the response of pre-polarized M1 and M2 macrophage subsets when challenged with LPS. Functional diversity is one of the key features of macrophages and can be attributed to their ability to respond to different microenvironmental cues by displaying equally diverse functional phenotypes (Gordon and Taylor, 2005). Macrophage polarization and disorders in bacterial recognition by macrophages are strongly correlated with the pathogenesis of IBD, and thus plays a vital role in the development and progression of inflammation with the imbalance between M1 and M2 switching a key point of disease initiation (Mahida, 2000; Rogler, 2004; You *et al.*, 2016). In IBD, macrophages migrate to the inflamed colonic mucosa, and following interaction with bacteria and bacterial products results in increased production of IL-1, IL-6, TNF-α, IL-12 and IL-23 (Seyedizade *et al.*, 2020).

In murine experimental models of DSS-induced colitis the population of M1 macrophages increases, while the M2 population decreases (Zhu *et al.*, 2014). This reduction of M2 macrophages attenuates colitis through inhibiting the production of IL-10 and subsequent upregulation of T-cell generation. M1 macrophage neutralization of IL-10 and its inhibition of LPS/TLR4-mediated production of TNF-α and IL-1β and down-regulate Th1 and Th17 responses by increasing CD4+ Foxp3+ Tregs in inflamed tissues reduces the effects of M2 macrophages (Bogdan *et al.*, 1992; Sica and Bronte, 2007). Thus, this disequilibrium of M1 and M2 phenotypes has been correlated with colitis progression in murine model of IBD (Zhu *et al.*, 2014). Therefore, it was of interest to complete the investigations by looking at the activation status of both phenotypes given this would be a recurrent situation within affected gastrointestinal tracts.

6.1. THP-1

6.1.1. Characterising LPS-activation of M1 THP-1-derived macrophages

Having pre-established a reliable protocol for the polarization of THP-1-derived macrophages to an M1 phenotype as was described in chapter 5 section 1.1, the next task was to understand how subsequent activation with LPS would affect the surface marker expression profile of the cells, to which the effects of minocycline could then be studied. For this investigation, and all subsequent work on this objective, the same markers as previously described were analysed which include CD14, CD11b (active conformation), CD80, CD86, CD163 and CD206. Here, THP-1 monocytes were differentiated to resting M0 macrophages via incubation with PMA (80nM) as described in chapter 5, section 1.1, then polarized to M1 using IFN-γ (20ng/mL) and LPS (10ng/mL) following the protocol also outlined in chapter 5 section 1.1. Once polarized, cells were then activated for a further 24hr with 100ng/mL LPS, consistent with that used when assessing the effect of minocycline on M0 activation in chapter 4. At this point supernatant was collected and stored at -70°c for cytokine determination and cells were collected and stained for surface marker analysis.

As a result of LPS activation of the polarized M1 macrophages, there was an upregulation of the percentage of $CD14^+$ cells as shown in Figure 6.1A and C and an increase in the density of CD14 expression (MFI) up by 1.3-fold versus the un-activated control (Figure 6.1B and D). No significant changes in expression were seen for the percentage of $CD11b^+$ cells following LPS activation of M1 macrophages, nor in the density of CD11b expression where replicates appear inconsistent (Figure 6.1A, B and F).

It is interesting to note that while in the model of M0 macrophages, LPS induced a decreased in CD14 expression, as shown in chapter 4, section 1.1, here in the model of polarized M1 macrophages, LPS exposure seems to promote an increase in CD14 expression (Figure 6.1A-C). In chapter 4, based on the presented data and in conjunction with the literature, a role of CD14 membrane shedding as an explanation for a decrease in expression following LPS activation of M0 macrophages was previously hypothesised considering CD14 is required for the macrophage response to endotoxin (Gangloff *et al.*, 2005; da Silva *et al.*,

2017). In this instance, however, when M1 macrophages were activated with LPS, a different mechanism was considered by which chronic exposure to LPS (during polarization and subsequent activation) may intensify CD14 upregulation as has been previously shown in different cellular models (Nockher and Scherberich, 1995; Brass *et al.*, 2007), perhaps through inhibition of membrane shedding as one possible mechanism (Delgado *et al.*, 1999; Ciesielska, Matyjek and Kwiatkowska, 2021).

The expression of CD80 and CD86, which were increased in M1 macrophages compared to M0 following polarization, were further increased after LPS activation of the pre-polarized M1 macrophages. Both the percentage of positive cells and density of expression for CD80 and CD86 were significantly increased following LPS activation compared to the expression in the non-activated M1 macrophage baseline (Figure 6.2A-F), As discussed previously, the literature supports the existence of high expression of CD80 and CD86 following M1 polarization, in addition to also being independently induced by LPS (Lim *et al.*, 2005; Rivellese *et al.*, 2014; Bertani, Mozetic, Fioramonti, Iuliani, *et al.*, 2017; Raggi *et al.*, 2017; Feito *et al.*, 2019; Taddio *et al.*, 2021). The data obtained during this model highlight a further enhancement of expression when these two independent stimuli are used in tandem.

Interesting, data was also obtained in relation to the M2-associated markers CD163 and CD206. Here, 24hr incubation of M1 macrophages with LPS resulted in expansion of the percentage of $CD163^+$ and $CD206^+$ cells, which was also reflected in the values pertaining to MFI (Figure 6.3A-F). This contrasted with the previous data from chapter 4 which showed LPS activation of M0 macrophages have an opposing influence on CD163 and CD206 expression. A possible explanation for these findings may again be attributed to the chronic exposure of the M1 macrophages to LPS in this model. Guzmán-Beltrán *et al* (2017) were able to show an altered and more M1-biased phenotype acquisition for macrophages following chronic exposure to LPS with the resultant cells displaying a $CD14^+CD206^+$ signature (Guzmán-Beltrán *et al.*, 2017). Other papers have also indicated an initial membrane shedding of CD163 from monocytes following LPS stimulation but which is followed by a recovery phase and secondary induction of surface CD163 to higher levels that of the un-activated baseline (Weaver *et al.*, 2007).

Therefore, a role of chronic LPS exposure on the procurement of M2-like marker signatures within this model was hypothesised which together present an activated M1 population possessing comparatively high levels of M2-associated markers CD163 and CD206.

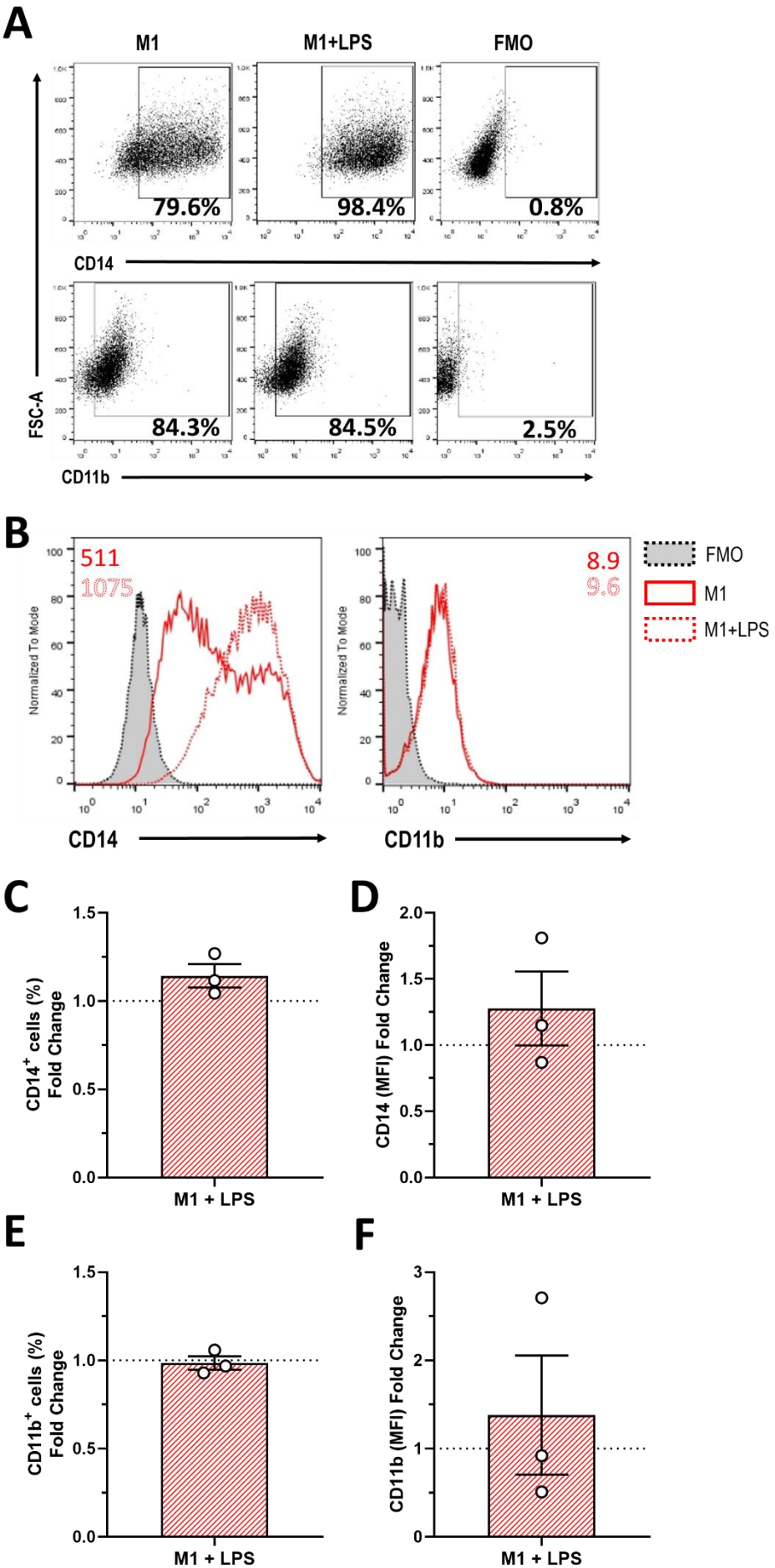
A
M1
M1+LPS
FMO
79.6%
98.4%
0.8%
CD14
84.3%
84.5%
2.5%
FSC-A
CD11b
B
511
1075
8.9
9.6
Normalized To Mode
FMO
M1
M1+LPS
CD14
CD11b
C
CD14+ cells (%) Fold Change
M1 + LPS
D
CD14 (MFI) Fold Change
M1 + LPS
E
CD11b+ cells (%) Fold Change
M1 + LPS
F
CD11b (MFI) Fold Change
M1 + LPS

Figure 6.1: CD14 and CD11b expression profile of LPS-activated M1 macrophages derived from THP-1. Data obtained after 24hr incubation of polarized M1 macrophages with LPS (100ng/mL). [A] Representative dot plots showing the percentage of $CD14^+$ (top) and $CD11b^+$ (bottom) cells. [B] Representative histograms showing mean fluorescent intensity (MFI) for CD14 (left) and CD11b (right). Numbers indicate MFI of live gated population. [C-F] Bar graphs showing the percentage of $CD14^+$ [C] and $CD11b^+$ [E] cells, and MFI values for CD14 [D] and CD11b [F]. Data normalised and displayed as fold change versus the non-activated M1 macrophage indicated at 1. Data represents 3 replicated experiments each comprising of triplicate values. Data presented as mean ± SEM. Unpaired *t* test applied versus the un-activated M1 macrophage.

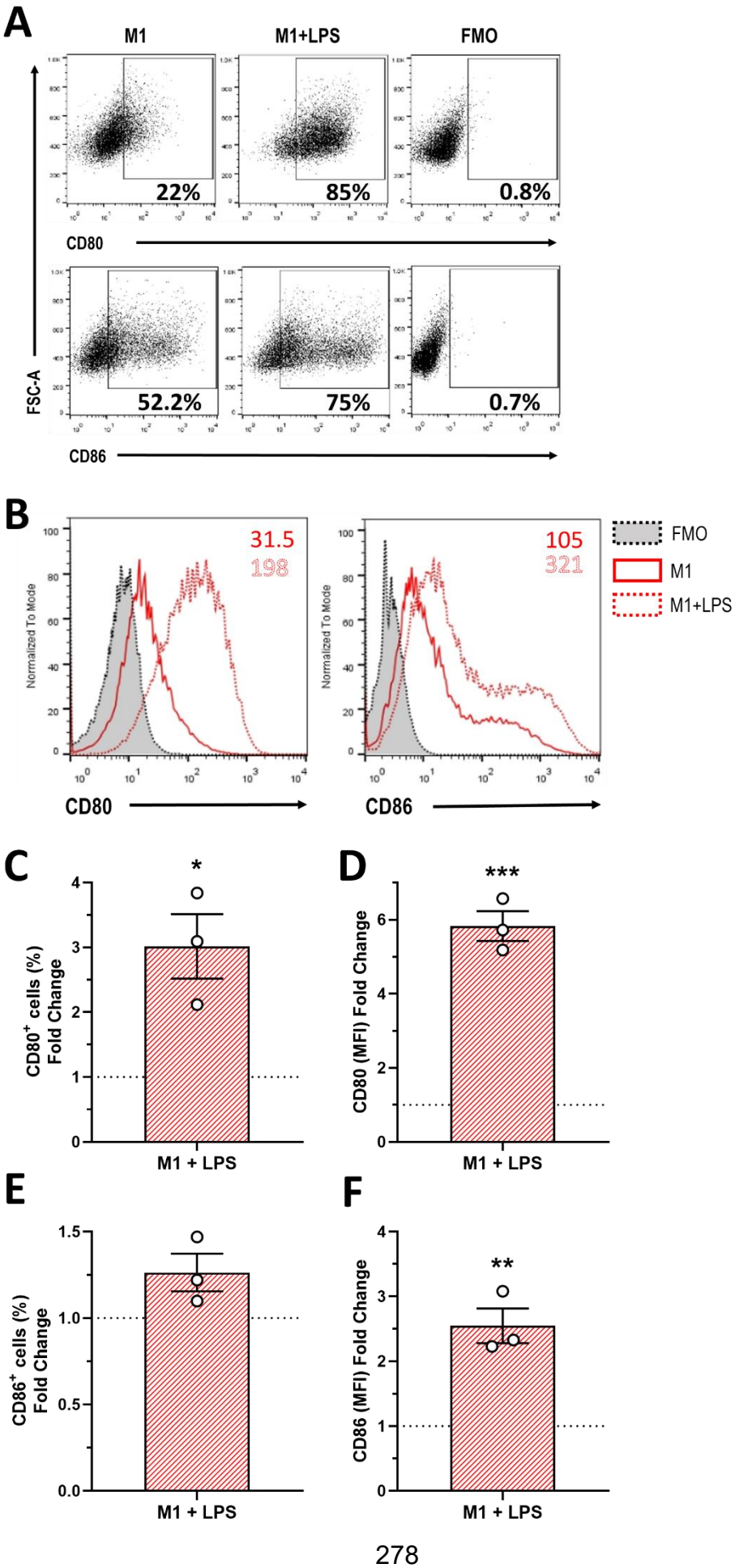
A
M1
M1+LPS
FMO
22%
85%
0.8%
CD80
52.2%
75%
0.7%
FSC-A
CD86
B
31.5
198
105
321
Normalized To Mode
FMO
M1
M1+LPS
CD80
CD86
C
*
CD80+ cells (%) Fold Change
M1 + LPS
D
***
CD80 (MFI) Fold Change
M1 + LPS
E
CD86+ cells (%) Fold Change
M1 + LPS
F
**
CD86 (MFI) Fold Change
M1 + LPS

Figure 6.2: CD80 and CD86 expression profile of LPS-activated M1 macrophages derived from THP-1. Data obtained after 24hr incubation of polarized M1 macrophages with LPS (100ng/mL). [A] Representative dot plots showing the percentage of $CD80^+$ (top) and $CD86^+$ (bottom) cells. [B] Representative histograms showing mean fluorescent intensity (MFI) for CD80 (left) and CD86 (right). Numbers indicate MFI of live gated population. [C-F] Bar graphs showing the percentage of $CD80^+$ [C] and $CD86^+$ [E] cells, and MFI values for CD80 [D] and CD86 [F]. Data normalised and displayed as fold change versus the non-activated M1 macrophage indicated at 1. Data represents 3 replicated experiments each comprising of triplicate values. Data presented as mean ± SEM. Unpaired *t* test applied versus the un-activated M1 macrophage. *p<0.05; **p<0.01; ***p<0.001.

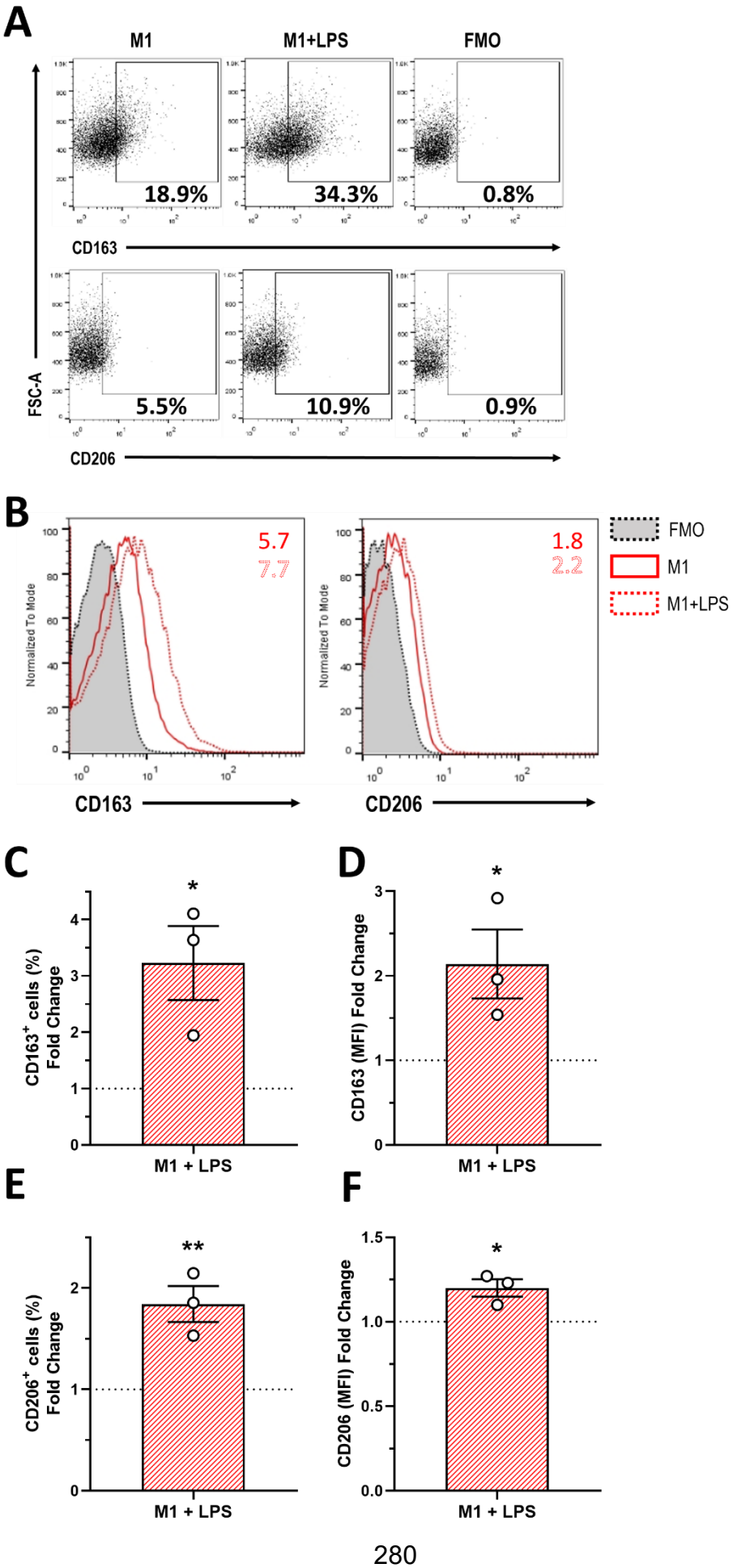
A
M1
M1+LPS
FMO
18.9%
34.3%
0.8%
CD163
FSC-A
5.5%
10.9%
0.9%
CD206
B
5.7
7.7
1.8
2.2
Normalized To Mode
FMO
M1
M1+LPS
CD163
CD206
C
CD163+ cells (%) Fold Change
M1 + LPS
D
CD163 (MFI) Fold Change
M1 + LPS
E
CD206+ cells (%) Fold Change
M1 + LPS
F
CD206 (MFI) Fold Change
M1 + LPS

Figure 6.3: CD163 and CD206 expression profile of LPS-activated M1 macrophages derived from THP-1. Data obtained after 24hr incubation of polarized M1 macrophages with LPS (100ng/mL). [A] Representative dot plots showing the percentage of $CD163^+$ (top) and $CD206^+$ (bottom) cells. [B] Representative histograms showing mean fluorescent intensity (MFI) for CD163 (left) and CD206 (right). Numbers indicate MFI of live gated population. [C-F] Bar graphs showing the percentage of $CD163^+$ [C] and $CD206^+$ [E] cells, and MFI values for CD163 [D] and CD206 [F]. Data normalised and displayed as fold change versus the non-activated M1 macrophage indicated at 1. Data represents 3 replicated experiments each comprising of triplicate values. Data presented as mean ± SEM. Unpaired *t* test applied versus the un-activated M1 macrophage. *p<0.05; **p<0.01.

6.1.2. Effect of Minocycline on LPS-activation of M1 THP-1-derived macrophages

Once the effect of LPS activation on M1 macrophage surface marker expression was determined, the effects of minocycline within this model were studied. For that, minocycline was administered to the M1 macrophage cultures at 10μM and 25μM, 2hr prior to the addition of LPS. This was left to incubate for a further 24hr at which point supernatants and cells were collected for further analysis.

In this model, minocycline did not seem to modify the percentage of $CD14^+$ cells following administration of both 10μM and 25μM versus LPS (Figure 6.4A and C). When analysing the mean fluorescent intensity (MFI) however, minocycline at both concentrations resulted in a decrease in CD14 expression versus the LPS-activated M1 group. Here, minocycline at 25μM was able to restore expression values back to the un-activated baseline and beyond, reducing the expression by 0.9-fold versus the LPS control group (p=0.3762) (Figure 6.4D). Despite no conclusive influence of LPS on the expression of CD11b in its activated form seen when administered alone, pre-incubation with minocycline at 25μM appeared to marginally reduce both the percentage of $CD11b^+$ cells and the density of CD11b expression compared to LPS but failed to reach significance (Figure 6.4B, E and F).

When assessing the M1-associated inflammatory markers CD80 and CD86 minocycline further increased their expression when compared to the LPS-activated M1 group. LPS alone increased the percentage of $CD80^+$ cells by 57.9% up from 32.1% in the non-activated control to 90% (Figure 6.5A and C). However, pre-treatment with minocycline surpassed this effect and resulted in a further increase to 99.3% and 99.8% exerted by 10μM and 25μM respectively

(Figure 6.5A and C). This increase in expression resulted in almost 100% of the population displaying a $CD80^+$ signature. Regarding MFI, upregulation of CD80 upon minocycline treatment was once again observed when compared to LPS alone, witnessing a positive correlation between increased minocycline concentration and increased CD80 upregulation (Figure 6.5B and D). Figure 6.5B and D illustrates minocycline at 10μM cause a 2-fold increase in CD80 expression, and 25μM a 6.3-fold increase (p=0.0374) versus the LPS control. Moreover, figure 6.5A, B, E and F show pre-incubation with 25μM minocycline caused a 6% and 0.3-fold increase in the percentage of $CD86^+$ cells and density of CD86 expression respectively when compared to the LPS control.

Regarding the expression of the M2-associated markers CD163 and CD206, which were increased upon LPS-activation as shown in section 4.1, minocycline intervention resulted in a further upregulation of the expression both proteins versus LPS. In the context of CD163, LPS alone increased the percentage of $CD163^+$ cells by 24% up from 12% in the non-activated control to 36% (Figure 6.5A and C). However, pre-treatment with minocycline exceeded this effect and resulted in a further increase to 83.3% (p=0.0016) and 97.6% (p=0.0002) exerted by 10μM and 25μM respectively (Figure 6.6A and C). Alike CD80, this increase in expression resulted in almost 100% of the population displaying a $CD163^+$ signature. Also, when assessing the density of CD163 expression there was again a positive correlation between an increase in minocycline concentration and an increase in CD163 expression, with 10μM eliciting a 3-fold increase, and 25μM a 13.7-fold (p=0.0043) increase versus LPS (Figure 6.6B and D). Data associated with CD206 expression also saw minocycline result in nearly all cells expressing CD206, with 10μM increasing the percentage by 56.8% (p=0.0043) and 25μM by 82.2% (p=0.0003) versus LPS alone (Figure 6.6E). Moreover, the previously described positive correlation between minocycline concentration and marker modification was again illustrated in the CD206 MFI data where minocycline at 10μM and 25μM elicited a 3.1-fold and 14.7-fold (p=0.0119) increase versus LPS respectively (Figure 6.6F).

This data communicates a similar narrative to that described in chapter 4 whereby minocycline seems to consolidate, and even exacerbate the effects of LPS in relation to upregulation of CD80, while also significantly increasing the expression of M2-associated markers CD163 and CD206, despite the potent pro-

inflammatory stimulus. It was also interesting to report a decrease in CD14 and CD11b expression upon minocycline treatment within this model, data which again suggests a possible influence of minocycline on the ability of these macrophages to continue responding to exogenous inflammatory ligands, in addition to their ability to mediate leukocyte adhesion, activation and accumulation in sites of infection (Khan, Khan and Gupta, 2018).

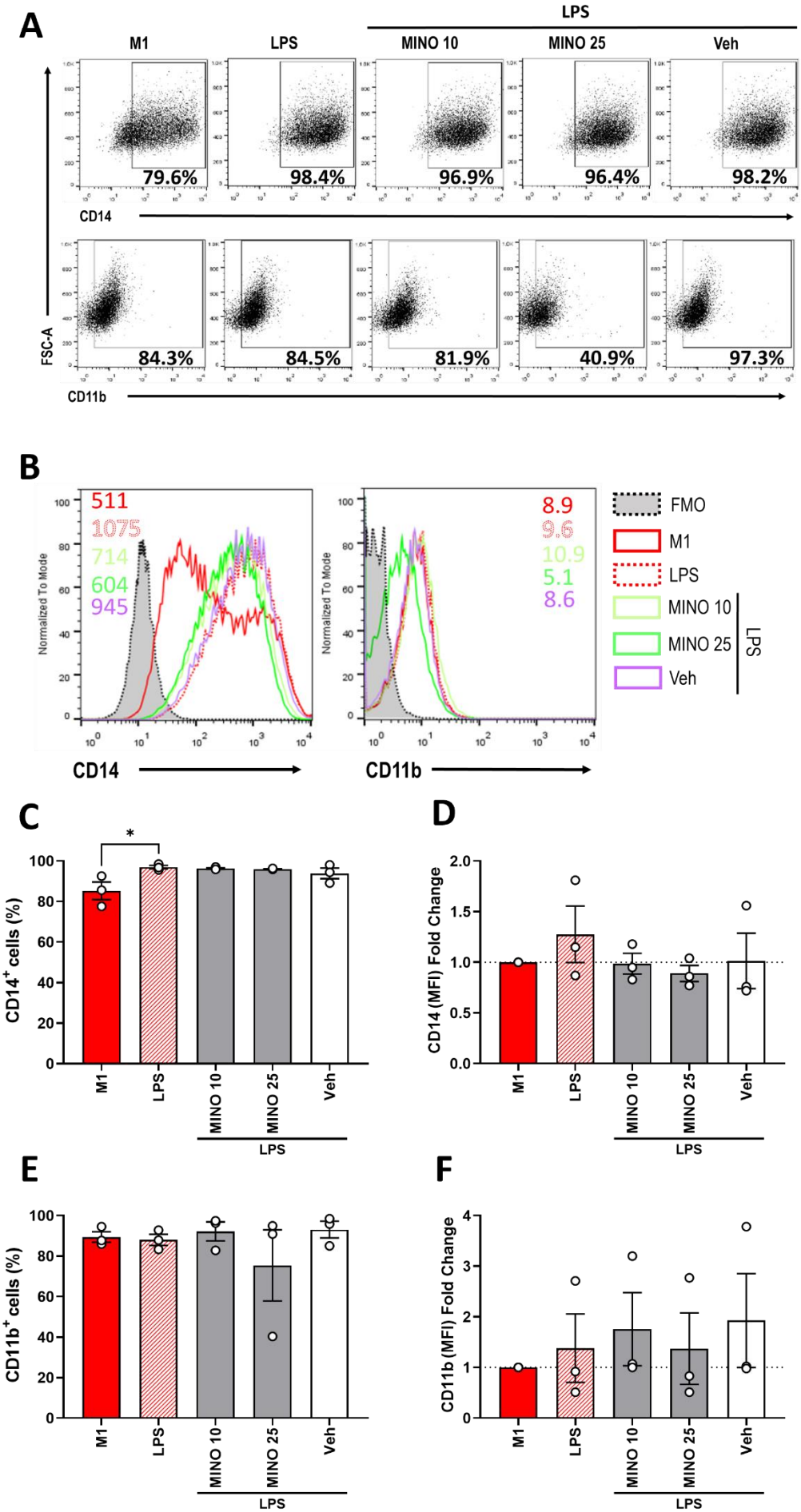
A
LPS
M1
LPS
MINO 10
MINO 25
Veh
79.6%
98.4%
96.9%
96.4%
98.2%
CD14
84.3%
84.5%
81.9%
40.9%
97.3%
FSC-A
CD11b
B
511
1075
714
604
945
8.9
9.6
10.9
5.1
8.6
Normalized To Mode
FMO
M1
LPS
MINO 10
MINO 25
Veh
LPS
CD14
CD11b
C
CD14+ cells (%)
*
M1
LPS
MINO 10
MINO 25
Veh
LPS
D
CD14 (MFI) Fold Change
E
CD11b+ cells (%)
F
CD11b (MFI) Fold Change

Figure 6.4: Effect of minocycline on CD14 and CD11b expression following LPS activation of M1 THP-1 macrophages. Data obtained after 24hr incubation of polarized M1 macrophages with LPS (100ng/mL). MINO 10 = Minocycline 10μM, MINO 25 = Minocycline 25μM, Veh = DMSO vehicle control 1:1000. [A] Representative dot plots showing the percentage of $CD14^+$ (top) and $CD11b^+$ (bottom) cells. [B] Representative histograms showing mean fluorescent intensity (MFI) for CD14 (left) and CD11b (right). Numbers indicate MFI of live gated population. [C-F] Bar graphs showing the percentage of $CD14^+$ [C] and $CD11b^+$ [E] cells, and MFI values for CD14 [D] and CD11b [F]. MFI values have been normalised and displayed as fold change versus the un-activated M1 macrophage control indicated at 1. Data representative of 3 repeated experiments each comprising triplicate values and presented as mean ± SEM. One-way ANOVA with post hoc Dunnett's applied versus the LPS-activated M1 macrophage. *p<0.05; **p<0.01; ***p<0.001; ****p<0.0001.

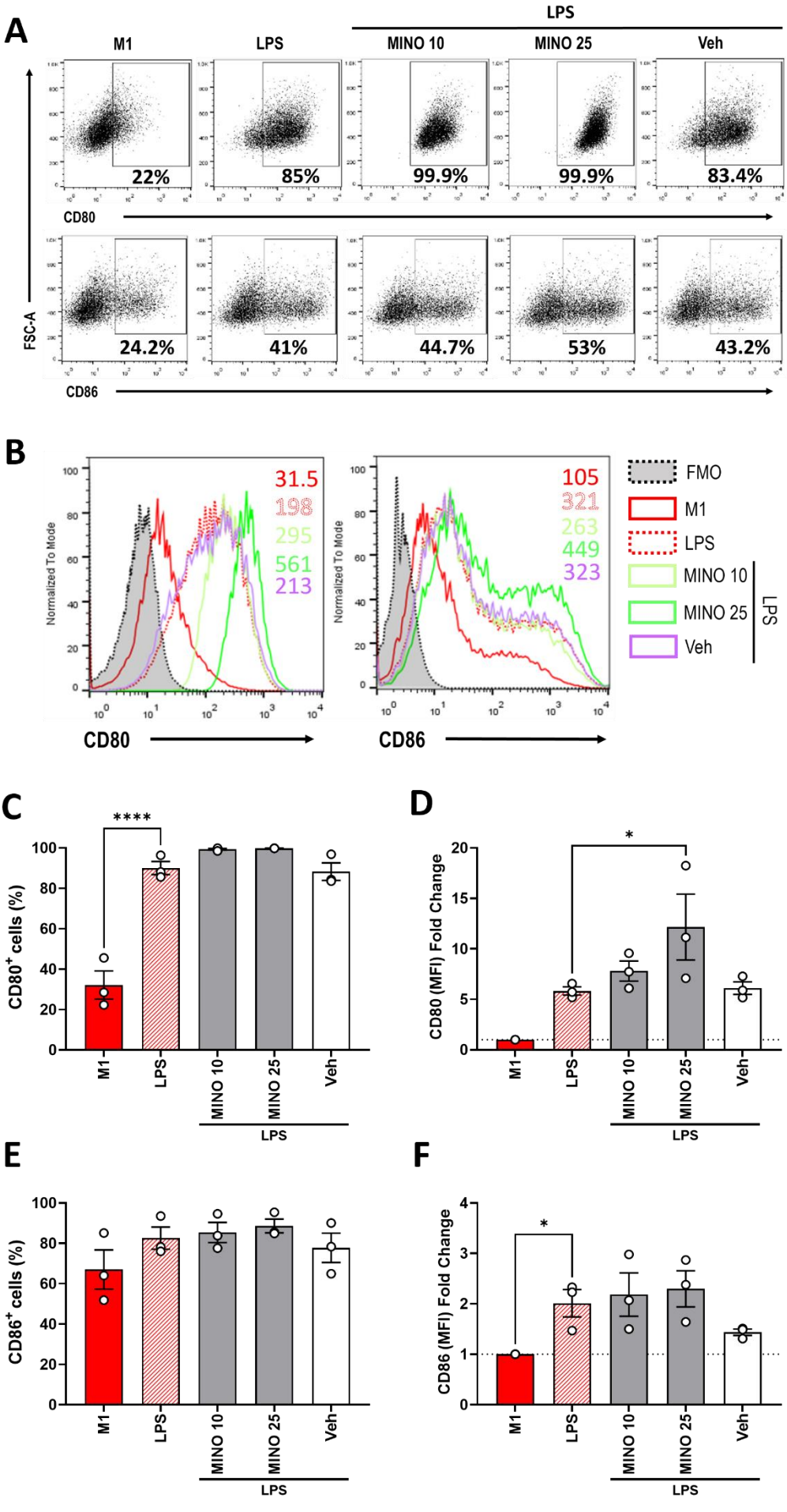
A
LPS
M1
LPS
MINO 10
MINO 25
Veh
22%
85%
99.9%
99.9%
83.4%
CD80
FSC-A
24.2%
41%
44.7%
53%
43.2%
CD86
B
Normalized To Mode
31.5
198
295
561
213
105
321
263
449
323
CD80
CD86
FMO
M1
LPS
MINO 10
MINO 25
Veh
LPS
C
CD80+ cells (%)
****
M1
LPS
MINO 10
MINO 25
Veh
LPS
D
CD80 (MFI) Fold Change
*
E
CD86+ cells (%)
F
CD86 (MFI) Fold Change
*

Figure 6.5: Effect of minocycline on CD80 and CD86 expression following LPS activation of M1 THP-1 macrophages. Data obtained after 24hr incubation of polarized M1 macrophages with LPS (100ng/mL). MINO 10 = Minocycline 10μM, MINO 25 = Minocycline 25μM, Veh = DMSO vehicle control 1:1000. [A] Representative dot plots showing the percentage of $CD80^+$ (top) and $CD86^+$ (bottom) cells. [B] Representative histograms showing mean fluorescent intensity (MFI) for CD80 (left) and CD86 (right). Numbers indicate MFI of live gated population. [C-F] Bar graphs showing the percentage of $CD80^+$ [C] and $CD86^+$ [E] cells, and MFI values for CD80 [D] and CD86 [F]. MFI values have been normalised and displayed as fold change versus the un-activated M1 macrophage control indicated at 1. Data representative of 3 repeated experiments each comprising triplicate values and presented as mean ± SEM. One-way ANOVA with post hoc Dunnett's applied versus the LPS-activated M1 macrophage. *p<0.05; ****p<0.0001.

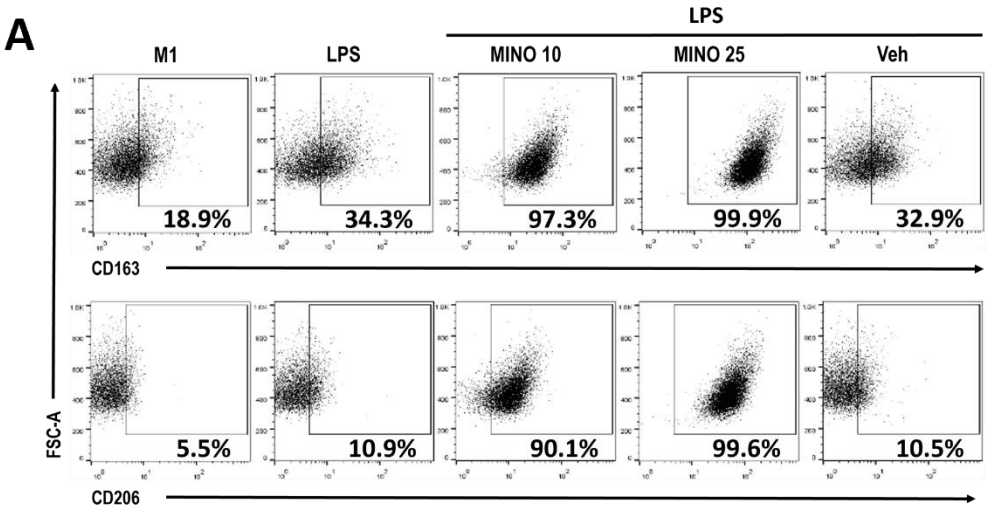
A
LPS
M1
LPS
MINO 10
MINO 25
Veh
18.9%
34.3%
97.3%
99.9%
32.9%
CD163
FSC-A
5.5%
10.9%
90.1%
99.6%
10.5%
CD206

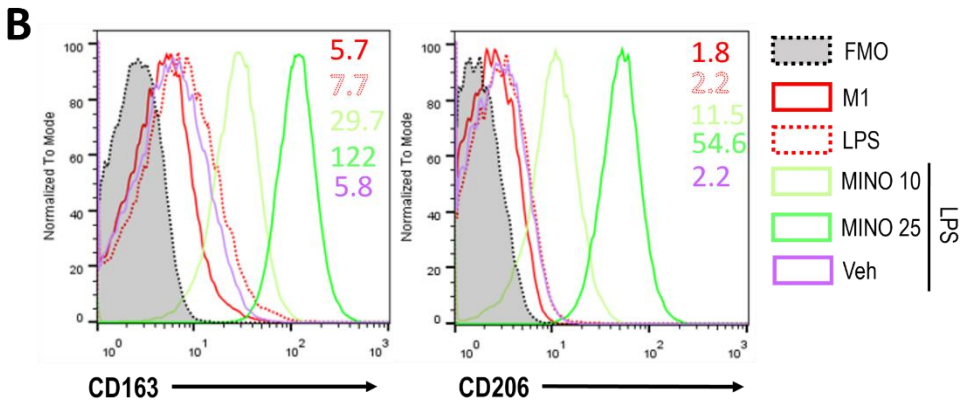
B
Normalized To Mode
5.7
7.7
29.7
122
5.8
1.8
2.2
11.5
54.6
2.2
CD163
CD206
FMO
M1
LPS
MINO 10
MINO 25
Veh
LPS

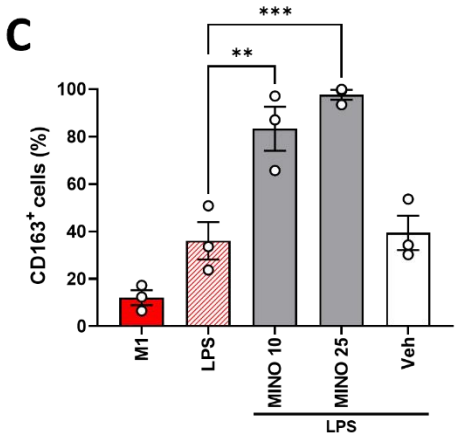
C
CD163+ cells (%)
M1
LPS
MINO 10
MINO 25
Veh
LPS

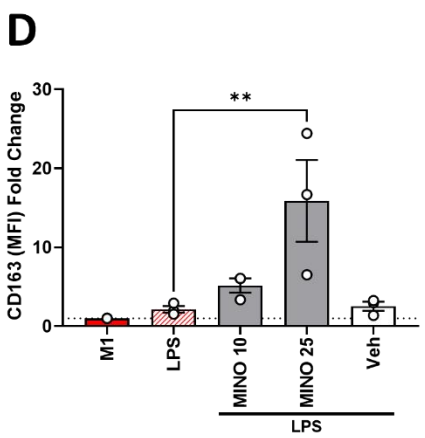
D
CD163 (MFI) Fold Change
M1
LPS
MINO 10
MINO 25
Veh
LPS

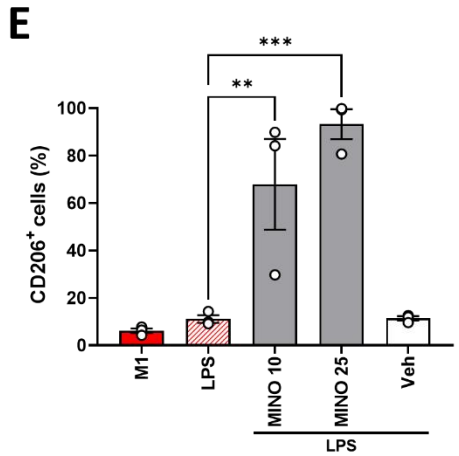
E
CD206+ cells (%)
M1
LPS
MINO 10
MINO 25
Veh
LPS

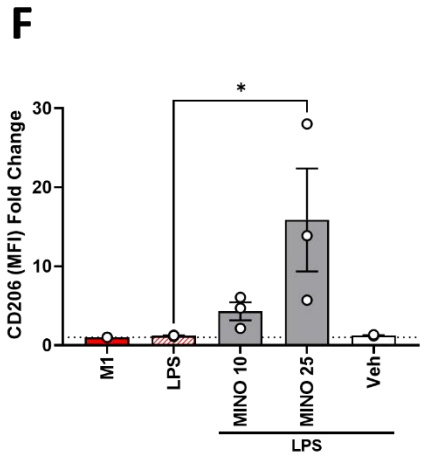
F
CD206 (MFI) Fold Change
M1
LPS
MINO 10
MINO 25
Veh
LPS

Figure 6.6: Effect of minocycline on CD163 and CD206 expression following LPS activation of M1 THP-1 macrophages. Data obtained after 24hr incubation of polarized M1 macrophages with LPS (100ng/mL). MINO 10 = Minocycline 10μM, MINO 25 = Minocycline 25μM, Veh = DMSO vehicle control 1:1000. [A] Representative contour plots showing the percentage of $CD163^+$ (top) and $CD206^+$ (bottom) cells. [B] Representative histograms showing mean fluorescent intensity (MFI) for CD163 (left) and CD206 (right). Numbers indicate MFI of live gated population. [C-F] Bar graphs showing the percentage of $CD163^+$ [C] and $CD206^+$ [E] cells, and MFI values for CD163 [D] and CD206 [F]. MFI values have been normalised and displayed as fold change versus the un-activated M1 macrophage control indicated at 1. Data representative of 3 repeated experiments each comprising triplicate values and presented as mean ± SEM. One-way ANOVA with post hoc Dunnett's applied versus the LPS-activated M1 macrophage. *p<0.05; **p<0.01; ***p<0.001.

6.2. PBMC

6.2.1. Characterising LPS-activation of M1/M2 PBMC-derived macrophage subsets

Primary macrophages in the form of M-CSF-expanded PBMCs were used to investigate if the THP-1 findings were translatable, and to study the effect of minocycline on M2 macrophage subsets. To maintain consistency between models the same protocol was used whereby PBMC monocytes were first differentiated to resting M0 macrophages following 6-day incubation with 50ng/mL M-CSF as described in chapter 2, section 2.2.2, and then polarized to either M1 or M2 subsets through 24hr incubation with IFN-γ (20ng/mL) + LPS (10ng/mL) or IL-4 (20ng/mL) respectively. Following 24hr polarization cells were then activated with LPS at 100ng/mL for an additional 24hr at which point supernatant and cells were collected for analysis.

In contrast to what was seen with the THP-1-derived M1 macrophages, no changes on CD14 expression were noted on M1 macrophages derived from PMBCs upon LPS activation when compared to the LPS control (Figure 6.7A-D). CD14 expression within the M2 cultures on the other hand was decreased following LPS activation, as evidenced by the reduced MFI by 0.8-fold (p<0.0001) (Figure 6.7B and D), and the subtle reduction in the percentage of $CD14^+$ cells (Figure 6.7A and C). A similar trend was also reflected by the data obtained for CD11b total protein, where the pre-polarized M1 cultures did not show any consistent change in expression when stimulated with LPS, while M2 cells appear

to downregulate both the percentage of $CD11b^+$ cells, in addition to the density of CD11b expression upon LPS activation (Figure 6.7A, B, E and F).

When assessing the M1-associated markers CD80 and CD86 it was interesting to report a significant upregulation of both markers within both M1 and M2 subsets, but with a more prominent response elicited by the M2 cells (Figure 6.8). Where the percentage of $CD80^+$ cells were increased by 1.1-fold versus the un-activated control in the M1 cultures, a greater increase was observed for the M2 cells, with a fold change of 5.9 versus the un-activated M2 control (Figure 6.8A and C). This expression signature was also reflected in the density of expression presented as MFI, whereby LPS resulted in a 1.2-fold increase in the M1 cultures, and 1.9-fold increase in the M2 (Figure 6.8B and D). Data pertaining to CD86 showed some disparity between donors relating to both the total percentage of $CD86^+$ cells and density of CD86 expression across both subsets (Figure 6.8A, B, E and F). However, continued to indicate an increase in expression following LPS activation, with the more prominent response originating from the M2 macrophages. Here, when challenged with LPS, M1 cultures had a minimal increase in the percentage of $CD86^+$ cells, while the M2 rose by 1.1-fold (Figure 6.8A and E). Regarding the density of CD86 expression, again, LPS elicited a subtle increase of 1.1-fold in the M1, but 1.4-fold in the M2 versus the un-activated control (Figure 6.8B and F).

Some modification of the M2-associated markers CD163 and CD206 was also reported following LPS activation of pre-polarized subsets. Here CD163 nor CD206 expression was significantly altered within the M1 cultures (Figure 6.9A-F), however both markers were significantly downregulated within the M2 cultures when compared to the un-activated control (Figure 6.9A-F). Although the results from the THP-1 model showed CD163 and CD206 increase within the M1 macrophage cultures following LPS activation, no conclusive data was obtained here using the PBMC-derived macrophages. Nonetheless, the significant upregulation of both pro-inflammatory markers CD80 and CD86, in addition to downregulation of the traditionally anti-inflammatory markers CD163 and CD206 with the M2-polarized macrophages following LPS stimulation, begins to suggest cellular plasticity and phenotype switching upon activation of M2 cells whereby cultures take on more classical M1 characteristics such as increased expression

of CD80 and CD86, and simultaneous downregulation of pro-fibrotic M2-like markers CD163 and CD206.

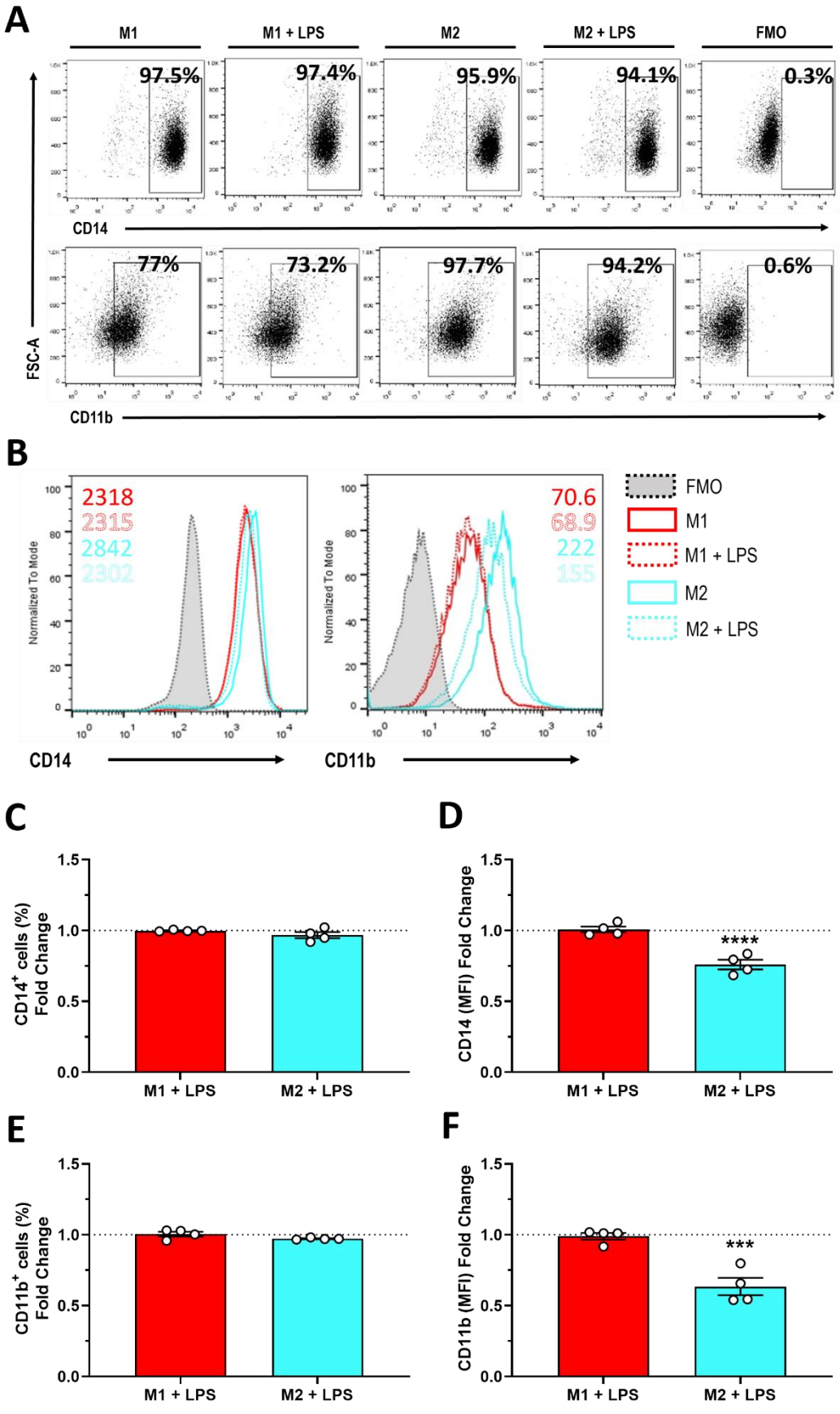

Figure 6.7: CD14 and CD11b expression profile of LPS-activated M1 and M2 polarized PBMC-derived macrophages. Data obtained after 24hr incubation of M1 and M2 polarized macrophages with LPS (100ng/mL). [A] Representative dot plots showing the percentage of $CD14^+$ (top) and $CD11b^+$ (bottom) cells. [B] Representative histograms showing mean fluorescent intensity (MFI) for CD14 (left) and CD11b (right). Numbers indicate MFI of live gated population. [C-F] Bar graphs showing the percentage of $CD14^+$ [C] and $CD11b^+$ [E] cells, and MFI values for CD14 [D] and CD11b [F]. Data normalised and displayed as fold change versus the un-activated M1 or M2 macrophage control indicated at 1. Plots and histograms illustrate one representative donor. Graphs represent data from 4 donors each comprising of duplicate values. Data presented as mean ± SEM. One-way ANOVA with post hoc Dunnett's applied versus the un-activated M1 or M2 macrophage. ***$p<0.001$; ****$p<0.0001$.

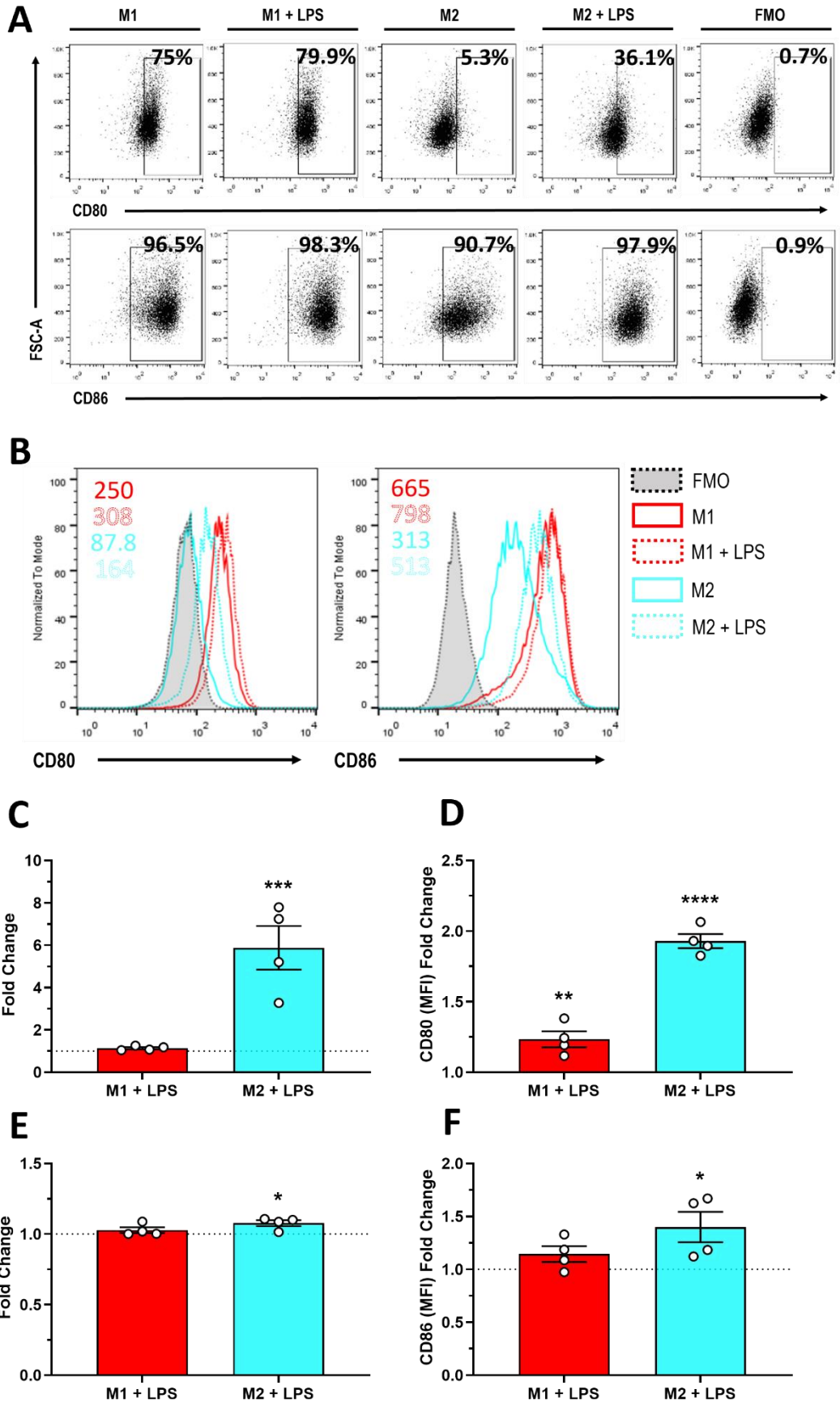
A
M1
M1 + LPS
M2
M2 + LPS
FMO
75%
79.9%
5.3%
36.1%
0.7%
CD80
96.5%
98.3%
90.7%
97.9%
0.9%
FSC-A
CD86
B
250
308
87.8
164
665
798
313
513
Normalized To Mode
FMO
M1
M1 + LPS
M2
M2 + LPS
CD80
CD86
C
CD80+ cells (%) Fold Change
***
M1 + LPS
M2 + LPS
D
CD80 (MFI) Fold Change
**
****
M1 + LPS
M2 + LPS
E
CD86+ cells (%) Fold Change
*
M1 + LPS
M2 + LPS
F
CD86 (MFI) Fold Change
*
M1 + LPS
M2 + LPS

Figure 6.8: CD80 and CD86 expression profile of LPS-activated M1 and M2 polarized PBMC-derived macrophages. Data obtained after 24hr incubation of M1 and M2 polarized macrophages with LPS (100ng/mL). [A] Representative dot plots showing the percentage of $CD80^+$ (top) and $CD86^+$ (bottom) cells. [B] Representative histograms showing mean fluorescent intensity (MFI) for CD80 (left) and CD86 (right). Numbers indicate MFI of live gated population. [C-F] Bar graphs showing the percentage of $CD80^+$ [C] and $CD86^+$ [E] cells, and MFI values for CD80 [D] and CD86 [F]. Data normalised and displayed as fold change versus the un-activated M1 or M2 macrophage control indicated at 1. Plots and histograms illustrate one representative donor. Graphs represent data from 4 donors each comprising of duplicate values. Data presented as mean ± SEM. One-way ANOVA with post hoc Dunnett's applied versus the un-activated M1 or M2 macrophage. *p<0.05; **p<0.01; ***p<0.001; ****p<0.0001.

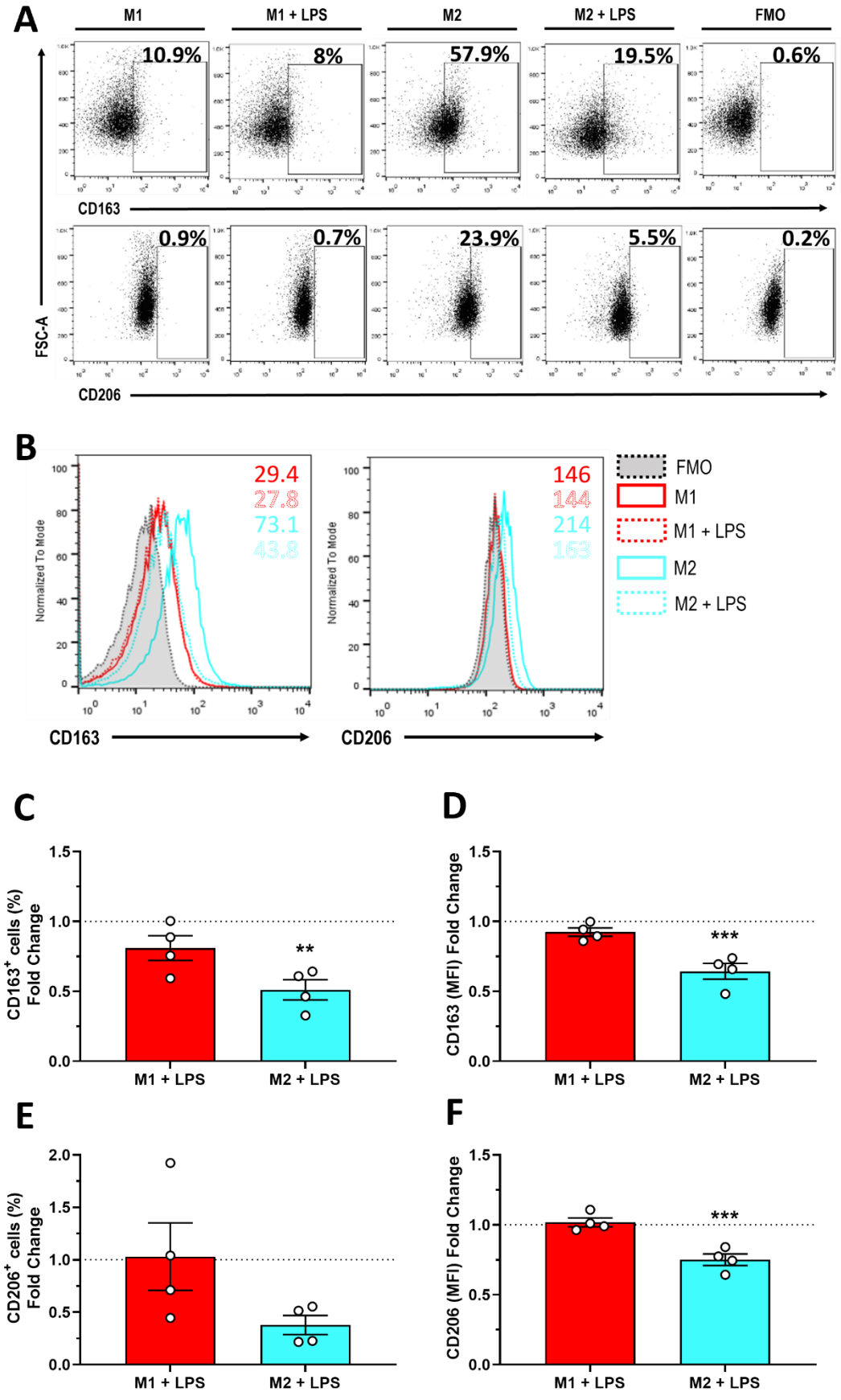

Figure 6.9: CD163 and CD206 expression profile of LPS-activated M1 and M2 polarized PBMC-derived macrophages. Data obtained after 24hr incubation of M1 and M2 polarized

macrophages with LPS (100ng/mL). [A] Representative dot plots showing the percentage of $CD163^+$ (top) and $CD206^+$ (bottom) cells. [B] Representative histograms showing mean fluorescent intensity (MFI) for CD163 (left) and CD206 (right). Numbers indicate MFI of live gated population. [C-F] Bar graphs showing the percentage of $CD163^+$ [C] and $CD206^+$ [E] cells, and MFI values for CD163 [D] and CD206 [F]. Data normalised and displayed as fold change versus the un-activated M1 or M2 macrophage indicated at 1. Plots and histograms illustrate one representative donor. Graphs represent data from 4 donors each comprising of duplicate values. Data presented as mean ± SEM. One-way ANOVA with post hoc Dunnett's applied versus the un-activated M1 or M2 macrophage. **$p<0.01$; ***$p<0.001$.

6.2.2. Effect of Minocycline during LPS-activation of PBMC-derived M1/M2 subsets

To study the effects of minocycline on the LPS-induced activation of PBMC-derived M1 and M2 macrophages minocycline was administered at 10μM and 25μM to pre-polarized M1 and M2 macrophages for 2hr prior to activation with LPS (100ng/mL) for a further 24hr. No conclusive alteration was noted for CD14 in either the M1 or M2 cultures when minocycline was introduced, with all data points from all donors remaining comparable to the LPS only control (Figure 6.10). For total CD11b expression, within the M1-polarized populations a subtle increase in the percentage of $CD11b^+$ cells was elicited by 25μM minocycline, with a 4.5% increase versus LPS (Figure 6.11A and C). A slight upregulation was also illustrated in the density of CD11b expression amongst the M1 population following treatment with 25μM minocycline, with a 0.1-fold increase in expression versus the control (Figure 6.11B and D). When assessing the M2 macrophages, minocycline at 25μM again upregulated the percentage of $CD11b^+$ cells (Figure 6.11A and E). This was also reflected to some degree in the density of CD11b, which was seen to increase comparable to that of the LPS control (Figure 6.11B and F). However, these margins remain very small so their significance should be considered carefully.

For the M1-associated markers CD80 and CD86, when assessing the M1 cultures no consistent change in the percentage of $CD80^+$ cells was found amongst donors (Figure 6.12A and C). Results for the M2 cultures were also inconclusive, with minocycline at 25μM seeming to increase CD80 expression but failing to reach significance (Figure 6.12A, B, D and F). When analysing CD86 expression there was again largely inconclusive data, with no consistent statistically significant changes observed regarding the percentage of $CD86^+$

cells (Figure 6.13A, C and E). Data pertaining to the density of CD86 expression was also inconclusive when compared to the LPS group (Figure 6.13B and D). As for the M2 model, minocycline appeared to have no influence on either the percentage of $CD86^+$ cells or density of CD86 expression across any of the donors tested (Figure 6.13A, B, E and F).

Finally, assessment of the M2-associated markers CD163 and CD206 yielded some promising data. Here intervention of M1-polarized macrophages with 25μM minocycline upregulated the density of CD163 expression, with eliciting a 0.3-fold increase versus the LPS control (p=0.0477) (Figure 6.14A and C). Minocycline also seemed to increase the percentage of $CD163^+$ cells although did not reach significance (Figure 6.14D). Modification by minocycline was also illustrated within the pre-polarized M2 cultures, whereby a small increase of 10.9% was noted following treatment with 25μM minocycline and compared to LPS alone (Figure 6.14A and E). This trend was not however reflected in data obtained for MFI (Figure 6.14B and F). This data suggests that LPS caused a reduction in CD163 expression within the M2 cultures, but minocycline may have acted to partially restore the expression. Results for CD206 expression were also somewhat inconclusive in regard to the percentage of $CD206^+$ cells or CD206 MFI whereby no change was observed by minocycline within the M1 cultures (Figure 6.15A, B, C and D). Furthermore, data obtained from the M2 cultures illustrated no definable change in the percentage of $CD206^+$ cells, or the density of CD206 expression due to minocycline intervention (Figure 6.15B and F).

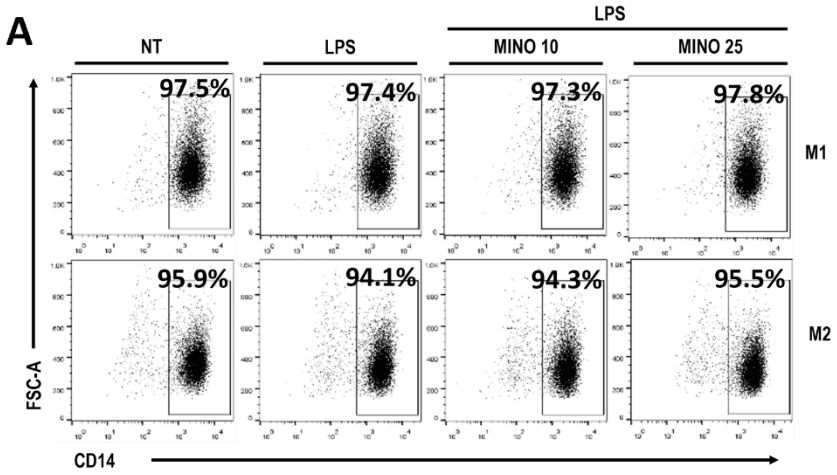
A
NT
LPS
LPS
MINO 10
MINO 25
97.5%
97.4%
97.3%
97.8%
M1
95.9%
94.1%
94.3%
95.5%
M2
FSC-A
CD14

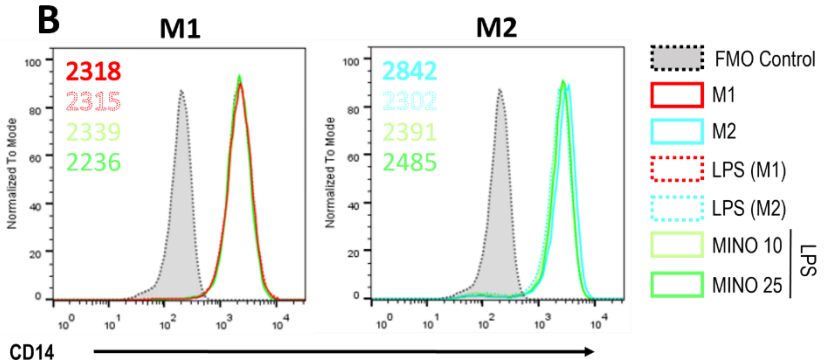
B
M1
M2
2318
2315
2339
2236
2842
2302
2391
2485
Normalized To Mode
CD14
FMO Control
M1
M2
LPS (M1)
LPS (M2)
MINO 10
MINO 25
LPS

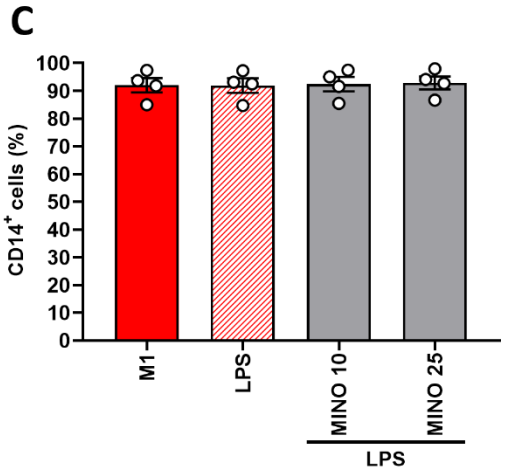
C
CD14+ cells (%)
M1
LPS
MINO 10
MINO 25
LPS

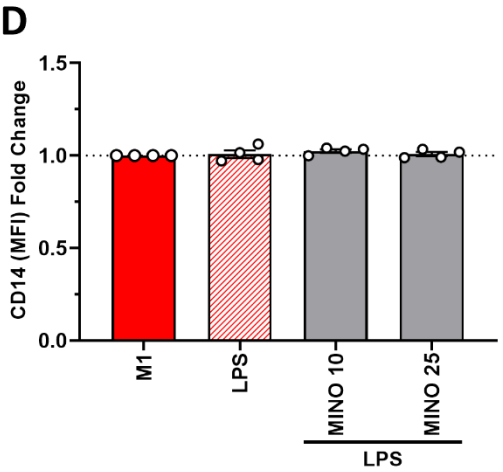
D
CD14 (MFI) Fold Change
M1
LPS
MINO 10
MINO 25
LPS

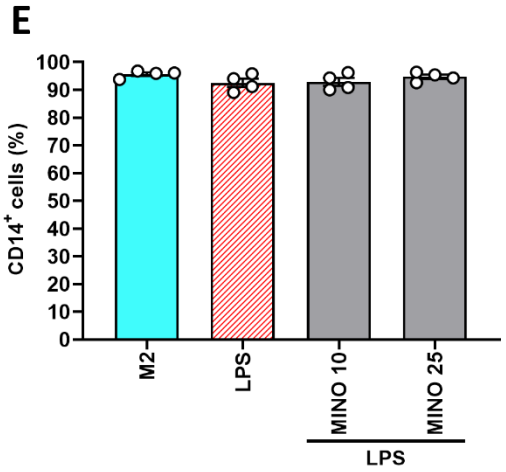
E
CD14+ cells (%)
M2
LPS
MINO 10
MINO 25
LPS

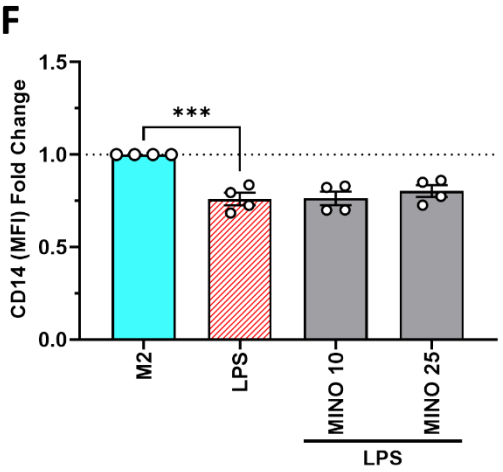
F
CD14 (MFI) Fold Change
***
M2
LPS
MINO 10
MINO 25
LPS

Figure 6.10: Effect of minocycline on CD14 expression following LPS-activation of M1 or M2 PBMC-derived macrophages. Data obtained after 2hr pre-treatment with minocycline and 24hr incubation of M1 or M2 macrophages with LPS (100ng/mL). NT = no treatment, MINO 10 = Minocycline 10μM, MINO 25 = Minocycline 25μM. [A] Representative dot plots showing the percentage of $CD14^+$ cells in M1 (top) or M2 (bottom) macrophage cultures following LPS-activation. [B] Representative histograms showing mean fluorescent intensity (MFI) for CD14 in M1 (left) or M2 (right) macrophages following LPS-activation. Numbers indicate MFI of live gated population. [C-F] Bar graphs showing the percentage of $CD14^+$ M1 macrophages [C] and $CD14^+$ M2 macrophages [E] and CD14 MFI values for M1 [D] and M2 [F] macrophages following LPS-activation. MFI normalised and displayed as fold change versus the un-activated M1 or M2 baseline indicated at 1. Plots and histograms illustrate one representative donor. Graphical data represent data from 4 donors each comprising of duplicate values. Data presented as mean ± SEM. One-way ANOVA with post hoc Dunnett's applied versus the LPS only group. ***$p<0.001$.

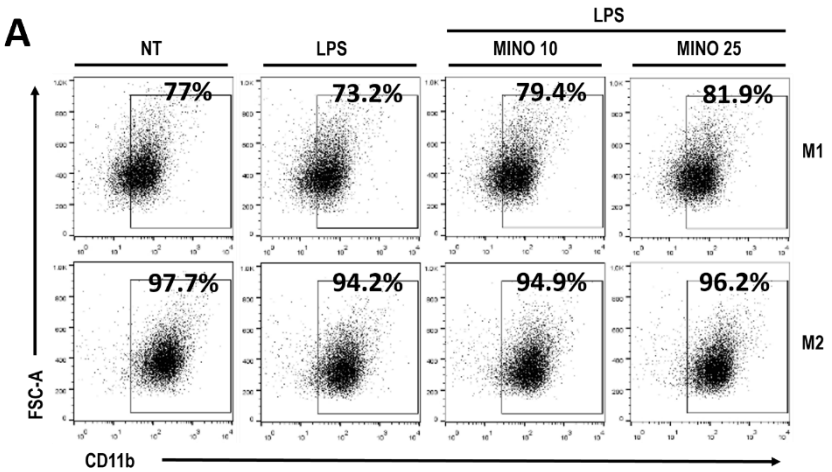
A
LPS
NT
LPS
MINO 10
MINO 25
77%
73.2%
79.4%
81.9%
M1
97.7%
94.2%
94.9%
96.2%
M2
FSC-A
CD11b

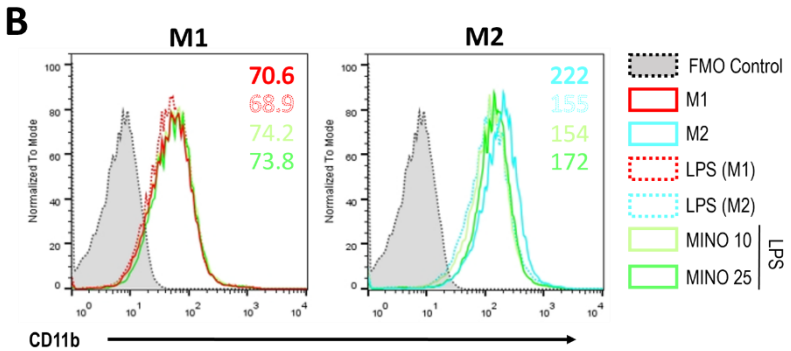
B
M1
M2
70.6
68.9
74.2
73.8
222
155
154
172
Normalized To Mode
CD11b
FMO Control
M1
M2
LPS (M1)
LPS (M2)
MINO 10
MINO 25
LPS

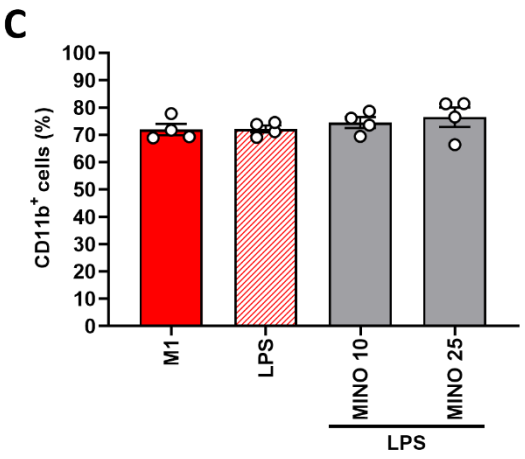
C
CD11b+ cells (%)
M1
LPS
MINO 10
MINO 25
LPS

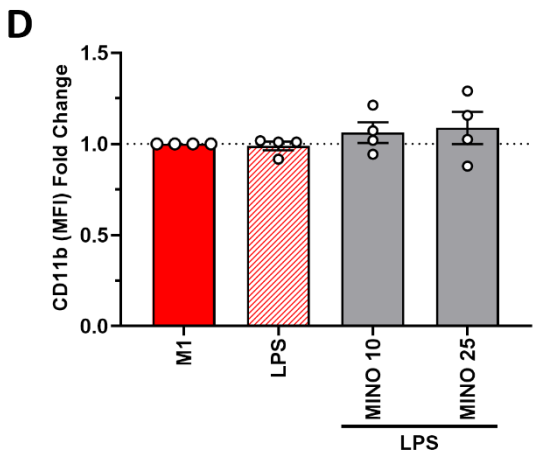
D
CD11b (MFI) Fold Change
M1
LPS
MINO 10
MINO 25
LPS

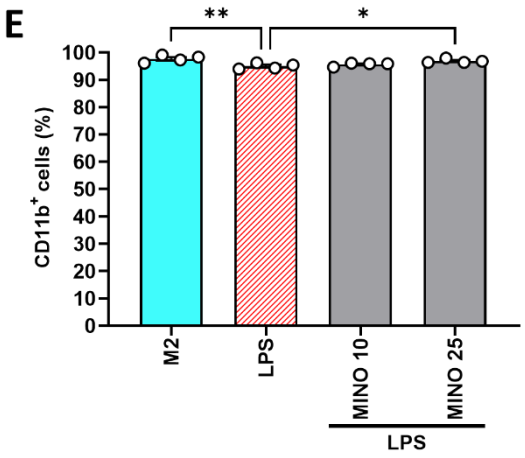
E
**
*
CD11b+ cells (%)
M2
LPS
MINO 10
MINO 25
LPS

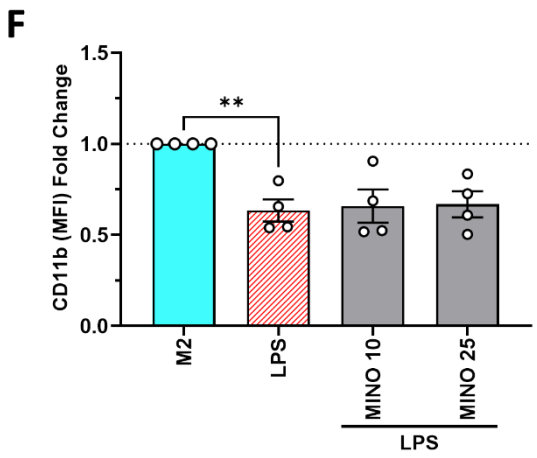
F
**
CD11b (MFI) Fold Change
M2
LPS
MINO 10
MINO 25
LPS

Figure 6.11: Effect of minocycline on CD11b expression following LPS-activation of M1 or M2 PBMC-derived macrophages. Data obtained after 2hr pre-incubation with minocycline and 24hr incubation of M1 or M2 macrophages with LPS (100ng/mL). NT = no treatment, MINO 10 = Minocycline 10μM, MINO 25 = Minocycline 25μM. [A] Representative dot plots showing the percentage of $CD11b^+$ cells in M1 (top) or M2 (bottom) macrophage cultures following LPS-activation. [B] Representative histograms showing mean fluorescent intensity (MFI) for CD11b in M1 (left) or M2 (right) macrophages following LPS-activation. Numbers indicate MFI of live gated population. [C-F] Bar graphs showing the percentage of $CD11b^+$ M1 macrophages [C] and $CD11b^+$ M2 macrophages [E] and CD11b MFI values for M1 [D] and M2 [F] macrophages following LPS-activation. MFI normalised and displayed as fold change versus the un-activated M1 or M2 baseline indicated at 1. Plots and histograms illustrate one representative donor. Graphical data represent data from 4 donors each comprising of duplicate values. Data presented as mean ± SEM. One-way ANOVA with post hoc Dunnett's applied versus the LPS only group. *$p<0.05$; **$p<0.01$.

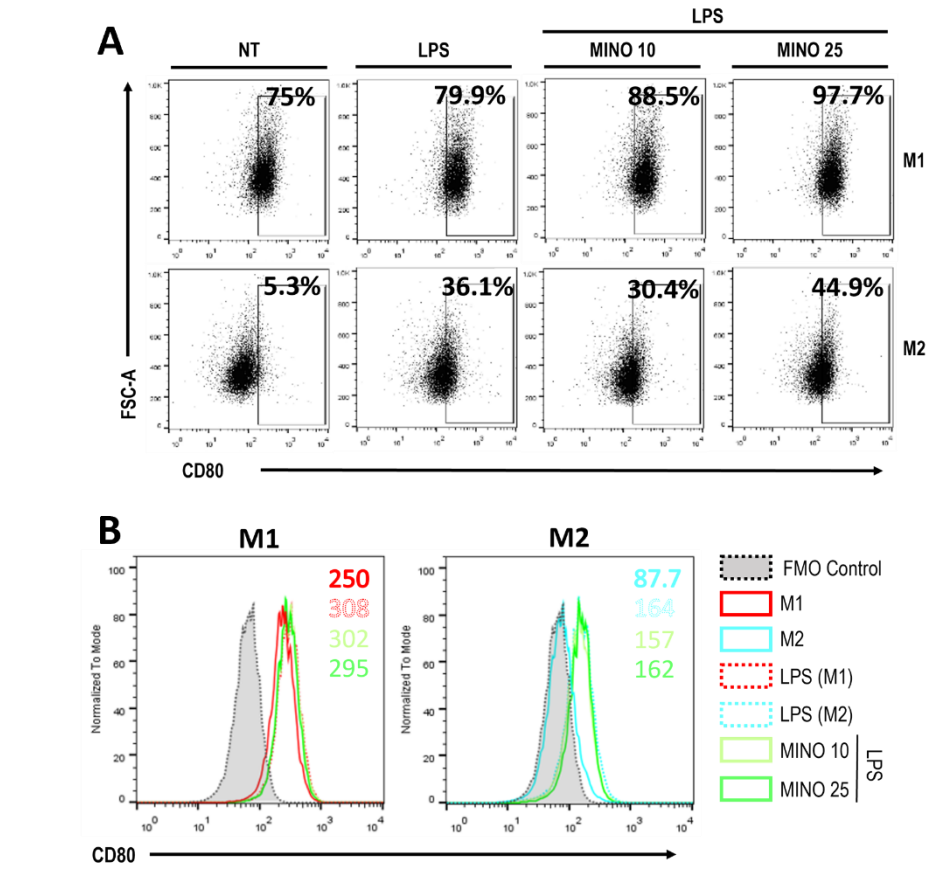
A
LPS
NT
LPS
MINO 10
MINO 25
75%
79.9%
88.5%
97.7%
M1
5.3%
36.1%
30.4%
44.9%
M2
FSC-A
CD80
B
M1
M2
250
308
302
295
87.7
164
157
162
Normalized To Mode
FMO Control
M1
M2
LPS (M1)
LPS (M2)
MINO 10
MINO 25
LPS
CD80

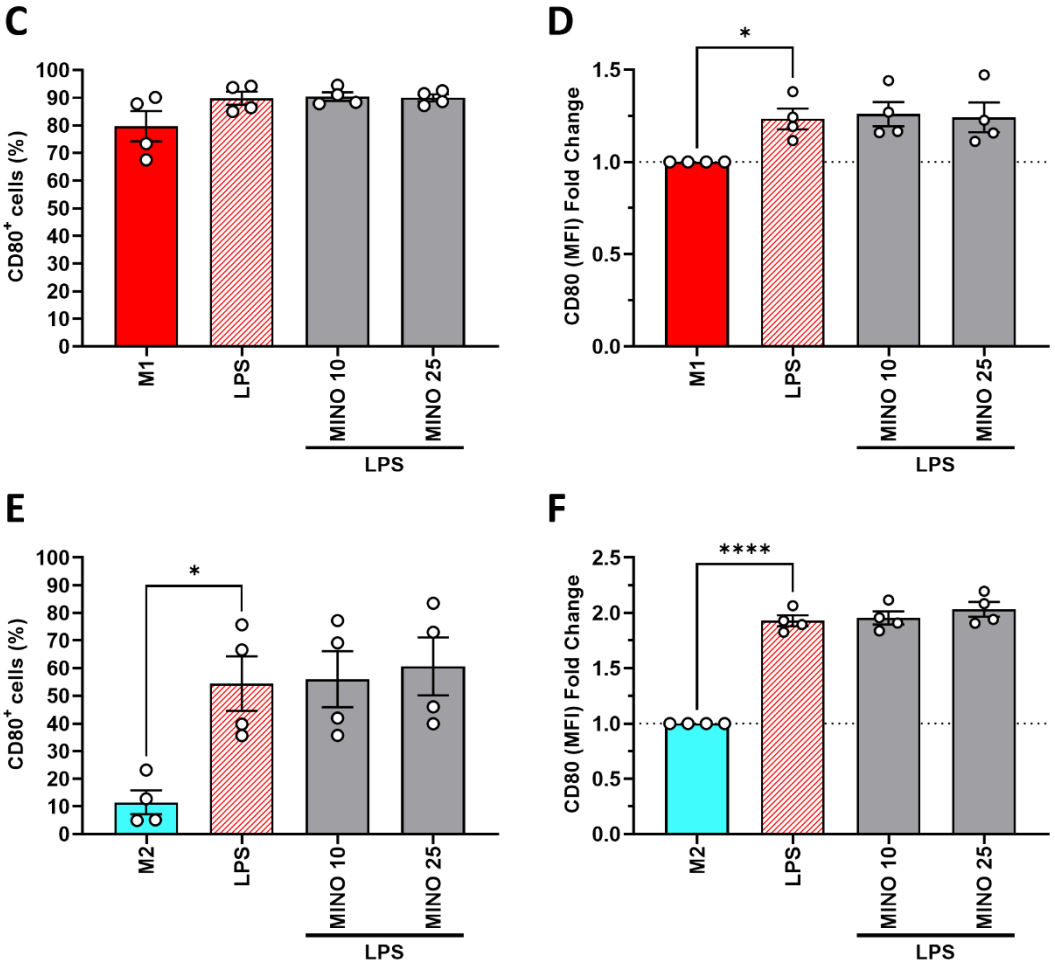
C
CD80+ cells (%)
M1
LPS
MINO 10
MINO 25
LPS
D
CD80 (MFI) Fold Change
*
M1
LPS
MINO 10
MINO 25
LPS
E
CD80+ cells (%)
*
M2
LPS
MINO 10
MINO 25
LPS
F
CD80 (MFI) Fold Change
****
M2
LPS
MINO 10
MINO 25
LPS

Figure 6.12: Effect of minocycline on CD80 expression following LPS-activation of M1 or M2 PBMC-derived macrophages. Data obtained after 2hr pre-incubation with minocycline and 24hr incubation of M1 or M2 macrophages with LPS (100ng/mL). NT = no treatment, MINO 10 = Minocycline 10μM, MINO 25 = Minocycline 25μM. [A] Representative dot plots showing the percentage of $CD80^+$ cells in M1 (top) or M2 (bottom) macrophage cultures following LPS-activation. [B] Representative histograms showing mean fluorescent intensity (MFI) for CD80 in M1 (left) or M2 (right) macrophages following LPS-activation. Numbers indicate MFI of live gated population. [C-F] Bar graphs showing the percentage of $CD80^+$ M1 macrophages [C] and $CD80^+$ M2 macrophages [E] and CD80 MFI values for M1 [D] and M2 [F] macrophages following LPS-activation. MFI normalised and displayed as fold change versus the un-activated M1 or M2 baseline indicated at 1. Plots and histograms illustrate one representative donor. Graphical data represent data from 4 donors each comprising of duplicate values. Data presented as mean ± SEM. One-way ANOVA with post hoc Dunnett's applied versus the LPS only group. *$p<0.05$; ****$p<0.0001$.

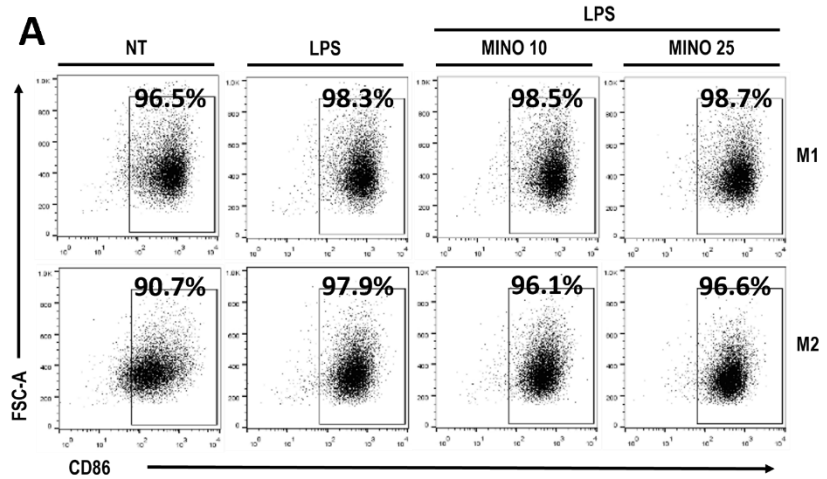
A
NT
LPS
LPS
MINO 10
MINO 25
96.5%
98.3%
98.5%
98.7%
M1
90.7%
97.9%
96.1%
96.6%
M2
FSC-A
CD86

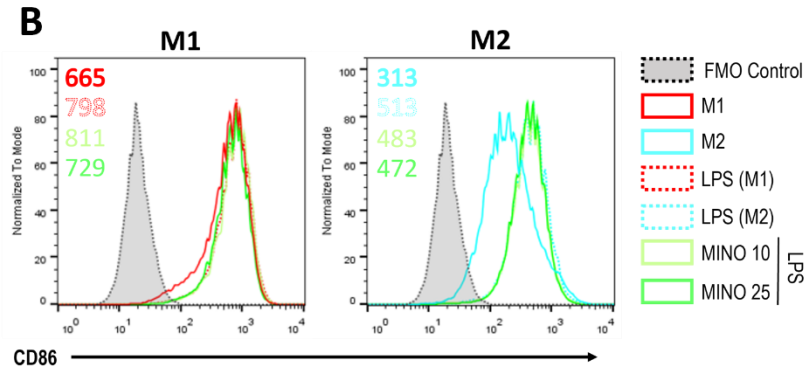
B
M1
M2
665
798
811
729
313
513
483
472
Normalized To Mode
CD86
FMO Control
M1
M2
LPS (M1)
LPS (M2)
MINO 10
MINO 25
LPS

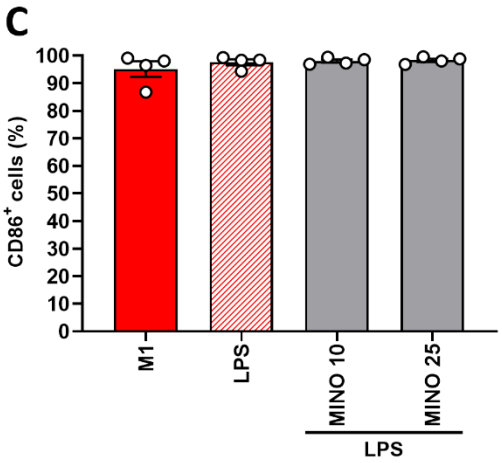
C
CD86+ cells (%)
M1
LPS
MINO 10
MINO 25
LPS

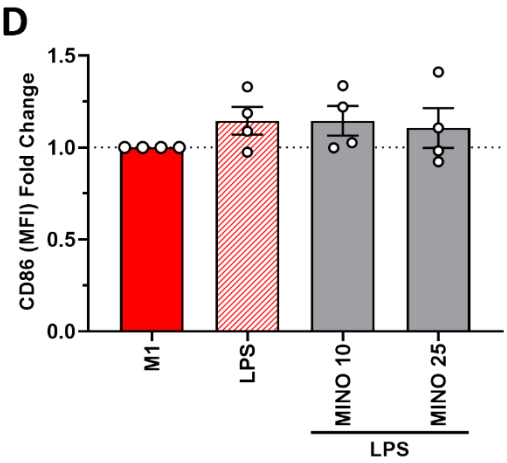
D
CD86 (MFI) Fold Change
M1
LPS
MINO 10
MINO 25
LPS

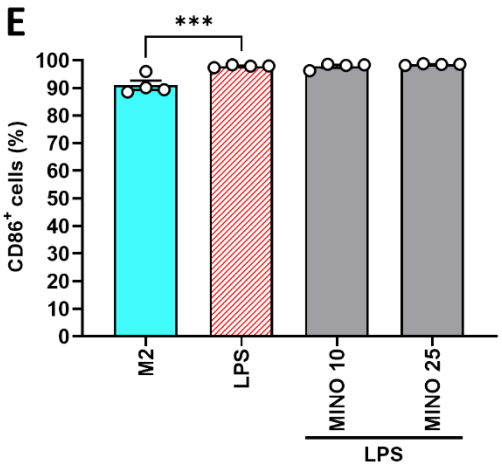
E
***
CD86+ cells (%)
M2
LPS
MINO 10
MINO 25
LPS

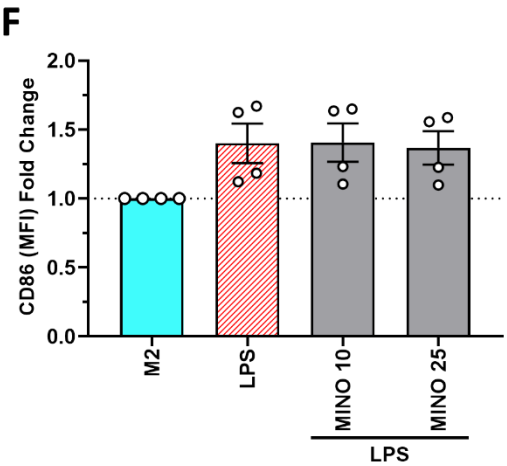
F
CD86 (MFI) Fold Change
M2
LPS
MINO 10
MINO 25
LPS

Figure 6.13: Effect of minocycline on CD86 expression following LPS-activation of M1 or M2 PBMC-derived macrophages. Data obtained after 2hr pre-incubation with minocycline and 24hr incubation of M1 or M2 macrophages with LPS (100ng/mL). NT = no treatment, MINO 10 = Minocycline 10μM, MINO 25 = Minocycline 25μM. [A] Representative dot plots showing the percentage of $CD86^+$ cells in M1 (top) or M2 (bottom) macrophage cultures following LPS-activation. [B] Representative histograms showing mean fluorescent intensity (MFI) for CD86 in M1 (left) or M2 (right) macrophages following LPS-activation. Numbers indicate MFI of live gated population. [C-F] Bar graphs showing the percentage of $CD86^+$ M1 macrophages [C] and $CD86^+$ M2 macrophages [E] and CD86 MFI values for M1 [D] and M2 [F] macrophages following LPS-activation. MFI normalised and displayed as fold change versus the un-activated M1 or M2 baseline indicated at 1. Plots and histograms illustrate one representative donor. Graphical data represent data from 4 donors each comprising of duplicate values. Data presented as mean ± SEM. One-way ANOVA with post hoc Dunnett's applied versus the LPS only group. ***$p<0.001$.

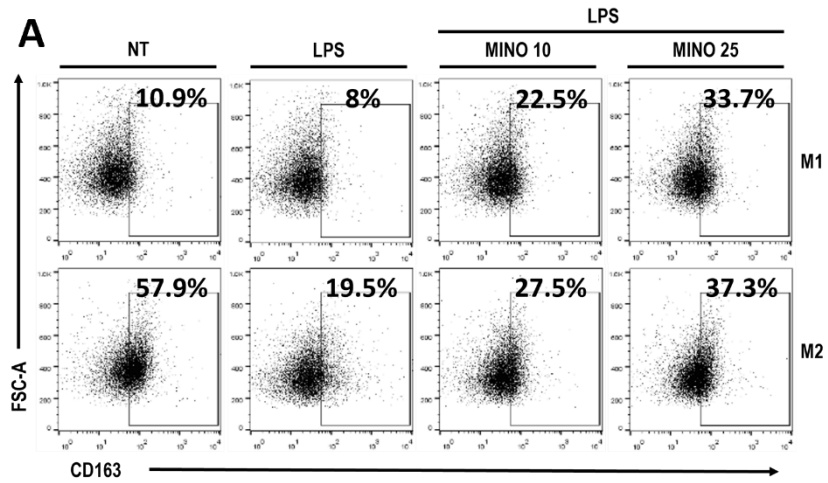
A
NT
LPS
LPS
MINO 10
MINO 25
10.9%
8%
22.5%
33.7%
M1
57.9%
19.5%
27.5%
37.3%
M2
FSC-A
CD163

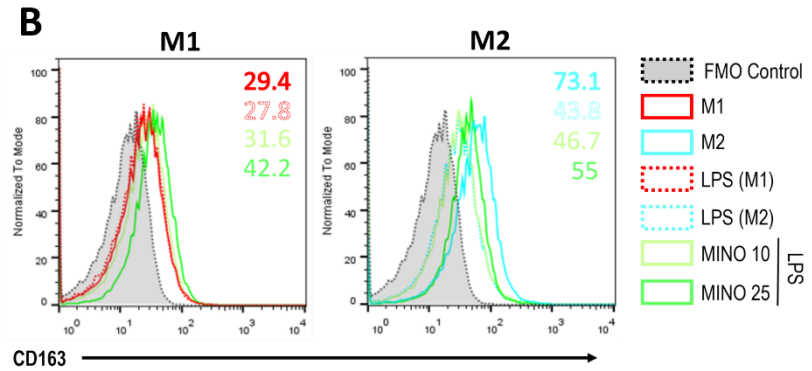
B
M1
M2
29.4
27.8
31.6
42.2
73.1
43.8
46.7
55
Normalized To Mode
FMO Control
M1
M2
LPS (M1)
LPS (M2)
MINO 10
MINO 25
LPS
CD163

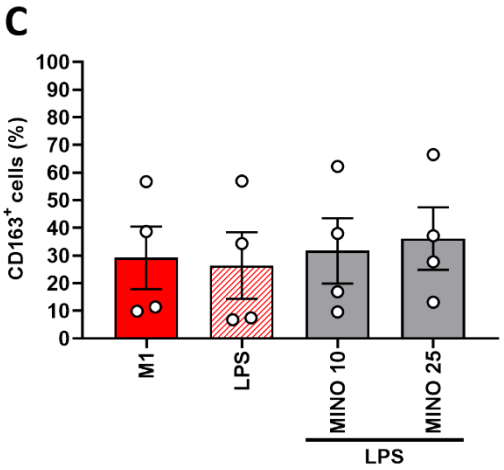
C
CD163+ cells (%)
M1
LPS
MINO 10
MINO 25
LPS

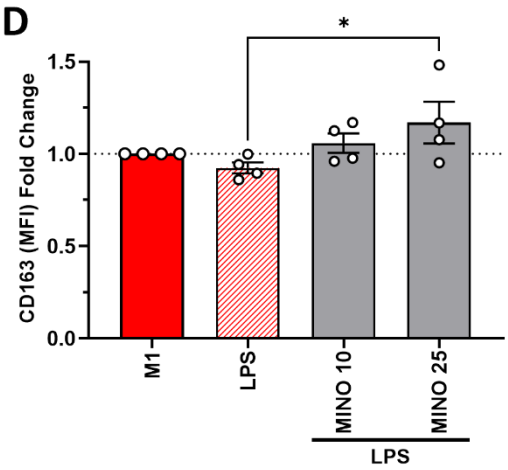
D
*
CD163 (MFI) Fold Change
M1
LPS
MINO 10
MINO 25
LPS

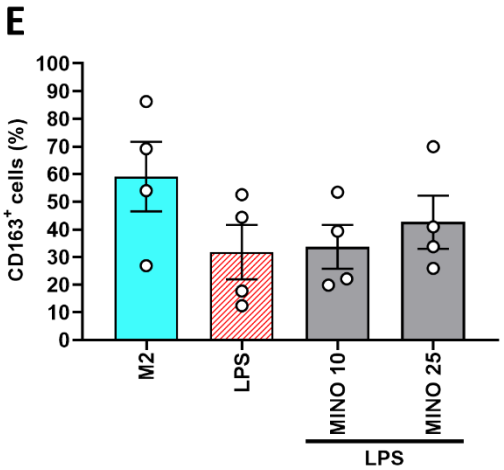
E
CD163+ cells (%)
M2
LPS
MINO 10
MINO 25
LPS

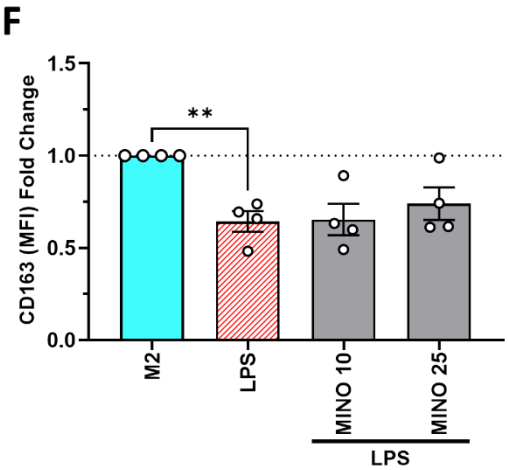
F
**
CD163 (MFI) Fold Change
M2
LPS
MINO 10
MINO 25
LPS

Figure 6.14: Effect of minocycline on CD163 expression following LPS-activation of M1 or M2 PBMC-derived macrophages. Data obtained after 2hr pre-incubation with minocycline and 24hr incubation of M1 or M2 macrophages with LPS (100ng/mL). NT = no treatment, MINO 10 = Minocycline 10μM, MINO 25 = Minocycline 25μM. [A] Representative dot plots showing the percentage of $CD163^+$ cells in M1 (top) or M2 (bottom) macrophage cultures following LPS-activation. [B] Representative histograms showing mean fluorescent intensity (MFI) for CD163 in M1 (left) or M2 (right) macrophages following LPS-activation. Numbers indicate MFI of live gated population. [C-F] Bar graphs showing the percentage of $CD163^+$ M1 macrophages [C] and $CD163^+$ M2 macrophages [E] and CD163 MFI values for M1 [D] and M2 [F] macrophages following LPS-activation. MFI normalised and displayed as fold change versus the un-activated M1 or M2 baseline indicated at 1. Plots and histograms illustrate one representative donor. Graphical data represent data from 4 donors each comprising of duplicate values. Data presented as mean ± SEM. One-way ANOVA with post hoc Dunnett's applied versus the LPS only group. *$p<0.05$; **$p<0.01$.

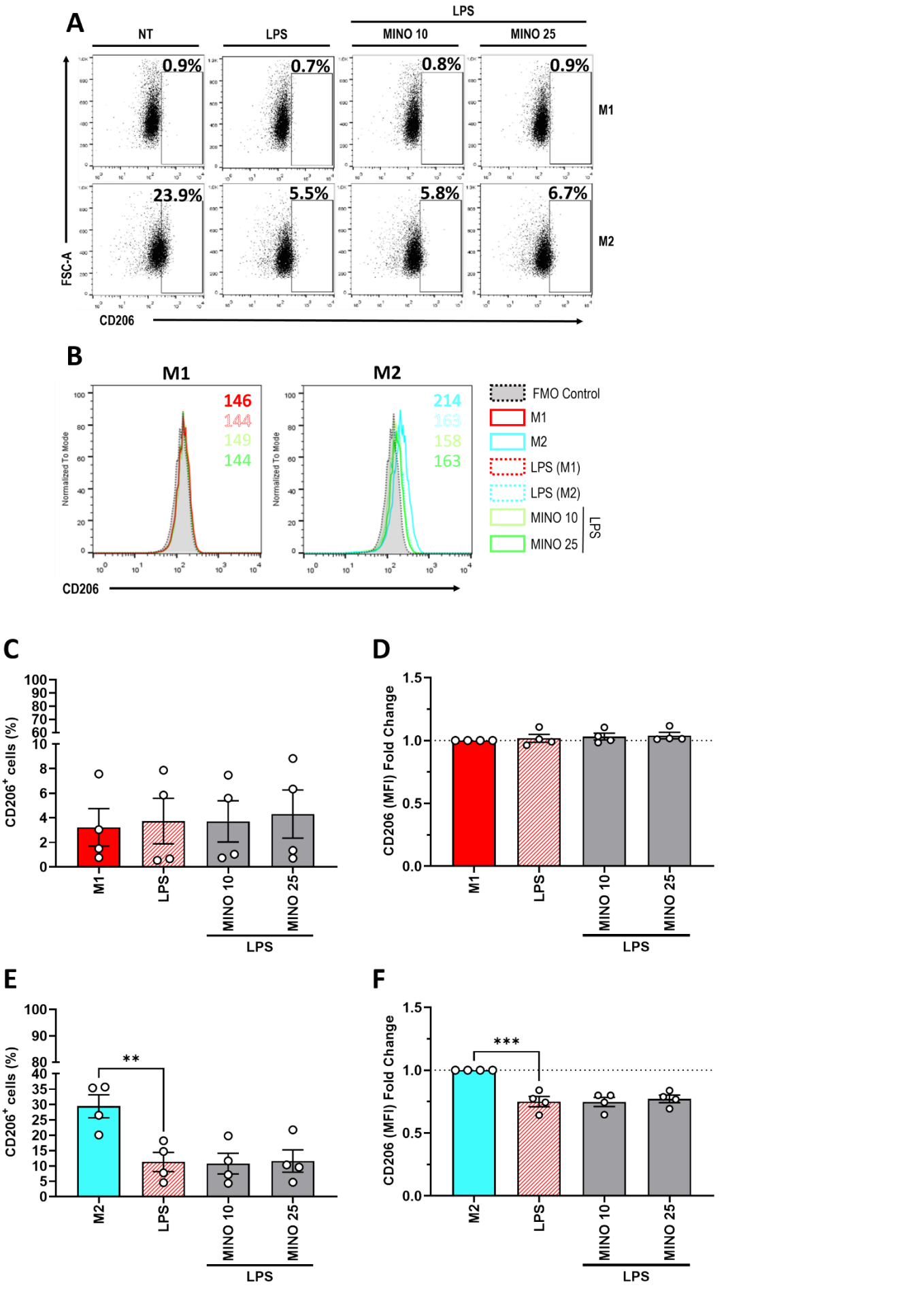
A
NT
LPS
LPS
MINO 10
MINO 25
0.9%
0.7%
0.8%
0.9%
M1
23.9%
5.5%
5.8%
6.7%
M2
FSC-A
CD206
B
M1
M2
146
144
149
144
214
163
158
163
Normalized To Mode
CD206
FMO Control
M1
M2
LPS (M1)
LPS (M2)
MINO 10
MINO 25
LPS
C
CD206+ cells (%)
M1
LPS
MINO 10
MINO 25
LPS
D
CD206 (MFI) Fold Change
M1
LPS
MINO 10
MINO 25
LPS
E
CD206+ cells (%)
**
M2
LPS
MINO 10
MINO 25
LPS
F
CD206 (MFI) Fold Change
***
M2
LPS
MINO 10
MINO 25
LPS

Figure 6.15: Effect of minocycline on CD206 expression following LPS-activation of M1 or M2 PBMC-derived macrophages. Data obtained after 2hr pre-incubation with minocycline and 24hr incubation of M1 or M2 macrophages with LPS (100ng/mL). NT = no treatment, MINO 10 = Minocycline 10μM, MINO 25 = Minocycline 25μM. [A] Representative dot plots showing the percentage of $CD206^+$ cells in M1 (top) or M2 (bottom) macrophage cultures following LPS-activation. [B] Representative histograms showing mean fluorescent intensity (MFI) for CD206 in M1 (left) or M2 (right) macrophages following LPS-activation. Numbers indicate MFI of live gated population. [C-F] Bar graphs showing the percentage of $CD206^+$ M1 macrophages [C] and $CD206^+$ M2 macrophages [E] and CD206 MFI values for M1 [D] and M2 [F] macrophages following LPS-activation. MFI normalised and displayed as fold change versus the un-activated M1 or M2 baseline indicated at 1. Plots and histograms illustrate one representative donor. Graphical data represent data from 4 donors each comprising of duplicate values. Data presented as mean ± SEM. One-way ANOVA with post hoc Dunnett's applied versus the LPS only group. **p<0.01; ***p<0.001.

6.3. Cytokine Production Profile of LPS-activated M1/M2 macrophage subsets

To assess the effect of minocycline on the response of both THP-1-derived, and PBMC-derived M1 and M2 macrophages to LPS-induced activation, the cytokine production profile of both the M1 and M2 macrophage cultures were first characterised to assess the effect of LPS. For cytokine determination both the THP-1 and PBMCs were first differentiated to resting M0 macrophages via PMA or M-CSF respectively, and then polarized to either M1 through 24hr incubation with IFN-γ (20ng/mL) + LPS (10ng/mL) or M2 with IL-4 (20ng/mL). Following 24hr polarization cells were then activated with LPS at 100ng/mL for an additional 24hr at which point supernatant was collected and cytokine concentration determined by ELISA. Here the concentration of IFN-γ, IL-1β, IL-6, TNF-α, IL-12p40 and IL-12p70, IL-4 and IL-10 was assessed.

When stimulated with LPS polarized M1 macrophages displayed upregulation of IL-1β, IL-6, and TNF-α both in the THP-1 (Figure 6.16 A2-A4) and PBMCs (Figure 6.16 B2-B4). Similarly, IL-12p40 production also increased following LPS-activation within the THP-1 experiments (Figure 6.16 A5), but to a lesser degree in the PBMCs (Figure 6.16 B5). Regarding the remaining 2 parameters, stimulation with LPS resulted in no clear change in the production of IFN-γ (Figure 6.16 A1 and B1), or IL-12p70, for which there was a lack of consistency between replicates which may in part be attributed to the data points remaining proximate to the lower detection limit of the assay (Figure 6.16 A6 and B6). Furthermore, of note, in THP-1 samples where a separate vehicle control was included (Veh+LPS), a similar or higher increase in cytokine production to that induced by LPS alone was seen (Figure 6.16A).

When assessing the production of the M2-associated cytokines IL-4 and IL-10 following LPS activation of M1 macrophages (Figure 6.17), LPS caused a significant reduction in IL-4 production by THP-1-derived M1 macrophages which was further exacerbated by the LPS+Veh control (Figure 6.17 A1). A similar effect was also observed in the PBMC-derived M1 macrophages although this was not statistically significant (Figure 6.17 B1). On the other hand, a significant increase in IL-10 production following LPS-activation was seen both in the THP-1-derived M1 macrophages (Figure 6.17 A2) and PBMC-derived M1 macrophages (Figure

6.17 B2), and in which case a higher concentration was detected in those co-treated with the DMSO vehicle control (LPS+Veh) (Figure 6.17 A2).

Having assessed the cytokine production signatures of the M1 macrophages upon LPS stimulation, the same panel of cytokines was next evaluated this time using the PBMC-derived M2 cultures. Figure 6.18 indicates increased production of all M1-associated cytokines IFN-γ, IL-1β, IL-6, TNF-α, IL-12p40 and IL-12p70 following administration of LPS (Figure 6.18 A1-6). This upregulation was also witnessed in the values for IL-10 (Figure 6.18 B2). On the contrary, there appeared to be no distinct change in the production of IL-4 within this LPS-activation model (Figure 6.18 B1). Interestingly, the magnitude of change in the production of these cytokines upon LPS stimulation was bigger in the M2 cultures versus the M1suggesting a more potent influence of LPS when administered to a pre-defined anti-inflammatory M2 phenotype.

These findings again relate this data to the current literary narrative which correlates upregulation of M1-associated cytokines with LPS activation. The increase in IL-10 production – traditionally understood to be a potent anti-inflammatory mediator, has also been reported for macrophages in response to TLR receptor ligands through involvement of MAPKs and transcription factors (Elcombe *et al.*, 2013; Vliet *et al.*, 2013; Sanin, Prendergast and Mountford, 2015). Furthermore, this characterisation strongly suggests that pre-defined anti-inflammatory cells such as M2 macrophages respond more potently to inflammatory stimuli, as seen by the more pronounced changes in cytokine signatures.

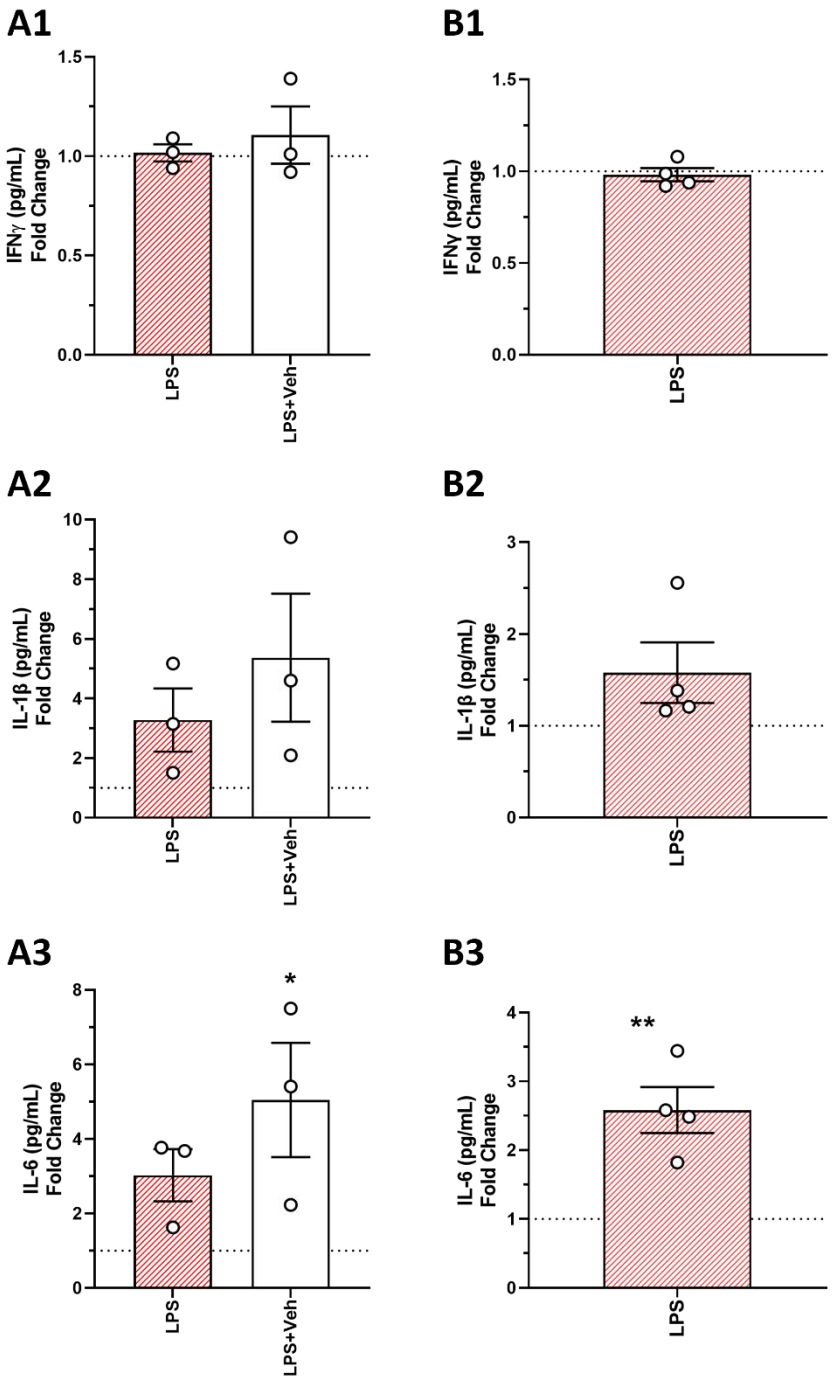
A1
IFNγ (pg/mL) Fold Change
1.5
1.0
0.5
0.0
LPS
LPS+Veh
B1
IFNγ (pg/mL) Fold Change
1.5
1.0
0.5
0.0
LPS
A2
IL-1β (pg/mL) Fold Change
10
8
6
4
2
0
LPS
LPS+Veh
B2
IL-1β (pg/mL) Fold Change
3
2
1
0
LPS
A3
IL-6 (pg/mL) Fold Change
8
6
4
2
0
*
LPS
LPS+Veh
B3
IL-6 (pg/mL) Fold Change
4
3
2
1
0
**
LPS

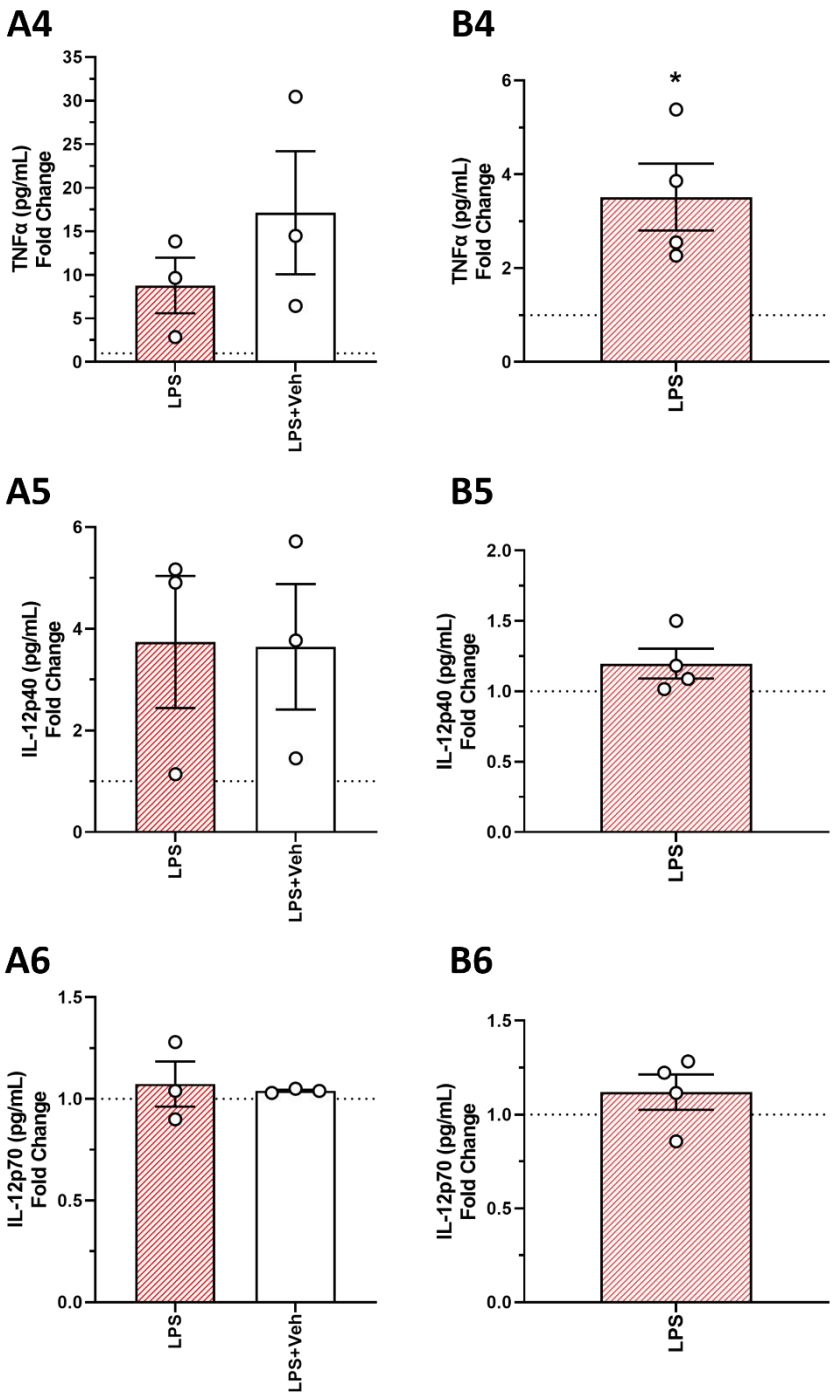

Figure 6.16: M1-associated cytokine production by LPS-activated M1 THP-1 (panel A) and PBMC-derived (panel B) macrophages. Data obtained from supernatant analysis after 24hr incubation of pre-polarized M1 macrophages with LPS (100ng/mL). Veh = DMSO vehicle control (1:1000). Bar graphs showing data for the M1-associated cytokines IFN-γ [1], IL-1β [2], IL-6 [3], TNF-α [4], IL-12p40 [5] and IL-12p70 [6]. Data presented as relative fold change versus the untreated M1 control indicated at 1. Graphs represent data from 3 repeated experiments each comprising triplicate readings for THP-1 [Panel A], and 4 donors each comprising of duplicate values for PBMCs [Panel B]. Data presented as mean ± SEM. One-way ANOVA with post hoc Dunnett's versus LPS applied. *p<0.05.

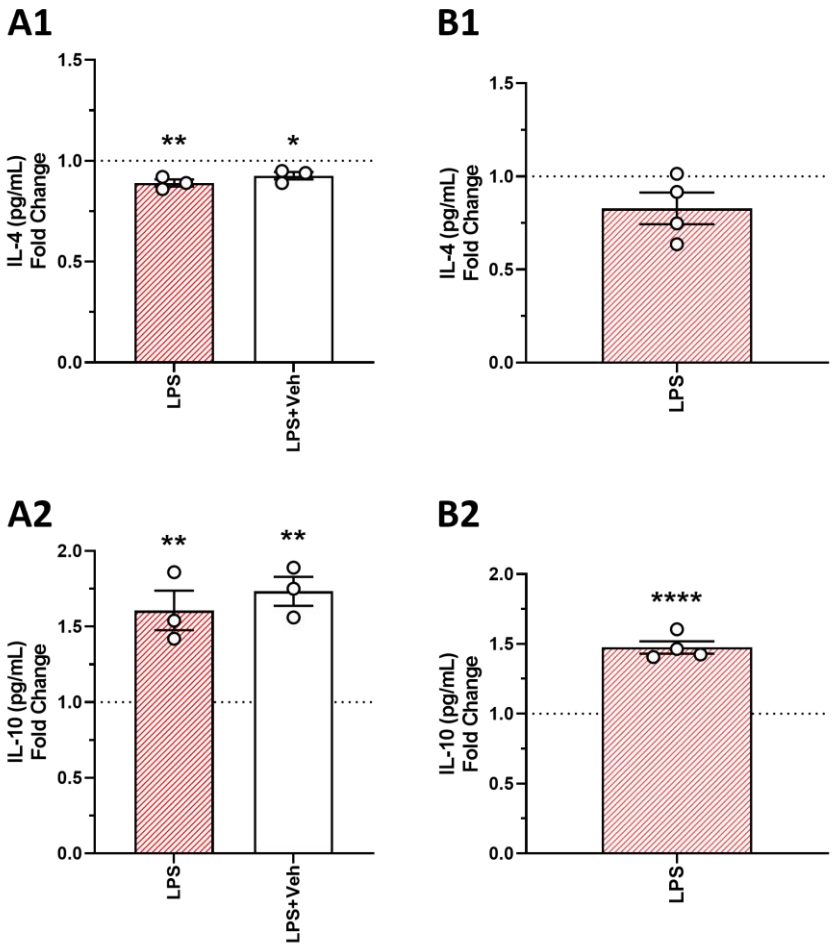

Figure 6.17: M2-associated cytokine production by LPS-activated M1 THP-1 (Panel A) and PBMC-derived (Panel B) macrophages. Data obtained from supernatant analysis after 24hr incubation of pre-polarized M1 macrophages with LPS (100ng/mL). Veh = DMSO vehicle control (1:1000). Bar graphs showing data for the M2-associated cytokines IL-4 [1] and IL-10 [2]. Data presented as relative fold change versus the untreated M1 control indicated at 1. Graphs represent data from 3 repeated experiments each comprising triplicate readings for THP-1 [Panel A], and 4 donors each comprising of duplicate values for PBMCs [Panel B]. Data presented as mean ± SEM. One-way ANOVA with post hoc Dunnett's versus LPS applied. *p<0.05; **p<0.01; ****p<0.0001.

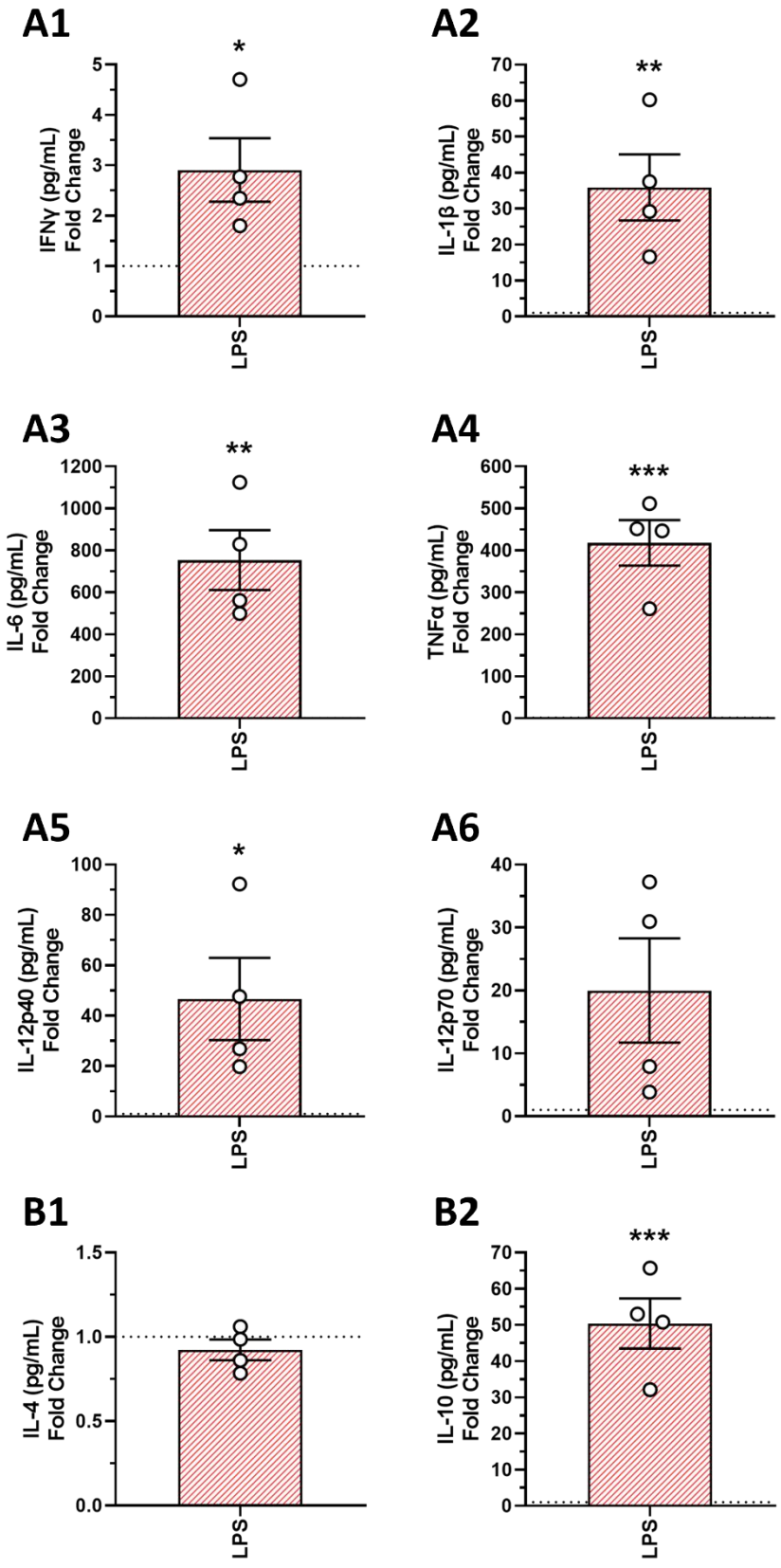

Figure 6.18: M1- and M2-associated cytokine production by LPS-activated M2 PBMC-derived macrophages. Data obtained from supernatant analysis after 24hr incubation of pre-polarized M2 macrophages with LPS (100ng/mL). Bar graphs showing data collected from PBMC experimental samples for M1-associated cytokines [Panel A] - IFN-γ [1], IL-1β [2], IL-6 [3], TNF-

α [4], IL-12p40 [5] and IL-12p70 [6], and M2-associated cytokines [Panel B] – IL-4 [1] and IL-10 [2]. Data presented as relative fold change versus the untreated M2 control indicated at 1. Graphs represent data from 4 donors each comprising of duplicate values. Data presented as mean ± SEM. One-way ANOVA with post hoc Dunnett's applied versus the M2 macrophage control. *p<0.05; **p<0.01; ***p<0.001.

6.4. Effect of Minocycline on cytokine production following LPS-activation of M1/M2 macrophage subsets

Having established baseline data and characterised the effect of LPS on pre-polarized M1 and M2 macrophage cytokine production, the next aim was to evaluate the effect of minocycline on these cytokine production signatures. As noted previously, to do this polarized M1 or M2 macrophages were pre-treated with minocycline at 10μM and 25μM for 2hr prior to the addition of LPS (100ng/mL) for a further 24hr, at which time supernatant was collected and analysed via ELISA. Considering the effect of the vehicle control on cytokine production seen previously in section 6.5, it was decided to consider the LPS+Veh group the comparison control in this instance.

When assessing the effect of minocycline upon the production of M1-associated cytokines from M1 macrophage THP-1 and PBMC cultures as displayed in Figure 6.19, an increase in the production of IFN-γ was found (Figure 6.19 A1 and B1). Here, 25μM minocycline caused a 1.2-fold increase in IFN-γ production versus the LPS+Veh control within the THP-1 model (Figure 6.19 A1). This was more pronounced in the PBMCs whereby both 10μM and 25μM resulted in a significant increase in production by 1.1- and 1.3-fold versus the LPS only control (p<0.0001) (Figure 6.19 B1). Inversely, minocycline treatment resulted in a reduced production of IL-1β by M1 THP-1-derived macrophages, which seemed to be concentration related when compared to the LPS+Veh control (Figure 6.19 A2), however, results for the PBMCs were inconclusive (Figure 6.19 B2).

For IL-6 and TNF-α different responses were seen for the THP-1 and PBMCs, whereby minocycline caused a decrease in production within the THP-1 (Figure 6.19 A3-4), whereas their production was increased within the PBMCs when compared to the LPS+Veh or LPS only controls respectively (Figure 6.19 B3-4) Again, a lack of consistency between models and replicates makes analysis and interpretation of the data difficult and thus requires further investigation with larger

data sets across increased replicates. Finally, as was mentioned previously, data points for the 2 subunits of IL-12 that were tested (p40 and p70) were on or very close to the lower detection limit of the assay used for this analysis, and as such data pertaining to these analytes should be interpreted with caution. This proximity to the assay detection limit may also explain why little to no response was noted for either analyte in either model following minocycline administration (Figure 6.19 A5-6).

For the M2-associated cytokines IL-4 and IL-10 within the M1 macrophage models no change was exerted by minocycline across either the THP-1 or PBMC data on the production of IL-4 when compared to the respective LPS+Veh or LPS only control (Figure 6.20 A1 and B1). Furthermore, although no change was seen with minocycline for IL-10 production within the PBMC-derived macrophages (Figure 6.20 B2), a significant reduction in IL-10 production following minocycline intervention was observed in the THP-1 cells, whereby a positive correlation was seen between minocycline concentration and the magnitude of IL-10 reduction versus the LPS+Veh group (Figure 6.20 A2). Here, minocycline at 25μM reduced the production of IL-10 by 0.56-fold (p=0.0148) versus the LPS+Veh group.

Changes induced by minocycline on cytokine production by M2 macrophages originating from the M2 PBMC-derived macrophages were next assessed and displayed in Figure 6.21. Here, there was again an increase in IFN-γ production following minocycline treatment when compared to LPS alone, increasing by 1.3-fold (p=0.0464) (Figure 6.20 A1). Furthermore, data pertaining to IL-1β was also like that observed in the M1 experiments as minocycline at 25μM again resulted in reduced production across all donors tested versus the LPS only control (Figure 6.20 A2). Here both 10μM and 25μM minocycline reduced the production of IL-1β by 0.9- (p=0.0041) and 0.7-fold (p<0.0001) respectively. Similarity in the response of both sets of macrophages also existed when assessing IL-6, and TNF-α, with minocycline causing a significant reduction in production of both cytokines versus LPS (Figure 6.20 A3-A5). Although some consistency was seen within the IL-12p40 and IL-12p70 data sets, there is disparity amongst donors, and thus given the proximity of the data points to the assay detection limit, it may be necessary to corroborate this data with a more sensitive technique.

Finally, Figure 6.21 panel B also outlines the results for the two M2-associated cytokines IL-4 and IL-10, and although the data for IL-4 noted no change in

expression by minocycline versus LPS (Figure 6.21 B1), there was downregulation of IL-10 following minocycline treatment when compared to LPS alone (Figure 6.21 B2). There was a 0.88-fold decrease in IL-10 production elicited by 25μM minocycline again with a positive correlation between minocycline concentration and the magnitude of IL-10 reduction seen. This potent reduction in IL-10 is consistent with the results obtained for the M1 macrophage experiments within the THP-1 model, in addition to those reported in chapter 5 when minocycline was administered prior to, and during polarization. Having corroborated a decrease in IL-10 across multiple experimental models utilizing distinct macrophage phenotypes further suggests that minocycline may be provoking direct modification of IL-10 production.

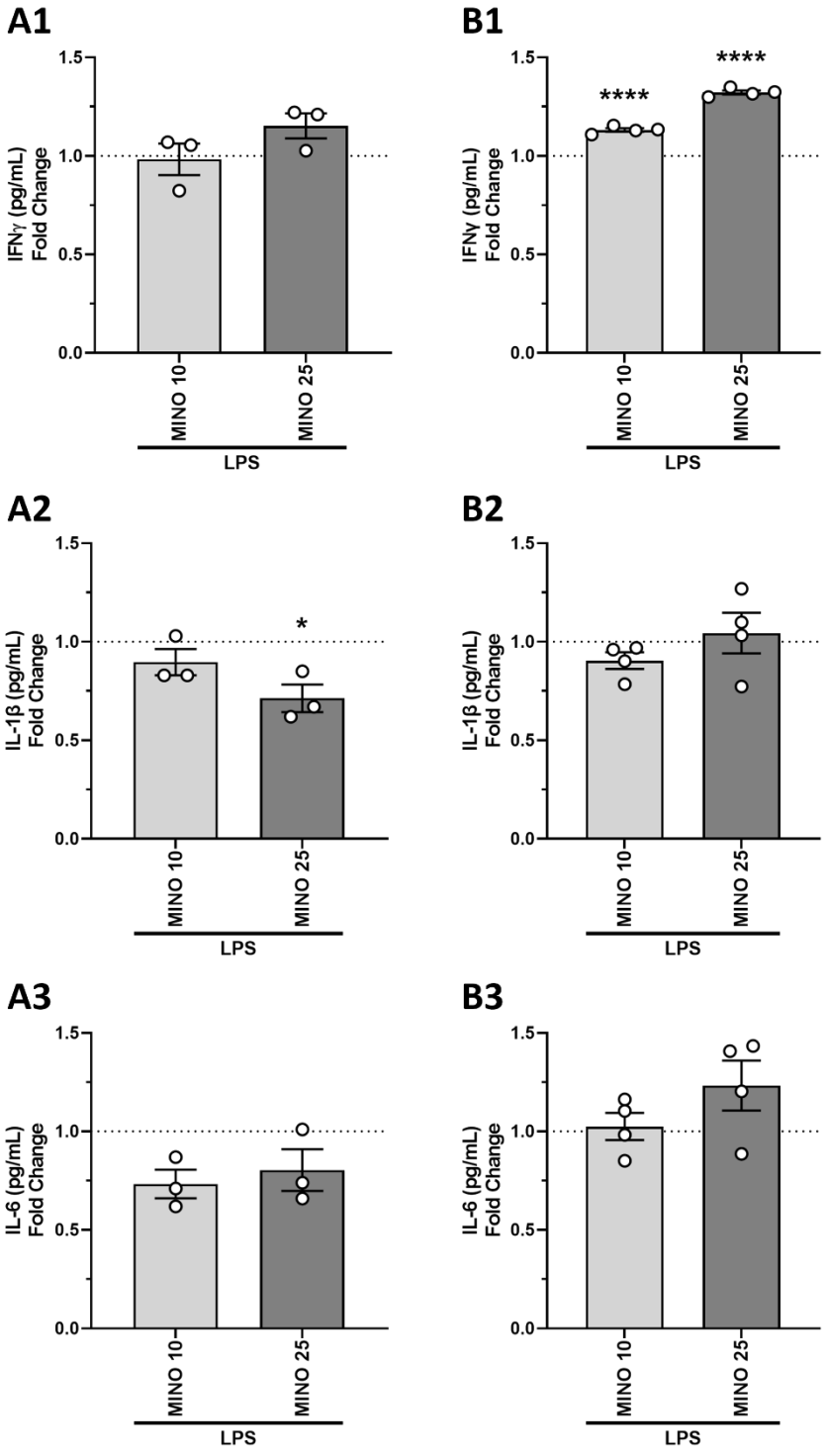
A1
IFNγ (pg/mL) Fold Change
1.5
1.0
0.5
0.0
MINO 10
MINO 25
LPS
B1
****
****
IFNγ (pg/mL) Fold Change
MINO 10
MINO 25
LPS
A2
IL-1β (pg/mL) Fold Change
*
MINO 10
MINO 25
LPS
B2
IL-1β (pg/mL) Fold Change
MINO 10
MINO 25
LPS
A3
IL-6 (pg/mL) Fold Change
MINO 10
MINO 25
LPS
B3
IL-6 (pg/mL) Fold Change
MINO 10
MINO 25
LPS

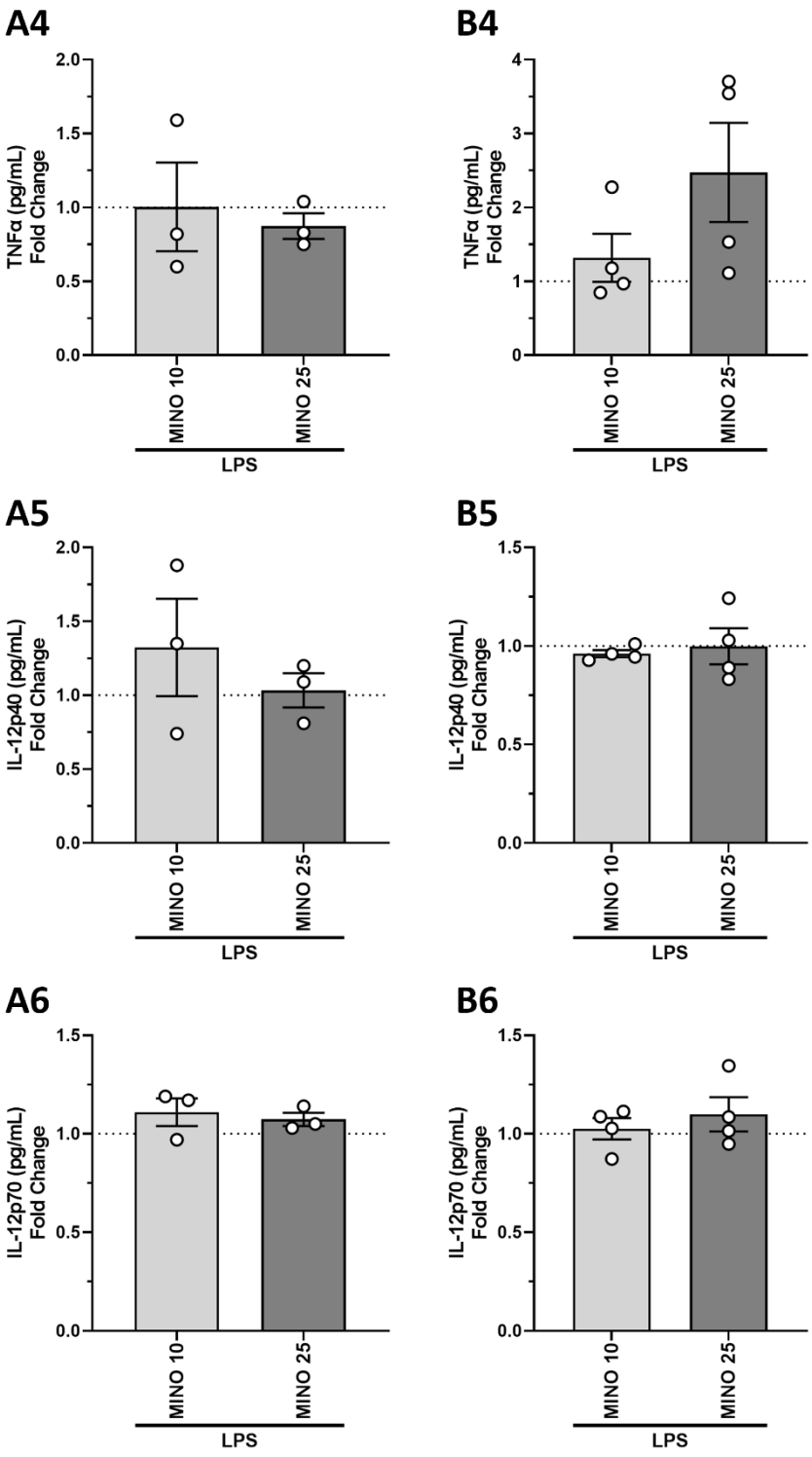

Figure 6.19: Effect of minocycline on M1-associated cytokine production by LPS-activated THP-1 (Panel A) and PBMC-derived (Panel B) M1 macrophages. Data obtained from supernatant analysis after 2hr pre-treatment with minocycline of M1 macrophages and a further 24hr incubation with LPS (100ng/mL). MINO 10 = minocycline 10μM, MINO 25 = minocycline 25μM, Veh = DMSO vehicle control (1:1000). Bar graphs showing data for M1-associated cytokines IFN-γ [1], IL-1β [2], IL-6 [3], TNF-α [4], IL-12p40 [5] and IL-12p70 [6]. Data presented as relative fold change versus the M1+Veh (Veh) [Panel A], or LPS- only [Panel B] control group

indicated at 1. Graphs represent data from 3 repeated experiments each comprising triplicate readings for THP-1 [Panel A], and 4 donors each comprising of duplicate values for PBMCs [Panel B]. Data presented as mean ± SEM. One-way ANOVA with post hoc Dunnett's applied versus the relevant control. *p<0.05; ****p<0.0001.

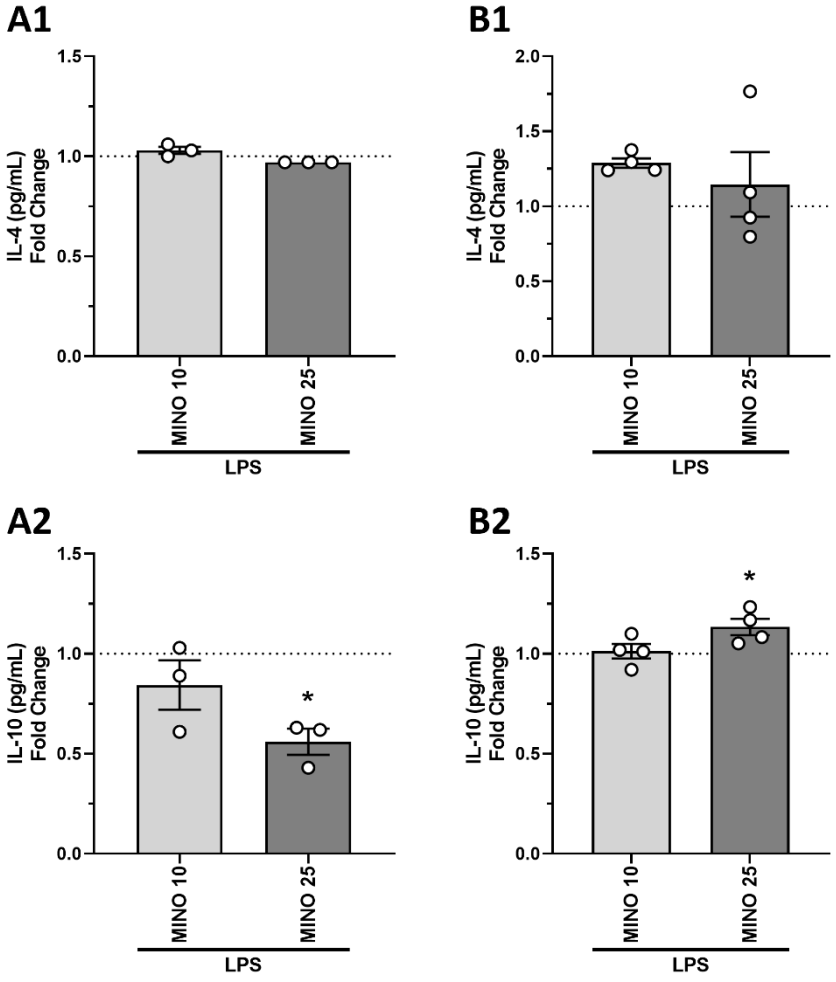

Figure 6.20: Effect of minocycline on M2-associated cytokine production from LPS-activated THP-1 [Panel A] and PBMC-derived [Panel B] M1 macrophages. Data obtained from supernatant analysis after 2hr pre-treatment with minocycline of M1 macrophages and a further 24hr incubation with LPS (100ng/mL). MINO 10 = minocycline 10μM, MINO 25 = minocycline 25μM, Veh = DMSO vehicle control (1:1000). Bar graphs showing data for M2-associated cytokines IL-4 [1] and IL-10 [2]. Data presented as relative fold change versus the M1+Veh (Veh) [Panel A], or LPS-only [Panel B] control group indicated at 1. Graphs represent data from 3 repeated experiments each comprising triplicate readings for THP-1 [Panel A], and 4 donors each comprising of duplicate values for PBMCs [Panel B]. Data presented as mean ± SEM. One-way ANOVA with post hoc Dunnett's applied versus the relevant control. *p<0.05.

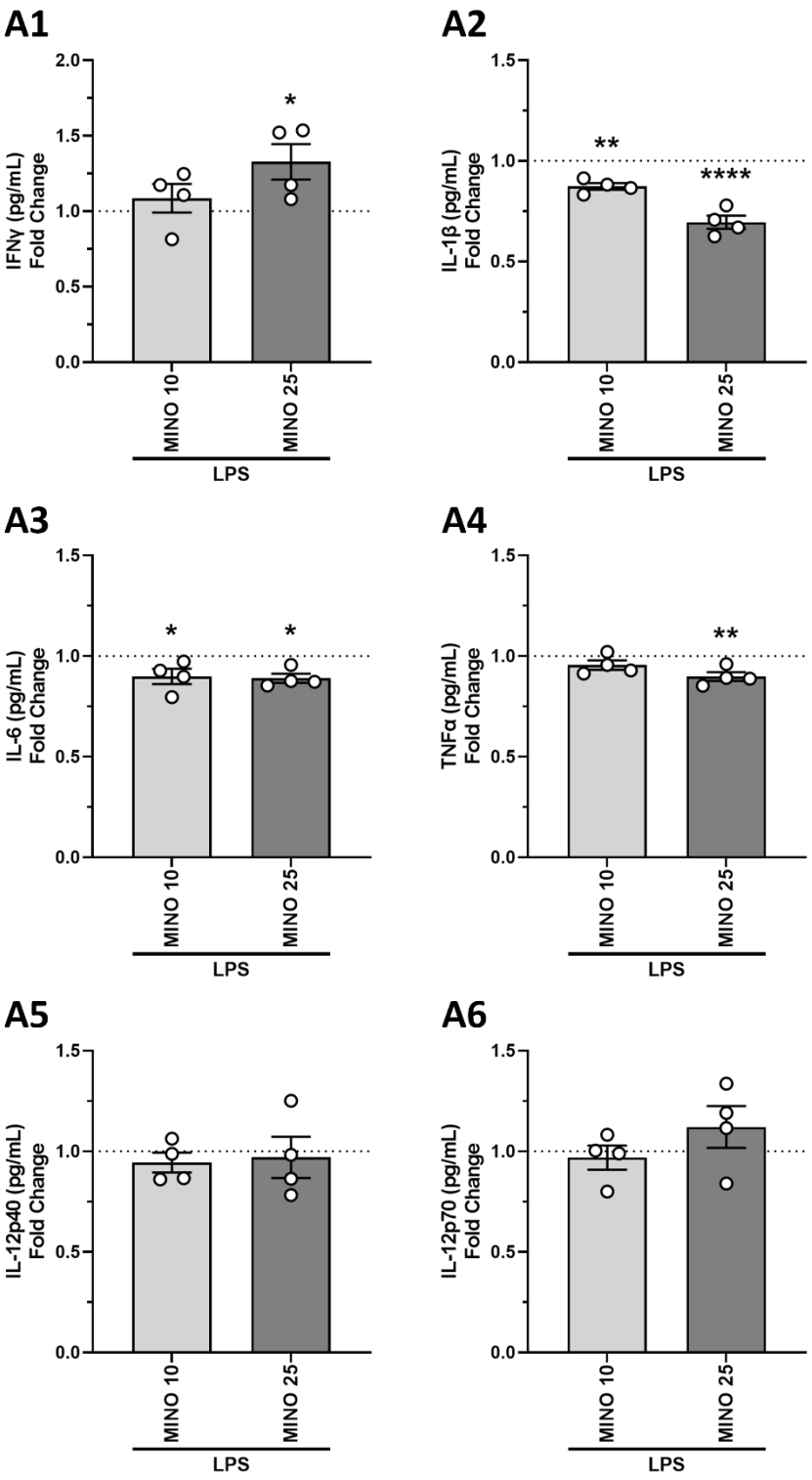
A1
IFNγ (pg/mL) Fold Change
2.0
1.5
1.0
0.5
0.0
*
MINO 10
MINO 25
LPS
A2
IL-1β (pg/mL) Fold Change
1.5
1.0
0.5
0.0
**
****
MINO 10
MINO 25
LPS
A3
IL-6 (pg/mL) Fold Change
1.5
1.0
0.5
0.0
*
*
MINO 10
MINO 25
LPS
A4
TNFα (pg/mL) Fold Change
1.5
1.0
0.5
0.0
**
MINO 10
MINO 25
LPS
A5
IL-12p40 (pg/mL) Fold Change
1.5
1.0
0.5
0.0
MINO 10
MINO 25
LPS
A6
IL-12p70 (pg/mL) Fold Change
1.5
1.0
0.5
0.0
MINO 10
MINO 25
LPS

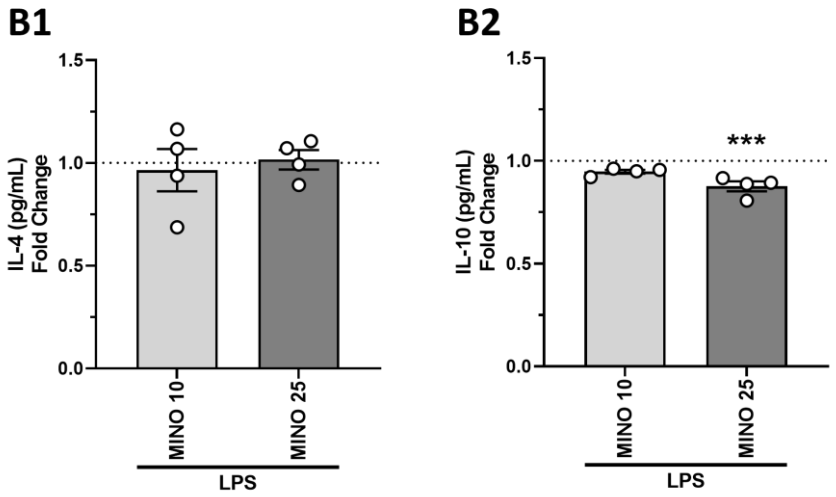

Figure 6.21: Effect of minocycline on M1- [Panel A] and M2-associated [Panel B] cytokine production from LPS-activated M2 PBMC-derived macrophages. Data obtained from supernatant analysis after 2hr pre-treatment of M2 macrophages with minocycline and a further 24hr incubation with LPS (100ng/mL). MINO 10 = minocycline 10μM, MINO 25 = minocycline 25μM, Veh = DMSO vehicle control (1:1000). Bar graphs showing data for M1-associated cytokines IFN-γ [1], IL-1β [2], IL-6 [3], TNF-α [4], IL-12p40 [5] and IL-12p70 [6], and M2-associated cytokines IL-4 [1] and IL-10 [2]. Data presented as relative fold change versus the LPS-only control group indicated at 1. Graphs represent data from 4 donors each comprising of duplicate values. Data presented as mean ± SEM. One-way ANOVA with post hoc Dunnett's applied versus the LPS only control. *p<0.05; **p<0.01; ***p<0.001; ****p<0.0001.

6.5. Chapter discussion

As referenced in the previous chapter, macrophages and their subsets identify different stimuli in the tissue microenvironment and respond appropriately with the goal of maintaining homeostasis, with classically-activated M1 macrophages displaying potent cytotoxic action, and alternatively-activated M2 cells acting to suppress the inflammatory response (Sica *et al.*, 2015; Shapouri-Moghaddam *et al.*, 2018; Moreira Lopes, Mosser and Gonçalves, 2020). Although the consensus also considers these macrophage populations to be transient and plastic, it is crucial in the avoidance of pathophysiology to maintain equilibrium between these distinct subsets (Camille and Dealtry, 2018).

Previous chapters discussed how during IBD, the intestinal mucosa becomes disrupted, encompassing compromised epithelial function, increased permeability, and the consequential invasion of luminal antigens into the underlying tissue (Moreira Lopes, Mosser and Gonçalves, 2020). If unresolved and left to enter a state of persistent 'chronic' inflammation, the contribution of

host inflammatory mechanisms, not exogenous pathogens, becomes chiefly responsible for resultant host pathophysiology, suggesting the existence of continual self-perpetuation of inflammatory cascades (Nathan and Ding, 2010). Thus, the development and progression of IBD can be partially attributed to a hindered ability of the host immune response to terminate and control inflammatory mechanisms, with a failure of macrophages to initiate appropriate resolution cascades resulting in prolonged damage to local tissue and the consequent development of chronic inflammation (Zhang and Mosser, 2008; Moreira Lopes, Mosser and Gonçalves, 2020).

In chapter 3 it was investigated if minocycline influenced monocyte-macrophage differentiation. Next, in chapter 4, the role of minocycline upon the activation of resting or naïve M0 macrophages when challenged with LPS was explored, and in the proceeding chapter 5 its influence in the polarization to M1 and M2 subsets was investigated. Here, in the final results chapter, minocycline's effect on the activation of pre-polarized subsets in response to LPS was assessed. By doing this some opposing roles of minocycline dependant on the time point and maturation phase at which it is introduced have been identified. Within this chapter, which looked at the effect of minocycline during LPS activation of pre-polarized macrophage subsets and if data that was corroborated either across cellular models or firmly between biological replicates only is considered, a few key findings from these investigations can be distinguished. Firstly, in sections 6.2. which assessed the effect of minocycline on surface marker expression in THP-1-derived M1 macrophages, and 6.4. which assessed minocycline on surface marker expression of PBMC-derived M1 and M2 macrophages, there is consistent upregulation of the surface marker CD163 seen across both the THP-1 and PBMC macrophage models and within both the M1 and M2 cultures.

It was previously discussed in chapter 4 how CD163 expression is highly expressed by macrophages and functions to bind a variety of ligands and promote the removal of non-self or altered-self antigens (PrabhuDas *et al.*, 2017). Although CD163 is a key feature of macrophage differentiation to an alternatively activated M2 phenotype, and which is directly modified by IL-10 stimulation, an increase in CD163 expression elicited by minocycline within both M1 and M2 cultures is reported here when compared to the LPS only control, which is also consistent with data obtained in chapter 5 in which minocycline was administered

during M1 and M2 polarization. However, despite reports describing a sensor-like function of CD163 in response to *Streptococcus* mutants, *Escherichia coli*, and *Staphylococcus aureus*, where CD163 promoted bacteria-induced production of pro-inflammatory cytokine TNF-α (Kneidl *et al.*, 2012), in this model there is in fact no correlation between an increase in CD163 expression and the production of IL-10 and TNF-α, with both cytokines actually appearing to be reduced within the THP-1 model of M1 macrophages and the PBMC-derived M2 macrophages upon treatment with minocycline and when compared with the LPS only group. This may suggest an independent mechanism of CD163 alteration exerted by minocycline considering minocycline within this setting was not shown to increase or decrease the production of IL-10 and TNF- α respectively, which are classic stimulators and effectors of CD163.

Potent modification of CD14, CD80 and CD206 within the THP-1 model was highlighted in section 6.1.2. which reiterates the previous implication of minocycline in the phenotypic switch from pro-inflammatory M1, to anti-inflammatory M2, in addition to rendering cells hyporesponsive to further TLR activation by LPS. This data, however, was again not mirrored by the PBMC data alike chapter 5 when minocycline was administered during polarization, and thus would benefit from replication using larger data sets or alternative cellular models.

Despite the inconsistencies between THP-1 and PBMC data regarding surface marker expression, as in earlier chapters, it was possible to obtain far more consistent data in relation to cytokine production with some very interesting results. The first key outcome described in section 6.6. was a consistent increase in IFN-γ production in response to LPS by both M1 and M2 macrophages and seen with both the THP-1 and PBMC models. In conjunction, additional downregulation of IL-10 within the THP-1-derived and PBMC-derived M1 and M2 macrophages was also observed when minocycline was administered during activation of pre-polarized subsets and compared to the LPS only control. In chapter 5 the same results were concluded, with an increase in IFN-γ and simultaneous decrease in IL-10 elicited by treatment with minocycline when administered during M1 and M2 polarization and compared to the un-treated group. Given their key roles in host protection and post-infection immunopathology which are discussed at length in chapter 3 (Burke and Young, 2019; Mezouar and Mege, 2020), a homeostatic role of minocycline on M2

macrophage phenotype was hypothesised, whereby minocycline regulates the usual biology of M2 subsets through limiting IL-10 production but promoting IFN-y. This finding was interesting given the lack of published reports also describing this effect. A 2018 paper by Tanita *et al*, correlated a clinical benefit of minocycline to its suppressive effects against the production of specific Th2 chemokines from M2 macrophages, which they hypothesized could contribute to the recruitment of Th2 cells and eosinophils in the lesional skin of bullous pemphigoid patients (Tanita *et al.*, 2018). However, this particular study did not directly measure IL-10, nor were any reports found associating modification of both IL-10 and IFN-γ from M2 macrophages to minocycline treatment. Given the limited literature it is speculated that simultaneous inhibition of IL-10 and promotion of IFN- γ may likewise contribute to the recruitment of both Th1 and Th2 effectors to sites of inflammation. It seems that minocycline, therefore, was able to modify the phenotype of the cells when administered during polarisation but also their response to LPS if administered to fully polarised cells which were subsequently challenged with LPS.

A further consistent feature of minocycline was the reduction of IL-1β. In section 6.6. a decrease in IL-1β production by M1 or M2 subsets when treated with minocycline during LPS activation when compared to the LPS only control was seen. This feature was consistent with both chapter 4 - in which minocycline was administered to resting M0 macrophages during LPS activation, and chapter 5 - whereby minocycline was administered during M1 and M2 polarization. As discussed in chapter 5, IL-1β is a potent pro-inflammatory cytokine crucial for host-defence responses to infection and injury, but which may also exacerbate damage during chronic disease and acute tissue injuries if left unregulated (Lopez-Castejon and Brough, 2011, p.). IL-1β has been shown to promote the differentiation of monocytes to M1-like macrophages, induce type 1 immune responses, polarize αβ $CD4^+$ T cells towards Th1, and favour the differentiation of αβ $CD4^+$ T cells towards Th17 (Acosta-Rodriguez *et al.*, 2007; Schenk *et al.*, 2014; Hutton *et al.*, 2016; Bent *et al.*, 2018).

Although largely beneficial, an over production can increase the risk of developing metabolic and autoinflammatory diseases with reports linking IL-1β overproduction to the development of Ulcerative colitis and Crohn's disease in both IBD patients and murine models (Mahida, Wu and Jewell, 1989). The

existence of consistent and corroborated downregulation of IL-1β following minocycline administration may underline a direct inhibitory function of minocycline on IL-1β production rather than an inhibitory action on the downstream activation of the NF-κB and MAPK pathways that upregulate additional pro-inflammatory cytokines such as IL-6 and TNF (Guarda and So, 2010; Sahoo *et al.*, 2011) which were demonstrated to be increased within this model of M1/M2 activation in response to minocycline. Thus, a reduction in IL-1β may limit both the further differentiation of macrophages to an M1 phenotype, and polarization and accumulation of other pro-inflammatory effects to the site of inflammation.

A key observation is the opposing influence of minocycline dependant on administration time point on the production of M1-associated cytokines TNF-α and IL-6 was identified. In chapter 5 minocycline decreased the production of both TNF-α and IL-6 when administered during M1 polarization without latter LPS activation in both the THP-1 and PBMC models. However, here, there is contrasting data illustrating an increase in these cytokines when minocycline is administered during LPS activation of pre-polarized M1 macrophages using the PBMC model. Both TNF-α and IL-6 have key roles in the development of chronic inflammation and have been specifically implicated in IBD. It was also discussed in detail in chapter 5 how IL-6 has been found at higher levels in various diseases, including IBD (Műzes *et al.*, 2012), with experimental models of colitis describing IL-6 as a major contributory cytokine within the chronic phase of inflammation (Atreya *et al.*, 2000; Yamamoto *et al.*, 2000). Moreover, additional research further implicates IL-6 in the maintenance of inflammation and onset of chronic disease as in the case of IBD relapse in part via control of leukocyte trafficking (Jones *et al.*, 2005; Kai *et al.*, 2005; Gabay, 2006).

Whereby bacterial pathogens and other noxious stimuli induce TNF-α via TLRs and NF-κB signalling, production of TNF-α is prominent in the subsequent initiation of a highly complex biological cascades involving chemokines, cytokines and endothelial adhesions that recruits and activates neutrophils, macrophages, and lymphocytes at sites of damage and infection (Locksley, Killeen and Lenardo, 2001; Akira and Takeda, 2004). Thus, while TNF-α is a critical component of innate and adaptive immunity, if unregulated, acts as a positive autocrine feedback signal to further activate NF-κB, and induce the production of more

TNF-α and other cytokines such as GM-CSF and IL-8, resulting in chronic inflammation and generalised wasting (Balkwill, 2006). In this regard, both pre-clinical and clinical trials have described an increase in TNF-α and its receptors at sites of chronic inflammation in conditions such as neuropathology, rheumatoid arthritis , cancer, and IBD., Increased levels of TNF-α have also been located in the intestinal mucosa, serum, and faeces of IBD juvenile patients (Pirenne *et al.*, 1992; Breese *et al.*, 1994). Further studies have also implicated TNF-α in the degradation of the epithelial barrier and subsequent regulation of tight-junctions (Ozaki *et al.*, 1999; Laukoetter *et al.*, 2007; Vetrano *et al.*, 2008).

Despite these implications of TNF-α and IL-6 in chronic inflammation, observing a decrease in their production when minocycline is administered during polarization, but an increase if administer during LPS activation of pre-polarized subsets may suggest a role of minocycline in initial exacerbation of inflammation through upregulation of potent pro-inflammatory mediators which may then allow for efficient exchange to pro-resolving mechanisms and the avoidance of chronic inflammation. With the data highlighting that M1 and M2 macrophages produce more cytokines in response to LPS when in the presence of minocycline strongly suggests that minocycline can exacerbate the response in this setting. However, if macrophages are polarised in the presence of minocycline, they conversely becoming less proinflammatory, suggesting a shift to more pro-resolving phenotype.

The data here alludes to a regulatory role of minocycline whereby it seems to exacerbate early acute inflammation via upregulation of M1-associated cytokines such as the production of TNF-α, IL-6 and IFN-γ if administered upon LPS activation, but simultaneously inhibits the development of chronic inflammation by dampening the expression of pro-inflammatory cytokines during polarization. Previous *in vivo* data provide further support of this modifying property of minocycline in which minocycline treatment of DSS-induced colitis in mice, resulted in increased IL-1β and IL-6 at 2 days post treatment, but decreased production at 4 days post treatment. Furthermore, minocycline seems to also limit the probability of aberrant M2-associated pathologies such as cancer and tumour formation through minimizing potent pro-resolving signatures such as IL-10 and CD206 allowing homeostatic regulation of each phenotype (Boyano *et al.*, 2000; Enninga *et al.*, 2018; Linde *et al.*, 2018; Yan *et al.*, 2018).

7. Discussion & conclusions

7.1. Project discussion

As was outlined in detail in chapter 1, section 1.3, the use of tetracyclines as immunomodulatory agents has gained increasing interest in the past two decades, with minocycline specifically reported to ameliorate experimental colitis through modulation of both the intestinal microbiota and the immune response (Garrido-Mesa, Camuesco, *et al.*, 2011a; Garrido-Mesa, Utrilla, *et al.*, 2011b). Furthermore, the studies conducted by Garrido Mesa and Garrido Mesa *et al* in 2011, 2015 and 2018 highlighted minocycline's effect on enhanced monocyte recruitment to the colon, phenotype switching of colonic macrophages from pro- to anti-inflammatory, and changes in the secretion of pro-inflammatory cytokines such as IL-1β and IL-6, seen using both *in vivo* and *in vitro* models (Garrido-Mesa, Camuesco, *et al.*, 2011a; Garrido-Mesa, Utrilla, *et al.*, 2011b; Garrido-Mesa, Algieri, Rodriguez-Nogales, Mª Pilar Utrilla, *et al.*, 2015; Garrido-Mesa, Rodríguez-Nogales, *et al.*, 2018b). However, despite these promising results, there remains no definitive data on the specific mechanism by which minocycline may influence macrophage development, function, and phenotype in the context of IBD. Therefore, the aim of this project was to "characterize the direct effects of minocycline on macrophage biology, with primary focus on macrophage differentiation, phenotype and function, and to subsequently investigate the mechanisms mediating these effects".

The key findings from the investigations conducted within this project are depicted below in Figure 7.1 and highlight the compound influence of minocycline on macrophage biology, from monocyte -macrophage differentiation, activation with bacterial LPS and polarization to M1 and M2 phenotypes.

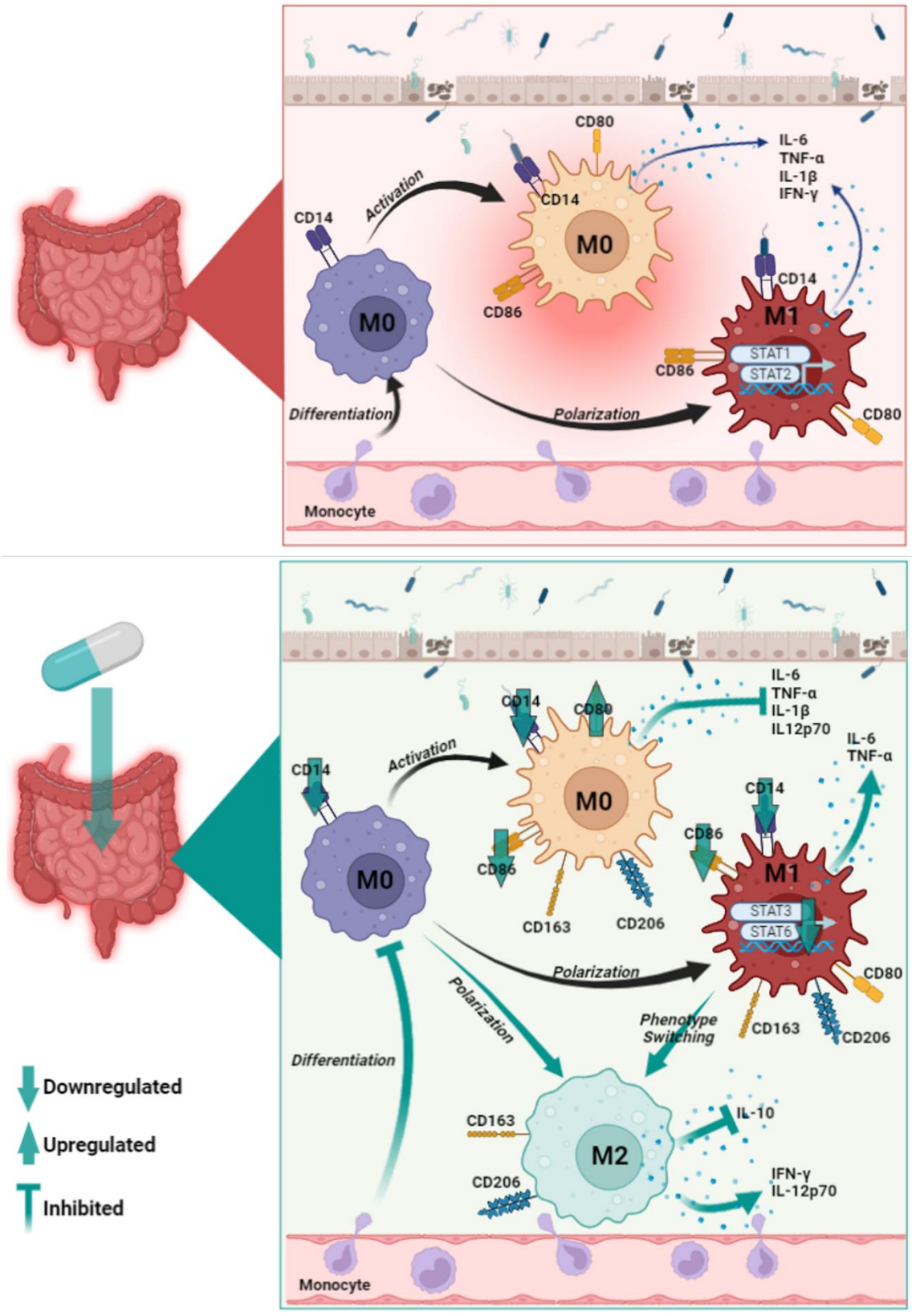
CD80
IL-6
TNF-α
IL-1β
IFN-γ
CD14
Activation
M0
CD14
CD86
M1
STAT1
STAT2
CD86
CD80
Differentiation
Polarization
Monocyte
IL-6
TNF-α
IL-1β
IL12p70
IL-6
TNF-α
CD14
CD80
Activation
CD14
M0
CD86
CD14
CD86
M1
STAT3
STAT6
CD163
CD206
Polarization
CD80
Polarization
Phenotype Switching
CD163
CD206
Differentiation
CD163
IL-10
M2
CD206
IFN-γ
IL-12p70
Monocyte
Downregulated
Upregulated
Inhibited

Figure 7.1: Key effects of minocycline on macrophage biology in the context of intestinal inflammation. In the context of IBD (top) local inflammation within the colon occurs which results in epithelial barrier dysfunction and infiltration of exogenous pathogens from the intestinal lumen. Under these inflammatory conditions circulating monocytes migrate into the lamina propria and differentiate into M0 macrophages. These M0 macrophages, upon stimulation with bacterial products such as LPS become activated and upregulate surface expression of the T cell co-stimulatory proteins CD86, CD80, as well as the LPS-response element CD14. Local IFN-γ and LPS also trigger polarization of M0 macrophages via STAT1/STAT2 transcription factors to pro-inflammatory M1, in which further upregulate CD80, CD86 and CD14. Both M0 and M1 macrophages dominate the compartment and produce high levels of pro-inflammatory cytokines IL-6, TNF-α, IL-1β and IFN-γ. Based on previous reports and *in vitro* investigations within this thesis, when treated with minocycline macrophage phenotype and function are altered, showing a shift towards an anti-inflammatory M2 phenotype. Monocyte-macrophage differentiation is disrupted resulting in less M0 accumulation, while simultaneously changing the terminal phenotype of both the resting and LPS-activated M0 macrophages reducing the expression of CD86 and CD14, but increasing CD80, CD163 and CD206. Polarization to M1 is also disrupted with downregulation in the transcription factors *stat3* and *stat6*, and changes in the acquired phenotype of these cells, with similar downregulation of CD86 and CD14, but enhancement of the M2-associated markers CD163 and CD206. In addition, minocycline inhibits the production of IL-6, TNF-α, IL-1β and IL12p70 from the activated M0 macrophages but under the same conditions enhances the production of IL-6 and TNF-α from the M1. Moreover, minocycline seems to preferentially drive polarization towards an M2 phenotype, which express high levels of CD206 and CD163. Interestingly, in this context minocycline also appears to limit typical IL-10 production from these cells but produces greater amounts of IFN-γ and IL-12p70. Overall, minocycline seems to modulate macrophage function in the context of intestinal inflammation through reducing pro-inflammatory phenotype acquisition and mediator release referencing an anti-inflammatory M2, but simultaneously controls over-production of potent anti-inflammatory mediators such as IL-10 thus limiting the chance of IL-10-mediated pathology.

Previous research has shown minocycline specifically influences the immune cell populations both circulating in the blood as well as those present in the lamina propria in the colon during intestinal inflammation using the mouse model of DSS-induced colitis. This study attributed minocycline's intestinal anti-inflammatory effect to a possible potentiation of the innate immune response in the intestine, leading to an earlier resolution of the inflammatory process due to a higher number of pro-inflammatory Ly6C^{+}MHC II+ macrophages located in the gut at initial stages of the inflammatory process, which then differentiated into a pro-resolving Ly6C^{-}MHCII^{+} phenotype (Garrido-Mesa, Rodríguez-Nogales, *et al.*,

2018a). Importantly, they also reported a higher percentage of monocytic cells in the blood stream of minocycline treated animals at both 2- and 4-days post treatment, therefore it was of interest to assess whether minocycline was directly influencing the monocyte-macrophage axis or whether this was an indirect outcome.

As discussed in chapter 3, mature macrophages in the adult mucosa have poor proliferative capacity suggesting an unlikely role of *in situ* self-renewal in macrophage replenishment and monocyte recruitment to be the key mechanism of replenishment for intestinal macrophage populations (Smythies *et al.*, 2006; Bain *et al.*, 2013; Calum C. Bain and Mowat, 2014). Therefore, investigations began by exploring the role of minocycline on monocyte-macrophage differentiation using an *in vitro* model of PMA-driven THP-1 and U-937 differentiation. The data in this model suggests that minocycline seems to inhibit the differentiation of monocytes to macrophages. This was reflected in the reduced number of adherent cells recovered when minocycline was administered to cultures during PMA-driven differentiation. A reduction in adherent cells suggests disruption of the differentiation process given this identifiable change in macrophage morphology acquisition. As mentioned above, the work published by Garrido-Mesa *et al* in 2018 reported a correlation between treatment with minocycline and both increased percentages of monocytes in the blood stream and a higher number of pro-inflammatory Ly6C^{+}MHC II+ macrophages located in the gut of colitic mice at initial stages of the inflammatory process (Garrido-Mesa, Rodríguez-Nogales, *et al.*, 2018b). In this regard, contradictory evidence was displayed whereby minocycline does not in fact directly promote monocyte-macrophage differentiation, but instead inhibits this process as seen by the reduction in adherent cells.

In addition to reducing the number of macrophages that differentiated from monocytes, it was reported in chapter 3 that minocycline influenced the terminal phenotype of the differentiated macrophages, significantly reducing CD14 and CD86 expression. This data partially coincided with the previous observations made by Garrido Mesa *et al*, in which minocycline was shown to influence the phenotype of M0 macrophage populations from that displaying an initial inflammatory signature to that which is more anti-inflammatory. However, this amendment in terminal phenotype was not limited to the investigations on

monocyte-macrophage differentiation and was reported across all 4 experimental protocols used.

Given the downregulation of CD14 seen in chapter 3, in chapter 4 the THP-1, U-937 *in vitro* systems were again used in combination with PBMC-derived macrophages to understand the role of minocycline on the response on resting M0 macrophages to LPS challenge. Previous data supported this avenue of investigation, with the article by Garrido Mesa *et al* reporting increased cytokine concentration in the culture supernatant of LPS-stimulated BMDM after 24hr of pre-incubation with minocycline (Garrido-Mesa, Rodríguez-Nogales, *et al.*, 2018a). With this accounted for, the influence of minocycline on the response of M0 macrophages when challenged with LPS was considered. A reduction in CD14 expression upon minocycline treatment was again observed in this setting. This result further extended into chapter 6 which then aimed to understand how different macrophage phenotypes respond to LPS challenge given the recurrent nature of IBD, and the previous evidence that minocycline *in vivo* promotes an early influx of pro-inflammatory Ly6C^{+}MHC II+ macrophages within the gut, which then differentiate into a pro-resolving Ly6C^{-}MHCII^{+} phenotype (Garrido-Mesa, Rodríguez-Nogales, *et al.*, 2018a). Here, again, the ability of minocycline to downregulate CD14 was highlighted.

CD14 plays a crucial role in pathogen recognition and immune cell activation, LPS binding, release of pro-inflammatory mediators, and phagocytic clearance and cellular apoptosis (Zamani *et al.*, 2013). Moreover, previous data also communicates that the innate immune system is poorly activated by LPS alone and requires both LPS binding protein and transfer on CD14. This leads to LPS being chaperoned by CD14 to the LPS receptor complex comprised of TLR4 MD2, resulting in the production of pro-inflammatory cytokines and type I interferons (Bode, Ehlting and Häussinger, 2012; Płóciennikowska *et al.*, 2015). Therefore, from the data generated in this project it was hypothesized that a significant reduction in this marker could correlate minocycline with a decrease in macrophage sensitivity to pathogenic stimulus, potentially suggesting a key role of minocycline in dampening the ability of macrophages to respond to invading bacteria.

Similarly, a downregulation in CD86 expression upon minocycline treatment was also reported, but which was conversely accompanied by upregulation of CD80 when studying both monocyte-macrophage differentiation (Chapter 3), and macrophage activation with LPS (Chapter 4 and 6). Given that CD86 and CD80 are the main co-stimulatory molecules expressed on the surface of macrophages and other APCs and are required for complete T-cell activation (Rivellese *et al.*, 2014; Taddio *et al.*, 2021), a downregulation of this marker could imply that minocycline treatment not only results in desensitization of macrophages to later stimulus, but also influences their ability to recruit additional immune cell populations and stimulate T-cell activation or the induction of tolerance. This furthers strengthens the hypothesis that minocycline modifies macrophage phenotype from a pro-inflammatory state ($CD14^{hi}CD86^{+}$) to a typical hypo-responsive intestinal macrophage baseline ($CD14^{low}$ $CD86^{low}$). Furthermore, this data, in combination with a lack of modification seen when studying *tlr4* gene expression suggests any alteration in cellular response to LPS was not necessarily due to direct modification of TLR4 expression by minocycline in this study, but rather an influence on its soluble counterpart CD14.

Considering the widely documented existence of increased macrophage CD14 expression in IBD patients and experimental models of colitis (Kamada *et al.*, 2008; Bain *et al.*, 2013; Lampinen *et al.*, 2013; Ogino *et al.*, 2013; Thiesen *et al.*, 2014), an inhibitory effect of minocycline on its expression may have beneficial therapeutic application in reducing innate cell LPS-sensitivity. Moreover, $CD14^{hi}$ monocyte and macrophage populations in the mucosa of IBD patients are thought to support pathogenic T cell function through the expression CD80 and CD86 (Rugtveit *et al.*, 1997) via binding to CD28 or CTLA-4 which promotes T cell activation resulting in downregulation of T cell function – a critical stage in inhibiting the immune response following infection resolution (Freeman *et al.*, 1995; Rugtveit *et al.*, 1997). The literature proposes different functional consequences of CD28 engagement by CD80 and CD86, the consensus suggesting a situation whereby CD80 co-stimulation promotes the development of Th1 cells, while co-stimulation with CD86 preferences Th2 differentiation (Slavik, Hutchcroft and Bierer, 1999). Based upon the data shown here in chapters 4, 5 and 6, it is hypothesised that minocycline may behave in a way that potentiates downstream humoral immunity in the form of Th1 recruitment and

activation through upregulation of CD80. It is considered that this may aid the initial acute response to inflammation which may counterintuitively support quicker resolution through mounting a strong pro-inflammatory response of macrophages to exogenous stimuli like LPS. This hypothesis is supported by the data disseminated by Garrido Mesa *et al* in which increased pro-inflammatory cytokines were noted at 2-days post treatment with minocycline, but which declined at 4-days (Garrido-Mesa, Rodríguez-Nogales, *et al.*, 2018a). It is thought that this pronounced acute response to inflammation may limit the development of chronic inflammation due to quick and efficient removal of pathogenic stimuli. The data in these chapters also highlighted the ability of minocycline in downregulating CD80's counterpart CD86, which may further correlate with reduced downstream Th2 populations, thus limiting the negative regulatory function of Th2 on the macrophages themselves. This possible attenuation of Th2 function by minocycline such as limited secretion of IL-4 and IL-13 may also help limit M2 macrophage associated pathology following phenotype switching such as fibrosis and tumour formation (Tjiu *et al.*, 2009).

The final crucial observation made regarding the effect of minocycline on macrophage phenotype was the pronounced acquisition of an M2-like phenotype via upregulation of CD163 and CD206 expression. In chapter 3, when studying the effect of minocycline on monocyte-macrophage differentiation, although not statistically significant, concentration dependant increases in the percentage of CD206 and CD163 expressing cells was observed. This highlights an ability of minocycline to not only disrupt the differentiation process itself as discussed above, but also modify the terminal phenotype of the macrophages themselves, preferencing the expression of M2-associated pro-regulatory proteins. This could suggest that in a non-inflammatory setting (absence of exogenous antigen stimulation) minocycline preferences the development of classical intestinal macrophages through acquisition of scavenger receptors such as CD163 and CD206 and development of hypo-responsiveness to TLR ligation $CD14^{low}$ (Bain et al., 2013).

This phenotype preferencing was further investigated throughout chapters 4, 5 and 6 in which macrophages were polarized and/or challenged with LPS considering the role of these scavenger receptors in the removal of non-self targets, and promotion of bacteria-induced pro-inflammatory cytokine production

(Fabriek *et al.*, 2009; PrabhuDas *et al.*, 2017; Nielson *et al.*, 2020). Interestingly, and as initially suggested from this data when exposing macrophages to minocycline during differentiation, minocycline continued to display a potent ability to upregulate the expression of both CD163 and CD206 in macrophages upon LPS challenge, and when administered during polarization to M1 and M2 phenotypes despite significant pro-inflammatory stimulus, with this data clear and pronounced in the THP-1 model.

It was discussed at length throughout this thesis how CD163 expression is restricted to the monocytic–macrophage linage and that $CD163^{+}$ macrophages may originate from extravasation of monocytes, or may represent macrophage activation switching (Porcheray *et al.*, 2005), with reports concluding upregulation of CD163 a feature of macrophage differentiation to 'alternatively activated' M2-type macrophages (Barros *et al.*, 2013). However, on the other hand, CD206 is noted in the literature to be an efficient endocytic receptor which recognises a wide variety of ligands including mannose, collagen and peptide hormones, in addition to allergens and microbial products such as LPS (Zamze *et al.*, 2002; Gazi and Martinez-Pomares, 2009; Martinez-Pomares, 2012). Witnessing consistent upregulation of these markers suggests minocycline is promoting an M2 macrophage phenotype that can maintain their ability to sense exogenous antigen, initiate the removal of these non-self targets but also maintain a level of self-regulation as to not become aberrantly pro-inflammatory in nature.

Crucially, this could be of therapeutic potential in the context of IBD, with previous reports indicating both a loss of $CD14^{hi}$ macrophages and accumulation of $CD206^{+}$ macrophages to current anti-TNF-α therapy whereby administration of adalimumab causes a possible phenotypic 'switch' in the context of IBD presented in Crohn's disease patients (Vos *et al.*, 2012). Additional studies have further corroborated these findings through data depicting increased levels of macrophage autophagy when compared to an IFN-γ-induced M1 macrophage control (Levin *et al.*, 2016).

The remaining protocol explored whether minocycline could influence the phenotype acquisition of macrophages if introduced during the polarization process. This was a key question raised not only by the data obtained within this project but also based upon the major reported finding that a higher number of pro-inflammatory $Ly6C^{+}$MHC II+ macrophages were located in the gut of

minocycline treated DSS-colitic mice at initial stages of the inflammatory process, which then differentiated into a pro-resolving Ly6C^{-}MHCII^{+} phenotype (Garrido-Mesa, Rodríguez-Nogales, *et al.*, 2018a).

With much of the literature depicting a concept of dual-purpose regarding macrophage polarization via advancing both inflammation and regeneration, in many pathophysiological conditions, macrophages do not neatly ascribe to this M1/M2 paradigm. It has been discussed how a balance between M1 and M2 phenotypic activity shifts over time with M1 macrophages generally behaving as first responders recruiting both effective defense against invasion, while M2 macrophages are essential for wound repair and tissue regeneration in the latter stages of inflammation resolution (Smith *et al.*, 2017). The importance of M1/M2 homeostasis is verified through evidence of delayed wound healing and fibrotic development when M1 or M2 subpopulations become unrestrained respectively. However, the M1/M2 nomenclature is a useful tool in describing macrophage population plasticity during inflammatory states and can be correlated with observable changes in biomarkers in relation to inflammatory progression and healing (Smith *et al.*, 2017).

During the investigations using THP-1, data categorically implied an influence of minocycline in the phenotypic switch from pro-inflammatory M1, to anti-inflammatory M2 as evidenced by decreased expression of CD86 and increase in CD163 and CD206. This data further supported the hypothesis that minocycline, regardless of the time-point of administration, or presence of strong pro-inflammatory stimuli (LPS and /or IFN-γ) drives macrophages to express M2-associated markers which may have therapeutically potent downstream influence on the progression of inflammation. However, although the phenotypic data was conclusive and corroborated across biological replicates when using the cell lines, the same marker modification was not witnessed when translating the investigation to primary PBMCs. Here, while some effects were consistent such as the upregulation of CD163 in M1 macrophages following LPS stimulation in the presence of minocycline (Chapter 6), and the increase in CD80 on M0 macrophages challenged with LPS and treated with minocycline (Chapter 4) there were some divergences noted. On these occasions there was not necessarily conflicting data obtained, simply a lack of statistical significance in the results obtained when compared to the relevant controls. Therefore, although

the data from the PBMCs were robust in nature constituting 4 donors and duplicate values, it would be valuable to replicate the data in additional donors to accurately assess the effect of minocycline in this setting.

Despite some disparity between models within this study, as previously outlined in chapter 5, accumulating evidence supports the idea that enforcing a pro-resolving M2 macrophage phenotype might be a novel therapeutic approach to control intestinal inflammation and restore tissue integrity (Na *et al.*, 2019b). For example, classic IBD therapies such as mesalazine and infliximab affect macrophage function through inhibition of inflammatory signalling pathways and/or inducing polarization of alternatively activated macrophages (Bantel *et al.*, 2000; Vos *et al.*, 2012). Furthermore, murine models of DSS colitis, whereby DSS-treated mice are deficient in M2 polarized macrophages, highlight higher susceptibility to the colitis stimuli (Takada *et al.*, 2010). Human studies also identify IBD susceptibility loci being strongly correlated with promotors regulated in response to LPS, and thus macrophage activation and phenotype acquisition (Baillie *et al.*, 2017). Additional evidence also suggests a causal link between altered macrophage phenotype and defects in the resolution of intestinal inflammation (Smith *et al.*, 2009b). Considering all this, the ability of minocycline to shift macrophage phenotype to pro-resolving M2 under pro-inflammatory conditions, as shown in the THP-1 model, represents an interesting immunomodulatory mechanism with potential in IBD treatment.

Cells of the innate immune system play vital roles in host defence against infection via activation of PRRs by exogenous ligands such as LPS, which result in the production of pro-inflammatory mediators and subsequent induction of adaptive immune responses (Iwasaki and Medzhitov, 2004; Cui *et al.*, 2015). In regard to cytokine production, minocycline repeatedly decreased the production of pro-inflammatory mediators TNF-α, IL-6, IL-1β and IL-12. This effect was witnessed when minocycline was administered to M0 macrophages challenged with LPS (chapter 4) and when introduced during M1 polarization (chapter 5). The phenotypic data obtained under the same conditions, as discussed above, highlights the role of minocycline in promoting an M2 phenotype via upregulation of CD163 and CD206, while also decreasing the expression of CD14 – a key molecule responsible for LPS-induced inflammatory cascades. Given this potent downregulation of CD14 elicited by minocycline, combined with consistent

decline in pro-inflammatory cytokine production may suggest a correlation between the two outcomes, whereby minocycline first decreases CD14, which ultimately disrupts the intracellular signalling pathways responsible for promoting the gene expression and secretion of pro-inflammatory mediators. Furthermore, previous data reports a similar role of minocycline whereby treatment of DSS-induced colitis in mice resulted in reduced TNF-α, IL-1β and IL-6, while *in vitro* data using RAW264.7 also highlighted a decline in IL-8 following administration of minocycline (Garrido-Mesa, Rodríguez-Nogales, *et al.*, 2018a). Combined, the data described in this project showed minocycline independently decreases TNF-α as well as promoting phenotype switching in the form of increased expression of CD163 and CD206.

When studied during induced M1 or M2 polarization shown in chapter 5, minocycline inhibited the production of pro-inflammatory cytokines IL-1β, IL-6 and TNF-α during both M1 and M2 polarization, which was also replicated across cellular models. Given this data it was hypothesized first that consistent inhibition of key inflammatory cytokines IL-1β, IL-6 and TNF-α following intervention of M1 or M2 polarization with minocycline may indicate a fundamental influence of minocycline on downstream inflammatory signalling. Chapter 5 contextualised these cytokines to IBD, providing evidence that over production of IL-1β can result in sterile inflammation, increasing the risk of developing metabolic and autoinflammatory diseases among IBD patients, with further reports linking an overproduction of IL-1β in both IBD patients and murine models and the development of mucosal inflammation (Mahida, Wu and Jewell, 1989). It has also been reported how IL-6 is a major contributory cytokine within the chronic phase of inflammation within experimental models of colitis and is a key protagonist to disease progression (Atreya *et al.*, 2000; Yamamoto *et al.*, 2000), while the IL-6/IL-6Rα complex was described to favour a transition from neutrophil to monocyte infiltration during early inflammatory events, and a disruption in IL-6 trans-signalling control of leucocyte trafficking may be significant at the onset of chronic disease such as IBD relapse (Hurst *et al.*, 2001; Marin *et al.*, 2001; Jones *et al.*, 2005; Gabay, 2006). Finally, clinical trials have described an increase in TNF-α and its receptors at sites of chronic inflammation, with increased levels of TNF-α found in the intestinal mucosa, serum, and faeces of IBD juvenile patients (Pirenne *et al.*, 1992; Breese *et al.*, 1994). While, in murine colitis models, TNF-

α has been implicated in the degradation of the epithelial barrier and subsequent regulation of tight-junctions (Ozaki *et al.*, 1999; Laukoetter *et al.*, 2007; Vetrano *et al.*, 2008; Su *et al.*, 2013).

Given the current literature, in combination with the data in this project, it is hypothesised that minocycline may have modulatory influence on pathological processes such as mucosal inflammation, tissue degradation, leukocyte trafficking, epithelial barrier dysfunction, and the activation of inflammatory resolution mechanisms via down regulation of these potent mediators. Furthermore, minocycline may again present as a viable option in the setting of IBD, given its ability to not only inhibit TNF-α secretion from macrophages, but also concurrently downregulate other contributory pro-inflammatory mediators.

Conversely, administration of minocycline during M2 macrophage polarization in PBMCs simultaneously caused increased production of typical pro-inflammatory mediators IFN-γ and IL-12, whilst inhibiting the potent anti-inflammatory cytokine IL-10. This was one of the more complex outcomes to explain given a lack of data in this setting. It was discussed how IFN-γ signalling is regulated via controlled expression of IFNGR1 and IFNGR2 (Kak, Raza and Tiwari, 2018) and activates macrophages, eliciting their polarization to M1 (Fultz *et al.*, 1993), while the coordination of IL-12 and IFN-γ link pathogen recognition by innate cells to the induction of specific immunity through amplifying or stabilizing the Th1 response via a positive feedback loop (Boehm *et al.*, 1997). Thus, macrophage-derived IFN-γ has been associated with restraint of bacterial growth (Rothfuchs *et al.*, 2001; Salins *et al.*, 2001) and a decreased resistance to bacterial, viral, and parasitic infections has been reported in animals lacking IFN-γ or IFNGR1 (Suzuki *et al.*, 1988; van den Broek *et al.*, 1995; Pearl *et al.*, 2001). In relation to IBD, IFN-γ is noted to be overproduced by macrophages in the lamina propria within colitis rodent models, which was also correlated with disproportional, dominant Th1 responses and thus is seen as a key contributor to IBD progression (Powrie and Leach, 1995; Fiocchi, 1998; Monteleone *et al.*, 1998). This dominance of Th1 phenotype and excessive secretion of INF-γ is also found observed in Crohn's disease patients when compared with healthy controls (Hugot *et al.*, 1996).

On the other hand, IL-10 is a pleiotropic and potent anti-inflammatory and immune-suppressive cytokine (Moore *et al.*, 2001; Mollazadeh *et al.*, 2019) and

inhibits the activity of Th1 cells, natural killer cells, and macrophages, and although all aforementioned cells are required for optimal pathogen clearance, dysregulation of these populations results in aberrant tissue damage. Consequently, IL-10 can both impede pathogen clearance but also ameliorate immunopathology. In models of rheumatoid arthritis IL-10 has been described to inhibit neutrophil migration and activation, and to preference an M2 macrophage phenotype through inhibition of key mediators such as TNF-α and IL-1β (Smallie *et al.*, 2010). In the setting of IBD, IL-10 plays an important physiological role in inflammation regulation, which is both supported by reports that genetic models of IL-10$^{-/-}$ mice spontaneously develop the disease (Berg *et al.*, 1996; Glocker *et al.*, 2009), while other reports correlating expansion of pro-inflammatory Th17 cells and suppression of Tregs in similar *in vivo* IL-10$^{-/-}$ models (Chaudhry and Rudensky, 2013).

The data disseminated in this thesis showed an inverse relationship of these cytokines, with a decrease in IL-10 and increase in IFN-γ and IL-12 when minocycline was administered during M2 polarization of PBMC-derived macrophages. Importantly, this effect was not observed when minocycline was administered during M1 polarisation. Given the current literature, in combination with these findings, it was concluded that minocycline may be having a homeostatic role on M2 macrophages, regulating their biology. Through limiting IL-10 production but promoting IFN-γ and IL-12, under M2 macrophage conditions, minocycline may consequently maintain CD4^{+} T cells and natural killer cell responses but also limit the macrophages' own ability to produce pathologically high levels of other pro-inflammatory mediators like IL-6, IL-1β and TNF-α, as seen under both M1 and M2 conditions. Furthermore, this premise is further supported by previous reports which have linked CD163^{+} TAMs to poor prognosis in the context of glioma, therefore the seeming ability of minocycline to limit the production of potent M2 cytokines like IL-10 in this project may limit the excessive polarization to M2 phenotypes and development of M2 associated pathologies such as tumour development.

Therefore, given the earlier hypothesis that minocycline may simultaneously promote acute inflammation allowing for quick transition to a pro-resolving state, whilst also limiting the development of M2-associated pathology via regulation of M2 phenotype acquisition, it may be possible that again in the context of cytokine

production, minocycline is able to tightly regulate macrophage phenotype. Here, it seems on the surface that minocycline promotes polarization to an M2 subset through CD163 and CD206 expression, but also potentially controls aberrant downstream Th2 responses through limitation of IL-10 secretion. Similarly, it appears that minocycline in the setting of M2 macrophages allows them to retain some pro-inflammatory capacity through production of IL-12, and help maintain antigen responsive cell populations within the near vicinity through production of IFN-y.

Aside from the perplexity of minocycline's effect on M2 cytokine production signatures, another major finding from this work was related to the disparity of cytokine production based on the timepoint of minocycline administration. It was outlined above that when added during M1 polarization, and prior to LPS challenge of M0 macrophages, minocycline resulted in potent inhibition of TNF-α and IL-6. However, when added to pre-polarized M1 macrophages challenged with LPS (chapter 6) the opposite effect was observed whereby minocycline resulted in enhanced production of these pro-inflammatory cytokines, while IL-1β remained decreased.

Firstly, IL-1β is a potent pro-inflammatory cytokine crucial for host-defence responses to infection and injury, but which may also exacerbate damage during chronic disease and acute tissue injuries if left unregulated (Lopez-Castejon and Brough, 2011). Therefore a consistent downregulation of this mediator following minocycline administration may underline a direct inhibitory function of minocycline on IL-1β production rather than downstream activation of NF-κB and MAPK pathways that upregulate additional pro-inflammatory cytokines such as IL-6 and TNF-α which were demonstrated to be increased within this model of M1 activation (Guarda and So, 2010; Sahoo *et al.*, 2011).

Next, as discussed in detail throughout this project, IL-6 has been found at high levels in various diseases, including IBD (Műzes *et al.*, 2012), while its inhibition in other autoimmune diseases such as rheumatoid arthritis has also proven to be beneficial. Moreover, *in vivo* studies and clinical trials have correlated an increase in TNF-α and its receptors at sites of chronic inflammation in IBD (Pirenne *et al.*, 1992; Breese *et al.*, 1994), whilst it has also been implicated in the degradation of the epithelial barrier and subsequent regulation of tight-junctions (Ozaki *et al.*, 1999; Laukoetter *et al.*, 2007; Vetrano *et al.*, 2008). Based on this data, and a

lack of supplementary information in the literature regarding this phenomenon, this opposing cytokine production signature dependant on administration point may therefore further vindicate the hypothesis that minocycline may cause an initial exacerbation of inflammation through upregulation of potent pro-inflammatory mediators as seen when M1 are challenged with LPS, but which may then allow for efficient exchange to pro-resolving mechanisms and the avoidance of chronic inflammation, as seen in the inhibition of mediator release when administered in the absence of antigenic stimulation.

Considering this data, it was finally decided to assess the genetic expression of transcription factors essential for macrophage functioning. As detailed in chapter 4, section 4.9, Ataie-Kachoie *et al* (2013) showed suppression of NF-κB in OVCAR-3 and SKOV-3 ovarian carcinoma cells when treated with minocycline (Ataie-Kachoie, P. *et al.*, 2013), while Weiler and Dittmar (2019) also confirmed that minocycline abrogated IκBα and p65 phosphorylation leading to suppression of NF-κB in MDA-MB0435-pFDR1 cancer cells and M13SV1-Cre breast epithelial cells (Weiler and Dittmar, 2019). In regard to macrophages, few reports exist, with one paper by Tai *et al* (2013), examining the effect of minocycline on cytokine and chemokine production in THP-1 monocytes when challenged with LPS. They showed that minocycline supressed TNF-α, IL-6, IFN-γ, IP-10, and MCP-1 production in a dose-dependent manner by inhibiting IκBα and IκBβ, but concluded that in THP-1 monocytes minocycline did not affect the phosphorylation of ERK1/2, JNK, p38 or TAK1 (Tai *et al.*, 2013). This data, in combination with the early findings of reduced CD14 expression with minocycline treatment suggest that minocycline may also be targeting this pathway in macrophages.

All the previously acquired data both presented in this thesis and reported within the literature suggests a potential role of minocycline in the context of intestinal inflammation whereby it could not only act to inhibit newly recruited 'patrolling' monocytes infiltrating into the inflamed intestine, but also modify the resultant macrophage phenotype, acting to simultaneously desensitise the cells to ongoing endogenous stimulus. Within this project a few modifications to key transcription factors responsible for macrophage polarization were observed. Firstly, in chapter 5 in which the role of minocycline upon this polarization process was assessed, minocycline was able to partially inhibit *stat3* and *stat6* gene

expression when administered during M1 polarization. Importantly, this depression of *stat3* and *stat6* gene expression was not replicated following M2 polarization. Binding of IL-10 to the IL-10 receptor results in activation of STAT3 (Riley *et al.*, 1999), with reports depicting STAT3 as a crucial protein for the transmission of anti-inflammatory signals in macrophages.

In that report, deletion of the *stat3* gene resulted in the spontaneous development of enterocolitis and increased susceptibility to LPS-mediated shock and septic peritonitis (Takeda *et al.*, 1999; Matsukawa *et al.*, 2003). On the other hand, while STAT6 is required for normal immune function, it has been implicated as a crucial factor in the development of pathological processes such as excessive mucus production, Th2 cell accumulation, tissue remodelling, and hyper-responsiveness (Thai *et al.*, 2005; Kuperman and Schleimer, 2008; Maier, Duschl and Horejs-Hoeck, 2012), in addition to colitis exacerbation (Elrod *et al.*, 2005).

The ability of minocycline within the models used in this project to partially inhibit both *stat3* and *stat6* could further support the hypothesis that sees minocycline exert a regulatory role over anti-inflammatory phenotype switching in respect to decreased *stat3* and *stat6,* given their central roles in M2-phenotype acquisition and anti-inflammatory functions. Crucially, this inhibitory function of minocycline was not seen when administered during M2 polarization, further suggesting a significant ability of minocycline to distinguish its functions depending on the initial phenotype of the macrophage – inhibiting M2-associated transcription in M1 macrophages and thus maintaining its ability to respond to exogenous insult but sparing transcription factor modification in M2 allowing for their maintenance. However, this hypothesis remains difficult to fully ascertain given that some of the earlier data in chapter 4 may correlate the initial increased *stat3* expression in the M1 cultures to autocrine signalling by IL-10 and IL-6, both of which were reported to be decreased by minocycline in this M1 model. As such, it may be hard to distinguish whether the downregulation of *stat3* in this setting is due to a direct inhibitory role of minocycline, or as a secondary bi-product of its inhibition of IL-10 and IL-6. Therefore, further verification would be required. Despite this, a reduction in *stat6* driven by minocycline may further indicate a regulatory function of minocycline over macrophage phenotype acquisition and plasticity.

Given the central function of *stat6* in M2 macrophage polarization, its inhibition by minocycline in M1 macrophages only could cooperatively allow the dampening

of further pro-inflammatory stimulation, in addition to limiting an aberrant switch to potent anti-inflammatory programmes which may result in the development of M2 macrophage pathophysiology. This is once again consistent with the postulation that minocycline could promote acute inflammation, as also indicated by increased IL-6 and TNF-α upon LPS challenge of M1 macrophages, but which then preferences a pro-resolving state through inhibition of IL-1β, IL-6 and TNF-α, but upregulation of CD163 and CD206, and simultaneously limits hyper-responsiveness to LPS via downregulation of CD14.

Finally, although failing to ascertain any defined effect of minocycline on IL-10 signalling mediated through the STAT3/SOCS3 axis in this project, these results may still render minocycline another safe and effective treatment strategy for IBD considering its well-established use as a pharmaceutical, impeccable safety record and pharmacokinetic profile, in addition to being an extremely cost-effective strategy when compared with anti-TNF therapies.

7.2. Project limitations & future work

As with all projects, various limitations were encountered throughout its course pertaining to experimental, financial, and contextual factors. The first key limitation of the study was the limited number of biological replicates in the form of donor PBMCs used. The use of the four individual donors for the experiments, in addition to the removal of certain variables such as DMSO an individual vehicle control, was dictated by cell availability, and as such it was required to slightly modify experimental parameters. The ability to use a greater number of donors and thus a greater number of cells would serve to substantiate the findings whilst also allowing better identification of anomalous data which may have skewed statistical values.

Another limitation of the study surrounded the use of PMA as a differentiation agent. It is noted in the literature that PMA-driven macrophage differentiation naturally preferences an M1-like phenotype given its role as a protein kinase C activator which subsequently results in downstream NF-κB signalling (Robinson, 1992). This may therefore mean the resting M0 macrophages within the THP-1 and U-937 studies would have obtained a more M1-like profile and would not necessarily represent a true naïve population prior to activation with LPS. However, this M0 population was still identifiably different to those cells generated

when inducing an M1 phenotype and clear changes in M0 macrophage biology were also measurable following LPS-stimulation. Furthermore, the M0 M-CSF expanded PBMCs were in the absence of PMA and were naturally more naïve in nature and as experimental findings were confirmed in this setting. Even so, it was an experimental variation worth noting during the analysis.

If time and resources had been no restraint it would also have been interesting to include greater number of minocycline titrations to identify an optimal dose or create full dose response curves in relation to the biomarkers tested. Moreover, given the identification of differing cytokine profiles at different time points in the previous reports by Garrido Mesa *et al* (Garrido-Mesa, Rodríguez-Nogales, *et al.*, 2018b), it may yield important evidence as to minocycline's influence on macrophage biology if cytokine production was measured at earlier time points. At present, data is only provided at 24hr post-stimulation – either following polarization or LPS-activation. This may thus only be providing a snapshot of the cytokine production signatures of the cells, and considering some cytokines are synthesised and released rapidly following induction it is possible that some vital information could be missing. Furthermore, there is evidence in the literature as discussed in chapter 5 of positive and negative feedback loops because of autocrine and paracrine signalling in the culture, therefore including earlier time points within the analysis may help remove the occurrence of such events.

With financial constraints within all projects including this one, it was not possible to utilise any omics analysis using the samples. However, given the preliminary findings from the RT-qPCR investigations it may be interesting to input such samples into a technique such as RNA sequencing which ultimately allows the detection and quantification of a far greater variety of genetic signatures currently unexplored in this project. Preliminary investigations were also launched in 2018 to assess the role of minocycline directly on murine BMDM cultures to provide proof-of-concept links to the previously reported *in vivo* data and those previously using BMDM. This, however, became economically unviable given the absence of licensing at the University of East London to breed animals on site, and thus required frequent purchasing of stocks from public suppliers which was not financially sustainable.

Moreover, a downstream role of minocycline on adaptive cell function was hypothesised, in which minocycline modifies macrophage biology which in turn

may influence T cell function, thus it may be a viable option to explore these thoughts using co-culture methods. Additionally, it is well understood that antigen presentation by major histocompatibility complexes (MHC) is a crucial step in adaptive immune cell activation (Clark, 1995; Holling, Schooten and van Den Elsen, 2004; Guerriero, 2019). Peptides presented via MHC molecules interact with T cell receptors (TCRs) and form specific peptide-MHC complexes, resulting in T cell proliferation and activation (Wieczorek *et al.*, 2017). Although the contribution of DC antigen cross-presentation to $CD8^+$ T cell activation in the context of immune defence against pathogens, viruses and tumours has been recognized, other immune cells such as macrophages have been shown capable of cross-presentation (Steinman *et al.*, 1999; Muntjewerff, Meesters and van den Bogaart, 2020). It has been reported that macrophages are able to cross-present antigens via similar cellular pathways as DCs, with proinflammatory macrophages noted to be involved in local reactivation of memory and effector $CD8^+$ T cells which may be related to immune tolerance (Embgenbroich and Burgdorf, 2018; Muntjewerff, Meesters and van den Bogaart, 2020).

Given this knowledge, it could be interesting to investigate whether minocycline has any influence on; a) MHC protein expression on all macrophage subsets, b) the ability of macrophages to process antigens and present peptide through assessing intracellular machinery involved within the endoplasmic reticulum, and c) the overall peptide repertoire presented by MHC proteins (Wieczorek *et al.*, 2017). There currently exists no data regarding minocycline on macrophage antigen presentation, and the data presented in this thesis that outlines clear changes in other T cell co-stimulatory molecules CD80 and CD86, thus could yield important insight into yet another possible mechanism of minocycline in the context of immune modulation.

Within this project healthy donor PBMCs were utilized for the investigations, which was perfectly adequate when aiming to assess cell-specific changes in response to minocycline. However, this may not be completely representative of colitic cells and as such, would be interesting to apply similar experimental protocols using isolated PBMCs or macrophages from IBD patients. Furthermore, there are currently no clinical trials utilising minocycline or any tetracycline derivative in the treatment of IBD, thus, a potential future trial may aim to explore minocycline intervention of IBD patients and consequently assess macrophage

phenotype and cytokine levels. It is also important to note the genetic abnormalities often associated with IBD onset and progression in genes such as NOD2. The intracellular pattern recognition receptor NOD2 (Nucleotide-binding oligomerization domain 2) plays a pivotal role in host–pathogen interactions and inflammatory response by activating pro-inflammatory pathways such as NF-κB, MAPKs, and Caspase-1 (Nabhani *et al.*, 2017). Recent genome-wide association studies have correlated polymorphisms conferring a hypofunctional NLRP3 phenotype with the development of Crohn's disease, and NOD2 is reported to be correlated with Crohn's disease (Ogura *et al.*, 2001; Zhen and Zhang, 2019). Existent of polymorphisms of genes within IBD patients may skew the response elicited by minocycline so it may be important to verify findings in appropriate disease models which account for these genetic variations.

A final hurdle encountered during this project was the emergence of COVID-19 and the global pandemic which resulted in a country-wide national lock-down in 2020. This undoubtedly had immense knock-on effects both professionally and personally, given the stay-at-home orders and closure of university campuses and research spaces. Having no access between the months of March-mid July, then restricted access through to 2021 of course was a huge limitation to the volume and frequency of work able to undertake in that time. Moreover, supply issues in the face of rapidly expanded COVID-19 testing via PCR resulted in extremely long lead times for certain laboratory reagents and equipment meaning some activities required adjusting to accommodate for this.

7.3. Project conclusion & impact

First discovered in the 1940s tetracycline's have undergone an assortment of structural modification not only to increase their antimicrobial activity but also to improve their absorption and half-life (Klein and Cunha, 1995b). Minocycline is a second-generation, semi-synthetic antibiotic analog of tetracycline with efficacy against both gram-positive and gram-negative bacterial strains through the inhibition of protein synthesis via acting on 16S rRNA (Kim and Suh, 2009). In addition to their antimicrobial properties, tetracyclines have been demonstrated to display a series of other effects unrelated to their antibiotic action, encompassing anti-inflammatory, anti-apoptotic, proteolytic and angiogenic properties (Sapadin and Fleischmajer, 2006c).

In the past 2 decades the therapeutic assets of minocycline beyond its function as an antibiotic have been well acknowledged within the literature, with both pre-clinical and clinical studies elucidating anti-inflammatory and immunomodulatory properties (Sapadin and Fleischmajer, 2006c; Garrido-Mesa, Camuesco, *et al.*, 2011a; Garrido-Mesa, Zarzuelo and Gálvez, 2013b). Minocycline has been verified to exert this immunomodulatory function via alteration of immune cell activation and the subsequent release of chemical compounds such as cytokines, chemokines, NO and MMPs, which successfully augment both inflammatory cascades and downstream immune responses.

Although there is plentiful data depicting the effects of minocycline on the innate immune system encompassing microglia and monocytes, data pertaining to macrophage-specific function remains unknown. Similarly, despite the articles described previously which depict minocycline's influence on transcriptional mechanisms involving NF-κB, STAT3, STAT1, and IRF1, there exists no data currently surrounding the effect of minocycline in relation to M1/M2 transcriptional regulation within the *in vitro* models selected in this project.

The data disseminated in this project has provided a novel insight into the direct influence of minocycline on macrophage differentiation, activation, and polarization status, showing for the first time that minocycline has a direct effect on macrophage differentiation, as shown by the reduced number of adherent macrophages that differentiated from THP-1 cells in the presence of minocycline. Furthermore, the data discussed in this thesis highlights a potent ability of minocycline to depress CD14 expression, whilst inducing an M2-bias phenotype through upregulation of CD163 and CD206. Moreover, the data also alludes to a highly regulatory role of minocycline whereby it exacerbates upregulation of M1-associated signatures such as the production of TNF-α, IL-6 and IFN-γ if administered prior to LPS activation in M1 and M2 macrophages, but simultaneously inhibits the expression of those same signatures– during polarization. Furthermore, minocycline seems to also limit the probability of aberrant M2-associated pathology through minimizing potent pro-resolving signatures such as IL-10 allowing homeostatic regulation of each phenotype. Novel data is also provided regarding LPS activation of pre-polarized subsets which at present does not appear in the literature. The data here highlights clear opposing effects of minocycline, in which minocycline under these conditions

results in increased production of TNF-α, IFN-γ and IL-6 in M1, whilst also increasing IFN-γ and reducing IL-10 in M2. This may be extremely valid for other pathologies where activation of cells is recurrent as in IBD.

As discussed in greater detail in chapter 1, section 1.2.4.3., isolated macrophages from the lamina propria of IBD patients are reported to have a more M1-like phenotype and produce large amounts of pro-inflammatory cytokines such as IL-12, IL-23, TNF and iNOS, and possess a strong response to bacterial stimuli (Reinecker *et al.*, 1993). They contribute to the disruption of the intestinal epithelial barrier via enhanced production of TNF, which impairs the structure and function of tight junctions (Lissner *et al.*, 2015), with research correlating aberrant M1 macrophage presence within a variety of pathologies including IBD rendering them a continued therapeutically viable target. M2 macrophages have thus been shown to contribute to the resolution of colitis via angiogenesis promotion, debris scavenging, and tissue repair (Hunter *et al.*, 2010; Weisser *et al.*, 2011; Leung *et al.*, 2013), and have therefore been frequently suggested as a possible collaborator in IBD immunotherapy for the re-establishment of mucosal tolerance and repair of injured mucosa (Haribhai *et al.*, 2016).

Moreover, a 2006 *in vivo* study conducted by Qualls *et al*, highlighted that depletion of colonic mononuclear phagocytes such as macrophages prior to colitis induction results in a more severe disease compared with mice that were not depleted of macrophages. They also reported a significant decrease in colonic transcript levels of IL-10 following mononuclear phagocyte depletion, whereas IFN-γ and TNF-α were not significantly affected, which suggested mononuclear phagocyte depletion led to a reduction in the M2 mature colonic macrophages, thus rendering mice more susceptible to DSS colitis (Qualls *et al.*, 2006). This narrative of M2 macrophage necessity in colitis regulation was further supported with studies correlating increased proportion of colonic M2 macrophages and the amelioration of colitis (Hunter *et al.*, 2010). These articles further endorse the crucial function of M2 macrophages in colitis regulation and provide a promising case for the results contained within this thesis in the argument of minocycline administration for colitis therapy given the evidence of M2 macrophage switching in this context, in combination with its potential regulatory activity on LPS signalling through potent downregulation of CD14 expression under any condition.

In addition, minocycline is an established antibiotic which may also prove pertinent in the treatment of IBD. In 2015, a report by Nakanishi, Sato and Ohteki suggested that gram-positive commensal bacteria in the colon are responsible for the recruitment of the proinflammatory monocytes and macrophages that propagate colitis. When compared with DSS-treated mice that did not receive antibiotic treatment, vancomycin-mediated depletion of commensal Gram-positive bacteria in mice undergoing DSS colitis reduced colonic monocyte and macrophage numbers, resulting in improved weight loss, colon shortening, colonic TNF-α and IL-6 levels, and histological damage (Nakanishi, Sato and Ohteki, 2015). Minocycline's recognised role as an antibiotic, effective against gram-positive and gram-negative bacteria, may render it an ideal candidate in its native state for the treatment of IBD. This, in conjunction with its established immunomodulatory function previously reported and outlined from the data in this project could also suggest a synergic role of its various functions in the regulation of IBD-related inflammation.

However, although effects on minocycline in macrophages are starting to be elucidated, not much is known in terms of mechanisms, and despite these previous reports, this project was unable to categorically identify any 1 clear mechanism of action, but rather suggests many events happen in tandem. From analysis of surface marker expression, cytokine production signatures, and gene expression of key transcription factors, it is difficult to ascertain whether these biological changes observed are as a direct result of minocycline on macrophage cellular machinery, or in fact resultant of modifications to signalling cascades. Although modulation of *stat3* and *stat6* was reported when minocycline was administered during M1 polarization, which suggested that minocycline may exert a regulatory role over anti-inflammatory phenotype switching in respect to this decreased *stat3* and *stat6,* this conclusion was difficult to fully ascertain given additional data in chapter 5 which was thought to correlate increased *stat3* expression to autocrine signalling by IL-10 and IL-6, both of which were reported to be decreased by minocycline in this M1 model.

Moreover, a reduction in *stat2* and *stat6* driven by minocycline may indicate a regulatory function of minocycline over the macrophage phenotype acquisition and plasticity, which could cooperatively allow the dampening of further pro-inflammatory stimulation. Furthermore, a simple lack of genetic modification by

minocycline within the M2 cultures in relation to either M1 or M2 associated transcription factors may indicate preferential function of minocycline on macrophages in pre-established pro-inflammatory states.

However, while this could prove therapeutically beneficial whereby minocycline does not seem to drastically alter the biology of anti-inflammatory macrophage populations but exerts potent modification of inflammatory subsets, this data would require corroboration using additional donors and replicate samples to fully support such conclusions. Although the data in this project was unable to identify distinct molecular targets of minocycline with unwavering certainty, it has added to the collective knowledge on minocycline's' immunomodulatory effects that can aid in the construction of a more detailed explanation as to how minocycline is specifically attributing to the anti-inflammatory effects seen in previous *in vivo* and *in vitro* models.

The data presented here supports future exploration of the potential of minocycline for immune mediated diseases. This concept of drug repurposing allows the exploration and identification of new applications for drugs that are already certified safe and in general circulation within society, ultimately allowing for rapid drug development and the proposition of new therapeutic alternatives. Innovation of further modified minocycline derivatives such as chemically modified tetracyclines (CMTs) that can not only be tailored to suit immunomodulatory functions, but also lack antibiotic function thus removing the ever-growing issue of antibiotic resistance.

Current therapies such as TNF antagonists which have been approved by the Food and Drug Administration of USA (FDA) for the treatment of IBD have revolutionized its medical management. The four inhibitors currently available; infliximab, adalimumab, certolizumab pegol, and golimumab, function by inhibiting disease activity resulting in mucosal healing (Slevin and Egan, 2015; Gajendran *et al.*, 2018). But, although proven to have good efficacy in relation to the induction of remission in moderately severe Crohn's disease patients who have previously failed treatment with standard therapies, registered systemic side effects linked with infection and inflammation in the skin and joints, development of non-Hodgkin's lymphoma, and activation of latent tuberculosis have been recorded (Cleynen and Vermeire, 2012; Targownik and Bernstein, 2013; Gubernatorova and Tumanov, 2016).

Data housed within this thesis supports the argument that minocycline may be an ideal clinical candidate for the treatment of IBD due to its immunomodulatory properties, in addition to its safety record, dual efficacy as an antibiotic and anti-inflammatory, and crucially in this economic climate, its affordability. Furthermore, the data outlined in this thesis showed superior immunomodulatory effects of minocycline when compared to the well-established immunosuppressant dexamethasone in the context of M0 macrophage response to LPS. Consequently, this advancement in knowledge and understanding of how minocycline directly influences macrophage function will ultimately aid the development of novel therapeutic strategies for those individuals that are burdened with diseases that are dominated by a dysregulated immune response as seen in diseases like IBD.

8. Bibliography

Abdalla, H.B. *et al.* (2020) 'Activation of PPAR-γ induces macrophage polarization and reduces neutrophil migration mediated by heme oxygenase 1', *International Immunopharmacology*, 84, p. 106565. Available at: https://doi.org/10.1016/j.intimp.2020.106565.

Acosta-Rodriguez, E.V. *et al.* (2007) 'Interleukins 1beta and 6 but not transforming growth factor-beta are essential for the differentiation of interleukin 17-producing human T helper cells', *Nature Immunology*, 8(9), pp. 942–949. Available at: https://doi.org/10.1038/ni1496.

Agwuh, K.N. and MacGowan, A. (2006) 'Pharmacokinetics and pharmacodynamics of the tetracyclines including glycylcyclines', *Journal of Antimicrobial Chemotherapy*, 58(2), pp. 256–265. Available at: https://doi.org/10.1093/jac/dkl224.

Ai, F. *et al.* (2020) 'Dexamethasone induces aberrant macrophage immune function and apoptosis', *Oncology Reports*, 43(2), pp. 427–436. Available at: https://doi.org/10.3892/or.2019.7434.

Akira, S. and Takeda, K. (2004) 'Toll-like receptor signalling', *Nature Reviews. Immunology*, 4(7), pp. 499–511. Available at: https://doi.org/10.1038/nri1391.

Akira, S., Uematsu, S. and Takeuchi, O. (2006) 'Pathogen recognition and innate immunity', *Cell*, 124(4), pp. 783–801. Available at: https://doi.org/10.1016/j.cell.2006.02.015.

Alano, C.C. *et al.* (2006) 'Minocycline inhibits poly(ADP-ribose) polymerase-1 at nanomolar concentrations', *Proceedings of the National Academy of Sciences of the United States of America*, 103(25), pp. 9685–9690. Available at: https://doi.org/10.1073/pnas.0600554103.

Albacker, L.A. *et al.* (2010) 'TIM-4, a Receptor for Phosphatidylserine, Controls Adaptive Immunity by Regulating the Removal of Antigen-Specific T Cells', *Journal of immunology (Baltimore, Md. : 1950)*, 185(11), pp. 6839–6849. Available at: https://doi.org/10.4049/jimmunol.1001360.

Ali, I. *et al.* (2018) 'Doxycycline as Potential Anti-cancer Agent', *Anti-Cancer Agents in Medicinal Chemistry*, 17(12). Available at: https://doi.org/10.2174/1871520617666170213111951.

Alivernini, S. *et al.* (2016) 'Tapering and discontinuation of TNF-α blockers without disease relapse using ultrasonography as a tool to identify patients with rheumatoid arthritis in clinical and histological remission', *Arthritis Research & Therapy*, 18, p. 39. Available at: https://doi.org/10.1186/s13075-016-0927-z.

Alvaro, T. *et al.* (2006) 'The presence of STAT1-positive tumor-associated macrophages and their relation to outcome in patients with follicular lymphoma', *Haematologica*, 91(12), pp. 1605–1612.

Andreadou, I. *et al.* (2019) ‘Immune cells as targets for cardioprotection: new players and novel therapeutic opportunities’, *Cardiovascular Research*, 115(7), pp. 1117–1130. Available at: https://doi.org/10.1093/cvr/cvz050.

Antonenko, Y.N. *et al.* (2010) ‘Minocycline chelates Ca2+, binds to membranes, and depolarizes mitochondria by formation of Ca2+-dependent ion channels’, *Journal of Bioenergetics and Biomembranes*, 42(2), pp. 151–163. Available at: https://doi.org/10.1007/s10863-010-9271-1.

Antoszczak, M. *et al.* (2020) ‘Old wine in new bottles: Drug repurposing in oncology’, *European Journal of Pharmacology*, 866, p. 172784. Available at: https://doi.org/10.1016/j.ejphar.2019.172784.

Aprahamian, T. *et al.* (2008) ‘Ageing is associated with diminished apoptotic cell clearance in vivo’, *Clinical & Experimental Immunology*, 152(3), pp. 448–455. Available at: https://doi.org/10.1111/j.1365-2249.2008.03658.x.

Arroyo-Espliguero, R. *et al.* (2004) ‘CD14 and toll-like receptor 4: a link between infection and acute coronary events?’, *Heart*, 90(9), pp. 983–988. Available at: https://doi.org/10.1136/hrt.2002.001297.

Artyomov, M., Sergushichev, A. and Schilling, J.D. (2016) ‘Integrating Immunometabolism and Macrophage Diversity’, *Seminars in immunology*, 28(5), pp. 417–424. Available at: https://doi.org/10.1016/j.smim.2016.10.004.

Asadi, A. *et al.* (2020) ‘Minocycline, focus on mechanisms of resistance, antibacterial activity, and clinical effectiveness: Back to the future’, *Journal of Global Antimicrobial Resistance*, 22, pp. 161–174. Available at: https://doi.org/10.1016/j.jgar.2020.01.022.

Ataie-Kachoie, P. *et al.* (2013) *Minocycline Targets the NF-κB Nexus through Suppression of TGF-β1-TAK1-IκB Signaling in Ovarian Cancer | Molecular Cancer Research*. Available at: https://mcr.aacrjournals.org/content/11/10/1279.long (Accessed: 25 June 2020).

Ataie-Kachoie, P. *et al.* (2015) ‘Minocycline attenuates hypoxia-inducible factor-1α expression correlated with modulation of p53 and AKT/mTOR/p70S6K/4E-BP1 pathway in ovarian cancer: in vitro and in vivo studies.’, *American Journal of Cancer Research*, 5(2), pp. 575–588.

Ataie-Kachoie, P., Morris, D.L. and Pourgholami, M.H. (2013) ‘Minocycline Suppresses Interleukine-6, Its Receptor System and Signaling Pathways and Impairs Migration, Invasion and Adhesion Capacity of Ovarian Cancer Cells: In Vitro and In Vivo Studies’, *PLoS ONE*, 8(4). Available at: https://doi.org/10.1371/journal.pone.0060817.

Atreya, R. *et al.* (2000) ‘Blockade of interleukin 6 trans signaling suppresses T-cell resistance against apoptosis in chronic intestinal inflammation: evidence in crohn disease and experimental colitis in vivo’, *Nature Medicine*, 6(5), pp. 583–588. Available at: https://doi.org/10.1038/75068.

Atri, C., Guerfali, F.Z. and Laouini, D. (2018) ‘Role of Human Macrophage Polarization in Inflammation during Infectious Diseases’, *International Journal of*

Molecular Sciences, 19(6), p. 1801. Available at: https://doi.org/10.3390/ijms19061801.

Auffray, C. *et al.* (2007) 'Monitoring of blood vessels and tissues by a population of monocytes with patrolling behavior', *Science (New York, N.Y.)*, 317(5838), pp. 666–670. Available at: https://doi.org/10.1126/science.1142883.

Babaev, V.R. *et al.* (2005) 'Conditional knockout of macrophage PPARgamma increases atherosclerosis in C57BL/6 and low-density lipoprotein receptor-deficient mice', *Arteriosclerosis, Thrombosis, and Vascular Biology*, 25(8), pp. 1647–1653. Available at: https://doi.org/10.1161/01.ATV.0000173413.31789.1a.

Babbin, B.A. *et al.* (2008) 'Annexin A1 Regulates Intestinal Mucosal Injury, Inflammation, and Repair', *Journal of immunology (Baltimore, Md. : 1950)*, 181(7), pp. 5035–5044.

Bahrami, F., Morris, D.L. and Pourgholami, M.H. (2012) 'Tetracyclines: drugs with huge therapeutic potential', *Mini Reviews in Medicinal Chemistry*, 12(1), pp. 44–52. Available at: https://doi.org/10.2174/138955712798868977.

Baillie, J.K. *et al.* (2017) 'Analysis of the human monocyte-derived macrophage transcriptome and response to lipopolysaccharide provides new insights into genetic aetiology of inflammatory bowel disease', *PLOS Genetics*, 13(3), p. e1006641. Available at: https://doi.org/10.1371/journal.pgen.1006641.

Bain, C.C. *et al.* (2013) 'Resident and pro-inflammatory macrophages in the colon represent alternative context-dependent fates of the same Ly6Chi monocyte precursors', *Mucosal Immunology*, 6(3), pp. 498–510. Available at: https://doi.org/10.1038/mi.2012.89.

Bain, C.C. *et al.* (2014) 'Constant replenishment from circulating monocytes maintains the macrophage pool in adult intestine', *Nature immunology*, 15(10), pp. 929–937. Available at: https://doi.org/10.1038/ni.2967.

Bain, Calum C and Mowat, A.M. (2014) 'Macrophages in intestinal homeostasis and inflammation', *Immunological Reviews*, 260(1), pp. 102–117. Available at: https://doi.org/10.1111/imr.12192.

Bain, Calum C. and Mowat, A.M. (2014) 'The monocyte-macrophage axis in the intestine', *Cellular Immunology*, 291(1), pp. 41–48. Available at: https://doi.org/10.1016/j.cellimm.2014.03.012.

Balic, J.J. *et al.* (2020) 'STAT3 serine phosphorylation is required for TLR4 metabolic reprogramming and IL-1β expression', *Nature Communications*, 11. Available at: https://doi.org/10.1038/s41467-020-17669-5.

Balkwill, F. (2006) 'TNF-α in promotion and progression of cancer', *Cancer and Metastasis Reviews*, 25(3), pp. 409–416. Available at: https://doi.org/10.1007/s10555-006-9005-3.

Bannerman, D.D. and Goldblum, S.E. (2003) 'Mechanisms of bacterial lipopolysaccharide-induced endothelial apoptosis', *American Journal of*

Physiology. Lung Cellular and Molecular Physiology, 284(6), pp. L899-914. Available at: https://doi.org/10.1152/ajplung.00338.2002.

Bantel, H. *et al.* (2000) 'Mesalazine inhibits activation of transcription factor NF-kappaB in inflamed mucosa of patients with ulcerative colitis', *The American Journal of Gastroenterology*, 95(12), pp. 3452–3457. Available at: https://doi.org/10.1111/j.1572-0241.2000.03360.x.

Barnig, C. *et al.* (2019) 'Activation of Resolution Pathways to Prevent and Fight Chronic Inflammation: Lessons From Asthma and Inflammatory Bowel Disease', *Frontiers in Immunology*, 10, p. 1699. Available at: https://doi.org/10.3389/fimmu.2019.01699.

Barros, M.H.M. *et al.* (2013) 'Macrophage Polarisation: an Immunohistochemical Approach for Identifying M1 and M2 Macrophages', *PLoS ONE*, 8(11), p. e80908. Available at: https://doi.org/10.1371/journal.pone.0080908.

Baseler, W.A. *et al.* (2016) 'Autocrine IL-10 functions as a rheostat for M1 macrophage glycolytic commitment by tuning nitric oxide production', *Redox Biology*, 10, pp. 12–23. Available at: https://doi.org/10.1016/j.redox.2016.09.005.

Bauer, C. *et al.* (2010) 'Colitis induced in mice with dextran sulfate sodium (DSS) is mediated by the NLRP3 inflammasome', *Gut*, 59(9), pp. 1192–1199. Available at: https://doi.org/10.1136/gut.2009.197822.

Bazil, V. and Strominger, J.L. (1991) 'Shedding as a mechanism of down-modulation of CD14 on stimulated human monocytes', *Journal of Immunology (Baltimore, Md.: 1950)*, 147(5), pp. 1567–1574.

Bellingan, G. (2000) 'Leukocytes: friend or foe', *Intensive Care Medicine*, 26(Suppl 1), pp. S111–S118. Available at: https://doi.org/10.1007/s001340051127.

Ben-Ari, Y. *et al.* (2010) 'The life of an mRNA in space and time', *Journal of Cell Science*, 123(10), pp. 1761–1774. Available at: https://doi.org/10.1242/jcs.062638.

Bent, R. *et al.* (2018) 'Interleukin-1 Beta—A Friend or Foe in Malignancies?', *International Journal of Molecular Sciences*, 19(8), p. 2155. Available at: https://doi.org/10.3390/ijms19082155.

Berg, D.J. *et al.* (1995) 'Interleukin-10 is a central regulator of the response to LPS in murine models of endotoxic shock and the Shwartzman reaction but not endotoxin tolerance', *The Journal of Clinical Investigation*, 96(5), pp. 2339–2347. Available at: https://doi.org/10.1172/JCI118290.

Berg, D.J. *et al.* (1996) 'Enterocolitis and colon cancer in interleukin-10-deficient mice are associated with aberrant cytokine production and CD4(+) TH1-like responses.', *Journal of Clinical Investigation*, 98(4), pp. 1010–1020. Available at: https://doi.org/10.1172/JCI118861.

Bernardo, D. *et al.* (2018) ‘Human intestinal pro-inflammatory CD11chighCCR2+CX3CR1+ macrophages, but not their tolerogenic CD11c-CCR2-CX3CR1- counterparts, are expanded in inflammatory bowel disease’, *Mucosal Immunology*, 11(4), pp. 1114–1126. Available at: https://doi.org/10.1038/s41385-018-0030-7.

Bertani, F.R., Mozetic, P., Fioramonti, M., Iuliani, M., *et al.* (2017) ‘Classification of M1/M2-polarized human macrophages by label-free hyperspectral reflectance confocal microscopy and multivariate analysis’, *Scientific Reports*, 7(1), p. 8965. Available at: https://doi.org/10.1038/s41598-017-08121-8.

Bertani, F.R., Mozetic, P., Fioramonti, M., Luliani, M., *et al.* (2017) *Classification of M1/M2-polarized human macrophages by label-free hyperspectral reflectance confocal microscopy and multivariate analysis | Scientific Reports*. Available at: https://www.nature.com/articles/s41598-017-08121-8 (Accessed: 2 September 2019).

Berthiaume, J.M. *et al.* (2012) ‘Normalizing the metabolic phenotype after myocardial infarction; impact of subchronic high fat feeding’, *Journal of Molecular and Cellular Cardiology*, 53(1), pp. 125–133. Available at: https://doi.org/10.1016/j.yjmcc.2012.04.005.

Beyer, M. *et al.* (2012) ‘High-Resolution Transcriptome of Human Macrophages’, *PLoS ONE*, 7(9), p. e45466. Available at: https://doi.org/10.1371/journal.pone.0045466.

Bhatt, L.K. and Addepalli, V. (2011) ‘Minocycline with Aspirin: An Approach to Attenuate Diabetic Nephropathy in Rats’, *Renal Failure*, 33(1), pp. 72–78. Available at: https://doi.org/10.3109/0886022X.2010.528117.

Blacker, D.J. *et al.* (2013) ‘Reducing Haemorrhagic Transformation after Thrombolysis for Stroke: A Strategy Utilising Minocycline’, *Stroke Research and Treatment*, 2013. Available at: https://doi.org/10.1155/2013/362961.

Bode, J.G., Ehlting, C. and Häussinger, D. (2012) ‘The macrophage response towards LPS and its control through the p38MAPK–STAT3 axis’, *Cellular Signalling*, 24(6), pp. 1185–1194. Available at: https://doi.org/10.1016/j.cellsig.2012.01.018.

Boehm, U. *et al.* (1997) ‘Cellular responses to interferon-gamma’, *Annual Review of Immunology*, 15, pp. 749–795. Available at: https://doi.org/10.1146/annurev.immunol.15.1.749.

Boehmer, E.D. *et al.* (2004) ‘Age-dependent decrease in Toll-like receptor 4-mediated proinflammatory cytokine production and mitogen-activated protein kinase expression’, *Journal of Leukocyte Biology*, 75(2), pp. 342–349. Available at: https://doi.org/10.1189/jlb.0803389.

Bogdan, C. *et al.* (1992) ‘Contrasting mechanisms for suppression of macrophage cytokine release by transforming growth factor-beta and interleukin-10’, *The Journal of Biological Chemistry*, 267(32), pp. 23301–23308.

Bollrath, J. and Powrie, F.M. (2013) ‘Controlling the frontier: regulatory T-cells and intestinal homeostasis’, *Seminars in Immunology*, 25(5), pp. 352–357. Available at: https://doi.org/10.1016/j.smim.2013.09.002.

Bolus, W.R. *et al.* (2015) ‘CCR2 deficiency leads to increased eosinophils, alternative macrophage activation, and type 2 cytokine expression in adipose tissue’, *Journal of Leukocyte Biology*, 98(4), pp. 467–477. Available at: https://doi.org/10.1189/jlb.3HI0115-018R.

Bonjoch, L. *et al.* (2015) ‘Minocycline inhibits peritoneal macrophages but activates alveolar macrophages in acute pancreatitis’, *Journal of Physiology and Biochemistry*, 71(4), pp. 839–846. Available at: https://doi.org/10.1007/s13105-015-0448-2.

Bonnardel, J. and Guilliams, M. (2018) ‘Developmental control of macrophage function’, *Current Opinion in Immunology*, 50, pp. 64–74. Available at: https://doi.org/10.1016/j.coi.2017.12.001.

Bortolanza, M. *et al.* (2018) ‘Tetracycline repurposing in neurodegeneration: focus on Parkinson’s disease’, *Journal of Neural Transmission*, 125(10), pp. 1403–1415. Available at: https://doi.org/10.1007/s00702-018-1913-1.

Borzutzky, A. *et al.* (2010) ‘NOD2-associated diseases: Bridging innate immunity and autoinflammation’, *Clinical Immunology (Orlando, Fla.)*, 134(3), pp. 251–261. Available at: https://doi.org/10.1016/j.clim.2009.05.005.

Bosco, A. *et al.* (2008) ‘Reduced Retina Microglial Activation and Improved Optic Nerve Integrity with Minocycline Treatment in the DBA/2J Mouse Model of Glaucoma’, *Investigative Ophthalmology & Visual Science*, 49(4), pp. 1437–1446. Available at: https://doi.org/10.1167/iovs.07-1337.

Bouhlel, M.A. *et al.* (2007a) ‘PPARgamma activation primes human monocytes into alternative M2 macrophages with anti-inflammatory properties’, *Cell Metabolism*, 6(2), pp. 137–143. Available at: https://doi.org/10.1016/j.cmet.2007.06.010.

Bouhlel, M.A. *et al.* (2007b) ‘PPARγ Activation Primes Human Monocytes into Alternative M2 Macrophages with Anti-inflammatory Properties’, *Cell Metabolism*, 6(2), pp. 137–143. Available at: https://doi.org/10.1016/j.cmet.2007.06.010.

Boutens, L. and Stienstra, R. (2016) ‘Adipose tissue macrophages: going off track during obesity’, *Diabetologia*, 59, pp. 879–894. Available at: https://doi.org/10.1007/s00125-016-3904-9.

Boyano, M.D. *et al.* (2000) ‘Soluble interleukin-2 receptor, intercellular adhesion molecule-1 and interleukin-10 serum levels in patients with melanoma’, *British Journal of Cancer*, 83(7), pp. 847–852. Available at: https://doi.org/10.1054/bjoc.2000.1402.

Boyette, L.B. *et al.* (2017) ‘Phenotype, function, and differentiation potential of human monocyte subsets’, *PLoS ONE*, 12(4), p. e0176460. Available at: https://doi.org/10.1371/journal.pone.0176460.

Boyle, J.J. *et al.* (2009) ‘Coronary Intraplaque Hemorrhage Evokes a Novel Atheroprotective Macrophage Phenotype’, *The American Journal of Pathology*, 174(3), pp. 1097–1108. Available at: https://doi.org/10.2353/ajpath.2009.080431.

Braga, T.T., Agudelo, J.S.H. and Camara, N.O.S. (2015) ‘Macrophages During the Fibrotic Process: M2 as Friend and Foe’, *Frontiers in Immunology*, 6, p. 602. Available at: https://doi.org/10.3389/fimmu.2015.00602.

Brahmachari, S. *et al.* (2016) ‘Activation of tyrosine kinase c-Abl contributes to α-synuclein–induced neurodegeneration’, *The Journal of Clinical Investigation*, 126(8), pp. 2970–2988. Available at: https://doi.org/10.1172/JCI85456.

Brass, D.M. *et al.* (2007) ‘CD14 is an essential mediator of LPS-induced airway disease’, *American Journal of Physiology-Lung Cellular and Molecular Physiology*, 293(1), pp. L77–L83. Available at: https://doi.org/10.1152/ajplung.00282.2006.

Breese, E.J. *et al.* (1994) ‘Tumor necrosis factor alpha-producing cells in the intestinal mucosa of children with inflammatory bowel disease’, *Gastroenterology*, 106(6), pp. 1455–1466. Available at: https://doi.org/10.1016/0016-5085(94)90398-0.

Bressenot, A. *et al.* (2013) ‘Microscopic features for initial diagnosis and disease activity evaluation in inflammatory bowel disease’, *Inflammatory Bowel Diseases*, 19(8), pp. 1745–1752. Available at: https://doi.org/10.1097/MIB.0b013e318281f2e8.

Broadhurst, M.J. *et al.* (2012) ‘Upregulation of Retinal Dehydrogenase 2 in Alternatively Activated Macrophages during Retinoid-dependent Type-2 Immunity to Helminth Infection in Mice’, *PLoS Pathogens*, 8(8), p. e1002883. Available at: https://doi.org/10.1371/journal.ppat.1002883.

van den Broek, M.F. *et al.* (1995) ‘Immune defence in mice lacking type I and/or type II interferon receptors’, *Immunological Reviews*, 148, pp. 5–18. Available at: https://doi.org/10.1111/j.1600-065x.1995.tb00090.x.

Brown, G.C. (2019) ‘The endotoxin hypothesis of neurodegeneration’, *Journal of Neuroinflammation*, 16, p. 180. Available at: https://doi.org/10.1186/s12974-019-1564-7.

Burke, J.D. and Young, H.A. (2019) ‘IFN-γ: A cytokine at the right time, is in the right place’, *Seminars in immunology*, 43, p. 101280. Available at: https://doi.org/10.1016/j.smim.2019.05.002.

Burke, N.N. *et al.* (2014) ‘Minocycline modulates neuropathic pain behaviour and cortical M1–M2 microglial gene expression in a rat model of depression’, *Brain, Behavior, and Immunity*, 42, pp. 147–156. Available at: https://doi.org/10.1016/j.bbi.2014.06.015.

Cai, Z. *et al.* (2011) ‘Increases in b-amyloid protein in the hippocampus caused by diabetic metabolic disorder are blocked by minocycline through inhibition of NF-kB pathway activation’, *Pharmacological Reports*, p. 11.

Cai, Z.-Y., Yan, Y. and Chen, R. (2010) 'Minocycline reduces astrocytic reactivation and neuroinflammation in the hippocampus of a vascular cognitive impairment rat model', *Neuroscience Bulletin*, 26(1), pp. 28–36. Available at: https://doi.org/10.1007/s12264-010-0818-2.

Camille, N. and Dealtry, G. (2018) 'Regulation of M1/M2 macrophage polarization by Sutherlandia frutescens via NFkB and MAPK signaling pathways', *South African Journal of Botany*, 116, pp. 42–51. Available at: https://doi.org/10.1016/j.sajb.2018.02.400.

Camilli, G. *et al.* (2016) 'Regulation and trafficking of the HLA-E molecules during monocyte-macrophage differentiation', *Journal of Leukocyte Biology*, 99(1), pp. 121–130. Available at: https://doi.org/10.1189/jlb.1A0415-172R.

Campana, L. *et al.* (2018) 'The STAT3-IL10-IL6 pathway is a novel regulator of macrophage efferocytosis and phenotypic conversion in sterile liver injury', *Journal of immunology (Baltimore, Md. : 1950)*, 200(3), pp. 1169–1187. Available at: https://doi.org/10.4049/jimmunol.1701247.

Campbell, J.H. *et al.* (2011) 'Minocycline inhibition of monocyte activation correlates with neuronal protection in SIV neuroAIDS', *PloS One*, 6(4), p. e18688. Available at: https://doi.org/10.1371/journal.pone.0018688.

Candelli, M. *et al.* (2021) 'Interaction between Lipopolysaccharide and Gut Microbiota in Inflammatory Bowel Diseases', *International Journal of Molecular Sciences*, 22(12), p. 6242. Available at: https://doi.org/10.3390/ijms22126242.

Cankaya, S. *et al.* (2019) 'The therapeutic role of minocycline in Parkinson's disease', *Drugs in Context*, 8. Available at: https://doi.org/10.7573/dic.212553.

Canli, Ö. *et al.* (2017) 'Myeloid Cell-Derived Reactive Oxygen Species Induce Epithelial Mutagenesis', *Cancer Cell*, 32(6), pp. 869-883.e5. Available at: https://doi.org/10.1016/j.ccell.2017.11.004.

Cao, C. *et al.* (2005) 'A specific role of integrin Mac-1 in accelerated macrophage efflux to the lymphatics', *Blood*, 106(9), pp. 3234–3241. Available at: https://doi.org/10.1182/blood-2005-03-1288.

Cao, S. *et al.* (2006) 'NF-κB1 (p50) Homodimers Differentially Regulate Pro- and Anti-inflammatory Cytokines in Macrophages', *The Journal of biological chemistry*, 281(36), pp. 26041–26050. Available at: https://doi.org/10.1074/jbc.M602222200.

Caprara, G., Allavena, P. and Erreni, M. (2020) 'Intestinal Macrophages at the Crossroad between Diet, Inflammation, and Cancer', *International Journal of Molecular Sciences*, 21(14), p. 4825. Available at: https://doi.org/10.3390/ijms21144825.

Carbone, M. *et al.* (2008) 'Poly(ADP-ribosyl)ation is implicated in the G0-G1 transition of resting cells', *Oncogene*, 27(47), pp. 6083–6092. Available at: https://doi.org/10.1038/onc.2008.221.

Carlin, L.M. *et al.* (2013) 'Nr4a1-Dependent Ly6Clow Monocytes Monitor Endothelial Cells and Orchestrate Their Disposal', *Cell*, 153(2), pp. 362–375. Available at: https://doi.org/10.1016/j.cell.2013.03.010.

Casarejos, M.J. *et al.* (2006) 'Susceptibility to rotenone is increased in neurons from parkin null mice and is reduced by minocycline', *Journal of Neurochemistry*, 97(4), pp. 934–946. Available at: https://doi.org/10.1111/j.1471-4159.2006.03777.x.

Castoldi, A. *et al.* (2016) 'The Macrophage Switch in Obesity Development', *Frontiers in Immunology*, 6, p. 637. Available at: https://doi.org/10.3389/fimmu.2015.00637.

Cevey, Á.C. *et al.* (2019) 'IL-10/STAT3/SOCS3 Axis Is Involved in the Anti-inflammatory Effect of Benznidazole', *Frontiers in Immunology*, 10, p. 1267. Available at: https://doi.org/10.3389/fimmu.2019.01267.

Chacón-Salinas, R. *et al.* (2005) 'Differential pattern of cytokine expression by macrophages infected in vitro with different Mycobacterium tuberculosis genotypes', *Clinical and Experimental Immunology*, 140(3), pp. 443–449. Available at: https://doi.org/10.1111/j.1365-2249.2005.02797.x.

Chakravarty, S. and Herkenham, M. (2005) 'Toll-Like Receptor 4 on Nonhematopoietic Cells Sustains CNS Inflammation during Endotoxemia, Independent of Systemic Cytokines', *The Journal of Neuroscience*, 25(7), pp. 1788–1796. Available at: https://doi.org/10.1523/JNEUROSCI.4268-04.2005.

Chang, C.H. *et al.* (1992) 'The activation of major histocompatibility complex class I genes by interferon regulatory factor-1 (IRF-1)', *Immunogenetics*, 35(6), pp. 378–384. Available at: https://doi.org/10.1007/BF00179793.

Chanput, W. *et al.* (2013) 'Characterization of polarized THP-1 macrophages and polarizing ability of LPS and food compounds', *Food Funct.*, 4(2), pp. 266–276. Available at: https://doi.org/10.1039/C2FO30156C.

Chanput, W., Mes, J.J. and Wichers, H.J. (2014) 'THP-1 cell line: An in vitro cell model for immune modulation approach', *International Immunopharmacology*, 23(1), pp. 37–45. Available at: https://doi.org/10.1016/j.intimp.2014.08.002.

Chaudhry, A. and Rudensky, A.Y. (2013) 'Control of inflammation by integration of environmental cues by regulatory T cells', *The Journal of Clinical Investigation*, 123(3), pp. 939–944. Available at: https://doi.org/10.1172/JCI57175.

Chawla, A. (2010) 'Control of macrophage activation and function by PPARs', *Circulation research*, 106(10), pp. 1559–1569. Available at: https://doi.org/10.1161/CIRCRESAHA.110.216523.

Chelvarajan, R.L. *et al.* (2006) 'Molecular basis of age-associated cytokine dysregulation in LPS-stimulated macrophages', *Journal of Leukocyte Biology*, 79(6), pp. 1314–1327. Available at: https://doi.org/10.1189/jlb.0106024.

Chen, B. and Frangogiannis, N.G. (2018) 'The Role of Macrophages in Nonischemic Heart Failure', *JACC: Basic to Translational Science*, 3(2), pp. 245–248. Available at: https://doi.org/10.1016/j.jacbts.2018.03.001.

Chen, L. and Flies, D.B. (2013) 'Molecular mechanisms of T cell co-stimulation and co-inhibition', *Nature reviews. Immunology*, 13(4), pp. 227–242. Available at: https://doi.org/10.1038/nri3405.

Chen, M. *et al.* (2000) 'Minocycline inhibits caspase-1 and caspase-3 expression and delays mortality in a transgenic mouse model of Huntington disease', *Nature Medicine*, 6(7), pp. 797–801. Available at: https://doi.org/10.1038/77528.

Chen, M.-C. *et al.* (2014) 'Retinoic acid and cancer treatment', *BioMedicine*, 4(4). Available at: https://doi.org/10.7603/s40681-014-0022-1.

Chen, X. *et al.* (2017) 'Paralemmin-3 contributes to lipopolysaccharide-induced inflammatory response and is involved in lipopolysaccharide-Toll-like receptor-4 signaling in alveolar macrophages.', *International journal of molecular medicine* [Preprint]. Available at: https://doi.org/10.3892/ijmm.2017.3161.

Chen, X. *et al.* (2020) 'Macrophage polarization and its role in the pathogenesis of acute lung injury/acute respiratory distress syndrome', *Inflammation Research*, pp. 1–13. Available at: https://doi.org/10.1007/s00011-020-01378-2.

Chinen, T. *et al.* (2011) 'Prostaglandin E2 and SOCS1 have a role in intestinal immune tolerance', *Nature Communications*, 2, p. 190. Available at: https://doi.org/10.1038/ncomms1181.

Chiu, Y.-H. *et al.* (2018) 'Phosphorylation of signal transducer and activator of transcription 3 induced by hyperglycemia is different with that induced by lipopolysaccharide or erythropoietin via receptor-coupled signaling in cardiac cells', *Molecular Medicine Reports*, 17(1), pp. 1311–1320. Available at: https://doi.org/10.3892/mmr.2017.7973.

Chiwunze, T.E. *et al.* (2016) 'Organocatalyzed Mannich reactions on minocycline: Towards novel tetracycline antibiotics', *South African Journal of Chemistry*, 69. Available at: https://doi.org/10.17159/0379-4350/2016/v69a9.

Cho, J.C. *et al.* (2018) 'Return of the tetracyclines: omadacycline, a novel aminomethylcycline antimicrobial', *Drugs of Today (Barcelona, Spain: 1998)*, 54(3), pp. 209–217. Available at: https://doi.org/10.1358/dot.2018.54.3.2800620.

Choi, Y. *et al.* (2007) 'Minocycline attenuates neuronal cell death and improves cognitive impairment in Alzheimer's disease models', *Neuropsychopharmacology: Official Publication of the American College of Neuropsychopharmacology*, 32(11), pp. 2393–2404. Available at: https://doi.org/10.1038/sj.npp.1301377.

Chopra, Ian and Roberts, M. (2001) 'Tetracycline Antibiotics: Mode of Action, Applications, Molecular Biology, and Epidemiology of Bacterial Resistance',

Microbiology and Molecular Biology Reviews, 65(2), pp. 232–260. Available at: https://doi.org/10.1128/MMBR.65.2.232-260.2001.

Chopra, I. and Roberts, M. (2001) 'Tetracycline antibiotics: mode of action, applications, molecular biology, and epidemiology of bacterial resistance', *Microbiology and molecular biology reviews: MMBR*, 65(2), pp. 232-260 ; second page, table of contents. Available at: https://doi.org/10.1128/MMBR.65.2.232-260.2001.

Chu, L.-S. *et al.* (2007) 'Minocycline inhibits 5-lipoxygenase activation and brain inflammation after focal cerebral ischemia in rats', *Acta Pharmacologica Sinica*, 28(6), pp. 763–772. Available at: https://doi.org/10.1111/j.1745-7254.2007.00578.x.

Ciesielska, A., Matyjek, M. and Kwiatkowska, K. (2021) 'TLR4 and CD14 trafficking and its influence on LPS-induced pro-inflammatory signaling', *Cellular and Molecular Life Sciences*, 78(4), pp. 1233–1261. Available at: https://doi.org/10.1007/s00018-020-03656-y.

Clark, B.R. (1995) 'Fate of intercellular MHC-peptide-T-cell receptor complexes during T-cell activation', *Journal of molecular recognition: JMR*, 8(1–2), pp. 63–66. Available at: https://doi.org/10.1002/jmr.300080111.

Clarke, N. *et al.* (2004) 'Retinoids: potential in cancer prevention and therapy', *Expert Reviews in Molecular Medicine*, 6(25), pp. 1–23. Available at: https://doi.org/10.1017/S1462399404008488.

Cleynen, I. and Vermeire, S. (2012) 'Paradoxical inflammation induced by anti-TNF agents in patients with IBD', *Nature Reviews. Gastroenterology & Hepatology*, 9(9), pp. 496–503. Available at: https://doi.org/10.1038/nrgastro.2012.125.

Cope, A.P. *et al.* (1992) 'Increased levels of soluble tumor necrosis factor receptors in the sera and synovial fluid of patients with rheumatic diseases', *Arthritis & Rheumatism*, 35(10), pp. 1160–1169. Available at: https://doi.org/10.1002/art.1780351008.

Copeland, K.F.T. and Brooks, J.I. (2010) 'A novel use for an old drug: the potential for minocycline as anti-HIV adjuvant therapy', *The Journal of Infectious Diseases*, 201(8), pp. 1115–1117. Available at: https://doi.org/10.1086/651278.

Corbin, A.L. *et al.* (2020) 'IRF5 guides monocytes towards an inflammatory CD11c+ macrophage phenotype and promotes intestinal inflammation', *Science immunology*, 5(47), p. eaax6085. Available at: https://doi.org/10.1126/sciimmunol.aax6085.

Couper, K.N., Blount, D.G. and Riley, E.M. (2008) 'IL-10: The Master Regulator of Immunity to Infection', *The Journal of Immunology*, 180(9), pp. 5771–5777. Available at: https://doi.org/10.4049/jimmunol.180.9.5771.

Covarrubias, A.J. *et al.* (2020) 'Senescent cells promote tissue NAD+ decline during ageing via the activation of CD38+ macrophages', *Nature metabolism*,

2(11), pp. 1265–1283. Available at: https://doi.org/10.1038/s42255-020-00305-3.

Crepaldi, L. *et al.* (2001) 'Up-Regulation of IL-10R1 Expression Is Required to Render Human Neutrophils Fully Responsive to IL-10', *The Journal of Immunology*, 167(4), pp. 2312–2322. Available at: https://doi.org/10.4049/jimmunol.167.4.2312.

Croasdell, A. *et al.* (2015) 'Resolvins attenuate inflammation and promote resolution in cigarette smoke-exposed human macrophages', *American Journal of Physiology - Lung Cellular and Molecular Physiology*, 309(8), pp. L888–L901. Available at: https://doi.org/10.1152/ajplung.00125.2015.

Cronin, J.G. *et al.* (2016) 'Signal transducer and activator of transcription-3 licenses Toll-like receptor 4-dependent interleukin (IL)-6 and IL-8 production via IL-6 receptor-positive feedback in endometrial cells', *Mucosal Immunology*, 9(5), pp. 1125–1136. Available at: https://doi.org/10.1038/mi.2015.131.

Cui, J. *et al.* (2015) 'Mechanisms and pathways of innate immune activation and regulation in health and cancer', *Human Vaccines & Immunotherapeutics*, 10(11), pp. 3270–3285. Available at: https://doi.org/10.4161/21645515.2014.979640.

Cui, Y. *et al.* (2008) 'A novel role of minocycline: attenuating morphine antinociceptive tolerance by inhibition of p38 MAPK in the activated spinal microglia', *Brain, Behavior, and Immunity*, 22(1), pp. 114–123. Available at: https://doi.org/10.1016/j.bbi.2007.07.014.

D'Agostino, P. *et al.* (1998) 'Tetracycline inhibits the nitric oxide synthase activity induced by endotoxin in cultured murine macrophages', *European Journal of Pharmacology*, 346(2–3), pp. 283–290.

Daley, J.M. *et al.* (2010) 'The phenotype of murine wound macrophages', *Journal of Leukocyte Biology*, 87(1), pp. 59–67. Available at: https://doi.org/10.1189/jlb.0409236.

Dalli, J. and Serhan, C.N. (2017) 'Pro-Resolving Mediators in Regulating and Conferring Macrophage Function', *Frontiers in Immunology*, 8, p. 1400. Available at: https://doi.org/10.3389/fimmu.2017.01400.

D'Amico, F. *et al.* (2021) 'International consensus on methodological issues in standardization of fecal calprotectin measurement in inflammatory bowel diseases', *United European Gastroenterology Journal*, 9(4), pp. 451–460. Available at: https://doi.org/10.1002/ueg2.12069.

Darnell, J.E., Kerr, I.M. and Stark, G.R. (1994) 'Jak-STAT pathways and transcriptional activation in response to IFNs and other extracellular signaling proteins', *Science (New York, N.Y.)*, 264(5164), pp. 1415–1421. Available at: https://doi.org/10.1126/science.8197455.

Davies, J.M. and Abreu, M.T. (2015) 'The innate immune system and inflammatory bowel disease', *Scandinavian Journal of Gastroenterology*, 50(1), pp. 24–33. Available at: https://doi.org/10.3109/00365521.2014.966321.

Daws, M.R. *et al.* (2003) 'Pattern Recognition by TREM-2: Binding of Anionic Ligands', *The Journal of Immunology*, 171(2), pp. 594–599. Available at: https://doi.org/10.4049/jimmunol.171.2.594.

De Santa, F. *et al.* (2007) 'The Histone H3 Lysine-27 Demethylase Jmjd3 Links Inflammation to Inhibition of Polycomb-Mediated Gene Silencing', *Cell*, 130(6), pp. 1083–1094. Available at: https://doi.org/10.1016/j.cell.2007.08.019.

De Vries, L.C.S. *et al.* (2019) 'A JAK1 Selective Kinase Inhibitor and Tofacitinib Affect Macrophage Activation and Function', *Inflammatory Bowel Diseases*, 25(4), pp. 647–660. Available at: https://doi.org/10.1093/ibd/izy364.

Defaux, A. *et al.* (2011) 'Minocycline promotes remyelination in aggregating rat brain cell cultures after interferon-γ plus lipopolysaccharide-induced demyelination', *Neuroscience*, 187, pp. 84–92. Available at: https://doi.org/10.1016/j.neuroscience.2011.04.053.

Defrancesco, I. and Arcaini, L. (2018) 'Overview on the management of non-gastric MALT lymphomas', *Best Practice & Research Clinical Haematology*, 31(1), pp. 57–64. Available at: https://doi.org/10.1016/j.beha.2017.11.001.

Degboé, Y. *et al.* (2019) 'Polarization of Rheumatoid Macrophages by TNF Targeting Through an IL-10/STAT3 Mechanism', *Frontiers in Immunology*, 10, p. 3. Available at: https://doi.org/10.3389/fimmu.2019.00003.

Del Rosso, J.Q. (2016) 'Topical and oral antibiotics for acne vulgaris', *Seminars in Cutaneous Medicine and Surgery*, 35(2), pp. 57–61. Available at: https://doi.org/10.12788/j.sder.2016.025.

Delgado, M. *et al.* (1999) 'Shedding of membrane-bound CD14 from lipopolysaccharide-stimulated macrophages by vasoactive intestinal peptide and pituitary adenylate cyclase activating polypeptide', *Journal of Neuroimmunology*, 99(1), pp. 61–71. Available at: https://doi.org/10.1016/s0165-5728(99)00105-8.

Deng, B. *et al.* (2014) 'Maresin Biosynthesis and Identification of Maresin 2, a New Anti-Inflammatory and Pro-Resolving Mediator from Human Macrophages', *PLoS ONE*, 9(7), p. e102362. Available at: https://doi.org/10.1371/journal.pone.0102362.

Dhein, S. *et al.* (2015) 'Organ-protective effects on the liver and kidney by minocycline in small piglets undergoing cardiopulonary bypass', *Naunyn-Schmiedeberg's Archives of Pharmacology*, 388(6), pp. 663–676. Available at: https://doi.org/10.1007/s00210-015-1115-4.

Di Cerbo, A. *et al.* (2019) 'Tetracyclines: Insights and Updates of their Use in Human and Animal Pathology and their Potential Toxicity', *The Open Biochemistry Journal*, 13. Available at: https://doi.org/10.2174/1874091X01913010001.

Dick, S.A. and Epelman, S. (2016) 'Chronic Heart Failure and Inflammation: What Do We Really Know?', *Circulation Research*, 119(1), pp. 159–176. Available at: https://doi.org/10.1161/CIRCRESAHA.116.308030.

Ding, S.-W. and Voinnet, O. (2007) ‘Antiviral immunity directed by small RNAs’, *Cell*, 130(3), pp. 413–426. Available at: https://doi.org/10.1016/j.cell.2007.07.039.

Doak, G.R., Schwertfeger, K.L. and Wood, D.K. (2018) ‘Distant Relations: Macrophage Functions in the Metastatic Niche’, *Trends in cancer*, 4(6), pp. 445–459. Available at: https://doi.org/10.1016/j.trecan.2018.03.011.

Dong, Z. *et al.* (2019) ‘Biological Functions and Molecular Mechanisms of Antibiotic Tigecycline in the Treatment of Cancers’, *International Journal of Molecular Sciences*, 20(14), p. 3577. Available at: https://doi.org/10.3390/ijms20143577.

Dorrington, M.G. and Fraser, I.D.C. (2019) ‘NF-κB Signaling in Macrophages: Dynamics, Crosstalk, and Signal Integration’, *Frontiers in Immunology*, 10. Available at: https://doi.org/10.3389/fimmu.2019.00705.

Drechsler, M. *et al.* (2015) ‘Annexin A1 Counteracts Chemokine-Induced Arterial Myeloid Cell Recruitment’, *Circulation research*, 116(5), pp. 827–835. Available at: https://doi.org/10.1161/CIRCRESAHA.116.305825.

Drewes, J.L. *et al.* (2014) ‘Attenuation of pathogenic immune responses during infection with human and simian immunodeficiency virus (HIV/SIV) by the tetracycline derivative minocycline’, *PloS One*, 9(4), p. e94375. Available at: https://doi.org/10.1371/journal.pone.0094375.

Du, B. *et al.* (2011) ‘Minocycline attenuates ototoxicity and enhances antitumor activity of cisplatin treatment in vitro’, *Otolaryngology--Head and Neck Surgery: Official Journal of American Academy of Otolaryngology-Head and Neck Surgery*, 144(5), pp. 719–725. Available at: https://doi.org/10.1177/0194599810395090.

Duerr, R.H. *et al.* (2006) ‘A Genome-Wide Association Study Identifies IL23R as an Inflammatory Bowel Disease Gene’, *Science (New York, N.Y.)*, 314(5804), pp. 1461–1463. Available at: https://doi.org/10.1126/science.1135245.

Duffy, M.J., McGowan, P.M. and Gallagher, W.M. (2008) ‘Cancer invasion and metastasis: changing views’, *The Journal of Pathology*, 214(3), pp. 283–293. Available at: https://doi.org/10.1002/path.2282.

Duggar, B.M. (1948) ‘Aureomycin; a product of the continuing search for new antibiotics’, *Annals of the New York Academy of Sciences*, 51(Art. 2), pp. 177–181.

Duluc, D. *et al.* (2007) ‘Tumor-associated leukemia inhibitory factor and IL-6 skew monocyte differentiation into tumor-associated macrophage-like cells’, *Blood*, 110(13), pp. 4319–4330. Available at: https://doi.org/10.1182/blood-2007-02-072587.

Dumont, E.A.W.J. *et al.* (2010) ‘Minocycline inhibits apoptotic cell death in a murine model of partial flap loss’, *Journal of Reconstructive Microsurgery*, 26(8), pp. 523–528. Available at: https://doi.org/10.1055/s-0030-1262952.

Dunne, J.L. *et al.* (2003) 'Mac-1, but not LFA-1, uses intercellular adhesion molecule-1 to mediate slow leukocyte rolling in TNF-alpha-induced inflammation', *Journal of Immunology (Baltimore, Md.: 1950)*, 171(11), pp. 6105–6111. Available at: https://doi.org/10.4049/jimmunol.171.11.6105.

Dunston, C.R. *et al.* (2011) 'Proteomic analysis of the anti-inflammatory action of minocycline', *Proteomics*, 11(1), pp. 42–51. Available at: https://doi.org/10.1002/pmic.201000273.

Durafourt, B.A. *et al.* (2012) 'Comparison of polarization properties of human adult microglia and blood-derived macrophages', *Glia*, 60(5), pp. 717–727. Available at: https://doi.org/10.1002/glia.22298.

Durbin, J.E. *et al.* (1996) 'Targeted disruption of the mouse Stat1 gene results in compromised innate immunity to viral disease', *Cell*, 84(3), pp. 443–450. Available at: https://doi.org/10.1016/s0092-8674(00)81289-1.

Dutta, K. *et al.* (2010) 'Minocycline differentially modulates viral infection and persistence in an experimental model of Japanese encephalitis', *Journal of Neuroimmune Pharmacology: The Official Journal of the Society on NeuroImmune Pharmacology*, 5(4), pp. 553–565. Available at: https://doi.org/10.1007/s11481-010-9233-8.

Dutta, K. and Basu, A. (2011) 'Use of minocycline in viral infections', *The Indian Journal of Medical Research*, 133, pp. 467–470.

Ebong, S.J. *et al.* (2001) 'Critical Role of CD14 for Production of Proinflammatory Cytokines and Cytokine Inhibitors during Sepsis with Failure To Alter Morbidity or Mortality', *Infection and Immunity*, 69(4), pp. 2099–2106. Available at: https://doi.org/10.1128/IAI.69.4.2099-2106.2001.

Edwards, J.P. *et al.* (2006) 'Biochemical and functional characterization of three activated macrophage populations', *Journal of Leukocyte Biology*, 80(6), pp. 1298–1307. Available at: https://doi.org/10.1189/jlb.0406249.

Elcombe, S.E. *et al.* (2013) 'Dectin-1 Regulates IL-10 Production via a MSK1/2 and CREB Dependent Pathway and Promotes the Induction of Regulatory Macrophage Markers', *PLOS ONE*, 8(3), p. e60086. Available at: https://doi.org/10.1371/journal.pone.0060086.

Elliott, M.R. *et al.* (2009) 'Nucleotides released by apoptotic cells act as a find-me signal to promote phagocytic clearance', *Nature*, 461(7261), pp. 282–286. Available at: https://doi.org/10.1038/nature08296.

Elrod, J.W. *et al.* (2005) 'DSS-Induced Colitis Is Exacerbated in STAT-6 Knockout Mice':, *Inflammatory Bowel Diseases*, 11(10), pp. 883–889. Available at: https://doi.org/10.1097/01.MIB.0000182871.76434.57.

Embgenbroich, M. and Burgdorf, S. (2018) 'Current Concepts of Antigen Cross-Presentation', *Frontiers in Immunology*, 9, p. 1643. Available at: https://doi.org/10.3389/fimmu.2018.01643.

Enninga, E.A.L. *et al.* (2018) ‘CD206-positive myeloid cells bind galectin-9 and promote a tumor-supportive microenvironment’, *The Journal of pathology*, 245(4), pp. 468–477. Available at: https://doi.org/10.1002/path.5093.

Esterly, N.B. *et al.* (1984) ‘Neutrophil chemotaxis in patients with acne receiving oral tetracycline therapy’, *Archives of Dermatology*, 120(10), pp. 1308–1313.

Esterly, N.B., Furey, N.L. and Flanagan, L.E. (1978) ‘THE EFFECT OF ANTIMICROBIAL AGENTS ON LEUKOCYTE CHEMOTAXIS’, *Journal of Investigative Dermatology*, 70(1), pp. 51–55. Available at: https://doi.org/10.1111/1523-1747.ep12543487.

Evans, R. and Alexander, P. (1970) ‘Cooperation of immune lymphoid cells with macrophages in tumour immunity’, *Nature*, 228(5272), pp. 620–622. Available at: https://doi.org/10.1038/228620a0.

Fabriek, B.O. *et al.* (2009) ‘The macrophage scavenger receptor CD163 functions as an innate immune sensor for bacteria’, *Blood*, 113(4), pp. 887–892. Available at: https://doi.org/10.1182/blood-2008-07-167064.

Fagan, S.C., Cronic, L.E. and Hess, D.C. (2011) ‘Minocycline Development for Acute Ischemic Stroke’, *Translational Stroke Research*, 2(2), pp. 202–208. Available at: https://doi.org/10.1007/s12975-011-0072-6.

Fahy, N. *et al.* (2014) ‘Human osteoarthritic synovium impacts chondrogenic differentiation of mesenchymal stem cells via macrophage polarisation state’, *Osteoarthritis and Cartilage*, 22(8), pp. 1167–1175. Available at: https://doi.org/10.1016/j.joca.2014.05.021.

Falagas, M.E. *et al.* (2015) ‘Tetracyclines for multidrug-resistant Acinetobacter baumannii infections’, *International Journal of Antimicrobial Agents*, 45(5), pp. 455–460. Available at: https://doi.org/10.1016/j.ijantimicag.2014.12.031.

Fan, X., Lo, E.H. and Wang, X. (2013) ‘Effects of Minocycline Plus Tissue Plasminogen Activator Combination Therapy After Focal Embolic Stroke in Type 1 Diabetic Rats’, *Stroke*, 44(3), pp. 745–752. Available at: https://doi.org/10.1161/STROKEAHA.111.000309.

Fan, Z. and Ley, K. (2015) ‘Leukocyte arrest: Biomechanics and molecular mechanisms of β2 integrin activation’, *Biorheology*, 52(5–6), pp. 353–377. Available at: https://doi.org/10.3233/BIR-15085.

Fares, M. *et al.* (2015) ‘DNA damage, lysosomal degradation and Bcl-xL deamidation in doxycycline- and minocycline-induced cell death in the K562 leukemic cell line’, *Biochemical and Biophysical Research Communications*, 463(3), pp. 268–274. Available at: https://doi.org/10.1016/j.bbrc.2015.05.043.

Farinha, P. *et al.* (2005) ‘Analysis of multiple biomarkers shows that lymphoma-associated macrophage (LAM) content is an independent predictor of survival in follicular lymphoma (FL)’, *Blood*, 106(6), pp. 2169–2174. Available at: https://doi.org/10.1182/blood-2005-04-1565.

Fearon, D.T. and Locksley, R.M. (1996) ‘The instructive role of innate immunity in the acquired immune response’, *Science (New York, N.Y.)*, 272(5258), pp. 50–53. Available at: https://doi.org/10.1126/science.272.5258.50.

Feito, M.J. *et al.* (2019) ‘Characterization of M1 and M2 polarization phenotypes in peritoneal macrophages after treatment with graphene oxide nanosheets’, *Colloids and Surfaces B: Biointerfaces*, 176, pp. 96–105. Available at: https://doi.org/10.1016/j.colsurfb.2018.12.063.

Feldmann, M., Brennan, F.M. and Maini, R.N. (1996) ‘Role of cytokines in rheumatoid arthritis’, *Annual Review of Immunology*, 14, pp. 397–440. Available at: https://doi.org/10.1146/annurev.immunol.14.1.397.

Fenton, M.J. and Golenbock, D.T. (1998) ‘LPS-binding proteins and receptors’, *Journal of Leukocyte Biology*, 64(1), pp. 25–32. Available at: https://doi.org/10.1002/jlb.64.1.25.

Fernandes, T.L. *et al.* (2020) ‘Macrophage: A Potential Target on Cartilage Regeneration’, *Frontiers in Immunology*, 11, p. 111. Available at: https://doi.org/10.3389/fimmu.2020.00111.

Ferrante, C.J. *et al.* (2013) ‘The Adenosine-Dependent Angiogenic Switch of Macrophages to an M2-Like Phenotype is Independent of Interleukin-4 Receptor Alpha (IL-4Rα) Signaling’, *Inflammation*, 36(4), pp. 921–931. Available at: https://doi.org/10.1007/s10753-013-9621-3.

Ferrero, E. *et al.* (1993) ‘Transgenic mice expressing human CD14 are hypersensitive to lipopolysaccharide.’, *Proceedings of the National Academy of Sciences of the United States of America*, 90(6), pp. 2380–2384.

Fiocchi, C. (1998) ‘Inflammatory bowel disease: etiology and pathogenesis’, *Gastroenterology*, 115(1), pp. 182–205. Available at: https://doi.org/10.1016/s0016-5085(98)70381-6.

Firestein, G.S. and McInnes, I.B. (2017) ‘Immunopathogenesis of Rheumatoid Arthritis’, *Immunity*, 46(2), pp. 183–196. Available at: https://doi.org/10.1016/j.immuni.2017.02.006.

Førland, D.T. *et al.* (2011) ‘Effect of an extract based on the medicinal mushroom Agaricus blazei Murill on expression of cytokines and calprotectin in patients with ulcerative colitis and Crohn’s disease’, *Scandinavian Journal of Immunology*, 73(1), pp. 66–75. Available at: https://doi.org/10.1111/j.1365-3083.2010.02477.x.

Forrester, M.A. *et al.* (2018) ‘Similarities and differences in surface receptor expression by THP-1 monocytes and differentiated macrophages polarized using seven different conditioning regimens’, *Cellular immunology*, 332, pp. 58–76. Available at: https://doi.org/10.1016/j.cellimm.2018.07.008.

Fournier, B.M. and Parkos, C.A. (2012) ‘The role of neutrophils during intestinal inflammation’, *Mucosal Immunology*, 5(4), pp. 354–366. Available at: https://doi.org/10.1038/mi.2012.24.

Fox, S. *et al.* (2010) ‘Neutrophil Apoptosis: Relevance to the Innate Immune Response and Inflammatory Disease’, *Journal of Innate Immunity*, 2(3), pp. 216–227. Available at: https://doi.org/10.1159/000284367.

Franceschi, C. *et al.* (2017) ‘Inflammaging and “Garb-aging”’, *Trends in Endocrinology & Metabolism*, 28(3), pp. 199–212. Available at: https://doi.org/10.1016/j.tem.2016.09.005.

Franke, A. *et al.* (2010) ‘Meta-Analysis Increases to 71 the Tally of Confirmed Crohn’s Disease Susceptibility Loci’, *Nature genetics*, 42(12), pp. 1118–1125. Available at: https://doi.org/10.1038/ng.717.

Freeman, G.J. *et al.* (1995) ‘B7-1 and B7-2 do not deliver identical costimulatory signals, since B7-2 but not B7-1 preferentially costimulates the initial production of IL-4’, *Immunity*, 2(5), pp. 523–532. Available at: https://doi.org/10.1016/1074-7613(95)90032-2.

Fujisaka, S. *et al.* (2009) ‘Regulatory Mechanisms for Adipose Tissue M1 and M2 Macrophages in Diet-Induced Obese Mice’, *Diabetes*, 58(11), pp. 2574–2582. Available at: https://doi.org/10.2337/db08-1475.

Fujisaka, S. *et al.* (2011) ‘Telmisartan improves insulin resistance and modulates adipose tissue macrophage polarization in high-fat-fed mice’, *Endocrinology*, 152(5), pp. 1789–1799. Available at: https://doi.org/10.1210/en.2010-1312.

Fujisaka, S. *et al.* (2013) ‘Adipose tissue hypoxia induces inflammatory M1 polarity of macrophages in an HIF-1α-dependent and HIF-1α-independent manner in obese mice’, *Diabetologia*, 56(6), pp. 1403–1412. Available at: https://doi.org/10.1007/s00125-013-2885-1.

Fullerton, J.N. and Gilroy, D.W. (2016) ‘Resolution of inflammation: a new therapeutic frontier’, *Nature Reviews. Drug Discovery*, 15(8), pp. 551–567. Available at: https://doi.org/10.1038/nrd.2016.39.

Fultz, M.J. *et al.* (1993) ‘Induction of IFN-gamma in macrophages by lipopolysaccharide’, *International Immunology*, 5(11), pp. 1383–1392. Available at: https://doi.org/10.1093/intimm/5.11.1383.

Funes, S.C. *et al.* (2018) ‘Implications of macrophage polarization in autoimmunity’, *Immunology*, 154(2), pp. 186–195. Available at: https://doi.org/10.1111/imm.12910.

van Furth, R. *et al.* (1972) ‘The mononuclear phagocyte system: a new classification of macrophages, monocytes, and their precursor cells’, *Bulletin of the World Health Organization*, 46(6), pp. 845–852.

van Furth, R. and Cohn, Z.A. (1968) ‘THE ORIGIN AND KINETICS OF MONONUCLEAR PHAGOCYTES’, *The Journal of Experimental Medicine*, 128(3), pp. 415–435.

Gabay, C. (2006) ‘Interleukin-6 and chronic inflammation’, *Arthritis Research & Therapy*, 8(2), p. S3. Available at: https://doi.org/10.1186/ar1917.

Gagliani, N. *et al.* (2015) ‘Th17 cells transdifferentiate into regulatory T cells during resolution of inflammation’, *Nature*, 523(7559), pp. 221–225. Available at: https://doi.org/10.1038/nature14452.

Gajendran, M. *et al.* (2018) ‘A comprehensive review and update on Crohn’s disease’, *Disease-a-Month*, 64(2), pp. 20–57. Available at: https://doi.org/10.1016/j.disamonth.2017.07.001.

Gajewski, T.F. (1996) ‘B7-1 but not B7-2 efficiently costimulates CD8+ T lymphocytes in the P815 tumor system in vitro’, *Journal of Immunology (Baltimore, Md.: 1950)*, 156(2), pp. 465–472.

Gangloff, S.C. *et al.* (2005) ‘Influence of CD14 on Ligand Interactions between Lipopolysaccharide and Its Receptor Complex’, *The Journal of Immunology*, 175(6), pp. 3940–3945. Available at: https://doi.org/10.4049/jimmunol.175.6.3940.

Gao, Y. *et al.* (2003) ‘γδ T Cells Provide an Early Source of Interferon γ in Tumor Immunity’, *The Journal of Experimental Medicine*, 198(3), pp. 433–442. Available at: https://doi.org/10.1084/jem.20030584.

Garrido-Mesa, J., Algieri, F., Rodriguez-Nogales, A., Utrilla, Maria Pilar, *et al.* (2015) ‘A new therapeutic association to manage relapsing experimental colitis: Doxycycline plus Saccharomyces boulardii’, *Pharmacological Research*, 97, pp. 48–63. Available at: https://doi.org/10.1016/j.phrs.2015.04.005.

Garrido-Mesa, J., Algieri, F., Rodriguez-Nogales, A., Utrilla, Mª Pilar, *et al.* (2015) ‘A new therapeutic association to manage relapsing experimental colitis: Doxycycline plus Saccharomyces boulardii’, *Pharmacological Research*, 97, pp. 48–63. Available at: https://doi.org/10.1016/j.phrs.2015.04.005.

Garrido-Mesa, J., Algieri, F., *et al.* (2018) ‘Immunomodulatory tetracyclines ameliorate DNBS-colitis: Impact on microRNA expression and microbiota composition’, *Biochemical Pharmacology*, 155, pp. 524–536. Available at: https://doi.org/10.1016/j.bcp.2018.07.044.

Garrido-Mesa, J., Rodríguez-Nogales, A., *et al.* (2018a) ‘Immunomodulatory tetracyclines shape the intestinal inflammatory response inducing mucosal healing and resolution’, *British Journal of Pharmacology* [Preprint]. Available at: https://doi.org/10.1111/bph.14494.

Garrido-Mesa, J., Rodríguez-Nogales, A., *et al.* (2018b) ‘Immunomodulatory tetracyclines shape the intestinal inflammatory response inducing mucosal healing and resolution’, *British Journal of Pharmacology* [Preprint]. Available at: https://doi.org/10.1111/bph.14494.

Garrido-Mesa, N., Utrilla, P., *et al.* (2011a) ‘The association of minocycline and the probiotic Escherichia coli Nissle 1917 results in an additive beneficial effect in a DSS model of reactivated colitis in mice’, *Biochemical Pharmacology*, 82(12), pp. 1891–1900. Available at: https://doi.org/10.1016/j.bcp.2011.09.004.

Garrido-Mesa, N., Utrilla, P., *et al.* (2011b) ‘The association of minocycline and the probiotic Escherichia coli Nissle 1917 results in an additive beneficial effect

in a DSS model of reactivated colitis in mice', *Biochemical Pharmacology*, 82(12), pp. 1891–1900. Available at: https://doi.org/10.1016/j.bcp.2011.09.004.

Garrido-Mesa, N., Camuesco, D., *et al.* (2011a) 'The intestinal anti-inflammatory effect of minocycline in experimental colitis involves both its immunomodulatory and antimicrobial properties', *Pharmacological Research*, 63(4), pp. 308–319. Available at: https://doi.org/10.1016/j.phrs.2010.12.011.

Garrido-Mesa, N., Camuesco, D., *et al.* (2011b) 'The intestinal anti-inflammatory effect of minocycline in experimental colitis involves both its immunomodulatory and antimicrobial properties', *Pharmacological Research*, 63(4), pp. 308–319. Available at: https://doi.org/10.1016/j.phrs.2010.12.011.

Garrido-Mesa, N., Zarzuelo, A. and Gálvez, J. (2013a) 'Minocycline: far beyond an antibiotic', *British Journal of Pharmacology*, 169(2), pp. 337–352. Available at: https://doi.org/10.1111/bph.12139.

Garrido-Mesa, N., Zarzuelo, A. and Gálvez, J. (2013b) 'What is behind the non-antibiotic properties of minocycline?', *Pharmacological Research*, 67(1), pp. 18–30. Available at: https://doi.org/10.1016/j.phrs.2012.10.006.

Garrido-Mesa, N., Zarzuelo, A. and Gálvez, J. (2013c) 'What is behind the non-antibiotic properties of minocycline?', *Pharmacological Research*, 67(1), pp. 18–30. Available at: https://doi.org/10.1016/j.phrs.2012.10.006.

Gatto, F. *et al.* (2017) 'PMA-Induced THP-1 Macrophage Differentiation is Not Impaired by Citrate-Coated Platinum Nanoparticles', *Nanomaterials*, 7(10). Available at: https://doi.org/10.3390/nano7100332.

Gazi, U. and Martinez-Pomares, L. (2009) 'Influence of the mannose receptor in host immune responses', *Immunobiology*, 214(7), pp. 554–561. Available at: https://doi.org/10.1016/j.imbio.2008.11.004.

Gazzinelli, R.T. *et al.* (1996) 'In the absence of endogenous IL-10, mice acutely infected with Toxoplasma gondii succumb to a lethal immune response dependent on CD4+ T cells and accompanied by overproduction of IL-12, IFN-gamma and TNF-alpha.', *The Journal of Immunology*, 157(2), pp. 798–805.

Geissmann, F., Jung, S. and Littman, D.R. (2003) 'Blood monocytes consist of two principal subsets with distinct migratory properties', *Immunity*, 19(1), pp. 71–82. Available at: https://doi.org/10.1016/s1074-7613(03)00174-2.

Genin, M. *et al.* (2015) 'M1 and M2 macrophages derived from THP-1 cells differentially modulate the response of cancer cells to etoposide', *BMC Cancer*, 15. Available at: https://doi.org/10.1186/s12885-015-1546-9.

Gensel, J.C. and Zhang, B. (2015) 'Macrophage activation and its role in repair and pathology after spinal cord injury', *Brain Research*, 1619, pp. 1–11. Available at: https://doi.org/10.1016/j.brainres.2014.12.045.

Geremia, A. *et al.* (2011) 'IL-23–responsive innate lymphoid cells are increased in inflammatory bowel disease', *The Journal of Experimental Medicine*, 208(6), pp. 1127–1133. Available at: https://doi.org/10.1084/jem.20101712.

Geremia, A. *et al.* (2014) 'Innate and adaptive immunity in inflammatory bowel disease', *Autoimmunity Reviews*, 13(1), pp. 3–10. Available at: https://doi.org/10.1016/j.autrev.2013.06.004.

Gilbertson-Beadling, S. *et al.* (1995) 'The tetracycline analogs minocycline and doxycycline inhibit angiogenesis in vitro by a non-metalloproteinase-dependent mechanism', *Cancer Chemotherapy and Pharmacology*, 36(5), pp. 418–424. Available at: https://doi.org/10.1007/BF00686191.

Giles, A.J. *et al.* (2018) 'Dexamethasone-induced immunosuppression: mechanisms and implications for immunotherapy', *Journal for Immunotherapy of Cancer*, 6, p. 51. Available at: https://doi.org/10.1186/s40425-018-0371-5.

Ginhoux, F. and Jung, S. (2014) 'Monocytes and macrophages: developmental pathways and tissue homeostasis', *Nature Reviews Immunology*, 14(6), pp. 392–404. Available at: https://doi.org/10.1038/nri3671.

Giuliani, F., Hader, W. and Yong, V.W. (2005a) 'Minocycline attenuates T cell and microglia activity to impair cytokine production in T cell-microglia interaction', *Journal of Leukocyte Biology*, 78(1), pp. 135–143. Available at: https://doi.org/10.1189/jlb.0804477.

Giuliani, F., Hader, W. and Yong, V.W. (2005b) 'Minocycline attenuates T cell and microglia activity to impair cytokine production in T cell-microglia interaction', *Journal of Leukocyte Biology*, 78(1), pp. 135–143. Available at: https://doi.org/10.1189/jlb.0804477.

Giurisato, E. *et al.* (2018) 'Myeloid ERK5 deficiency suppresses tumor growth by blocking protumor macrophage polarization via STAT3 inhibition', *Proceedings of the National Academy of Sciences*, 115(12), pp. E2801–E2810. Available at: https://doi.org/10.1073/pnas.1707929115.

Gleissner, C.A. *et al.* (2010) 'CXCL4 induces a unique transcriptome in monocyte-derived macrophages', *Journal of immunology (Baltimore, Md. : 1950)*, 184(9), pp. 4810–4818. Available at: https://doi.org/10.4049/jimmunol.0901368.

Glocker, E.-O. *et al.* (2009) 'Inflammatory Bowel Disease and Mutations Affecting the Interleukin-10 Receptor', *The New England journal of medicine*, 361(21), pp. 2033–2045. Available at: https://doi.org/10.1056/NEJMoa0907206.

Godson, C. *et al.* (2000) 'Cutting Edge: Lipoxins Rapidly Stimulate Nonphlogistic Phagocytosis of Apoptotic Neutrophils by Monocyte-Derived Macrophages', *The Journal of Immunology*, 164(4), pp. 1663–1667. Available at: https://doi.org/10.4049/jimmunol.164.4.1663.

Goenka, S. and Kaplan, M.H. (2011) 'Transcriptional regulation by STAT6', *Immunologic research*, 50(1), pp. 87–96. Available at: https://doi.org/10.1007/s12026-011-8205-2.

Gold, L.S. *et al.* (2020) 'Minocycline 1.5% foam for the topical treatment of moderate to severe papulopustular rosacea: Results of 2 phase 3, randomized,

clinical trials', *Journal of the American Academy of Dermatology*, 82(5), pp. 1166–1173. Available at: https://doi.org/10.1016/j.jaad.2020.01.043.

Golub, L.M. *et al.* (1991) 'Tetracyclines inhibit connective tissue breakdown: new therapeutic implications for an old family of drugs', *Critical Reviews in Oral Biology and Medicine: An Official Publication of the American Association of Oral Biologists*, 2(3), pp. 297–321.

Golub, L.M. *et al.* (1998) 'Tetracyclines Inhibit Connective Tissue Breakdown by Multiple Non-Antimicrobial Mechanisms', *Advances in Dental Research*, 12(1), pp. 12–26. Available at: https://doi.org/10.1177/08959374980120010501.

Golub, L.M., Suomalainen, K. and Sorsa, T. (1992) 'Host modulation with tetracyclines and their chemically modified analogues', *Current Opinion in Dentistry*, 2, pp. 80–90.

Gomes, P.S. and Fernandes, M.H. (2007) 'Effect of therapeutic levels of doxycycline and minocycline in the proliferation and differentiation of human bone marrow osteoblastic cells', *Archives of Oral Biology*, 52(3), pp. 251–259. Available at: https://doi.org/10.1016/j.archoralbio.2006.10.005.

Gomez, C.R. *et al.* (2008) 'Innate immunity and aging', *Experimental Gerontology*, 43(8), pp. 718–728. Available at: https://doi.org/10.1016/j.exger.2008.05.016.

Gordon, S. (2003) 'Alternative activation of macrophages', *Nature Reviews Immunology*, 3(1), pp. 23–35. Available at: https://doi.org/10.1038/nri978.

Gordon, S. and Martinez, F.O. (2010) 'Alternative Activation of Macrophages: Mechanism and Functions', *Immunity*, 32(5), pp. 593–604. Available at: https://doi.org/10.1016/j.immuni.2010.05.007.

Gordon, S. and Plüddemann, A. (2018) 'Macrophage Clearance of Apoptotic Cells: A Critical Assessment', *Frontiers in Immunology*, 0. Available at: https://doi.org/10.3389/fimmu.2018.00127.

Gordon, S. and Taylor, P.R. (2005) 'Monocyte and macrophage heterogeneity', *Nature Reviews. Immunology*, 5(12), pp. 953–964. Available at: https://doi.org/10.1038/nri1733.

Gracie, J.A. *et al.* (1999) 'A proinflammatory role for IL-18 in rheumatoid arthritis', *Journal of Clinical Investigation*, 104(10), pp. 1393–1401. Available at: https://doi.org/10.1172/JCI7317.

Grainger, J.R. *et al.* (2017) 'Macrophages in gastrointestinal homeostasis and inflammation', *Pflugers Archiv*, 469(3), pp. 527–539. Available at: https://doi.org/10.1007/s00424-017-1958-2.

Greenwald, R.A. *et al.* (1987) 'Tetracyclines inhibit human synovial collagenase in vivo and in vitro', *The Journal of Rheumatology*, 14(1), pp. 28–32.

Greenwald, R.A. *et al.* (1992) 'Tetracyclines suppress matrix metalloproteinase activity in adjuvant arthritis and in combination with flurbiprofen, ameliorate bone damage', *The Journal of Rheumatology*, 19(6), pp. 927–938.

Greenwald, R.A. (1994) ‘Treatment of destructive arthritic disorders with MMP inhibitors. Potential role of tetracyclines’, *Annals of the New York Academy of Sciences*, 732, pp. 181–198.

Griffin, M.O. *et al.* (2010) ‘Tetracyclines: a pleitropic family of compounds with promising therapeutic properties. Review of the literature’, *American Journal of Physiology. Cell Physiology*, 299(3), pp. C539-548. Available at: https://doi.org/10.1152/ajpcell.00047.2010.

Griffin, M.O., Ceballos, G. and Villarreal, F.J. (2011) ‘Tetracycline compounds with non-antimicrobial organ protective properties: Possible mechanisms of action’, *Pharmacological Research*, 63(2), pp. 102–107. Available at: https://doi.org/10.1016/j.phrs.2010.10.004.

Grimm, M.C. *et al.* (1995) ‘Direct evidence of monocyte recruitment to inflammatory bowel disease mucosa’, *Journal of Gastroenterology and Hepatology*, 10(4), pp. 387–395. Available at: https://doi.org/10.1111/j.1440-1746.1995.tb01589.x.

Guarda, G. and So, A. (2010) ‘Regulation of inflammasome activity’, *Immunology*, 130(3), pp. 329–336. Available at: https://doi.org/10.1111/j.1365-2567.2010.03283.x.

Gubernatorova, E.O. and Tumanov, A.V. (2016) ‘Tumor necrosis factor and lymphotoxin in regulation of intestinal inflammation’, *Biochemistry (Moscow)*, 81(11), pp. 1309–1325. Available at: https://doi.org/10.1134/S0006297916110092.

Gude, D.R. *et al.* (2008) ‘Apoptosis induces expression of sphingosine kinase 1 to release sphingosine-1-phosphate as a “come-and-get-me” signal’, *The FASEB Journal*, 22(8), pp. 2629–2638. Available at: https://doi.org/10.1096/fj.08-107169.

Guerin, C. *et al.* (1992) ‘Selective endothelial growth inhibition by tetracyclines that inhibit collagenase’, *Biochemical and Biophysical Research Communications*, 188(2), pp. 740–745.

Guerriero, J.L. (2019) ‘Macrophages: Their Untold Story in T Cell Activation and Function’, *International Review of Cell and Molecular Biology*, 342, pp. 73–93. Available at: https://doi.org/10.1016/bs.ircmb.2018.07.001.

Guo, H., Jin, D. and Chen, X. (2014) ‘Lipocalin 2 is a Regulator Of Macrophage Polarization and NF-κB/STAT3 Pathway Activation’, *Molecular Endocrinology*, 28(10), pp. 1616–1628. Available at: https://doi.org/10.1210/me.2014-1092.

Guo, X. *et al.* (2017) ‘Single tumor-initiating cells evade immune clearance by recruiting type II macrophages’, *Genes & Development*, 31(3), pp. 247–259. Available at: https://doi.org/10.1101/gad.294348.116.

Guo, Y. *et al.* (2020) ‘Abnormal polarization of macrophage-like cells in the peripheral blood of patients with glioma’, *Oncology Letters*, 20(1), pp. 947–954. Available at: https://doi.org/10.3892/ol.2020.11602.

Guzmán-Beltrán, S. *et al.* (2017) 'Human macrophages chronically exposed to LPS can be reactivated by stimulation with MDP to acquire an antimicrobial phenotype', *Cellular Immunology*, 315, pp. 45–55. Available at: https://doi.org/10.1016/j.cellimm.2017.02.004.

Hadis, U. *et al.* (2011) 'Intestinal Tolerance Requires Gut Homing and Expansion of FoxP3+ Regulatory T Cells in the Lamina Propria', *Immunity*, 34(2), pp. 237–246. Available at: https://doi.org/10.1016/j.immuni.2011.01.016.

Hagemann, T. *et al.* (2008) '"Re-educating" tumor-associated macrophages by targeting NF-κB', *The Journal of Experimental Medicine*, 205(6), pp. 1261–1268. Available at: https://doi.org/10.1084/jem.20080108.

Haghi-Aminjan, H. (2017) 'A systematic review on potential mechanisms of minocycline in kidney diseases', *Pharmacological Reports*, p. 8.

Haltmayer, E. *et al.* (2019) 'Co-culture of osteochondral explants and synovial membrane as in vitro model for osteoarthritis', *PLoS ONE*, 14(4), p. e0214709. Available at: https://doi.org/10.1371/journal.pone.0214709.

Hambardzumyan, D., Gutmann, D.H. and Kettenmann, H. (2016) 'The role of microglia and macrophages in glioma maintenance and progression', *Nature Neuroscience*, 19(1), pp. 20–27. Available at: https://doi.org/10.1038/nn.4185.

Hampe, J. *et al.* (2007) 'A genome-wide association scan of nonsynonymous SNPs identifies a susceptibility variant for Crohn disease in ATG16L1', *Nature Genetics*, 39(2), pp. 207–211. Available at: https://doi.org/10.1038/ng1954.

Hampton, R.Y. *et al.* (1991) 'Recognition and plasma clearance of endotoxin by scavenger receptors', *Nature*, 352(6333), pp. 342–344. Available at: https://doi.org/10.1038/352342a0.

Han, M.S. *et al.* (2013) 'JNK Expression by Macrophages Promotes Obesity-induced Insulin Resistance and Inflammation', *Science (New York, N.Y.)*, 339(6116), p. 10.1126/science.1227568. Available at: https://doi.org/10.1126/science.1227568.

Han, S. *et al.* (2013) 'PMA and Ionomycin Induce Glioblastoma Cell Death: Activation-Induced Cell-Death-Like Phenomena Occur in Glioma Cells', *PLoS ONE*, 8(10), p. e76717. Available at: https://doi.org/10.1371/journal.pone.0076717.

Hanna, R.N. *et al.* (2011) 'The transcription factor NR4A1 (Nur77) controls bone marrow differentiation and the survival of Ly6C− monocytes', *Nature Immunology*, 12(8), pp. 778–785. Available at: https://doi.org/10.1038/ni.2063.

Hao, N.-B. *et al.* (2012) *Macrophages in Tumor Microenvironments and the Progression of Tumors*, *Journal of Immunology Research*. Available at: https://doi.org/10.1155/2012/948098.

Haribhai, D. *et al.* (2016) 'Alternatively activated macrophages boost iTreg and Th17 cell responses during immunotherapy for colitis', *Journal of immunology*

(Baltimore, Md. : 1950), 196(8), pp. 3305–3317. Available at: https://doi.org/10.4049/jimmunol.1501956.

Harris, D.P. *et al.* (2005) 'Regulation of IFN-gamma production by B effector 1 cells: essential roles for T-bet and the IFN-gamma receptor', *Journal of Immunology (Baltimore, Md.: 1950)*, 174(11), pp. 6781–6790. Available at: https://doi.org/10.4049/jimmunol.174.11.6781.

Harwani, S.C. (2018a) 'Macrophages under pressure: the role of macrophage polarization in hypertension', *Translational Research*, 191, pp. 45–63. Available at: https://doi.org/10.1016/j.trsl.2017.10.011.

Harwani, S.C. (2018b) 'Macrophages Under Pressure: The Role of Macrophage Polarization in Hypertension', *Translational research : the journal of laboratory and clinical medicine*, 191, pp. 45–63. Available at: https://doi.org/10.1016/j.trsl.2017.10.011.

Haziot, A. *et al.* (1988) 'The monocyte differentiation antigen, CD14, is anchored to the cell membrane by a phosphatidylinositol linkage', *Journal of Immunology (Baltimore, Md.: 1950)*, 141(2), pp. 547–552.

Haziot, A. *et al.* (1996) 'Resistance to endotoxin shock and reduced dissemination of gram-negative bacteria in CD14-deficient mice', *Immunity*, 4(4), pp. 407–414. Available at: https://doi.org/10.1016/s1074-7613(00)80254-x.

He, Y. *et al.* (2020) 'IL-4 Switches Microglia/macrophage M1/M2 Polarization and Alleviates Neurological Damage by Modulating the JAK1/STAT6 Pathway Following ICH', *Neuroscience*, 437, pp. 161–171. Available at: https://doi.org/10.1016/j.neuroscience.2020.03.008.

Heaney, M., Mahoney, M.V. and Gallagher, J.C. (2019) 'Eravacycline: The Tetracyclines Strike Back', *Annals of Pharmacotherapy*, 53(11), pp. 1124–1135. Available at: https://doi.org/10.1177/1060028019850173.

Hemmati, S., Haque, T. and Gritsman, K. (2017) 'Inflammatory Signaling Pathways in Preleukemic and Leukemic Stem Cells', *Frontiers in Oncology*, 7. Available at: https://doi.org/10.3389/fonc.2017.00265.

Henry, C.J. *et al.* (2008) 'Minocycline attenuates lipopolysaccharide (LPS)-induced neuroinflammation, sickness behavior, and anhedonia', *Journal of Neuroinflammation*, 5, p. 15. Available at: https://doi.org/10.1186/1742-2094-5-15.

Heo, K. *et al.* (2006) 'Minocycline inhibits caspase-dependent and -independent cell death pathways and is neuroprotective against hippocampal damage after treatment with kainic acid in mice', *Neuroscience Letters*, 398(3), pp. 195–200. Available at: https://doi.org/10.1016/j.neulet.2006.01.027.

Herbert, D.R. *et al.* (2004) 'Alternative Macrophage Activation Is Essential for Survival during Schistosomiasis and Downmodulates T Helper 1 Responses and Immunopathology', *Immunity*, 20(5), pp. 623–635. Available at: https://doi.org/10.1016/S1074-7613(04)00107-4.

van Herk, E.H. and Te Velde, A.A. (2016) ‘Treg subsets in inflammatory bowel disease and colorectal carcinoma: Characteristics, role, and therapeutic targets’, *Journal of Gastroenterology and Hepatology*, 31(8), pp. 1393–1404. Available at: https://doi.org/10.1111/jgh.13342.

Hermann, M., Flammer, A. and Lüscher, T.F. (2006) ‘Nitric oxide in hypertension’, *Journal of Clinical Hypertension (Greenwich, Conn.)*, 8(12 Suppl 4), pp. 17–29. Available at: https://doi.org/10.1111/j.1524-6175.2006.06032.x.

Herrera, M. and Garvin, J.L. (2005) ‘Recent advances in the regulation of nitric oxide in the kidney’, *Hypertension (Dallas, Tex.: 1979)*, 45(6), pp. 1062–1067. Available at: https://doi.org/10.1161/01.HYP.0000159760.88697.1e.

Hesketh, M. *et al.* (2017) ‘Macrophage Phenotypes Regulate Scar Formation and Chronic Wound Healing’, *International Journal of Molecular Sciences*, 18(7), p. 1545. Available at: https://doi.org/10.3390/ijms18071545.

Hettinger, J. *et al.* (2013) ‘Origin of monocytes and macrophages in a committed progenitor’, *Nature Immunology*, 14(8), pp. 821–830. Available at: https://doi.org/10.1038/ni.2638.

Hidalgo, M. and Eckhardt, S.G. (2001) ‘Development of Matrix Metalloproteinase Inhibitors in Cancer Therapy’, *JNCI Journal of the National Cancer Institute*, 93(3), pp. 178–193. Available at: https://doi.org/10.1093/jnci/93.3.178.

Higashi, Y. *et al.* (2019) ‘Minocycline inhibits PDGF-BB-induced human aortic smooth muscle cell proliferation and migration by reversing miR-221- and -222-mediated RECK suppression’, *Cellular Signalling*, 57, pp. 10–20. Available at: https://doi.org/10.1016/j.cellsig.2019.01.014.

Hine, A.M. and Loke, P. (2019) ‘Intestinal macrophages in resolving inflammation’, *Journal of immunology (Baltimore, Md. : 1950)*, 203(3), pp. 593–599. Available at: https://doi.org/10.4049/jimmunol.1900345.

Ho, G. *et al.* (2020) ‘Resolution of Inflammation and Gut Repair in IBD: Translational Steps Towards Complete Mucosal Healing’, *Inflammatory Bowel Diseases*, 26(8), pp. 1131–1143. Available at: https://doi.org/10.1093/ibd/izaa045.

Ho, M.K. and Springer, T.A. (1982) ‘Mac-1 antigen: quantitative expression in macrophage populations and tissues, and immunofluorescent localization in spleen’, *Journal of Immunology (Baltimore, Md.: 1950)*, 128(5), pp. 2281–2286.

Holling, T.M., Schooten, E. and van Den Elsen, P.J. (2004) ‘Function and regulation of MHC class II molecules in T-lymphocytes: of mice and men’, *Human Immunology*, 65(4), pp. 282–290. Available at: https://doi.org/10.1016/j.humimm.2004.01.005.

Hong, S. *et al.* (2016) ‘Complement and Microglia Mediate Early Synapse Loss in Alzheimer Mouse Models’, *Science (New York, N.Y.)*, 352(6286), pp. 712–716. Available at: https://doi.org/10.1126/science.aad8373.

Hoshino, Y. *et al.* (2007) ‘Mechanisms of polymorphonuclear neutrophil-mediated induction of HIV-1 replication in macrophages during pulmonary tuberculosis’, *The Journal of Infectious Diseases*, 195(9), pp. 1303–1310. Available at: https://doi.org/10.1086/513438.

Hotamisligil, G.S. (2006) ‘Inflammation and metabolic disorders’, *Nature*, 444(7121), pp. 860–867. Available at: https://doi.org/10.1038/nature05485.

Hou, L. *et al.* (2017) ‘Complement receptor 3 mediates NADPH oxidase activation and dopaminergic neurodegeneration through a Src-Erk-dependent pathway’, *Redox Biology*, 14, pp. 250–260. Available at: https://doi.org/10.1016/j.redox.2017.09.017.

Hu, B. and Guo, Y. (2019) ‘Inhibition of mitochondrial translation as a therapeutic strategy for human ovarian cancer to overcome chemoresistance’, *Biochemical and Biophysical Research Communications*, 509(2), pp. 373–378. Available at: https://doi.org/10.1016/j.bbrc.2018.12.127.

Hu, X. *et al.* (2010) ‘Minocycline protects against myocardial ischemia and reperfusion injury by inhibiting high mobility group box 1 protein in rats’, *European Journal of Pharmacology*, 638(1), pp. 84–89. Available at: https://doi.org/10.1016/j.ejphar.2010.03.059.

Huang, T.-Y. *et al.* (2009) ‘Minocycline attenuates experimental colitis in mice by blocking expression of inducible nitric oxide synthase and matrix metalloproteinases’, *Toxicology and Applied Pharmacology*, 237(1), pp. 69–82. Available at: https://doi.org/10.1016/j.taap.2009.02.026.

Hughes, E.L. *et al.* (2017) ‘Mast cells mediate early neutrophil recruitment and exhibit anti-inflammatory properties via the formyl peptide receptor 2/lipoxin A4 receptor’, *British Journal of Pharmacology*, 174(14), pp. 2393–2408. Available at: https://doi.org/10.1111/bph.13847.

Hugot, J.P. *et al.* (1996) ‘Mapping of a susceptibility locus for Crohn’s disease on chromosome 16’, *Nature*, 379(6568), pp. 821–823. Available at: https://doi.org/10.1038/379821a0.

Hung, Y.-L. *et al.* (2017) ‘Corylin protects LPS-induced sepsis and attenuates LPS-induced inflammatory response’, *Scientific Reports*, 7, p. 46299. Available at: https://doi.org/10.1038/srep46299.

Hunter, C.A. *et al.* (1997) ‘IL-10 is required to prevent immune hyperactivity during infection with Trypanosoma cruzi.’, *The Journal of Immunology*, 158(7), pp. 3311–3316.

Hunter, M.M. *et al.* (2010) ‘In Vitro-Derived Alternatively Activated Macrophages Reduce Colonic Inflammation in Mice’, *Gastroenterology*, 138(4), pp. 1395–1405. Available at: https://doi.org/10.1053/j.gastro.2009.12.041.

Hurst, S.M. *et al.* (2001) ‘Il-6 and its soluble receptor orchestrate a temporal switch in the pattern of leukocyte recruitment seen during acute inflammation’, *Immunity*, 14(6), pp. 705–714. Available at: https://doi.org/10.1016/s1074-7613(01)00151-0.

Hutton, H.L. *et al.* (2016) 'The NLRP3 inflammasome in kidney disease and autoimmunity', *Nephrology (Carlton, Vic.)*, 21(9), pp. 736–744. Available at: https://doi.org/10.1111/nep.12785.

Hynes, R.O. (2002) 'Integrins: bidirectional, allosteric signaling machines', *Cell*, 110(6), pp. 673–687. Available at: https://doi.org/10.1016/s0092-8674(02)00971-6.

Ingersoll, M.A. *et al.* (2010) 'Comparison of gene expression profiles between human and mouse monocyte subsets', *Blood*, 115(3), pp. e10–e19. Available at: https://doi.org/10.1182/blood-2009-07-235028.

Ingham, E., Turnbull, L. and Kearney, J.N. (1991) 'The effects of minocycline and tetracycline on the mitotic response of human peripheral blood-lymphocytes', *The Journal of Antimicrobial Chemotherapy*, 27(5), pp. 607–617.

Ip, W.K.E. *et al.* (2017) 'Anti-inflammatory effect of IL-10 mediated by metabolic reprogramming of macrophages', *Science*, 356(6337), pp. 513–519. Available at: https://doi.org/10.1126/science.aal3535.

Iqbal, S. and Kumar, A. (2015) 'Characterization of In vitro Generated Human Polarized Macrophages', *Journal of Clinical & Cellular Immunology*, 06(06). Available at: https://doi.org/10.4172/2155-9899.1000380.

Isidro, R.A. and Appleyard, C.B. (2016) 'Colonic macrophage polarization in homeostasis, inflammation, and cancer', *American Journal of Physiology - Gastrointestinal and Liver Physiology*, 311(1), pp. G59–G73. Available at: https://doi.org/10.1152/ajpgi.00123.2016.

Italiani, P. *et al.* (2014) 'Transcriptomic Profiling of the Development of the Inflammatory Response in Human Monocytes In Vitro', *PLoS ONE*, 9(2), p. e87680. Available at: https://doi.org/10.1371/journal.pone.0087680.

Iwasaki, A. and Medzhitov, R. (2004) 'Toll-like receptor control of the adaptive immune responses', *Nature Immunology*, 5(10), pp. 987–995. Available at: https://doi.org/10.1038/ni1112.

Jabłońska-Trypuć, A., Matejczyk, M. and Rosochacki, S. (2016) 'Matrix metalloproteinases (MMPs), the main extracellular matrix (ECM) enzymes in collagen degradation, as a target for anticancer drugs', *Journal of Enzyme Inhibition and Medicinal Chemistry*, 31(sup1), pp. 177–183. Available at: https://doi.org/10.3109/14756366.2016.1161620.

Jackaman, C. *et al.* (2017) 'Aging and cancer: The role of macrophages and neutrophils', *Ageing Research Reviews*, 36, pp. 105–116. Available at: https://doi.org/10.1016/j.arr.2017.03.008.

Jakubzick, C. *et al.* (2013) 'Minimal differentiation of classical monocytes as they survey steady state tissues and transport antigen to lymph nodes', *Immunity*, 39(3), p. 10.1016/j.immuni.2013.08.007. Available at: https://doi.org/10.1016/j.immuni.2013.08.007.

Jaworska, K. *et al.* (2019) ‘Inflammatory bowel disease is associated with increased gut-to-blood penetration of short-chain fatty acids: A new, non-invasive marker of a functional intestinal lesion’, *Experimental Physiology*, 104(8), pp. 1226–1236. Available at: https://doi.org/10.1113/EP087773.

Jimenez-Uribe, A.P. *et al.* (2019) *CD80 Expression Correlates with IL-6 Production in THP-1-Like Macrophages Costimulated with LPS and Dialyzable Leukocyte Extract (Transferon®)*. Available at: https://www.hindawi.com/journals/jir/2019/2198508/ (Accessed: 2 September 2019).

Jinnouchi, H. *et al.* (2020) ‘Diversity of macrophage phenotypes and responses in atherosclerosis’, *Cellular and molecular life sciences: CMLS*, 77(10), pp. 1919–1932. Available at: https://doi.org/10.1007/s00018-019-03371-3.

Johnson, D.R. and Pober, J.S. (1990) ‘Tumor necrosis factor and immune interferon synergistically increase transcription of HLA class I heavy- and light-chain genes in vascular endothelium.’, *Proceedings of the National Academy of Sciences of the United States of America*, 87(13), pp. 5183–5187.

Joks, R. *et al.* (2010) ‘Tetracycline-mediated IgE isotype-specific suppression of ongoing human and murine IgE responses in vivo and murine memory IgE responses induced in vitro’, *International Immunology*, 22(4), pp. 281–288. Available at: https://doi.org/10.1093/intimm/dxq004.

Joks, R. and Durkin, H.G. (2011) ‘Non-antibiotic properties of tetracyclines as anti-allergy and asthma drugs’, *Pharmacological Research*, 64(6), pp. 602–609. Available at: https://doi.org/10.1016/j.phrs.2011.04.001.

Jones, G.-R. *et al.* (2018) ‘Dynamics of Colon Monocyte and Macrophage Activation During Colitis’, *Frontiers in Immunology*, 9, p. 2764. Available at: https://doi.org/10.3389/fimmu.2018.02764.

Jones, S.A. *et al.* (2005) ‘IL-6 transsignaling: the in vivo consequences’, *Journal of Interferon & Cytokine Research: The Official Journal of the International Society for Interferon and Cytokine Research*, 25(5), pp. 241–253. Available at: https://doi.org/10.1089/jir.2005.25.241.

Jouanguy, E. *et al.* (1999) ‘IL-12 and IFN-gamma in host defense against mycobacteria and salmonella in mice and men’, *Current Opinion in Immunology*, 11(3), pp. 346–351. Available at: https://doi.org/10.1016/s0952-7915(99)80055-7.

Jubin, T. *et al.* (2017) ‘Poly ADP-ribose polymerase-1: Beyond transcription and towards differentiation’, *Seminars in Cell & Developmental Biology*, 63, pp. 167–179. Available at: https://doi.org/10.1016/j.semcdb.2016.07.027.

Jung, H.-J. *et al.* (2014) ‘Minocycline inhibits angiogenesis in vitro through the translational suppression of HIF-1α’, *Archives of Biochemistry and Biophysics*, 545, pp. 74–82. Available at: https://doi.org/10.1016/j.abb.2013.12.023.

Junttila, I.S. *et al.* (2008) ‘Tuning sensitivity to IL-4 and IL-13: differential expression of IL-4Ralpha, IL-13Ralpha1, and gammac regulates relative

cytokine sensitivity', *The Journal of Experimental Medicine*, 205(11), pp. 2595–2608. Available at: https://doi.org/10.1084/jem.20080452.

Kadigamuwa, C. *et al.* (2019) 'Role of Retinoic Acid Receptor-γ in DNA Damage-Induced Necroptosis', *iScience*, 17, pp. 74–86. Available at: https://doi.org/10.1016/j.isci.2019.06.019.

Kadl, A. *et al.* (2010) 'Identification of a novel macrophage phenotype that develops in response to atherogenic phospholipids via Nrf2', *Circulation research*, 107(6), pp. 737–746. Available at: https://doi.org/10.1161/CIRCRESAHA.109.215715.

Kai, Y. *et al.* (2005) 'Colitis in mice lacking the common cytokine receptor γ chain is mediated by IL-6-producing CD4+ T cells', *Gastroenterology*, 128(4), pp. 922–934. Available at: https://doi.org/10.1053/j.gastro.2005.01.013.

Kak, G., Raza, M. and Tiwari, B.K. (2018) 'Interferon-gamma (IFN-γ): Exploring its implications in infectious diseases', *Biomolecular Concepts*, 9(1), pp. 64–79. Available at: https://doi.org/10.1515/bmc-2018-0007.

Kalliolias, G.D. and Ivashkiv, L.B. (2016) 'TNF biology, pathogenic mechanisms and emerging therapeutic strategies', *Nature reviews. Rheumatology*, 12(1), pp. 49–62. Available at: https://doi.org/10.1038/nrrheum.2015.169.

Kamada, N. *et al.* (2008) 'Unique CD14+ intestinal macrophages contribute to the pathogenesis of Crohn disease via IL-23/IFN-γ axis', *The Journal of Clinical Investigation*, 118(6), pp. 2269–2280. Available at: https://doi.org/10.1172/JCI34610.

Kang, K. *et al.* (2008) 'Adipocyte-Derived Th2 Cytokines and Myeloid PPARδ Regulate Macrophage Polarization and Insulin Sensitivity', *Cell Metabolism*, 7(6), pp. 485–495. Available at: https://doi.org/10.1016/j.cmet.2008.04.002.

Kapoor, N. *et al.* (2015) 'Transcription Factors STAT6 and KLF4 Implement Macrophage Polarization via the Dual Catalytic Powers of MCPIP', *The Journal of Immunology*, 194(12), pp. 6011–6023. Available at: https://doi.org/10.4049/jimmunol.1402797.

Karimi, Y. *et al.* (2020) 'IFN-β signalling regulates RAW 264.7 macrophage activation, cytokine production, and killing activity', *Innate Immunity*, 26(3), pp. 172–182. Available at: https://doi.org/10.1177/1753425919878839.

Kasahara, T. *et al.* (1983) 'Interleukin 2-mediated immune interferon (IFN-gamma) production by human T cells and T cell subsets', *Journal of Immunology (Baltimore, Md.: 1950)*, 130(4), pp. 1784–1789.

Keffer, J. *et al.* (1991) 'Transgenic mice expressing human tumour necrosis factor: A predictive genetic model of arthritis', *EMBO Journal*, 10(13), pp. 4025–4031. Available at: https://doi.org/10.1002/j.1460-2075.1991.tb04978.x.

Keubler, L.M. *et al.* (2015) 'A Multihit Model: Colitis Lessons from the Interleukin-10–deficient Mouse', *Inflammatory Bowel Diseases*, 21(8), pp. 1967–1975. Available at: https://doi.org/10.1097/MIB.0000000000000468.

Khan, S.Q., Khan, I. and Gupta, V. (2018) ‘CD11b Activity Modulates Pathogenesis of Lupus Nephritis’, *Frontiers in Medicine*, 5, p. 52. Available at: https://doi.org/10.3389/fmed.2018.00052.

Kiecolt-Glaser, J.K. *et al.* (2018) ‘Marital Distress, Depression, and a Leaky Gut: Translocation of Bacterial Endotoxin as a Pathway to Inflammation’, *Psychoneuroendocrinology*, 98, pp. 52–60. Available at: https://doi.org/10.1016/j.psyneuen.2018.08.007.

Kim, H.-S. and Suh, Y.-H. (2009) ‘Minocycline and neurodegenerative diseases’, *Behavioural Brain Research*, 196(2), pp. 168–179. Available at: https://doi.org/10.1016/j.bbr.2008.09.040.

Kim, N. *et al.* (2016) ‘Minocycline promotes the generation of dendritic cells with regulatory properties’, *Oncotarget*, 7(33), pp. 52818–52831. Available at: https://doi.org/10.18632/oncotarget.10810.

Kinsner, A. *et al.* (2006) ‘Highly purified lipoteichoic acid induced pro-inflammatory signalling in primary culture of rat microglia through Toll-like receptor 2: selective potentiation of nitric oxide production by muramyl dipeptide’, *Journal of Neurochemistry*, 99(2), pp. 596–607. Available at: https://doi.org/10.1111/j.1471-4159.2006.04085.x.

Kircik, L.H. (2010) ‘Doxycycline and minocycline for the management of acne: a review of efficacy and safety with emphasis on clinical implications’, *Journal of drugs in dermatology: JDD*, 9(11), pp. 1407–1411.

Kiszewski, A.E. *et al.* (2006) ‘The local immune response in ulcerative lesions of Buruli disease’, *Clinical and Experimental Immunology*, 143(3), pp. 445–451. Available at: https://doi.org/10.1111/j.1365-2249.2006.03020.x.

Klein, N.C. and Cunha, B.A. (1995a) ‘Tetracyclines’, *The Medical Clinics of North America*, 79(4), pp. 789–801.

Klein, N.C. and Cunha, B.A. (1995b) ‘Tetracyclines’, *The Medical Clinics of North America*, 79(4), pp. 789–801.

Kloppenburg, M. *et al.* (1994) ‘Minocycline in active rheumatoid arthritis’, *Arthritis & Rheumatism*, 37(5), pp. 629–636. Available at: https://doi.org/10.1002/art.1780370505.

Kloppenburg, M., Verweij, C.L., Miltenburg, A.M., *et al.* (1995) ‘The influence of tetracyclines on T cell activation’, *Clinical and Experimental Immunology*, 102(3), pp. 635–641.

Kloppenburg, M., Verweij, C.L., Miltenburg, A.M.M., *et al.* (1995) ‘The influence of tetracyclines on T cell activation’, *Clinical & Experimental Immunology*, 102(3), pp. 635–641. Available at: https://doi.org/10.1111/j.1365-2249.1995.tb03864.x.

Kloppenburg, M. *et al.* (1996) ‘The tetracycline derivative minocycline differentially affects cytokine production by monocytes and T lymphocytes’, *Antimicrobial Agents and Chemotherapy*, 40(4), pp. 934–940.

Kmieć, Z., Cyman, M. and Ślebioda, T.J. (2017) ‘Cells of the innate and adaptive immunity and their interactions in inflammatory bowel disease’, *Advances in Medical Sciences*, 62(1), pp. 1–16. Available at: https://doi.org/10.1016/j.advms.2016.09.001.

Kneidl, J. *et al.* (2012) ‘Soluble CD163 promotes recognition, phagocytosis and killing of Staphylococcus aureus via binding of specific fibronectin peptides’, *Cellular Microbiology*, 14(6), pp. 914–936. Available at: https://doi.org/10.1111/j.1462-5822.2012.01766.x.

Ko, J.-C. *et al.* (2015) ‘Minocycline enhances mitomycin C-induced cytotoxicity through down-regulating ERK1/2-mediated Rad51 expression in human non-small cell lung cancer cells’, *Biochemical Pharmacology*, 97(3), pp. 331–340. Available at: https://doi.org/10.1016/j.bcp.2015.07.025.

Kobayashi, K. *et al.* (2013) ‘Minocycline selectively inhibits M1 polarization of microglia’, *Cell Death & Disease*, 4(3), pp. e525–e525. Available at: https://doi.org/10.1038/cddis.2013.54.

Koelink, P.J. *et al.* (2020) ‘Anti-TNF therapy in IBD exerts its therapeutic effect through macrophage IL-10 signalling’, *Gut*, 69(6), pp. 1053–1063. Available at: https://doi.org/10.1136/gutjnl-2019-318264.

Komohara, Y. *et al.* (2008) ‘Possible involvement of the M2 anti-inflammatory macrophage phenotype in growth of human gliomas’, *The Journal of Pathology*, 216(1), pp. 15–24. Available at: https://doi.org/10.1002/path.2370.

Komohara, Y. *et al.* (2012) ‘Importance of direct macrophage - Tumor cell interaction on progression of human glioma’, *Cancer Science*, 103(12), pp. 2165–2172. Available at: https://doi.org/10.1111/cas.12015.

Kondo, Y. *et al.* (2005) ‘The role of autophagy in cancer development and response to therapy’, *Nature Reviews Cancer*, 5(9), pp. 726–734. Available at: https://doi.org/10.1038/nrc1692.

Kondo, Y. and Kondo, S. (2006) ‘Autophagy and cancer therapy’, *Autophagy*, 2(2), pp. 85–90. Available at: https://doi.org/10.4161/auto.2.2.2463.

Kong, D. *et al.* (2016) ‘PKA regulatory IIα subunit is essential for PGD2-mediated resolution of inflammation’, *The Journal of Experimental Medicine*, 213(10), pp. 2209–2226. Available at: https://doi.org/10.1084/jem.20160459.

Kraakman, M.J. *et al.* (2014) ‘Macrophage Polarization in Obesity and Type 2 Diabetes: Weighing Down Our Understanding of Macrophage Function?’, *Frontiers in Immunology*, 5, p. 470. Available at: https://doi.org/10.3389/fimmu.2014.00470.

Krady, J.K. *et al.* (2005) ‘Minocycline reduces proinflammatory cytokine expression, microglial activation, and caspase-3 activation in a rodent model of diabetic retinopathy’, *Diabetes*, 54(5), pp. 1559–1565. Available at: https://doi.org/10.2337/diabetes.54.5.1559.

Krausgruber, T. *et al.* (2011) 'IRF5 promotes inflammatory macrophage polarization and TH1-TH17 responses', *Nature Immunology*, 12(3), pp. 231–238. Available at: https://doi.org/10.1038/ni.1990.

Kredel, L.I. *et al.* (2013) 'Adipokines from local fat cells shape the macrophage compartment of the creeping fat in Crohn's disease', *Gut*, 62(6), pp. 852–862. Available at: https://doi.org/10.1136/gutjnl-2011-301424.

Kuchroo, V.K. *et al.* (1995) 'B7-1 and B7-2 costimulatory molecules activate differentially the Th1/Th2 developmental pathways: application to autoimmune disease therapy', *Cell*, 80(5), pp. 707–718. Available at: https://doi.org/10.1016/0092-8674(95)90349-6.

Kühl, A.A. *et al.* (2015) 'Diversity of Intestinal Macrophages in Inflammatory Bowel Diseases', *Frontiers in Immunology*, 6. Available at: https://doi.org/10.3389/fimmu.2015.00613.

Kühn, R. *et al.* (1993) 'Interleukin-10-deficient mice develop chronic enterocolitis', *Cell*, 75(2), pp. 263–274. Available at: https://doi.org/10.1016/0092-8674(93)80068-p.

Kujawski, M. *et al.* (2008) 'Stat3 mediates myeloid cell–dependent tumor angiogenesis in mice', *The Journal of Clinical Investigation*, 118(10), pp. 3367–3377. Available at: https://doi.org/10.1172/JCI35213.

Kuperman, D.A. and Schleimer, R.P. (2008) 'Interleukin-4, Interleukin-13, Signal Transducer and Activator of Transcription factor 6, and Allergic Asthma', *Current molecular medicine*, 8(5), pp. 384–392.

Kurokawa, I. *et al.* (2009) 'New developments in our understanding of acne pathogenesis and treatment', *Experimental Dermatology*, 18(10), pp. 821–832. Available at: https://doi.org/10.1111/j.1600-0625.2009.00890.x.

Labro, M.T. and Abdelghaffar, H. (2001) 'Immunomodulation by macrolide antibiotics', *Journal of Chemotherapy (Florence, Italy)*, 13(1), pp. 3–8. Available at: https://doi.org/10.1179/joc.2001.13.1.3.

Lampinen, M. *et al.* (2013) 'CD14+CD33+ myeloid cell-CCL11-eosinophil signature in ulcerative colitis', *Journal of Leukocyte Biology*, 94(5), pp. 1061–1070. Available at: https://doi.org/10.1189/jlb.1212640.

Landmann, R. *et al.* (1991) 'Effect of cytokines and lipopolysaccharide on CD14 antigen expression in human monocytes and macrophages', *Journal of Cellular Biochemistry*, 47(4), pp. 317–329. Available at: https://doi.org/10.1002/jcb.240470406.

Lane, P. and Williamson, D.M. (1969) 'Treatment of Acne Vulgaris with Tetracyline Hydrochloride: a Double-blind Trial with 51 Patients', *BMJ*, 2(5649), pp. 76–79. Available at: https://doi.org/10.1136/bmj.2.5649.76.

Lang, R. *et al.* (2002) 'Shaping gene expression in activated and resting primary macrophages by IL-10', *Journal of Immunology*, 169(5), pp. 2253–2263. Available at: https://doi.org/10.4049/jimmunol.169.5.2253.

Lang, R. (2005) ‘Tuning of macrophage responses by Stat3-inducing cytokines: molecular mechanisms and consequences in infection’, *Immunobiology*, 210(2–4), pp. 63–76. Available at: https://doi.org/10.1016/j.imbio.2005.05.001.

Lanier, L.L. *et al.* (1995) ‘CD80 (B7) and CD86 (B70) provide similar costimulatory signals for T cell proliferation, cytokine production, and generation of CTL’, *Journal of Immunology (Baltimore, Md.: 1950)*, 154(1), pp. 97–105.

Larabi, A., Barnich, N. and Nguyen, H.T.T. (2019) ‘New insights into the interplay between autophagy, gut microbiota and inflammatory responses in IBD’, *Autophagy*, 16(1), pp. 38–51. Available at: https://doi.org/10.1080/15548627.2019.1635384.

Laskar, A. *et al.* (2013) ‘SPION primes THP1 derived M2 macrophages towards M1-like macrophages’, *Biochemical and Biophysical Research Communications*, 441(4), pp. 737–742. Available at: https://doi.org/10.1016/j.bbrc.2013.10.115.

Lauber, K. *et al.* (2003) ‘Apoptotic cells induce migration of phagocytes via caspase-3-mediated release of a lipid attraction signal’, *Cell*, 113(6), pp. 717–730. Available at: https://doi.org/10.1016/s0092-8674(03)00422-7.

Laukoetter, M.G. *et al.* (2007) ‘JAM-A regulates permeability and inflammation in the intestine in vivo’, *Journal of Experimental Medicine*, 204(13), pp. 3067–3076. Available at: https://doi.org/10.1084/jem.20071416.

Lawrence, T. and Gilroy, D.W. (2007) ‘Chronic inflammation: a failure of resolution?’, *International Journal of Experimental Pathology*, 88(2), pp. 85–94. Available at: https://doi.org/10.1111/j.1365-2613.2006.00507.x.

Lawrence, T. and Natoli, G. (2011) ‘Transcriptional regulation of macrophage polarization: enabling diversity with identity’, *Nature Reviews Immunology*, 11(11), pp. 750–761. Available at: https://doi.org/10.1038/nri3088.

Lech, M. and Anders, H.-J. (2013) ‘Macrophages and fibrosis: How resident and infiltrating mononuclear phagocytes orchestrate all phases of tissue injury and repair’, *Biochimica et Biophysica Acta (BBA) - Molecular Basis of Disease*, 1832(7), pp. 989–997. Available at: https://doi.org/10.1016/j.bbadis.2012.12.001.

Lee, J.-H. *et al.* (2017) ‘Tolerogenic dendritic cells are efficiently generated using minocycline and dexamethasone’, *Scientific Reports*, 7. Available at: https://doi.org/10.1038/s41598-017-15569-1.

Lee, S.J. (2002) ‘Mannose Receptor-Mediated Regulation of Serum Glycoprotein Homeostasis’, *Science*, 295(5561), pp. 1898–1901. Available at: https://doi.org/10.1126/science.1069540.

LeFebvre, J.M. *et al.* (1991) ‘Kt/V: patients do not get what the physician prescribes’, *ASAIO transactions*, 37(3), pp. M132-3.

Lehrke, M. *et al.* (2004) ‘An Inflammatory Cascade Leading to Hyperresistinemia in Humans’, *PLoS Medicine*, 1(2), p. e45. Available at: https://doi.org/10.1371/journal.pmed.0010045.

Lehrke, M. and Lazar, M.A. (2005) ‘The many faces of PPARgamma’, *Cell*, 123(6), pp. 993–999. Available at: https://doi.org/10.1016/j.cell.2005.11.026.

Lennard-Jones, J.E. (1989) ‘Classification of Inflammatory Bowel Disease’, *Scandinavian Journal of Gastroenterology*, 24(sup170), pp. 2–6. Available at: https://doi.org/10.3109/00365528909091339.

Leung, G. *et al.* (2013) ‘Bone marrow-derived alternatively activated macrophages reduce colitis without promoting fibrosis: participation of IL-10’, *American Journal of Physiology-Gastrointestinal and Liver Physiology*, 304(9), pp. G781–G792. Available at: https://doi.org/10.1152/ajpgi.00055.2013.

Levin, A.D. *et al.* (2016) ‘Autophagy Contributes to the Induction of Anti-TNF Induced Macrophages’, *Journal of Crohn’s & Colitis*, 10(3), pp. 323–329. Available at: https://doi.org/10.1093/ecco-jcc/jjv174.

Levkovitch-Verbin, H. *et al.* (2006) ‘Minocycline delays death of retinal ganglion cells in experimental glaucoma and after optic nerve transection’, *Archives of Ophthalmology (Chicago, Ill.: 1960)*, 124(4), pp. 520–526. Available at: https://doi.org/10.1001/archopht.124.4.520.

Levy, B.D. *et al.* (2001) ‘Lipid mediator class switching during acute inflammation: signals in resolution’, *Nature Immunology*, 2(7), pp. 612–619. Available at: https://doi.org/10.1038/89759.

Ley, K. *et al.* (2007) ‘Getting to the site of inflammation: the leukocyte adhesion cascade updated’, *Nature Reviews. Immunology*, 7(9), pp. 678–689. Available at: https://doi.org/10.1038/nri2156.

Li, C. *et al.* (2017) ‘IRF6 Regulates Alternative Activation by Suppressing PPARγ in Male Murine Macrophages’, *Endocrinology*, 158(9), pp. 2837–2847. Available at: https://doi.org/10.1210/en.2017-00053.

Li, C. *et al.* (2018) ‘Macrophage polarization and meta-inflammation’, *Translational Research*, 191, pp. 29–44. Available at: https://doi.org/10.1016/j.trsl.2017.10.004.

Li, C., Corraliza, I. and Langhorne, J. (1999) ‘A Defect in Interleukin-10 Leads to Enhanced Malarial Disease in Plasmodium chabaudi chabaudi Infection in Mice’, *Infection and Immunity*, 67(9), pp. 4435–4442. Available at: https://doi.org/10.1128/IAI.67.9.4435-4442.1999.

Li, C.-H. *et al.* (2014) ‘Minocycline accelerates hypoxia-inducible factor-1 alpha degradation and inhibits hypoxia-induced neovasculogenesis through prolyl hydroxylase, von Hippel–Lindau-dependent pathway’, *Archives of Toxicology*, 88(3), pp. 659–671. Available at: https://doi.org/10.1007/s00204-013-1175-5.

Li, H. *et al.* (2018) ‘Transcriptional Regulation of Macrophages Polarization by MicroRNAs’, *Frontiers in Immunology*, 9. Available at: https://doi.org/10.3389/fimmu.2018.01175.

Li, J. *et al.* (2018) ‘Regulatory T-Cells: Potential Regulator of Tissue Repair and Regeneration’, *Frontiers in Immunology*, 9, p. 585. Available at: https://doi.org/10.3389/fimmu.2018.00585.

Li, Y. *et al.* (2021) ‘Minocycline alleviates peripheral nerve adhesion by promoting regulatory macrophage polarization via the TAK1 and its downstream pathway’, *Life Sciences*, 276, p. 119422. Available at: https://doi.org/10.1016/j.lfs.2021.119422.

Liang, Y.-B. *et al.* (2017) ‘Downregulated SOCS1 expression activates the JAK1/STAT1 pathway and promotes polarization of macrophages into M1 type’, *Molecular Medicine Reports*, 16(5), pp. 6405–6411. Available at: https://doi.org/10.3892/mmr.2017.7384.

Liao, X. *et al.* (2011) ‘Krüppel-like factor 4 regulates macrophage polarization’, *The Journal of Clinical Investigation*, 121(7), pp. 2736–2749. Available at: https://doi.org/10.1172/JCI45444.

Libioulle, C. *et al.* (2007) ‘Novel Crohn Disease Locus Identified by Genome-Wide Association Maps to a Gene Desert on 5p13.1 and Modulates Expression of PTGER4’, *PLoS Genetics*, 3(4), p. e58. Available at: https://doi.org/10.1371/journal.pgen.0030058.

Ligumsky, M. *et al.* (1990) ‘Role of interleukin 1 in inflammatory bowel disease--enhanced production during active disease.’, *Gut*, 31(6), pp. 686–689.

Lim, W. *et al.* (2005) ‘Regulation of B7.1 costimulatory molecule is mediated by the IFN regulatory factor-7 through the activation of JNK in lipopolysaccharide-stimulated human monocytic cells’, *Journal of immunology (Baltimore, Md.*, 175(9), pp. 5690–5700. Available at: https://doi.org/10.4049/jimmunol.175.9.5690.

Lin, Q., Dong, C. and Cooper, M.D. (1998) ‘Impairment of T and B Cell Development by Treatment with a Type I Interferon’, *The Journal of Experimental Medicine*, 187(1), pp. 79–87.

Linde, N. *et al.* (2018) ‘Macrophages orchestrate breast cancer early dissemination and metastasis’, *Nature Communications*, 9, p. 21. Available at: https://doi.org/10.1038/s41467-017-02481-5.

Liou, G.-Y. *et al.* (2017) ‘Presence of Interleukin-13 at pancreatic ADM/PanIN lesions alters macrophage populations and mediates pancreatic tumorigenesis’, *Cell reports*, 19(7), pp. 1322–1333. Available at: https://doi.org/10.1016/j.celrep.2017.04.052.

Lissner, D. *et al.* (2015) ‘Monocyte and M1 Macrophage-induced Barrier Defect Contributes to Chronic Intestinal Inflammation in IBD’:, *Inflammatory Bowel Diseases*, p. 1. Available at: https://doi.org/10.1097/MIB.0000000000000384.

Liu, D. and Yang, P.S. (2012) ‘Minocycline hydrochloride nanoliposomes inhibit the production of TNF-α in LPS-stimulated macrophages’, *International Journal of Nanomedicine*, 7, pp. 4769–4775. Available at: https://doi.org/10.2147/IJN.S34036.

Liu, H. *et al.* (2019) ‘Subsets of mononuclear phagocytes are enriched in the inflamed colons of patients with IBD’, *BMC Immunology*, 20, p. 42. Available at: https://doi.org/10.1186/s12865-019-0322-z.

Liu, H.-Y. *et al.* (2018) ‘Chronic minocycline treatment reduces the anxiety-like behaviors induced by repeated restraint stress through modulating neuroinflammation’, *Brain Research Bulletin*, 143, pp. 19–26. Available at: https://doi.org/10.1016/j.brainresbull.2018.08.015.

Liu, J. and Cao, X. (2015) ‘Regulatory dendritic cells in autoimmunity: A comprehensive review’, *Journal of Autoimmunity*, 63, pp. 1–12. Available at: https://doi.org/10.1016/j.jaut.2015.07.011.

Liu, L. *et al.* (2020) ‘Progranulin inhibits LPS-induced macrophage M1 polarization via NF-κB and MAPK pathways’, *BMC Immunology*, 21, p. 32. Available at: https://doi.org/10.1186/s12865-020-00355-y.

Liu, W.-T. *et al.* (2011) ‘Minocycline inhibits the growth of glioma by inducing autophagy’, *Autophagy*, 7(2), pp. 166–175. Available at: https://doi.org/10.4161/auto.7.2.14043.

Liu, W.-T. *et al.* (2013) ‘Inhibition of glioma growth by minocycline is mediated through endoplasmic reticulum stress-induced apoptosis and autophagic cell death’, *Neuro-Oncology*, 15(9), pp. 1127–1141. Available at: https://doi.org/10.1093/neuonc/not073.

Liu, X. *et al.* (2018) ‘LPS-induced proinflammatory cytokine expression in human airway epithelial cells and macrophages via NF-κB, STAT3 or AP-1 activation’, *Molecular Medicine Reports*, 17(4), pp. 5484–5491. Available at: https://doi.org/10.3892/mmr.2018.8542.

Lloberas, J. and Celada, A. (2002) ‘Effect of aging on macrophage function’, *Experimental Gerontology*, 37(12), pp. 1325–1331. Available at: https://doi.org/10.1016/S0531-5565(02)00125-0.

Llorens, S., Jordán, J. and Nava, E. (2002) ‘The nitric oxide pathway in the cardiovascular system’, *Journal of Physiology and Biochemistry*, 58(3), pp. 179–188. Available at: https://doi.org/10.1007/BF03179855.

Lobo-Silva, D. *et al.* (2017) ‘Interferon-β regulates the production of IL-10 by toll-like receptor-activated microglia’, *Glia*, 65(9), pp. 1439–1451. Available at: https://doi.org/10.1002/glia.23172.

Locati, M., Curtale, G. and Mantovani, A. (2020) ‘Diversity, Mechanisms and Significance of Macrophage Plasticity’, *Annual review of pathology*, 15, pp. 123–147. Available at: https://doi.org/10.1146/annurev-pathmechdis-012418-012718.

Locati, M., Mantovani, A. and Sica, A. (2013) ‘Macrophage activation and polarization as an adaptive component of innate immunity’, *Advances in Immunology*, 120, pp. 163–184. Available at: https://doi.org/10.1016/B978-0-12-417028-5.00006-5.

Locksley, R.M., Killeen, N. and Lenardo, M.J. (2001) ‘The TNF and TNF Receptor Superfamilies: Integrating Mammalian Biology’, *Cell*, 104(4), pp. 487–501. Available at: https://doi.org/10.1016/S0092-8674(01)00237-9.

Lokeshwar, B.L. (1999) ‘MMP Inhibition in Prostate Cancer’, *Annals of the New York Academy of Sciences*, 878(1), pp. 271–289. Available at: https://doi.org/10.1111/j.1749-6632.1999.tb07690.x.

Lopez-Castejon, G. and Brough, D. (2011) ‘Understanding the mechanism of IL-1β secretion’, *Cytokine & Growth Factor Reviews*, 22(4), pp. 189–195. Available at: https://doi.org/10.1016/j.cytogfr.2011.10.001.

Lu, C.-S. *et al.* (2020) ‘Oct4 promotes M2 macrophage polarization through upregulation of macrophage colony-stimulating factor in lung cancer’, *Journal of Hematology & Oncology*, 13, p. 62. Available at: https://doi.org/10.1186/s13045-020-00887-1.

Lu, L., Barbi, J. and Pan, F. (2017) ‘The regulation of immune tolerance by FOXP3’, *Nature reviews. Immunology*, 17(11), pp. 703–717. Available at: https://doi.org/10.1038/nri.2017.75.

Lu, Y.-C. *et al.* (2009) ‘Differential Role for c-Rel and C/EBPβ/δ in TLR-Mediated Induction of Proinflammatory Cytokines’, *Journal of immunology (Baltimore, Md. : 1950)*, 182(11), pp. 7212–7221. Available at: https://doi.org/10.4049/jimmunol.0802971.

Lu, Z. *et al.* (2017) ‘Inhibition of autophagy enhances the selective anti-cancer activity of tigecycline to overcome drug resistance in the treatment of chronic myeloid leukemia’, *Journal of Experimental & Clinical Cancer Research : CR*, 36. Available at: https://doi.org/10.1186/s13046-017-0512-6.

Lukácsi, S. *et al.* (2020) ‘The differential role of CR3 (CD11b/CD18) and CR4 (CD11c/CD18) in the adherence, migration and podosome formation of human macrophages and dendritic cells under inflammatory conditions’, *PLOS ONE*, 15(5), p. e0232432. Available at: https://doi.org/10.1371/journal.pone.0232432.

Lund, M.E. *et al.* (2016) ‘The choice of phorbol 12-myristate 13-acetate differentiation protocol influences the response of THP-1 macrophages to a pro-inflammatory stimulus’, *Journal of Immunological Methods*, 430, pp. 64–70. Available at: https://doi.org/10.1016/j.jim.2016.01.012.

Luo, W. *et al.* (2017) ‘Effect of modulation of PPAR-γ activity on Kupffer cells M1/M2 polarization in the development of non-alcoholic fatty liver disease’, *Scientific Reports*, 7, p. 44612. Available at: https://doi.org/10.1038/srep44612.

Ma, R. *et al.* (2018) ‘Inhibition of autophagy enhances the antitumour activity of tigecycline in multiple myeloma’, *Journal of Cellular and Molecular Medicine*, 22(12), pp. 5955–5963. Available at: https://doi.org/10.1111/jcmm.13865.

Ma, X. (2001) ‘TNF-α and IL-12:a balancing act in macrophage functioning’, *Microbes and Infection*, 3(2), pp. 121–129. Available at: https://doi.org/10.1016/S1286-4579(00)01359-9.

Macdonald, H. *et al.* (1973) ‘Pharmacokinetic studies on minocycline in man’, *Clinical Pharmacology & Therapeutics*, 14(5), pp. 852–861. Available at: https://doi.org/10.1002/cpt1973145852.

MacDonald, T.T. and Pender, S.L.F. (1998) ‘Lamina Propria T Cells’, *Mucosal T Cells*, 71, pp. 103–117. Available at: https://doi.org/10.1159/000058721.

Machado, L.S. *et al.* (2006) ‘Delayed minocycline inhibits ischemia-activated matrix metalloproteinases 2 and 9 after experimental stroke’, *BMC Neuroscience*, 7, p. 56. Available at: https://doi.org/10.1186/1471-2202-7-56.

Maffeis, L. and Veraldi, S. (2010) ‘Minocycline in the treatment of acne: latest findings’, *Giornale Italiano Di Dermatologia E Venereologia: Organo Ufficiale, Societa Italiana Di Dermatologia E Sifilografia*, 145(3), pp. 425–429.

Mahbub, S., Deburghgraeve, C.R. and Kovacs, E.J. (2012) ‘Advanced Age Impairs Macrophage Polarization’, *Journal of Interferon & Cytokine Research*, 32(1), pp. 18–26. Available at: https://doi.org/10.1089/jir.2011.0058.

Mahida, Y.R. (2000) ‘The Key Role of Macrophages in the Immunopathogenesis of Inflammatory Bowel Disease’:, *Inflammatory Bowel Diseases*, 6(1), pp. 21–33. Available at: https://doi.org/10.1097/00054725-200002000-00004.

Mahida, Y.R., Wu, K. and Jewell, D.P. (1989) ‘Enhanced production of interleukin 1-beta by mononuclear cells isolated from mucosa with active ulcerative colitis of Crohn’s disease.’, *Gut*, 30(6), pp. 835–838.

Mahnke, K. *et al.* (1997) ‘CD14 is expressed by subsets of murine dendritic cells and upregulated by lipopolysaccharide’, *Advances in Experimental Medicine and Biology*, 417, pp. 145–159. Available at: https://doi.org/10.1007/978-1-4757-9966-8_25.

Maier, E., Duschl, A. and Horejs-Hoeck, J. (2012) ‘STAT6-dependent and -independent mechanisms in Th2 polarization’, *European Journal of Immunology*, 42(11), pp. 2827–2833. Available at: https://doi.org/10.1002/eji.201242433.

Maiti, P. *et al.* (2014) ‘Molecular Chaperone Dysfunction in Neurodegenerative Diseases and Effects of Curcumin’, *BioMed Research International*, 2014. Available at: https://doi.org/10.1155/2014/495091.

Manferdini, C. *et al.* (2016) ‘From osteoarthritic synovium to synovial-derived cells characterization: synovial macrophages are key effector cells’, *Arthritis Research & Therapy*, 18, p. 83. Available at: https://doi.org/10.1186/s13075-016-0983-4.

Mantovani, A. *et al.* (2004) 'The chemokine system in diverse forms of macrophage activation and polarization', *Trends in Immunology*, 25(12), pp. 677–686. Available at: https://doi.org/10.1016/j.it.2004.09.015.

Mantovani, A. *et al.* (2008) 'Cancer-related inflammation', *Nature*, 454(7203), pp. 436–444. Available at: https://doi.org/10.1038/nature07205.

Mantovani, A. *et al.* (2017) 'Tumor-Associated Macrophages as Treatment Targets in Oncology', *Nature reviews. Clinical oncology*, 14(7), pp. 399–416. Available at: https://doi.org/10.1038/nrclinonc.2016.217.

Mantovani, A. and Allavena, P. (2015) 'The interaction of anticancer therapies with tumor-associated macrophages', *The Journal of Experimental Medicine*, 212(4), pp. 435–445. Available at: https://doi.org/10.1084/jem.20150295.

Mantovani, A., Bonecchi, R. and Locati, M. (2006) 'Tuning inflammation and immunity by chemokine sequestration: decoys and more', *Nature Reviews Immunology*, 6(12), pp. 907–918. Available at: https://doi.org/10.1038/nri1964.

Mantovani, A. and Marchesi, F. (2014) 'IL-10 and macrophages orchestrate gut homeostasis', *Immunity*, 40(5), pp. 637–639. Available at: https://doi.org/10.1016/j.immuni.2014.04.015.

Mao, Y. *et al.* (2015) 'Glycyrrhizic Acid Promotes M1 Macrophage Polarization in Murine Bone Marrow-Derived Macrophages Associated with the Activation of JNK and NF-κB', *Mediators of Inflammation*, 2015, p. 372931. Available at: https://doi.org/10.1155/2015/372931.

Marin, V. *et al.* (2001) 'The IL-6-Soluble IL-6Rα Autocrine Loop of Endothelial Activation as an Intermediate Between Acute and Chronic Inflammation: an Experimental Model Involving Thrombin', *The Journal of Immunology*, 167(6), pp. 3435–3442. Available at: https://doi.org/10.4049/jimmunol.167.6.3435.

Markovic, D.S. *et al.* (2011) 'Minocycline reduces glioma expansion and invasion by attenuating microglial MT1-MMP expression', *Brain, Behavior, and Immunity*, 25(4), pp. 624–628. Available at: https://doi.org/10.1016/j.bbi.2011.01.015.

Marks, D.J. *et al.* (2006) 'Defective acute inflammation in Crohn's disease: a clinical investigation', *The Lancet*, 367(9511), pp. 668–678. Available at: https://doi.org/10.1016/S0140-6736(06)68265-2.

Marrack, P., Kappler, J. and Mitchell, T. (1999) 'Type I Interferons Keep Activated T Cells Alive', *The Journal of Experimental Medicine*, 189(3), pp. 521–530.

Martinez, F.O. *et al.* (2006) 'Transcriptional profiling of the human monocyte-to-macrophage differentiation and polarization: new molecules and patterns of gene expression', *Journal of Immunology (Baltimore, Md.: 1950)*, 177(10), pp. 7303–7311.

Martinez, F.O. and Gordon, S. (2014) 'The M1 and M2 paradigm of macrophage activation: time for reassessment', *F1000Prime Rep*, 6(13). Available at: https://doi.org/10.12703/P6-13.

Martinez, F.O., Helming, L. and Gordon, S. (2009) 'Alternative activation of macrophages: an immunologic functional perspective', *Annual Review of Immunology*, 27, pp. 451–483. Available at: https://doi.org/10.1146/annurev.immunol.021908.132532.

Martinez-Pomares, L. (2012) 'The mannose receptor', *Journal of Leukocyte Biology*, 92(6), pp. 1177–1186. Available at: https://doi.org/10.1189/jlb.0512231.

Masumori, N. *et al.* (1994) 'Inhibitory Effect of Minocycline on in Vitro Invasion and Experimental Metastasis of Mouse Renal Adenocarcinoma', *The Journal of Urology*, 151(5), pp. 1400–1404. Available at: https://doi.org/10.1016/S0022-5347(17)35268-0.

Matsukawa, A. *et al.* (2003) 'Aberrant Inflammation and Lethality to Septic Peritonitis in Mice Lacking STAT3 in Macrophages and Neutrophils 1', *The Journal of Immunology* [Preprint]. Available at: https://doi.org/10.4049/jimmunol.171.11.6198.

Matsukawa, A. *et al.* (2005) 'Stat3 in Resident Macrophages as a Repressor Protein of Inflammatory Response', *The Journal of Immunology*, 175(5), pp. 3354–3359. Available at: https://doi.org/10.4049/jimmunol.175.5.3354.

Matsuoka, K. and Kanai, T. (2015) 'The gut microbiota and inflammatory bowel disease', *Seminars in Immunopathology*, 37(1), pp. 47–55. Available at: https://doi.org/10.1007/s00281-014-0454-4.

de Mattos, B.R.R. *et al.* (2015) 'Inflammatory Bowel Disease: An Overview of Immune Mechanisms and Biological Treatments', *Mediators of Inflammation*, 2015. Available at: https://doi.org/10.1155/2015/493012.

Matulonis, U. *et al.* (1996) 'B7-1 is superior to B7-2 costimulation in the induction and maintenance of T cell-mediated antileukemia immunity. Further evidence that B7-1 and B7-2 are functionally distinct', *Journal of Immunology (Baltimore, Md.: 1950)*, 156(3), pp. 1126–1131.

Maylia, E. and Nokes, L.D. (1999) 'The use of ultrasonics in orthopaedics--a review', *Technology and Health Care: Official Journal of the European Society for Engineering and Medicine*, 7(1), pp. 1–28.

Melief, J. *et al.* (2012) 'Phenotyping primary human microglia: tight regulation of LPS responsiveness', *Glia*, 60(10), pp. 1506–1517. Available at: https://doi.org/10.1002/glia.22370.

Melief, J. *et al.* (2013) 'Microglia in normal appearing white matter of multiple sclerosis are alerted but immunosuppressed', *Glia*, 61(11), pp. 1848–1861. Available at: https://doi.org/10.1002/glia.22562.

Meng, F. and Lowell, C.A. (1997) 'Lipopolysaccharide (LPS)-induced Macrophage Activation and Signal Transduction in the Absence of Src-Family

Kinases Hck, Fgr, and Lyn', *The Journal of Experimental Medicine*, 185(9), pp. 1661–1670.

Meraz, M.A. *et al.* (1996) 'Targeted disruption of the Stat1 gene in mice reveals unexpected physiologic specificity in the JAK-STAT signaling pathway', *Cell*, 84(3), pp. 431–442. Available at: https://doi.org/10.1016/s0092-8674(00)81288-x.

Metz, L.M. *et al.* (2017) 'Trial of Minocycline in a Clinically Isolated Syndrome of Multiple Sclerosis', *New England Journal of Medicine*, 376(22), pp. 2122–2133. Available at: https://doi.org/10.1056/NEJMoa1608889.

Mezouar, S. and Mege, J. (2020) 'Changing the paradigm of IFN-γ at the interface between innate and adaptive immunity: Macrophage-derived IFN-γ', *Journal of Leukocyte Biology*, 108(1), pp. 419–426. Available at: https://doi.org/10.1002/JLB.4MIR0420-619RR.

Mildner, A. *et al.* (2017) 'Genomic Characterization of Murine Monocytes Reveals C/EBPβ Transcription Factor Dependence of Ly6C- Cells', *Immunity*, 46(5), pp. 849-862.e7. Available at: https://doi.org/10.1016/j.immuni.2017.04.018.

Mily, A. *et al.* (2020) 'Polarization of M1 and M2 Human Monocyte-Derived Cells and Analysis with Flow Cytometry upon Mycobacterium tuberculosis Infection', *Journal of Visualized Experiments: JoVE* [Preprint], (163). Available at: https://doi.org/10.3791/61807.

Mircic, M. and Kavanaugh, A. (2009) 'The clinical efficacy of tocilizumab in rheumatoid arthritis', *Drugs of Today (Barcelona, Spain: 1998)*, 45(3), pp. 189–197. Available at: https://doi.org/10.1358/dot.2009.45.3.1343794.

Mirza, R. and Koh, T.J. (2011) 'Dysregulation of monocyte/macrophage phenotype in wounds of diabetic mice', *Cytokine*, 56(2), pp. 256–264. Available at: https://doi.org/10.1016/j.cyto.2011.06.016.

Mitsialis, V. *et al.* (2020) 'Single-Cell Analyses of Colon and Blood Reveal Distinct Immune Cell Signatures of Ulcerative Colitis and Crohn's Disease', *Gastroenterology*, 159(2), pp. 591-608.e10. Available at: https://doi.org/10.1053/j.gastro.2020.04.074.

Mollazadeh, H. *et al.* (2019) 'Immune modulation by curcumin: The role of interleukin-10', *Critical Reviews in Food Science and Nutrition*, 59(1), pp. 89–101. Available at: https://doi.org/10.1080/10408398.2017.1358139.

Molteni, M., Gemma, S. and Rossetti, C. (2016) 'The Role of Toll-Like Receptor 4 in Infectious and Noninfectious Inflammation', *Mediators of Inflammation*, 2016, pp. 1–9. Available at: https://doi.org/10.1155/2016/6978936.

Monk, E., Shalita, A. and Siegel, D.M. (2011) 'Clinical applications of non-antimicrobial tetracyclines in dermatology', *Pharmacological Research*, 63(2), pp. 130–145. Available at: https://doi.org/10.1016/j.phrs.2010.10.007.

Monteleone, G. *et al.* (1998) ‘Response of human intestinal lamina propria T lymphocytes to interleukin 12: additive effects of interleukin 15 and 7’, *Gut*, 43(5), pp. 620–628.

Moore, K.W. *et al.* (2001) ‘Interleukin-10 and the interleukin-10 receptor’, *Annual Review of Immunology*, 19, pp. 683–765. Available at: https://doi.org/10.1146/annurev.immunol.19.1.683.

Morales, J.C. *et al.* (2014) ‘Review of Poly (ADP-ribose) Polymerase (PARP) Mechanisms of Action and Rationale for Targeting in Cancer and Other Diseases’, *Critical reviews in eukaryotic gene expression*, 24(1), pp. 15–28.

Morantz, R.A. *et al.* (1979) ‘Macrophages in experimental and human brain tumors. Part 2: studies of the macrophage content of human brain tumors’, *Journal of Neurosurgery*, 50(3), pp. 305–311. Available at: https://doi.org/10.3171/jns.1979.50.3.0305.

Moreira Lopes, T.C., Mosser, D.M. and Gonçalves, R. (2020) ‘Macrophage polarization in intestinal inflammation and gut homeostasis’, *Inflammation Research: Official Journal of the European Histamine Research Society ... [et Al.]*, 69(12), pp. 1163–1172. Available at: https://doi.org/10.1007/s00011-020-01398-y.

Mortha, A. *et al.* (2014) ‘Microbiota-Dependent Crosstalk Between Macrophages and ILC3 Promotes Intestinal Homeostasis’, *Science (New York, N.Y.)*, 343(6178), p. 1249288. Available at: https://doi.org/10.1126/science.1249288.

Mosser, D.M. and Edwards, J.P. (2008) ‘Exploring the full spectrum of macrophage activation’, *Nature Reviews Immunology*, 8(12), pp. 958–969. Available at: https://doi.org/10.1038/nri2448.

Mosser, D.M. and Gonçalves, R. (2015) ‘Activation of Murine Macrophages’, *Current Protocols in Immunology*, 111(1), p. 14.2.1-14.2.10. Available at: https://doi.org/10.1002/0471142735.im1402s111.

Mouton, A.J. *et al.* (2020) ‘Obesity, Hypertension, and Cardiac Dysfunction: Novel Roles of Immunometabolism in Macrophage Activation and Inflammation’, *Circulation research*, 126(6), pp. 789–806. Available at: https://doi.org/10.1161/CIRCRESAHA.119.312321.

Mulcahy Levy, J.M., Towers, C.G. and Thorburn, A. (2017) ‘Targeting Autophagy in Cancer’, *Nature reviews. Cancer*, 17(9), pp. 528–542. Available at: https://doi.org/10.1038/nrc.2017.53.

Muller, P.A., Matheis, F. and Mucida, D. (2020) ‘Gut Macrophages: Key Players in Intestinal Immunity and Tissue Physiology’, *Current opinion in immunology*, 62, pp. 54–61. Available at: https://doi.org/10.1016/j.coi.2019.11.011.

Muntjewerff, E.M., Meesters, L.D. and van den Bogaart, G. (2020) ‘Antigen Cross-Presentation by Macrophages’, *Frontiers in Immunology*, 11, p. 1276. Available at: https://doi.org/10.3389/fimmu.2020.01276.

Murai, M. *et al.* (2009) ‘Interleukin 10 acts on regulatory T cells to maintain expression of the transcription factor Foxp3 and suppressive function in mice with colitis’, *Nature Immunology*, 10(11), pp. 1178–1184. Available at: https://doi.org/10.1038/ni.1791.

Murata, Y. *et al.* (2008) ‘Extension of the Thrombolytic Time Window With Minocycline in Experimental Stroke’, *Stroke; a journal of cerebral circulation*, 39(12), pp. 3372–3377. Available at: https://doi.org/10.1161/STROKEAHA.108.514026.

Murphy, J.T. *et al.* (2006) ‘Gene expression profiling of monocyte-derived macrophages following infection with Mycobacterium avium subspecies avium and Mycobacterium avium subspecies paratuberculosis’, *Physiological Genomics*, 28(1), pp. 67–75. Available at: https://doi.org/10.1152/physiolgenomics.00098.2006.

Murray, P.J. *et al.* (2014) ‘Macrophage Activation and Polarization: Nomenclature and Experimental Guidelines’, *Immunity*, 41(1), pp. 14–20. Available at: https://doi.org/10.1016/j.immuni.2014.06.008.

Műzes, G. *et al.* (2012) ‘Changes of the cytokine profile in inflammatory bowel diseases’, *World Journal of Gastroenterology : WJG*, 18(41), pp. 5848–5861. Available at: https://doi.org/10.3748/wjg.v18.i41.5848.

Na, Y.R. *et al.* (2019a) ‘Macrophages in intestinal inflammation and resolution: a potential therapeutic target in IBD’, *Nature Reviews Gastroenterology & Hepatology*, 16(9), pp. 531–543. Available at: https://doi.org/10.1038/s41575-019-0172-4.

Na, Y.R. *et al.* (2019b) ‘Macrophages in intestinal inflammation and resolution: a potential therapeutic target in IBD’, *Nature Reviews. Gastroenterology & Hepatology*, 16(9), pp. 531–543. Available at: https://doi.org/10.1038/s41575-019-0172-4.

Nabhani, Z.A. *et al.* (2017) ‘Nod2: The intestinal gate keeper’, *PLOS Pathogens*, 13(3), p. e1006177. Available at: https://doi.org/10.1371/journal.ppat.1006177.

Nakanishi, Y., Sato, T. and Ohteki, T. (2015) ‘Commensal Gram-positive bacteria initiates colitis by inducing monocyte/macrophage mobilization’, *Mucosal Immunology*, 8(1), pp. 152–160. Available at: https://doi.org/10.1038/mi.2014.53.

Nakano, Y. *et al.* (2015) ‘Astrocytic TLR4 expression and LPS-induced nuclear translocation of STAT3 in the sensory circumventricular organs of adult mouse brain’, *Journal of Neuroimmunology*, 278, pp. 144–158. Available at: https://doi.org/10.1016/j.jneuroim.2014.12.013.

Nathan, C. and Ding, A. (2010) ‘Nonresolving Inflammation’, *Cell*, 140(6), pp. 871–882. Available at: https://doi.org/10.1016/j.cell.2010.02.029.

Nelson, M.L. (1998a) ‘Chemical and biological dynamics of tetracyclines’, *Advances in Dental Research*, 12(2), pp. 5–11. Available at: https://doi.org/10.1177/08959374980120011901.

Nelson, M.L. (1998b) ‘Chemical and biological dynamics of tetracyclines’, *Advances in Dental Research*, 12(2), pp. 5–11. Available at: https://doi.org/10.1177/08959374980120011901.

Nelson, M.L. and Levy, S.B. (2011) ‘The history of the tetracyclines’, *Annals of the New York Academy of Sciences*, 1241(1), pp. 17–32. Available at: https://doi.org/10.1111/j.1749-6632.2011.06354.x.

Neurath, M.F. (2019) ‘Targeting immune cell circuits and trafficking in inflammatory bowel disease’, *Nature Immunology*, 20(8), pp. 970–979. Available at: https://doi.org/10.1038/s41590-019-0415-0.

Neuvonen, P.J. (1976) ‘Interactions with the absorption of tetracyclines’, *Drugs*, 11(1), pp. 45–54. Available at: https://doi.org/10.2165/00003495-197611010-00004.

Newman, T.A. *et al.* (2001) ‘T-cell- and macrophage-mediated axon damage in the absence of a CNS-specific immune response: involvement of metalloproteinases’, *Brain: A Journal of Neurology*, 124(Pt 11), pp. 2203–2214. Available at: https://doi.org/10.1093/brain/124.11.2203.

NEWTON, S. *et al.* (2004) ‘Sepsis-Induced Changes in Macrophage Co-Stimulatory Molecule Expression’, *Surgical infections*, 5(4), pp. 375–383. Available at: https://doi.org/10.1089/sur.2004.5.375.

Nielson *et al.* (2020) ‘Macrophage Activation Markers, CD163 and CD206, in Acute-on-Chronic Liver Failure’.

Nikodemova, M., Duncan, I.D. and Watters, J.J. (2006) ‘Minocycline exerts inhibitory effects on multiple mitogen-activated protein kinases and IkappaBalpha degradation in a stimulus-specific manner in microglia’, *Journal of Neurochemistry*, 96(2), pp. 314–323. Available at: https://doi.org/10.1111/j.1471-4159.2005.03520.x.

Nishiki, S. *et al.* (2004) ‘Selective activation of STAT3 in human monocytes stimulated by G-CSF: implication in inhibition of LPS-induced TNF-α production’, *American Journal of Physiology-Cell Physiology*, 286(6), pp. C1302–C1311. Available at: https://doi.org/10.1152/ajpcell.00387.2003.

Niu, G. *et al.* (2008) ‘The combined effects of celecoxib and minocycline hydrochloride on inhibiting the osseous metastasis of breast cancer in nude mice’, *Cancer Biotherapy & Radiopharmaceuticals*, 23(4), pp. 469–476. Available at: https://doi.org/10.1089/cbr.2008.0475.

Nockher, W.A. and Scherberich, J.E. (1995) ‘Monocyte cell-surface CD14 expression and soluble CD14 antigen in hemodialysis: Evidence for chronic exposure to LPS’, *Kidney International*, 48(5), pp. 1469–1476. Available at: https://doi.org/10.1038/ki.1995.436.

Nolan, A. *et al.* (2008) 'CD40 and CD80/86 Act Synergistically to Regulate Inflammation and Mortality in Polymicrobial Sepsis', *American Journal of Respiratory and Critical Care Medicine*, 177(3), pp. 301–308. Available at: https://doi.org/10.1164/rccm.200703-515OC.

Nolan, A. *et al.* (2009) 'Differential Role for CD80 and CD86 in the Regulation of the Innate Immune Response in Murine Polymicrobial Sepsis', *PLOS ONE*, 4(8), p. e6600. Available at: https://doi.org/10.1371/journal.pone.0006600.

Novak, M.L. and Koh, T.J. (2013) 'Macrophage phenotypes during tissue repair', *Journal of Leukocyte Biology*, 93(6), pp. 875–881. Available at: https://doi.org/10.1189/jlb.1012512.

Nowarski, R. *et al.* (2013) 'Innate Immune Cells in Inflammation and Cancer', *Cancer Immunology Research*, 1(2), pp. 77–84. Available at: https://doi.org/10.1158/2326-6066.CIR-13-0081.

Noy, R. and Pollard, J.W. (2014) 'Tumor-associated macrophages: from mechanisms to therapy', *Immunity*, 41(1), pp. 49–61. Available at: https://doi.org/10.1016/j.immuni.2014.06.010.

O'Brien, K. *et al.* (2017) 'Enumeration and Localization of Mesenchymal Progenitor Cells and Macrophages in Synovium from Normal Individuals and Patients with Pre-Osteoarthritis or Clinically Diagnosed Osteoarthritis', *International Journal of Molecular Sciences*, 18(4), p. 774. Available at: https://doi.org/10.3390/ijms18040774.

Ochsendorf, F. (2010) 'Minocycline in acne vulgaris: benefits and risks', *American Journal of Clinical Dermatology*, 11(5), pp. 327–341. Available at: https://doi.org/10.2165/11319280-000000000-00000.

Odegaard, J.I. *et al.* (2007) 'Macrophage-specific PPARγ controls alternative activation and improves insulin resistance', *Nature*, 447(7148), pp. 1116–1120. Available at: https://doi.org/10.1038/nature05894.

Oft, M. (2014) 'IL-10: Master Switch from Tumor-Promoting Inflammation to Antitumor Immunity', *Cancer Immunology Research*, 2(3), pp. 194–199. Available at: https://doi.org/10.1158/2326-6066.CIR-13-0214.

Ogino, T. *et al.* (2013) 'Increased Th17-Inducing Activity of CD14+ CD163low Myeloid Cells in Intestinal Lamina Propria of Patients With Crohn's Disease', *Gastroenterology*, 145(6), pp. 1380-1391.e1. Available at: https://doi.org/10.1053/j.gastro.2013.08.049.

Ogura, Y. *et al.* (2001) 'A frameshift mutation in NOD2 associated with susceptibility to Crohn's disease', *Nature*, 411(6837), pp. 603–606. Available at: https://doi.org/10.1038/35079114.

Oh, H. *et al.* (2019) 'Asaronic Acid Attenuates Macrophage Activation toward M1 Phenotype through Inhibition of NF-κB Pathway and JAK-STAT Signaling in Glucose-Loaded Murine Macrophages', *Journal of Agricultural and Food Chemistry*, 67(36), pp. 10069–10078. Available at: https://doi.org/10.1021/acs.jafc.9b03926.

Ohmori, Y. and Hamilton, T.A. (1997) 'IL-4-induced STAT6 suppresses IFN-gamma-stimulated STAT1-dependent transcription in mouse macrophages.', *The Journal of Immunology*, 159(11), pp. 5474–5482.

Ohshima, S. *et al.* (2010) 'Effect of an antimicrobial agent on atherosclerotic plaques: assessment of metalloproteinase activity by molecular imaging', *Journal of the American College of Cardiology*, 55(12), pp. 1240–1249. Available at: https://doi.org/10.1016/j.jacc.2009.11.056.

Olefsky, J.M. and Glass, C.K. (2010) 'Macrophages, Inflammation, and Insulin Resistance', *Annual Review of Physiology*, 72(1), pp. 219–246. Available at: https://doi.org/10.1146/annurev-physiol-021909-135846.

Oliveira, A.G. *et al.* (2013) 'Acute exercise induces a phenotypic switch in adipose tissue macrophage polarization in diet-induced obese rats', *Obesity (Silver Spring, Md.)*, 21(12), pp. 2545–2556. Available at: https://doi.org/10.1002/oby.20402.

Onali, S., Favale, A. and Fantini, M.C. (2019) 'The Resolution of Intestinal Inflammation: The Peace-Keeper's Perspective', *Cells*, 8(4), p. 344. Available at: https://doi.org/10.3390/cells8040344.

O'Neill, L.A.J., Golenbock, D. and Bowie, A.G. (2013) 'The history of Toll-like receptors — redefining innate immunity', *Nature Reviews Immunology*, 13(6), pp. 453–460. Available at: https://doi.org/10.1038/nri3446.

Orecchioni, M. *et al.* (2019) 'Macrophage Polarization: Different Gene Signatures in M1(LPS+) vs. Classically and M2(LPS–) vs. Alternatively Activated Macrophages', *Frontiers in Immunology*, 10. Available at: https://doi.org/10.3389/fimmu.2019.01084.

Osborn, O. and Olefsky, J.M. (2012) 'The cellular and signaling networks linking the immune system and metabolism in disease', *Nature Medicine*, 18(3), pp. 363–374. Available at: https://doi.org/10.1038/nm.2627.

Ozaki, H. *et al.* (1999) 'Cutting edge: Combined treatment of TNF-α and IFN-γ causes redistribution of junctional adhesion molecule in human endothelial cells', *Journal of Immunology*, 163(2), pp. 553–557.

Pålsson-McDermott, E.M. and O'Neill, L.A.J. (2004) 'Signal transduction by the lipopolysaccharide receptor, Toll-like receptor-4', *Immunology*, 113(2), pp. 153–162. Available at: https://doi.org/10.1111/j.1365-2567.2004.01976.x.

Pannellini, T. *et al.* (2004) 'The expression of LEC/CCL16, a powerful inflammatory chemokine, is upregulated in ulcerative colitis', *International Journal of Immunopathology and Pharmacology*, 17(2), pp. 171–180. Available at: https://doi.org/10.1177/039463200401700209.

Park, C. *et al.* (2000) 'Immune Response in Stat2 Knockout Mice', *Immunity*, 13(6), pp. 795–804. Available at: https://doi.org/10.1016/S1074-7613(00)00077-7.

Park, J.H. *et al.* (2017) 'IBD immunopathogenesis: A comprehensive review of inflammatory molecules', *Autoimmunity Reviews*, 16(4), pp. 416–426. Available at: https://doi.org/10.1016/j.autrev.2017.02.013.

Park, S. *et al.* (2016) 'Histological Disease Activity as a Predictor of Clinical Relapse Among Patients With Ulcerative Colitis: Systematic Review and Meta-Analysis', *The American Journal of Gastroenterology*, 111(12), pp. 1692–1701. Available at: https://doi.org/10.1038/ajg.2016.418.

Parker, D. (2019) *CD80/CD86 signaling contributes to the proinflammatory response of Staphylococcus aureus in the airway*. Available at: https://www.ncbi.nlm.nih.gov/pmc/articles/PMC5916031/ (Accessed: 2 September 2019).

Pascual, G. *et al.* (2005) 'A SUMOylation-dependent pathway mediates transrepression of inflammatory response genes by PPAR-gamma', *Nature*, 437(7059), pp. 759–763. Available at: https://doi.org/10.1038/nature03988.

Patel, L. *et al.* (2003) 'Resistin is expressed in human macrophages and directly regulated by PPARγ activators', *Biochemical and Biophysical Research Communications*, 300(2), pp. 472–476. Available at: https://doi.org/10.1016/S0006-291X(02)02841-3.

Patel, R.N. *et al.* (1999) 'A novel mechanism of action of chemically modified tetracyclines: inhibition of COX-2-mediated prostaglandin E2 production', *Journal of Immunology (Baltimore, Md.: 1950)*, 163(6), pp. 3459–3467.

Pauleau, A.-L. *et al.* (2004) 'Enhancer-mediated control of macrophage-specific arginase I expression', *Journal of immunology (Baltimore, Md.*, 172(12), pp. 7565–7573. Available at: https://doi.org/10.4049/jimmunol.172.12.7565.

Pearl, J.E. *et al.* (2001) 'Inflammation and Lymphocyte Activation during Mycobacterial Infection in the Interferon-γ-Deficient Mouse', *Cellular Immunology*, 211(1), pp. 43–50. Available at: https://doi.org/10.1006/cimm.2001.1819.

Pederzoli-Ribeil, M. *et al.* (2010) 'Design and characterization of a cleavage-resistant Annexin A1 mutant to control inflammation in the microvasculature', *Blood*, 116(20), pp. 4288–4296. Available at: https://doi.org/10.1182/blood-2010-02-270520.

Perretti, M. and Flower, R.J. (2004) 'Annexin 1 and the biology of the neutrophil', *Journal of Leukocyte Biology*, 76(1), pp. 25–29. Available at: https://doi.org/10.1189/jlb.1103552.

Perrier, C. *et al.* (2012) 'Neutralization of membrane TNF, but not soluble TNF, is crucial for the treatment of experimental colitis', *Inflammatory Bowel Diseases*, n/a(n/a). Available at: https://doi.org/10.1002/ibd.23023.

Peyrin–Biroulet, L. *et al.* (2008) 'Efficacy and Safety of Tumor Necrosis Factor Antagonists in Crohn's Disease: Meta-Analysis of Placebo-Controlled Trials', *Clinical Gastroenterology and Hepatology*, 6(6), pp. 644–653. Available at: https://doi.org/10.1016/j.cgh.2008.03.014.

Pi, R. *et al.* (2004) ‘Minocycline prevents glutamate-induced apoptosis of cerebellar granule neurons by differential regulation of p38 and Akt pathways’, *Journal of Neurochemistry*, 91(5), pp. 1219–1230. Available at: https://doi.org/10.1111/j.1471-4159.2004.02796.x.

Pinney, S.P. *et al.* (2003) ‘Minocycline inhibits smooth muscle cell proliferation, migration and neointima formation after arterial injury’, *Journal of Cardiovascular Pharmacology*, 42(4), pp. 469–476.

Pirenne, H. *et al.* (1992) ‘Comparison of T cell functional changes during childhood with the ontogeny of CDw29 and CD45RA expression on CD4+ T cells’, *Pediatric research*, 32(1), pp. 81–86. Available at: https://doi.org/10.1203/00006450-199207000-00016.

Platt, A.M. *et al.* (2010) ‘An independent subset of TLR expressing CCR2-dependent macrophages promotes colonic inflammation’, *Journal of Immunology (Baltimore, Md.: 1950)*, 184(12), pp. 6843–6854. Available at: https://doi.org/10.4049/jimmunol.0903987.

Płóciennikowska, A. *et al.* (2015) ‘Co-operation of TLR4 and raft proteins in LPS-induced pro-inflammatory signaling’, *Cellular and Molecular Life Sciences*, 72(3), pp. 557–581. Available at: https://doi.org/10.1007/s00018-014-1762-5.

Popa, C. *et al.* (2007) ‘The role of TNF-α in chronic inflammatory conditions, intermediary metabolism, and cardiovascular risk’, *Journal of Lipid Research*, 48(4), pp. 751–762. Available at: https://doi.org/10.1194/jlr.R600021-JLR200.

Popovic, N. *et al.* (2002) ‘Inhibition of autoimmune encephalomyelitis by a tetracycline’, *Annals of Neurology*, 51(2), pp. 215–223.

Porcheray, F. *et al.* (2005) ‘Macrophage activation switching: an asset for the resolution of inflammation’, *Clinical and Experimental Immunology*, 142(3), pp. 481–489. Available at: https://doi.org/10.1111/j.1365-2249.2005.02934.x.

Porta, C. *et al.* (2009) ‘Tolerance and M2 (alternative) macrophage polarization are related processes orchestrated by p50 nuclear factor κB’, *Proceedings of the National Academy of Sciences*, 106(35), pp. 14978–14983. Available at: https://doi.org/10.1073/pnas.0809784106.

Pourgholami, M.H. *et al.* (2012) ‘Minocycline inhibits growth of epithelial ovarian cancer’, *Gynecologic Oncology*, 125(2), pp. 433–440. Available at: https://doi.org/10.1016/j.ygyno.2012.01.006.

Pourgholami, M.H. *et al.* (2013) ‘Minocycline inhibits malignant ascites of ovarian cancer through targeting multiple signaling pathways’, *Gynecologic Oncology*, 129(1), pp. 113–119. Available at: https://doi.org/10.1016/j.ygyno.2012.12.031.

Powrie, F. and Leach, M.W. (1995) ‘Genetic and spontaneous models of inflammatory bowel disease in rodents: evidence for abnormalities in mucosal immune regulation’, *Therapeutic Immunology*, 2(2), pp. 115–123.

PrabhuDas, M.R. *et al.* (2017) ‘A Consensus Definitive Classification of Scavenger Receptors and Their Roles in Health and Disease’, *Journal of immunology (Baltimore, Md. : 1950)*, 198(10), pp. 3775–3789. Available at: https://doi.org/10.4049/jimmunol.1700373.

Proto, J.D. *et al.* (2018) ‘Regulatory T cells promote macrophage efferocytosis during inflammation resolution’, *Immunity*, pp. S1074-7613(18)30335–2. Available at: https://doi.org/10.1016/j.immuni.2018.07.015.

Pugin, J. *et al.* (1993) ‘Lipopolysaccharide activation of human endothelial and epithelial cells is mediated by lipopolysaccharide-binding protein and soluble CD14’, *Proceedings of the National Academy of Sciences of the United States of America*, 90(7), pp. 2744–2748. Available at: https://doi.org/10.1073/pnas.90.7.2744.

Purton, L.E. *et al.* (2006) ‘RARγ is critical for maintaining a balance between hematopoietic stem cell self-renewal and differentiation’, *Journal of Experimental Medicine*, 203(5), pp. 1283–1293. Available at: https://doi.org/10.1084/jem.20052105.

Qualls, J.E. *et al.* (2006) ‘Suppression of experimental colitis by intestinal mononuclear phagocytes’, *Journal of Leukocyte Biology*, 80(4), pp. 802–815. Available at: https://doi.org/10.1189/jlb.1205734.

Quintero-Fabián, S. *et al.* (2019) ‘Role of Matrix Metalloproteinases in Angiogenesis and Cancer’, *Frontiers in Oncology*, 9, p. 1370. Available at: https://doi.org/10.3389/fonc.2019.01370.

Racke, M.K. *et al.* (1995) ‘Distinct roles for B7-1 (CD-80) and B7-2 (CD-86) in the initiation of experimental allergic encephalomyelitis.’, *Journal of Clinical Investigation*, 96(5), pp. 2195–2203.

Radad, K., Moldzio, R. and Rausch, W.-D. (2010) ‘Minocycline protects dopaminergic neurons against long-term rotenone toxicity’, *The Canadian Journal of Neurological Sciences. Le Journal Canadien Des Sciences Neurologiques*, 37(1), pp. 81–85. Available at: https://doi.org/10.1017/s0317167100009690.

Raggi, F. *et al.* (2017) ‘Regulation of Human Macrophage M1–M2 Polarization Balance by Hypoxia and the Triggering Receptor Expressed on Myeloid Cells-1’, *Frontiers in Immunology*, 8. Available at: https://doi.org/10.3389/fimmu.2017.01097.

Ramseyer, V.D. *et al.* (2016) ‘Angiotensin II-mediated hypertension impairs nitric oxide-induced NKCC2 inhibition in thick ascending limbs’, *American Journal of Physiology - Renal Physiology*, 310(8), pp. F748–F754. Available at: https://doi.org/10.1152/ajprenal.00473.2015.

Rauch, I., Müller, M. and Decker, T. (2013) ‘The regulation of inflammation by interferons and their STATs’, *JAK-STAT*, 2(1), p. e23820. Available at: https://doi.org/10.4161/jkst.23820.

Regen, F. *et al.* (2014) ‘Striking Growth-inhibitory Effects of Minocycline on Human Prostate Cancer Cell Lines’, *Urology*, 83(2), p. 509.e1-509.e6. Available at: https://doi.org/10.1016/j.urology.2013.10.029.

Reglodi, D. *et al.* (2017) ‘Novel tactics for neuroprotection in Parkinson’s disease: Role of antibiotics, polyphenols and neuropeptides’, *Progress in Neurobiology*, 155, pp. 120–148. Available at: https://doi.org/10.1016/j.pneurobio.2015.10.004.

Reijnders, T.D.Y. *et al.* (2020) ‘Immunomodulation by macrolides: therapeutic potential for critical care’, *The Lancet. Respiratory Medicine*, 8(6), pp. 619–630. Available at: https://doi.org/10.1016/S2213-2600(20)30080-1.

Reinecker, H.C. *et al.* (1993) ‘Enhanced secretion of tumour necrosis factor-alpha, IL-6, and IL-1 beta by isolated lamina propria mononuclear cells from patients with ulcerative colitis and Crohn’s disease.’, *Clinical and Experimental Immunology*, 94(1), pp. 174–181.

Ren, W. *et al.* (2019) ‘Glutamine Metabolism in Macrophages: A Novel Target for Obesity/Type 2 Diabetes’, *Advances in Nutrition*, 10(2), pp. 321–330. Available at: https://doi.org/10.1093/advances/nmy084.

Renshaw, M. *et al.* (2002) ‘Cutting Edge: Impaired Toll-Like Receptor Expression and Function in Aging’, *The Journal of Immunology*, 169(9), pp. 4697–4701. Available at: https://doi.org/10.4049/jimmunol.169.9.4697.

Ricote, M. *et al.* (1998) ‘The peroxisome proliferator-activated receptor-gamma is a negative regulator of macrophage activation’, *Nature*, 391(6662), pp. 79–82. Available at: https://doi.org/10.1038/34178.

Ricote, M. *et al.* (1999) ‘The peroxisome proliferator-activated receptor(PPARgamma) as a regulator of monocyte/macrophage function’, *Journal of Leukocyte Biology*, 66(5), pp. 733–739. Available at: https://doi.org/10.1002/jlb.66.5.733.

Riley, J.K. *et al.* (1999) ‘Interleukin-10 receptor signaling through the JAK-STAT pathway. Requirement for two distinct receptor-derived signals for anti-inflammatory action’, *The Journal of Biological Chemistry*, 274(23), pp. 16513–16521. Available at: https://doi.org/10.1074/jbc.274.23.16513.

Rivellese, F. *et al.* (2014) ‘IgE and IL-33−mediated triggering of human basophils inhibits TLR4−induced monocyte activation’, *European Journal of Immunology*, 44(10), pp. 3045–3055. Available at: https://doi.org/10.1002/eji.201444731.

Rivollier, A. *et al.* (2012) ‘Inflammation switches the differentiation program of Ly6Chi monocytes from antiinflammatory macrophages to inflammatory dendritic cells in the colon’, *Journal of Experimental Medicine*, 209(1), pp. 139–155. Available at: https://doi.org/10.1084/jem.20101387.

Robinson, C.M. *et al.* (2009) ‘Cytokines Involved in Interferon-γ Production by Human Macrophages’, *Journal of Innate Immunity*, 2(1), pp. 56–65. Available at: https://doi.org/10.1159/000247156.

Robinson, P.J. (1992) ‘Differential stimulation of protein kinase C activity by phorbol ester or calcium/phosphatidylserine in vitro and in intact synaptosomes.’, *Journal of Biological Chemistry*, 267(30), pp. 21637–21644. Available at: https://doi.org/10.1016/S0021-9258(19)36659-1.

Roggendorf, W., Strupp, S. and Paulus, W. (1996) ‘Distribution and characterization of microglia/macrophages in human brain tumors’, *Acta Neuropathologica*, 92(3), pp. 288–293. Available at: https://doi.org/10.1007/s004010050520.

Rogler, G. (2004) ‘Update in inflammatory bowel disease pathogenesis’, *Current Opinion in Gastroenterology*, 20(4), pp. 311–317.

Rogler, G. (2015) ‘Where are we heading to in pharmacological IBD therapy?’, *Pharmacological Research*, 100, pp. 220–227. Available at: https://doi.org/10.1016/j.phrs.2015.07.005.

Rokita, E. and Menzel, E.J. (1997) ‘Characteristics of CD14 shedding from human monocytes: Evidence for the competition of soluble CD14 (sCD14) with CD14 receptors for lipopolysaccharide (LPS) binding’, *APMIS*, 105(7–12), pp. 510–518. Available at: https://doi.org/10.1111/j.1699-0463.1997.tb05048.x.

Romagnani, S. (2000) ‘T-cell subsets (Th1 versus Th2)’, *Annals of Allergy, Asthma & Immunology*, 85(1), pp. 9–21. Available at: https://doi.org/10.1016/S1081-1206(10)62426-X.

Romero-Perez, D. *et al.* (2008) ‘Cardiac Uptake of Minocycline and Mechanisms for In Vivo Cardioprotection’, *Journal of the American College of Cardiology*, 52(13), pp. 1086–1094. Available at: https://doi.org/10.1016/j.jacc.2008.06.028.

Rossi, M.L. *et al.* (1987) ‘Immunohistological study of mononuclear cell infiltrate in malignant gliomas’, *Acta Neuropathologica*, 74(3), pp. 269–277. Available at: https://doi.org/10.1007/BF00688191.

Rossol, M. *et al.* (2011) ‘LPS-induced Cytokine Production in Human Monocytes and Macrophages’, *Critical Reviews™ in Immunology*, 31(5), pp. 379–446. Available at: https://doi.org/10.1615/CritRevImmunol.v31.i5.20.

Rőszer, T. (2015) *Understanding the Mysterious M2 Macrophage through Activation Markers and Effector Mechanisms*, *Mediators of Inflammation*. Available at: https://doi.org/10.1155/2015/816460.

Rothfuchs, A.G. *et al.* (2001) ‘IFN-αβ-Dependent, IFN-γ Secretion by Bone Marrow-Derived Macrophages Controls an Intracellular Bacterial Infection’, *The Journal of Immunology*, 167(11), pp. 6453–6461. Available at: https://doi.org/10.4049/jimmunol.167.11.6453.

Rottenberg, M.E. and Carow, B. (2014) ‘SOCS3 and STAT3, major controllers of the outcome of infection with Mycobacterium tuberculosis’, *Seminars in Immunology*, 26(6), pp. 518–532. Available at: https://doi.org/10.1016/j.smim.2014.10.004.

Ruffell, D. *et al.* (2009) 'A CREB-C/EBPβ cascade induces M2 macrophage-specific gene expression and promotes muscle injury repair', *Proceedings of the National Academy of Sciences*, 106(41), pp. 17475–17480. Available at: https://doi.org/10.1073/pnas.0908641106.

Rugtveit, J. *et al.* (1997) 'Cytokine profiles differ in newly recruited and resident subsets of mucosal macrophages from inflammatory bowel disease', *Gastroenterology*, 112(5), pp. 1493–1505. Available at: https://doi.org/10.1016/s0016-5085(97)70030-1.

Ruiz-Moreno, C., Velez-Pardo, C. and Jimenez-Del-Rio, M. (2018) 'Minocycline induces apoptosis in acute lymphoblastic leukemia Jurkat cells', *Toxicology in Vitro*, 50, pp. 336–346. Available at: https://doi.org/10.1016/j.tiv.2018.03.012.

Sadowski, T. and Steinmeyer, J. (2001) 'Minocycline Inhibits the Production of Inducible Nitric Oxide Synthase in Articular Chondrocytes', *The Journal of Rheumatology*, p. 5.

Sahoo, A.K. *et al.* (2018) 'Features and outcomes of drugs for combination therapy as multi-targets strategy to combat Alzheimer's disease', *Journal of Ethnopharmacology*, 215, pp. 42–73. Available at: https://doi.org/10.1016/j.jep.2017.12.015.

Sahoo, M. *et al.* (2011) 'Role of the Inflammasome, IL-1β, and IL-18 in Bacterial Infections', *The Scientific World Journal*, 11, pp. 2037–2050. Available at: https://doi.org/10.1100/2011/212680.

Saikali, Z. and Singh, G. (2003) 'Doxycycline and other tetracyclines in the treatment of bone metastasis', *Anti-Cancer Drugs*, 14(10), pp. 773–778. Available at: https://doi.org/10.1097/00001813-200311000-00001.

Saivin, S. and Houin, G. (1988) 'Clinical pharmacokinetics of doxycycline and minocycline', *Clinical Pharmacokinetics*, 15(6), pp. 355–366. Available at: https://doi.org/10.2165/00003088-198815060-00001.

Salins, S. *et al.* (2001) 'Differential Induction of Gamma Interferon in Legionella pneumophila- Infected Macrophages from BALB/c and A/J Mice', *Infection and Immunity*, 69(6), pp. 3605–3610. Available at: https://doi.org/10.1128/IAI.69.6.3605-3610.2001.

Salkowski, C. *et al.* (1999) 'IL-12 is dysregulated in macrophages from IRF-1 and IRF-2 knockout mice.', *Journal of immunology* [Preprint].

Samatar, A.A. and Poulikakos, P.I. (2014) 'Targeting RAS-ERK signalling in cancer: promises and challenges', *Nature Reviews. Drug Discovery*, 13(12), pp. 928–942. Available at: https://doi.org/10.1038/nrd4281.

Sambrano, G.R. and Steinberg, D. (1995) 'Recognition of oxidatively damaged and apoptotic cells by an oxidized low density lipoprotein receptor on mouse peritoneal macrophages: role of membrane phosphatidylserine.', *Proceedings of the National Academy of Sciences*, 92(5), pp. 1396–1400. Available at: https://doi.org/10.1073/pnas.92.5.1396.

Sanin, D.E., Prendergast, C.T. and Mountford, A.P. (2015) 'IL-10 Production in Macrophages Is Regulated by a TLR-Driven CREB-Mediated Mechanism That Is Linked to Genes Involved in Cell Metabolism', *The Journal of Immunology*, 195(3), pp. 1218–1232. Available at: https://doi.org/10.4049/jimmunol.1500146.

Santa-Cecília, F.V. *et al.* (2016) 'Doxycycline Suppresses Microglial Activation by Inhibiting the p38 MAPK and NF-kB Signaling Pathways', *Neurotoxicity Research*, 29(4), pp. 447–459. Available at: https://doi.org/10.1007/s12640-015-9592-2.

Sapadin, A.N. and Fleischmajer, R. (2006a) 'Tetracyclines: Nonantibiotic properties and their clinical implications', *Journal of the American Academy of Dermatology*, 54(2), pp. 258–265. Available at: https://doi.org/10.1016/j.jaad.2005.10.004.

Sapadin, A.N. and Fleischmajer, R. (2006b) 'Tetracyclines: Nonantibiotic properties and their clinical implications', *Journal of the American Academy of Dermatology*, 54(2), pp. 258–265. Available at: https://doi.org/10.1016/j.jaad.2005.10.004.

Sapadin, A.N. and Fleischmajer, R. (2006c) 'Tetracyclines: Nonantibiotic properties and their clinical implications', *Journal of the American Academy of Dermatology*, 54(2), pp. 258–265. Available at: https://doi.org/10.1016/j.jaad.2005.10.004.

Sasaki, A. *et al.* (1998) 'Expression of interleukin-1beta mRNA and protein in human gliomas assessed by RT-PCR and immunohistochemistry', *Journal of Neuropathology and Experimental Neurology*, 57(7), pp. 653–663. Available at: https://doi.org/10.1097/00005072-199807000-00002.

Sasaki, A. (2017) 'Microglia and brain macrophages: An update', *Neuropathology*, 37(5), pp. 452–464. Available at: https://doi.org/10.1111/neup.12354.

Satoh, T. *et al.* (2010) 'The Jmjd3-Irf4 axis regulates M2 macrophage polarization and host responses against helminth infection', *Nature Immunology*, 11(10), pp. 936–944. Available at: https://doi.org/10.1038/ni.1920.

Satoh, T. and Akira, S. (2016) 'Toll-Like Receptor Signaling and Its Inducible Proteins', *Microbiology Spectrum*, 4(6). Available at: https://doi.org/10.1128/microbiolspec.MCHD-0040-2016.

Savage, D.B. *et al.* (2001) 'Resistin / Fizz3 Expression in Relation to Obesity and Peroxisome Proliferator–Activated Receptor-γ Action in Humans', *Diabetes*, 50(10), pp. 2199–2202. Available at: https://doi.org/10.2337/diabetes.50.10.2199.

Savitsky, D.A. *et al.* (2009) 'Regulation of immunity and oncogenesis by the IRF transcription factor family', *Cancer Immunology, Immunotherapy* [Preprint]. Available at: https://doi.org/10.1007/s00262-009-0804-6.

Scannell, M. *et al.* (2007) 'Annexin-1 and Peptide Derivatives Are Released by Apoptotic Cells and Stimulate Phagocytosis of Apoptotic Neutrophils by

Macrophages', *The Journal of Immunology*, 178(7), pp. 4595–4605. Available at: https://doi.org/10.4049/jimmunol.178.7.4595.

Scarabelli, T.M. *et al.* (2004) 'Minocycline inhibits caspase activation and reactivation, increases the ratio of XIAP to smac/DIABLO, and reduces the mitochondrial leakage of cytochrome C and smac/DIABLO', *Journal of the American College of Cardiology*, 43(5), pp. 865–874. Available at: https://doi.org/10.1016/j.jacc.2003.09.050.

Schädlich, H. *et al.* (1999) 'Anti-inflammatory effects of systemic anti-tumour necrosis factor α treatment in human/murine SCID arthritis', *Annals of the Rheumatic Diseases*, 58(7), pp. 428–434. Available at: https://doi.org/10.1136/ard.58.7.428.

Schandené, L. *et al.* (1994) 'B7/CD28-dependent IL-5 production by human resting T cells is inhibited by IL-10.', *The Journal of Immunology*, 152(9), pp. 4368–4374.

Schenk, M. *et al.* (2014) 'Interleukin-1β triggers the differentiation of macrophages with enhanced capacity to present mycobacterial antigen to T cells', *Immunology*, 141(2), pp. 174–180. Available at: https://doi.org/10.1111/imm.12167.

Schett, G. and Neurath, M.F. (2018) 'Resolution of chronic inflammatory disease: universal and tissue-specific concepts', *Nature Communications*, 9, p. 3261. Available at: https://doi.org/10.1038/s41467-018-05800-6.

Schiering, C. *et al.* (2014) 'The Alarmin IL-33 Promotes Regulatory T Cell Function in the Intestine', *Nature*, 513(7519), pp. 564–568. Available at: https://doi.org/10.1038/nature13577.

Schiffrin, E.L. (2014) 'Immune mechanisms in hypertension and vascular injury', *Clinical Science (London, England: 1979)*, 126(4), pp. 267–274. Available at: https://doi.org/10.1042/CS20130407.

Schif-Zuck, S. *et al.* (2011) 'Satiated-efferocytosis generates pro-resolving CD11blow macrophages: modulation by resolvins and glucocorticoids', *European journal of immunology*, 41(2), pp. 366–379. Available at: https://doi.org/10.1002/eji.201040801.

Schlereth, S.L. *et al.* (2016) 'Characterization of Antigen-Presenting Macrophages and Dendritic Cells in the Healthy Human Sclera', *Investigative Ophthalmology & Visual Science*, 57(11), pp. 4878–4885. Available at: https://doi.org/10.1167/iovs.15-18552.

Schmid, M.C. *et al.* (2018) 'Integrin CD11b activation drives anti-tumor innate immunity', *Nature Communications*, 9. Available at: https://doi.org/10.1038/s41467-018-07387-4.

Schnappinger, D. and Hillen, W. (1996) 'Tetracyclines: antibiotic action, uptake, and resistance mechanisms', *Archives of Microbiology*, 165(6), pp. 359–369. Available at: https://doi.org/10.1007/s002030050339.

Schroder, K. *et al.* (2004) ‘Interferon-γ: an overview of signals, mechanisms and functions’, *Journal of Leukocyte Biology*, 75(2), pp. 163–189. Available at: https://doi.org/10.1189/jlb.0603252.

Schulz, O. *et al.* (2009) ‘Intestinal CD103+, but not CX3CR1+, antigen sampling cells migrate in lymph and serve classical dendritic cell functions’, *Journal of Experimental Medicine*, 206(13), pp. 3101–3114. Available at: https://doi.org/10.1084/jem.20091925.

Schwende, H. *et al.* (1996) ‘Differences in the state of differentiation of THP-1 cells induced by phorbol ester and 1,25-dihydroxyvitamin D3’, *Journal of Leukocyte Biology*, 59(4), pp. 555–561.

Schwerd, T. *et al.* (2017) ‘Impaired antibacterial autophagy links granulomatous intestinal inflammation in Niemann–Pick disease type C1 and XIAP deficiency with NOD2 variants in Crohn’s disease’, *Gut*, 66(6), pp. 1060–1073. Available at: https://doi.org/10.1136/gutjnl-2015-310382.

Seabrook, T.J. *et al.* (2006) ‘Minocycline affects microglia activation, Abeta deposition, and behavior in APP-tg mice’, *Glia*, 53(7), pp. 776–782. Available at: https://doi.org/10.1002/glia.20338.

Seftor, E.A. *et al.* (1998) ‘Application of chemically modified tetracyclines (CMTs) in experimental models of cancer and arthritis’, *Advances in Dental Research*, 12(2), pp. 103–110. Available at: https://doi.org/10.1177/08959374980120010101.

Serbina, N.V. and Pamer, E.G. (2006) ‘Monocyte emigration from bone marrow during bacterial infection requires signals mediated by chemokine receptor CCR2’, *Nature Immunology*, 7(3), pp. 311–317. Available at: https://doi.org/10.1038/ni1309.

Serhan, C.N. and Savill, J. (2005) ‘Resolution of inflammation: the beginning programs the end’, *Nature Immunology*, 6(12), pp. 1191–1197. Available at: https://doi.org/10.1038/ni1276.

Seyedizade, S.S. *et al.* (2020) ‘Current Status of M1 and M2 Macrophages Pathway as Drug Targets for Inflammatory Bowel Disease’, *Archivum Immunologiae Et Therapiae Experimentalis*, 68(2), p. 10. Available at: https://doi.org/10.1007/s00005-020-00576-4.

Shahzad, K. *et al.* (2011) ‘Minocycline reduces plaque size in diet induced atherosclerosis via p27(Kip1)’, *Atherosclerosis*, 219(1), pp. 74–83. Available at: https://doi.org/10.1016/j.atherosclerosis.2011.05.041.

Shapouri-Moghaddam, A. *et al.* (2018) ‘Macrophage plasticity, polarization, and function in health and disease’, *Journal of Cellular Physiology*, 233(9), pp. 6425–6440. Available at: https://doi.org/10.1002/jcp.26429.

Sharma, N. *et al.* (2012) ‘Myeloid KLF4 deficiency augments atherogenesis in ApoE-/- mice’, *Arteriosclerosis, thrombosis, and vascular biology*, 32(12), pp. 2836–2838. Available at: https://doi.org/10.1161/ATVBAHA.112.300471.

Shaughnessy, L.M. and Swanson, J.A. (2007) ‘THE ROLE OF THE ACTIVATED MACROPHAGE IN CLEARING LISTERIA MONOCYTOGENES INFECTION’, *Frontiers in bioscience : a journal and virtual library*, 12, pp. 2683–2692.

Shiratori, H. *et al.* (2017) ‘THP-1 and human peripheral blood mononuclear cell-derived macrophages differ in their capacity to polarize in vitro’, *Molecular Immunology*, 88, pp. 58–68. Available at: https://doi.org/10.1016/j.molimm.2017.05.027.

Sica, A. *et al.* (2015) ‘Macrophage polarization in pathology’, *Cellular and Molecular Life Sciences*, 72(21), pp. 4111–4126. Available at: https://doi.org/10.1007/s00018-015-1995-y.

Sica, A. and Bronte, V. (2007) ‘Altered macrophage differentiation and immune dysfunction in tumor development’, *The Journal of Clinical Investigation*, 117(5), pp. 1155–1166. Available at: https://doi.org/10.1172/JCI31422.

Sica, A. and Mantovani, A. (2012) ‘Macrophage plasticity and polarization: in vivo veritas’, *The Journal of Clinical Investigation*, 122(3), pp. 787–795. Available at: https://doi.org/10.1172/JCI59643.

da Silva, T.A. *et al.* (2017) ‘CD14 is critical for TLR2-mediated M1 macrophage activation triggered by N-glycan recognition’, *Scientific Reports*, 7, p. 7083. Available at: https://doi.org/10.1038/s41598-017-07397-0.

Sindrilaru, A. and Scharffetter-Kochanek, K. (2013) ‘Disclosure of the Culprits: Macrophages—Versatile Regulators of Wound Healing’, *Advances in Wound Care*, 2(7), pp. 357–368. Available at: https://doi.org/10.1089/wound.2012.0407.

Singh, M. *et al.* (2014) ‘Minocycline attenuates HIV-1 infection and suppresses chronic immune activation in humanized NOD/LtsZ-scidIL-2Rγnull mice’, *Immunology*, 142(4), pp. 562–572. Available at: https://doi.org/10.1111/imm.12246.

Sinha-Hikim, I. *et al.* (2011) ‘Minocycline suppresses oxidative stress and attenuates fetal cardiac myocyte apoptosis triggered by in utero cocaine exposure’, *Apoptosis*, 16(6), pp. 563–573. Available at: https://doi.org/10.1007/s10495-011-0590-4.

Siouti, E. and Andreakos, E. (2019) ‘The many facets of macrophages in rheumatoid arthritis’, *Biochemical Pharmacology*, 165, pp. 152–169. Available at: https://doi.org/10.1016/j.bcp.2019.03.029.

Skelly, D.T. *et al.* (2013) ‘A Systematic Analysis of the Peripheral and CNS Effects of Systemic LPS, IL-1B, TNF-α and IL-6 Challenges in C57BL/6 Mice’, *PLoS ONE*, 8(7), p. e69123. Available at: https://doi.org/10.1371/journal.pone.0069123.

Skidmore, R. *et al.* (2003) ‘Effects of subantimicrobial-dose doxycycline in the treatment of moderate acne’, *Archives of Dermatology*, 139(4), pp. 459–464. Available at: https://doi.org/10.1001/archderm.139.4.459.

Slavik, J.M., Hutchcroft, J.E. and Bierer, B.E. (1999) 'CD80 and CD86 Are Not Equivalent in Their Ability to Induce the Tyrosine Phosphorylation of CD28 *', *Journal of Biological Chemistry*, 274(5), pp. 3116–3124. Available at: https://doi.org/10.1074/jbc.274.5.3116.

Slevin, S.M. and Egan, L.J. (2015) 'New Insights into the Mechanisms of Action of Anti–Tumor Necrosis Factor-α Monoclonal Antibodies in Inflammatory Bowel Disease':, *Inflammatory Bowel Diseases*, 21(12), pp. 2909–2920. Available at: https://doi.org/10.1097/MIB.0000000000000533.

Smallie, T. *et al.* (2010) 'IL-10 inhibits transcription elongation of the human TNF gene in primary macrophages', *The Journal of Experimental Medicine*, 207(10), pp. 2081–2088. Available at: https://doi.org/10.1084/jem.20100414.

Smith, A.M. *et al.* (2009a) 'Disordered macrophage cytokine secretion underlies impaired acute inflammation and bacterial clearance in Crohn's disease', *The Journal of Experimental Medicine*, 206(9), pp. 1883–1897. Available at: https://doi.org/10.1084/jem.20091233.

Smith, A.M. *et al.* (2009b) 'Disordered macrophage cytokine secretion underlies impaired acute inflammation and bacterial clearance in Crohn's disease', *The Journal of Experimental Medicine*, 206(9), pp. 1883–1897. Available at: https://doi.org/10.1084/jem.20091233.

Smith, K. and Leyden, J.J. (2005) 'Safety of doxycycline and minocycline: a systematic review', *Clinical Therapeutics*, 27(9), pp. 1329–1342. Available at: https://doi.org/10.1016/j.clinthera.2005.09.005.

Smith, T.D. *et al.* (2017) 'Harnessing macrophage plasticity for tissue regeneration', *Advanced Drug Delivery Reviews*, 114, pp. 193–205. Available at: https://doi.org/10.1016/j.addr.2017.04.012.

Smith-Norowitz, T.A. *et al.* (2002) 'Effect of minocycline and doxycycline on IgE responses', *Annals of Allergy, Asthma & Immunology*, 89(2), pp. 172–179. Available at: https://doi.org/10.1016/S1081-1206(10)61934-5.

Smythies, L.E. *et al.* (2005) 'Human intestinal macrophages display profound inflammatory anergy despite avid phagocytic and bacteriocidal activity', *Journal of Clinical Investigation*, 115(1), pp. 66–75. Available at: https://doi.org/10.1172/JCI200519229.

Smythies, L.E. *et al.* (2006) 'Mucosal IL-8 and TGF-beta recruit blood monocytes: evidence for cross-talk between the lamina propria stroma and myeloid cells', *Journal of Leukocyte Biology*, 80(3), pp. 492–499. Available at: https://doi.org/10.1189/jlb.1005566.

Smythies, L.E. *et al.* (2010) 'Inflammation anergy in human intestinal macrophages is due to Smad-induced IkappaBalpha expression and NF-kappaB inactivation', *The Journal of biological chemistry*, 285(25), pp. 19593–19604. Available at: https://doi.org/10.1074/jbc.m109.069955.

Socias, S.B. *et al.* (2018) 'Exploiting the therapeutic potential of ready-to-use drugs: Repurposing antibiotics against amyloid aggregation in

neurodegenerative diseases', *Progress in Neurobiology*, 162, pp. 17–36. Available at: https://doi.org/10.1016/j.pneurobio.2017.12.002.

Soehnlein, O. *et al.* (2008) 'Neutrophil secretion products pave the way for inflammatory monocytes', *Blood*, 112(4), pp. 1461–1471. Available at: https://doi.org/10.1182/blood-2008-02-139634.

Soehnlein, O. *et al.* (2017) 'Neutrophils as protagonists and targets in chronic inflammation', *Nature Reviews. Immunology*, 17(4), pp. 248–261. Available at: https://doi.org/10.1038/nri.2017.10.

Solovjov, D.A., Pluskota, E. and Plow, E.F. (2005) 'Distinct Roles for the α and β Subunits in the Functions of Integrin αMβ2*', *Journal of Biological Chemistry*, 280(2), pp. 1336–1345. Available at: https://doi.org/10.1074/jbc.M406968200.

Song, H. *et al.* (2014) 'Cytotoxic effects of tetracycline analogues (doxycycline, minocycline and COL-3) in acute myeloid leukemia HL-60 cells', *PloS One*, 9(12), p. e114457. Available at: https://doi.org/10.1371/journal.pone.0114457.

Song, Y. *et al.* (2004) 'Minocycline protects PC12 cells from ischemic-like injury and inhibits 5-lipoxygenase activation', *Neuroreport*, 15(14), pp. 2181–2184.

Song, Y. *et al.* (2006a) 'Minocycline protects PC12 cells against NMDA-induced injury via inhibiting 5-lipoxygenase activation', *Brain Research*, 1085(1), pp. 57–67. Available at: https://doi.org/10.1016/j.brainres.2006.02.042.

Song, Y. *et al.* (2006b) 'Minocycline protects PC12 cells against NMDA-induced injury via inhibiting 5-lipoxygenase activation', *Brain Research*, 1085(1), pp. 57–67. Available at: https://doi.org/10.1016/j.brainres.2006.02.042.

de Souza, H.S.P. and Fiocchi, C. (2016) 'Immunopathogenesis of IBD: current state of the art', *Nature Reviews. Gastroenterology & Hepatology*, 13(1), pp. 13–27. Available at: https://doi.org/10.1038/nrgastro.2015.186.

Spoettl, T. *et al.* (2006) 'Monocyte chemoattractant protein-1 (MCP-1) inhibits the intestinal-like differentiation of monocytes', *Clinical and Experimental Immunology*, 145(1), pp. 190–199. Available at: https://doi.org/10.1111/j.1365-2249.2006.03113.x.

Spöttl, T. *et al.* (2001) 'Monocyte differentiation in intestine-like macrophage phenotype induced by epithelial cells', *Journal of Leukocyte Biology*, 70(2), pp. 241–251. Available at: https://doi.org/10.1189/jlb.70.2.241.

Sriram, K., Miller, D.B. and O'Callaghan, J.P. (2006) 'Minocycline attenuates microglial activation but fails to mitigate striatal dopaminergic neurotoxicity: role of tumor necrosis factor-α', *Journal of Neurochemistry*, 96(3), pp. 706–718. Available at: https://doi.org/10.1111/j.1471-4159.2005.03566.x.

Starr, T. *et al.* (2018) 'The phorbol 12-myristate-13-acetate differentiation protocol is critical to the interaction of THP-1 macrophages with Salmonella Typhimurium', *PLOS ONE*, 13(3), p. e0193601. Available at: https://doi.org/10.1371/journal.pone.0193601.

Steevels, T.A.M. and Meyaard, L. (2011) ‘Immune inhibitory receptors: essential regulators of phagocyte function’, *European Journal of Immunology*, 41(3), pp. 575–587. Available at: https://doi.org/10.1002/eji.201041179.

Steinman, R.M. *et al.* (1999) ‘Antigen capture, processing, and presentation by dendritic cells: recent cell biological studies’, *Human Immunology*, 60(7), pp. 562–567. Available at: https://doi.org/10.1016/s0198-8859(99)00030-0.

Stirling, D.P. *et al.* (2005) ‘Minocycline as a neuroprotective agent’, *Neuroscientist*, 11(4), pp. 308–322. Available at: https://doi.org/10.1177/1073858405275175.

Su, L. *et al.* (2013) ‘TNFR2 Activates MLCK-Dependent Tight Junction Dysregulation to Cause Apoptosis-Mediated Barrier Loss and Experimental Colitis’, *Gastroenterology*, 145(2), pp. 407–415. Available at: https://doi.org/10.1053/j.gastro.2013.04.011.

Subauste, C.S., Malefyt, R. de W. and Fuh, F. (1998) ‘Role of CD80 (B7.1) and CD86 (B7.2) in the Immune Response to an Intracellular Pathogen’, p. 11.

Sugimoto, M.A. *et al.* (2016) ‘Resolution of Inflammation: What Controls Its Onset?’, *Frontiers in Immunology*, 7, p. 160. Available at: https://doi.org/10.3389/fimmu.2016.00160.

Sun, C. *et al.* (2013) ‘Neuroprotective effect of minocycline in a rat model of branch retinal vein occlusion’, *Experimental Eye Research*, 113, pp. 105–116. Available at: https://doi.org/10.1016/j.exer.2013.05.018.

Sun, K. *et al.* (2016) ‘IRF5 regulates lung macrophages M2 polarization during severe acute pancreatitis in vitro’, *World Journal of Gastroenterology*, 22(42), pp. 9368–9377. Available at: https://doi.org/10.3748/wjg.v22.i42.9368.

Sunakawa, Y. *et al.* (2015) ‘Variations in genes regulating tumor-associated macrophages (TAMs) to predict outcomes of bevacizumab-based treatment in patients with metastatic colorectal cancer: results from TRIBE and FIRE3 trials’, *Annals of Oncology*, 26(12), pp. 2450–2456. Available at: https://doi.org/10.1093/annonc/mdv474.

Sunderkotter, C. *et al.* (2004) ‘Subpopulations of Mouse Blood Monocytes Differ in Maturation Stage and Inflammatory Response’, *The Journal of Immunology*, 172(7), pp. 4410–4417. Available at: https://doi.org/10.4049/jimmunol.172.7.4410.

Suzuki, Y. *et al.* (1988) ‘Interferon-gamma: the major mediator of resistance against Toxoplasma gondii’, *Science (New York, N.Y.)*, 240(4851), pp. 516–518. Available at: https://doi.org/10.1126/science.3128869.

Svajger, U., Obermajer, N. and Jeras, M. (2010) ‘Novel findings in drug-induced dendritic cell tolerogenicity’, *International Reviews of Immunology*, 29(6), pp. 574–607. Available at: https://doi.org/10.3109/08830185.2010.522280.

Svendsen, U.G. (1977) ‘The importance of thymus in the pathogenesis of the chronic phase of hypertension in mice following partial infarction of the kidney’,

Acta Pathologica Et Microbiologica Scandinavica. Section A, Pathology, 85(4), pp. 539–547. Available at: https://doi.org/10.1111/j.1699-0463.1977.tb03886.x.

Switzer, J.A. *et al.* (2011) 'MMP-9 in an Exploratory Trial of Intravenous Minocycline for Acute Ischemic Stroke', *Stroke; a journal of cerebral circulation*, 42(9), pp. 2633–2635. Available at: https://doi.org/10.1161/STROKEAHA.111.618215.

Szanto, A. *et al.* (2010) 'STAT6 Transcription Factor Is a Facilitator of the Nuclear Receptor PPARγ-Regulated Gene Expression in Macrophages and Dendritic Cells', *Immunity*, 33(5), pp. 699–712. Available at: https://doi.org/10.1016/j.immuni.2010.11.009.

Szekanecz, Z. *et al.* (1995) 'Increased Synovial Expression of Transforming Growth Factor (TGF)-β Receptor Endoglin and TGF-β1 in Rheumatoid Arthritis: Possible Interactions in the Pathogenesis of the Disease', *Clinical Immunology and Immunopathology*, 76(2), pp. 187–194. Available at: https://doi.org/10.1006/clin.1995.1114.

Szeto, G.L. *et al.* (2010) 'Minocycline attenuates HIV infection and reactivation by suppressing cellular activation in human CD4+ T cells', *The Journal of Infectious Diseases*, 201(8), pp. 1132–1140. Available at: https://doi.org/10.1086/651277.

Szeto, G.L. *et al.* (2011a) 'Minocycline suppresses activation of nuclear factor of activated T cells 1 (NFAT1) in human CD4+ T cells', *The Journal of Biological Chemistry*, 286(13), pp. 11275–11282. Available at: https://doi.org/10.1074/jbc.M110.210518.

Szeto, G.L. *et al.* (2011b) 'Minocycline Suppresses Activation of Nuclear Factor of Activated T Cells 1 (NFAT1) in Human CD4+ T Cells *', *Journal of Biological Chemistry*, 286(13), pp. 11275–11282. Available at: https://doi.org/10.1074/jbc.M110.210518.

Szulzewsky, F. *et al.* (2015) 'Glioma-Associated Microglia/Macrophages Display an Expression Profile Different from M1 and M2 Polarization and Highly Express Gpnmb and Spp1', *PLoS ONE*, 10(2), p. e0116644. Available at: https://doi.org/10.1371/journal.pone.0116644.

Taddio, M.F. *et al.* (2021) 'In Vivo Imaging of Local Inflammation: Monitoring LPS-Induced CD80/CD86 Upregulation by PET', *Molecular Imaging and Biology*, 23(2), pp. 196–207. Available at: https://doi.org/10.1007/s11307-020-01543-3.

Tai, K. *et al.* (2013) 'Minocycline modulates cytokine and chemokine production in lipopolysaccharide-stimulated THP-1 monocytic cells by inhibiting IκB kinase α/β phosphorylation', *Translational Research*, 161(2), pp. 99–109. Available at: https://doi.org/10.1016/j.trsl.2012.10.001.

Takada, Y. *et al.* (2010) 'Monocyte chemoattractant protein-1 contributes to gut homeostasis and intestinal inflammation by composition of IL-10-producing regulatory macrophage subset', *Journal of Immunology (Baltimore, Md.: 1950)*, 184(5), pp. 2671–2676. Available at: https://doi.org/10.4049/jimmunol.0804012.

Takeda, K. *et al.* (1996) ‘Impaired IL-13-mediated functions of macrophages in STAT6-deficient mice.’, *The Journal of Immunology*, 157(8), pp. 3220–3222.

Takeda, K. *et al.* (1999) ‘Enhanced Th1 Activity and Development of Chronic Enterocolitis in Mice Devoid of Stat3 in Macrophages and Neutrophils’, *Immunity*, 10(1), pp. 39–49. Available at: https://doi.org/10.1016/S1074-7613(00)80005-9.

Takeuchi, O. and Akira, S. (2010) ‘Pattern recognition receptors and inflammation’, *Cell*, 140(6), pp. 805–820. Available at: https://doi.org/10.1016/j.cell.2010.01.022.

Tamura, Y. *et al.* (1999) ‘CD14 transgenic mice expressing membrane and soluble forms: comparisons of levels of cytokines and lethalities in response to lipopolysaccharide between transgenic and non-transgenic mice’, *International Immunology*, 11(3), pp. 333–339. Available at: https://doi.org/10.1093/intimm/11.3.333.

Tang, C. *et al.* (2014) ‘Antibiotic drug tigecycline inhibited cell proliferation and induced autophagy in gastric cancer cells’, *Biochemical and Biophysical Research Communications*, 446(1), pp. 105–112. Available at: https://doi.org/10.1016/j.bbrc.2014.02.043.

Tanita, K. *et al.* (2018) ‘Minocycline decreases Th2 chemokines from M2 macrophages: Possible mechanisms for the suppression of bullous pemphigoid by traditional bullous disease drugs’, *Experimental Dermatology*, 27(11), pp. 1268–1272. Available at: https://doi.org/10.1111/exd.13779.

Tao, R. *et al.* (2010) ‘Minocycline protects cardiac myocytes against simulated ischemia–reperfusion injury by inhibiting poly(ADP-ribose) polymerase-1’, *Journal of Cardiovascular Pharmacology*, 56(6), pp. 659–668. Available at: https://doi.org/10.1097/FJC.0b013e3181faeaf0.

Tao, T. *et al.* (2013) ‘Minocycline promotes axonal regeneration through suppression of RGMa in rat MCAO/reperfusion model’, *Synapse*, 67(4), pp. 189–198. Available at: https://doi.org/10.1002/syn.21629.

Targownik, L. and Bernstein, C. (2013) *Infectious and malignant complications of TNF inhibitor therapy in IBD.* Available at: https://reference.medscape.com/medline/abstract/24042192 (Accessed: 27 August 2021).

Tariq, S., Rizvi, S.F.A. and Anwar, U. (2018) ‘Tetracycline: Classification, Structure Activity Relationship and Mechanism of Action as a Theranostic Agent for Infectious Lesions-A Mini Review’, *Biomedical Journal of Scientific & Technical Research*, 7(2), pp. 001–010. Available at: https://doi.org/10.26717/BJSTR.2018.07.001475.

Tarique, A.A. *et al.* (2015) ‘Phenotypic, Functional, and Plasticity Features of Classical and Alternatively Activated Human Macrophages’, *American Journal of Respiratory Cell and Molecular Biology*, 53(5), pp. 676–688. Available at: https://doi.org/10.1165/rcmb.2015-0012OC.

Taylor, M.E. *et al.* (1990) ‘Primary structure of the mannose receptor contains multiple motifs resembling carbohydrate-recognition domains’, *The Journal of Biological Chemistry*, 265(21), pp. 12156–12162.

Taylor, P., Gordon, S. and Martinezpomares, L. (2005) ‘The mannose receptor: linking homeostasis and immunity through sugar recognition’, *Trends in Immunology*, 26(2), pp. 104–110. Available at: https://doi.org/10.1016/j.it.2004.12.001.

Teng, Y.D. *et al.* (2004) ‘Minocycline inhibits contusion-triggered mitochondrial cytochrome c release and mitigates functional deficits after spinal cord injury’, *Proceedings of the National Academy of Sciences of the United States of America*, 101(9), pp. 3071–3076. Available at: https://doi.org/10.1073/pnas.0306239101.

Thai, P. *et al.* (2005) ‘Differential Regulation of MUC5AC/Muc5ac and hCLCA-1/mGob-5 Expression in Airway Epithelium’, *American Journal of Respiratory Cell and Molecular Biology*, 33(6), pp. 523–530. Available at: https://doi.org/10.1165/rcmb.2004-0220RC.

Thiesen, S. *et al.* (2014) ‘CD14(hi)HLA-DR(dim) macrophages, with a resemblance to classical blood monocytes, dominate inflamed mucosa in Crohn’s disease’, *Journal of Leukocyte Biology*, 95(3), pp. 531–541. Available at: https://doi.org/10.1189/jlb.0113021.

Thomas, G.D. *et al.* (2016) ‘Deleting an Nr4a1 Super-Enhancer Subdomain Ablates Ly6Clow Monocytes while Preserving Macrophage Gene Function’, *Immunity*, 45(5), pp. 975–987. Available at: https://doi.org/10.1016/j.immuni.2016.10.011.

Thompson, C.D. *et al.* (2013) ‘The Therapeutic Role of Interleukin-10 after Spinal Cord Injury’, *Journal of Neurotrauma*, 30(15), pp. 1311–1324. Available at: https://doi.org/10.1089/neu.2012.2651.

Thomson, A.W. and Ezzelarab, M.B. (2018) ‘Regulatory dendritic cells: profiling, targeting and therapeutic application’, *Current opinion in organ transplantation*, 23(5), pp. 538–545. Available at: https://doi.org/10.1097/MOT.0000000000000565.

Thong, Y.H. and Ferrante, A. (1980) ‘Effect of tetracycline treatment on immunological responses in mice’, *Clinical and Experimental Immunology*, 39(3), pp. 728–732.

Ti, D. *et al.* (2015) ‘LPS-preconditioned mesenchymal stromal cells modify macrophage polarization for resolution of chronic inflammation via exosome-shuttled let-7b’, *Journal of Translational Medicine*, 13, p. 308. Available at: https://doi.org/10.1186/s12967-015-0642-6.

Tikka, T.M. and Koistinaho, J.E. (2001) ‘Minocycline provides neuroprotection against N-methyl-D-aspartate neurotoxicity by inhibiting microglia’, *Journal of Immunology (Baltimore, Md.: 1950)*, 166(12), pp. 7527–7533.

Tilley, B.C. (1995) 'Minocycline in Rheumatoid Arthritis: A 48-Week, Double-Blind, Placebo-Controlled Trial', *Annals of Internal Medicine*, 122(2), p. 81. Available at: https://doi.org/10.7326/0003-4819-122-2-199501150-00001.

Titos, E. *et al.* (2011) 'Resolvin D1 and Its Precursor Docosahexaenoic Acid Promote Resolution of Adipose Tissue Inflammation by Eliciting Macrophage Polarization toward an M2-Like Phenotype', *The Journal of Immunology*, 187(10), pp. 5408–5418. Available at: https://doi.org/10.4049/jimmunol.1100225.

Tjiu, J.-W. *et al.* (2009) 'Tumor-Associated Macrophage-Induced Invasion and Angiogenesis of Human Basal Cell Carcinoma Cells by Cyclooxygenase-2 Induction', *Journal of Investigative Dermatology*, 129(4), pp. 1016–1025. Available at: https://doi.org/10.1038/jid.2008.310.

Togo, T. *et al.* (2000) 'Expression of CD40 in the brain of Alzheimer's disease and other neurological diseases', *Brain Research*, 885(1), pp. 117–121. Available at: https://doi.org/10.1016/S0006-8993(00)02984-X.

Toshchakov, V. *et al.* (2002) 'TLR4, but not TLR2, mediates IFN-β–induced STAT1α/β-dependent gene expression in macrophages', *Nature Immunology* [Preprint]. Available at: https://doi.org/10.1038/ni774.

Truman, L.A. *et al.* (2008) 'CX3CL1/fractalkine is released from apoptotic lymphocytes to stimulate macrophage chemotaxis', *Blood*, 112(13), pp. 5026–5036. Available at: https://doi.org/10.1182/blood-2008-06-162404.

Tsukamoto, H. *et al.* (2018) 'Lipopolysaccharide (LPS)-binding protein stimulates CD14-dependent Toll-like receptor 4 internalization and LPS-induced TBK1-IKKε-IRF3 axis activation', *The Journal of Biological Chemistry*, 293(26), pp. 10186–10201. Available at: https://doi.org/10.1074/jbc.M117.796631.

Tugal Derin, Liao Xudong, and Jain Mukesh K. (2013) 'Transcriptional Control of Macrophage Polarization', *Arteriosclerosis, Thrombosis, and Vascular Biology*, 33(6), pp. 1135–1144. Available at: https://doi.org/10.1161/ATVBAHA.113.301453.

University of Florida (2020) *Angiotensin and Neuroimmune Activation in Hypertension*. Clinical trial registration NCT02133885. clinicaltrials.gov. Available at: https://clinicaltrials.gov/ct2/show/NCT02133885 (Accessed: 10 March 2021).

Vaure, C. and Liu, Y. (2014) 'A Comparative Review of Toll-Like Receptor 4 Expression and Functionality in Different Animal Species', *Frontiers in Immunology*, 5, p. 316. Available at: https://doi.org/10.3389/fimmu.2014.00316.

Veloso, P. *et al.* (2020) 'Macrophages skew towards M1 profile through reduced CD163 expression in symptomatic apical periodontitis', *Clinical Oral Investigations*, 24(12), pp. 4571–4581. Available at: https://doi.org/10.1007/s00784-020-03324-2.

Verreck, F.A.W. *et al.* (2006) 'Phenotypic and functional profiling of human proinflammatory type-1 and anti-inflammatory type-2 macrophages in response

to microbial antigens and IFN-gamma- and CD40L-mediated costimulation', *Journal of Leukocyte Biology*, 79(2), pp. 285–293. Available at: https://doi.org/10.1189/jlb.0105015.

Vetrano, S. *et al.* (2008) 'Unique Role of Junctional Adhesion Molecule-A in Maintaining Mucosal Homeostasis in Inflammatory Bowel Disease', *Gastroenterology*, 135(1), pp. 173–184. Available at: https://doi.org/10.1053/j.gastro.2008.04.002.

Villanueva, C.J. and Tontonoz, P. (2010) 'Licensing PPARγ to work in macrophages', *Immunity*, 33(5), pp. 647–649. Available at: https://doi.org/10.1016/j.immuni.2010.11.017.

Viola, M.F. and Boeckxstaens, G. (2020) 'Intestinal resident macrophages: Multitaskers of the gut', *Neurogastroenterology and Motility*, 32(8), p. e13843. Available at: https://doi.org/10.1111/nmo.13843.

Vliet, S.J. van *et al.* (2013) 'MGL signaling augments TLR2-mediated responses for enhanced IL-10 and TNF-α secretion', *Journal of Leukocyte Biology*, 94(2), pp. 315–323. Available at: https://doi.org/10.1189/jlb.1012520.

Vogel, D.Y.S. *et al.* (2014) 'Human macrophage polarization in vitro: Maturation and activation methods compared', *Immunobiology*, 219(9), pp. 695–703. Available at: https://doi.org/10.1016/j.imbio.2014.05.002.

Vong, L. *et al.* (2010) 'A pro-resolution mediator, prostaglandin D2, is specifically up-regulated in individuals in long-term remission from ulcerative colitis', *Proceedings of the National Academy of Sciences of the United States of America*, 107(26), pp. 12023–12027. Available at: https://doi.org/10.1073/pnas.1004982107.

Vos, A.C.W. *et al.* (2012) 'Regulatory Macrophages Induced by Infliximab Are Involved in Healing In Vivo and In Vitro', *Inflammatory Bowel Diseases*, 18(3), pp. 401–408. Available at: https://doi.org/10.1002/ibd.21818.

Waddell, A. *et al.* (2011) 'Colonic eosinophilic inflammation in experimental colitis is mediated by Ly6Chigh CCR2+ inflammatory monocyte/macrophage-derived CCL11', *Journal of immunology (Baltimore, Md. : 1950)*, 186(10), pp. 5993–6003. Available at: https://doi.org/10.4049/jimmunol.1003844.

Walker, D.G. and Lue, L.-F. (2015) 'Immune phenotypes of microglia in human neurodegenerative disease: challenges to detecting microglial polarization in human brains', *Alzheimer's Research & Therapy*, 7(1), p. 56. Available at: https://doi.org/10.1186/s13195-015-0139-9.

Wallace, K.L. *et al.* (2014) 'Immunopathology of inflammatory bowel disease', *World Journal of Gastroenterology : WJG*, 20(1), pp. 6–21. Available at: https://doi.org/10.3748/wjg.v20.i1.6.

Walz, W. and Cayabyab, F.S. (2017) 'Neutrophil Infiltration and Matrix Metalloproteinase-9 in Lacunar Infarction', *Neurochemical Research*, 42(9), pp. 2560–2565. Available at: https://doi.org/10.1007/s11064-017-2265-1.

Wan, S. and Sun, H. (2019) ‘Glucagon-like peptide-1 modulates RAW264.7 macrophage polarization by interfering with the JNK/STAT3 signaling pathway’, *Experimental and Therapeutic Medicine*, 17(5), pp. 3573–3579. Available at: https://doi.org/10.3892/etm.2019.7347.

Wang, B. *et al.* (2017) ‘Inhibition of mitochondrial translation effectively sensitizes renal cell carcinoma to chemotherapy’, *Biochemical and Biophysical Research Communications*, 490(3), pp. 767–773. Available at: https://doi.org/10.1016/j.bbrc.2017.06.115.

Wang, F. *et al.* (2018) ‘Interferon Gamma Induces Reversible Metabolic Reprogramming of M1 Macrophages to Sustain Cell Viability and Pro-Inflammatory Activity’, *EBioMedicine*, 30, pp. 303–316. Available at: https://doi.org/10.1016/j.ebiom.2018.02.009.

Wang, J. (2018) ‘Neutrophils in tissue injury and repair’, *Cell and Tissue Research*, 371(3), pp. 531–539. Available at: https://doi.org/10.1007/s00441-017-2785-7.

Wang, J., Chen, W.-D. and Wang, Y.-D. (2020) ‘The Relationship Between Gut Microbiota and Inflammatory Diseases: The Role of Macrophages’, *Frontiers in Microbiology*, 11, p. 1065. Available at: https://doi.org/10.3389/fmicb.2020.01065.

Wang, N., Liang, H. and Zen, K. (2014a) ‘Molecular Mechanisms That Influence the Macrophage M1–M2 Polarization Balance’, *Frontiers in Immunology*, 5. Available at: https://doi.org/10.3389/fimmu.2014.00614.

Wang, N., Liang, H. and Zen, K. (2014b) ‘Molecular Mechanisms That Influence the Macrophage M1–M2 Polarization Balance’, *Frontiers in Immunology*, 5. Available at: https://doi.org/10.3389/fimmu.2014.00614.

Wang, X. *et al.* (2003) ‘Minocycline inhibits caspase-independent and -dependent mitochondrial cell death pathways in models of Huntington’s disease’, *Proceedings of the National Academy of Sciences of the United States of America*, 100(18), pp. 10483–10487. Available at: https://doi.org/10.1073/pnas.1832501100.

Wang, Y. *et al.* (2019) ‘M1 and M2 macrophage polarization and potentially therapeutic naturally occurring compounds’, *International Immunopharmacology*, 70, pp. 459–466. Available at: https://doi.org/10.1016/j.intimp.2019.02.050.

Wang, Y. *et al.* (2020) ‘Interleukin-6 knockout reverses macrophage differentiation imbalance and alleviates cardiac dysfunction in aging mice’, *Aging (Albany NY)*, 12(20), pp. 20184–20197. Available at: https://doi.org/10.18632/aging.103749.

Wang, Y.-M. *et al.* (2019) ‘Paclitaxel alleviated sepsis-induced acute lung injury by activating MUC1 and suppressing TLR-4/NF-κB pathway’, *Drug Design, Development and Therapy*, 13, pp. 3391–3404. Available at: https://doi.org/10.2147/DDDT.S222296.

Warren, C.F.A., Wong-Brown, M.W. and Bowden, N.A. (2019) 'BCL-2 family isoforms in apoptosis and cancer', *Cell Death & Disease*, 10(3), pp. 1–12. Available at: https://doi.org/10.1038/s41419-019-1407-6.

Wasserman, J.K. and Schlichter, L.C. (2007) 'Minocycline protects the blood–brain barrier and reduces edema following intracerebral hemorrhage in the rat', *Experimental Neurology*, 207(2), pp. 227–237. Available at: https://doi.org/10.1016/j.expneurol.2007.06.025.

Watanabe, S. *et al.* (2019) 'The role of macrophages in the resolution of inflammation', *The Journal of Clinical Investigation*, 129(7), pp. 2619–2628. Available at: https://doi.org/10.1172/JCI124615.

Weaver, L.K. *et al.* (2007) 'Up-regulation of human monocyte CD163 upon activation of cell-surface Toll-like receptors', *Journal of Leukocyte Biology*, 81(3), pp. 663–671. Available at: https://doi.org/10.1189/jlb.0706428.

Webster, G. and Del Rosso, J.Q. (2007) 'Anti-inflammatory activity of tetracyclines', *Dermatologic Clinics*, 25(2), pp. 133–135, v. Available at: https://doi.org/10.1016/j.det.2007.01.012.

Webster, G.F., McGinley, K.J. and Leyden, J.J. (1981) 'Inhibition of lipase production in Propionibacterium acnes by sub-minimal-inhibitory concentrations of tetracycline and erythromycin', *The British Journal of Dermatology*, 104(4), pp. 453–457.

Wei, Y. and Bechhofer, D.H. (2002) 'Tetracycline Induces Stabilization of mRNA in Bacillus subtilis', *Journal of Bacteriology*, 184(4), pp. 889–894. Available at: https://doi.org/10.1128/jb.184.4.889-894.2002.

Weiler, J. and Dittmar, T. (2019) 'Minocycline impairs TNF-α-induced cell fusion of M13SV1-Cre cells with MDA-MB-435-pFDR1 cells by suppressing NF-κB transcriptional activity and its induction of target-gene expression of fusion-relevant factors', *Cell Communication and Signaling : CCS*, 17. Available at: https://doi.org/10.1186/s12964-019-0384-9.

Weisberg, S.P. *et al.* (2003) 'Obesity is associated with macrophage accumulation in adipose tissue', *Journal of Clinical Investigation*, 112(12), pp. 1796–1808. Available at: https://doi.org/10.1172/JCI200319246.

Weisser, S.B. *et al.* (2011) 'SHIP-deficient, alternatively activated macrophages protect mice during DSS-induced colitis', *Journal of Leukocyte Biology*, 90(3), pp. 483–492. Available at: https://doi.org/10.1189/jlb.0311124.

Werdin, F. *et al.* (2009) 'Evidence-based management strategies for treatment of chronic wounds', *Eplasty*, 9.

Wieczorek, M. *et al.* (2017) 'Major Histocompatibility Complex (MHC) Class I and MHC Class II Proteins: Conformational Plasticity in Antigen Presentation', *Frontiers in Immunology*, 8, p. 292. Available at: https://doi.org/10.3389/fimmu.2017.00292.

Wienerroither, S. *et al.* (2015) ‘Cooperative Transcriptional Activation of Antimicrobial Genes by STAT and NF-κB Pathways by Concerted Recruitment of the Mediator Complex’, *Cell Reports*, 12(2), pp. 300–312. Available at: https://doi.org/10.1016/j.celrep.2015.06.021.

Williams, D.N., Laughlin, L.W. and Lee, Y.H. (1974) ‘Minocycline: Possible vestibular side-effects’, *Lancet (London, England)*, 2(7883), pp. 744–746. Available at: https://doi.org/10.1016/s0140-6736(74)90941-6.

Williams, R.O., Feldmann, M. and Maini, R.N. (1992) ‘Anti-tumor necrosis factor ameliorates joint disease in murine collagen-induced arthritis.’, *Proceedings of the National Academy of Sciences*, 89(20), pp. 9784–9788. Available at: https://doi.org/10.1073/pnas.89.20.9784.

Wolf, D. *et al.* (2018) ‘A ligand-specific blockade of the integrin Mac-1 selectively targets pathologic inflammation while maintaining protective host-defense’, *Nature Communications*, 9(1), p. 525. Available at: https://doi.org/10.1038/s41467-018-02896-8.

Wu, D.C. *et al.* (2002) ‘Blockade of Microglial Activation Is Neuroprotective in the 1-Methyl-4-Phenyl-1,2,3,6-Tetrahydropyridine Mouse Model of Parkinson Disease’, *The Journal of Neuroscience*, 22(5), pp. 1763–1771. Available at: https://doi.org/10.1523/JNEUROSCI.22-05-01763.2002.

Wu, H. *et al.* (2012) ‘Tumor-associated macrophages promote angiogenesis and lymphangiogenesis of gastric cancer’, *Journal of Surgical Oncology*, 106(4), pp. 462–468. Available at: https://doi.org/10.1002/jso.23110.

Wynn, T.A. (2004) ‘FIBROTIC DISEASE AND THE TH1/TH2 PARADIGM’, *Nature reviews. Immunology*, 4(8), pp. 583–594. Available at: https://doi.org/10.1038/nri1412.

Wynn, T.A., Chawla, A. and Pollard, J.W. (2013) ‘Origins and Hallmarks of Macrophages: Development, Homeostasis, and Disease’, *Nature*, 496(7446), pp. 445–455. Available at: https://doi.org/10.1038/nature12034.

Xia, D. *et al.* (2011) ‘Administration of minocycline ameliorates damage in a renal ischemia/reperfusion injury model’, *Clinical and Investigative Medicine. Medecine Clinique Et Experimentale*, 34(2), pp. E55-63. Available at: https://doi.org/10.25011/cim.v34i1.15101.

Xu, W. *et al.* (2013) ‘Reversible differentiation of pro- and anti-inflammatory macrophages’, *Molecular Immunology*, 53(3), pp. 179–186. Available at: https://doi.org/10.1016/j.molimm.2012.07.005.

Xue, J. *et al.* (2014) ‘Transcriptome-Based Network Analysis Reveals a Spectrum Model of Human Macrophage Activation’, *Immunity*, 40(2), pp. 274–288. Available at: https://doi.org/10.1016/j.immuni.2014.01.006.

Yamamoto, M. *et al.* (2000) ‘IL-6 Is Required for the Development of Th1 Cell-Mediated Murine Colitis’, *The Journal of Immunology*, 164(9), pp. 4878–4882. Available at: https://doi.org/10.4049/jimmunol.164.9.4878.

Yamamoto, Y. *et al.* (2011) 'Septic Shock Is Associated with Receptor for Advanced Glycation End Products Ligation of LPS', *The Journal of Immunology*, 186(5), pp. 3248–3257. Available at: https://doi.org/10.4049/jimmunol.1002253.

Yan, G. *et al.* (2018) 'Levels of peripheral Th17 cells and serum Th17-related cytokines in patients with colorectal cancer: a meta-analysis', *Cellular and Molecular Biology (Noisy-Le-Grand, France)*, 64(6), pp. 94–102.

Yan, T.-D. *et al.* (2010) 'Oncogenic Potential of Retinoic Acid Receptor-γ in Hepatocellular Carcinoma', *Cancer Research*, 70(6), pp. 2285–2295. Available at: https://doi.org/10.1158/0008-5472.CAN-09-2968.

Yang, J. *et al.* (2018) 'Sphingosine 1-Phosphate (S1P)/S1P Receptor2/3 Axis Promotes Inflammatory M1 Polarization of Bone Marrow-Derived Monocyte/Macrophage via G(α)i/o/PI3K/JNK Pathway', *Cellular Physiology and Biochemistry: International Journal of Experimental Cellular Physiology, Biochemistry, and Pharmacology*, 49(5), pp. 1677–1693. Available at: https://doi.org/10.1159/000493611.

Yang, T. *et al.* (2015) 'Gut dysbiosis is linked to hypertension', *Hypertension (Dallas, Tex.: 1979)*, 65(6), pp. 1331–1340. Available at: https://doi.org/10.1161/HYPERTENSIONAHA.115.05315.

Yang, Y. *et al.* (2013) 'Colon Macrophages Polarized by Commensal Bacteria Cause Colitis and Cancer through the Bystander Effect', *Translational Oncology*, 6(5), pp. 596-IN8. Available at: https://doi.org/10.1593/tlo.13412.

Yang, Y. *et al.* (2021) 'Cross-talk between the gut microbiota and monocyte-like macrophages mediates an inflammatory response to promote colitis-associated tumourigenesis', *Gut*, 70(8), pp. 1495–1506. Available at: https://doi.org/10.1136/gutjnl-2020-320777.

Yang, Y. *et al.* (2015) 'Attenuation of acute stroke injury in rat brain by minocycline promotes blood–brain barrier remodeling and alternative microglia/macrophage activation during recovery', *Journal of Neuroinflammation*, 12(1), p. 26. Available at: https://doi.org/10.1186/s12974-015-0245-4.

Yao, J.S. *et al.* (2007) 'Comparison of doxycycline and minocycline in the inhibition of VEGF-induced smooth muscle cell migration', *Neurochemistry International*, 50(3), pp. 524–530. Available at: https://doi.org/10.1016/j.neuint.2006.10.008.

Yao, S., Zhu, Y. and Chen, L. (2013) 'Advances in targeting cell surface signalling molecules for immune modulation', *Nature reviews. Drug discovery*, 12(2), pp. 130–146. Available at: https://doi.org/10.1038/nrd3877.

Yoon, P. *et al.* (2004) 'Macrophage hypo-responsiveness to interferon-γ in aged mice is associated with impaired signaling through Jak-STAT', *Mechanisms of Ageing and Development*, 125(2), pp. 137–143. Available at: https://doi.org/10.1016/j.mad.2003.11.010.

You, Y. *et al.* (2016) ‘Sorting nexin 10 acting as a novel regulator of macrophage polarization mediates inflammatory response in experimental mouse colitis’, *Scientific Reports*, 6(1), p. 20630. Available at: https://doi.org/10.1038/srep20630.

Yrjänheikki, J. *et al.* (1998) ‘Tetracyclines inhibit microglial activation and are neuroprotective in global brain ischemia’, *Proceedings of the National Academy of Sciences of the United States of America*, 95(26), pp. 15769–15774.

Yrjänheikki, J. *et al.* (1999) ‘A tetracycline derivative, minocycline, reduces inflammation and protects against focal cerebral ischemia with a wide therapeutic window’, *Proceedings of the National Academy of Sciences of the United States of America*, 96(23), pp. 13496–13500.

Yu, J. *et al.* (2006) ‘Pro- and antiinflammatory cytokine signaling: reciprocal antagonism regulates interferon-gamma production by human natural killer cells’, *Immunity*, 24(5), pp. 575–590. Available at: https://doi.org/10.1016/j.immuni.2006.03.016.

Yu, T. *et al.* (2019) ‘Modulation of M2 macrophage polarization by the crosstalk between Stat6 and Trim24’, *Nature Communications*, 10, p. 4353. Available at: https://doi.org/10.1038/s41467-019-12384-2.

Yuan, Z. *et al.* (2019) ‘The anti-inflammatory effect of minocycline on endotoxin-induced uveitis and retinal inflammation in rats’, *Molecular Vision*, 25, pp. 359–372.

Yunna, C. *et al.* (2020) ‘Macrophage M1/M2 polarization’, *European Journal of Pharmacology*, 877, p. 173090. Available at: https://doi.org/10.1016/j.ejphar.2020.173090.

Zakeri, B. and Wright, G.D. (2008) ‘Chemical biology of tetracycline antibiotics’, *Biochemistry and Cell Biology = Biochimie Et Biologie Cellulaire*, 86(2), pp. 124–136. Available at: https://doi.org/10.1139/O08-002.

Zamani, F. *et al.* (2013) ‘Induction of CD14 Expression and Differentiation to Monocytes or Mature Macrophages in Promyelocytic Cell Lines: New Approach’, *Advanced Pharmaceutical Bulletin*, 3(2), pp. 329–332. Available at: https://doi.org/10.5681/apb.2013.053.

Zamze, S. *et al.* (2002) ‘Recognition of bacterial capsular polysaccharides and lipopolysaccharides by the macrophage mannose receptor’, *The Journal of Biological Chemistry*, 277(44), pp. 41613–41623. Available at: https://doi.org/10.1074/jbc.M207057200.

Zhang, B. *et al.* (2019) ‘Low-intensity pulsed ultrasound suppresses synovitis by modulating polarization of synovial macrophages in mice with osteoarthritis’, 第三军医大学学报, 41(08), pp. 747–756. Available at: https://doi.org/10.16016/j.1000-5404.201901091.

Zhang, C. *et al.* (2004) ‘Neuroprotection of photoreceptors by minocycline in light-induced retinal degeneration’, *Investigative Ophthalmology & Visual*

Science, 45(8), pp. 2753–2759. Available at: https://doi.org/10.1167/iovs.03-1344.

Zhang, J. *et al.* (2020) 'Bone marrow mesenchymal stem cell-derived exosomes prevent osteoarthritis by regulating synovial macrophage polarization', *Aging (Albany NY)*, 12(24), pp. 25138–25152. Available at: https://doi.org/10.18632/aging.104110.

Zhang, L. and Li, S. (2020) 'Lactic acid promotes macrophage polarization through MCT-HIF1α signaling in gastric cancer', *Experimental Cell Research*, 388(2), p. 111846. Available at: https://doi.org/10.1016/j.yexcr.2020.111846.

Zhang, M.-Z. *et al.* (2017) 'IL-4/IL-13–mediated polarization of renal macrophages/dendritic cells to an M2a phenotype is essential for recovery from acute kidney injury', *Kidney international*, 91(2), pp. 375–386. Available at: https://doi.org/10.1016/j.kint.2016.08.020.

Zhang, X. and Mosser, D.M. (2008) 'Macrophage activation by endogenous danger signals', *The Journal of Pathology*, 214(2), pp. 161–178. Available at: https://doi.org/10.1002/path.2284.

Zhang, Y. *et al.* (2013) 'ROS play a critical role in the differentiation of alternatively activated macrophages and the occurrence of tumor-associated macrophages', *Cell Research*, 23(7), pp. 898–914. Available at: https://doi.org/10.1038/cr.2013.75.

Zhang, Y. and Rom, W.N. (1993) 'Regulation of the interleukin-1 beta (IL-1 beta) gene by mycobacterial components and lipopolysaccharide is mediated by two nuclear factor-IL6 motifs.', *Molecular and Cellular Biology*, 13(6), pp. 3831–3837.

Zhao, S. *et al.* (2020) 'Tumor-derived exosomal miR-934 induces macrophage M2 polarization to promote liver metastasis of colorectal cancer', *Journal of Hematology & Oncology*, 13, p. 156. Available at: https://doi.org/10.1186/s13045-020-00991-2.

Zhao, Y. *et al.* (2015) 'Minocycline upregulates cyclic AMP response element binding protein and brain-derived neurotrophic factor in the hippocampus of cerebral ischemia rats and improves behavioral deficits', *Neuropsychiatric Disease and Treatment*, 11, pp. 507–516. Available at: https://doi.org/10.2147/NDT.S73836.

Zhen, Y. and Zhang, H. (2019) 'NLRP3 Inflammasome and Inflammatory Bowel Disease', *Frontiers in Immunology*, 10, p. 276. Available at: https://doi.org/10.3389/fimmu.2019.00276.

Zhong, Z., Wen, Z. and Darnell, J.E. (1994) 'Stat3: a STAT family member activated by tyrosine phosphorylation in response to epidermal growth factor and interleukin-6', *Science (New York, N.Y.)*, 264(5155), pp. 95–98. Available at: https://doi.org/10.1126/science.8140422.

Zhou, D. *et al.* (2014) 'Macrophage polarization and function with emphasis on the evolving roles of coordinated regulation of cellular signaling pathways',

Cellular Signalling, 26(2), pp. 192–197. Available at: https://doi.org/10.1016/j.cellsig.2013.11.004.

Zhou, H. *et al.* (2013) 'CD11b/CD18 (Mac-1) Is a Novel Surface Receptor for Extracellular Double-stranded RNA to Mediate Cellular Inflammatory Responses', *Journal of immunology (Baltimore, Md. : 1950)*, 190(1), pp. 115–125. Available at: https://doi.org/10.4049/jimmunol.1202136.

Zhou, Y.-Q. *et al.* (2018) 'Minocycline as a promising therapeutic strategy for chronic pain', *Pharmacological Research*, 134, pp. 305–310. Available at: https://doi.org/10.1016/j.phrs.2018.07.002.

Zhu, J. (2015) 'T helper 2 (Th2) cell differentiation, type 2 innate lymphoid cell (ILC2) development and regulation of interleukin-4 (IL-4) and IL-13 production', *Cytokine*, 75(1), pp. 14–24. Available at: https://doi.org/10.1016/j.cyto.2015.05.010.

Zhu, J. and Paul, W.E. (2008) 'CD4 T cells: fates, functions, and faults', *Blood*, 112(5), pp. 1557–1569. Available at: https://doi.org/10.1182/blood-2008-05-078154.

Zhu, S. *et al.* (2002) 'Minocycline inhibits cytochrome c release and delays progression of amyotrophic lateral sclerosis in mice', *Nature*, 417(6884), pp. 74–78. Available at: https://doi.org/10.1038/417074a.

Zhu, S., Davis, T.N. and Kung, A.L. (2009) 'Activation of PI3K p110α by minocycline leads to cell dysfunction and cell death in 9L glioma', *Cancer Research*, 69(23 Supplement), pp. A69–A69. Available at: https://doi.org/10.1158/0008-5472.FBCR09-A69.

Zhu, W. *et al.* (2014) 'Disequilibrium of M1 and M2 Macrophages Correlates with the Development of Experimental Inflammatory Bowel Diseases', *Immunological investigations* [Preprint]. Available at: https://doi.org/10.3109/08820139.2014.909456.

Zigmond, E. *et al.* (2012) 'Ly6C hi monocytes in the inflamed colon give rise to proinflammatory effector cells and migratory antigen-presenting cells', *Immunity*, 37(6), pp. 1076–1090. Available at: https://doi.org/10.1016/j.immuni.2012.08.026.

Zigmond, E. *et al.* (2014) 'Macrophage-restricted interleukin-10 receptor deficiency, but not IL-10 deficiency, causes severe spontaneous colitis', *Immunity*, 40(5), pp. 720–733. Available at: https://doi.org/10.1016/j.immuni.2014.03.012.

Zigmond, E. and Jung, S. (2013) 'Intestinal macrophages: well educated exceptions from the rule', *Trends in Immunology*, 34(4), pp. 162–168. Available at: https://doi.org/10.1016/j.it.2013.02.001.

Zimmermann, P. *et al.* (2018) 'The Immunomodulatory Effects of Macrolides—A Systematic Review of the Underlying Mechanisms', *Frontiers in Immunology*, 9, p. 302. Available at: https://doi.org/10.3389/fimmu.2018.00302.

9. Appendix

A1: Product information table

Application	Product	Supplier
Cell Culture	Gibco™ RPMI 1640 Media	Thermo Fisher Scientific, UK
	Foetal Bovine Serum	Sigma Aldrich/Merck, UK
	Dimethyl Sulfoxide	Sigma Aldrich/Merck, UK
	Minocycline Hydrochloride	Sigma Aldrich/Merck, UK
	Dexamethasone	Sigma Aldrich/Merck, UK
	Corning™ Trypan Blue	Thermo Fisher Scientific, UK
	Phorbol 12-myristate 13-acetate	Apollo Scientific Ltd, UK
	Recombinant Human IFN-γ (carrier-free)	BioLegend®, UK
	Recombinant Human IL-4 (293E-expressed) (carrier-free)	BioLegend®, UK
	Recombinant Human IL-13 (carrier-free)	BioLegend®, UK
	Lipopolysaccharides from *Escherichia coli* O55:B5	Sigma Aldrich/Merck, UK
	Accutase® Cell Detachment Solution	BioLegend®, UK
	Recombinant Human M-CSF	PeproTech Inc, UK
	Histopaque-1077	Scientific Laboratory Supplies (SLS), UK
	Histopaque®-1119	Sigma Aldrich/Merck, UK
PBS	Potassium Chloride	Sigma Aldrich/Merck, UK
	Sodium Chloride	Sigma Aldrich/Merck, UK
	Sodium Phosphate Dibasic	Sigma Aldrich/Merck, UK
	Potassium Phosphate Monobasic	Sigma Aldrich/Merck, UK
Flow Cytometry	BD™ CD&T Beads	BD Biosciences, UK
	Anti-Mouse Ig, κ/Negative Control Compensation Particles Set	BD Biosciences, UK
	CD80 Brilliant Violet 650™ (2D10)	BioLegend®, UK
	CD163 Brilliant Violet 711™ (VI M38)	BioLegend®, UK
	CD206 Brilliant Violet 785™ (15-2)	BioLegend®, UK
	CD11b PE/Cyanine7 (CBRM1/5)	BioLegend®, UK
	CD86 PE (BU63)	BioLegend®, UK
	CD14 FITC (63D3)	BioLegend®, UK
	CD11b Brilliant Violet 785™ (ICRF44)	BioLegend®, UK
	CD206 PerCP/Cyanine5.5 (15-2)	BioLegend®, UK
	Human TruStain FcX™	BioLegend®, UK
	Zombie Aqua™ Fixable Viability Kit	BioLegend®, UK
	FluoroFix™ Buffer	BioLegend®, UK
RT-qPCR	KicqStart® SYBR® Green Primers	Sigma Aldrich/Merck, UK
	LunaScript® RT SuperMix Kit	New England Biolabs (NEB), UK

	Luna® Universal qPCR Master Mix	New England Biolabs (NEB), UK
	Monarch Total RNA Miniprep Kit	New England Biolabs (NEB), UK
	RNaseZAP™	Sigma Aldrich/Merck, UK
	Nuclease-free Water	Sigma Aldrich/Merck, UK
ELISA	LEGENDplex™ Human Macrophage/Microglia Panel (13-plex) with V-bottom Plate	BioLegend®, UK
	Human IL-12 (p70) ELISA MAX™ Deluxe Set	BioLegend®, UK
	Human IL-12/IL-23 (p40) ELISA MAX™ Deluxe Set	BioLegend®, UK
	Human IL-10 ELISA MAX™ Deluxe Set	BioLegend®, UK
	Human IL-4 ELISA MAX™ Deluxe Set	BioLegend®, UK
	Human IFN-γ ELISA MAX™ Deluxe Set	BioLegend®, UK
	Human TNF-α Uncoated ELISA	Invitrogen, Thermo Fisher Scientific, UK
	Human IL-6 Uncoated ELISA	Invitrogen, Thermo Fisher Scientific, UK
	Human IL-1β Uncoated ELISA	Invitrogen, Thermo Fisher Scientific, UK
	Stop Solution for TMB Substrate	BioLegend®, UK
	TWEEN® 20	Sigma Aldrich/Merck, UK
	Nunc Immuno Plate F96 Maxisorp	SLS Scientific Laboratory Supplies, UK
ICFC	Cell Staining Buffer	BioLegend®, UK
	Fixation Buffer	BioLegend®, UK
	True-Phos™ Perm Buffer	BioLegend®, UK
	FITC anti-STAT3 Phospho (Tyr705) (13A3-1)	BioLegend®, UK
	PE anti-human STAT3 (15H2B45)	BioLegend®, UK
	FITC Mouse IgG1, κ isotype Ctrl (MOPC-21)	BioLegend®, UK
	PE Mouse IgG1, κ isotype Ctrl (MOPC-21)	BioLegend®, UK

A2: U-937 PMA-induced monocyte-macrophage differentiation: protocol optimization

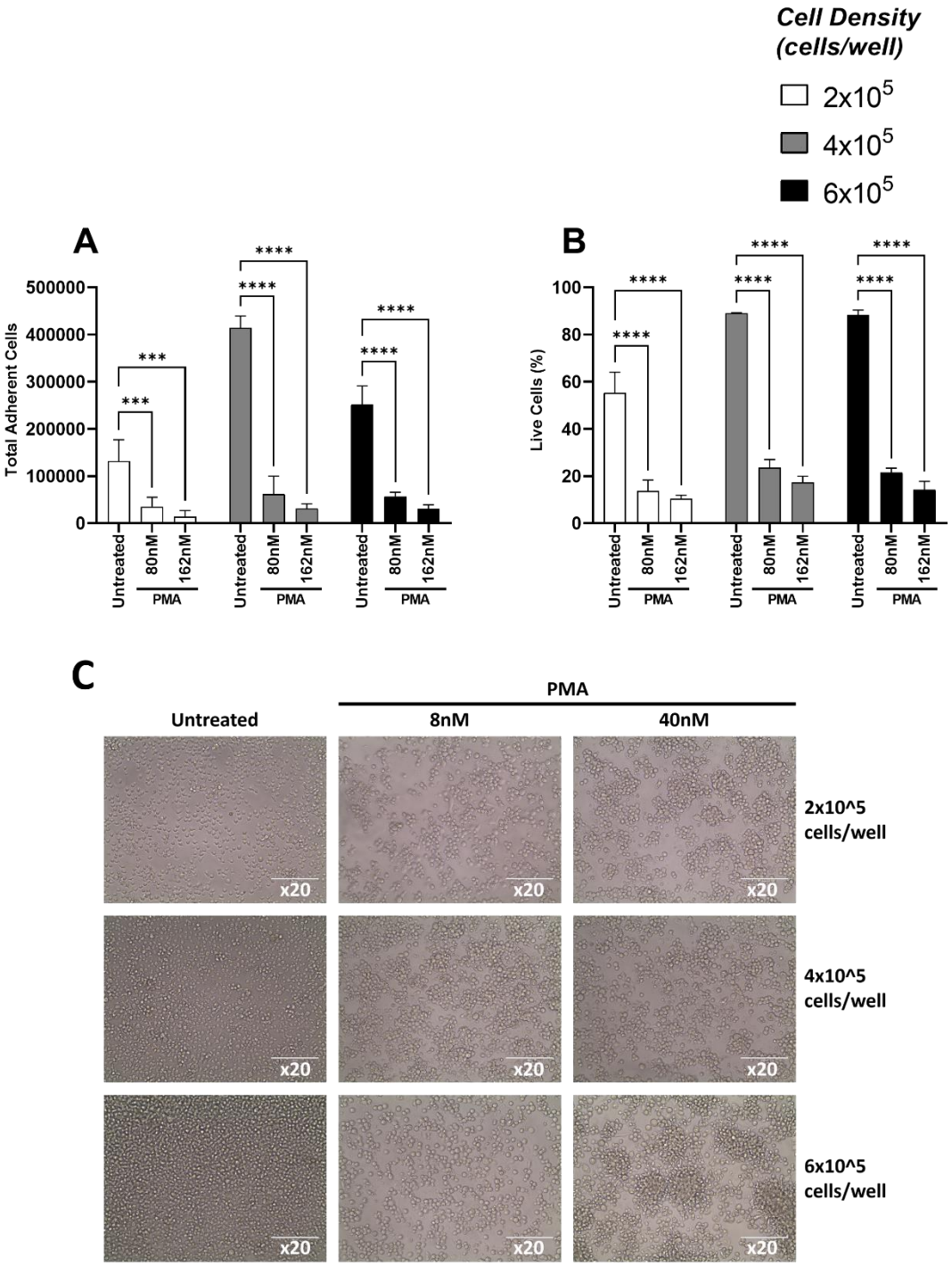

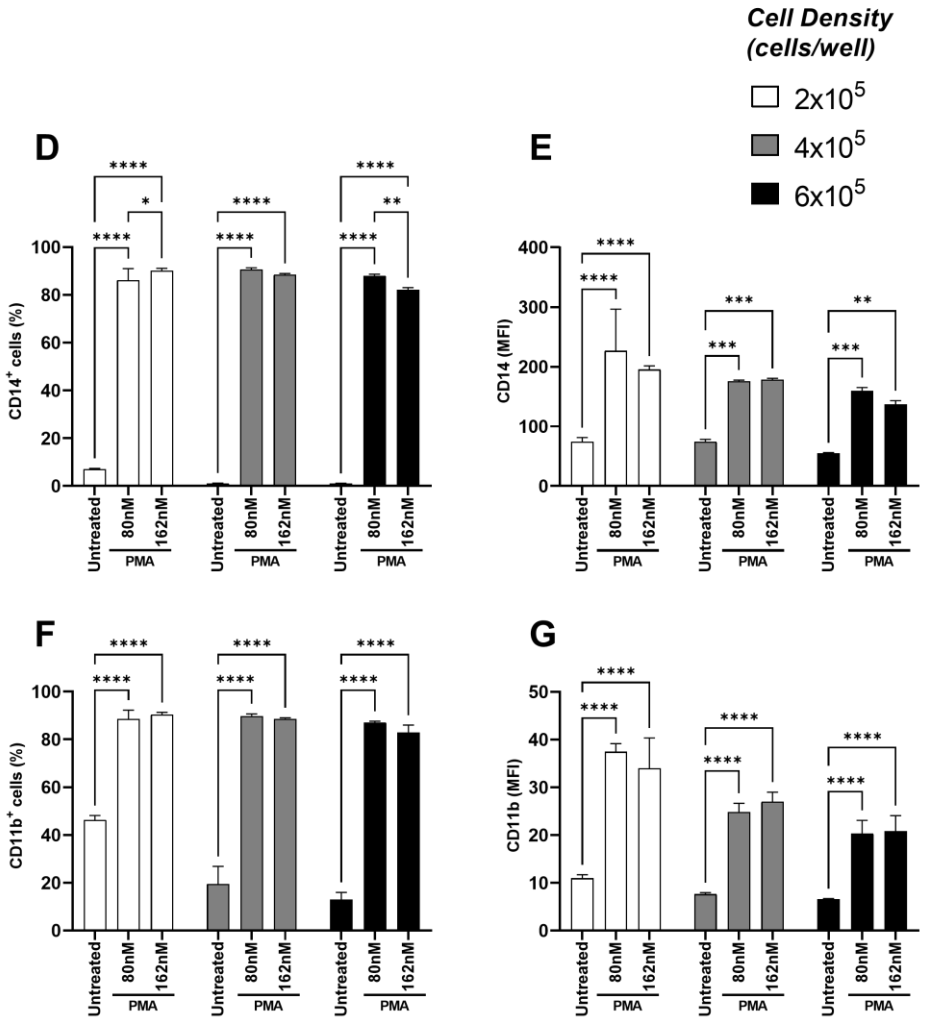

A2.1: Optimization 1 - Assessment of total adherent cell counts, viability, and CD14 and CD11b surface marker expression with different cell seeding densities and PMA titrations. Data obtained after 48hr PMA treatment at either 80nM or 162nM, followed by 72hr resting in replenished media. Bar graphs showing; [A] total number of adherent cells recovered [B] adherent cell viability [C] Microscopic images taken at x20 magnification [D] percentage of $CD14^+$ cells [E] percentage of $CD11b^+$ cells [F] MFI values for CD14 [G] MFI values for CD11b. Data represents 1 experiment comprising triplicate values. Data presented as Mean ± SD. Images present 1 representative well from each condition. One-way ANOVA with post hoc Bonferroni. *p<0.05; **p<0.01; ***p<0.001; ****p<0.0001.

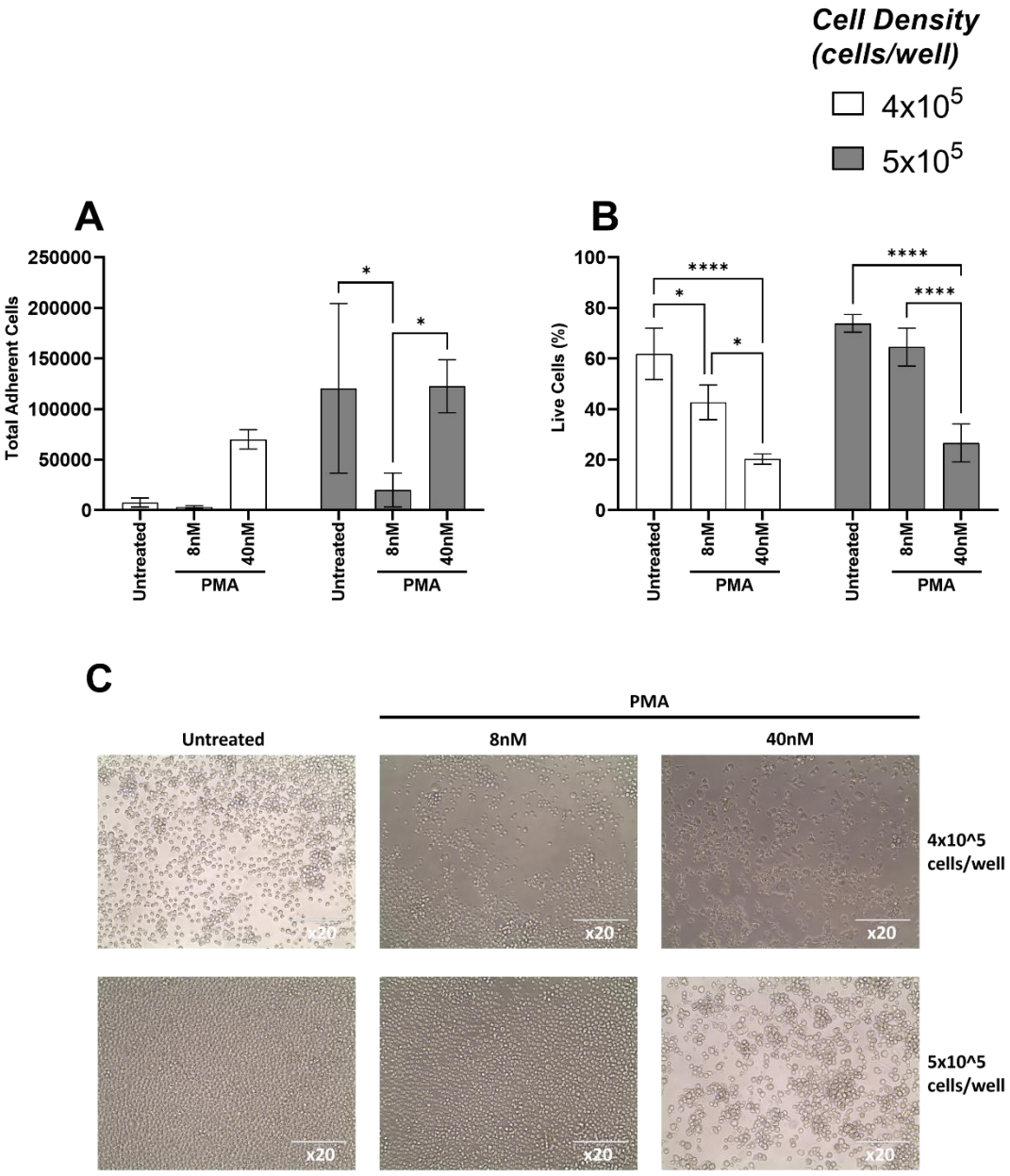
Cell Density
(cells/well)
4x10^5
5x10^5
A
Total Adherent Cells
250000
200000
150000
100000
50000
0
Untreated
8nM
40nM
PMA
B
Live Cells (%)
100
80
60
40
20
0
****
*
C
PMA
Untreated
8nM
40nM
4x10^5
cells/well
5x10^5
cells/well
x20

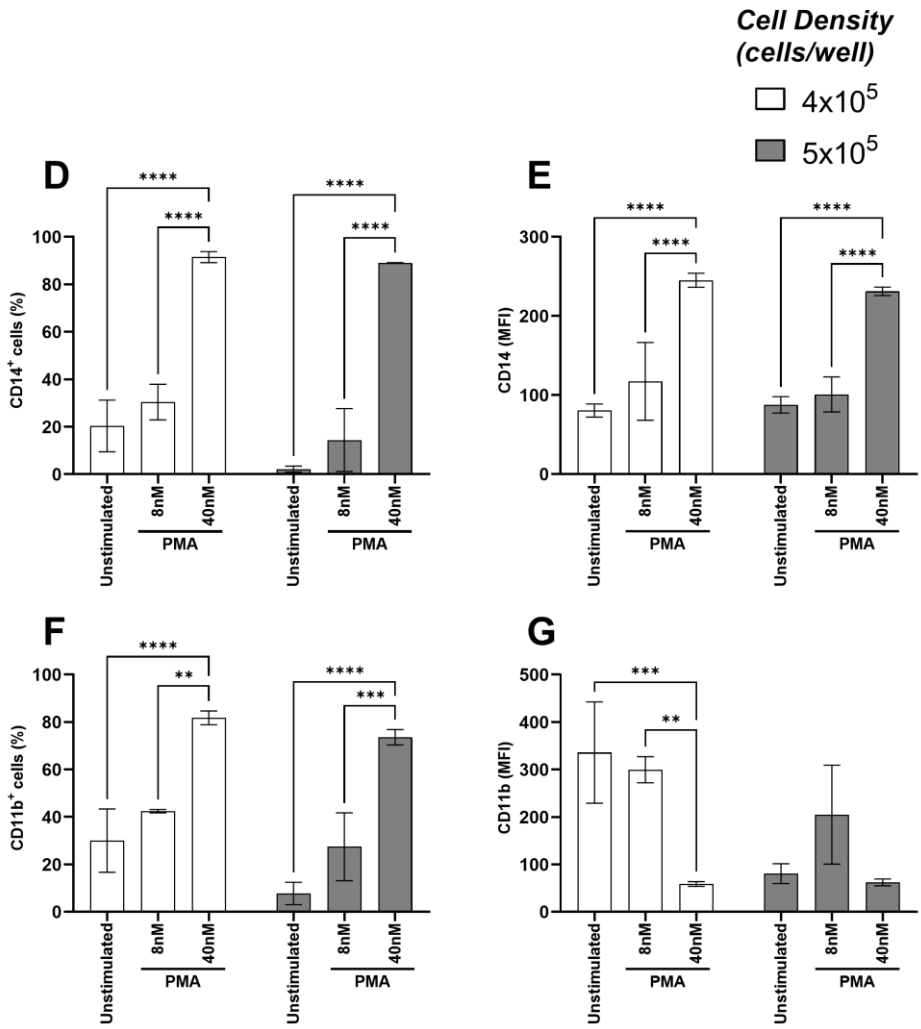

A2.2: Optimization 2 - Assessment of total adherent cell counts, viability, and CD14 and CD11b surface marker expression with different cell seeding densities and PMA titrations. Data obtained after 48hr PMA treatment at either 8nM or 40nM, followed by 72hr resting in replenished media. Bar graphs showing; [A] total number of adherent cells recovered [B] adherent cell viability [C] Microscopic images taken at x20 magnification [D] percentage of $CD14^+$ cells [E] percentage of $CD11b^+$ cells [F] MFI values for CD14 [G] MFI values for CD11b. Data represents 1 experiment comprising triplicate values. Data presented as Mean ± SD. Images present 1 representative well from each condition. One-way ANOVA with post hoc Bonferroni. *p<0.05; **p<0.01; ***p<0.001; ****p<0.0001.

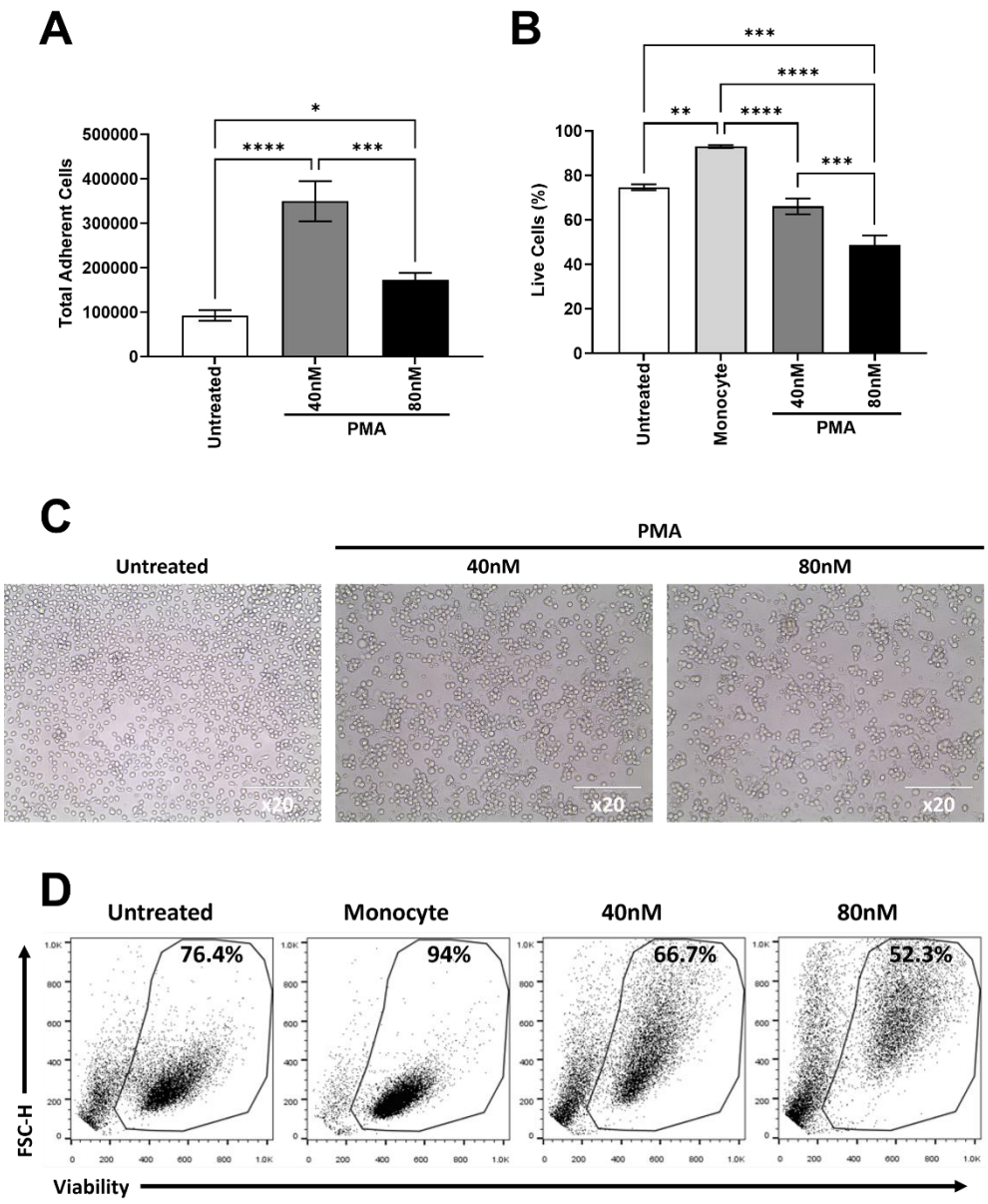

A2.3: Optimization 3 - Assessment of total adherent cell counts, and viability with different PMA titrations. Data obtained after cells seeded at $4x10^5$ cells/well with 48hr PMA treatment at either 40nM or 80nM, followed by 72hr resting in replenished media. Bar graphs showing; [A] total number of adherent cells recovered [B] adherent cell viability [C] Microscopic images taken at x20 magnification [D] percentage of live cells (Zombie Aqua negative). Data represents 1 experiment comprising triplicate values. Data presented as Mean ± SD. Images and plots present 1 representative well from each condition. One-way ANOVA with post hoc Bonferroni. *p<0.05; **p<0.01; ***p<0.001; ****p<0.0001.

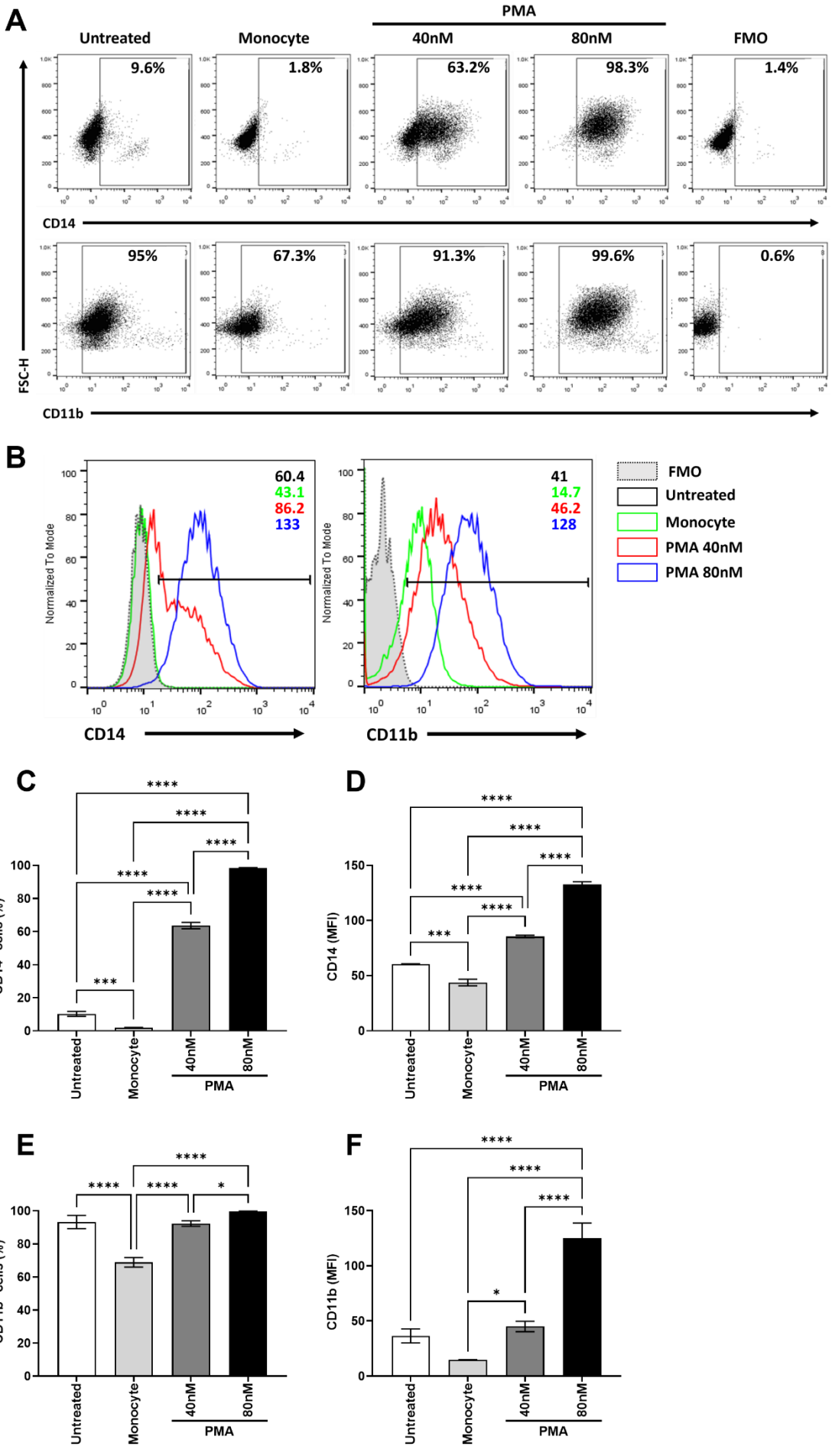
A
PMA
Untreated
Monocyte
40nM
80nM
FMO
9.6%
1.8%
63.2%
98.3%
1.4%
CD14
95%
67.3%
91.3%
99.6%
0.6%
FSC-H
CD11b
B
60.4
43.1
86.2
133
41
14.7
46.2
128
Normalized To Mode
FMO
Untreated
Monocyte
PMA 40nM
PMA 80nM
CD14
CD11b
C
CD14+ cells (%)
D
CD14 (MFI)
E
CD11b+ cells (%)
F
CD11b (MFI)
Untreated
Monocyte
40nM
80nM
PMA

A2.4: Optimization 4: CD14 and CD11b expression profile of cells treated with 40nM or 80nM PMA. Data obtained from adherent cells after cells initially seeded at $4x10^5$ cells/well with 48hr PMA treatment at either 40nM or 80nM, and 72hr resting. [A**]** Representative contour plots showing the percentage of $CD14^+$ (top) and $CD11b^+$ (bottom) cells. [B] Representative histograms showing mean fluorescent intensity (MFI) for CD14 (left) and CD11b (right). Numbers indicate MFI of live gated population. [C—F] Bar graphs showing the percentage of $CD14^+$ [C] and $CD11b^+$ [E] cells, and MFI values for CD14 [D] and CD11b [F] displayed as fold change versus the untreated control. Plots and histograms illustrate one representative experiment. Bar graphs represent 1 experiment comprising of triplicate values. Data presented as mean ± SD. One-way ANOVA with post hoc Bonferroni applied. *p<0.05; ***p<0.001; ****p<0.0001.

A3: U-937 macrophage characterization: Surface marker evaluation

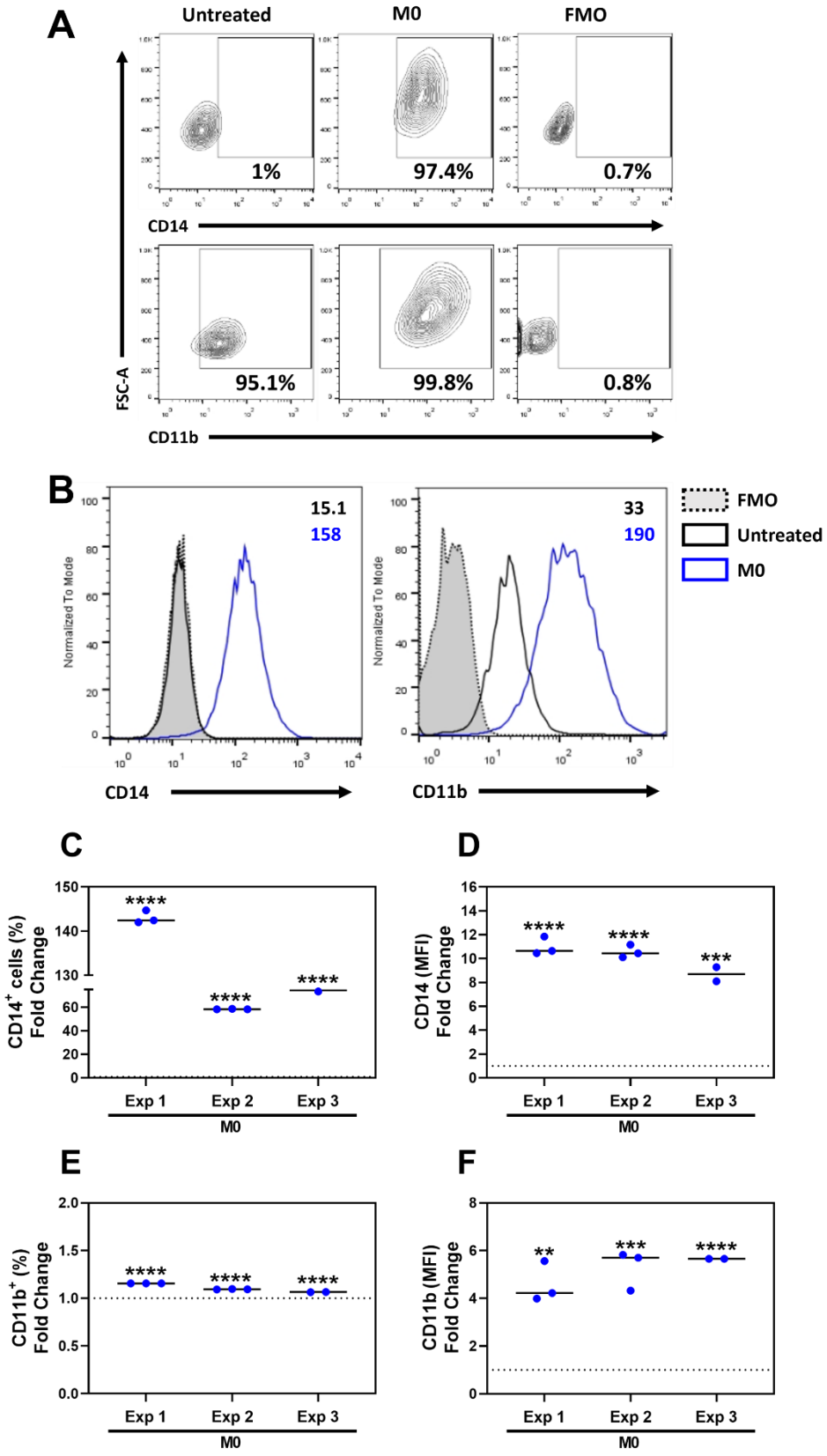

A3.1: CD14 and CD11b expression profile of PMA- differentiated U-937 macrophages**.** Data obtained from adherent cells after 48hr of 80nM PMA treatment and 72hr resting. [A] Representative contour plots showing the percentage of $CD14^+$ (top) and $CD11b^+$ (bottom) cells. [B] Representative histograms showing mean fluorescent intensity (MFI) for CD14 (left) and CD11b (right). Numbers indicate MFI of live gated population. [C—F] Nested bar graphs showing the percentage of $CD14^+$ [C] and $CD11b^+$ [E] cells, and MFI values for CD14 [D] and CD11b [F]. Data displayed as fold change versus the U-937 monocyte. Data compares U-937 monocytes from culture and PMA-differentiated M0 macrophages. Plots and histograms illustrate one representative experiment. Nested data represent 3 experiments each comprising of triplicate values. Data presented as mean ± SD. One-way ANOVA with post hoc Dunnett's applied versus the unstimulated U-937 monocyte. ***p*<0.01; ****p*<0.001; *****p*<0.0001.

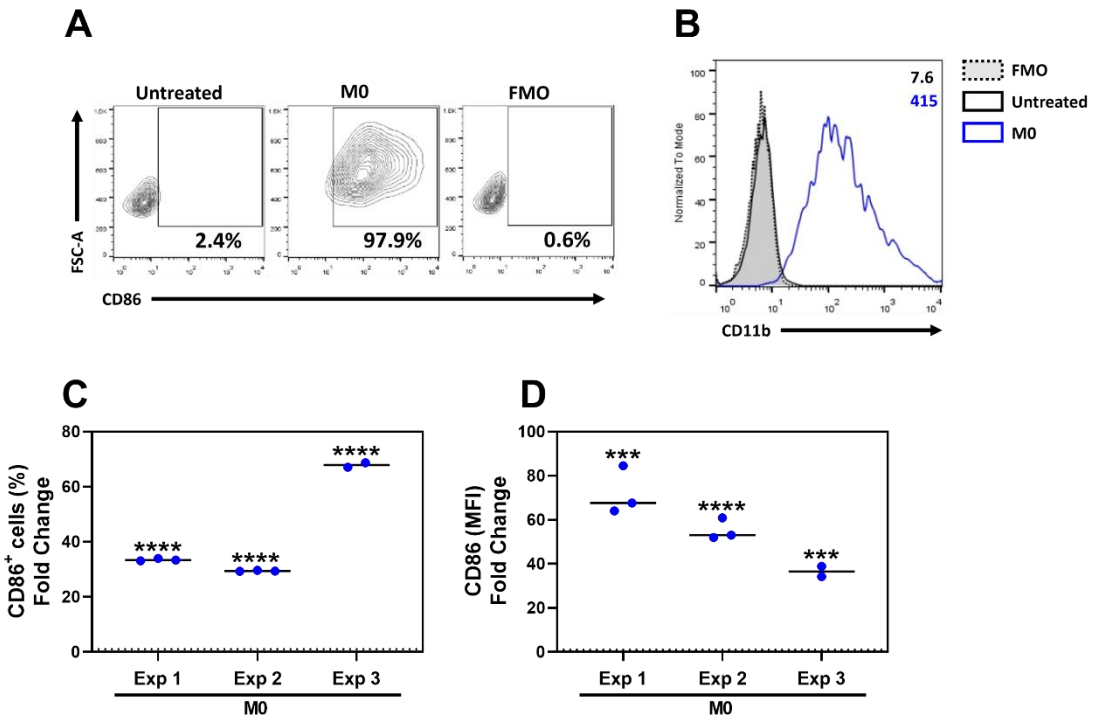

A3.2: CD86 expression profile of PMA- differentiated U-937 macrophages**.** Data obtained from adherent cells after 48hr of 80nM PMA treatment and 72hr resting. [A] Representative contour plots showing the percentage of $CD86^+$ cells. [B] Representative histogram showing mean fluorescent intensity (MFI) for CD86. Numbers indicate MFI of live gated population. [C and D] Nested bar graphs showing the percentage of $CD86^+$ [C] cells, and MFI values for CD86 [D]. Data displayed as fold change versus the U-937 monocyte. Data compares U-937 monocytes from culture and PMA-differentiated M0 macrophages. Plots and histograms illustrate one representative experiment. Nested data represent 3 experiments each comprising of triplicate values. Data presented as mean ± SD. One-way ANOVA with post hoc Dunnett's applied versus the unstimulated U-937 monocyte. ***p<0.001; ****p<0.0001.

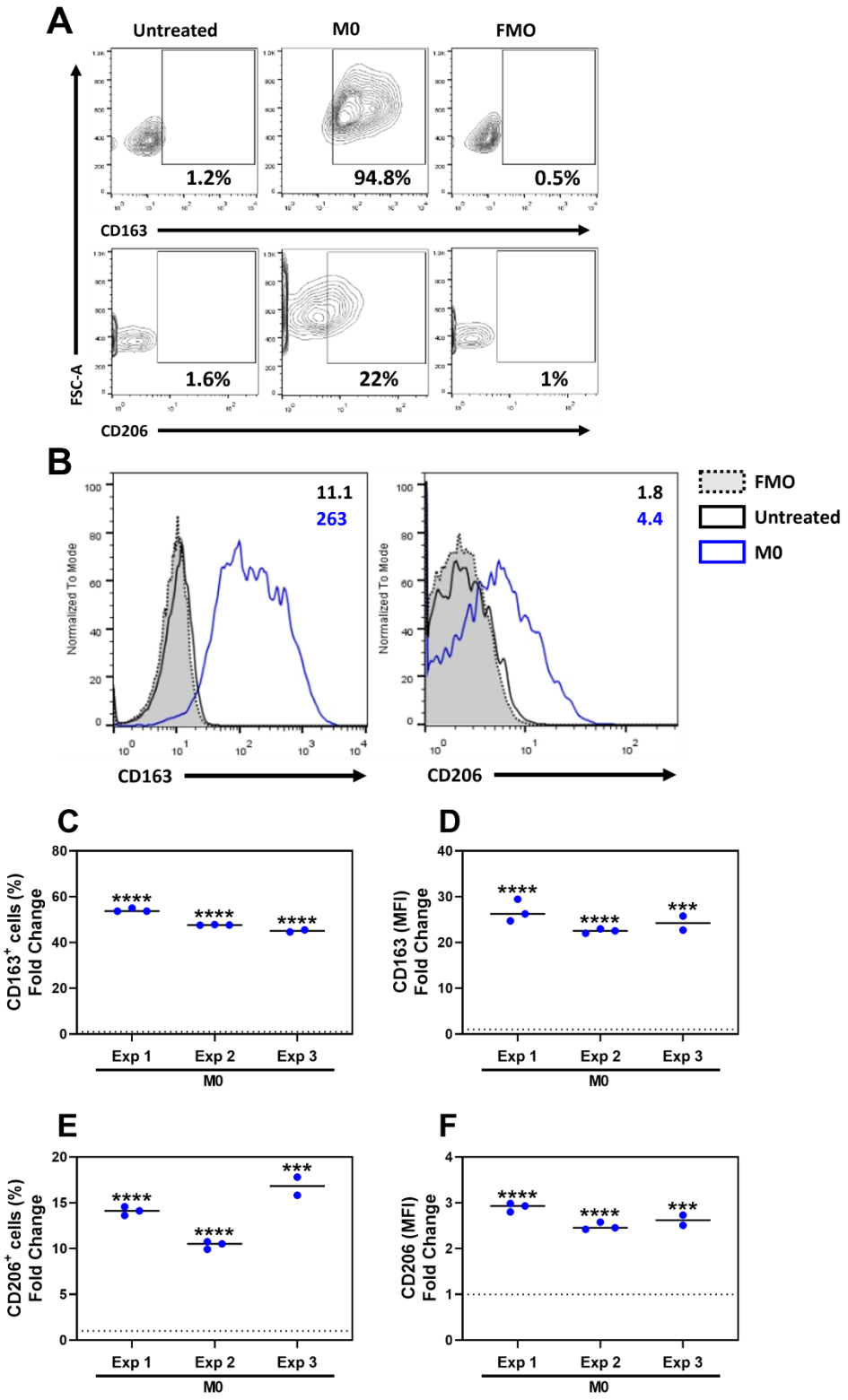

A3.3: CD163 and CD206 expression profile of PMA- differentiated U-937 macrophages**.** Data obtained from adherent cells after 48hr of 80nM PMA treatment and 72hr resting. [A] Representative contour plots showing the percentage of $CD163^+$ (top) and $CD206^+$ (bottom) cells. [B] Representative histograms showing mean fluorescent intensity (MFI) for CD163 (left) and CD206 (right). Numbers indicate MFI of live gated population.

[C—F] Nested bar graphs showing the percentage of CD163^{+} [C] and CD206^{+} [E] cells, and MFI values for CD163 [D] and CD206 [F]. Data displayed as fold change versus the U-937 monocyte. Data compares U-937 monocytes from culture and PMA-differentiated M0 macrophages. Plots and histograms illustrate one representative experiment. Nested data represent 3 experiments each comprising of triplicate values. Data presented as mean ± SD. One-way ANOVA with post hoc Dunnett's applied versus the unstimulated U-937 monocyte. ***p<0.001; ****p<0.0001.

A4: Effect of minocycline on cell viability during PMA-induced U-937 differentiation

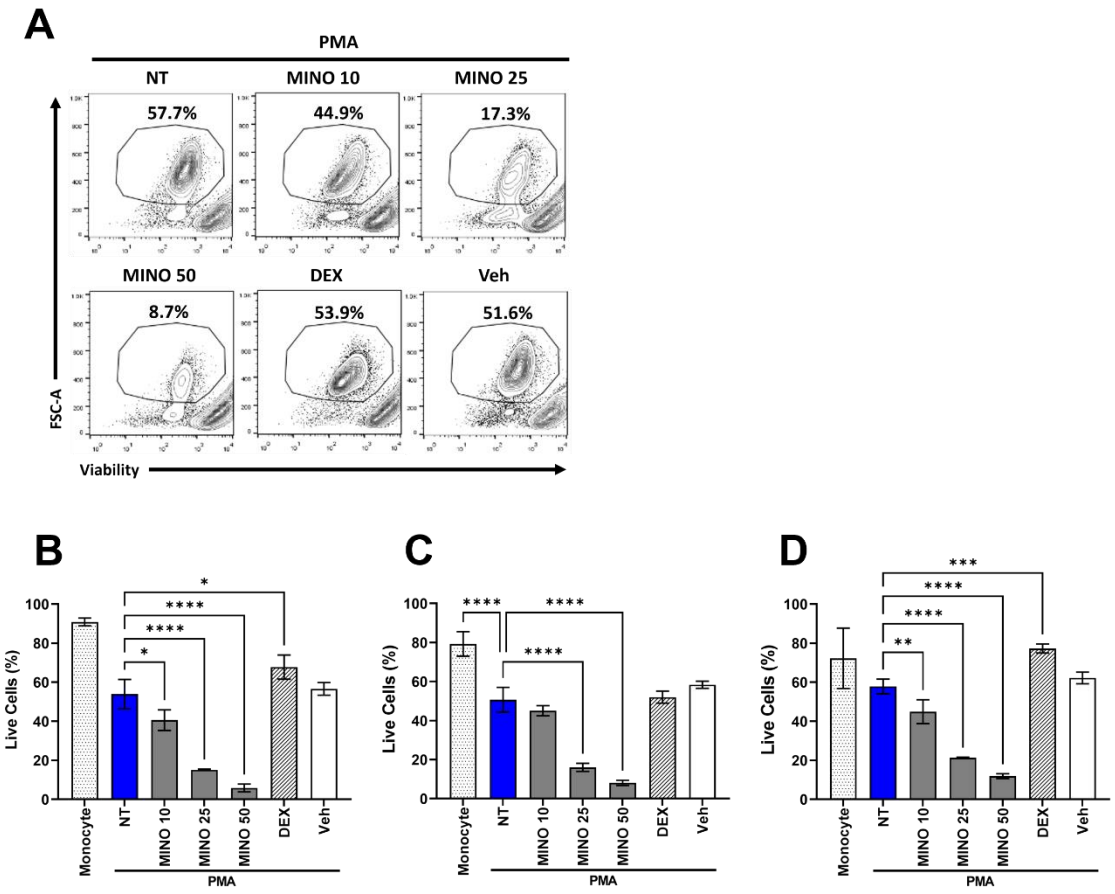

A4: Effect of minocycline on cell viability during PMA-induced U-937 differentiation**.** [A] Representative contour plots showing the percentage of live adherent cells (%) (Zombie Aqua^{neg}) at 72hr. [B-D] Bar graphs showing the percentage of live cells (%) (Zombie Aqua^{neg}) after 48hr 80nM PMA treatment and 72hr resting. NT = untreated PMA-induced macrophage, MINO 10 = Minocycline 10μM, MINO 25 = Minocycline 25μM, MINO 50 = Minocycline 50μM, DEX = Dexamethasone 50μM, Veh = DMSO vehicle control 1:1000. Each graph represents 1 experiment comprising of triplicate values and is presented as mean ± SD. Plots illustrate one representative experiment. One-way ANOVA with post hoc Dunnett's applied versus the NT group. *p<0.05; **p<0.01; ***p<0.001; ****p<0.0001.

A5: Effect of minocycline on cellular adherence during PMA-induced U-937 monocyte differentiation

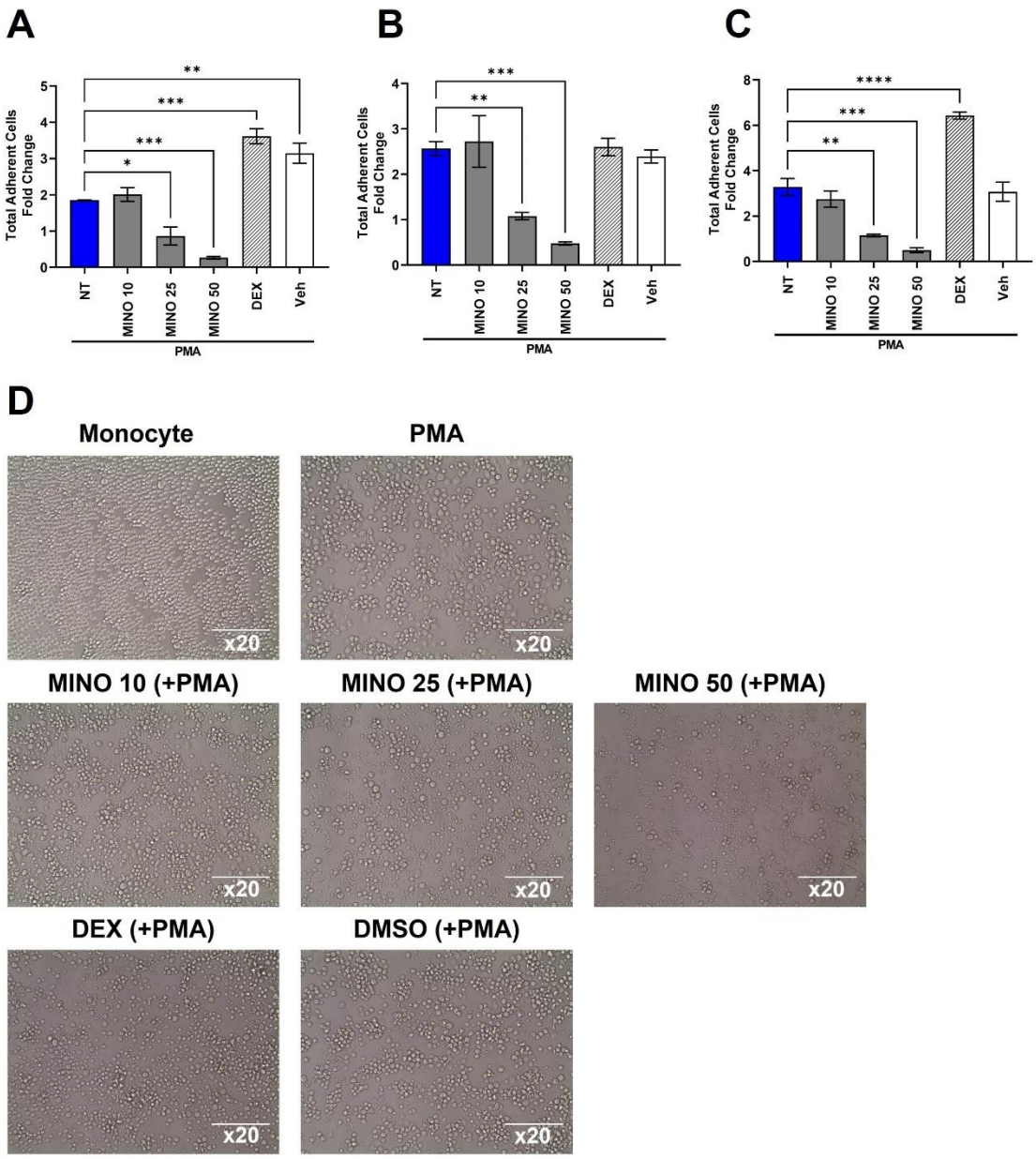

A5: Effect of minocycline on cellular adherence and morphology during PMA-induced U-937 monocyte differentiation**.** [A-C] Bar graphs showing the total number of adherent cells after 48h of 80nM PMA treatment and72hr resting. Data showed as fold change versus the untreated U-937 monocyte control [D] Representative microscopic images at x20. NT = untreated PMA-induced macrophage, MINO 10 = Minocycline 10μM, MINO 25 = Minocycline 25μM, MINO 50 = Minocycline 50μM, DEX = Dexamethasone 50μM, Veh = DMSO vehicle control 1:1000. Each graph represents 1 experiment comprising of triplicate values and is presented as mean ± SD. Images present one representative well. One-way ANOVA with post hoc Dunnett's applied versus the NT group. *p<0.05; **p<0.01; ***p<0.001; ****p<0.0001.

A6: Effect of minocycline on surface marker expression of PMA-differentiated U-937 macrophages

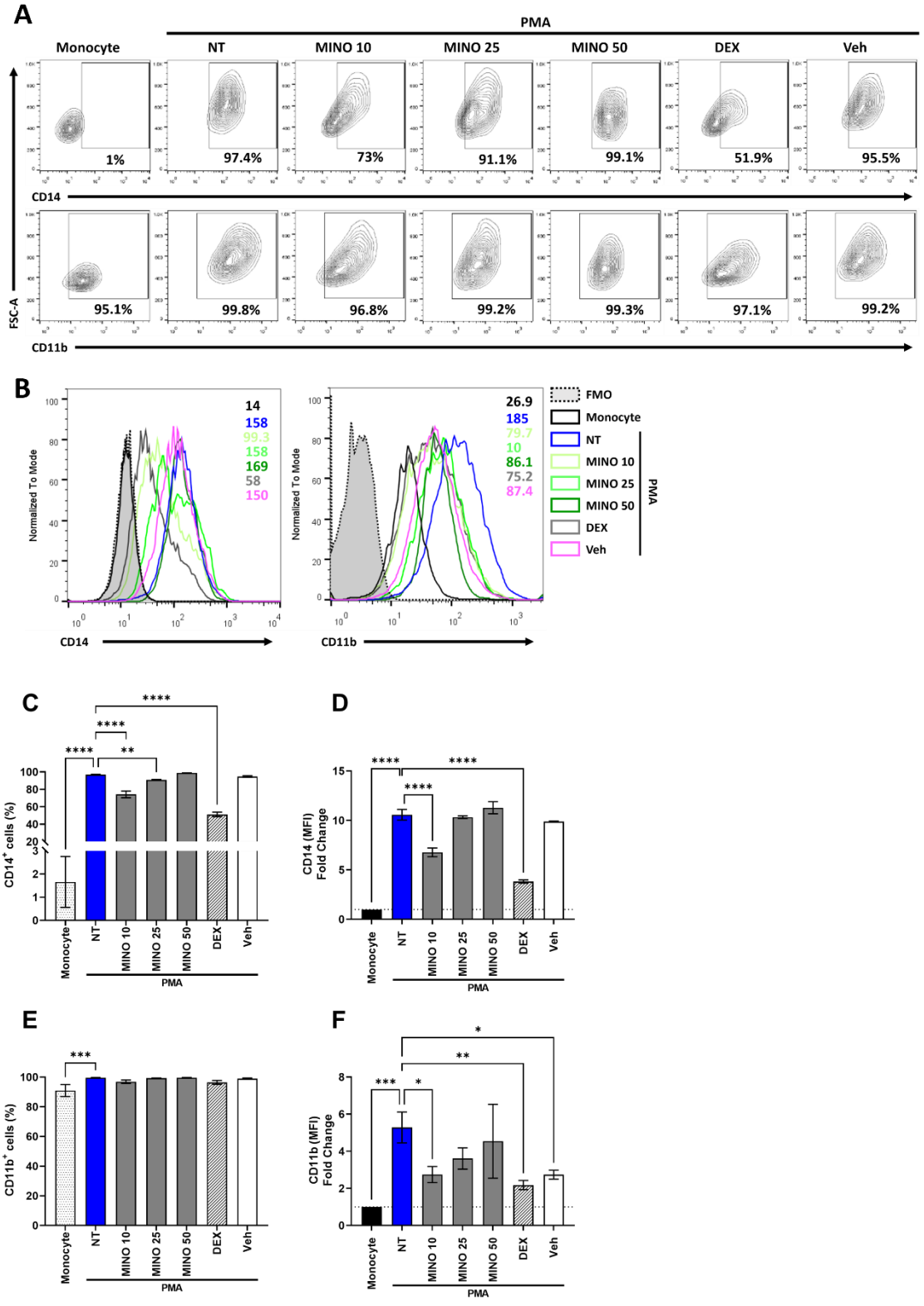

A6.1: Effect of minocycline on CD14 and CD11b expression of PMA-differentiated U-937 macrophages: replicate 1. Data obtained from adherent cells after 48hr of 80nM PMA treatment and 72hr resting. [A] Representative contour plots showing the percentage of $CD14^+$ (top) and $CD11b^+$ (bottom) cells. [B] Representative histograms showing mean fluorescent intensity (MFI) of CD14 (left) and CD11b (right). Numbers indicate MFI of live gated population. [C-F] Bar graphs showing the percentage of $CD14^+$ [C] and $CD11b^+$ [E] cells, and MFI values for CD14 [D] and CD11b [F] displayed as fold change versus the U-937 monocyte. NT = untreated PMA-differentiated M0 macrophage, MINO 10 = Minocycline 10μM, MINO 25 = Minocycline 25μM, MINO 50 = Minocycline 50μM, DEX = Dexamethasone 50μM, Veh = DMSO vehicle control 1:1000. Plots and histograms illustrate one representative experiment. Graphical data represent 1 experiment comprising of triplicate values. Data presented as mean ± SD. One-way ANOVA with post hoc Dunnett's applied versus the unstimulated U-937 monocyte. *p<0.05; **p<0.01; ***p<0.001; ****p<0.0001.

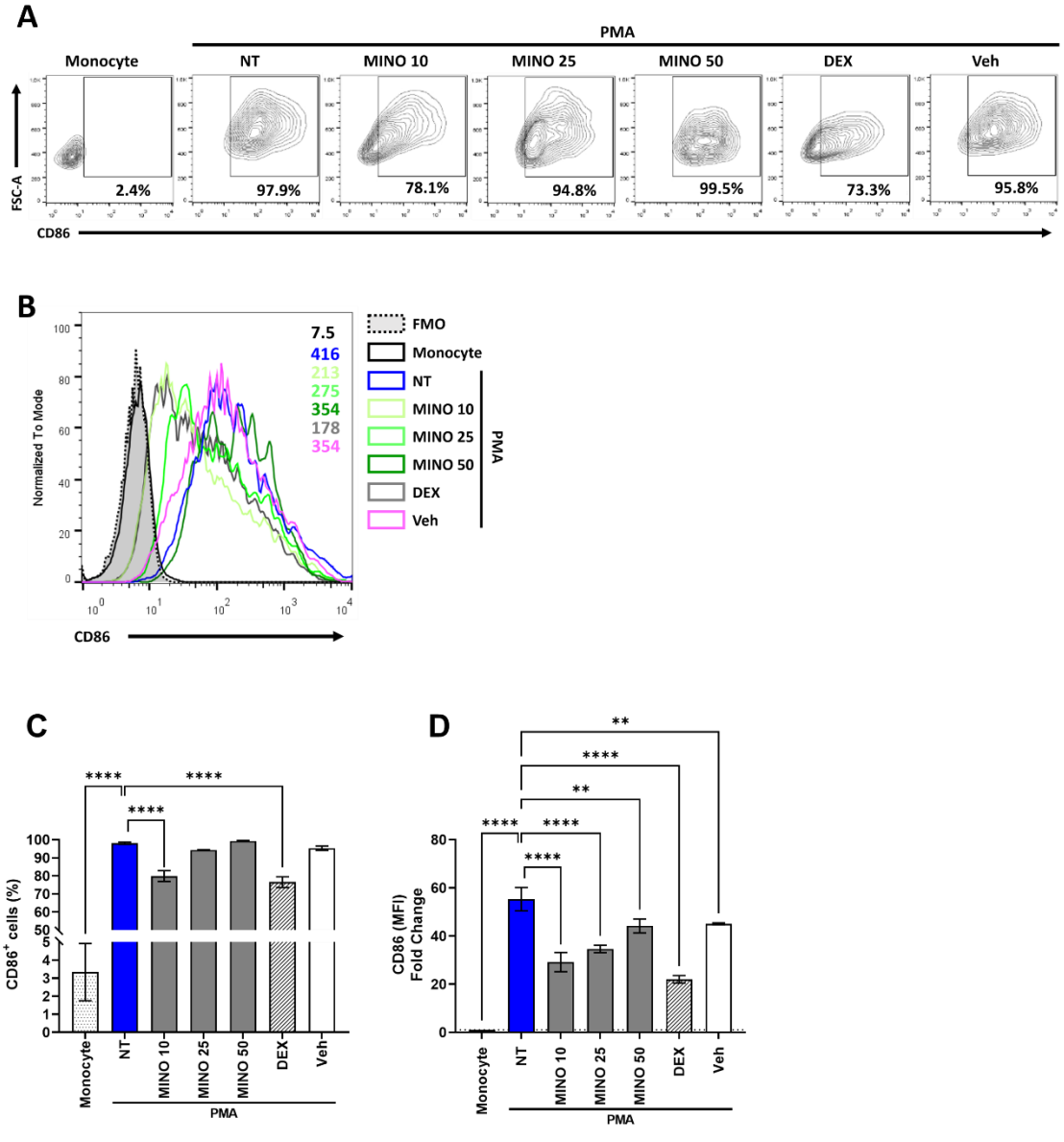

A6.2: Effect of minocycline on CD86 expression of PMA-differentiated U-937 macrophages: replicate 1. Data obtained from adherent cells after 48hr of 80nM PMA treatment and 72hr resting. [A] Representative contour plots showing the percentage of $CD86^+$ cells. [B] Representative histogram showing mean fluorescent intensity (MFI) of CD86. Numbers indicate MFI of live gated population. [C and D] Bar graphs showing the percentage of $CD86^+$ cells [C] and MFI values for CD86 [D]. MFI displayed as fold change versus the U-937 monocyte. NT = untreated PMA-differentiated M0 macrophage, MINO 10 = Minocycline 10μM, MINO 25 = Minocycline 25μM, MINO 50 = Minocycline 50μM, DEX = Dexamethasone 50μM, Veh = DMSO vehicle control 1:1000. Plots and histograms illustrate one representative experiment. Graphical data represent 1 experiment comprising of triplicate values. Data presented as mean ± SD. One-way ANOVA with post hoc Dunnett's applied versus the unstimulated U-937 monocyte. *p<0.05; **p<0.01; ****p<0.0001.

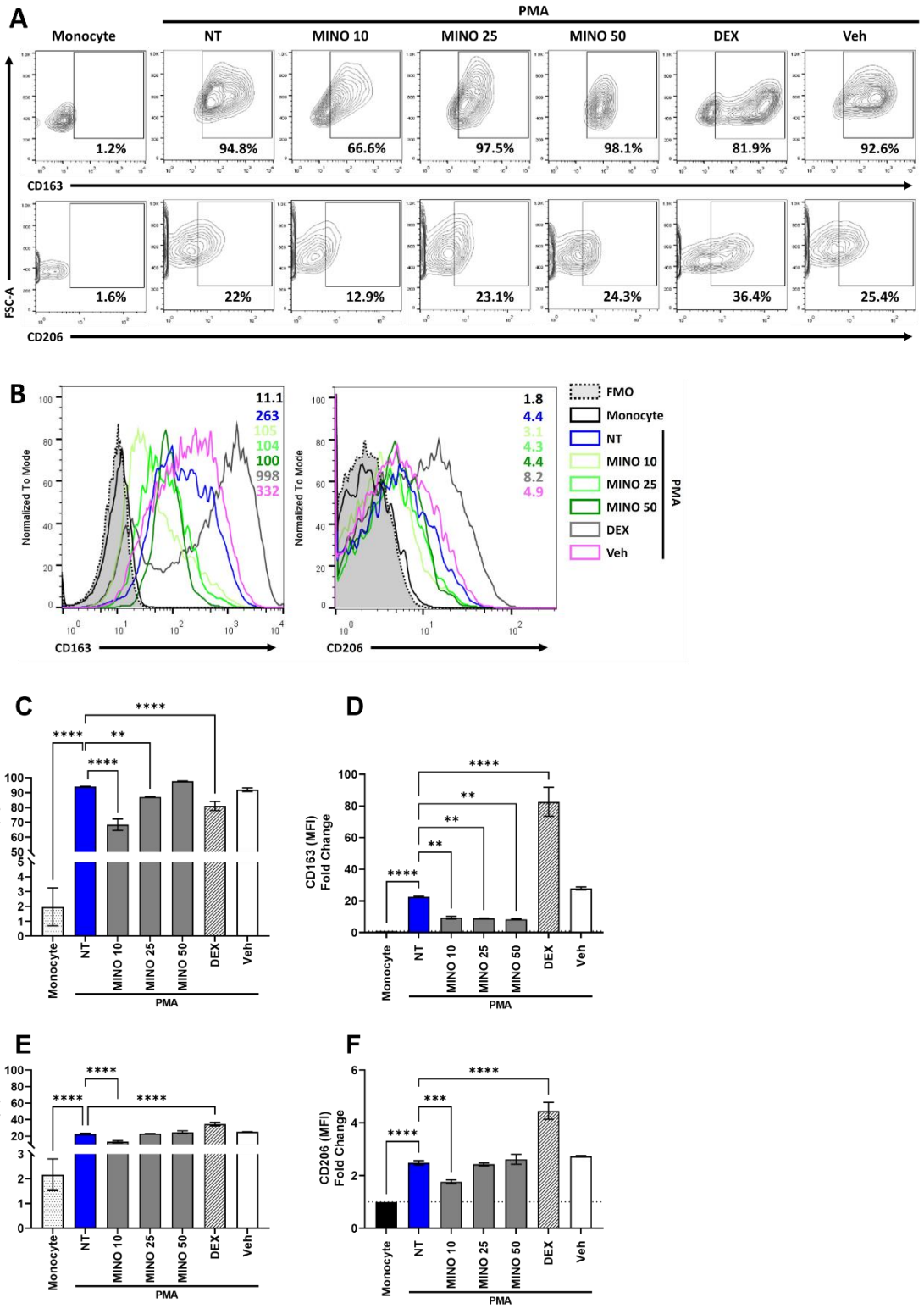

A6.3: Effect of minocycline on CD163 and CD206 expression of PMA-differentiated U-937 macrophages: replicate 1. Data obtained from adherent cells after 48hr of 80nM PMA treatment and 72hr resting. [A] Representative contour plots showing the percentage of $CD163^+$ (top) and $CD206^+$ (bottom) cells. [B] Representative histograms showing mean fluorescent intensity (MFI) of CD163 (left) and CD206 (right). Numbers indicate MFI of live gated population. [C-F] Bar graphs showing the percentage of $CD163^+$ [C] and $CD206^+$ [E] cells, and MFI values for CD163 [D] and CD206 [F] displayed as fold change versus the U-937 monocyte.

NT = untreated PMA-differentiated M0 macrophage, MINO 10 = Minocycline 10μM, MINO 25 = Minocycline 25μM, MINO 50 = Minocycline 50μM, DEX = Dexamethasone 50μM, Veh = DMSO vehicle control 1:1000. Plots and histograms illustrate one representative experiment. Graphical data represent 1 experiment comprising of triplicate values. Data presented as mean ± SD. One-way ANOVA with post hoc Dunnett's applied versus the unstimulated U-937 monocyte. **p<0.01; ***p<0.001; ****p<0.0001.

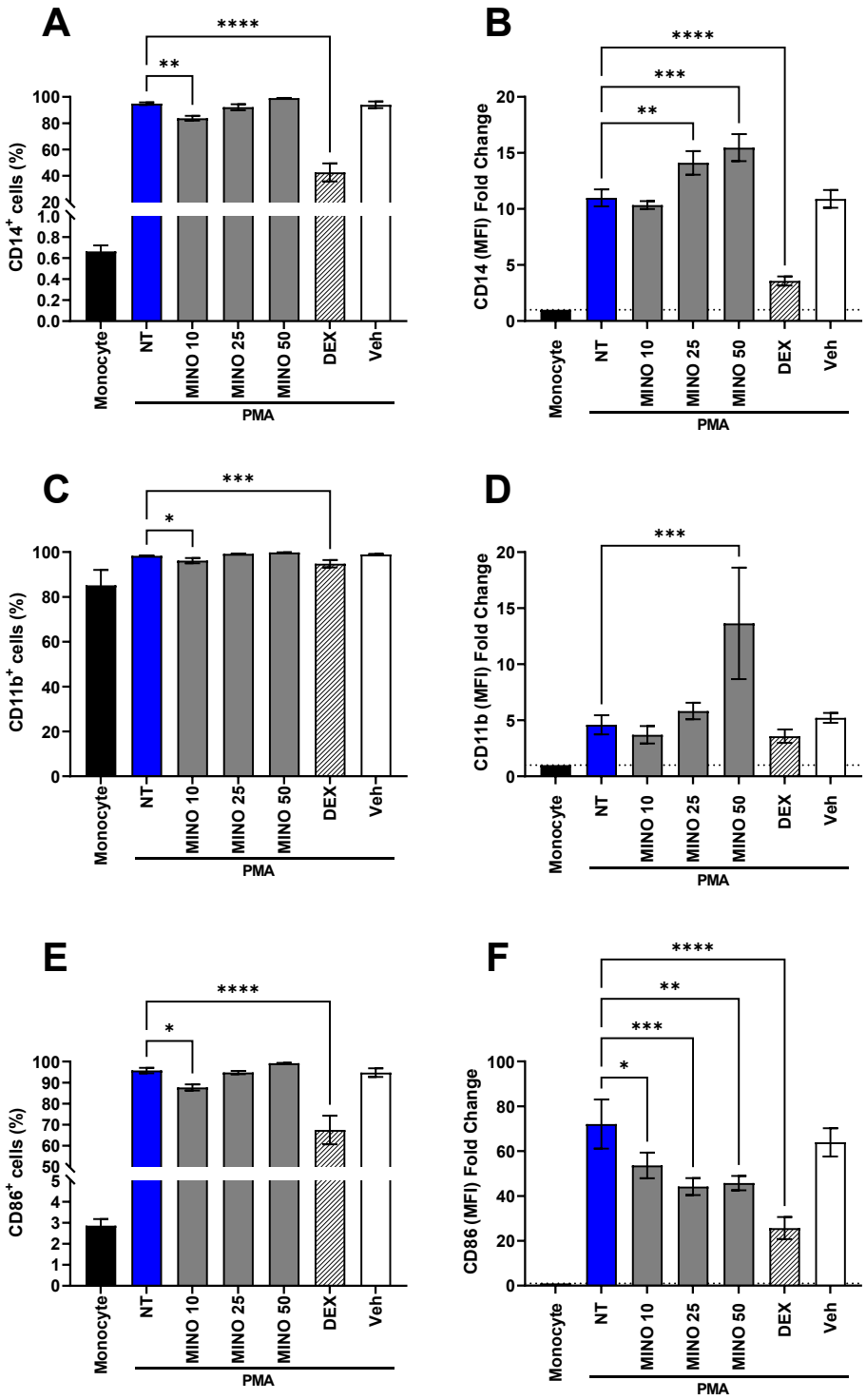

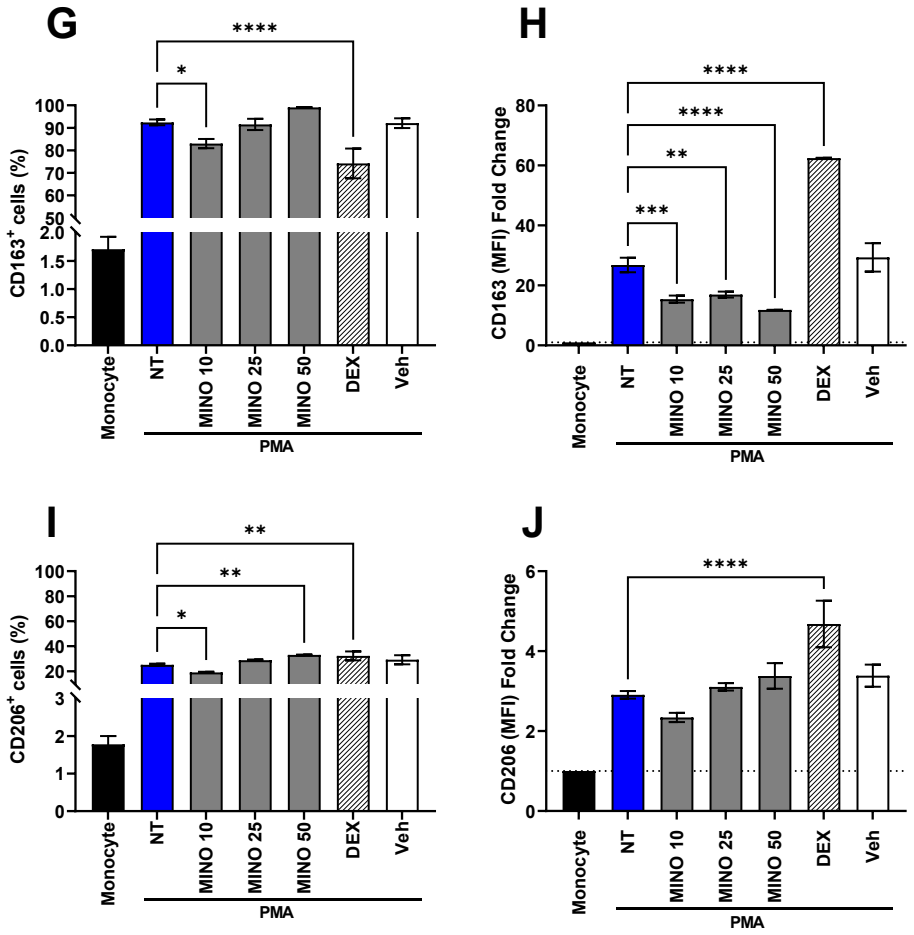

A6.4: Effect of minocycline on surface marker expression of PMA-differentiated U-937 macrophages: biological replicate 2. Data obtained from adherent cells after 48hr of 80nM PMA treatment and 72hr resting. [A-L] Bar graphs showing the percentage of $CD14^+$ [A], $CD11b^+$ [C], $CD86^+$ [E], $CD163^+$ [G] and $CD206^+$ [I] cells, and MFI values for CD14 [B], CD11b [D], CD86 [F], CD163 [H] and CD206 [J]. MFI displayed as fold change versus the U-937 monocyte. NT = untreated PMA-differentiated M0 macrophage, MINO 10 = Minocycline 10μM, MINO 25 = Minocycline 25μM, MINO 50 = Minocycline 50μM, DEX = Dexamethasone 50μM, Veh = DMSO vehicle control 1:1000. Data presented as mean ± SD. One-way ANOVA with post hoc Dunnett's applied versus the unstimulated U-937 monocyte. *p<0.05; **p<0.01; ***p<0.001; ****p<0.0001.

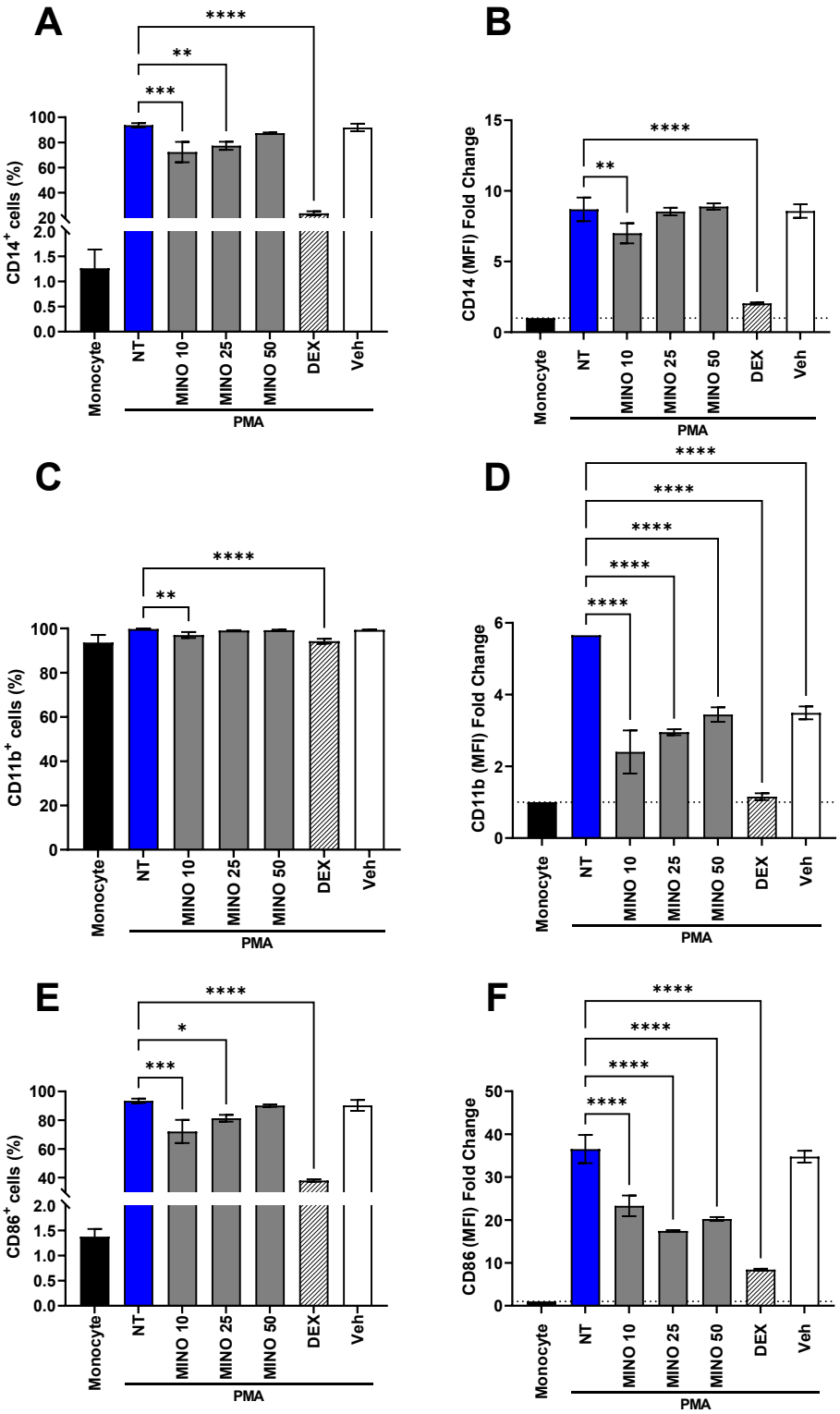
A
B
C
D
E
F
CD14+ cells (%)
CD14 (MFI) Fold Change
CD11b+ cells (%)
CD11b (MFI) Fold Change
CD86+ cells (%)
CD86 (MFI) Fold Change
Monocyte
NT
MINO 10
MINO 25
MINO 50
DEX
Veh
PMA

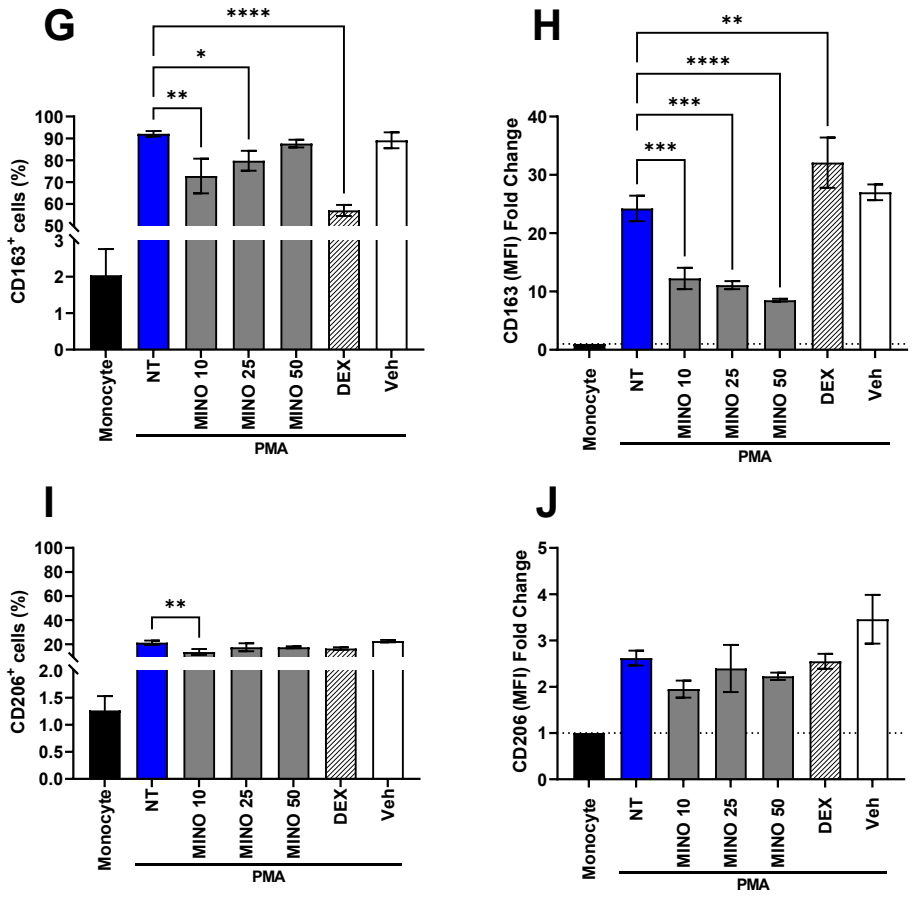

A6.5: Effect of minocycline on surface marker expression of PMA-differentiated U-937 macrophages: biological replicate 3. Data obtained from adherent cells after 48hr of 80nM PMA treatment and 72hr resting. [A-L] Bar graphs showing the percentage of $CD14^+$ [A], $CD11b^+$ [C], $CD86^+$ [E], $CD163^+$ [G] and $CD206^+$ [I] cells, and MFI values for CD14 [B], CD11b [D], CD86 [F], CD163 [H] and CD206 [J]. MFI displayed as fold change versus the U-937 monocyte. NT = untreated PMA-differentiated M0 macrophage, MINO 10 = Minocycline 10μM, MINO 25 = Minocycline 25μM, MINO 50 = Minocycline 50μM, DEX = Dexamethasone 50μM, Veh = DMSO vehicle control 1:1000. Data presented as mean ± SD. One-way ANOVA with post hoc Dunnett's applied versus the unstimulated U-937 monocyte. *p<0.05; **p<0.01; ***p<0.001; ****p<0.0001.

A7: U-937 LPS-activation characterization: Surface marker evaluation

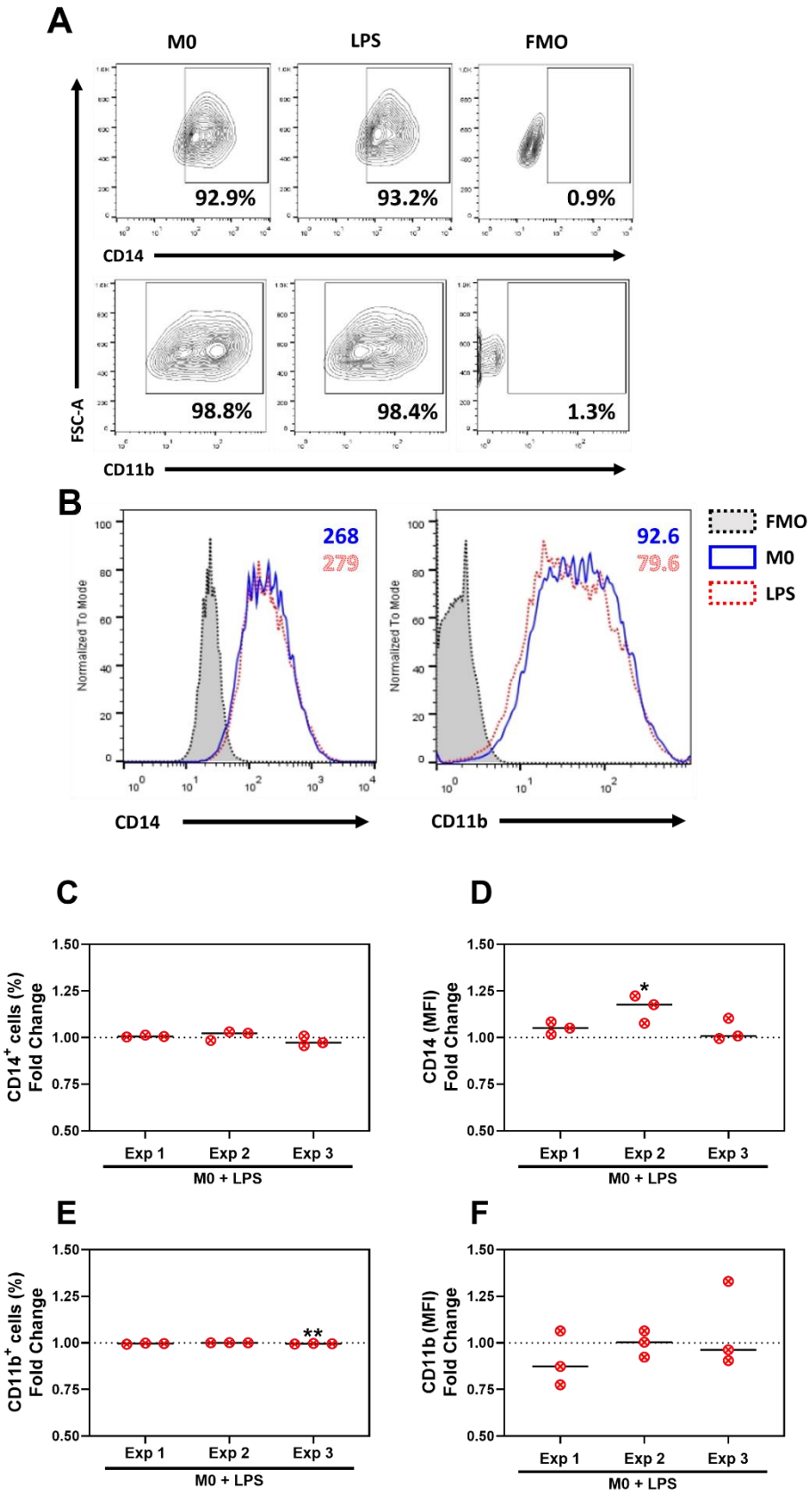

A7.1: CD14 and CD11b expression profile of LPS-activated U-937 macrophages**.** Data obtained after 24hr incubation of differentiated M0 macrophages with LPS (100ng/mL). [A] Representative contour plots showing the percentage of $CD14^+$ (top) and $CD11b^+$ (bottom) cells. [B] Representative histograms showing mean fluorescent intensity (MFI) of CD14 (left) and CD11b (right). Numbers indicate MFI of live gated population. [C-F] Nested bar graphs showing the percentage of $CD14^+$ [C] and $CD11b^+$ [E] cells, and MFI values for CD14 [D] and CD11b [F]. MFI data displayed as fold change versus the un-activated M0 macrophage. Plots and histograms illustrate one representative experiment. Nested data represents 3 replicated experiments each comprising of triplicate values. Data presented as mean ± SD. One-way ANOVA with post hoc Dunnett's applied versus the un-activated M0 macrophage. *$p<0.05$; **$p<0.01$.

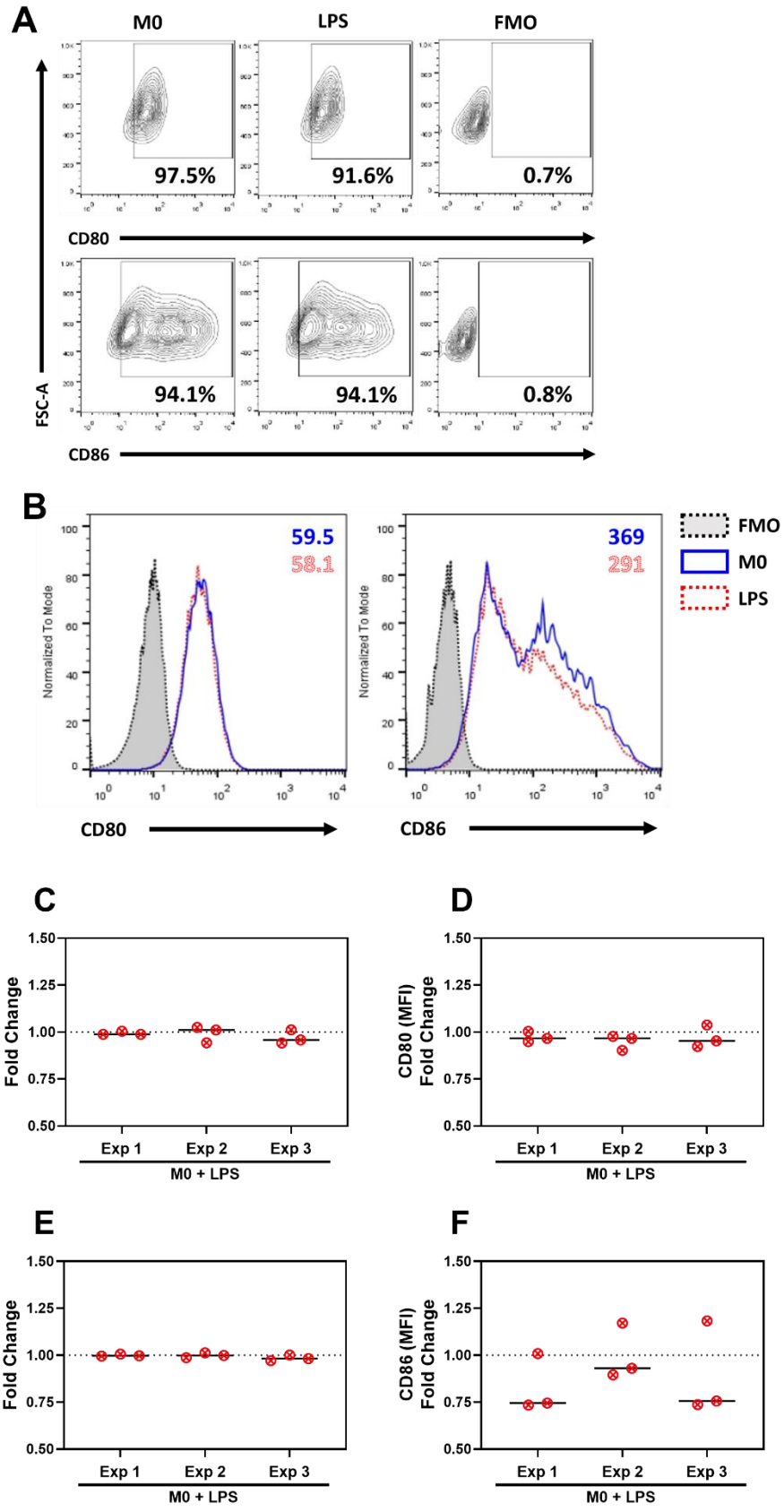
A
M0
LPS
FMO
97.5%
91.6%
0.7%
CD80
94.1%
94.1%
0.8%
FSC-A
CD86
B
59.5
58.1
369
291
FMO
M0
LPS
Normalized To Mode
CD80
CD86
C
D
E
F
CD80+ cells (%) Fold Change
CD80 (MFI) Fold Change
CD86+ cells (%) Fold Change
CD86 (MFI) Fold Change
1.50
1.25
1.00
0.75
0.50
Exp 1
Exp 2
Exp 3
M0 + LPS

A7.2: CD80 and CD86 expression profile of LPS-activated U-937 macrophages**.** Data obtained after 24hr incubation of differentiated M0 macrophages with LPS (100ng/mL). [A] Representative contour plots showing the percentage of $CD80^+$ (top) and $CD86^+$ (bottom) cells. [B] Representative histograms showing mean fluorescent intensity (MFI) of CD80 (left) and CD86 (right). Numbers indicate MFI of live gated population. [C-F] Nested bar graphs showing the percentage of $CD80^+$ [C] and $CD86^+$ [E] cells, and MFI values for CD80 [D] and CD86 [F]. MFI data displayed as fold change versus the un-activated M0 macrophage. Plots and histograms illustrate one representative experiment. Nested data represents 3 replicated experiments each comprising of triplicate values. Data presented as mean ± SD. One-way ANOVA with post hoc Dunnett's applied versus the un-activated M0 macrophage.

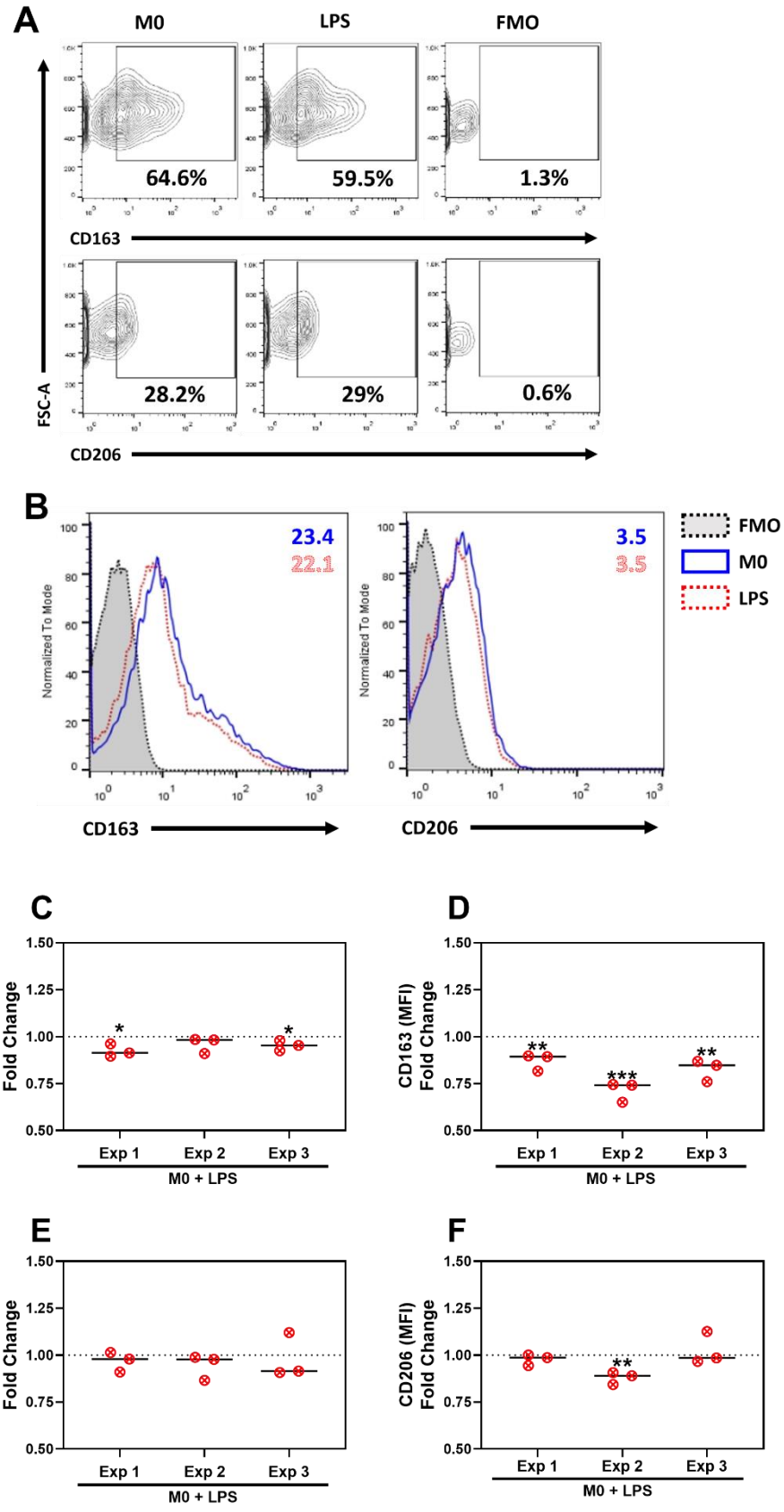
A
M0
LPS
FMO
64.6%
59.5%
1.3%
CD163
28.2%
29%
0.6%
FSC-A
CD206
B
23.4
22.1
3.5
3.5
Normalized To Mode
FMO
M0
LPS
CD163
CD206
C
CD163+ cells (%) Fold Change
Exp 1
Exp 2
Exp 3
M0 + LPS
D
CD163 (MFI) Fold Change
E
CD206+ cells (%) Fold Change
F
CD206 (MFI) Fold Change

A7.3: CD163 and CD206 expression profile of LPS-activated U-937 macrophages**.** Data obtained after 24hr incubation of differentiated M0 macrophages with LPS (100ng/mL). [A] Representative contour plots showing the percentage of $CD63^+$ (top) and $CD206^+$ (bottom) cells. [B] Representative histograms showing mean fluorescent intensity (MFI) of CD163 (left) and CD206 (right). Numbers indicate MFI of live gated population. [C-F] Nested bar graphs showing the percentage of $CD163^+$ [C] and $CD206^+$ [E] cells, and MFI values for CD163 [D] and CD206 [F]. MFI data displayed as fold change versus the un-activated M0 macrophage. Plots and histograms illustrate one representative experiment. Nested data represents 3 replicated experiments each comprising of triplicate values. Data presented as mean ± SD. One-way ANOVA with post hoc Dunnett's applied versus the un-activated M0 macrophage. *p<0.05; **p<0.01; ***p<0.001.

A8: Effect of minocycline on adherent cell viability following LPS activation of THP-1 macrophages

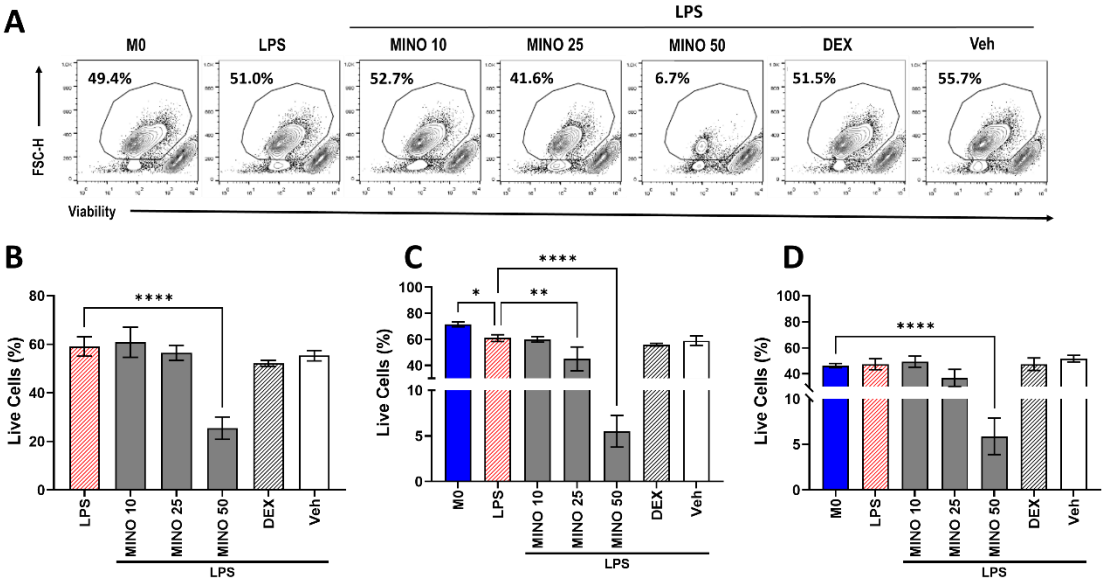

A8: Effect of minocycline on adherent cell viability following LPS activation of THP-1 macrophages**.** Data obtained from adherent cells after 24hr incubation of differentiated M0 macrophages with LPS (100ng/mL). [A] Representative contour plots showing the percentage of live cells (Zombie $Aqua^{neg}$) cells. [B-D] Bar graphs showing the percentage of live cells. M0 = untreated PMA-differentiated M0 macrophage, MINO 10 = Minocycline 10μM, MINO 25 = Minocycline 25μM, MINO 50 = Minocycline 50μM, DEX = Dexamethasone 50μM, Veh = DMSO vehicle control 1:1000. Plots illustrate one representative experiment. Each graph represents 1 experiment comprising of triplicate values. Data presented as mean ± SD. One-way ANOVA with post hoc Dunnett's applied versus the LPS-activated M0 macrophage. *p<0.05; **p<0.01; ****p<0.0001.

A9: Effect of minocycline on adherent cell viability following LPS activation of U-937 macrophages

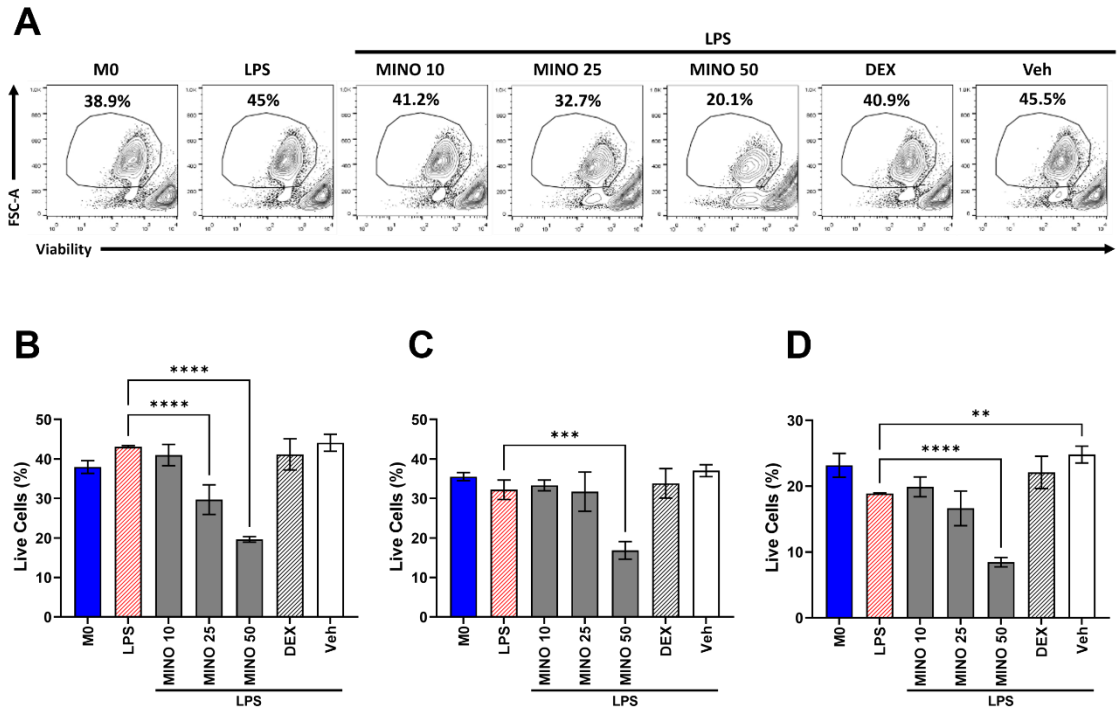

A9: Effect of minocycline on adherent cell viability following LPS activation of U-937 macrophages**.** Data obtained from adherent cells after 24hr incubation of differentiated M0 macrophages with LPS (100ng/mL). [A] Representative contour plots showing the percentage of live cells (Zombie Aqua^{neg}) cells. [B-D] Bar graphs showing the percentage of live cells. M0 = untreated PMA-differentiated M0 macrophage, MINO 10 = Minocycline 10μM, MINO 25 = Minocycline 25μM, MINO 50 = Minocycline 50μM, DEX = Dexamethasone 50μM, Veh = DMSO vehicle control 1:1000. Plots illustrate one representative experiment. Each graph represents 1 experiment comprising of triplicate values. Data presented as mean ± SD. One-way ANOVA with post hoc Dunnett's applied versus the LPS-activated M0 macrophage. **p<0.01; ***p<0.001; ****p<0.0001.

A10: Effect of minocycline on surface marker expression following LPS-activation of U-937 macrophages

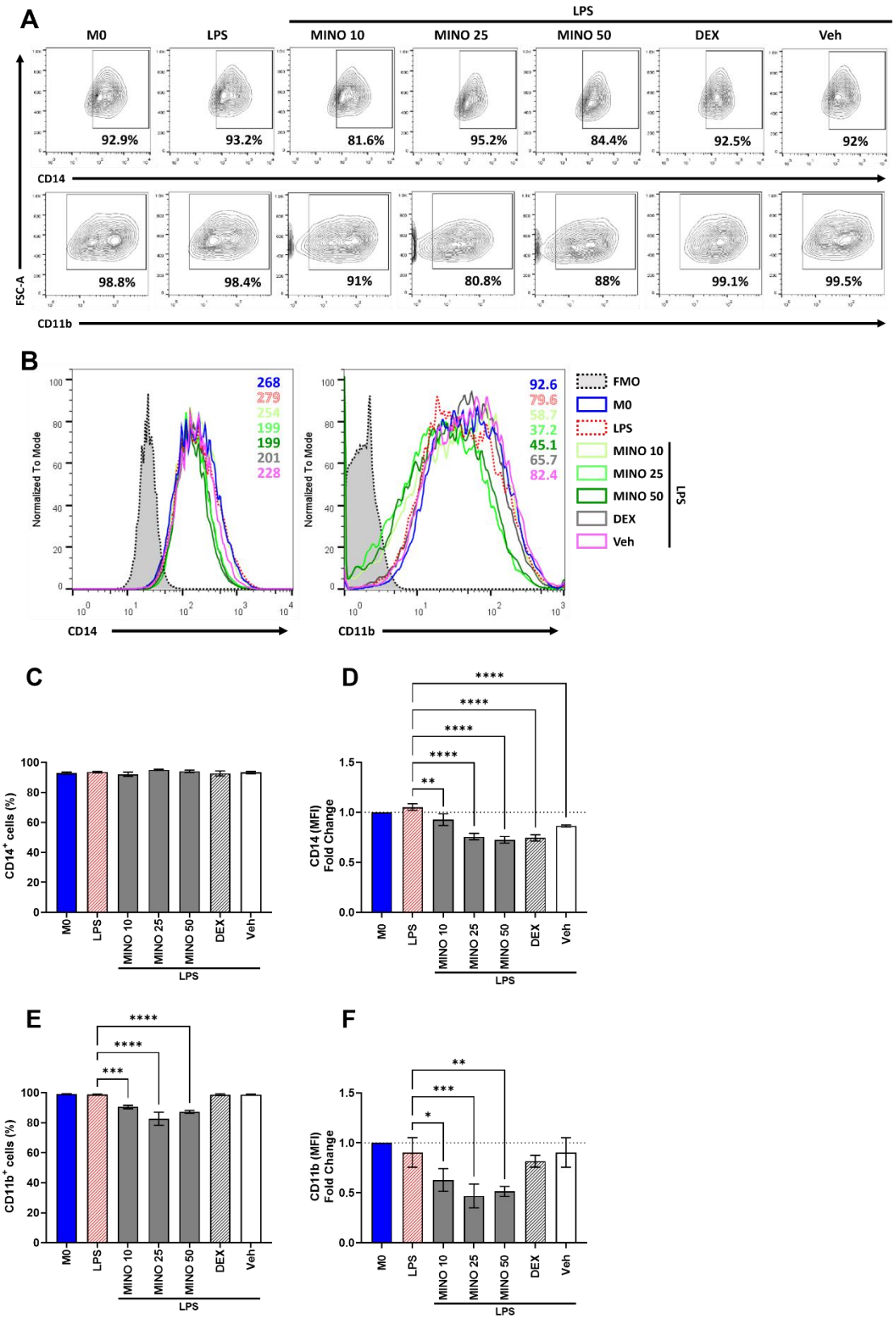

A10.1: Effect of minocycline on CD14 and CD11b expression following LPS-activation of U-937 macrophages: biological replicate 1**.** Data obtained after 24hr incubation of differentiated M0 macrophages with LPS (100ng/mL). [A] Representative contour plots showing the percentage of $CD14^+$ (top) and $CD11b^+$ (bottom) cells. [B] Representative histograms showing mean fluorescent intensity (MFI) of CD14 (left) and CD11b (right). Numbers indicate MFI of live gated population. [C-F] Bar graphs showing the percentage of $CD14^+$ [C] and $CD11b^+$ [E] cells, and MFI values for CD14 [D] and CD11b [F]. MFI values displayed as fold change versus the un-activated M0 macrophage control. MINO 10 = Minocycline 10μM, MINO 25 = Minocycline 25μM, MINO 50 = Minocycline 50μM, DEX = Dexamethasone 50μM, Veh = DMSO vehicle control 1:1000. Plots and histograms illustrate one representative experiment. Graphical data represent 1 experiment comprising of triplicate values. Data presented as mean ± SD. One-way ANOVA with post hoc Dunnett's applied versus the LPS-activated M0 macrophage. *p<0.05; **p<0.01; ***p<0.001; ****p<0.0001.

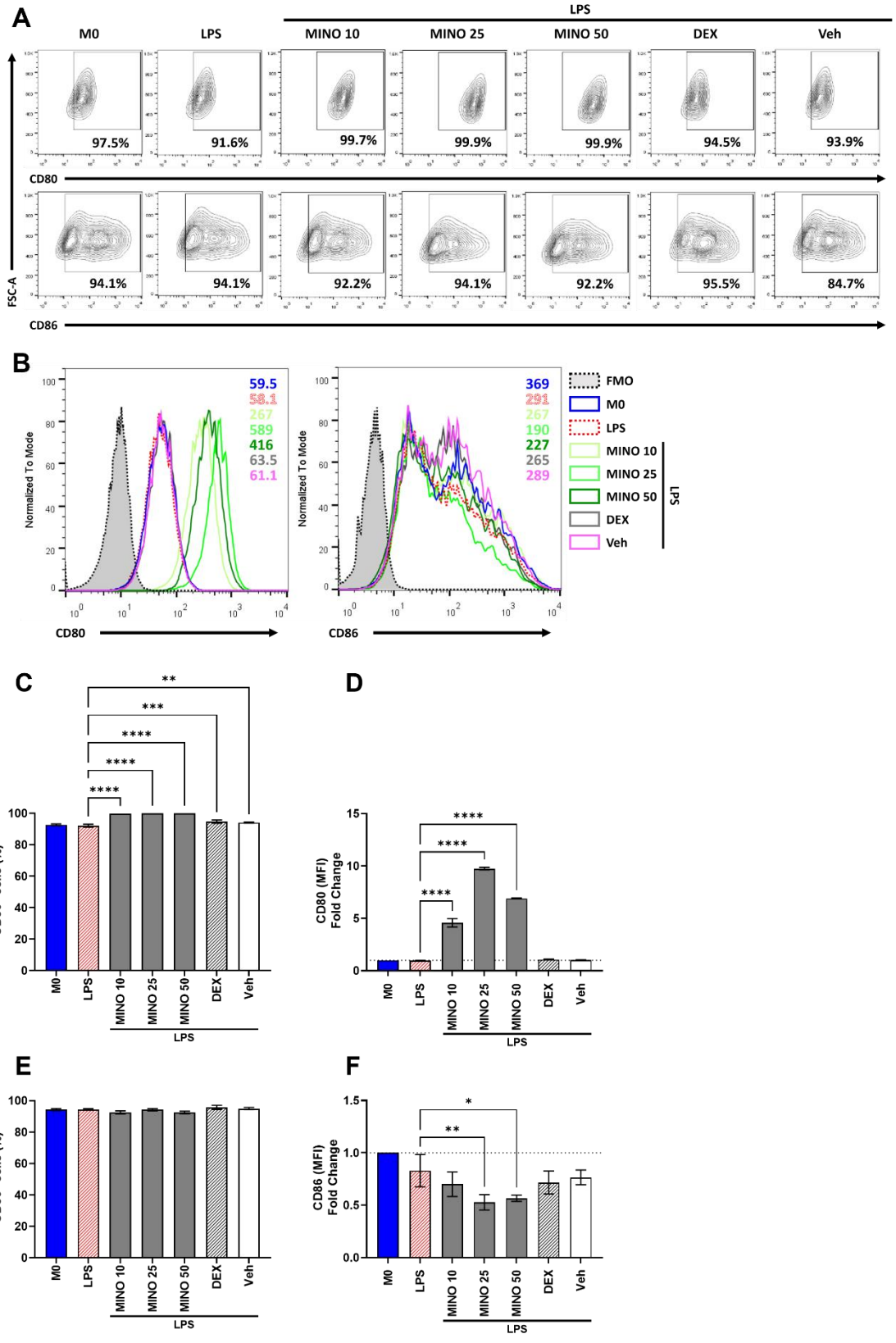
A
LPS
M0
LPS
MINO 10
MINO 25
MINO 50
DEX
Veh
97.5%
91.6%
99.7%
99.9%
99.9%
94.5%
93.9%
CD80
94.1%
94.1%
92.2%
94.1%
92.2%
95.5%
84.7%
FSC-A
CD86
B
Normalized To Mode
59.5
58.1
267
589
416
63.5
61.1
369
291
267
190
227
265
289
CD80
CD86
FMO
M0
LPS
MINO 10
MINO 25
MINO 50
DEX
Veh
LPS
C
CD80+ cells (%)
D
CD80 (MFI) Fold Change
E
CD86+ cells (%)
F
CD86 (MFI) Fold Change

A10.2: Effect of minocycline on CD80 and CD86 expression following LPS-activation of U-937 macrophages: biological replicate 1**.** Data obtained after 24hr incubation of differentiated M0 macrophages with LPS (100ng/mL). [A] Representative contour plots showing the percentage of $CD80^+$ (top) and $CD86^+$ (bottom) cells. [B] Representative histograms showing mean fluorescent intensity (MFI) of CD80 (left) and CD86 (right). Numbers indicate MFI of live gated population. [C-F] Bar graphs showing the percentage of $CD80^+$ [C] and $CD86^+$ [E] cells, and MFI values for CD80 [D] and CD86 [F]. MFI values displayed as fold change versus the un-activated M0 macrophage control. MINO 10 = Minocycline 10μM, MINO 25 = Minocycline 25μM, MINO 50 = Minocycline 50μM, DEX = Dexamethasone 50μM, Veh = DMSO vehicle control 1:1000. Plots and histograms illustrate one representative experiment. Graphical data represent 1 experiment comprising of triplicate values. Data presented as mean ± SD. One-way ANOVA with post hoc Dunnett's applied versus the LPS-activated M0 macrophage. *p<0.05; **p<0.01; ***p<0.001; ****p<0.0001.

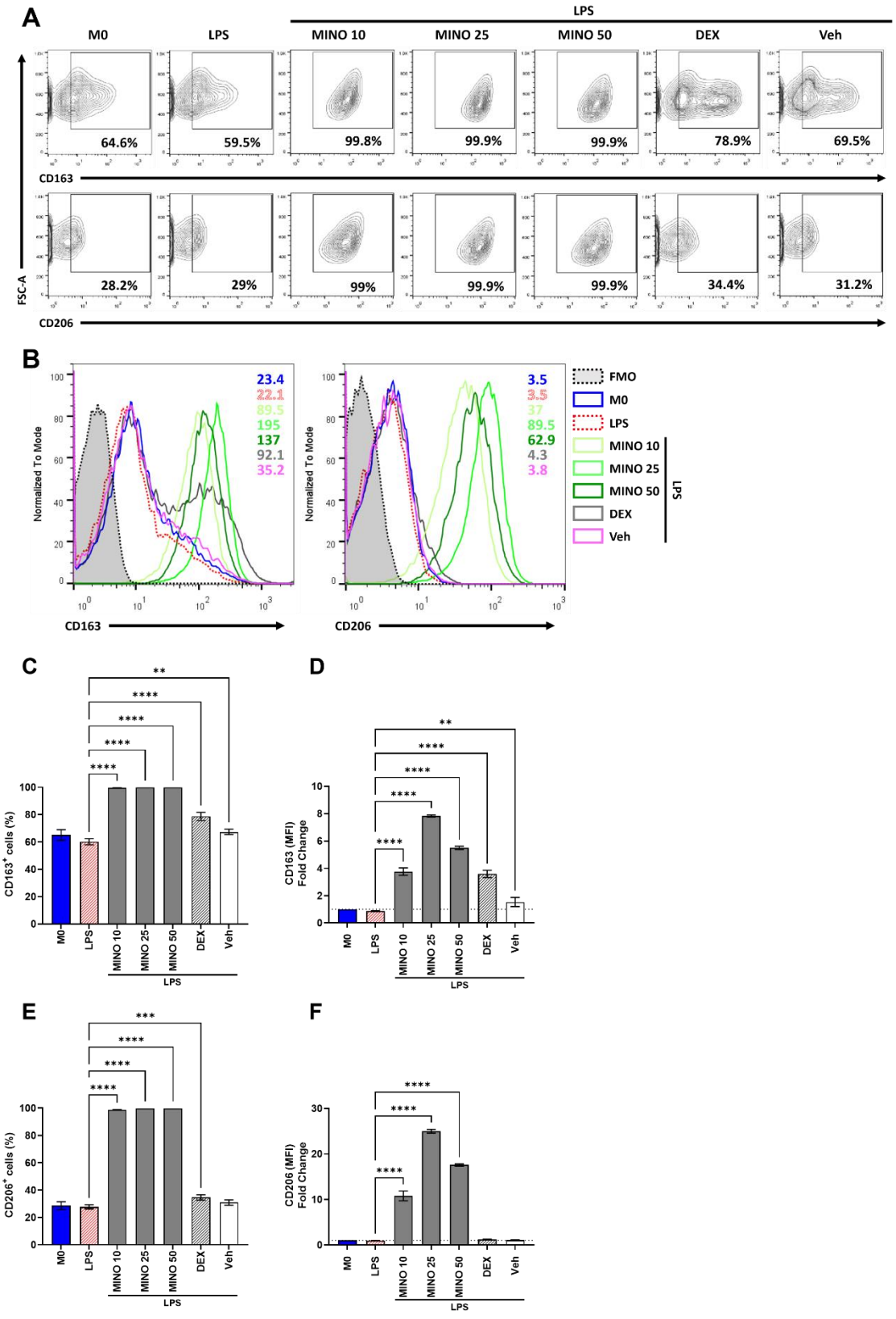
A
LPS
M0
LPS
MINO 10
MINO 25
MINO 50
DEX
Veh
64.6%
59.5%
99.8%
99.9%
99.9%
78.9%
69.5%
CD163
28.2%
29%
99%
99.9%
99.9%
34.4%
31.2%
FSC-A
CD206
B
23.4
22.1
89.5
195
137
92.1
35.2
3.5
3.5
37
89.5
62.9
4.3
3.8
Normalized To Mode
CD163
CD206
FMO
M0
LPS
MINO 10
MINO 25
MINO 50
DEX
Veh
LPS
C
CD163+ cells (%)
D
CD163 (MFI) Fold Change
E
CD206+ cells (%)
F
CD206 (MFI) Fold Change

A10.3: Effect of minocycline on CD163 and CD206 expression following LPS-activation of U-937 macrophages: biological replicate 1**.** Data obtained after 24hr incubation of differentiated M0 macrophages with LPS (100ng/mL). [A] Representative contour plots showing the percentage of $CD163^+$ (top) and $CD206^+$ (bottom) cells. [B] Representative histograms showing mean fluorescent intensity (MFI) of CD163 (left) and CD206 (right). Numbers indicate MFI of live gated population. [C-F] Bar graphs showing the percentage of $CD163^+$ [C] and $CD206^+$ [E] cells, and MFI values for CD163 [D] and CD206 [F]. MFI values displayed as fold change versus the un-activated M0 macrophage control. MINO 10 = Minocycline 10μM, MINO 25 = Minocycline 25μM, MINO 50 = Minocycline 50μM, DEX = Dexamethasone 50μM, Veh = DMSO vehicle control 1:1000. Plots and histograms illustrate one representative experiment. Graphical data represent 1 experiment comprising of triplicate values. Data presented as mean ± SD. One-way ANOVA with post hoc Dunnett's applied versus the LPS-activated M0 macrophage. $^{**}p<0.01$; $^{***}p<0.001$; $^{****}p<0.0001$.

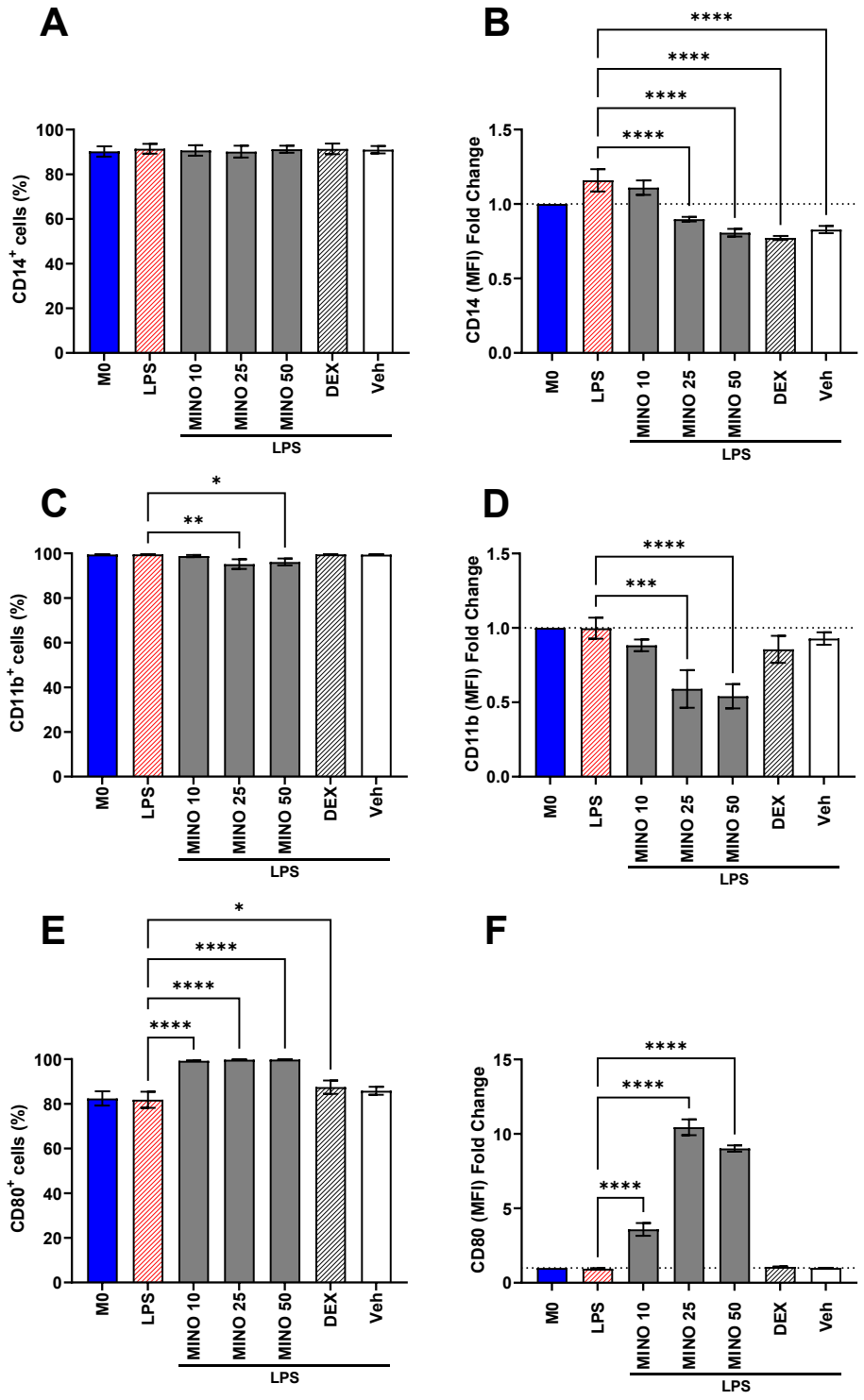
A
CD14+ cells (%)
100
80
60
40
20
0
M0
LPS
MINO 10
MINO 25
MINO 50
DEX
Veh
LPS
B
CD14 (MFI) Fold Change
1.5
1.0
0.5
0.0
****
****
****
****
M0
LPS
MINO 10
MINO 25
MINO 50
DEX
Veh
LPS
C
CD11b+ cells (%)
100
80
60
40
20
0
*
**
M0
LPS
MINO 10
MINO 25
MINO 50
DEX
Veh
LPS
D
CD11b (MFI) Fold Change
1.5
1.0
0.5
0.0
****
***
M0
LPS
MINO 10
MINO 25
MINO 50
DEX
Veh
LPS
E
CD80+ cells (%)
100
80
60
40
20
0
*
****
****
****
M0
LPS
MINO 10
MINO 25
MINO 50
DEX
Veh
LPS
F
CD80 (MFI) Fold Change
15
10
5
0
****
****
****
M0
LPS
MINO 10
MINO 25
MINO 50
DEX
Veh
LPS

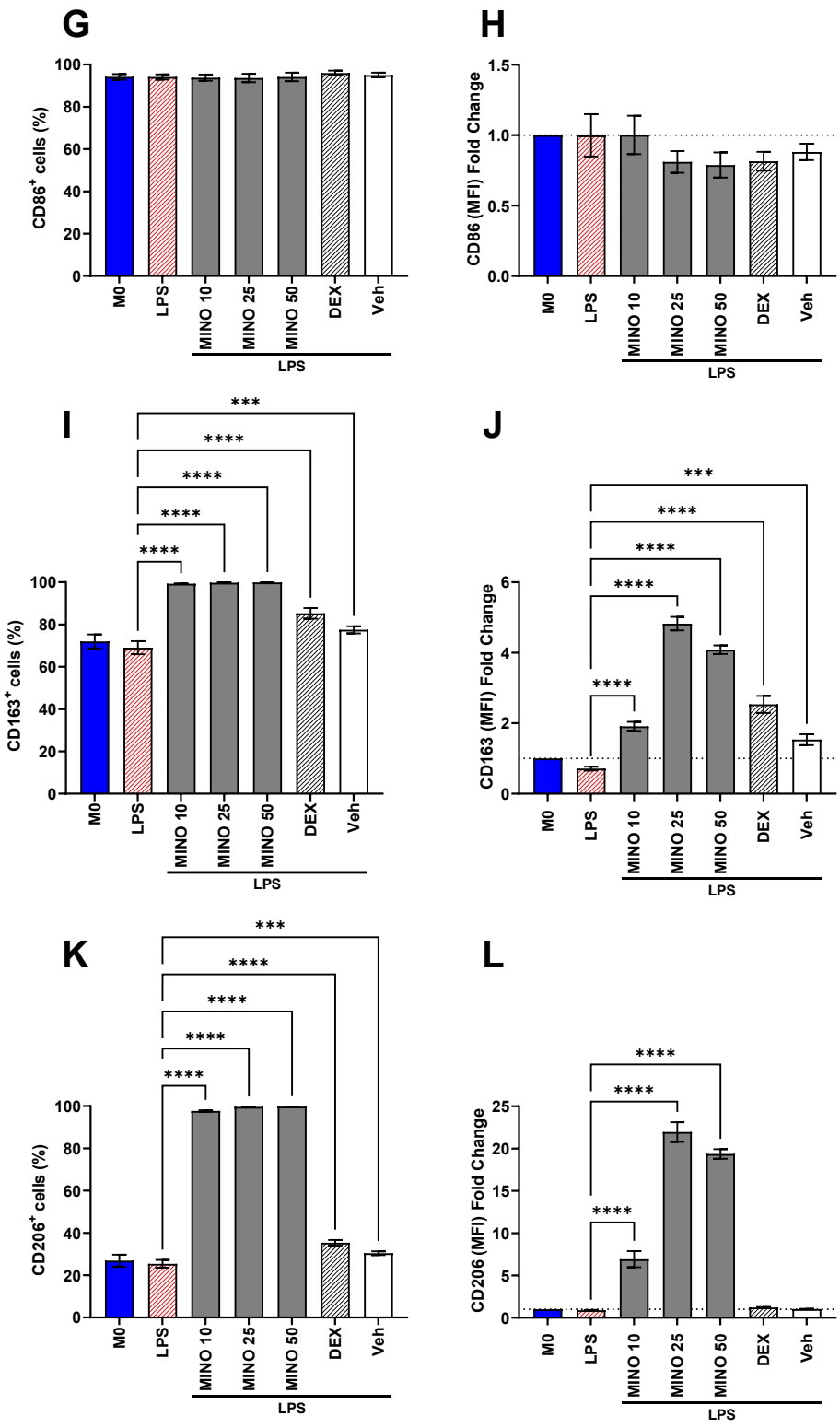

A10.4: Effect of minocycline on surface marker expression following LPS-activation of U-937 macrophages: biological replicate 2. Data obtained from adherent cells after 24hr incubation of differentiated M0 macrophages with LPS (100ng/mL). [A-L] Bar graphs showing the percentage of $CD14^+$ [A], $CD11b^+$ [C], $CD80^+$ [E], $CD86^+$ [G], $CD163^+$ [I] and $CD206^+$ [K] cells, and MFI values for CD14 [B], CD11b [D], CD80 [F], CD86 [H], CD163 [J] and CD206 [L].

MINO 10 = Minocycline 10μM, MINO 25 = Minocycline 25μM, MINO 50 = Minocycline 50μM, DEX = Dexamethasone 50μM, Veh = DMSO vehicle control 1:1000. Data presented as mean ± SD. MFI values displayed as fold change versus the un-activated M0 macrophage control. One-way ANOVA with post hoc Dunnett's applied versus the LPS-activated M0 macrophage. **p*<0.05; ***p*<0.01; ****p*<0.001; *****p*<0.0001.

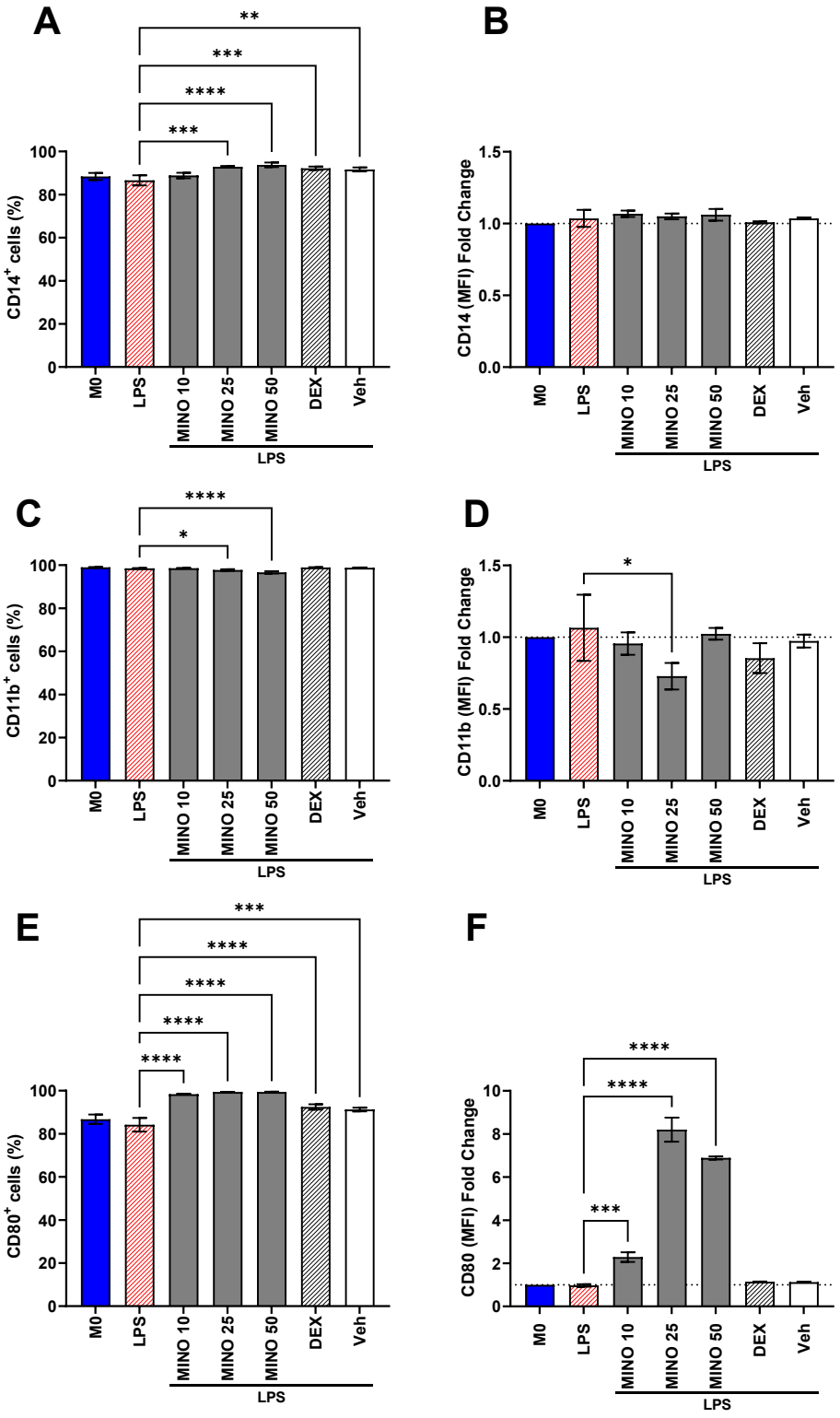

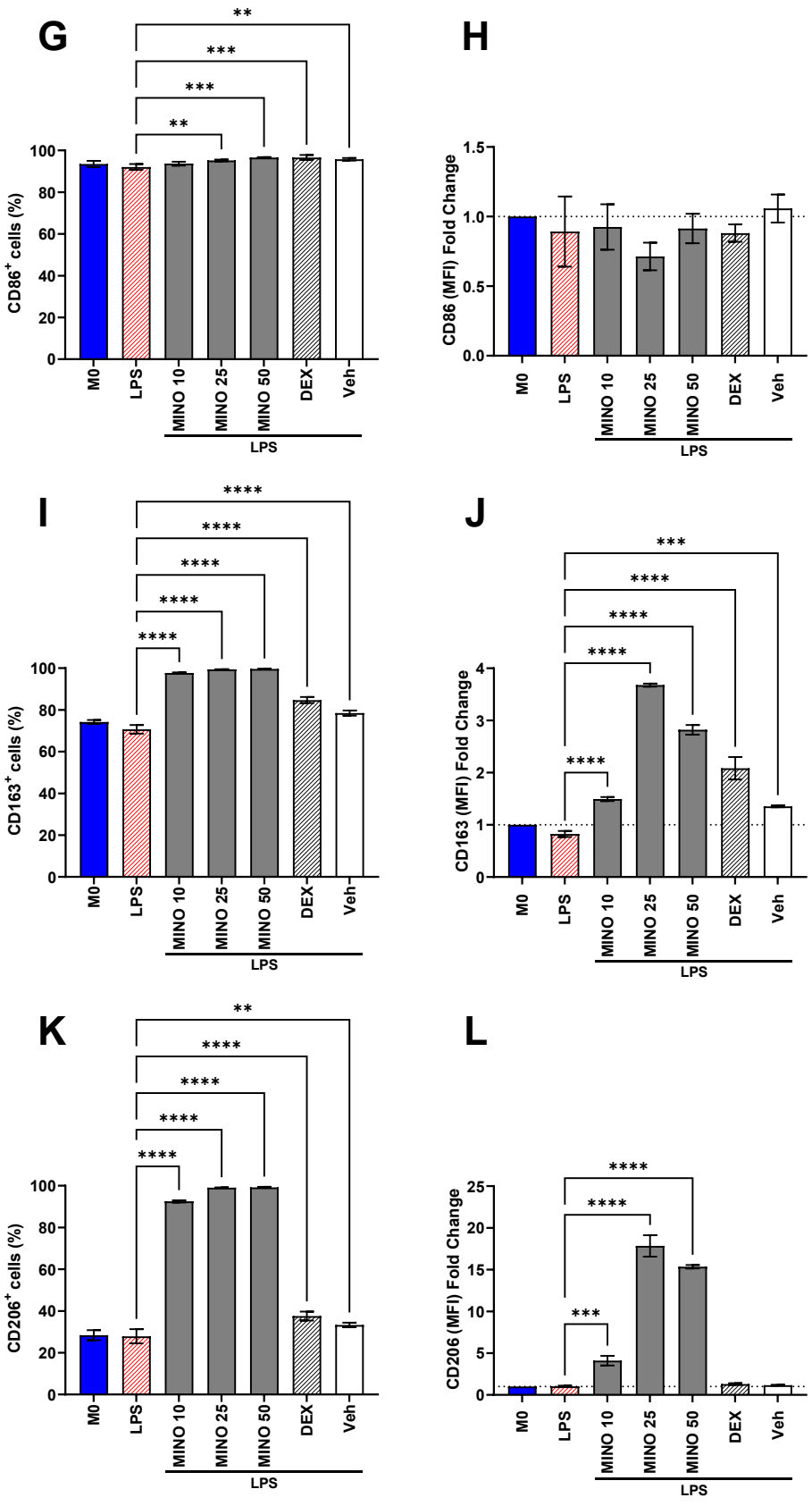
G
CD86+ cells (%)
M0
LPS
MINO 10
MINO 25
MINO 50
DEX
Veh
LPS
H
CD86 (MFI) Fold Change
I
CD163+ cells (%)
J
CD163 (MFI) Fold Change
K
CD206+ cells (%)
L
CD206 (MFI) Fold Change

A10.5: Effect of minocycline on surface marker expression following LPS-activation of U-937 macrophages: biological replicate 3. Data obtained from adherent cells after 24hr incubation of differentiated M0 macrophages with LPS (100ng/mL). [A-L] Bar graphs showing the percentage of $CD14^+$ [A], $CD11b^+$ [C], $CD80^+$ [E], $CD86^+$ [G], $CD163^+$ [I] and $CD206^+$ [K] cells, and MFI values for CD14 [B], CD11b [D], CD80 [F], CD86 [H], CD163 [J] and CD206 [L]. MINO 10 = Minocycline 10μM, MINO 25 = Minocycline 25μM, MINO 50 = Minocycline 50μM, DEX = Dexamethasone 50μM, Veh = DMSO vehicle control 1:1000. Data presented as mean ± SD. MFI values displayed as fold change versus the un-activated M0 macrophage control. One-way ANOVA with post hoc Dunnett's applied versus the LPS-activated M0 macrophage. *p<0.05; **p<0.01; ***p<0.001; ****p<0.0001.

A11: M1 and M2 polarization of THP-1 PMA-differentiated M0 macrophages: protocol optimization

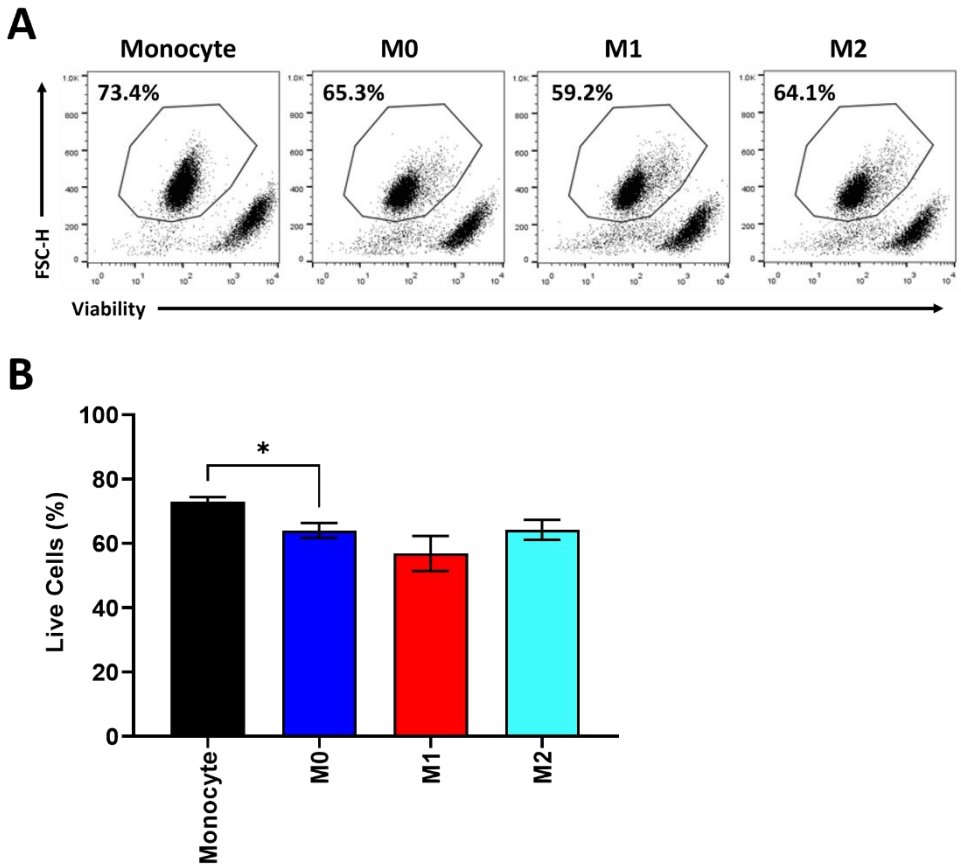

A11.1: Optimization 1 - Assessment of M1 and M2 polarization on total adherent cell viability. Data obtained after 24hr incubation of differentiated THP-1 M0 macrophages with M1 polarizing agents IFN-γ (20ng/mL) + LPS (10ng/mL), or M2 polarizing agent IL-4 (20ng/mL). [A] Representative contour plots showing the percentage of live cells (Zombie $Aqua^{neg}$) cells. [B] Bar graph showing the percentage of live cells. Plots illustrate one representative value. Graph represents 1 experiment comprising of triplicate values. Data presented as mean ± SD. One-way ANOVA with post hoc Dunnett's applied versus the unpolarized M0 macrophage. *p<0.05.

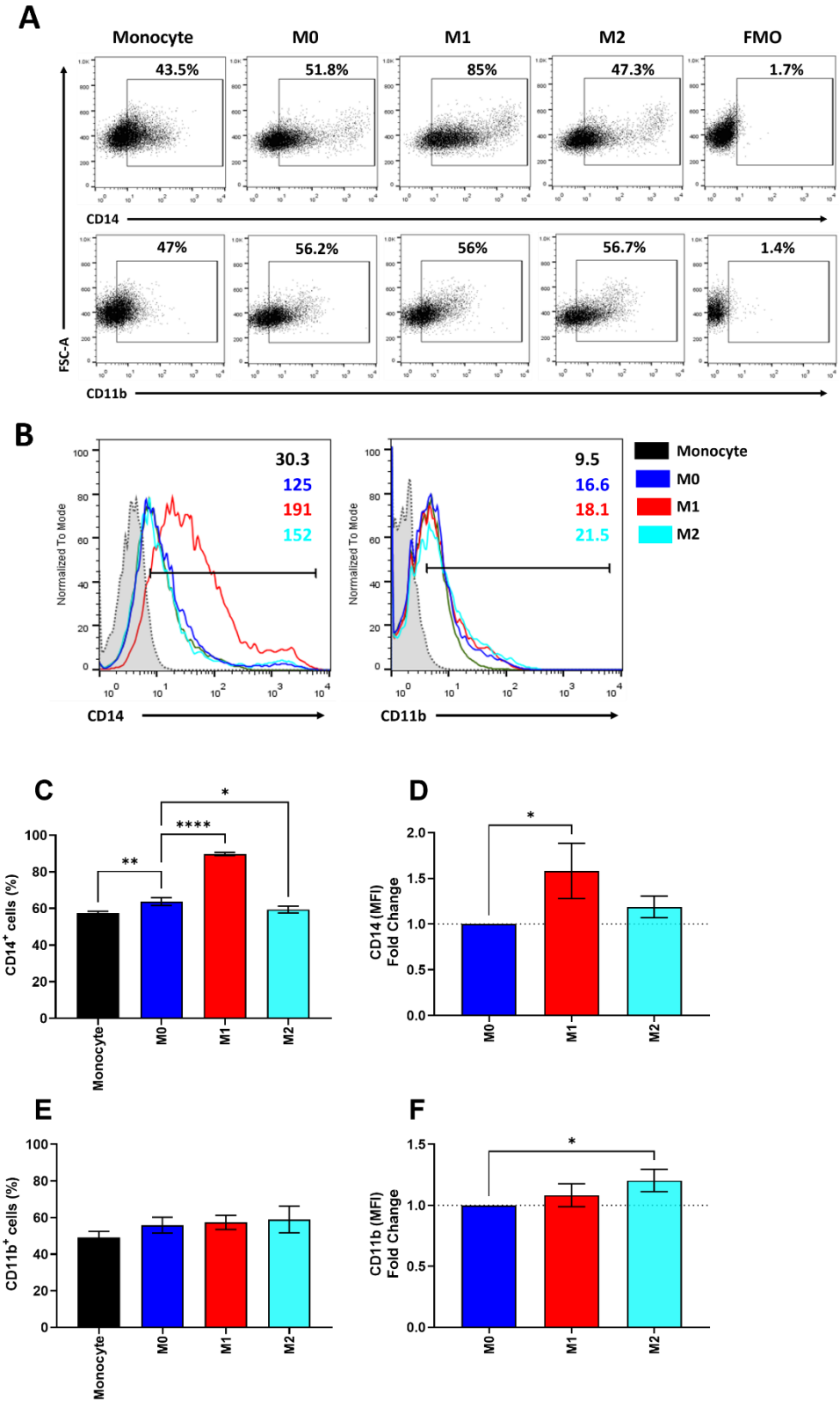
A
Monocyte
M0
M1
M2
FMO
43.5%
51.8%
85%
47.3%
1.7%
CD14
47%
56.2%
56%
56.7%
1.4%
FSC-A
CD11b
B
30.3
125
191
152
9.5
16.6
18.1
21.5
Normalized To Mode
CD14
CD11b
Monocyte
M0
M1
M2
C
CD14+ cells (%)
D
CD14 (MFI) Fold Change
E
CD11b+ cells (%)
F
CD11b (MFI) Fold Change

A11.2: Optimization 1 - Assessment of M1 and M2 polarization on CD14 and CD11b surface marker expression. Data obtained after 24hr incubation of differentiated M0 macrophages with M1 polarizing agents IFN-γ (20ng/mL) + LPS (10ng/mL), or M2 polarizing agent IL-4 (20ng/mL). [A] Representative contour plots showing the percentage of $CD14^+$ (top) and $CD11b^+$ (bottom) cells. [B] Representative histograms showing mean fluorescent intensity (MFI) of CD14 (left) and CD11b (right). Numbers indicate MFI of live gated population. [C-F] Bar graphs showing the percentage of $CD14^+$ [C] and $CD11b^+$ [E] cells, and MFI values for CD14 [D] and CD11b [F]. MFI values displayed as fold change versus the un-polarized M0 macrophage control. Plots and histograms illustrate one representative condition. Graphical data represent 1 experiment comprising of triplicate values. Data presented as mean ± SD. One-way ANOVA with post hoc Dunnett's applied versus the unpolarized M0 macrophage. *p<0.05; **p<0.01; ****p<0.0001.

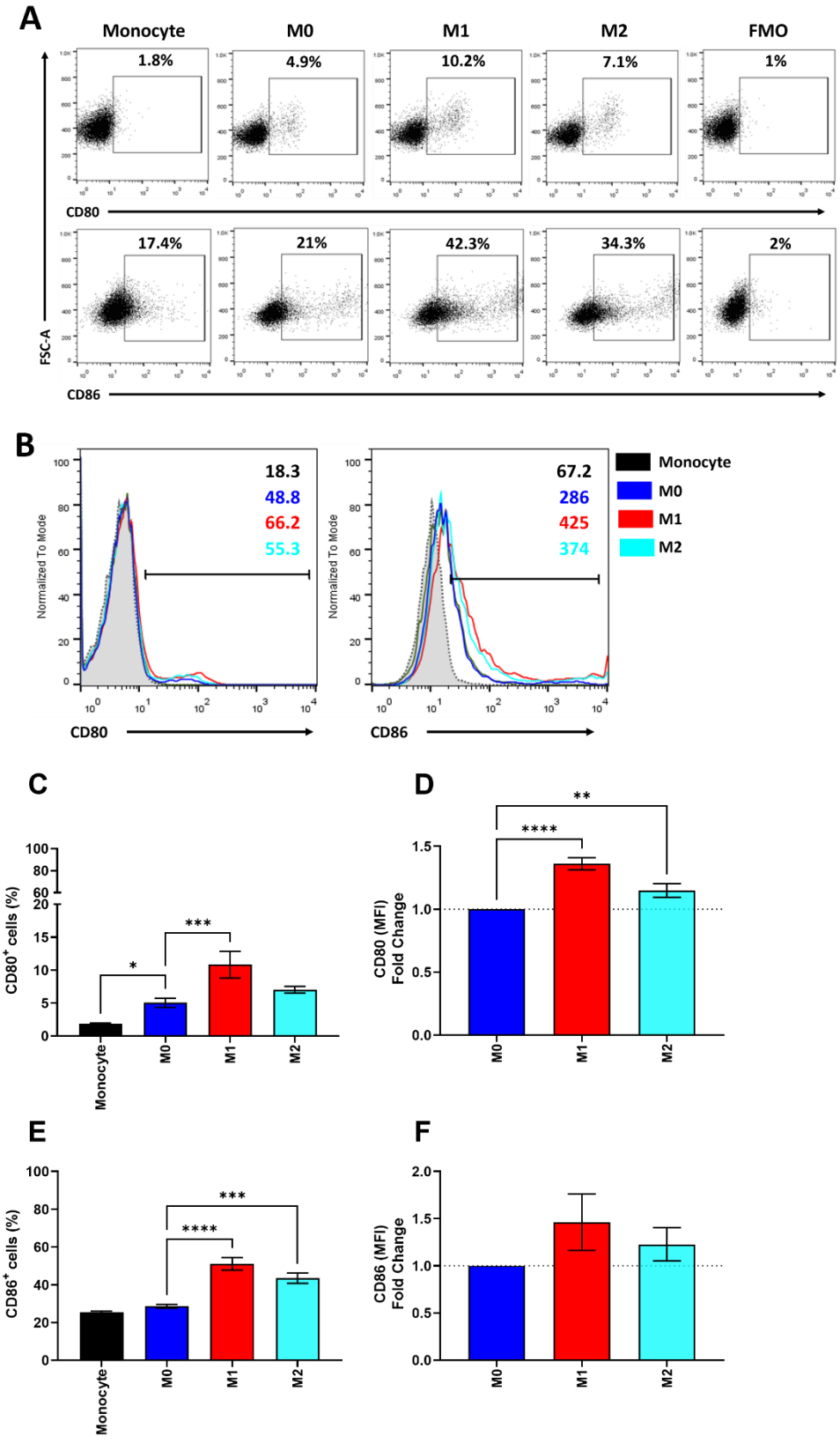
A
Monocyte
M0
M1
M2
FMO
1.8%
4.9%
10.2%
7.1%
1%
CD80
17.4%
21%
42.3%
34.3%
2%
FSC-A
CD86
B
18.3
48.8
66.2
55.3
67.2
286
425
374
Monocyte
M0
M1
M2
Normalized To Mode
CD80
CD86
C
CD80+ cells (%)
*
***
Monocyte
M0
M1
M2
D
**
****
CD80 (MFI) Fold Change
M0
M1
M2
E
CD86+ cells (%)
***
****
Monocyte
M0
M1
M2
F
CD86 (MFI) Fold Change
M0
M1
M2

A11.3: Optimization 1 - Assessment of M1 and M2 polarization on CD80 and CD86 surface marker expression. Data obtained after 24hr incubation of differentiated M0 macrophages with M1 polarizing agents IFN-γ (20ng/mL) + LPS (10ng/mL), or M2 polarizing agent IL-4 (20ng/mL). [A] Representative contour plots showing the percentage of $CD80^+$ (top) and $CD86^+$ (bottom) cells. [B] Representative histograms showing mean fluorescent intensity (MFI) of CD80 (left) and CD86 (right). Numbers indicate MFI of live gated population. [C-F] Bar graphs showing the percentage of $CD80^+$ [C] and $CD86^+$ [E] cells, and MFI values for CD80 [D] and CD86 [F]. MFI values displayed as fold change versus the un-polarized M0 macrophage control. Plots and histograms illustrate one representative condition. Graphical data represent 1 experiment comprising of triplicate values. Data presented as mean ± SD. One-way ANOVA with post hoc Dunnett's applied versus the unpolarized M0 macrophage. *p<0.05; **p<0.01; ***p<0.001; ****p<0.0001.

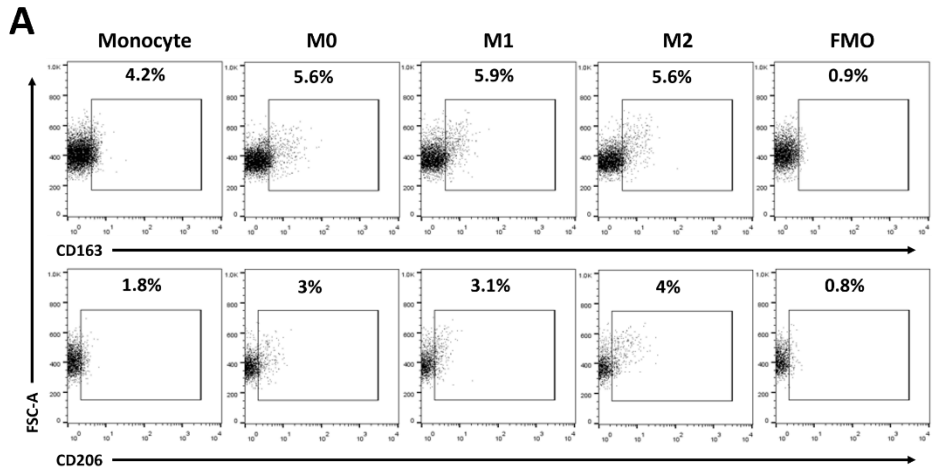
A
Monocyte
M0
M1
M2
FMO
4.2%
5.6%
5.9%
5.6%
0.9%
CD163
1.8%
3%
3.1%
4%
0.8%
FSC-A
CD206

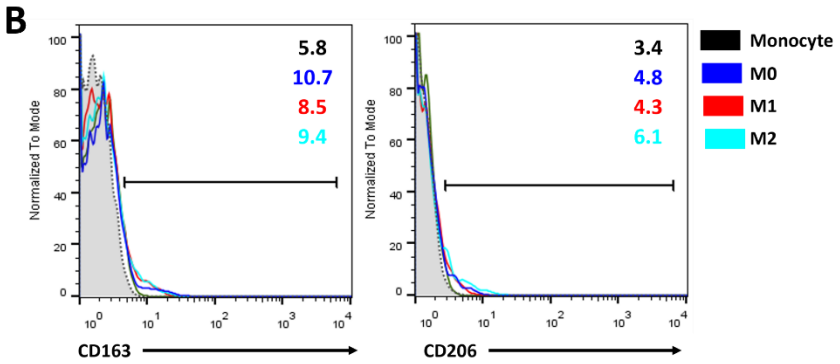
B
5.8
10.7
8.5
9.4
3.4
4.8
4.3
6.1
Monocyte
M0
M1
M2
Normalized To Mode
CD163
CD206

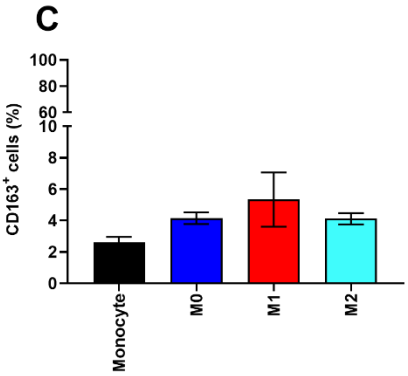
C
CD163+ cells (%)
Monocyte
M0
M1
M2

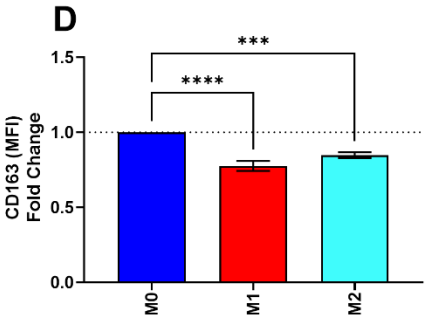
D
CD163 (MFI) Fold Change
***
****
M0
M1
M2

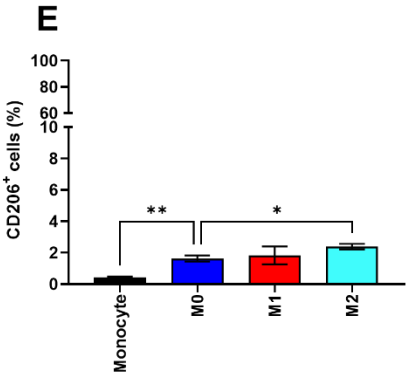
E
CD206+ cells (%)
**
*
Monocyte
M0
M1
M2

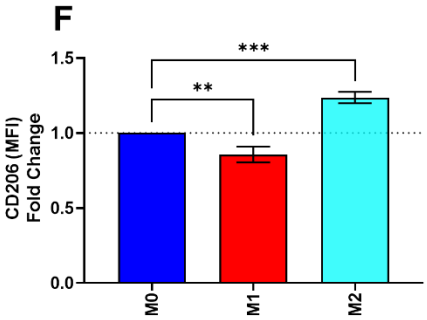
F
CD206 (MFI) Fold Change
***
**
M0
M1
M2

A11.4: Optimization 1 - Assessment of M1 and M2 polarization on CD163 and CD206 surface marker expression. Data obtained after 24hr incubation of differentiated M0 macrophages with M1 polarizing agents IFN-γ (20ng/mL) + LPS (10ng/mL), or M2 polarizing agent IL-4 (20ng/mL). [A] Representative contour plots showing the percentage of $CD163^+$ (top) and $CD206^+$ (bottom) cells. [B] Representative histograms showing mean fluorescent intensity (MFI) of CD163 (left) and CD206 (right). Numbers indicate MFI of live gated population. [C-F] Bar graphs showing the percentage of $CD163^+$ [C] and $CD206^+$ [E] cells, and MFI values for CD163 [D] and CD206 [F]. MFI values displayed as fold change versus the un-polarized M0 macrophage control. Plots and histograms illustrate one representative condition. Graphical data represent 1 experiment comprising of triplicate values. Data presented as mean ± SD. One-way ANOVA with post hoc Dunnett's applied versus the unpolarized M0 macrophage. *p<0.05; **p<0.01; ***p<0.001; ****p<0.0001.

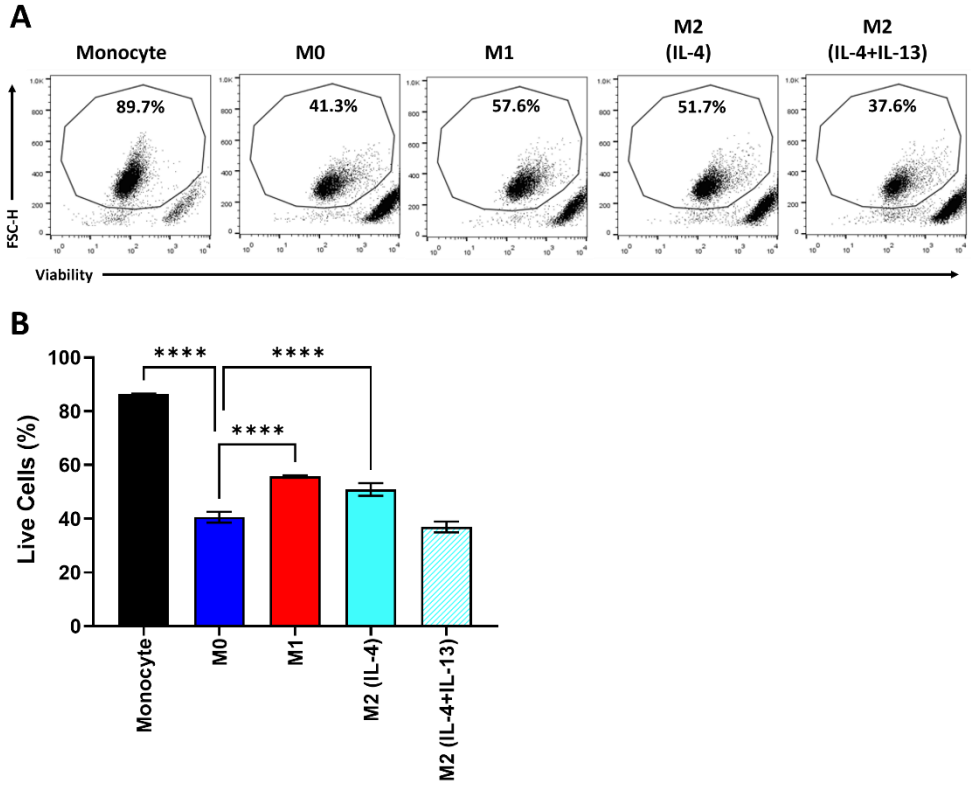

A11.5: Optimization 2 - Assessment of M1 and different M2 polarization protocols on total adherent cell viability. Data obtained after 24hr incubation of differentiated THP-1 M0 macrophages with M1 polarizing agents IFN-γ (20ng/mL) + LPS (10ng/mL), or M2 polarizing agents IL-4 (20ng/mL), or IL-4 (20ng/mL) + IL-13 (20ng/mL). [A] Representative contour plots showing the percentage of live cells (Zombie $Aqua^{neg}$) cells. [B] Bar graph showing the percentage of live cells. Plots illustrate one representative value. Graph represents 1 experiment comprising of triplicate values. Data presented as mean ± SD. One-way ANOVA with post hoc Dunnett's applied versus the unpolarized M0 macrophage. ****p<0.0001.

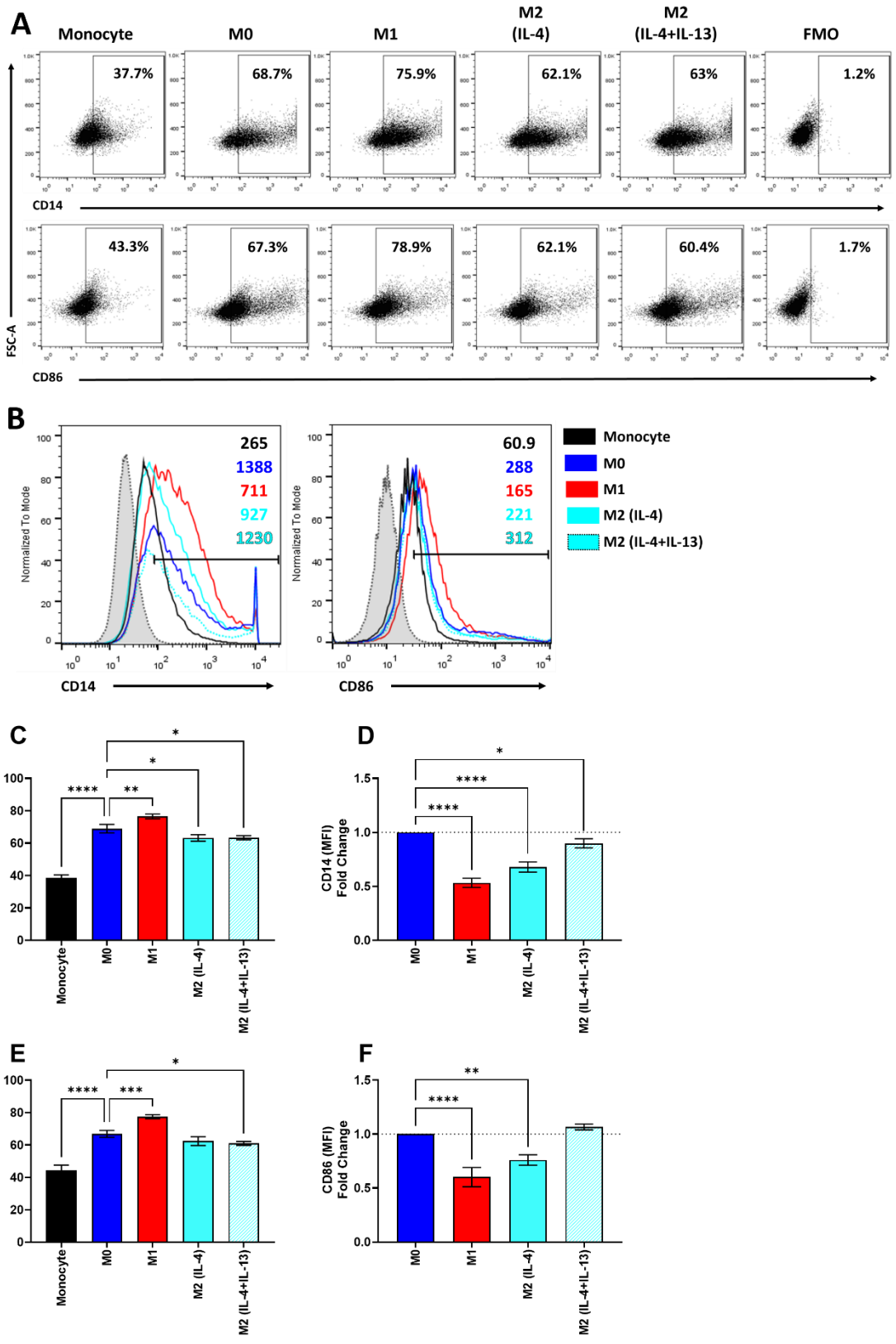
A
Monocyte
M0
M1
M2 (IL-4)
M2 (IL-4+IL-13)
FMO
37.7%
68.7%
75.9%
62.1%
63%
1.2%
43.3%
67.3%
78.9%
62.1%
60.4%
1.7%
CD14
CD86
FSC-A
B
265
1388
711
927
1230
60.9
288
165
221
312
Normalized To Mode
Monocyte
M0
M1
M2 (IL-4)
M2 (IL-4+IL-13)
C
CD14+ cells (%)
D
CD14 (MFI) Fold Change
E
CD86+ cells (%)
F
CD86 (MFI) Fold Change

A11.6: Optimization 2 - Assessment of M1 and different M2 polarization protocols on CD14 and CD86 surface marker expression. Data obtained after 24hr incubation of differentiated M0 macrophages with M1 polarizing agents IFN-γ (20ng/mL) + LPS (10ng/mL), or M2 polarizing agents IL-4 (20ng/mL), or IL-4 (20ng/mL) + IL-13 (20ng/mL). [A] Representative contour plots showing the percentage of $CD14^+$ (top) and $CD86^+$ (bottom) cells. [B] Representative histograms showing mean fluorescent intensity (MFI) of CD14 (left) and CD86 (right). Numbers indicate MFI of live gated population. [C-F] Bar graphs showing the percentage of $CD14^+$ [C] and $CD86^+$ [E] cells, and MFI values for CD14 [D] and CD86 [F]. MFI values displayed as fold change versus the un-polarized M0 macrophage control. Plots and histograms illustrate one representative condition. Graphical data represent 1 experiment comprising of triplicate values. Data presented as mean ± SD. One-way ANOVA with post hoc Dunnett's applied versus the unpolarized M0 macrophage. *p<0.05; **p<0.01; ***p<0.001; ****p<0.0001.

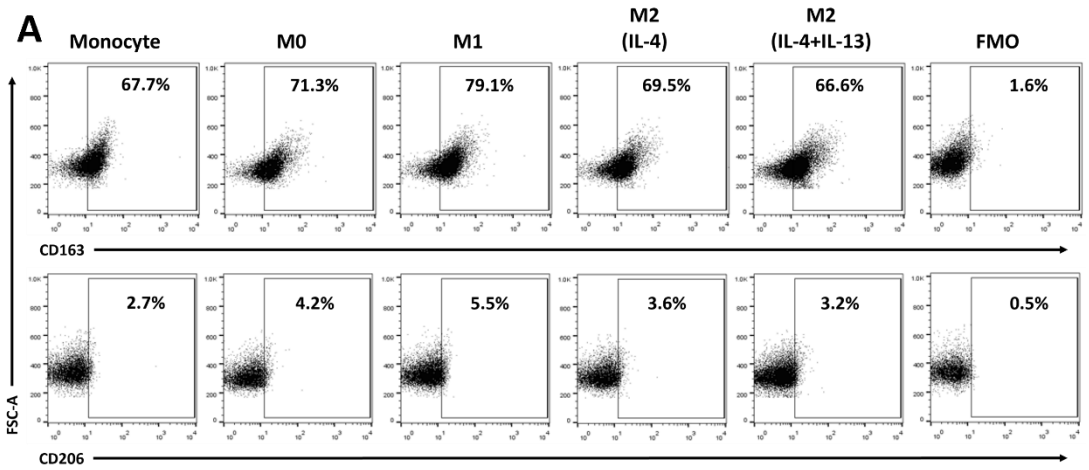
A
Monocyte
M0
M1
M2 (IL-4)
M2 (IL-4+IL-13)
FMO
67.7%
71.3%
79.1%
69.5%
66.6%
1.6%
CD163
2.7%
4.2%
5.5%
3.6%
3.2%
0.5%
FSC-A
CD206

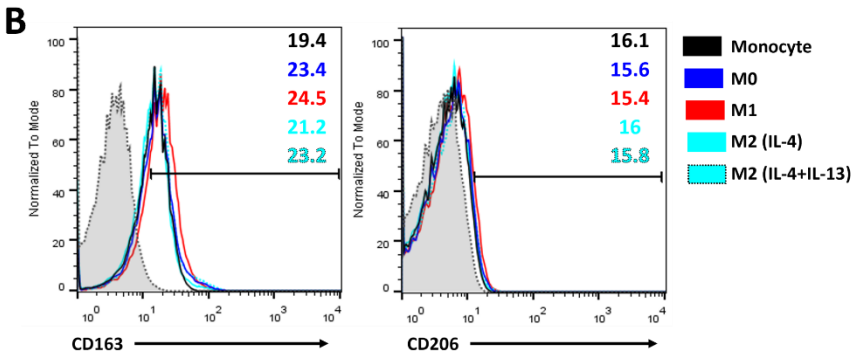
B
19.4
23.4
24.5
21.2
23.2
16.1
15.6
15.4
16
15.8
Normalized To Mode
CD163
CD206
Monocyte
M0
M1
M2 (IL-4)
M2 (IL-4+IL-13)

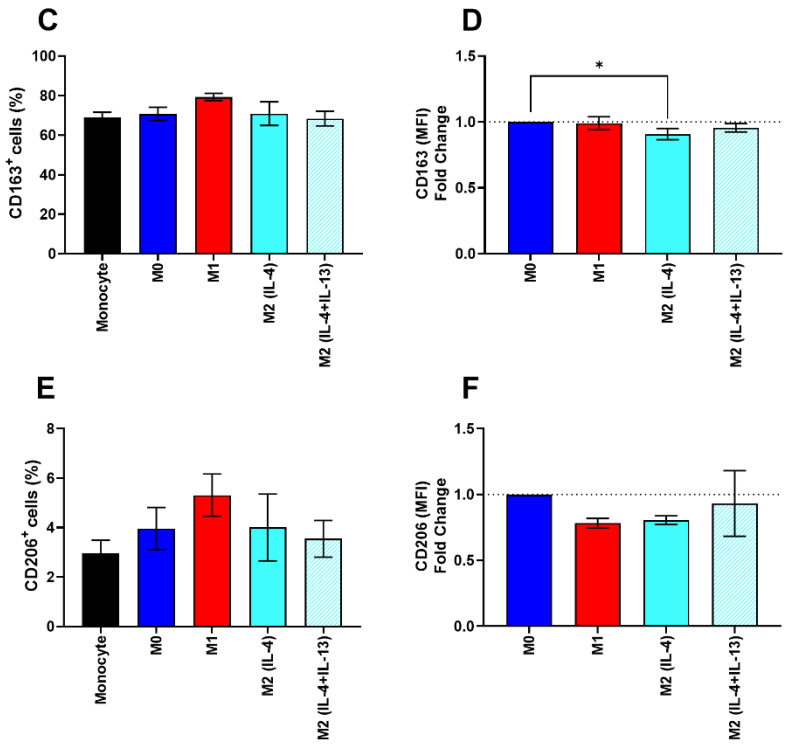
C
CD163+ cells (%)
Monocyte
M0
M1
M2 (IL-4)
M2 (IL-4+IL-13)
D
CD163 (MFI) Fold Change
*

E
CD206+ cells (%)
F
CD206 (MFI) Fold Change

A11.7: Optimization 2 - Assessment of M1 and different M2 polarization protocols on CD163 and CD206 surface marker expression. Data obtained after 24hr incubation of differentiated M0 macrophages with M1 polarizing agents IFN-γ (20ng/mL) + LPS (10ng/mL), or M2 polarizing agents IL-4 (20ng/mL), or IL-4 (20ng/mL) + IL-13 (20ng/mL). [A] Representative contour plots showing the percentage of $CD163^+$ (top) and $CD206^+$ (bottom) cells. [B] Representative histograms showing mean fluorescent intensity (MFI) of CD163 (left) and CD206 (right). Numbers indicate MFI of live gated population. [C-F] Bar graphs showing the percentage of $CD163^+$ [C] and $CD206^+$ [E] cells, and MFI values for CD163 [D] and CD206 [F]. MFI values displayed as fold change versus the un-polarized M0 macrophage control. Plots and histograms illustrate one representative condition. Graphical data represent 1 experiment comprising of triplicate values. Data presented as mean ± SD. One-way ANOVA with post hoc Dunnett's applied versus the unpolarized M0 macrophage. *p<0.05.

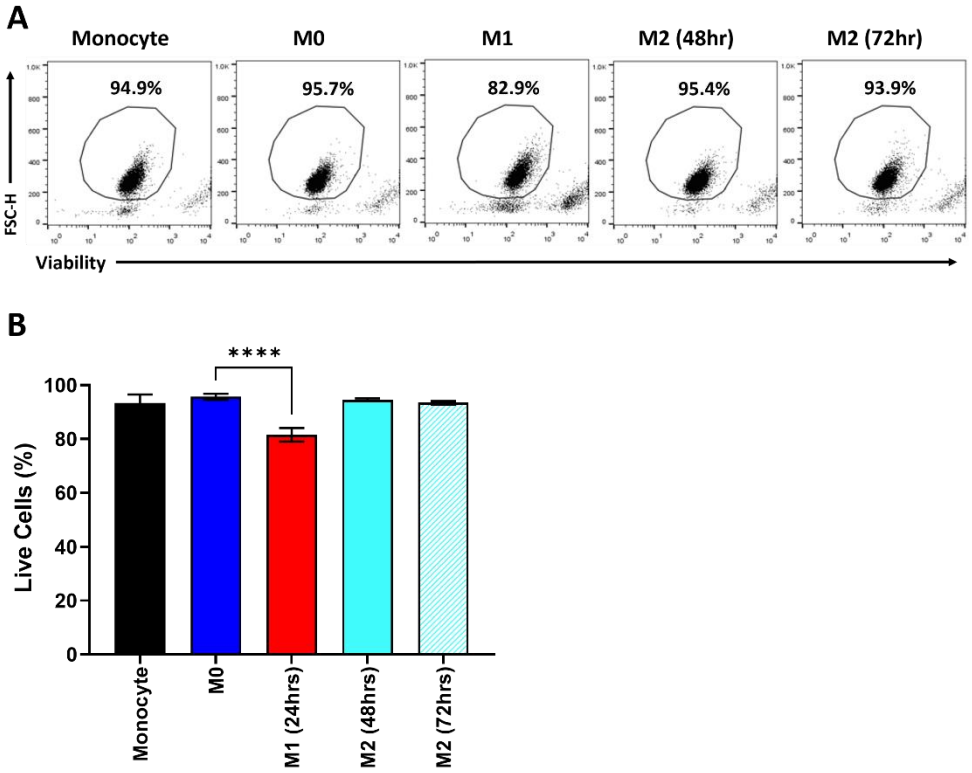

A11.8: Optimization 3 - Assessment of M1 and different M2 polarization protocols on total adherent cell viability. Data obtained after 24hr incubation of differentiated THP-1 M0 macrophages with M1 polarizing agents IFN-γ (20ng/mL) + LPS (10ng/mL), or M2 polarizing agent IL-4 (20ng/mL) incubated for 24hr or 48hr. [A] Representative contour plots showing the percentage of live cells (Zombie $Aqua^{neg}$) cells. [B] Bar graph showing the percentage of live cells. Plots illustrate one representative value. Graph represents 1 experiment comprising of triplicate values. Data presented as mean ± SD. One-way ANOVA with post hoc Dunnett's applied versus the unpolarized M0 macrophage. ****p<0.0001.

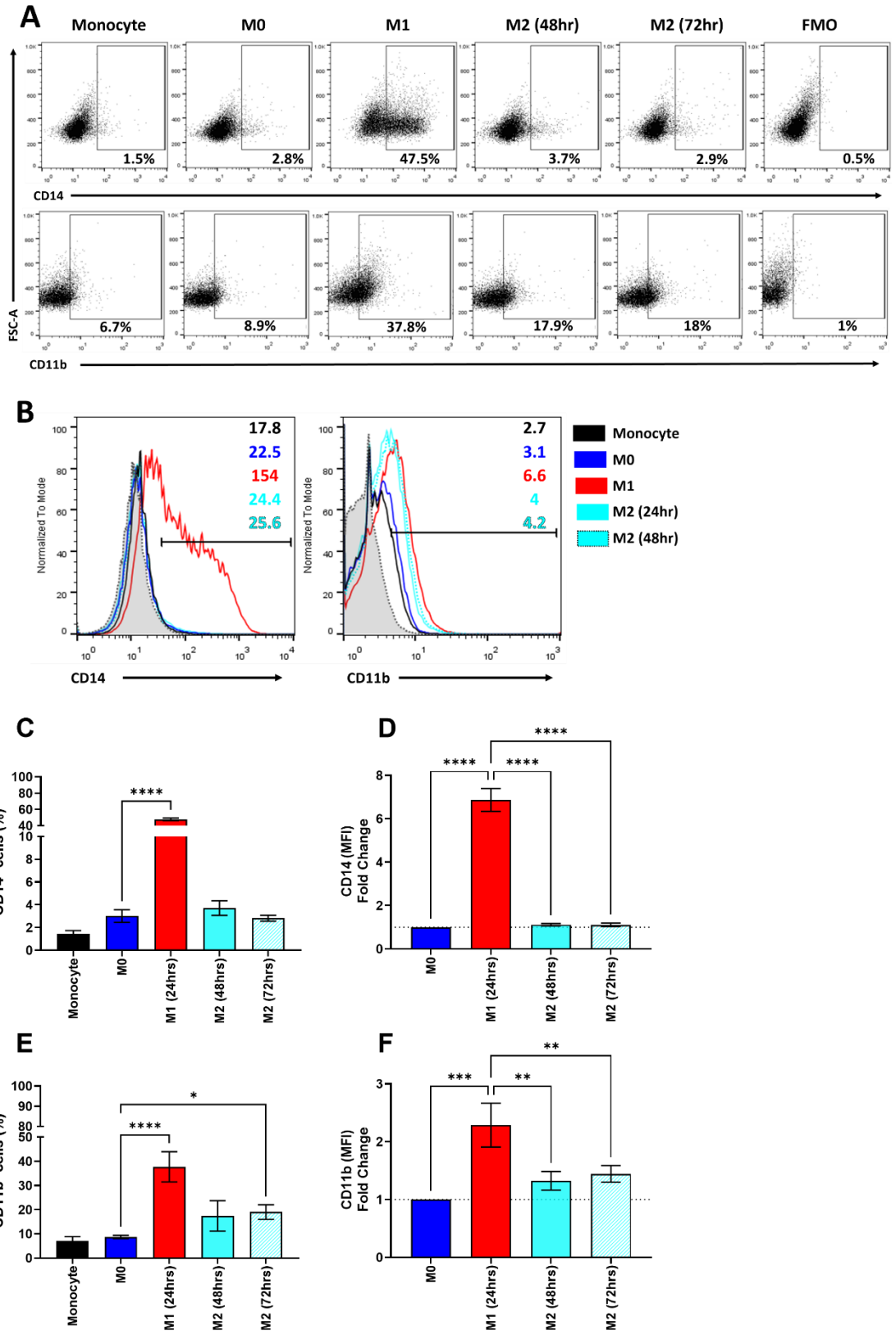
A
Monocyte
M0
M1
M2 (48hr)
M2 (72hr)
FMO
1.5%
2.8%
47.5%
3.7%
2.9%
0.5%
CD14
6.7%
8.9%
37.8%
17.9%
18%
1%
FSC-A
CD11b
B
17.8
22.5
154
24.4
25.6
2.7
3.1
6.6
4
4.2
Normalized To Mode
CD14
CD11b
Monocyte
M0
M1
M2 (24hr)
M2 (48hr)
C
CD14+ cells (%)
****
Monocyte
M0
M1 (24hrs)
M2 (48hrs)
M2 (72hrs)
D
CD14 (MFI) Fold Change
****
****
****
E
CD11b+ cells (%)
*
****
F
CD11b (MFI) Fold Change
**
***
**

A11.9: Optimization 3 - Assessment of M1 and different M2 polarization protocols on CD14 and CD11b surface marker expression. Data obtained after 24hr incubation of differentiated THP-1 M0 macrophages with M1 polarizing agents IFN-γ (20ng/mL) + LPS (10ng/mL), or M2 polarizing agent IL-4 (20ng/mL) incubated for 24hr or 48hr. [A] Representative contour plots showing the percentage of $CD14^+$ (top) and $CD11b^+$ (bottom) cells. [B] Representative histograms showing mean fluorescent intensity (MFI) of CD14 (left) and CD11b (right). Numbers indicate MFI of live gated population. [C-F] Bar graphs showing the percentage of $CD14^+$ [C] and $CD11b^+$ [E] cells, and MFI values for CD14 [D] and CD11b [F]. MFI values displayed as fold change versus the un-polarized M0 macrophage control. Plots and histograms illustrate one representative condition. Graphical data represent 1 experiment comprising of triplicate values. Data presented as mean ± SD. One-way ANOVA with post hoc Dunnett's applied versus the unpolarized M0 macrophage. *p<0.05; **p<0.01; ***p<0.001; ****p<0.0001.

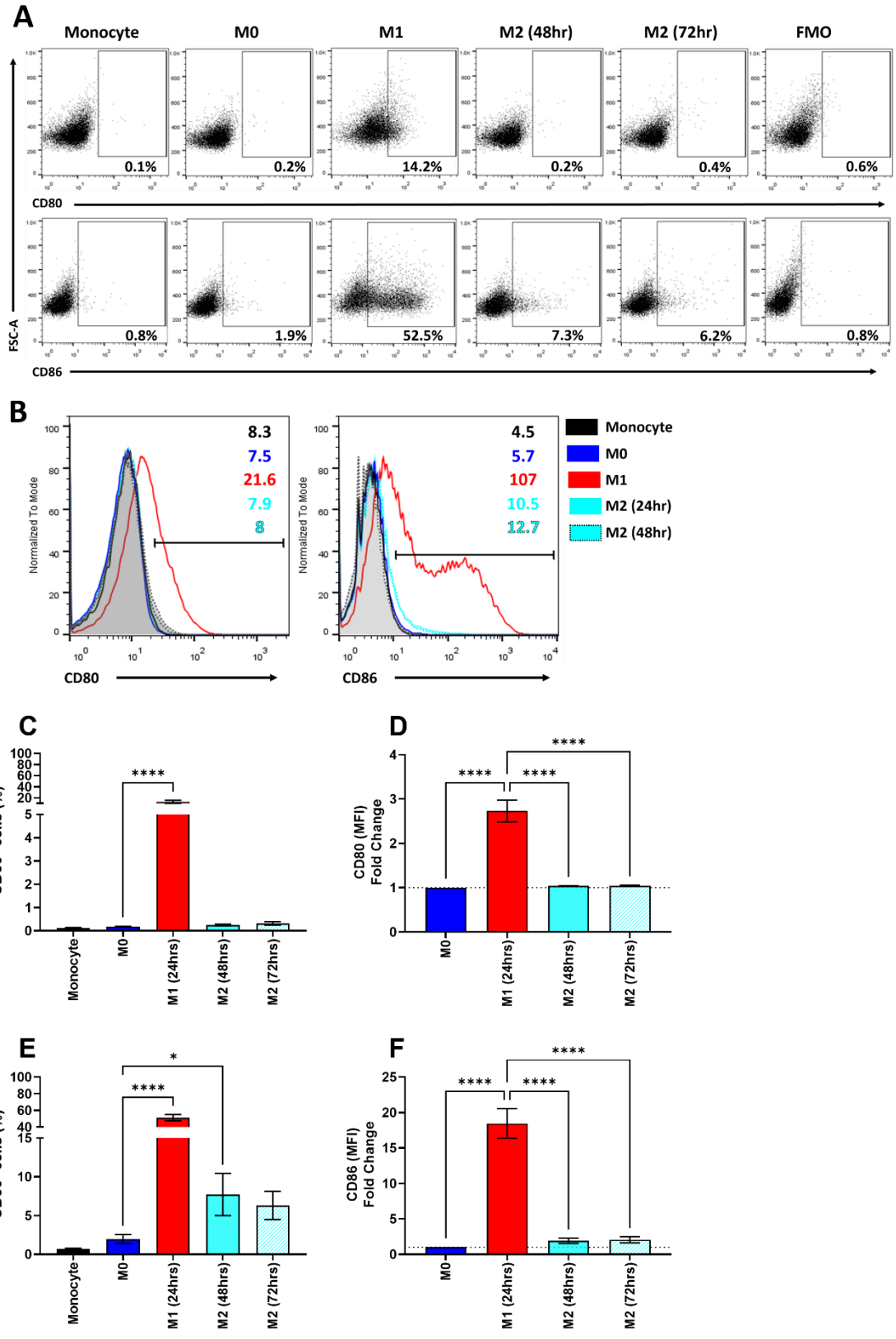
A
Monocyte
M0
M1
M2 (48hr)
M2 (72hr)
FMO
0.1%
0.2%
14.2%
0.2%
0.4%
0.6%
CD80
FSC-A
0.8%
1.9%
52.5%
7.3%
6.2%
0.8%
CD86
B
8.3
7.5
21.6
7.9
8
4.5
5.7
107
10.5
12.7
Normalized To Mode
CD80
CD86
Monocyte
M0
M1
M2 (24hr)
M2 (48hr)
C
CD80+ cells (%)
****
Monocyte
M0
M1 (24hrs)
M2 (48hrs)
M2 (72hrs)
D
CD80 (MFI) Fold Change
****
E
CD86+ cells (%)
*
F
CD86 (MFI) Fold Change

A11.10: Optimization 3 - Assessment of M1 and different M2 polarization protocols on CD80 and CD86 surface marker expression. Data obtained after 24hr incubation of differentiated THP-1 M0 macrophages with M1 polarizing agents IFN-γ (20ng/mL) + LPS (10ng/mL), or M2 polarizing agent IL-4 (20ng/mL) incubated for 24hr or 48hr. [A] Representative contour plots showing the percentage of $CD80^+$ (top) and $CD86^+$ (bottom) cells. [B] Representative histograms showing mean fluorescent intensity (MFI) of CD80 (left) and CD86 (right). Numbers indicate MFI of live gated population. [C-F] Bar graphs showing the percentage of $CD80^+$ [C] and $CD86^+$ [E] cells, and MFI values for CD80 [D] and CD86 [F]. MFI values displayed as fold change versus the un-polarized M0 macrophage control. Plots and histograms illustrate one representative condition. Graphical data represent 1 experiment comprising of triplicate values. Data presented as mean ± SD. One-way ANOVA with post hoc Dunnett's applied versus the unpolarized M0 macrophage. *p<0.05; ****p<0.0001.

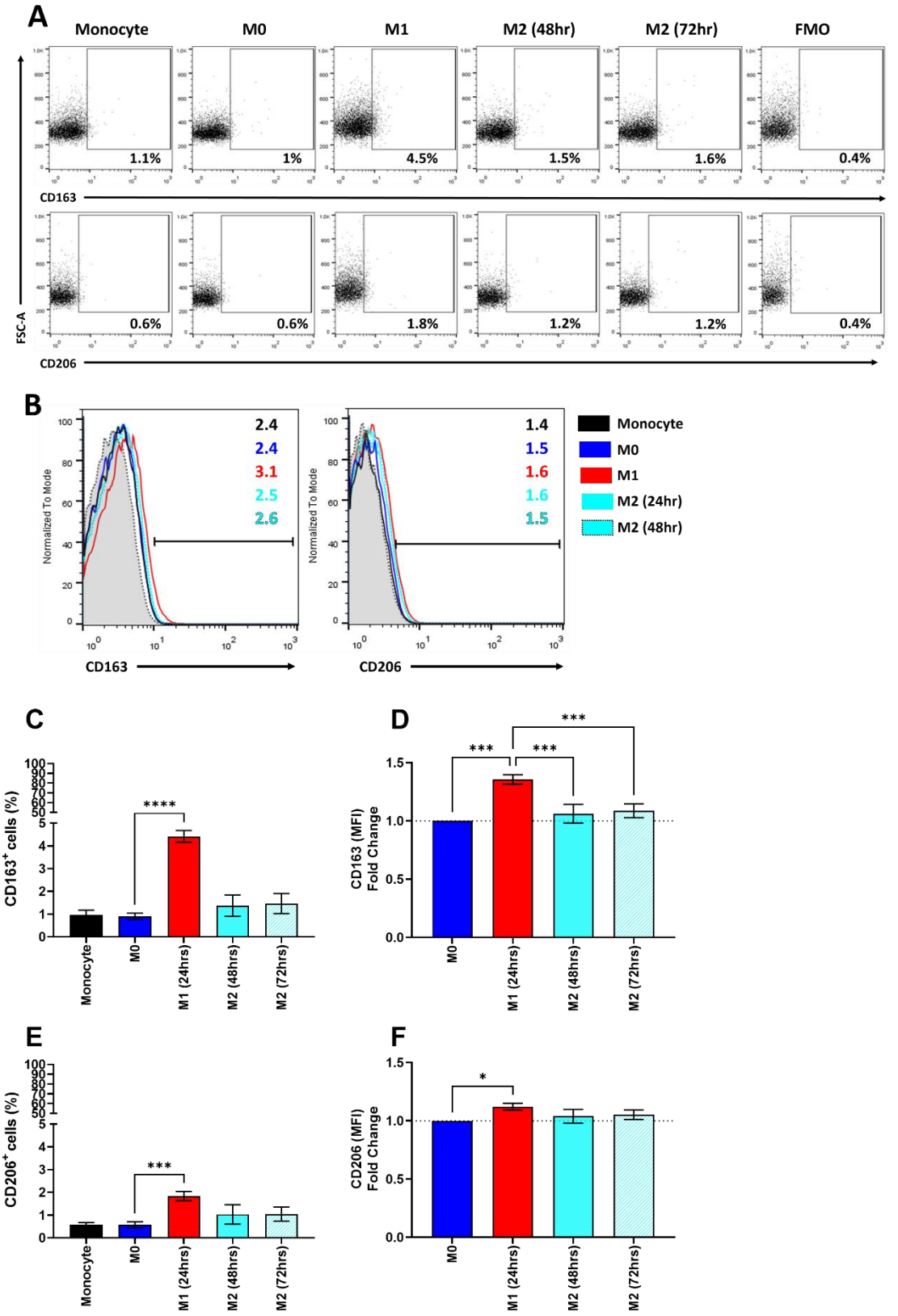

A11.11: Optimization 3 - Assessment of M1 and different M2 polarization protocols on CD163 and CD206 surface marker expression. Data obtained after 24hr incubation of differentiated THP-1 M0 macrophages with M1 polarizing agents IFN-γ (20ng/mL) + LPS (10ng/mL), or M2 polarizing agent IL-4 (20ng/mL) incubated for 24hr or 48hr. [A] Representative contour plots showing the percentage of $CD163^+$ (top) and $CD206^+$ (bottom) cells.

[B] Representative histograms showing mean fluorescent intensity (MFI) of CD163 (left) and CD206 (right). Numbers indicate MFI of live gated population. [C-F] Bar graphs showing the percentage of $CD163^{+}$ [C] and $CD206^{+}$ [E] cells, and MFI values for CD163 [D] and CD206 [F]. MFI values displayed as fold change versus the un-polarized M0 macrophage control. Plots and histograms illustrate one representative condition. Graphical data represent 1 experiment comprising of triplicate values. Data presented as mean ± SD. One-way ANOVA with post hoc Dunnett's applied versus the unpolarized M0 macrophage. *p<0.05; ***p<0.001; ****p<0.0001.

A12: M1 and M2 polarization of U-937 PMA-differentiated M0 macrophages: protocol optimization

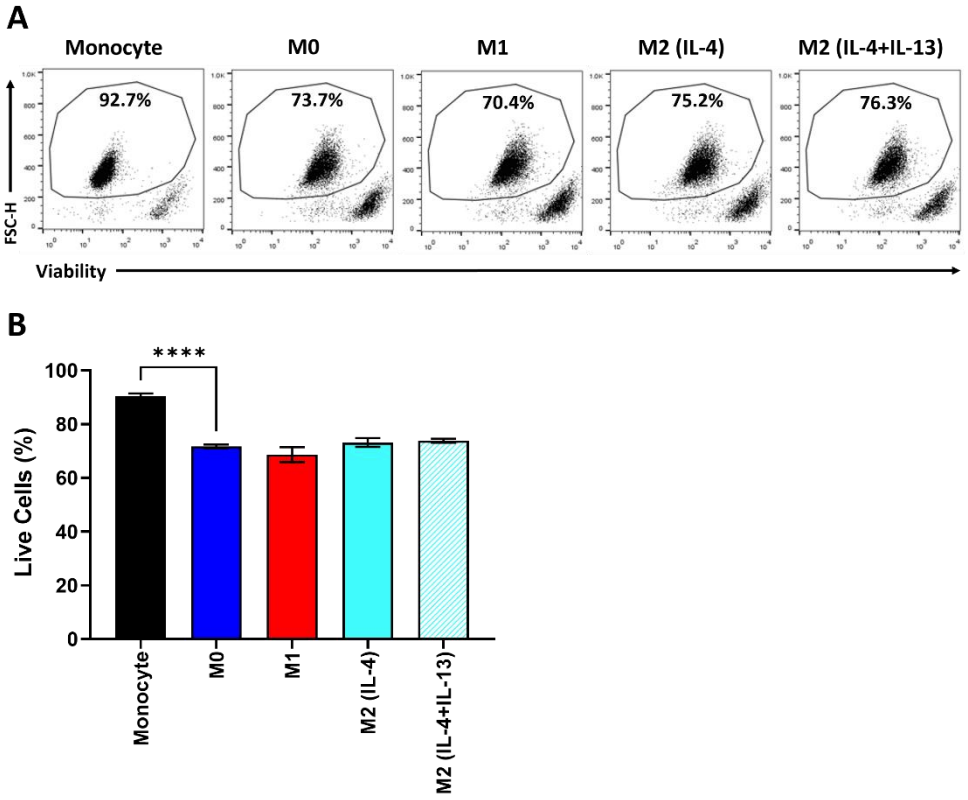

A12.1: Optimization 1 - Assessment of M1 and different M2 polarization protocols on total adherent cell viability. Data obtained after 24hr incubation of differentiated THP-1 M0 macrophages with M1 polarizing agents IFN-γ (20ng/mL) + LPS (10ng/mL), or M2 polarizing agents IL-4 (20ng/mL), or IL-4 (20ng/mL) + IL-13 (20ng/mL). [A] Representative contour plots showing the percentage of live cells (Zombie $Aqua^{neg}$) cells. [B] Bar graph showing the percentage of live cells. Plots illustrate one representative value. Graph represents 1 experiment comprising of triplicate values. Data presented as mean ± SD. One-way ANOVA with post hoc Dunnett's applied versus the unpolarized M0 macrophage. ****p<0.0001.

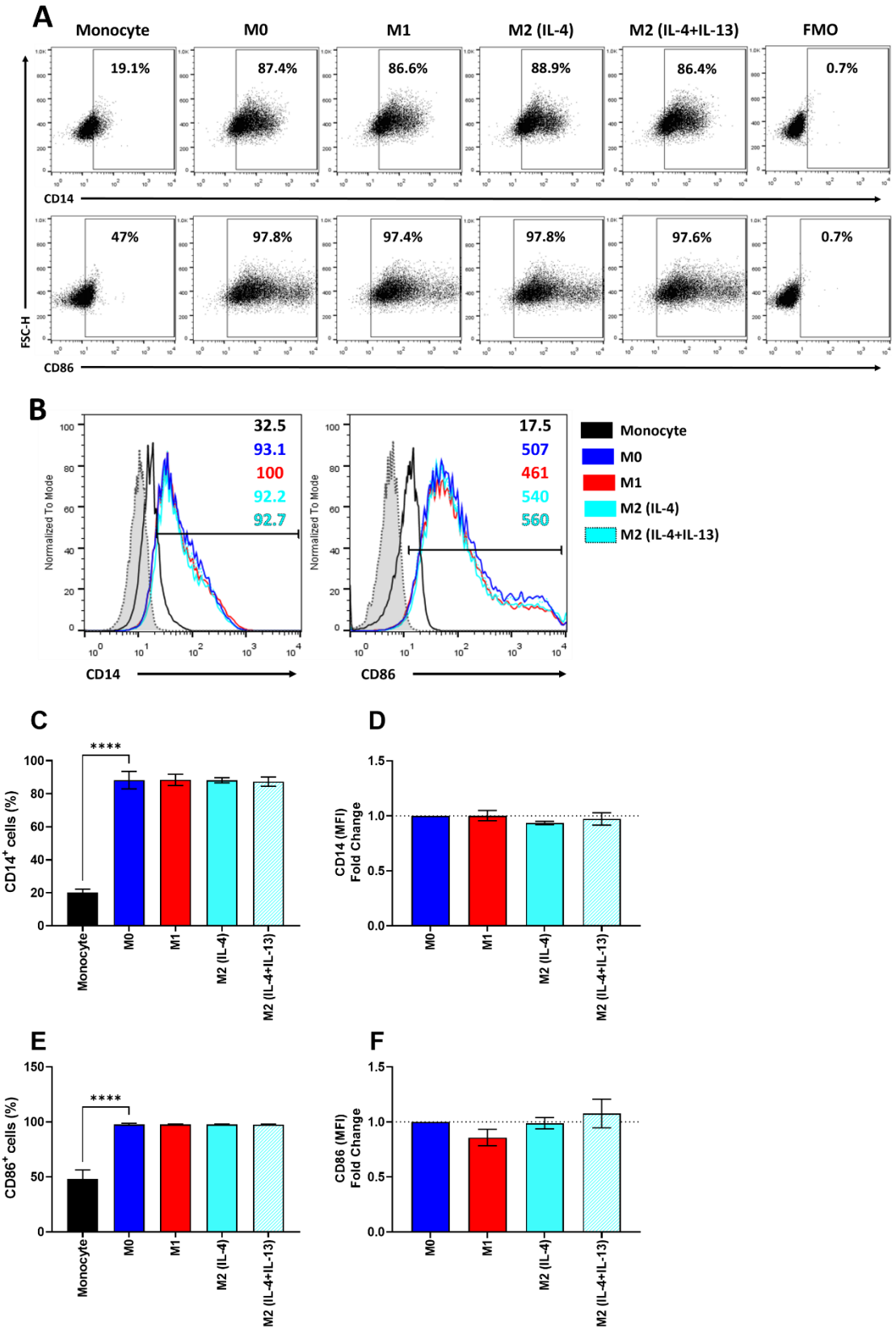
A
Monocyte
M0
M1
M2 (IL-4)
M2 (IL-4+IL-13)
FMO
19.1%
87.4%
86.6%
88.9%
86.4%
0.7%
47%
97.8%
97.4%
97.8%
97.6%
0.7%
CD14
CD86
FSC-H
B
32.5
93.1
100
92.2
92.7
17.5
507
461
540
560
Normalized To Mode
Monocyte
M0
M1
M2 (IL-4)
M2 (IL-4+IL-13)
C
D
CD14+ cells (%)
CD14 (MFI) Fold Change
****
E
F
CD86+ cells (%)
CD86 (MFI) Fold Change

A12.2: Optimization 1 - Assessment of M1 and different M2 polarization protocols on CD14 and CD86 surface marker expression. Data obtained after 24hr incubation of differentiated M0 macrophages with M1 polarizing agents IFN-γ (20ng/mL) + LPS (10ng/mL), or M2 polarizing agents IL-4 (20ng/mL), or IL-4 (20ng/mL) + IL-13 (20ng/mL). [A] Representative contour plots showing the percentage of $CD14^+$ (top) and $CD86^+$ (bottom) cells. [B] Representative histograms showing mean fluorescent intensity (MFI) of CD14 (left) and CD86 (right). Numbers indicate MFI of live gated population. [C-F] Bar graphs showing the percentage of $CD14^+$ [C] and $CD86^+$ [E] cells, and MFI values for CD14 [D] and CD86 [F]. MFI values displayed as fold change versus the un-polarized M0 macrophage control. Plots and histograms illustrate one representative condition. Graphical data represent 1 experiment comprising of triplicate values. Data presented as mean ± SD. One-way ANOVA with post hoc Dunnett's applied versus the unpolarized M0 macrophage. ****$p<0.0001$.

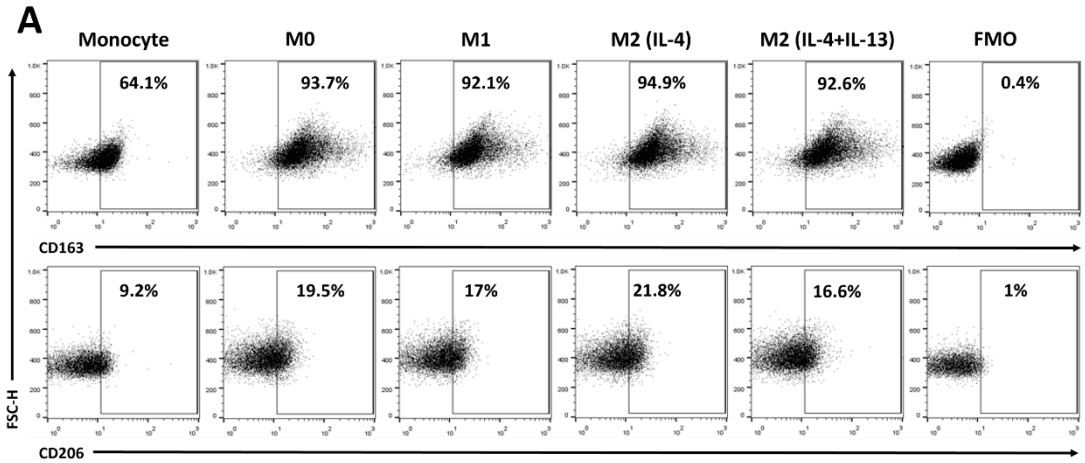
A
Monocyte
M0
M1
M2 (IL-4)
M2 (IL-4+IL-13)
FMO
64.1%
93.7%
92.1%
94.9%
92.6%
0.4%
CD163
9.2%
19.5%
17%
21.8%
16.6%
1%
FSC-H
CD206

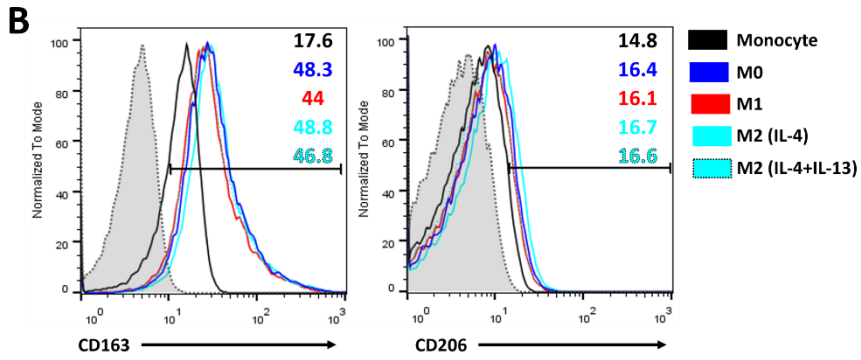
B
17.6
48.3
44
48.8
46.8
14.8
16.4
16.1
16.7
16.6
Normalized To Mode
CD163
CD206
Monocyte
M0
M1
M2 (IL-4)
M2 (IL-4+IL-13)

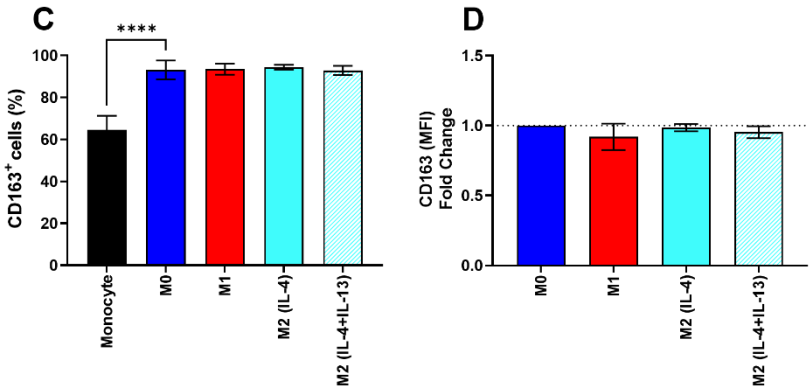
C
****
CD163+ cells (%)
Monocyte
M0
M1
M2 (IL-4)
M2 (IL-4+IL-13)

D
CD163 (MFI) Fold Change
M0
M1
M2 (IL-4)
M2 (IL-4+IL-13)

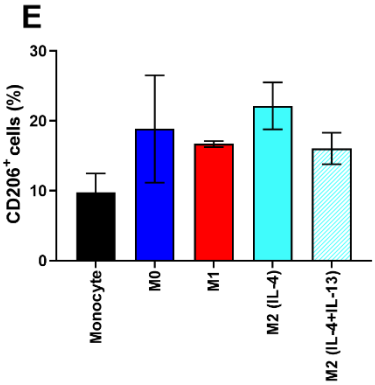
E
CD206+ cells (%)
Monocyte
M0
M1
M2 (IL-4)
M2 (IL-4+IL-13)

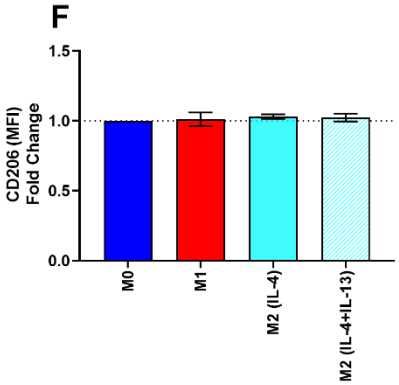
F
CD206 (MFI) Fold Change
M0
M1
M2 (IL-4)
M2 (IL-4+IL-13)

A12.3: Optimization 1 - Assessment of M1 and different M2 polarization protocols on CD163 and CD206 surface marker expression. Data obtained after 24hr incubation of differentiated M0 macrophages with M1 polarizing agents IFN-γ (20ng/mL) + LPS (10ng/mL), or M2 polarizing agents IL-4 (20ng/mL), or IL-4 (20ng/mL) + IL-13 (20ng/mL). [A] Representative contour plots showing the percentage of $CD163^+$ (top) and $CD206^+$ (bottom) cells. [B] Representative histograms showing mean fluorescent intensity (MFI) of CD163 (left) and CD206 (right). Numbers indicate MFI of live gated population. [C-F] Bar graphs showing the percentage of $CD163^+$ [C] and $CD206^+$ [E] cells, and MFI values for CD163 [D] and CD206 [F]. MFI values displayed as fold change versus the un-polarized M0 macrophage control. Plots and histograms illustrate one representative condition. Graphical data represent 1 experiment comprising of triplicate values. Data presented as mean ± SD. One-way ANOVA with post hoc Dunnett's applied versus the unpolarized M0 macrophage. ****p<0.0001.

A13: Effect of minocycline on adherent cell viability following M1-polarization of THP-1 macrophages

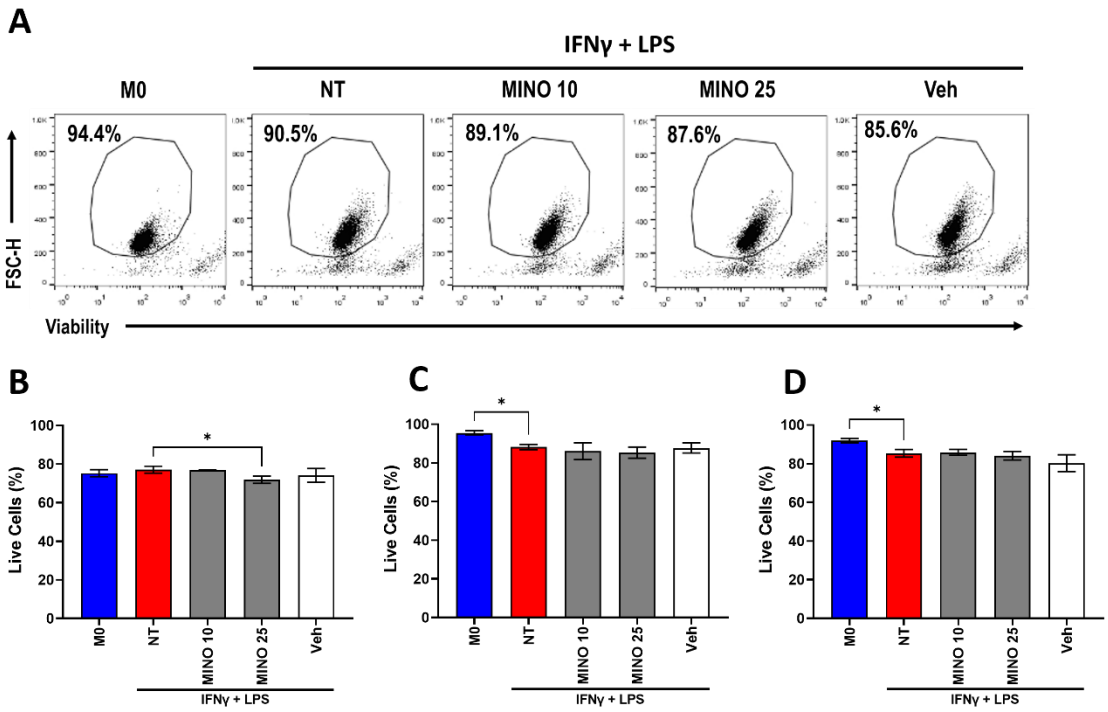

A13: Effect of minocycline on adherent cell viability following M1 polarization of THP-1 macrophages**.** Data obtained from adherent cells after 24hr incubation of differentiated M0 macrophages with M1 polarizing agents IFN-γ (20ng/mL) and LPS (10ng/mL). [A] Representative contour plots showing the percentage of live cells ($Zombie\ Aqua^{neg}$) cells. [B-D] Bar graphs showing the percentage of live cells. M0 = untreated PMA-differentiated M0 macrophage, NT = untreated M1-polarized macrophage, MINO 10 = Minocycline 10μM, MINO 25 = Minocycline 25μM, Veh = DMSO vehicle control 1:1000. Plots illustrate one representative experiment. Each graph represents 1 experiment comprising of triplicate values. Data presented as mean ± SD. One-way ANOVA with post hoc Dunnett's applied versus the untreated (NT) M1-polarized macrophage. *p<0.05.

A14: Effect of minocycline on adherent cell viability following M1 or M2 polarization of PBMC-derived macrophages

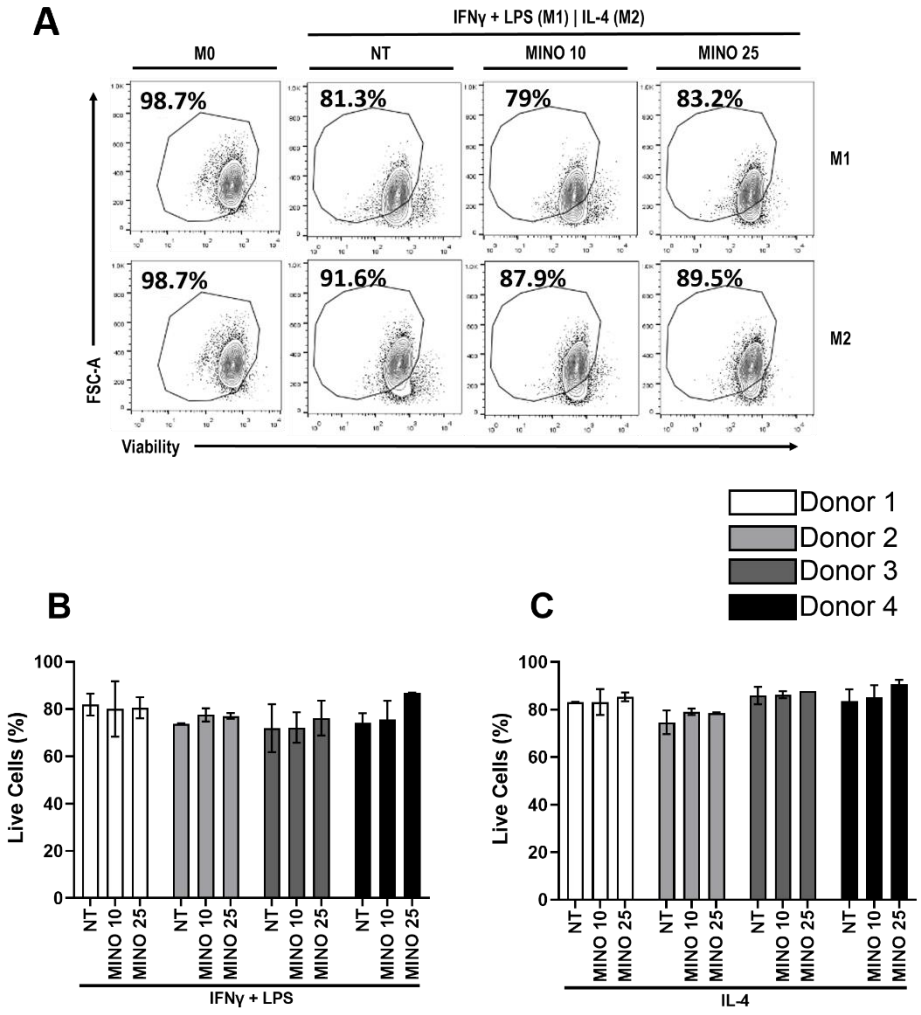

A14: Effect of minocycline on adherent cell viability following M1 or M2 polarization of PBMC-derived macrophages**.** Data obtained after 24hr incubation of M-CSF-expanded M0 macrophages with M1 (IFN-γ 20ng/mL + LPS 10mg/mL) or M2 (IL-4 20ng/mL) polarizing agents. [A] Representative contour plots showing the percentage of live (Zombie Aqua^{neg}) cells following the addition of M1 (top) or M2 (bottom) polarizing agents. [B and C] Bar graphs showing the percentage of live cells of M1 [B] and M2 [C] polarized macrophages. NT = no treatment, MINO 10 = Minocycline 10μM, MINO 25 = Minocycline 25μM. Plots illustrate one representative donor. Graphical data represent data from 4 donors each comprising of duplicate values. Data presented as mean ± SD. Two-way ANOVA with post hoc Dunnett's applied versus the un-treated M1 or M2 control.

A15: Effect of minocycline on adherent cell viability following LPS-activation of M1 polarized THP-1 macrophages

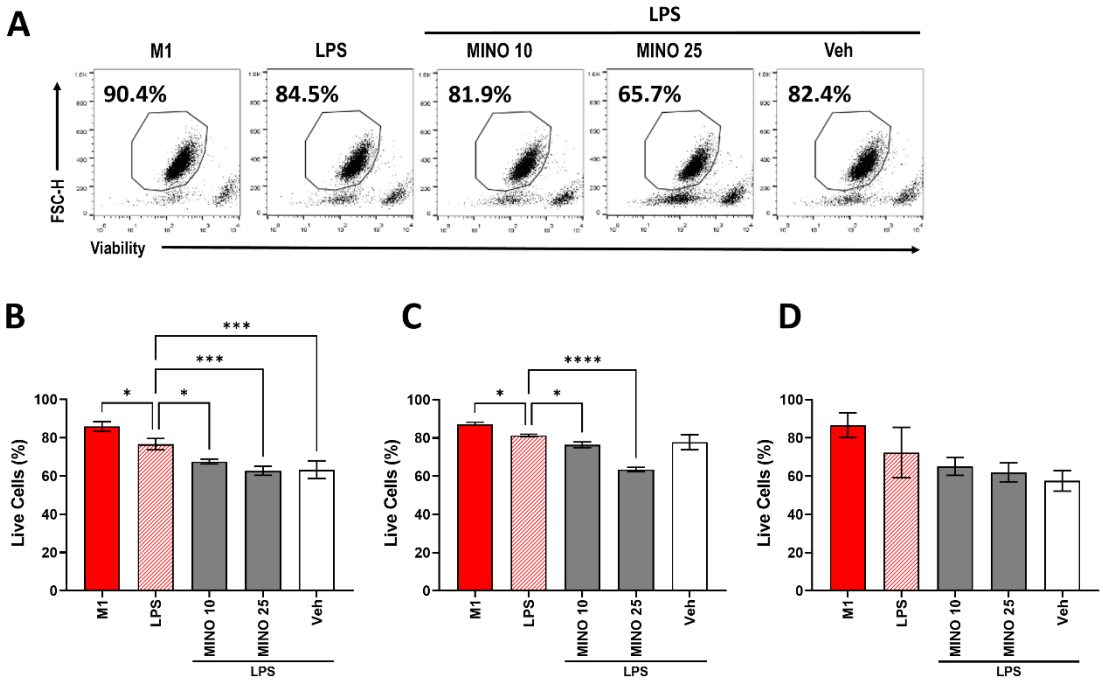

A15: Effect of minocycline on adherent cell viability following LPS-activation of M1 polarized THP-1 macrophages**.** Data obtained from adherent cells after 24hr incubation of pre-polarized M1 macrophages with LPS (100ng/mL). [A] Representative contour plots showing the percentage of live cells (Zombie Aqua^{neg}) cells. [B-D] Bar graphs showing the percentage of live cells. MINO 10 = Minocycline 10μM, MINO 25 = Minocycline 25μM, Veh = DMSO vehicle control 1:1000. Plots illustrate one representative experiment. Each graph represents 1 experiment comprising of triplicate values. Data presented as mean ± SD. One-way ANOVA with post hoc Dunnett's applied versus the un-activated M1-polarized macrophage. *p<0.05; ***p<0.001; ****p<0.0001.

A16: Effect of minocycline on adherent cell viability following LPS-activation of M1 or M2 polarized PBMC-derived macrophages

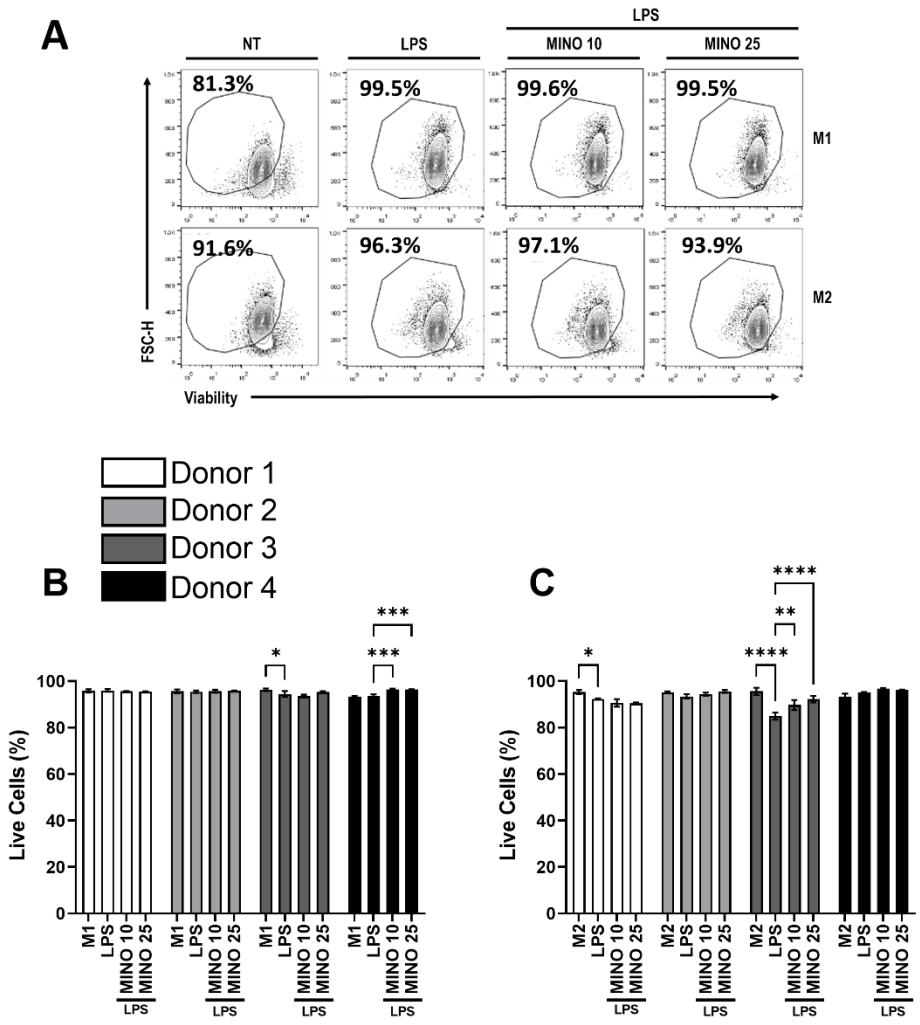

A16: Effect of minocycline on adherent cell viability following LPS-activation of M1 or M2 polarized PBMC-derived macrophages**.** Data obtained after 24hr incubation of M1 or M2 polarized PBMC-derived macrophages with LPS (100ng/mL). [A] Representative contour plots showing the percentage of live (Zombie Aqua^{neg}) cells following LPS-activation of M1 (top) or M2 (bottom) macrophages. [B and C] Bar graphs showing the percentage of live cells of M1 [B] and M2 [C] polarized macrophages following LPS-activation. MINO 10 = Minocycline 10μM, MINO 25 = Minocycline 25μM. Plots illustrate one representative donor. Graphical data represent data from 4 donors each comprising of duplicate values. Data presented as mean ± SD. Two-way ANOVA with post hoc Dunnett's applied versus the LPS-activated M1 or M2 control. *p<0.05; **p<0.01; ***p<0.001; ****p<0.0001.

A17: Effect of minocycline on cytokine production using the LEGENDPlex™ Assay

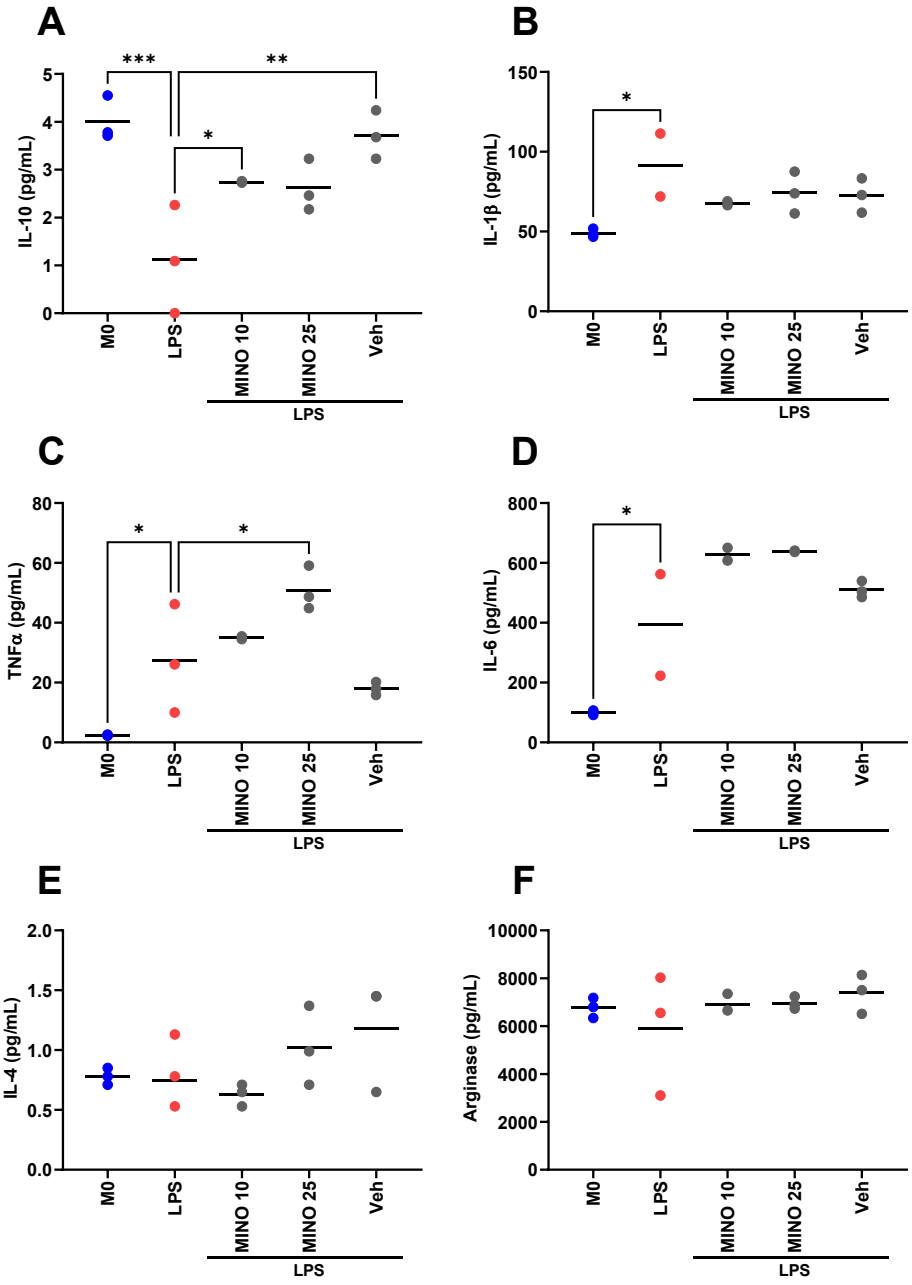

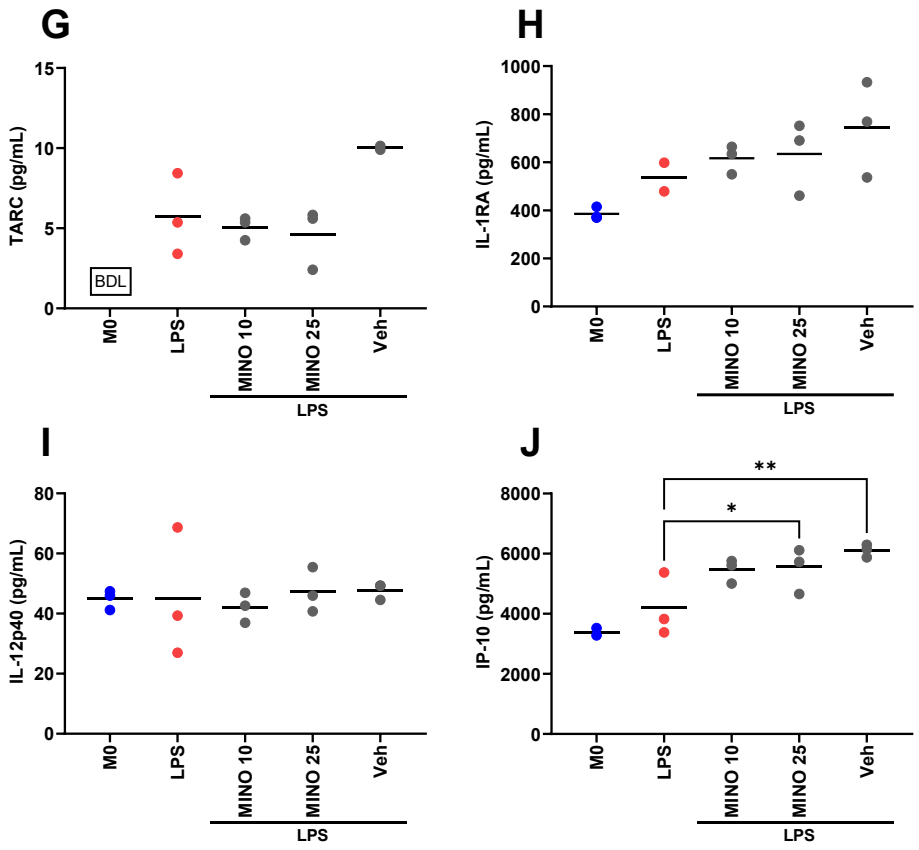

A17.1: Effect of minocycline on cytokine production from LPS-activated M0 THP-1 macrophages. Data obtained after 24hr incubation of differentiated M0 macrophages with LPS (100ng/mL). MINO 10 = minocycline 10μM, MINO 25 = minocycline 25μM, Veh = DMSO vehicle control (1:1000). Graphs showing data collected from THP-1 experimental samples for cytokines IL-10 [A], IL-1β [B], TNF-α [C], IL-6 [D], IL-4 [E], Arginase [F], TARC [G], IL-1RA [H], IL-12p40 [I] and IP-10 [J]. Graphs represent data from 1 experiment comprising triplicate values. One-way ANOVA with post hoc Dunnett's applied versus the LPS-activated control. *p<0.05; **p<0.01; ***p<0.001.

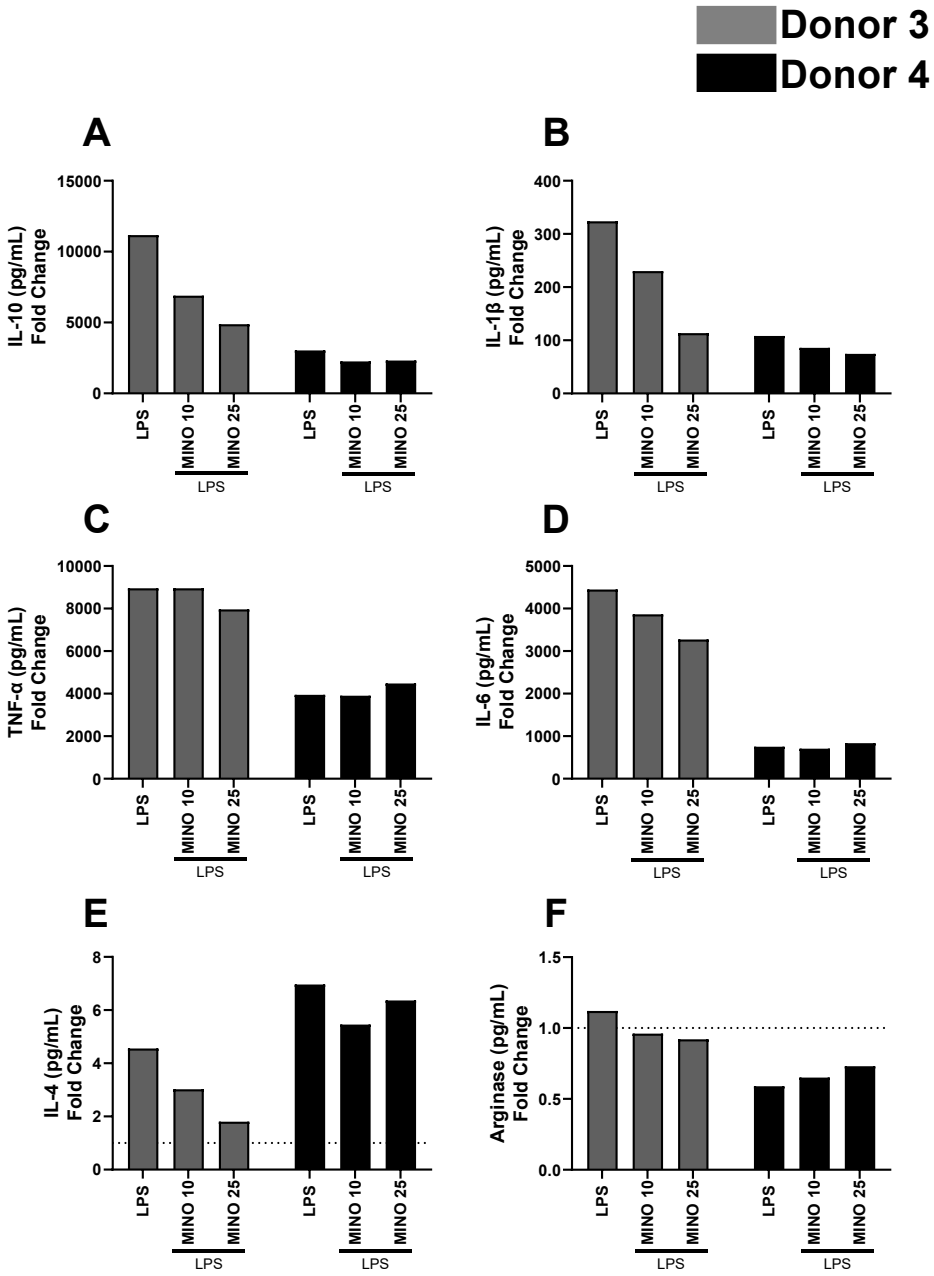
Donor 3
Donor 4
A
IL-10 (pg/mL) Fold Change
15000
10000
5000
0
LPS
MINO 10
MINO 25
LPS
MINO 10
MINO 25
LPS
LPS
B
IL-1β (pg/mL) Fold Change
400
300
200
100
0
C
TNF-α (pg/mL) Fold Change
10000
8000
6000
4000
2000
0
D
IL-6 (pg/mL) Fold Change
5000
4000
3000
2000
1000
0
E
IL-4 (pg/mL) Fold Change
8
6
4
2
0
F
Arginase (pg/mL) Fold Change
1.5
1.0
0.5
0.0

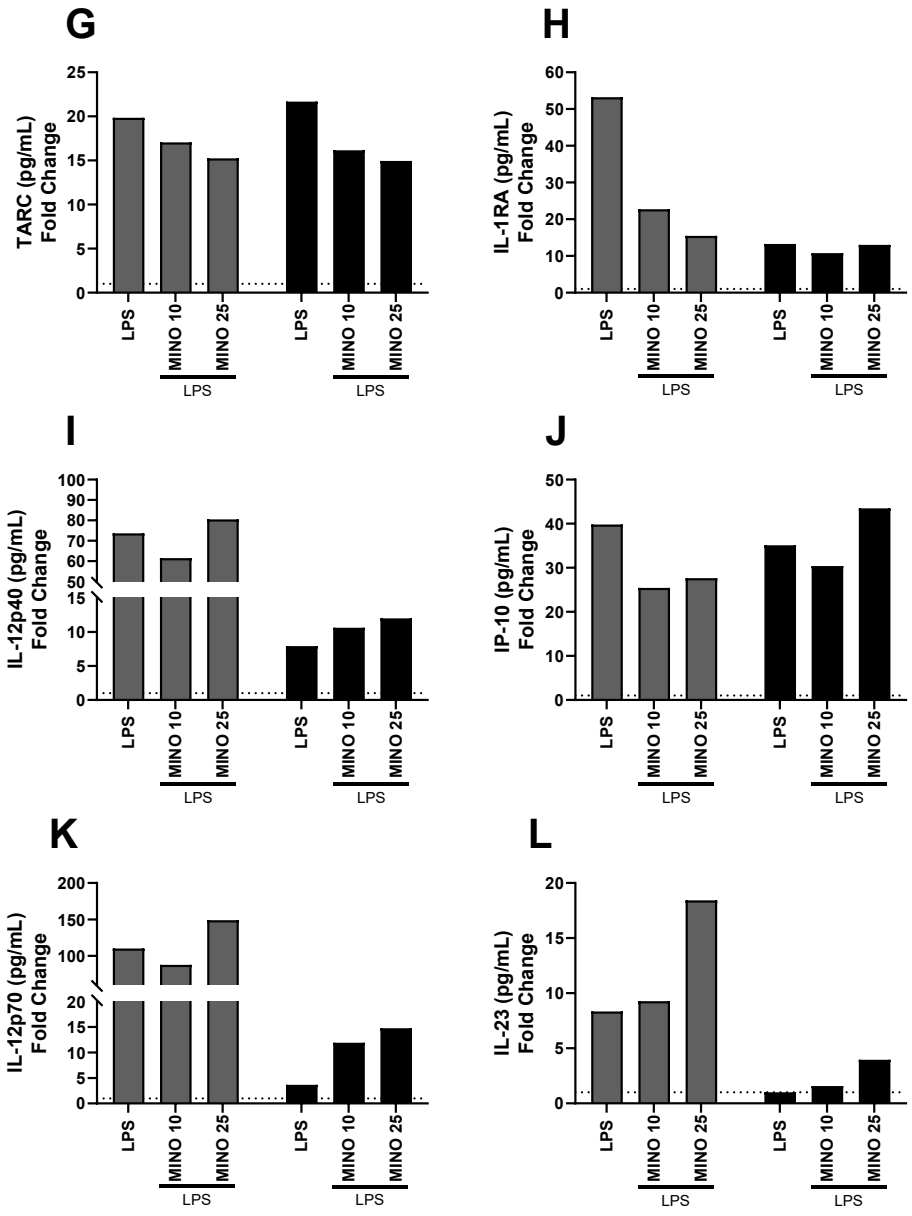

A17.2: Effect of minocycline on cytokine production from LPS-activated M0 PBMC-derived macrophages. Data obtained after 24hr incubation of differentiated M0 macrophages with LPS (100ng/mL). MINO 10 = minocycline 10μM, MINO 25 = minocycline 25μM. Bar graphs showing data collected from PBMC experimental samples for cytokines IL-10 [A], IL-1β [B], TNF-α [C], IL-6 [D], IL-4 [E], Arginase [F], TARC [G], IL-1RA [H], IL-12p40 [I], IP-10 [J], IL-12p70 [K] and IL-23 [L]. Graphs represent data from 2 individual donors each comprising one value. No statistics available.

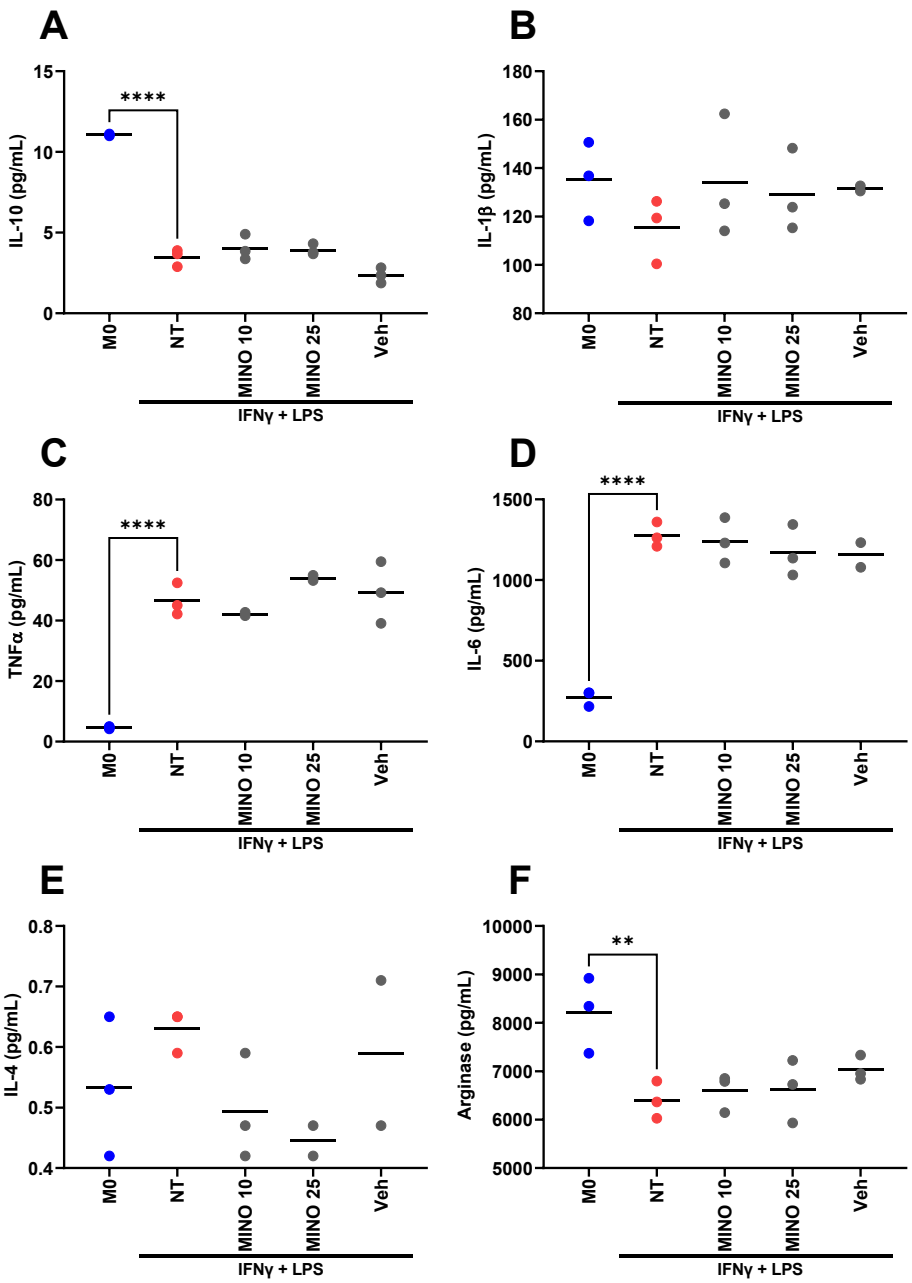
A
IL-10 (pg/mL)
15
10
5
0
****
M0
NT
MINO 10
MINO 25
Veh
IFNγ + LPS
B
IL-1β (pg/mL)
180
160
140
120
100
80
M0
NT
MINO 10
MINO 25
Veh
IFNγ + LPS
C
TNFα (pg/mL)
80
60
40
20
0
****
M0
NT
MINO 10
MINO 25
Veh
IFNγ + LPS
D
IL-6 (pg/mL)
1500
1000
500
0
****
M0
NT
MINO 10
MINO 25
Veh
IFNγ + LPS
E
IL-4 (pg/mL)
0.8
0.7
0.6
0.5
0.4
M0
NT
MINO 10
MINO 25
Veh
IFNγ + LPS
F
Arginase (pg/mL)
10000
9000
8000
7000
6000
5000
**
M0
NT
MINO 10
MINO 25
Veh
IFNγ + LPS

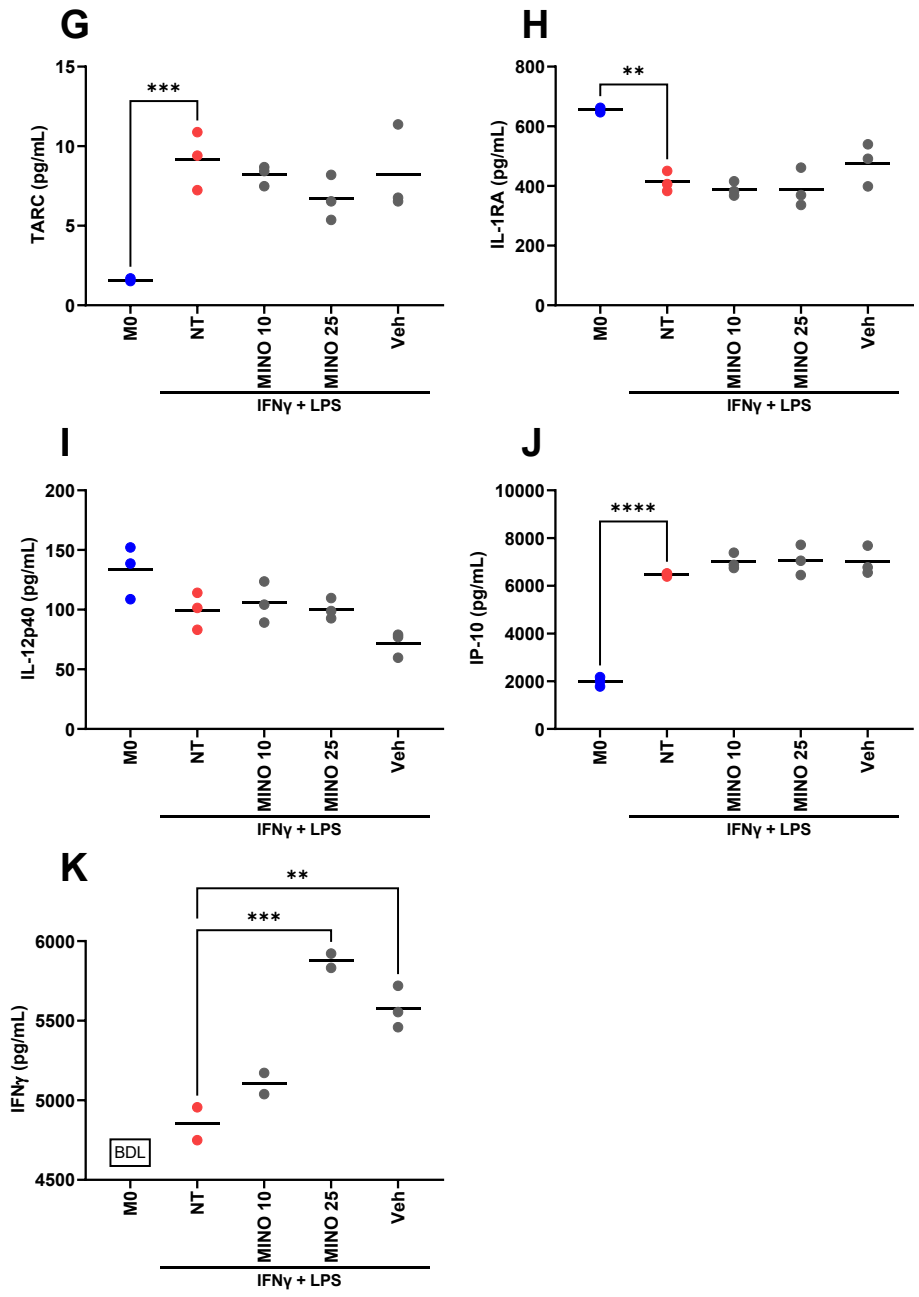

A17.3: Effect of minocycline on cytokine production from M1-polarized THP-1 macrophages. Data obtained from adherent cells after 24hr incubation of differentiated M0 macrophages with M1 polarizing agents IFN-γ (20ng/mL) and LPS (10ng/mL). NT = untreated M1 macrophage, MINO 10 = minocycline 10μM, MINO 25 = minocycline 25μM, Veh = DMSO vehicle control (1:1000). Graphs showing data collected from THP-1 experimental samples for cytokines IL-10 [A], IL-1β [B], TNF-α [C], IL-6 [D], IL-4 [E], Arginase [F], TARC [G], IL-1RA [H], IL-12p40 [I], IP-10 [J] and IFN-γ [K]. Graphs represent data from 1 experiment comprising triplicate values. One-way ANOVA with post hoc Dunnett's applied versus the M1-polarized control. **p<0.01; ***p<0.001; ****p<0.0001.

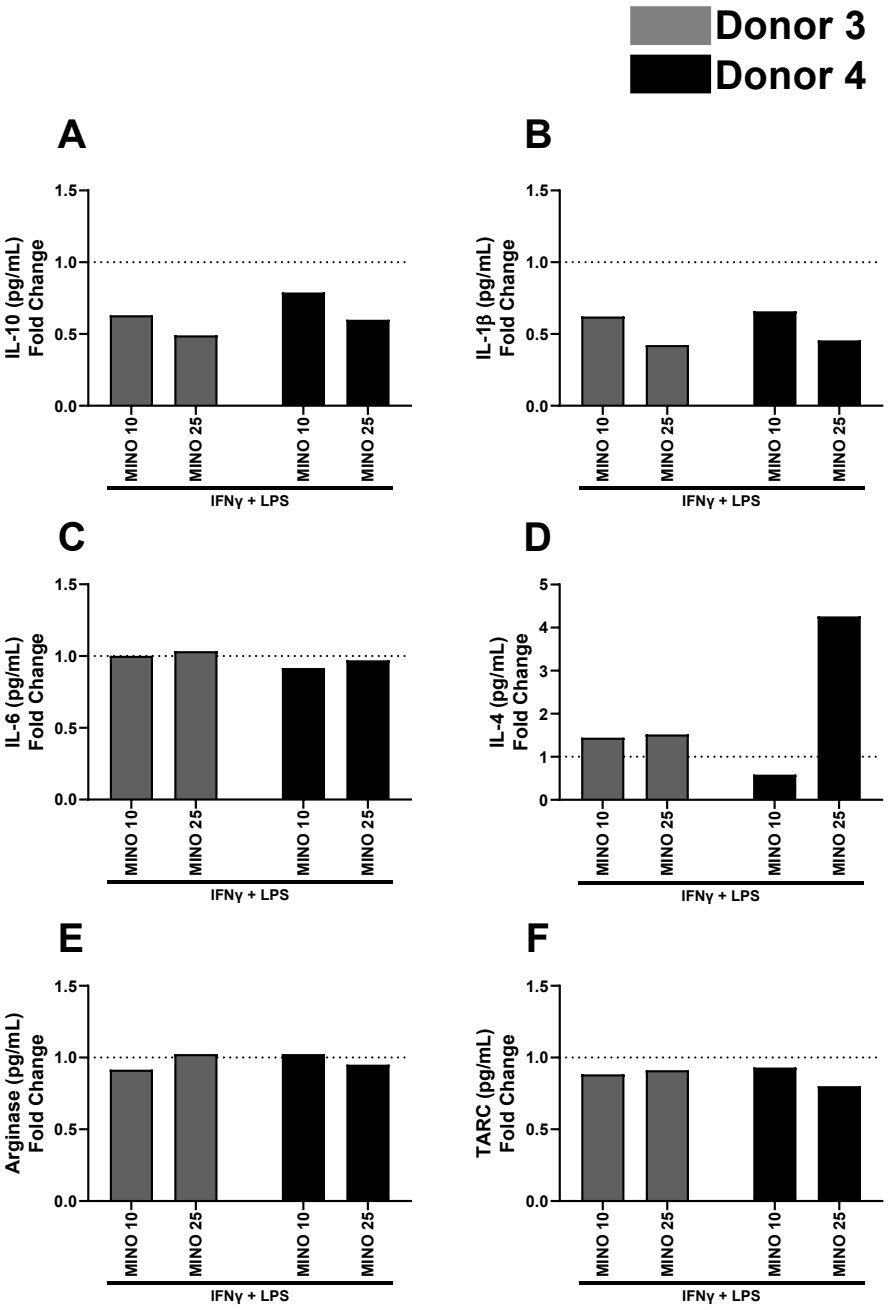
Donor 3
Donor 4
A
IL-10 (pg/mL) Fold Change
1.5
1.0
0.5
0.0
MINO 10
MINO 25
MINO 10
MINO 25
IFNγ + LPS
B
IL-1β (pg/mL) Fold Change
1.5
1.0
0.5
0.0
MINO 10
MINO 25
MINO 10
MINO 25
IFNγ + LPS
C
IL-6 (pg/mL) Fold Change
1.5
1.0
0.5
0.0
MINO 10
MINO 25
MINO 10
MINO 25
IFNγ + LPS
D
IL-4 (pg/mL) Fold Change
5
4
3
2
1
0
MINO 10
MINO 25
MINO 10
MINO 25
IFNγ + LPS
E
Arginase (pg/mL) Fold Change
1.5
1.0
0.5
0.0
MINO 10
MINO 25
MINO 10
MINO 25
IFNγ + LPS
F
TARC (pg/mL) Fold Change
1.5
1.0
0.5
0.0
MINO 10
MINO 25
MINO 10
MINO 25
IFNγ + LPS

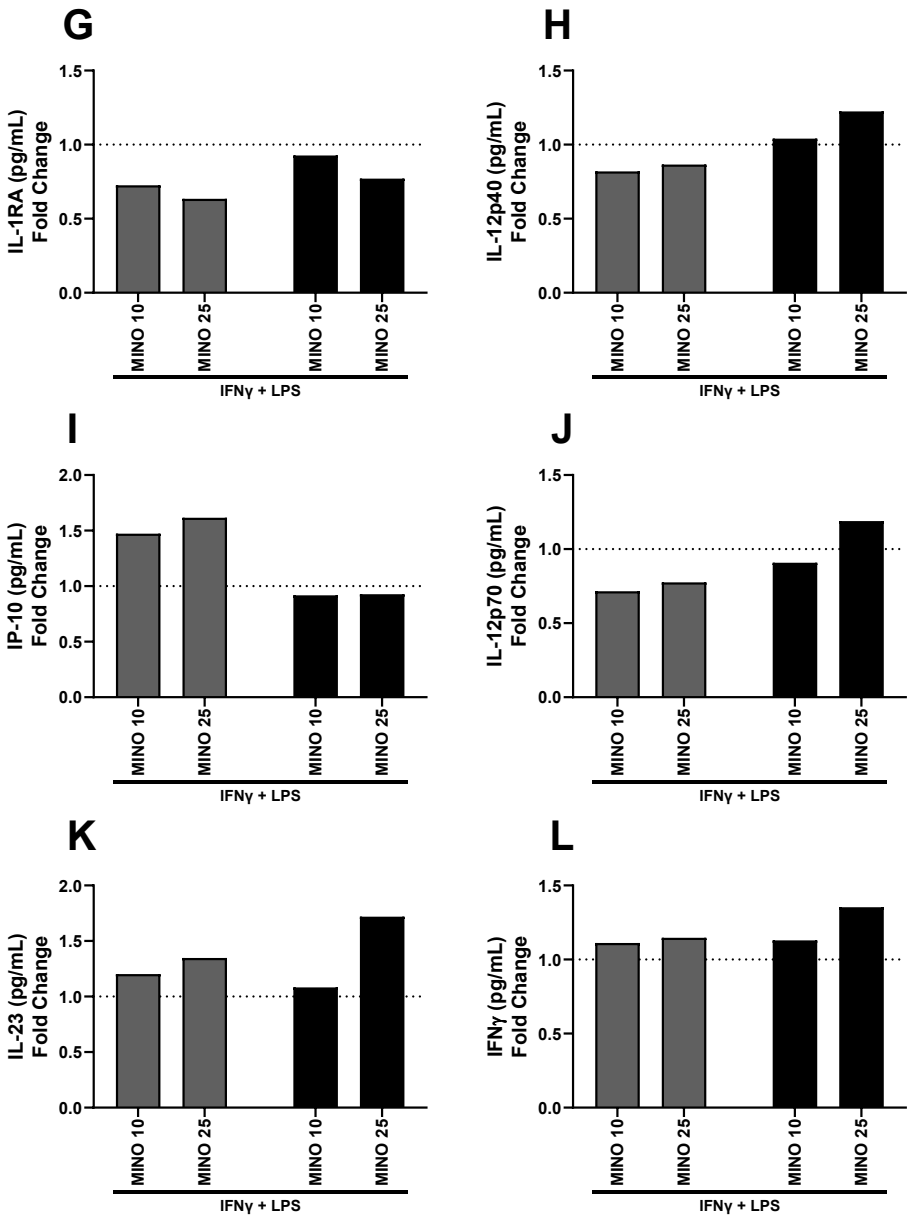

A17.4: Effect of minocycline on cytokine production from M1-polarized PBMC-derived macrophages. Data obtained from adherent cells after 24hr incubation of differentiated M0 macrophages with M1 polarizing agents IFN-γ (20ng/mL) and LPS (10ng/mL). MINO 10 = minocycline 10μM, MINO 25 = minocycline 25μM. Bar graphs showing data collected from PBMC experimental samples for cytokines IL-10 [A], IL-1β [B], IL-6 [C], IL-4 [D], Arginase [E], TARC [F], IL-1RA [G], IL-12p40 [H], IP-10 [I], IL-12p70 [J], IL-23 [K] and IFN-γ [L]. Graphs represent data from 2 individual donors each comprising one value. No statistics available.

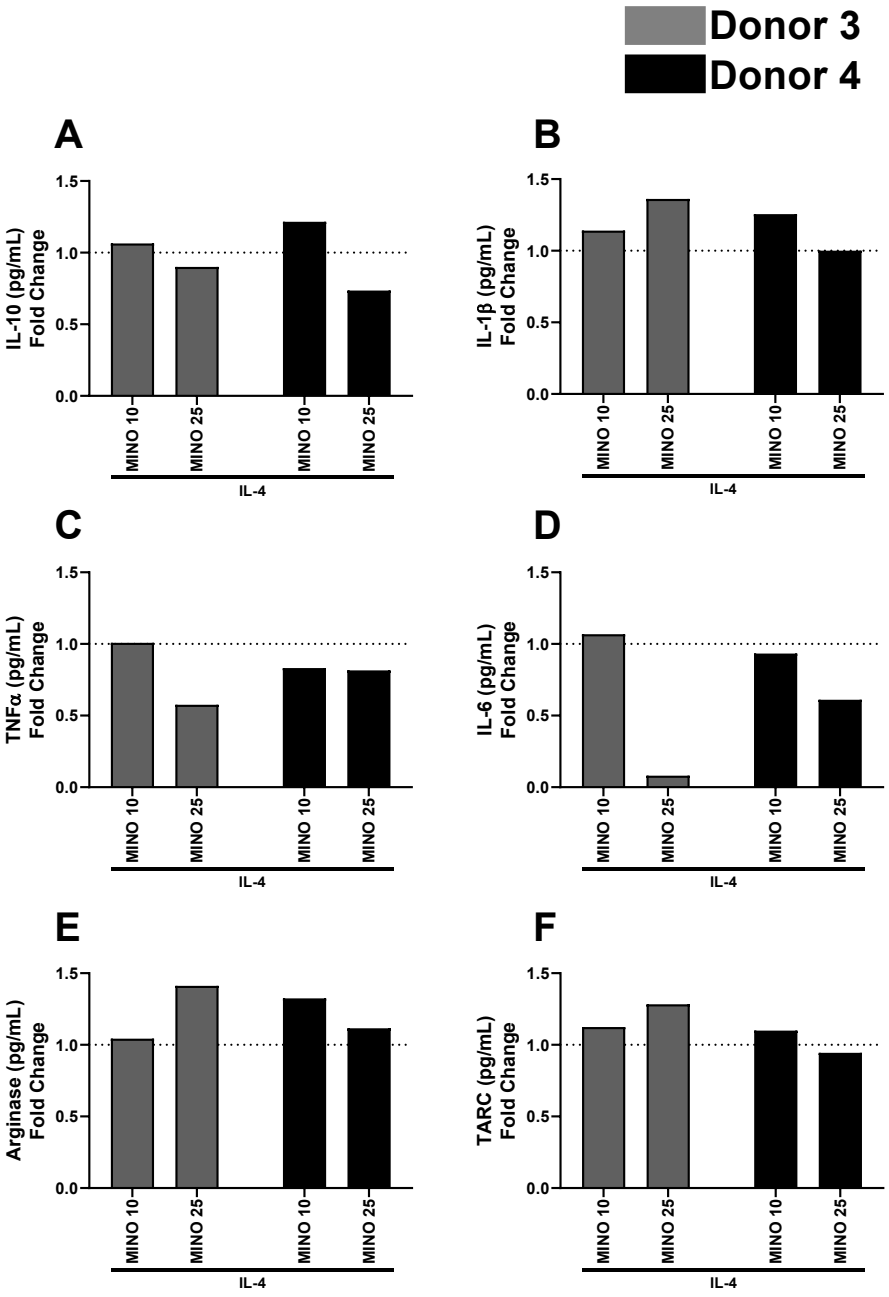
Donor 3
Donor 4
A
IL-10 (pg/mL) Fold Change
B
IL-1β (pg/mL) Fold Change
C
TNFα (pg/mL) Fold Change
D
IL-6 (pg/mL) Fold Change
E
Arginase (pg/mL) Fold Change
F
TARC (pg/mL) Fold Change
1.5
1.0
0.5
0.0
MINO 10
MINO 25
MINO 10
MINO 25
IL-4

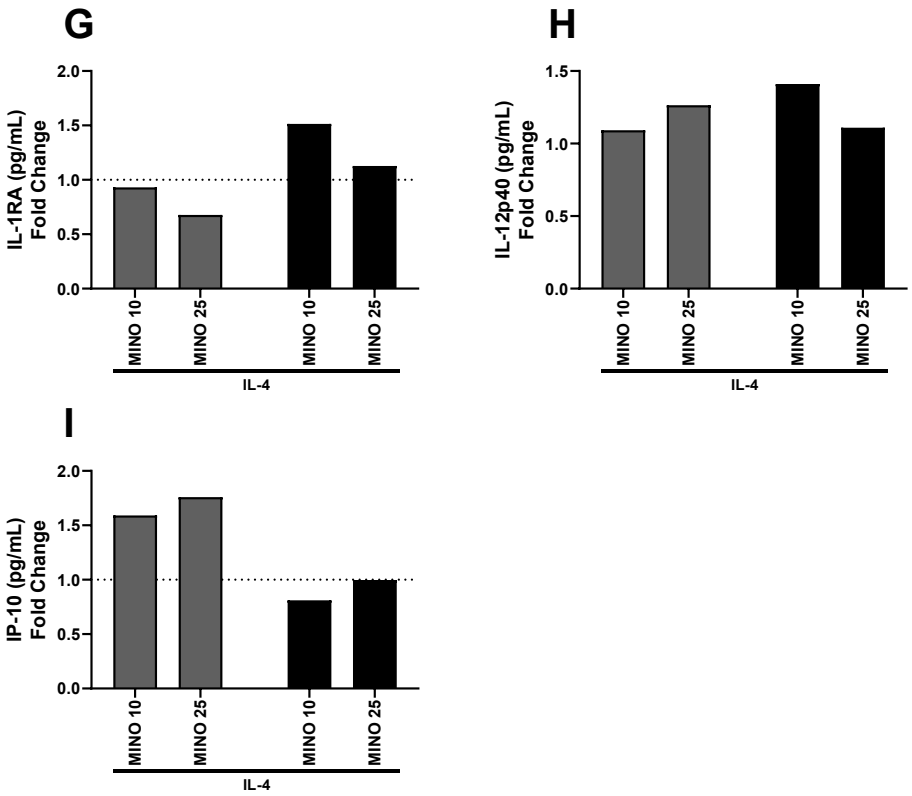

A17.5: Effect of minocycline on cytokine production from M2-polarized PBMC-derived macrophages. Data obtained from adherent cells after 24hr incubation of differentiated M0 macrophages with M2 polarizing agent IL-4 (20ng/mL). MINO 10 = minocycline 10μM, MINO 25 = minocycline 25μM. Bar graphs showing data collected from PBMC experimental samples for cytokines IL-10 [A], IL-1β [B], TNF-α [C], IL-6 [D], Arginase [E], TARC [F], IL-1RA [G], IL-12p40 [H], IP-10 [I]. Graphs represent data from 2 individual donors each comprising one value. No statistics available.

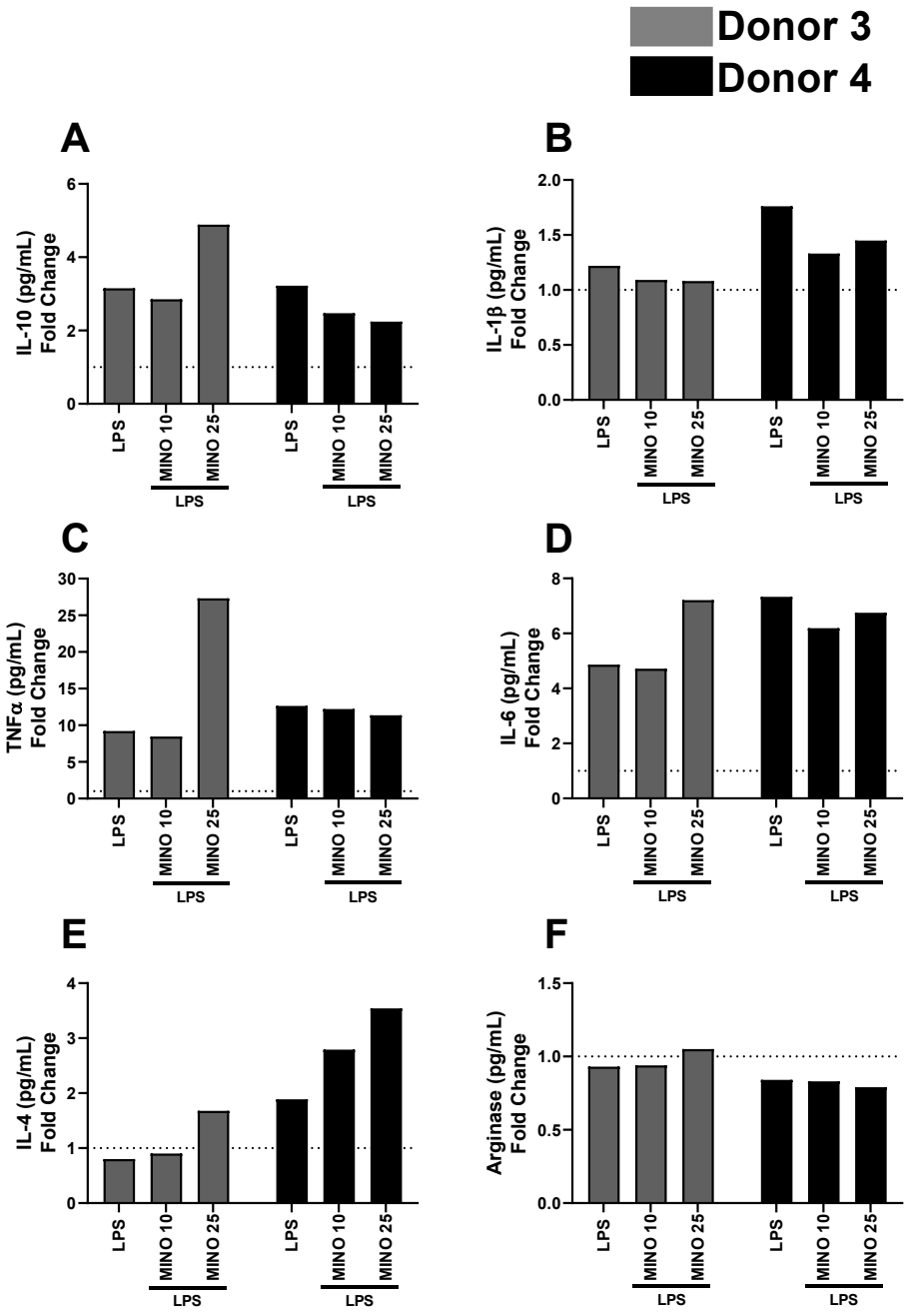
Donor 3
Donor 4
A
IL-10 (pg/mL) Fold Change
0
2
4
6
LPS
MINO 10
MINO 25
LPS
MINO 10
MINO 25
LPS
LPS
B
IL-1β (pg/mL) Fold Change
0.0
0.5
1.0
1.5
2.0
LPS
MINO 10
MINO 25
LPS
MINO 10
MINO 25
LPS
LPS
C
TNFα (pg/mL) Fold Change
0
5
10
15
20
25
30
LPS
MINO 10
MINO 25
LPS
MINO 10
MINO 25
LPS
LPS
D
IL-6 (pg/mL) Fold Change
0
2
4
6
8
LPS
MINO 10
MINO 25
LPS
MINO 10
MINO 25
LPS
LPS
E
IL-4 (pg/mL) Fold Change
0
1
2
3
4
LPS
MINO 10
MINO 25
LPS
MINO 10
MINO 25
LPS
LPS
F
Arginase (pg/mL) Fold Change
0.0
0.5
1.0
1.5
LPS
MINO 10
MINO 25
LPS
MINO 10
MINO 25
LPS
LPS

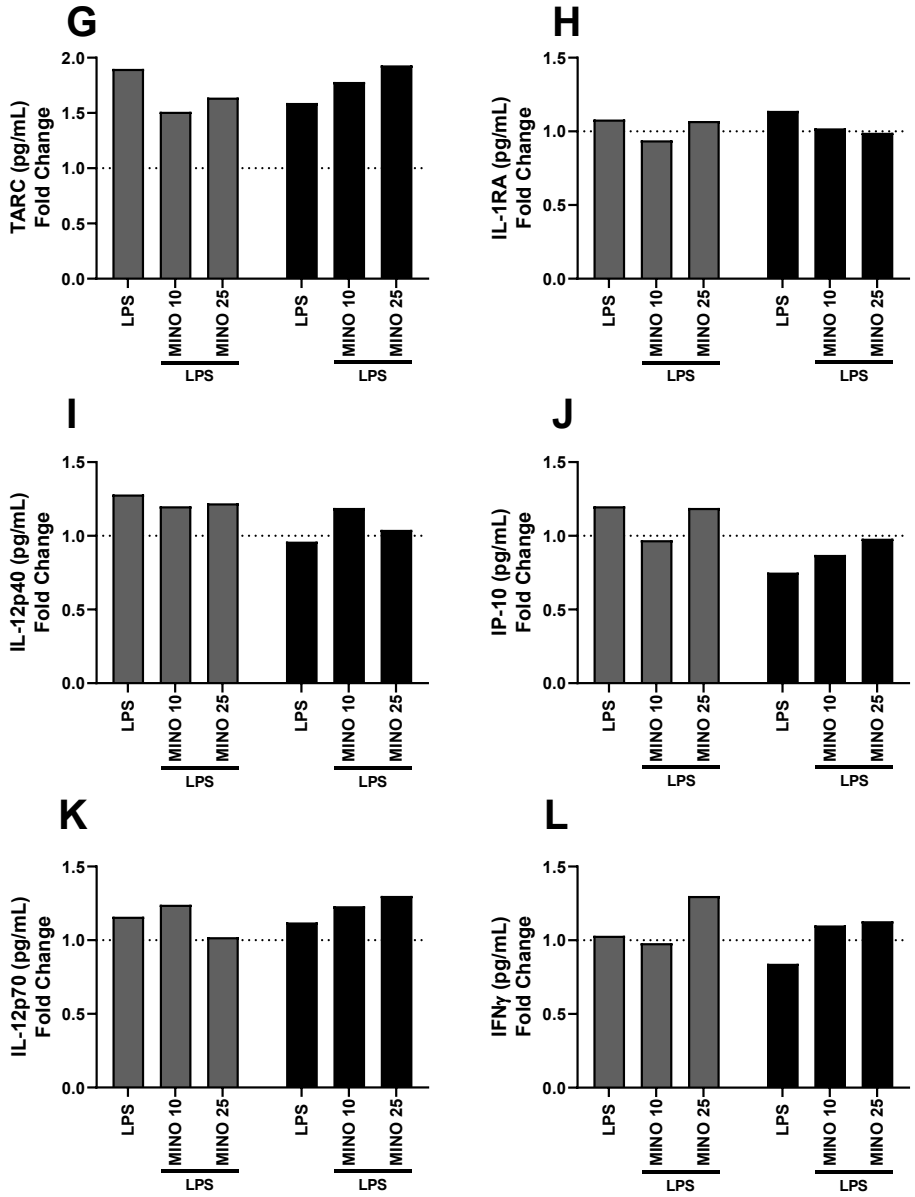

A17.6: Effect of minocycline on cytokine production from LPS-activated PBMC-derived M1 macrophages. Data obtained from adherent cells after 24hr incubation of polarized M1 macrophages with LPS (100ng/mL). MINO 10 = minocycline 10μM, MINO 25 = minocycline 25μM. Bar graphs showing data collected from PBMC experimental samples for cytokines IL-10 [A], IL-1β [B], TNF-α [C], IL-6 [D], IL-4 [E], Arginase [F], TARC [G], IL-1RA [H], IL-12p40 [I], IP-10 [J], IL-12p70 [K], IFN-γ [L]. Graphs represent data from 2 individual donors each comprising one value. No statistics available.

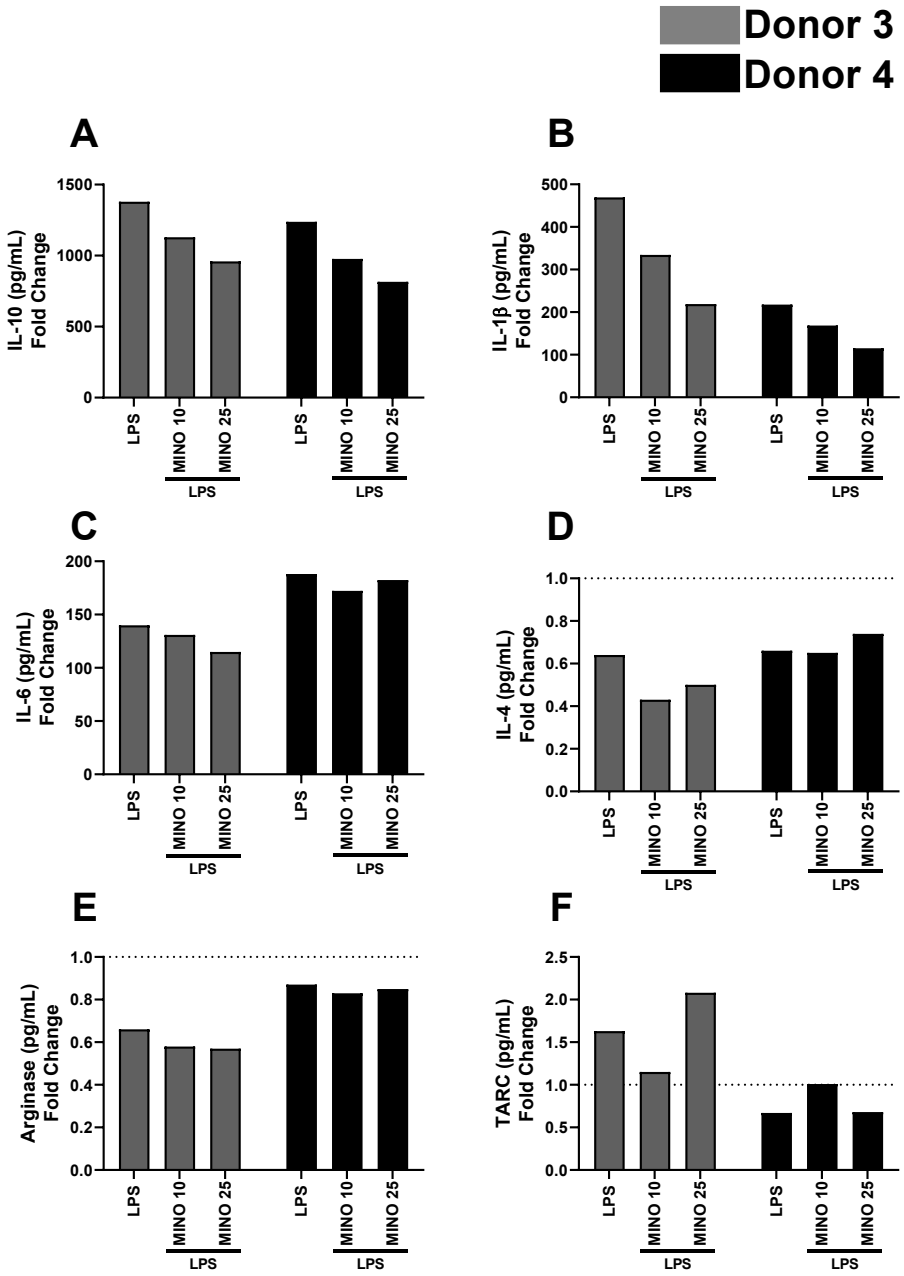
Donor 3
Donor 4
A
IL-10 (pg/mL) Fold Change
1500
1000
500
0
B
IL-1β (pg/mL) Fold Change
500
400
300
200
100
0
C
IL-6 (pg/mL) Fold Change
200
150
100
50
0
D
IL-4 (pg/mL) Fold Change
1.0
0.8
0.6
0.4
0.2
0.0
E
Arginase (pg/mL) Fold Change
1.0
0.8
0.6
0.4
0.2
0.0
F
TARC (pg/mL) Fold Change
2.5
2.0
1.5
1.0
0.5
0.0
LPS
MINO 10
MINO 25
LPS
LPS
LPS

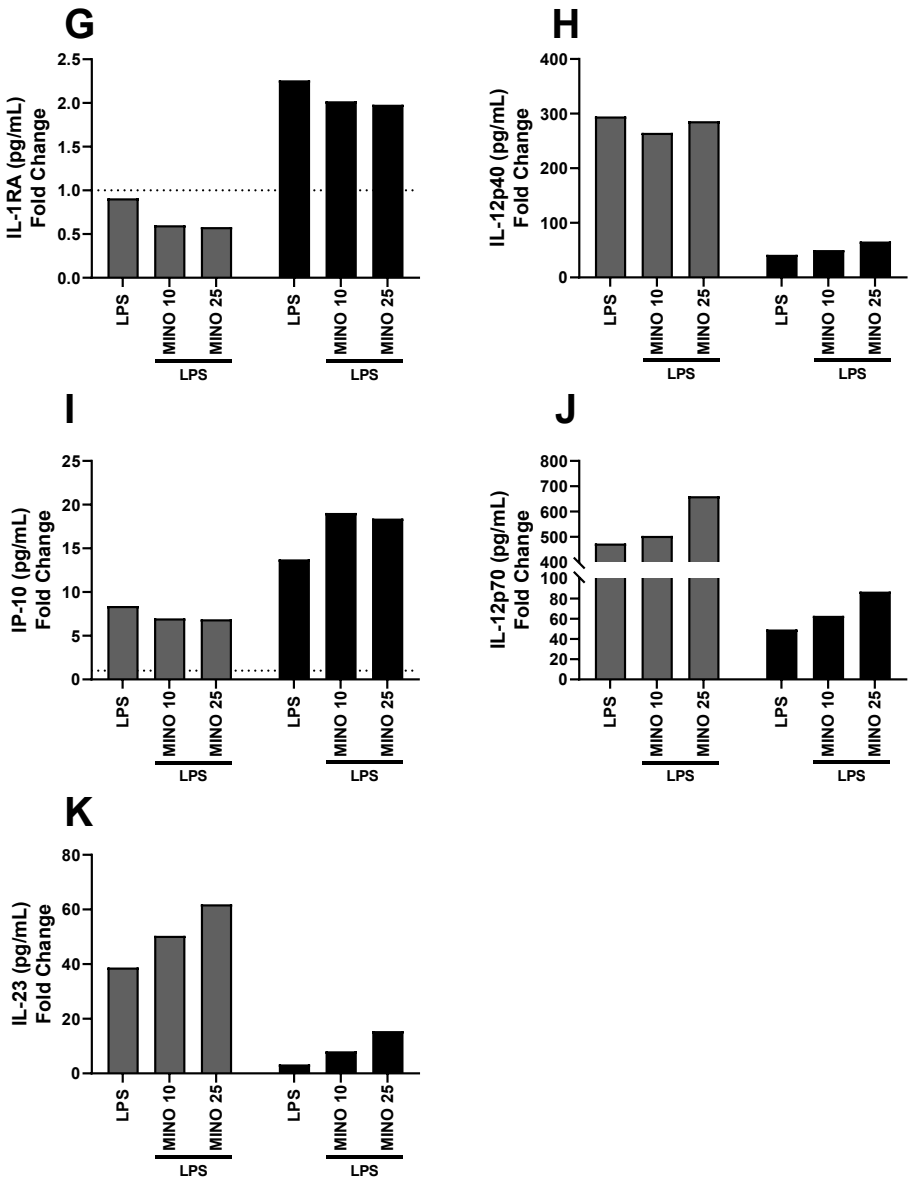

A17.7: Effect of minocycline on cytokine production from LPS-activated PBMC-derived M2 macrophages. Data obtained from adherent cells after 24hr incubation of polarized M2 macrophages with LPS (100ng/mL). MINO 10 = minocycline 10μM, MINO 25 = minocycline 25μM. Bar graphs showing data collected from PBMC experimental samples for cytokines IL-10 [A], IL-1β [B], IL-6 [C], IL-4 [D], Arginase [E], TARC [F], IL-1RA [G], IL-12p40 [H], IP-10 [I], IL-12p70 [J], Il-23 [K]. Graphs represent data from 2 individual donors each comprising one value. No statistics available.